Dissertation zur Erlangung des Doktorgrades

der Fakultät für Chemie und Pharmazie

der Ludwig-Maximilians-Universität München

Quantifying the Electrophilic Reactivities of Quinone Methides:

From One-Bond Electrophilicities to Limitations

Christoph Philipp Groß

aus

München, Bayern

2025

Erklärung

Diese Dissertation wurde im Sinne von § 7 der Promotionsordnung vom 28. November 2011 von Herrn PD Dr. Armin R. Ofial betreut.

Eidesstattliche Versicherung

Diese Dissertation wurde eigenständig und ohne unerlaubte Hilfe erarbeitet.

München, den 14.08.2025

X _____
  Christoph Groß

Dissertation eingereicht am: 21.08.2025

1. Gutachter: PD Dr. Armin R. Ofial

2. Gutachter: Prof. Dr. Hendrik Zipse

Mündliche Prüfung am: 30.10.2025

Acknowledgement

Publications

Parts of this thesis have been published in scientific journals:

(1) "**Defining the Synthetic Scope of *ortho*-Quinone Methides by Quantifying Their Electrophilicity**"
C. Gross, A. Eitzinger, N. Hampel, P. Mayer, A. R. Ofial, *Chem. Eur. J.* **2025**, *31*, e202403785.

(2) "**Asymmetric isochalcogenourea-catalysed (4+2)-cycloadditions of *ortho*-quinone methides and allenoates**"
A. Scheucher, C. Gross, M. Piringer, J. Novacek, A. R. Ofial, M. Waser, *Org. Biomol. Chem.* **2025**, *23*, 827.

(3) "**Reactivity of *δ*-Functionalized *para*-Quinone Methides in Nucleophilic Addition Reactions**"
C. Gross, A. Eitzinger, P. Mayer, A. R. Ofial, *Chem. Eur. J.* **2025**, *31*, e202501224.

Contributions to Conferences

Parts of this work were presented at scientific conferences:

2022-07   17th Belgium Organic Synthesis Symposium (XVII BOSS), Namur (Belgium)

Poster presentation: "Electrophilic Reactivity of 7-Cyano-*p*-Quinone Methides"

2023-09   19th European Symposium on Organic Reactivity (ESOR2023), Amsterdam (Netherlands)

Poster presentation: "Electrophilic Reactivities of *ortho*-Quinone Methides"

2024-09   23th Lecture Conference ORCHEM 2024, Regensburg (Germany)

Poster presentation: "Electrophilic Reactivities of *ortho*-Quinone Methides"

External research visit

2024-01 – 2024-02   with Prof. Dr. Mario Waser at the Johannes Kepler Universität (JKU) Linz (Austria)

Research project: "Asymmetric isochalcogenourea catalysed (4+2) cycloadditions of *ortho*-quinone methides and allenoates"

Abbreviations

$\%V_{bur}$	Buried volume		HSQC	Heteronuclear single quantum coherence
18-c-6	18-Crown-6 ether		HMBC	Heteronuclear multiple bond correlation
A	Absorbance		Nuc	Nucleophile
Abs	Absorbance		oQM	*ortho*-quinone methide
Ac	Acetyl		pQM	*para*-quinone methide
Acc	Acceptor		r.t.	Room temperature
aq. sat.	Aqueous saturated		Ref.	Reference
ATR	Attenuated Total Reflection		R_f	Retardation factor
Bn	Benzyl		scXRD	Single crystal X-Ray diffraction
Bu	Butyl		refls.	Reflections
C	Constant		R_{int}	Mean error of symmetry Equivalent reflections
c	concentration		R_w	Weighted R-value
calcd. or calc.	calculated		S	Goodness of fit
d	Optical path length		Z	Number of units
DCM	Dichloromethane		μ	Absorption coefficient
DMSO	Dimethylsulfoxide		SET	Single electron transfer
DNA	Desoxyribonucleic acid		T	temperature
d.r.	Diastereomeric ratio		t	time
$E_{1/2}$	Half-wave potential		THF	Tetrahydrofuran
EI	Electron Ionization or Electrophile		TLC	Thin-layer chromatography
E_p^{ox}	Oxidation peak potential		TMS	Trimethylsilane
E_p^{red}	Reduction peak potential		Unit Prefixes	
Eq. or eq	Equation		c	Centi
equiv.	Equivalence		k	Kilo
e.r.	Enantiomeric ratio		M	Mega
ESI	Electrospray Ionization		m	Milli
exp	Exponential or experimental		n	Nano
Exptl.	experimental		μ	Micro
F	Faraday constant		Units	
GC	Gas chromatography		%	percent
HRMS	High resolution mass spectrometry		°C	Degree Celsius
I	Intensity of light		Å	Angstrom
I_0	Intensity of incoming light		e	Elementary charge
IChU	Isochalcogenureas		g	gram
IR	Infrared		h	hour
J	Coupling constant		Hz	Hertz
k_2	Second-order rate constant		K	Kelvin
k_{obs}	Observed rate constant		L	Liter
LCC	Lignin-carbohydrate-complex		M	Molar concentration
lg	Common logarithm		m	Meter
M	mass peak		min	Minute
m.p.	Melting point		mol	Mole
max	Maximum		ppm	Parts per million
m/z	Mass-to-charge ratio		s	Second
MAA	Methyl anion affinity		V	Volt
MeCN	Acetonitrile		UV/Vis	Ultraviolet-Visible
MOM	Methoxymethyl ether		V	Volume
n	Integer number		vs	versus
n.d.	not defined		ϕ	Dihedral Angle
NMR	Nuclear Magnetic Resonance		δ	Chemical shift or position in the molecule
C_q	Quaternary carbon		σ or σ^+	Hammett substituent constants
d	Doublet		$\Delta G^{\ddagger}$	Gibbs activation energy
m	Multiplet		ΔG_R	Gibbs reaction energy
q	Quartet		λ	wavelength
s	Singlet		ρ	density
t	Triplet		ε	Molar absorption coefficient
COSY	Correlated spectroscopy		$\tilde{\nu}$	Wavenumber

Table of contents

Chapter 1. Summary

1.1. Reactivity of *δ*-Functionalized *para*-Quinone Methides in Nucleophilic Addition Reactions

The electrophilic reactivities of six *δ*-functionalized *para*-quinone methides (*δ*-FG-*p*QMs) have been characterized from the kinetics of addition reactions of carbanionic reference nucleophiles to the QMs' exocyclic double bond. The progress of these rate-determining carbon-carbon bond-forming reactions was monitored photometrically in DMSO at 20°C (Figure 1).
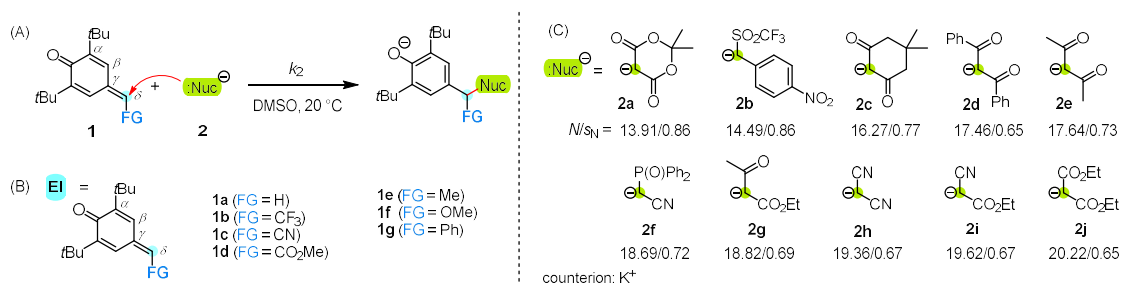
Figure 1. (A) Nucleophilic addition reaction at the exocyclic double bond of *δ*-functionalized *p*QMs; (B) Overview of investigated *p*QMs and (C) carbanionic reference nucleophiles used. The electrophilicity parameter *E* of *p*QM **1b** was characterized in ref. *EJOC* **2020**, *2020*, 3812-3817.

The conversion of the colored *p*QMs was observed at or near their absorbance maxima under pseudo first-order reaction conditions where the concentration of the carbanions exceeded the concentration of the *p*QMs by at least a factor of ten (Figure 2A, B). Experimental second-order rate constants k_2 of these bimolecular reactions were determined by plotting the first order rate constants k_{obs} against the corresponding nucleophile concentrations (Figure 2C). Finally, the electrophilicity descriptors *E* of the *p*QMs were quantified by using the Mayr-Patz equation $\lg k_2 = s_N(N + E)$ and a linear regression analysis. Plots of $(\lg k_2)/s_N$ against the nucleophilicity parameters *N* gave linear correlations with a unity slope as required for electrophiles (Figure 2D).
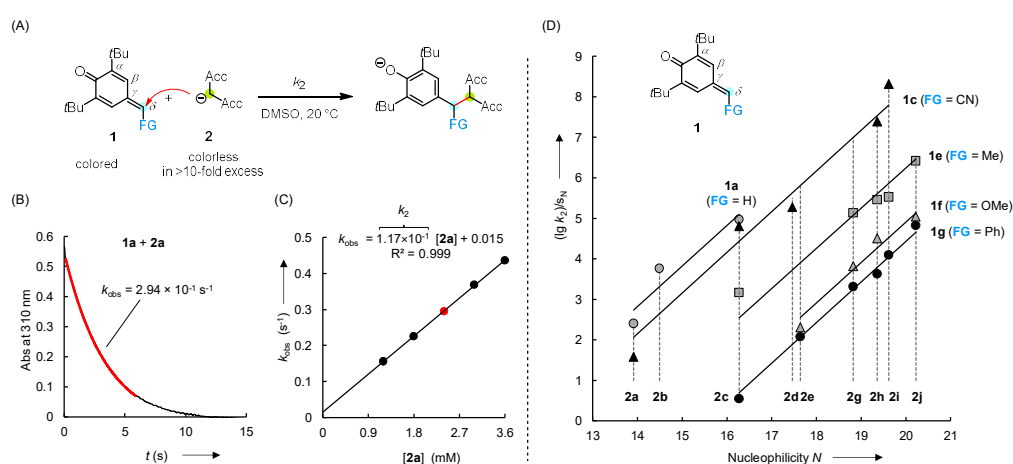
Figure 2. (A) Nucleophilic addition reaction of an electrophilic *p*QM **1** with an acceptor-substituted carbanion **2** in DMSO at 20°C; (B) The time-dependent decay of the absorbance of **1a** ([**1a**]$_0$ = 2.50 × 10^{-5} M) at 310 nm for the reaction with **2a** ([**2a**]$_0$ = 2.40 × 10^{-3} M) in DMSO at 20°C; (C) Linear correlation of experimentally determined k_{obs} values with concentrations of **2a**, the slope represents the second-order rate constant k_2; (D) Linear correlations of $(\lg k_2)/s_N$ for the reactions of *p*QMs **1a**, **1c** and **1e**-**1g** with carbanionic reference nucleophiles **2** against the nucleophilicity parameters *N* of **2** (DMSO, 20 °C).

The kinetic investigations were additionally corroborated by product studies which usually confirmed simple Michael additions, except of the δ-methoxy-substituted pQM which undergoes subsequent elimination sequences to form benzylidene-type products. Interestingly, a reaction performed in a CCl$_4$/DMSO mixture led to formation of a spirocyclopropane and a bis-spiro cyclopentane adduct. The analogous reaction in a n-pentane/DMSO mixture formed the 1:1 and 2:1 Michael adducts. This formation of the spirocyclic products under the former conditions is interpreted as initial Michael additions followed by ring-forming reactions involving radical intermediates.

Comparison of the Mayr electrophilicities E of the δ-FG-pQMs with those of analogously substituted phenylogous pQMs shows that the simpler δ-FG-pQMs are generally one to four orders of magnitude more reactive (Figure 3). The electronic substituent effects are much stronger if the functional groups are bound directly to the electrophilic centre than being attached at a more remote position of the phenyl ring. The δ-donor-substituted pQMs (Me, OMe) show only a moderate increase in electrophilic reactivity whereas the δ-acceptor-substituted pQMs (CF$_3$, CN, CO$_2$Me) are up to three units on the Mayr scale more reactive than analogously aryl-substituted pQMs. Surprisingly, the simple hydrogen-substituted pQM **1a** outperforms the phenylogous pQM by more than four orders of magnitude and is an even stronger electrophile than the δ-acceptor-substituted pQMs.
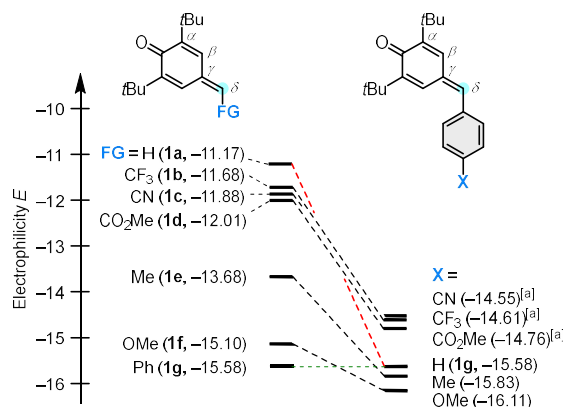
Figure 3. Comparison of the electrophilic reactivities E of δ-functionalized pQMs **1** with those of phenylogous pQMs (Electrophilicity parameters E of phenylogous pQMs with X = CN, CF$_3$ and CO$_2$Me were extrapolated by a Hammett correlation).

This unorthodox reactivity sequence cannot be explained solely by electronic effects. Quantum-chemical calculations were used to unravel the seemingly unsystematic δ-FG effects on the electrophilic reactivities of δ-FG pQMs. It was shown that the electrophilicity E of the δ-FG pQMs is described by a linear combination of buried volumes (%V_{bur}) and methyl anion affinities (MAAs) which adequately assesses for variable steric and electronic effects of these different functional groups. Plotting the electrophilicity E against the linear combination of %V_{bur} and MAAs leads to an excellent linear correlation and will subsequently enable chemists to tailor novel pQMs with predictable reactivity properties (Figure 4).
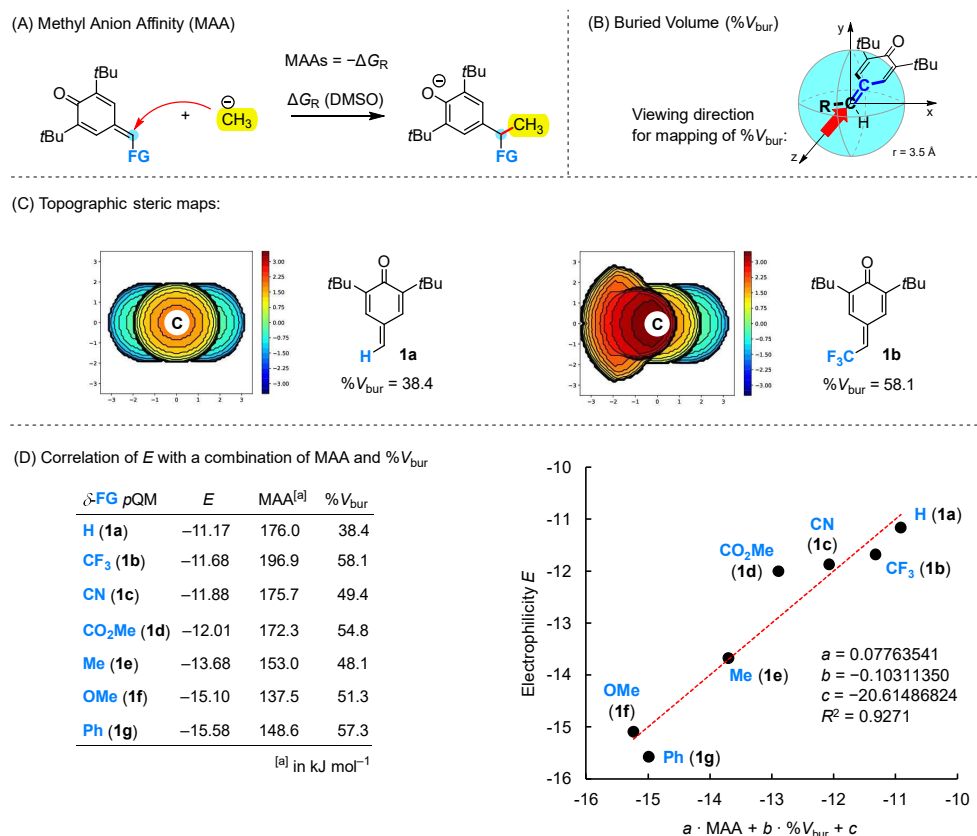
Figure 4. (A) Gibbs reaction energy ΔG_R (MAA = $-\Delta G_R$) of the addition of the methyl anion to the δ-FG pQMs. (B) Viewing direction for mapping of buried volume (%V_{bur}). (C) Topographic steric maps. (D) Correlation of Mayr electrophilicity E with a linear combination of MAA and %V_{bur}.

1.2. Electrophilic Reactivities of δ-Disubstituted *para*-Quinone Methides – A Limitation to the Mayr-Patz Equation

The electrophilic reactivities of a series of δ-cyano-δ-aryl disubstituted *para*-quinone methides (CN pQMs) and one δ-trifluoromethyl-δ-aryl disubstituted *para*-quinone methide (CF$_3$ pQM) have been quantified from the kinetics of their addition reactions with carbanionic reference nucleophiles and additionally in two cases with (heteroatom)-nucleophiles such as primary amines and ring-substituted thiophenolates (Figure 5).
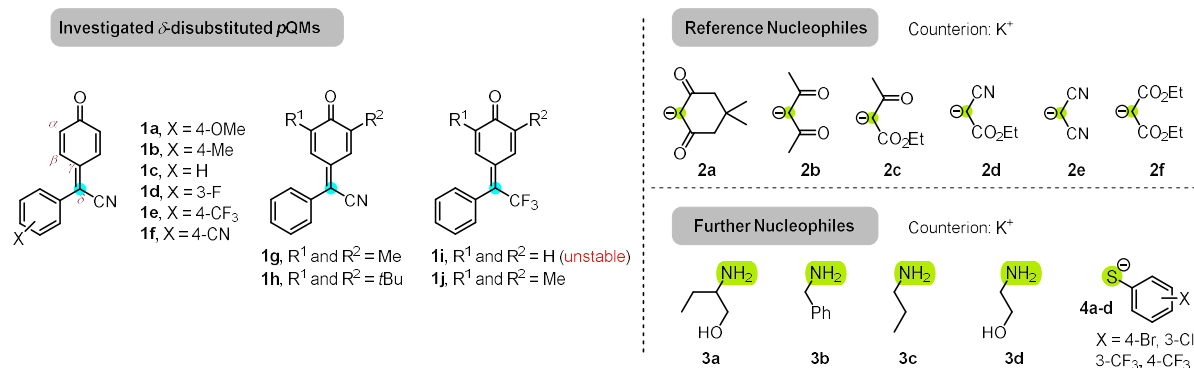
Figure 5. Overview of investigated δ-disubstituted pQMs (**1a**-**1h** and **1i**-**1j**) and reference nucleophiles used.

The rates of the addition reactions (k_{obs}) were monitored by means of UV/Vis spectroscopy by following the time-dependent decay of the colored pQMs under pseudo first-order reaction conditions (Figure 6B). The second order rate constants k_2 were determined from plots of k_{obs} vs. the concentration of the nucleophile (Figure 6C). Plotting of the logarithmic second order rate constants k_2 against the nucleophilicity parameters N leads to linear correlations with slope parameters deviating from the unity slope for electrophiles as defined by the Mayr-Patz equation (lg $k_2 = s_N(N + E)$) (Figure 6D).
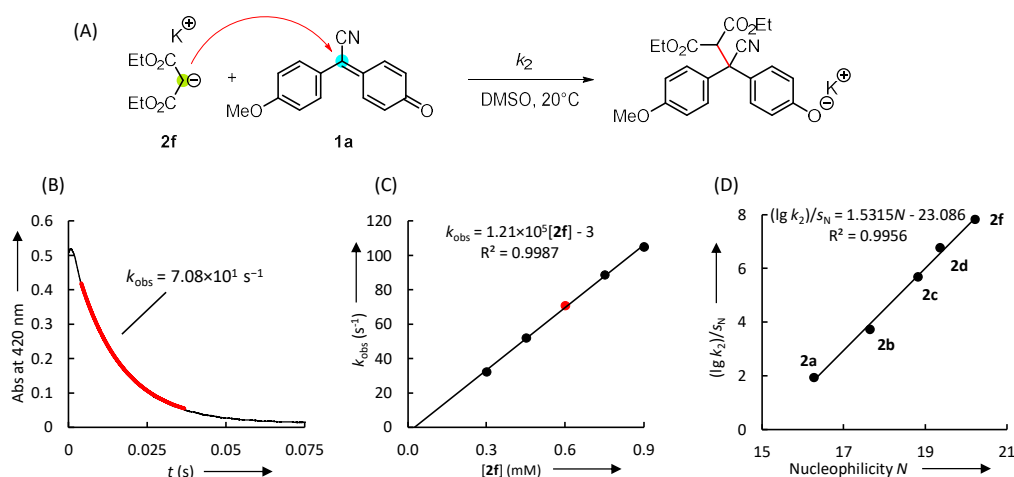
Figure 6. (A) Rate-determining addition reaction of carbanionic nucleophile **2f** to CN pQM **1a** in DMSO at 20°C; (B) Time-dependent decay of the colored CN pQM at 420 nm and observed rate constant; (C) Linear correlation of experimentally determined first-order rate constants k_{obs} with concentrations of carbanion **2f**; (D) Linear correlation of (lg k_2)/s_N vs nucleophilicity N to determine E and s_E values of the CN pQM.

Hence, two electrophilicity parameters (s_E and E of the extended Mayr-Patz equation lg $k_2 = s_E s_N(N + E)$) were used to classify the reactivities of the δ-disubstituted pQMs. The investigated CN pQMs and CF$_3$ pQMs have electrophile-specific sensitivity parameters s_E of greater than unity ($s_E = 1.49 - 1.57$). These pQMs are more sensitive (higher steric demand) towards nucleophile variations than unsubstituted pQMs or structurally related diarylcarbenium ions. Visualizing the second-order rate constants k_2 of the reactions between CN pQMs and carbanionic nucleophiles in plots with Hammett substituent constants of the substituted aryl moieties as well as the experimentally determined half-wave reduction potentials $E_{1/2}$ of the CN pQMs led to excellent linear correlations (Figure 7A).

Interestingly, despite the negative inductive effect (-I) of the nitrile group on the reactive center, the electrophilicity of CN pQMs is reduced relative to that of analogously substituted pQMs without nitrile group (Figure 7B). This effect is even more pronounced for CF$_3$ pQMs, which are less reactive than CN pQMs. Though the CF$_3$ functional group is a strong electron-withdrawing substituent, it is a weaker π-electron donor compared to a nitril group and should therefore increase the electrophilic reactivity. It is assumed that the increasing steric bulk at the reactive carbon center on the pQMs (H < CN < CF$_3$) is mainly responsible for the reduced electrophilic reactivities.
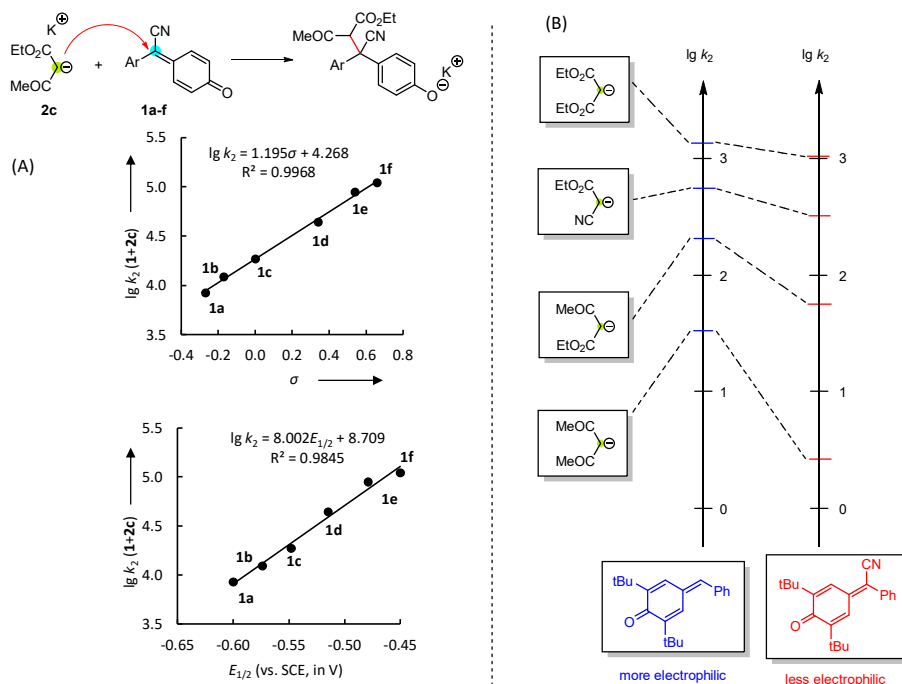
Figure 7. (A) Linear correlations of experimental rate constants k_2 of reactions of **1+2c** vs. Hammett substituent constants and experimentally determined reduction potentials $E_{1/2}$ of CN pQMs. (B) Comparison of relative reactivities of a CN pQM with an analogously substituted pQM without nitril group.

Primary amines and ring-substituted thiophenolates were used as additional nucleophiles to test the validity of the electrophilicity parameters E (s_E) of the CN pQMs calibrated against carbanionic reference nucleophiles. For the reactions with these additional nucleophiles, linear correlations of (lg k_2)/s_N vs. N with only slightly higher slope parameters than that for the reference system were observed, and the deviations of the experimentally determined rate constants of these reactions are still within the error tolerance of less than two orders of magnitude on the Mayr scale (Figure 8). Although all three nucleophile classes investigated have different steric demands, the observed slope parameters in the correlations of (lg k_2)/s_N vs. N are all very similar. This shows that the electrophilicity parameters E (s_E) of the CN pQMs, determined from their reactions with carbanions, are reasonable and they will allow to semi-quantitatively predict the rates of reactions with other novel nucleophile classes.
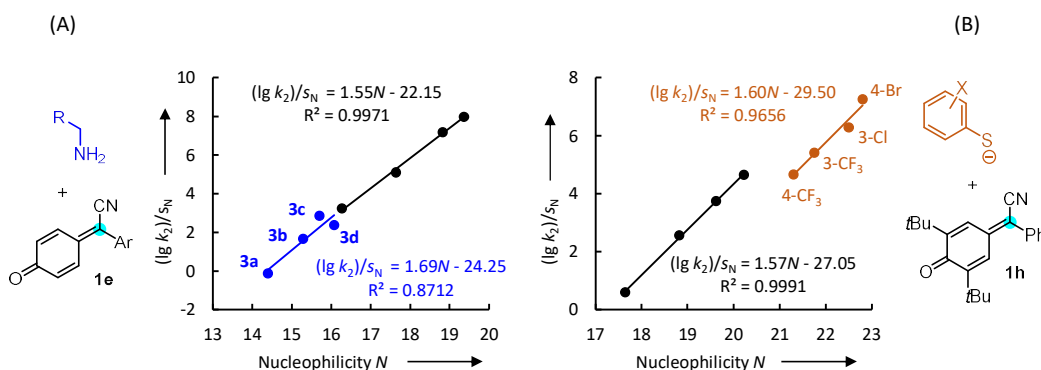
Figure 8. (A) Linear correlations of (lg k_2)/s_N against N for reactions of CN pQM **1e** with primary amines **3** (blue dots) and carbanionic reference nucleophiles (black dots) measured in DMSO at 20°C; (B) Linear correlations of (lg k_2)/s_N against N for reactions of CN pQM **1h** with substituted thiophenolates (orange dots) and carbanionic reference nucleophiles (black dots) measured in DMSO at 20°C.

1.3. Defining the Synthetic Scope of *ortho*-Quinone Methides by Quantifying Their Electrophilicity

Eight aryl-substituted *ortho*-quinone methides (*o*QMs) were synthesized, isolated and characterized by spectroscopic methods (Figure 9A). Kinetic studies of the nucleophilic additions of carbanionic nucleophiles to *o*QMs were investigated photometrically in DMSO at 20°C (Figure 9B). The experimental second-order rate constants k_2 for the carbon-carbon bond forming reactions at the *o*QMs' exocyclic π-bond were determined by plotting the pseudo-first-order rate constants k_{obs} against the carbanion concentrations. The electrophilic reactivities E of the *o*QMs were evaluated by the linear free-energy relationship $\lg k_2 = s_N(N + E)$ from plots of $(\lg k_2)/s_N$ against the nucleophilicity parameters N of the carbanionic reference nucleophiles (Figure 10).
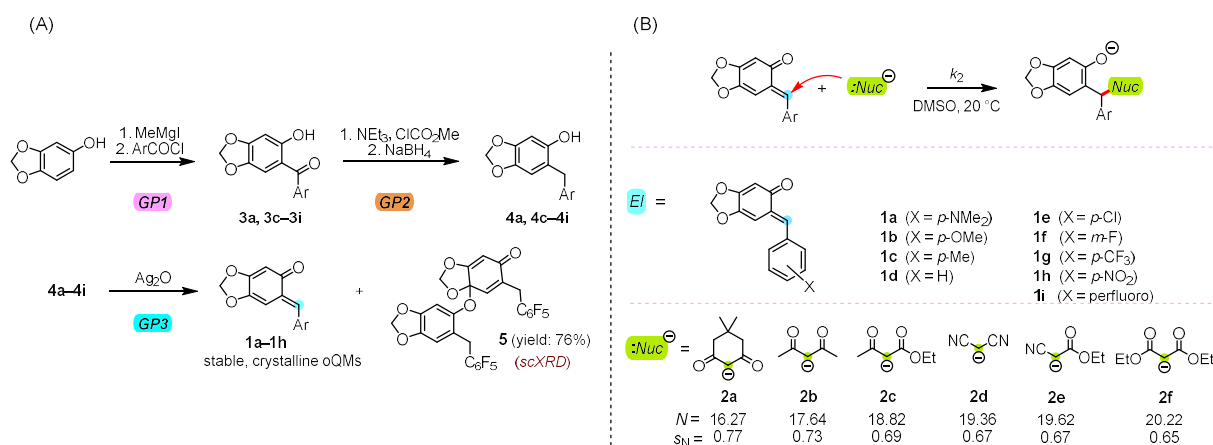
Figure 9. (A) Novel three-step synthetic procedure to obtain stable and crystalline *o*QMs; (B) Carbon-carbon bond-forming reaction of *o*QM with nucleophile and overview of investigated aryl-substituted *o*QMs and carbanionic reference nucleophiles used.
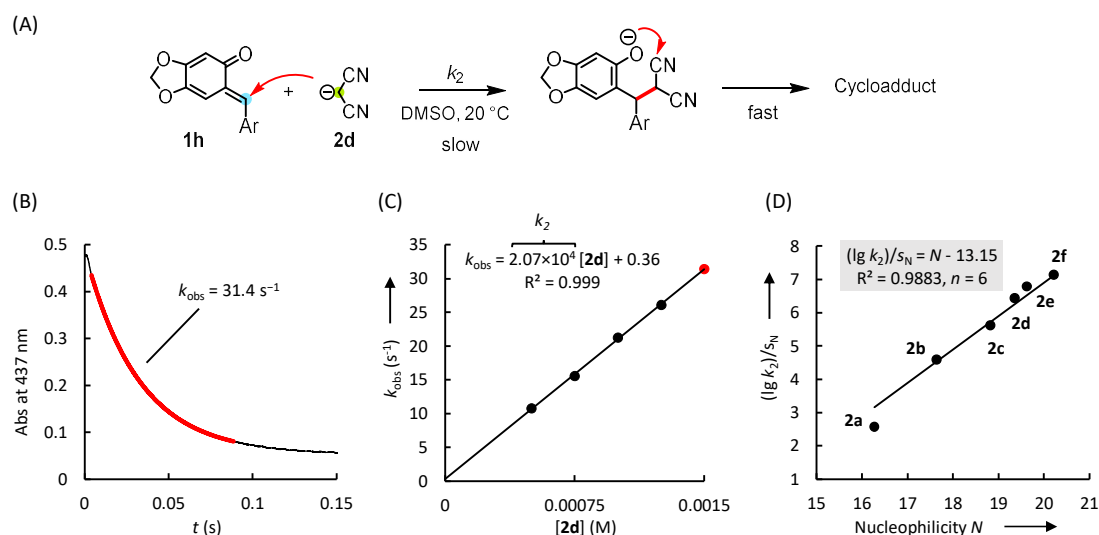
Figure 10. (A) Rate-determining Michael addition of a carbanion to *o*QMs' exocyclic π-bond and subsequent fast intramolecular ring-closure to form a cycloadduct; (B) Determination of the observed rate constant k_{obs} (s^{-1}) from the exponential decay of the *o*QM absorbance A at 437 nm versus time for the reaction between *o*QM **1h** ($c_0 =$ 4.30 × 10^{-5} M) and carbanion **2d** ($c_0 =$ 1.50 × 10^{-3} M); (C) The slope of the linear correlation of k_{obs} with [**2d**] corresponds to the second-order rate constant k_2; (D) Linear correlation of $(\lg k_2)/s_N$ for the reaction of *o*QM **1h** with carbanionic reference nucleophiles **2a-f** against the nucleophilicity parameters N of **2a-f** (DMSO, 20 °C) and a slope parameter of unity as required by the Mayr-Patz equation.

The electrophilicities E of the oQMs correlate linearly with Hammett substituent constants and experimentally determined one-electron reduction potentials E_p^{red} (Figure 11A). Interestingly, the electronic effects of substituents at the aromatic ring in oQMs exactly mirror those in *para*-quinone methides (pQMs) as indicated by the unity slope of the linear relationship in Figure 11B. The investigated oQMs have electrophilicity parameters between $E = -13.15$ (p-NO$_2$-substituted derivative) and $E = -16.07$ (p-NMe$_2$ substituted derivative). Compared to other electrophiles, their reactivity is located in a reactivity range which is also covered by compounds like *N*-methylmaleimide, 1,1-bissulfonyl-activated styrene and some previously characterized pQMs (Figure 11C).

Further anionic or neutral C-, S-, or N-centered nucleophiles such as S-ylides, P-ylides, thiophenolates and some amines were used to assess the validity of the oQMs' electrophilicity parameters E determined from their reactions with carbanionic reference nucleophiles. The experimental rates of the investigated electrophile-nucleophile combinations deviated by only one order of magnitude or less from the calculated second-order rate constants and are still within the error limits of the Mayr scale.

Consequently, the electrophilicity parameters E of the oQMs are of high accuracy and can be used to predict the rates of Michael additions with other nucleophiles. Furthermore, the linear correlations in Figure 11 will be useful to tailor further novel oQMs with predictable properties.
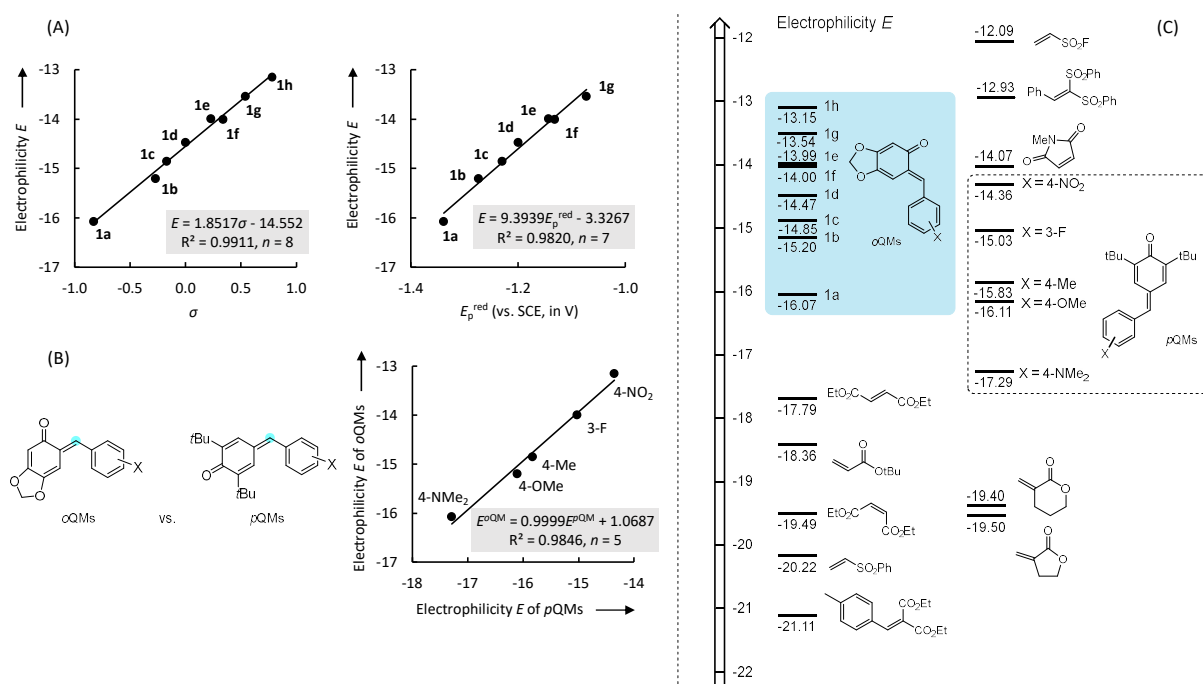
Figure 11. (A) Linear correlations of the electrophilicity E of oQMs against the Hammett substituent constants σ and their experimentally determined one-electron reduction potentials E_p^{red}; (B) Linear correlation of the electrophilicities E of oQMs with those of analogously ring-substituted pQMs; (C) oQMs **1** embedded on Mayr's reactivity scale to compare their reactivity to other novel Michael acceptors.

1.4. Asymmetric isochalcogenourea-catalysed (4+2)-cycloadditions of *ortho*-quinone methides and allenoates

A total of four additional benzodioxole-based *ortho*-quinone methides (*o*QMs), three of them with heteroaryl rings (furanyl, pyrrolyl, indolyl) and one of them with extended π-system (cinnamyl) were synthesized and characterized by spectroscopic methods. The reactivities of the *o*QMs were quantified by kinetic experiments of their carbon-carbon bond forming reactions with acceptor-substituted carbanionic reference nucleophiles (Figure 12). The second-order rate constants k_2 of these addition reactions were determined in DMSO at 20°C by using photometric methods. Then, the electrophilicities E of *o*QMs were calculated from the experimentally determined k_2 and the reported nucleophilicity parameters (N and s_N) of the reference nucleophiles according to the linear free-energy relationship $\lg k_2 = s_N(N + E)$. Additionally to the previously characterized aryl-substituted *o*QMs, all four newly investigated *o*QMs are located in a relative narrow reactivity range of approximately four orders of magnitude (Figure 12C). It can be expected that all *o*QMs will perform comparable well in further Michael additions.
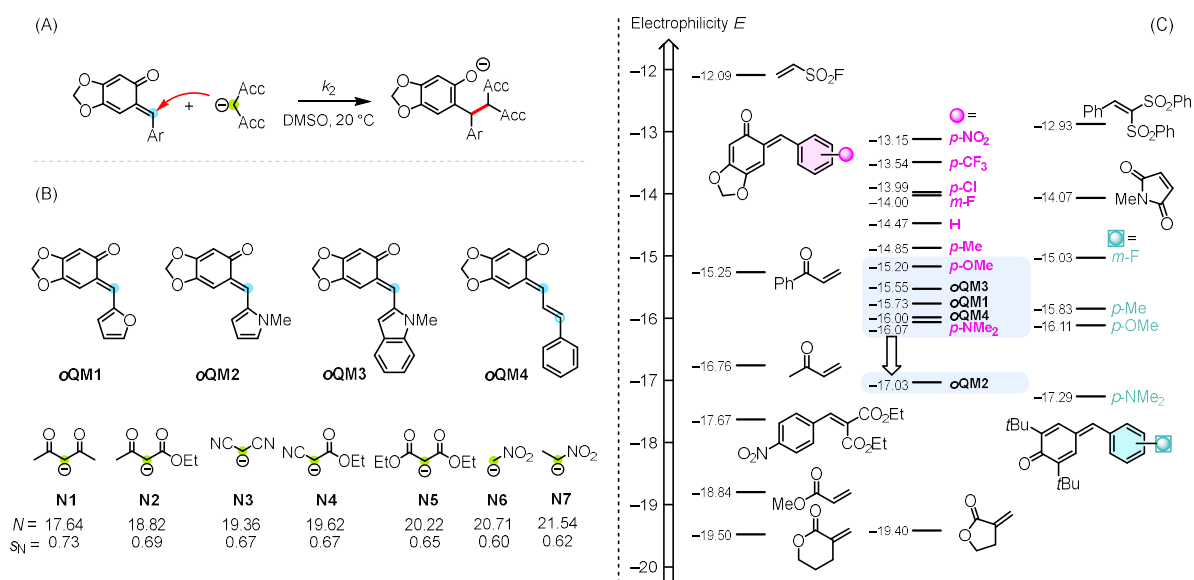
Figure 12. (A) Carbon-carbon bond forming reaction of an *o*QM and an acceptor-substituted carbanionic reference nucleophile. (B) Investigated heteroaryl- and cinnamyl derived *o*QMs and carbanions (reference nucleophiles) used. (C) An electrophilicity scale to compare the electrophilic reactivity of **oQM1**-**oQM4** with previously characterized aryl-substituted *o*QMs and further Michael acceptors.

Furthermore, in collaboration with the group of Prof. Dr. Mario Waser at the JKU Linz, it was demonstrated that the electrophilicity parameters E of the *o*QMs can be successfully used to reliably evaluate the scope of their reactions with structurally diverse nucleophiles. A series of 11 benzodioxole-based *o*QMs was employed in Michael additions with isochalcogenourea (IChU)-activated allenoates (Figure 13). The betaine intermediates, preformed from the IChU attached to the beta-position of the allenoates, reacted with the *o*QMs to form (4+2) cycloadducts. Optimal reaction conditions were obtained for HyperBTM (ITU1) catalyzed reactions, which mainly afforded the γ-annulated cycloadducts with an exocyclic double bond in *Z*-configuration and in all cases with excellent enantiomeric ratios (e.r. 99:1).
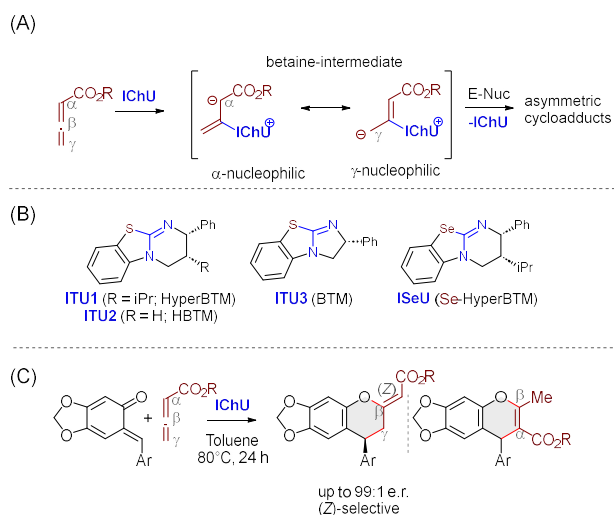
Figure 13. (A) Allenoate activation by an isochalcogenourea catalyst (IChU) to form a α- or γ-nucleophilic betaine intermediate and its subsequent asymmetric reaction with electrophiles; (B) Isochalcogenourea-type catalysts used in the optimization protocol; (C) Prototypical reaction between benzodioxole-based *o*QM and allenoate, activated by IChU, to form an asymmetric (4+2)-cycloadduct.

1.5. [4+2] Cycloadditions of *o*QMs with Enamines and Determining the Free Energy of Concert

The [4+2]-cycloaddition reactivities of a series of aryl-substituted *ortho*-quinone methides (*o*QMs) in reactions with enamines (electron-rich dienophiles) were investigated (Figure 14). Product analyses for reactions between aryl-substituted *o*QMs and enamines were performed in CH_2Cl_2 at room temperature. In all cases, the corresponding cycloaddition products (dihydrochromanes) were isolated. According to spectroscopic and crystallographic methods, the cycloaddition products were often obtained as mixtures of exo/endo diastereomers, although the proportion of endo isomers predominated, which is consistent with *Alder's endo rule*.
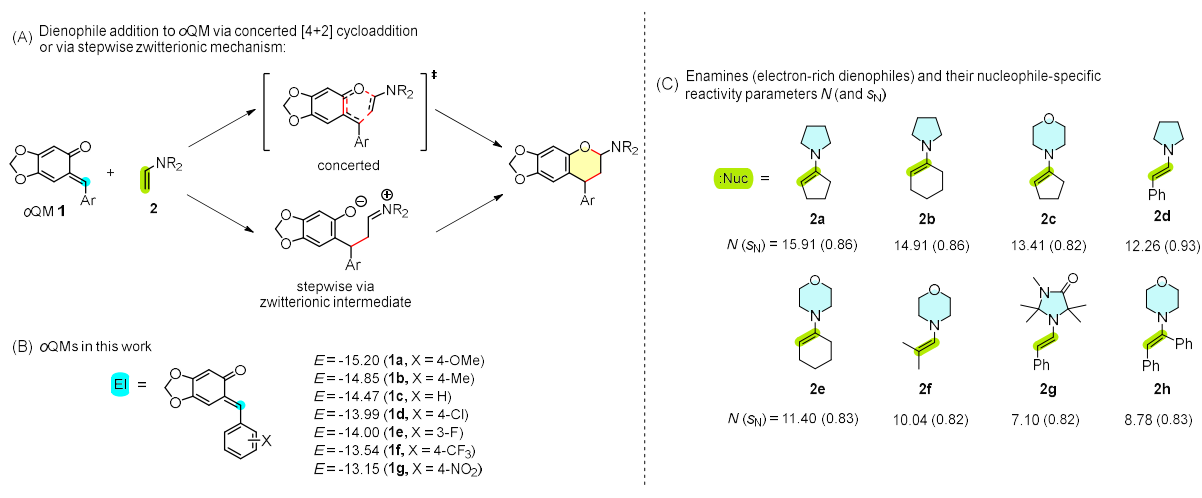
Figure 14. (A) Illustration of an inverse hetero-Diels-Alder reaction of an *o*QM with an enamine (electron-rich dienophile) following either a concerted or stepwise mechanism. (B) Structures and electrophilicity parameters *E* of *o*QMs **1a-1g**. (C) Enamines **2a-h** (electron-rich dienophiles) used in this work (nucleophilicity parameters *N* and sensitivity parameters s_N of enamines **2a-2f**, **2h** in CH_2Cl_2, **2g** in MeCN.

Subsequently, kinetic studies of these electrophile-nucleophile combinations were carried out in CH_2Cl_2 at 20°C and monitored by using UV/Vis spectroscopy. The kinetic measurements were observed at the absorbance maxima of the colored oQMs under pseudo-first-order reaction conditions using the enamines in large excess over the oQMs and experimental second-order rate constants k_2 were derived from plots of first-order rate constants k_{obs} vs. the enamine concentrations (Figure 15).
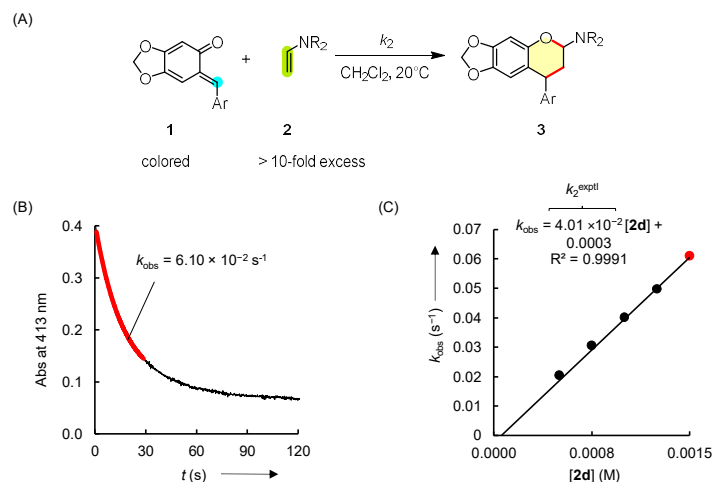
Figure 15. (A) [4+2] cycloaddition reaction of an oQM **1** with an enamine **2** in CH_2Cl_2 at 20 °C. (B) Time-dependent decay of the absorbance of **1c** ([**1c**]$_0$ = 5.69 × 10^{-5} M) at 413 nm for the reaction with **2d** ([**2d**]$_0$ = 1.50 × 10^{-3} M) in CH_2Cl_2 at 20°C. (C) Linear correlation of experimentally determined k_{obs} values with concentrations of **2d**, the slope represents the second-order rate constant k_2.

By analyzing the experimental second-order rate constants k_2 with the Mayr-Patz equation lg $k_2 = s_N(N + E)$ (1), it was found that the experimental rate constants deviate significantly, that is, by more than two orders of magnitude from the rate constants calculated by equation (1) for a hypothetical stepwise mechanism involving zwitterion intermediates (Figure 16). This observation was made both for reactions of an oQM with a series of enamines and in the opposite way for reactions of an enamine with a series of oQMs, as illustrated in two Mayr correlations (Figure 16B, C). It would be expected that the data points of the enamines and the oQMs would lie on the black correlation lines if they reacted as one-bond nucleophiles and one-bond electrophiles, respectively. However, all data points were found to lie well above the correlation lines, indicating that the transition state of these reactions is more favorable than that leading to the formation of zwitterions. Consequently, it is assumed in both cases that the reactions most likely follow a concerted mechanism.

An alternative explanation for the unexpectedly high rate constants such as a single-electron transfer (SET) mechanism involving radical intermediates can be ruled out. Experimental redox potentials of the oQM-enamine pairs were determined, and the corresponding Gibbs energies for electron transfer were calculated. In all cases, these Gibbs energies were substantially higher than the experimental Gibbs activation energies derived from the kinetic data.
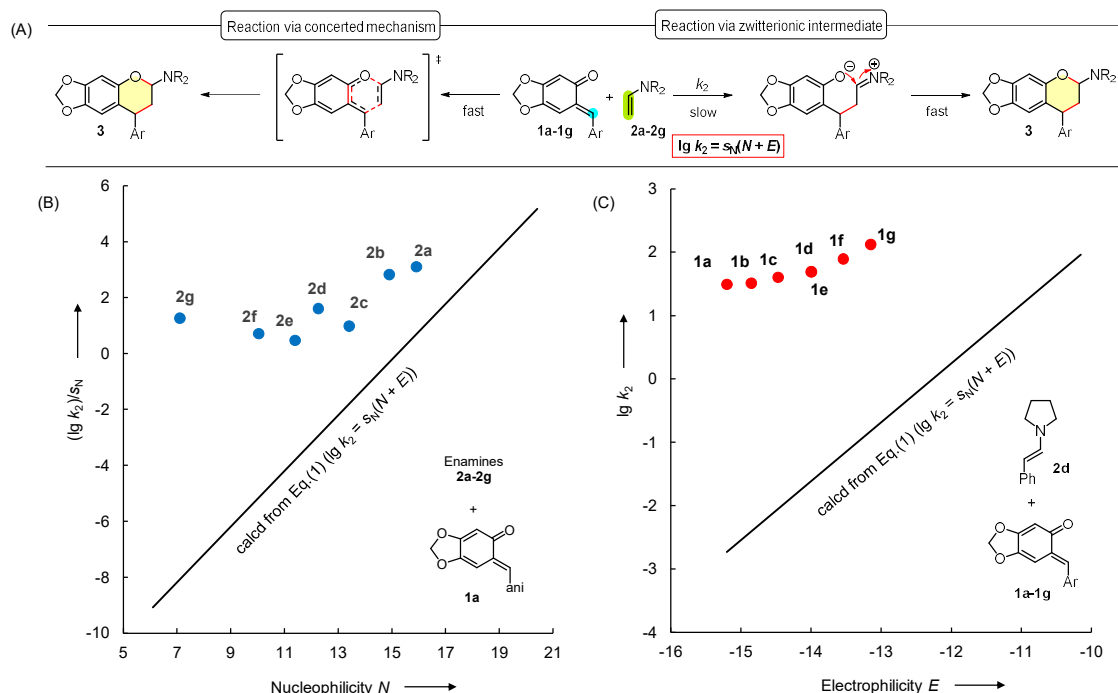
Figure 16. (A) Overview of a concerted and a stepwise mechanism for the reactions between oQMs **1** and enamines **2**; (B) Correlation of (lg k_2)/s_N for the reactions of oQM **1a** with enamines **2a**-**2g** against the one-bond nucleophilicity parameters N of the enamines; (C) Correlation of lg k_2 for the reactions of enamine **2d** with oQMs **1a**-**1g** against the one-bond electrophilicity parameters E of the oQMs. (The black correlation lines were drawn with data points calculated from the known one-bond reactivity parameters E, N (and s_N) of oQMs and enamines according to the Mayr-Patz equation lg $k_2 = s_N(N + E)$.

Interestingly, the difference between experimental and calculated rate constants increases with decreasing nucleophilicity N of the enamines or electrophilicity E of the oQMs. This observation can also be seen from a correlation of Gibbs activation energies $\Delta G^{\ddagger}$ against the enamines one-bond nucleophilicity parameters N (Figure 17). The orange line represents activation energies derived from rate constants calculated by equation (1) for a stepwise mechanism, while the blue line shows the corresponding energies derived from the experimentally determined rate constants k_2. The difference between those two activation energies reflects for an energy of concert as illustrated by the grey correlation line. Thus, the energy of concert decreases steadily with increasing nucleophilicity N of the enamines. It is a likely explanation, therefore, that the concerted formation of both σ-bonds becomes more and more asynchronous with higher N of the enamine.
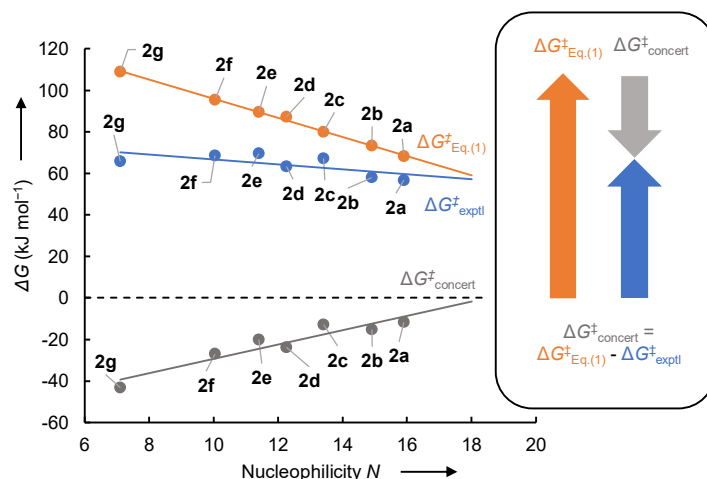
Figure 17. Correlation of Gibbs activation energies $\Delta G^{\ddagger}$ for the reactions of oQM **1b** with enamines **2a**-**2g** at 20°C against the one-bond nucleophilicity parameters N of enamines.

Furthermore, the [4+2] cycloaddition reaction of oQMs with enamines was tested in five additional solvents. Rate constants were determined which, despite the different polarity of the solvents, deviated only slightly from each other and also agreed well with the previously determined reaction rate in CH_2Cl_2. This observation is consistent with previous studies that the rates of concerted reactions are generally not significantly affected by solvents and emphasizes that the investigated cycloaddition reactions between oQMs and enamines are most likely of a concerted nature.

Further types of dienophiles such as enol ethers, vinyl-sulfides and vinyl-azides allowed to form the corresponding cycloaddition products with oQMs, while the corresponding kinetic experiments were not performed. Nonetheless, the known one-bond reactivity parameters E, N (and s_N) could be used to semi-quantitatively predict the probability of the product formation. The rule of thumb, that is $E + N > -5$, is usually the lower threshold for observable reactivity at room temperature. However, for some of the reactions investigated here, this rule is not fulfilled and the sum of the reactivity parameters $E + N$ often lies well below this empirical limit. The fact that cycloaddition products are nevertheless observed under mild conditions strongly suggests that these reactions do not proceed via stepwise bond formation and it can therefore be assumed that such reactions are likely to proceed according to concerted mechanisms.

_____

Chapter 2. Introduction and Objectives

2.1. Reactivities of Quinone Methides

Development of reactivity scales.

The valence bond theory developed by LEWIS,[1] along with the BRØNSTED–LOWRY acid-base theory**,** laid the groundwork for understanding the mechanisms of organic chemical reactions.[2] Building on these foundations, in the 1930s INGOLD expanded the conceptual framework by classifying chemical species as either electrophilic (electron-withdrawing) or nucleophilic (electron-donating).[3] This distinction greatly simplified the interpretation of reaction mechanisms, as most organic reactions involve an interaction between a nucleophile and an electrophile.

Following this concept, SWAIN and SCOTT started in 1953 the first empirical approach to quantify the term nucleophilicity.[4] They proposed a two-parameter equation (1) and compared the rate of an S_N2 reaction between a substrate such as an alkyl halide, acyl halide, or others with water in water (defined as k^0) with the rate of the reaction involving nucleophiles other than water (defined as k). The nucleophilic constant n is then defined as a measure of the reactivity of a given nucleophile ($n = 0$ for water) and s describes the electrophile-specific sensitivity ($s = 1$ for methyl bromide at 25°C).

$$\lg (k/k^0) = sn \tag{1}$$

Unfortunately, this equation remained of minor use as shortly afterwards, more factors were found that influence the reactivity, such as basicity, polarization of the nucleophiles, solvent effects and many more as reported by EDWARDS[5], BUNNETT[6] and PARKER.[7]

In 1972, RITCHIE introduced a new approach. Instead of using reaction partners that follow displacement reactions (S_N2), he used carbocations (e.g. tritylium and tropylium ions) and aryldiazonium ions and studied their simple addition reactions with a variety of nucleophiles.[8] Subsequently, he proposed a new linear free-energy relationship, equation (2), in which k is the rate constant for a reaction of a cation with a given nucleophile in a given solvent, while k_0 is the rate constant for the reaction of the same cation with water in aqueous solution at 23°C. N_+ defines the reactivity of nucleophiles and is independent of the cation used. Importantly $\lg k_0$ can be seen in principle as an electrophile specific parameter in the correlation. Remarkably, constant selectivity relationships were observed, but it was later found that the equation is not strictly valid and better correlations are obtained when different types of electrophiles are treated separately.[9]

$$\lg k = \lg k_0 + N_+ \tag{2}$$

This problem was finally solved by introducing an additional s parameter as described by MAYR and PATZ, which reflects the sensitivity of the nucleophile to electrophilic variation. Thus, in Equation (3), k_2 is the second-order rate constant of a polar reaction at 20°C, E represents the electrophilicity of the electrophile, and nucleophiles are characterized by two solvent-dependent parameters, the nucleophilicity N and the nucleophile-specific sensitivity parameter s_N.[10] To develop a comprehensive and broadly applicable reactivity scale, Mayr and co-workers initially employed benzhydrylium ions and later structurally related neutral electrophiles such as Michael acceptors with constant steric shielding at the reaction center as further model electrophiles.[11] This framework allowed the systematic characterization of a wide variety of nucleophiles under consistent conditions. To date,

_____

Equation (3) covers the most comprehensive data collection of polar organic reactivity and has successfully been applied to characterize the reactivity of more than 1300 nucleophiles and more than 350 electrophiles that cover a range of 40 orders of magnitude.[12]

$$\lg k_2 \,(20°C) = s_N(N + E) \tag{3}$$

It is also worth noting that Equation (3) is specifically valid to reactions where one new σ-bond is formed in the rate-determining step.[13] Reactions that proceed via fundamentally different mechanisms such as S_N2 reactions[14] or concerted cycloadditions[15] are outside the scope of this model.

Michael additions.

A particularly important class of electrophiles featured in Mayr's reactivity scales are Michael acceptors. The Michael addition is a fundamental reaction in organic chemistry that involves the conjugate addition of a nucleophile (Michael donor) to an α,β-unsaturated organic compound (Michael acceptor) which typically contains electron-withdrawing groups that activate the double bond toward nucleophilic attack.[16] First described by ARTHUR MICHAEL in 1887 (Scheme 1),[17] this reaction has become a powerful tool for forming carbon-carbon and carbon-heteroatom bonds in a regio- and stereoselective manner.[18] It typically involves the addition of enolates (or other stabilized carbanions) or other nucleophiles (often base-mediated) like thiols, amines, phosphines to electrophilic alkenes like enones, acrylates or a variety of further electron-deficient alkenes such as nitroalkenes, unsaturated nitriles (such as acrylonitrile), benzylidene malononitriles and quinone methides.[19]
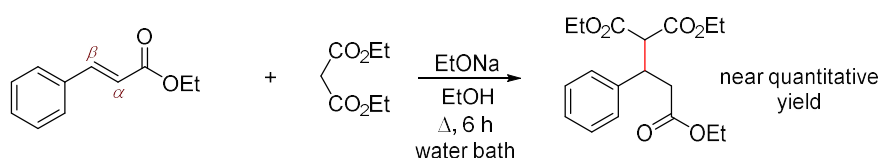
Scheme 1. Example for the nucleophilic addition of ethyl malonate to ethyl cinnamate as described by A. Michael.[17]

The significance of the Michael addition lies in its mild reaction conditions and broad substrate scope, making it a key step in many synthetic pathways, including the synthesis of natural products[20], pharmaceuticals[21], and complex molecular frameworks.[22]

From a mechanistic standpoint, the Michael addition is particularly suited to reactivity studies using the Mayr-Patz equation, as it involves the formation of a single σ-bond in the rate-determining step, allowing for quantitative comparison of nucleophilic reactivities under well-defined conditions.

Quinone methides in general.

Quinone methides represent a class of Michael acceptors that consist of a cyclohexadiene core bearing a carbonyl and an exocyclic methylene group. Structurally, they are closely related to quinones, in which one of the carbonyl oxygen atoms is exchanged by a CH_2-unit, or to quinone dimethides where a carbon-carbon double bond is replaced by a carbonyl group (Scheme 2).[23]

_____

Quinone   Quinone methide   Quinone dimethide
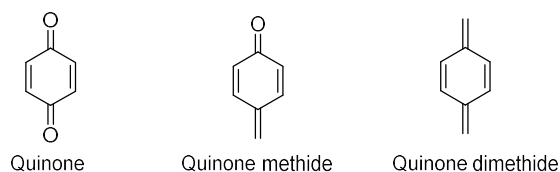
Scheme 2. Structural relation of quinone methides to quinones and quinone dimethides.

Depending on the relative position of the exocyclic methylene group and carbonyl residue at the cyclohexadiene core, quinone methides are mostly subclassified in 1,4- and 1,2-quinone methides also known as *para-* and *ortho*-quinone methides. This structural assembly leads to high polarization and the formally neutral compounds possess strong zwitterionic character. The zwitterionic resonance structure is of great importance as it exemplifies their general reactivity. They behave like Michael acceptors, although their reactivity is much more pronounced. Their high reactivity is mainly driven by the increase in π-stabilization energy which results from the formation of a fully aromatic ring when a nucleophile attacks at the exocyclic double bond.[24]

The third but less common isomer is the 1,3-quinone methide (*meta*-quinone methide) which displays quite different structural and electronic features. Due to the lack of direct electronic orbital interaction between the carbonyl group and exocyclic methylene group in the meta position, the molecule does not benefit from the same resonance stabilization. Consequently, *meta*-quinone methides are described as triplet biradical species in their neutral form, which makes these compounds very reactive and highly difficult to isolate (Scheme 3).[25]

1,4-quinone methide (*p*QM)   1,2-quinone methide (*o*QM)   1,3-quinone methide (*m*QM)
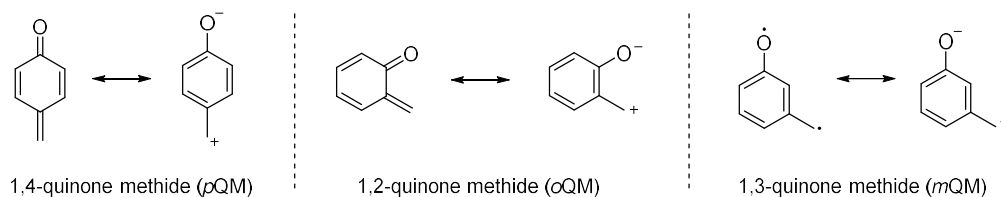
Scheme 3. Quinone methides are categorized into three isomers, the *para-*, *ortho-* and *meta*-quinone methides. Each isomer is shown in its neutral and zwitterionic resonance structure.

Due to their exceptional reactivity compared to classical Michael acceptors, quinone methides could establish themselves as extremely versatile compounds in organic chemistry.

Historical background on quinone methides.

The origins of quinone methide chemistry trace back to the early years of the 20th century when the first compounds with quinonoid character and methylene functionality were discovered.

In 1902, ZINCKE reported in his pioneering study *"Ueber die Einwirkung von Brom und von Chlor auf Phenole: Substitutionsproducte Pseudobromide und Pseudochloride"* on the formation of unusual phenol-halogen compounds with pronounced quinonoid character.[26] These compounds, which he described as "pseudobromides" or "bromoketones", were obtained for example by treating tetrachloro-*p*-cresol with bromine. The pseudobromide could thus be converted into an addition product via reaction with methanol (Scheme 4). He deduced the formation of this by the existence of a reactive intermediate, a compound which he considered to be a "methylenequinone" formed by elimination of HBr from the corresponding pseudobromide.
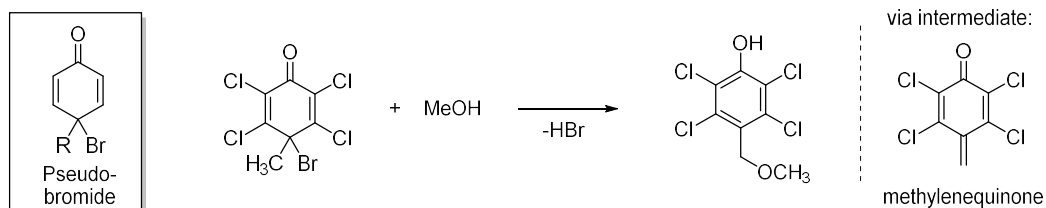
Scheme 4. Reaction of the pseudobromide with methanol leads to the formation of a 1,6 addition product, which must be formed via formation of a reactive intermediate, the methylenquinone.

Although, direct detection of the methylenequinone intermediate was initially not possible, ZINCKE reported in the course of his studies that further phenols such as bisphenol F, *p*-benzylphenol, isoeugenol and others could be converted into pseudobromides with quinonoid character. Thus, elimination of HBr from the pseudobromides gave rise to methylenequinone-type species, some of which could even be isolated. These highly reactive species readily reacted with nucleophiles such as water, alcohols, or acetic acid to form colorless products (Scheme 5).
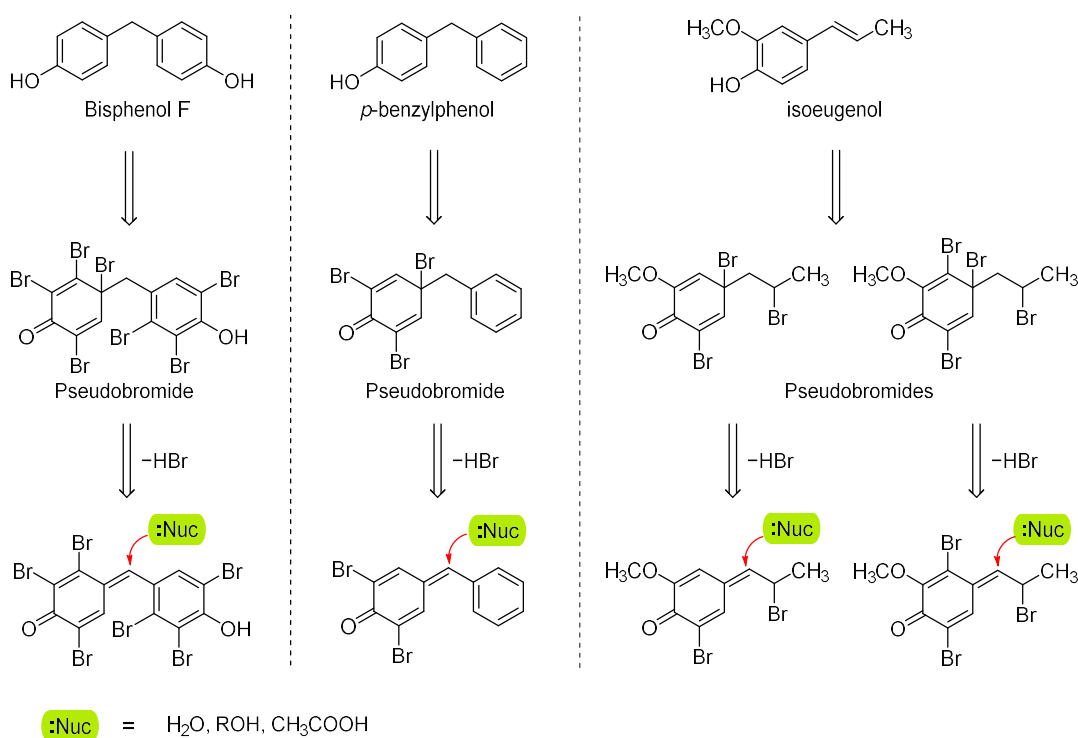
Scheme 5. Generation of further methylenequinone-type species from phenols such as bisphenol F, *p*-benzylphenol and isoeugenol via the corresponding pseudobromides. The methylenequinones undergo addition reactions with nucleophiles such as water, alcohols and acetic acid.[26]

Shortly after, in 1903 BISTRZYCKI and HERBST reported a quinonoid compound which they identified as a methylenquinone.[27] They introduced a new term for this class of compounds as "Chinomethan", which is mostly known today under the English term "quinone methide". The 7,7-diphenylquinone methide which they isolated represented one of the first structurally well-established examples of this class. At the same time, BAEYER and VILLIGER reported on the formation of the same quinone methide and investigated its subsequent reactions.[28]

While these very first reports in quinone methide chemistry focused on *para*-quinone methides, the concept of the ortho isomers emerged only a few years later. In 1907, FRIES and KANN suggested the formation of an *ortho*-quinone methide but were unable to isolate the proposed species.[29]

_____

Direct evidence for *o*QMs remained elusive until 1963, when GARDNER et al. provided the first solid proof of their existence.[30] They successfully generated an *o*QM by pyrolysis from *o*-(methoxymethyl)phenol in a quartz tube under reduced pressure at temperatures of 500-650°C. The resulting yellow pyrolysate was trapped at −196°C and remained stable up to a temperature of 0°C. Reactions with nucleophiles such as LiAlH₄ or CH₃MgI afforded the *o*-cresol and *o*-ethylphenol products, leading to the conclusion that the yellow pyrolysate must have been an *ortho*-quinone methide (Scheme 6A). Nevertheless, the *o*QM generated from *o*-(methoxymethyl)phenol could only be generated and observed under highly specific conditions, which limited its accessibility.

A key contribution came in 1977, when JURD synthesized the first stabilized *o*QM.[31] It was obtained via a two-step synthesis involving a Friedel-crafts-type alkylation and a subsequent oxidation under mild conditions (Scheme 6B). The thus obtained *o*QM remained stable even under ambient conditions and could be handled and studied without special precautions. For the first time it was demonstrated that the right structural design yielded persistent *o*QMs.

(A)

P.D. Gardner (1963)

(B)

Leonard Jurd (1977)
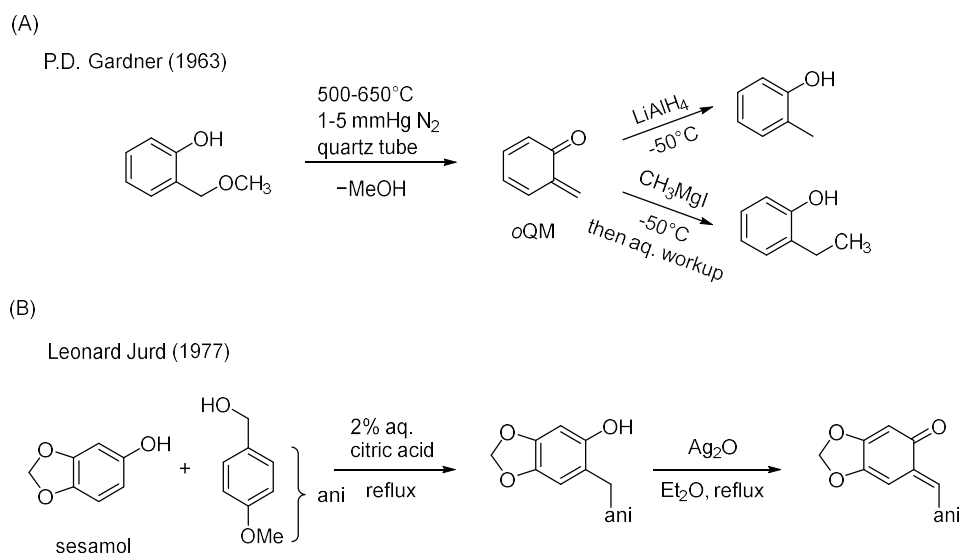
Scheme 6. (A) First generation of an *ortho*-quinone methide (*o*QM) by pyrolysis and subsequent reactions of the *o*QM with the nucleophiles LiAlH₄ and CH₃MgI in diethyl ether.[30] (B) First stable *o*QM synthesized by a two-step procedure from sesamol and a benzylic alcohol.[31]

The early investigations by ZINCKE,[26] BISTRZYCKI[27] and BAEYER[28] as well as by FRIES,[29] GARDNER[30] and JURD[31] laid the experimental and conceptual foundation for the development of quinone methide chemistry and firmly established these species as a distinct class of highly reactive Michael acceptors.

2.2. Synthetic Approaches to Quinone Methides

Over the past decades, a wide variety of synthetic strategies has been developed to access both *ortho*- and *para*-quinone methides. The choice of method typically depends on the substitution pattern, stability of the intermediates and reaction conditions.[25, 32] The most important approaches are outlined below.

_____

2.2.1. Synthesis of *ortho*-Quinone Methides

Due to the fact that only a limited number of stabilized *o*QMs are known to date, most synthetic routes are restricted to in-situ generation, where the highly reactive intermediates are directly captured by a nucleophile (Scheme 7). Among the most common strategies is the base-induced β-elimination (a) from suitable benzylic precursors such as *o*-hydroxy benzyl halides[33] and benzylic derivatives bearing other leaving groups (e.g. tosylate[34], acetates[35]). Treatment of these *o*QM-precursors with bases results in the elimination of hydrogen halides, TsOH or acetic acid, respectively, to generate the highly reactive *o*QM species.

A similar pathway can be accessed under acidic conditions, in which a substituent is transformed upon protonation into a good leaving group (b). For example, *o*-hydroxy benzyl ethers can be activated and transformed into *o*QMs with slightly acidic phyllosilicates like montmorillonite.[36] Additionally, *o*-hydroxy benzyl alcohol derivatives are protected on the phenolic residue by -TMS[37] or -MOM[38], prior to creation of a good leaving group at the benzylic position. Acid treatment then triggers both deprotection and elimination, forming the *o*QM. In some cases, both the phenolic and benzylic hydroxyl group are protected and unmasked simultaneously under acidic conditions.[39] In general, base-mediated methods are preferred over acid-mediated strategies, as *o*QMs tend to be acid-sensitive and prone to side reactions such as hydration or decomposition. In addition, basic conditions offer broader functional group tolerance and are more compatible with diverse nucleophiles.[32a]

Oxidative methods (c) also provide access to *o*QMs, typically from *o*-alkylphenols using one-electron oxidants such as Ag_2O[40], or aqueous $K_3[Fe(CN)_6]$ solutions.[41] However, these approaches are less broadly applicable due to poor tolerance of *para*-substituents bearing α-protons, which instead favor *p*QM formation.[32a]

Thermolysis (d) represents another widely used strategy to access *o*QMs. Upon heating, suitable precursors undergo fragmentation to release the *o*QM and a by-product. Reported precursor classes include benzooxazines[42], benzooxetanes[43], benzodioxins[44], 2-vinyl phenols[45], Mannich bases[46] and sulfonates.[47] Photochemical activation (e), provides a complementary approach. Here, precursors such as *o*-hydroxybenzyl alcohols[48] or ethers[49] are exposed to UV light, leading to bond-cleavage and the formation of *o*QMs along with by-products such as water or alcohols. This method is particularly valuable for triggering *o*QM formation under mild and spatially controlled conditions.[32a]

Less common, but mechanistically practical is the tautomerization method (f). In this approach, α-substituted *p*-quinones bearing an allylic proton adjacent to the carbonyl group can undergo a 1,5-hydrogen shift to generate the corresponding *o*QM. Though not broadly applied, this method has found utility in natural product synthesis, where it is used to initiate downstream transformations such as intramolecular cyclizations.[50]

_____
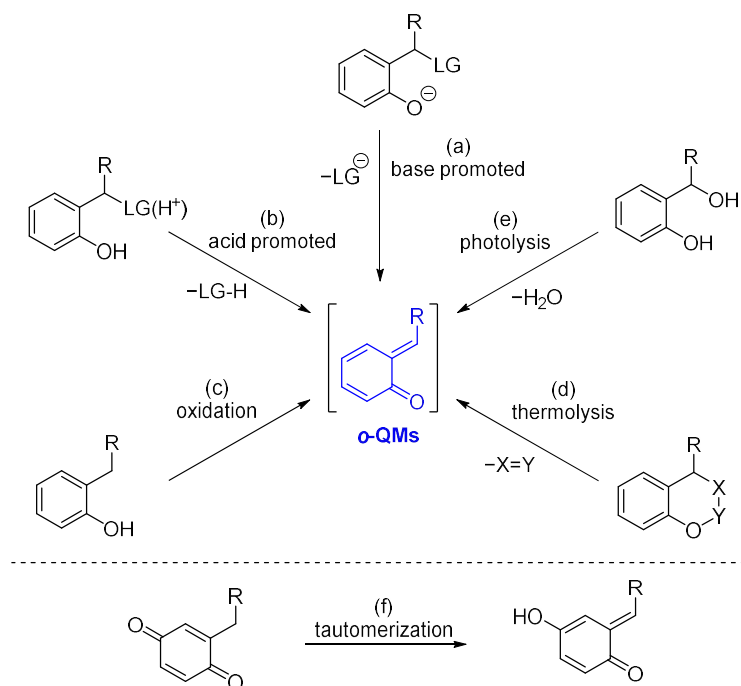
Scheme 7. Brief overview of valuable synthetic approaches to access *o*QMs.

2.2.2. Synthesis of *para*-Quinone Methides

Interestingly, some of the methods applied to *o*QMs can, in principle, be directly adopted for the generation of *p*QMs. One of the most common strategies involves again base-induced elimination, mostly starting from *para*-substituted benzylic alcohols (Scheme 8A).[32b]

The benzylic alcohols may be converted into benzhydryl chlorides using thionyl chloride[51], or into sulfone derivatives by treatment with sodium phenylsulfinate.[52] Both transformations install suitable leaving groups that can be eliminated upon deprotonation using bases like NEt_3 or NaOH. Alternatively, benzylic alcohols can be activated by ethereal HBF_4 to generate a carbenium ion, which then undergoes deprotonation under basic conditions to form the *p*QM.[51]

Furthermore, stabilized aryl *p*QMs bearing *tert*-butyl groups at the 2,6-positions can be synthesized by a simple base-promoted (e.g. piperidine) condensation reaction between the substituted phenol and an aromatic aldehyde which goes through a Mannich base intermediate (Scheme 8B).[53] This approach can also be adapted to access more functionally diverse *p*QMs.[54] Oxidative methods using DDQ[55], metal oxides[56], or $K_3[Fe(CN)_6]$[57] are also effective in *p*QM synthesis. Photochemical methods have been reported but remain of minor practical importance.[58]

(A)   base-induced pathways

(B)   condensation reaction
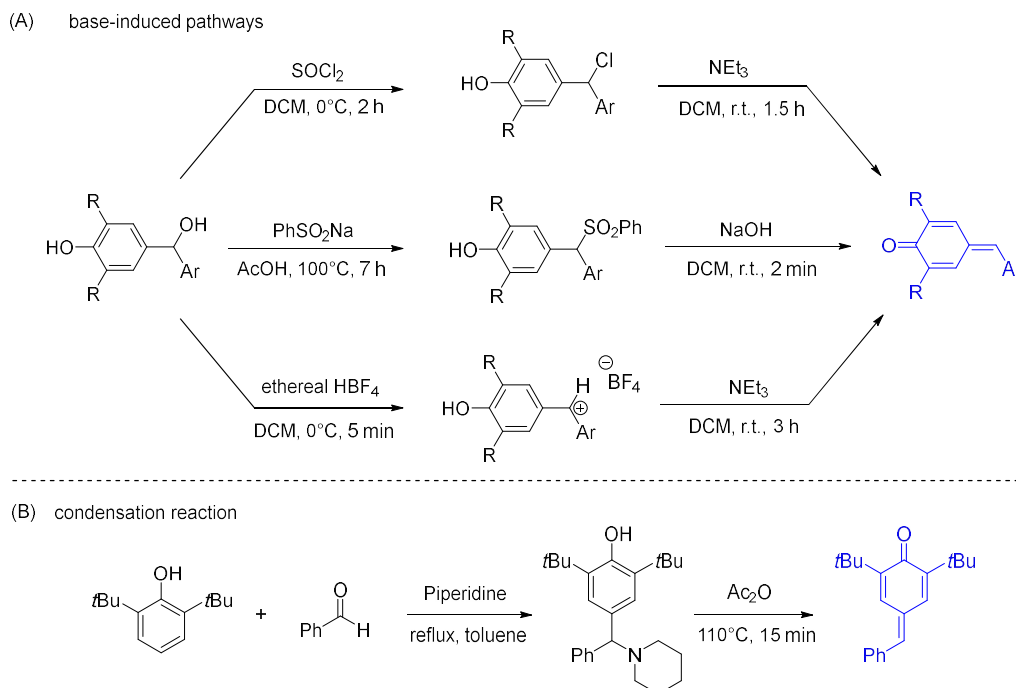
Scheme 8. Illustration of valuable synthetic methods to access substituted *p*QMs.

2.3. Applications of Quinone Methides

Owing to their unique structural features, QMs act as electrophilic Michael acceptors that enable a diverse array of reactions. *Para*-quinone methides typically undergo 1,6-nucleophilic additions while in contrast, *ortho*-quinone methides exhibit a broader reaction profile. Beyond 1,4-nucleophilic additions, *o*QMs readily participate in [4+2] cycloadditions and 6π-electrocyclizations, enabling rapid access to complex polycyclic systems. Their unique reactivity makes them valuable intermediates that are utilized in fields like organic synthesis, medicinal chemistry, and biology (Scheme 9).[59]

_____

1,6-nucleophilic addition to *p*QMs:

1,4-nucleophilic addition to *o*QMs:

[4+2] cycloaddition involving *o*QMs:

6π-electrocyclization of *o*QMs:
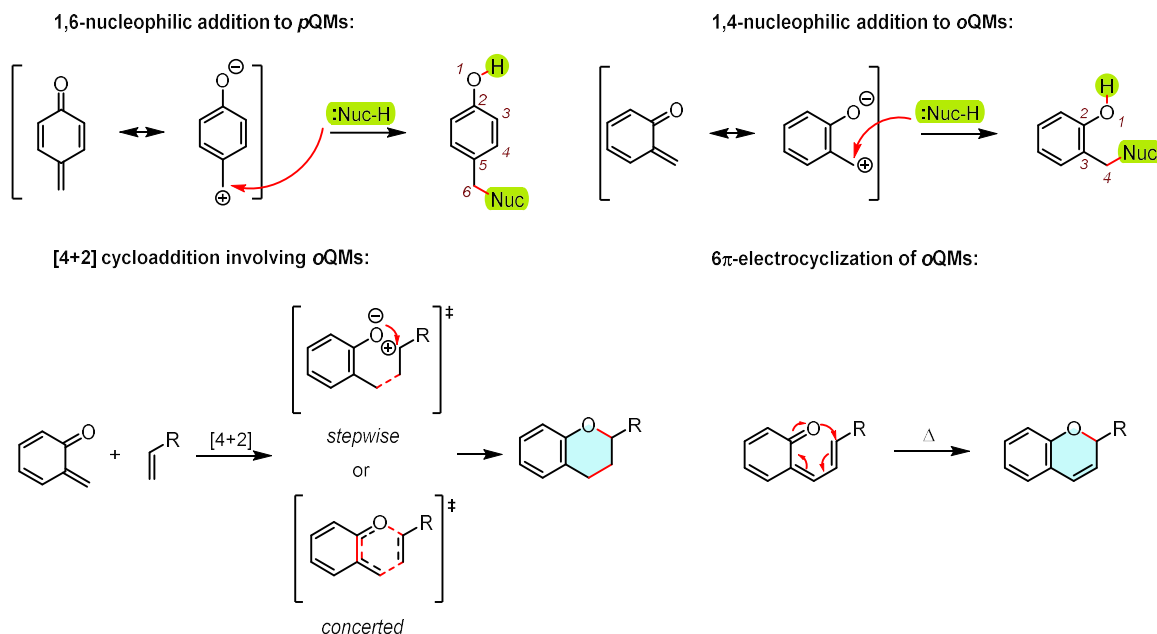
Scheme 9. Representative reactivities of *para-* and *ortho*-quinone methides: *p*QMs typically undergo 1,6-nucleophilic additions, while *o*QMs can participate in 1,4-nucleophilic additions, [4+2] cycloadditions and 6π-electrocyclizations.

2.3.1. Quinone Methides in Biology and Medicinal Chemistry

One of the most intriguing natural applications of quinone methides is observed in the biosynthesis of lignin, a major phenolic biopolymer that constitutes a central component of plant cell walls and provides essential mechanical support, water transport capability and resistance against microbial attack to the plant.[60] During lignification, *p*QMs arise as transient intermediates formed through radical coupling reactions of monolignols primarily such as coniferyl, sinapyl and *p*-coumaryl alcohols (Scheme 10A). These monolignols are first oxidized enzymatically by peroxidases (involving H_2O_2) or laccases (involving O_2), leading to formation of resonance-stabilized phenoxyl radicals (Scheme 10B).[61] These radicals can then undergo a variety of coupling modes, the exact type depends on the structure of the monolignol involved. For coniferyl units however, the β-O-4 or β-5 linkages are particularly common.[62] For β-O-4 coupling, a combination of two radicals results in a new C−O bond and the formation of a reactive *p*QM intermediate (Scheme 10C). The transient *p*QM can then undergo subsequent Michael additions typically involving nucleophiles such as water, alcohols (from other lignin units) or hydroxy groups from polysaccharides (lignin-carbohydrate-complex (LCC)).[62] These additions occur under rearomatization, driving the formation of C−O linkages that ultimately contribute in building up the complex, cross-linked three-dimensional lignin polymer.

It is important to note that the biosynthesis of lignin is a highly complex process, involving not only the three primary monolignols mentioned but also various other modified and acylated derivatives as well as oligomeric lignin fragments that can participate in further coupling reactions.[63]

_____
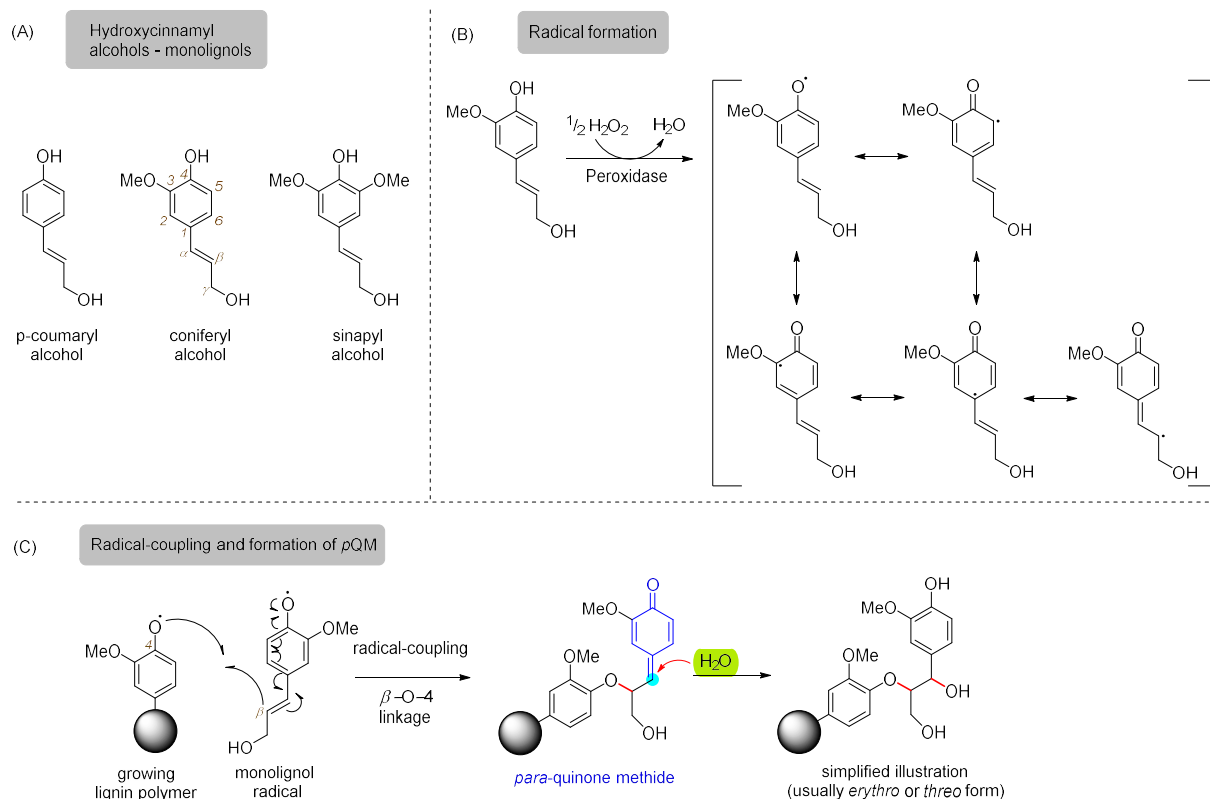
Scheme 10. (A) Most abundant hydroxycinnamyl alcohols involved in the biosynthesis of lignin. (B) Phenoxyl radical formation by peroxidase and H_2O_2 from coniferyl alcohol and corresponding resonance structures. (C) Example for radical coupling between a growing lignin polymer and a monolignol unit under formation of a *para*-quinone methide. Nucleophilic addition of water to the *p*QM contributes in building up the complex lignin polymer.

Beyond their central role in lignin biosynthesis, quinone methide moieties are key structural features in a variety of naturally occurring terpenoids, particularly among diterpenes and triterpenes (Scheme 11).[23] Notable examples for diterpenoids include *taxodone* and its oxidized analog *taxodione* isolated from plants like *taxodium distichum*.[64] Among triterpenoids, *celastrol* and *pristimerin* extracted from plants such as *Tripterygium wilfordii* and *Celastrus orbiculatus Thunb*. are prominent representatives and are traditionally used in Chinese medicine.[65] All these compounds exhibit a broad range of biological activities including anti-inflammatory, antimicrobial and particularly anticancer effects.[65, 66] The electrophilic QM motif enables covalent modification of nucleophilic biomolecules, particularly protein thiols (e.g. cysteine moieties) and DNA bases (e.g. guanine).[67] This results in DNA alkylation, inhibition of cell proliferation, and, ultimately, induction of apoptosis.[65c] For instance, celastrol, one of the most extensively studied triterpenoids, has demonstrated potent cytotoxicity against various cancer types including breast, prostate, lung and brain cancer cell lines by inhibiting signaling pathways such as NF-κB and Hsp90.[65c, 68] However, the same reactivity responsible for beneficial effects can also lead to off-target toxicity in healthy cells, emphasizing the importance for selective delivery and careful dosing.[65c]

_____

diterpenes   triterpenes

taxodone (R = OH)
taxodione (R = O as carbonyl group)

celastrol (R = H)
pristimerin (R = Me)
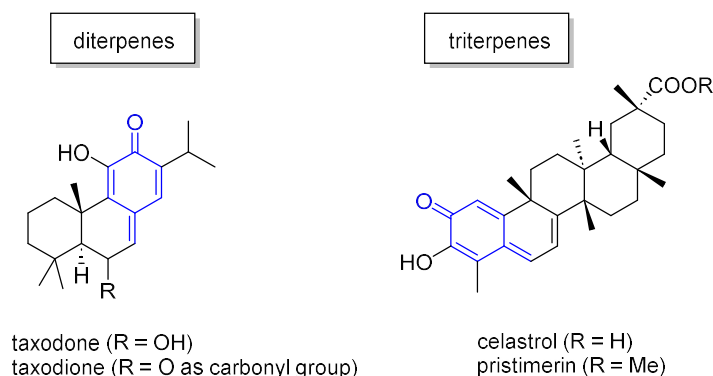
Scheme 11. Naturally occurring diterpenoids and triterpenoids with embedded QM structure which have biological activities.

In addition to these natural abundant QM-bearing compounds, quinone methides appear in prodrugs where QMs are released *in vivo* via enzymatic activation. A prominent example is Mitomycin C, a naturally occurring antibiotic and antitumor agent originally isolated from *Streptomyces caespitosus*.[69] Reductive enzymes such as NADPH-cytochrome P-450 reductase convert its quinone core to a hydroquinone, which then undergoes elimination of methanol to form a highly reactive *o*-quinone methide intermediate (Scheme 12).[70] This species can alkylate DNA and form interstrand crosslinks, thereby blocking replication and transcription, arresting the cell cycle, and triggering apoptosis.[71] However, its potent reactivity also raises concerns of systemic toxicity.[70]

Mitomycin C

Mitomycin C
Hydroquinone

ortho-Quinone methide
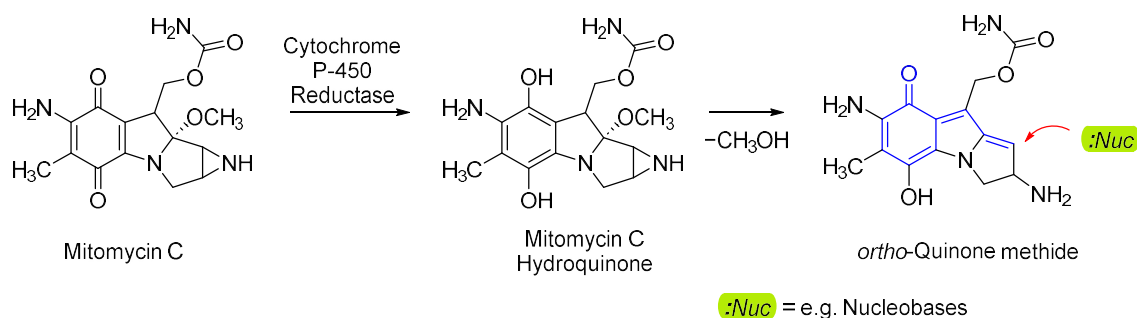
:Nuc = e.g. Nucleobases

Scheme 12. Transformation of Mitomycin C into the *o*QM, initiated by the cytochrome P-450 reductase. The transient *o*QM can react with nucleophiles such as nucleobases (first step of DNA alkylation is shown).[71a]

These examples of naturally occurring and bioactive QMs highlight their therapeutic promise and the toxicological challenges that arise from their electrophilicity.

2.3.2. Quinone Methides in Organic Synthesis

Their diverse reactivity is further exploited in the biomimetic synthesis of natural products.[72] A classic example is the total synthesis of Carpanone, first reported by CHAPMAN and co-workers in 1971.[73] In this synthesis, an oxidative homocoupling of a phenolic precursor generates an *o*QM intermediate, which subsequently undergoes an intramolecular [4+2] cycloaddition, efficiently assembling a complex polycyclic framework in a single step (Scheme 13A). Similarly, the synthesis of Mollugin, a bioactive naphthohydroquinone, proceeds via a quinone that is deprotonated at its prenyl moiety by NEt₃ and can delocalize to form an *o*QM species (Scheme 13B). The *o*QM intermediate then undergoes a 6π-

electrocyclization, engaging with the extended π-system to construct the fused polycyclic ring structure.[74]
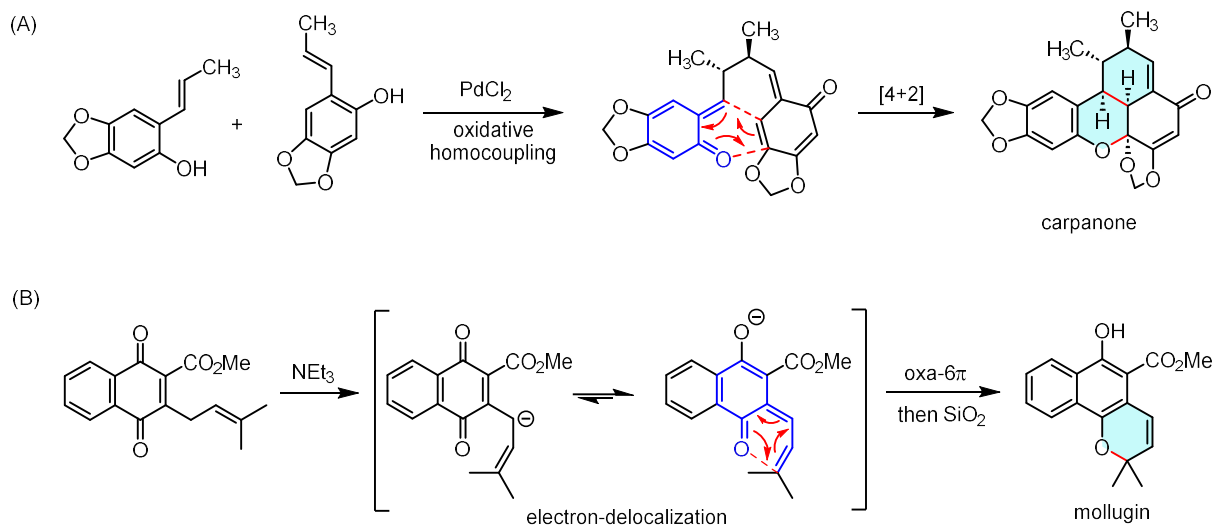
Scheme 13. (A) Synthesis of natural product Carpanone via intramolecular [4+2] cyclization of an *o*QM. (B) Synthesis of natural product Mollugin through oxa-6π electrocyclization of an *o*QM intermediate.[73, 74]

Furthermore, the chemistry of quinone methides is remarkably diverse and continues to be exploited in the development of modern synthetic methodologies. *o*QMs are frequently employed in asymmetric transformations, particularly in (4 + n) cycloaddition reactions, to construct valuable molecular scaffolds.[75, 76] For example, *o*QMs have proven useful in the synthesis of 3,4-dihydrocoumarins, a structural motif commonly encountered in biologically active compounds.[77] These coumarin derivatives can be accessed via (4+2) cycloadditions between *o*QMs and α-cyano ketones[78] or β-keto acyl pyrazoles[79], often catalyzed by squaramide-based organocatalysts, providing products in excellent yield and high enantiomeric excess.

In addition, more extended ring systems such as caprolactones, which are key structures in the synthesis of biodegradable polymers and also exhibit interesting biological activity[80], can be constructed through (4+3) cycloaddition reactions involving *o*QMs and enals (Scheme 14A).[81] Beyond these two representative examples, a broad range of other cycloaddition pathways have been reported, including not only further (4+2) and (4+3) but also (4+1) and even (4+4) reactions.[76]

In contrast, the reactivity of *p*QMs is typically governed by simple 1,6-nucleophilic addition reactions.[59a] However, several remarkable and more complex transformations have also been described. With appropriate reaction partners, *p*QMs can participate in the formation of spirocyclic frameworks. For instance, spirocyclopropanes can be obtained from reaction with α-bromo malonate or related substrates[32b, 82], while an interesting hetero-spirocyclopentane with an isoxazole was observed in a 1,3 dipolar cycloaddition reaction with benzonitrile oxide.[83]

Additionally, the reactivity of *p*QMs becomes significantly more diverse when the *p*QM carry an aryl moiety with *ortho*-substituents such as hydroxy, amino or olefinic groups.[32b] With an *ortho*-hydroxy group, intramolecular ring closures can occur, which give rise to benzopyran or benzofuran derivatives. For example, the reaction with ethyl benzimidate catalyzed by a Lewis acid leads to formation of a benzoxazine scaffold (Scheme 14B).[32b]
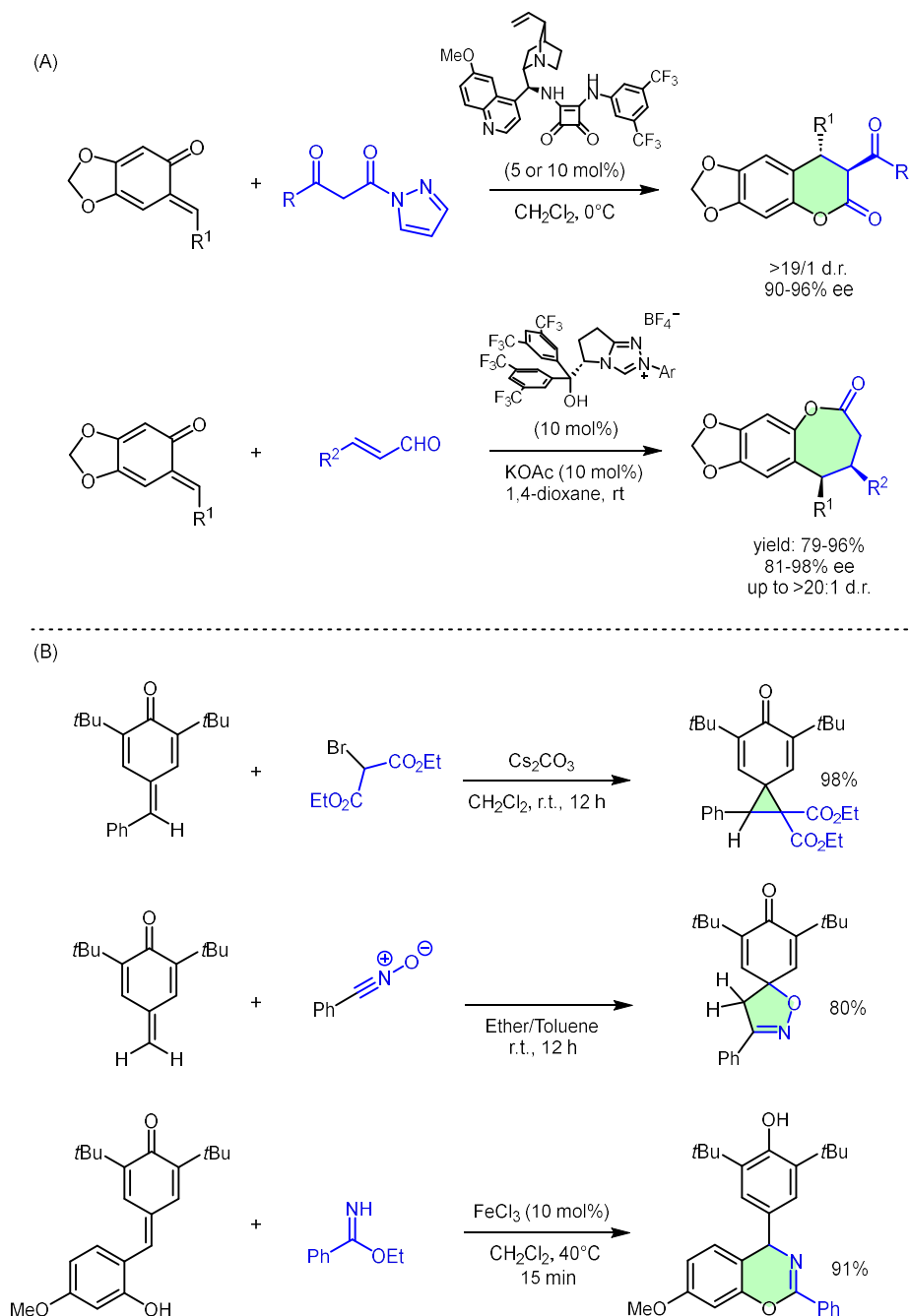
Scheme 14. (A) Selected examples of asymmetric (4 + 2 and 4 + 3) cycloadditions involving *o*QMs. (B) Selected transformations of *p*QMs leading to spirocyclic and heterocyclic structures.[32b, 78, 79, 81, 82, 83]

2.4. Objectives

WAN[48a,b], KRESGE[48c,d, 49, 58], FRECCERO[67a] and RICHARD[84] conducted a few fundamental reactivity studies on some simple *para-* and *ortho-*quinone methides in aqueous media by exploring their reactions with O-, N-, S- and halide nucleophiles. MAYR and co-workers later introduced a set of aryl-substituted *para-*quinone methides as structural analogs of benzhydrylium ions for the construction and extension of their comprehensive reactivity scales.[51, 85] However, systematic and detailed knowledge of the reactivities of a broader spectrum of quinone methides remained scarce.

The primary objective of this thesis was to investigate and characterize the electrophilic reactivities of quinone methides, focusing on *ortho*- and *para*-quinone methides (*o*QMs and *p*QMs), in the context of the Mayr-Patz equation $\lg k_2 = s_N(N + E)$. Scheme 15 illustrates the overall strategy of how to achieve this goal, summarizing the key approaches and outcomes envisioned in the course of this work.
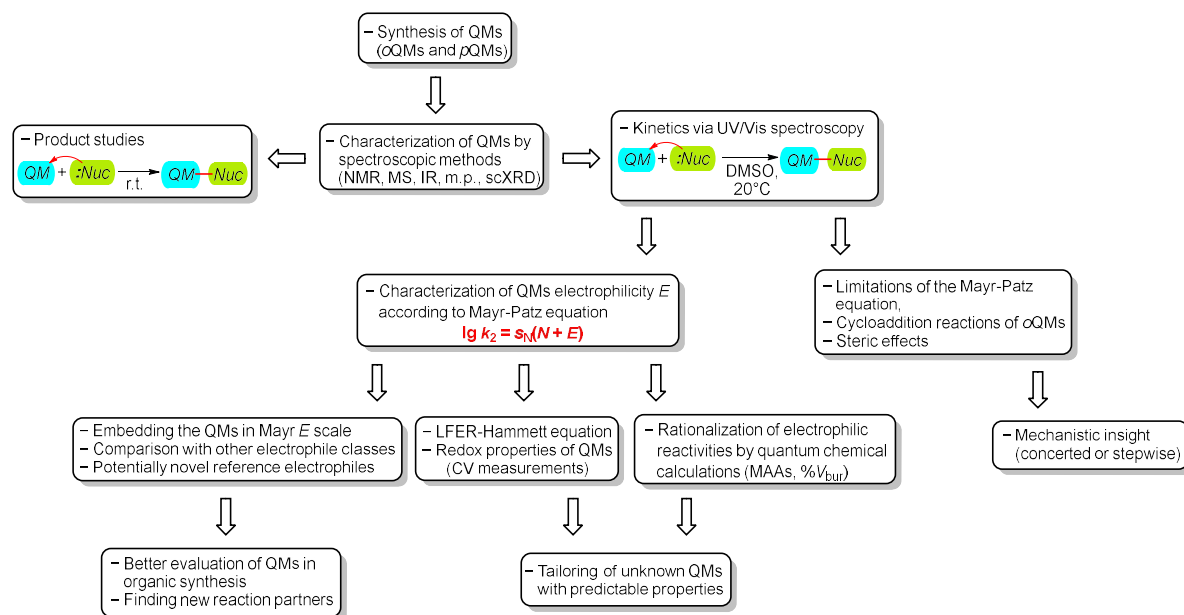
Scheme 15. Schematic overview of the studies conducted on quinone methides (QMs) in this PhD thesis and the insights gained from them.

The first part of this thesis focused on δ-functionalized *p*QMs. In contrast to aryl-substituted *p*QMs which serve as structural analogs of benzhydrylium ions, simple δ-functional group-substituted *para*-quinone methides (δ-FG *p*QMs) bear only functional groups such as -CN, -CF$_3$, -Me, -OMe directly at the exocyclic double bond. Although the majority of these compounds have been known since the 1960s through the work of WINSTEIN[56] and ERSHOV[57a], their synthetic applications had remained surprisingly underdeveloped. The lack of information on their reactivities has hindered a broader use of these compounds in organic synthesis. Chapter 3 addresses this gap by characterizing their electrophilic reactivities toward C-centered reference nucleophiles and reaction products with carbon and heteroatom nucleophiles. Quantum chemical methodology was used to further rationalize their reactivity behavior.

Chapter 4 extends this study to δ-disubstituted *p*QMs, which typically lack bulky substituents at the 2,6-positions adjacent to the carbonyl group, but feature aryl groups combined with electron-withdrawing substituents such as CN or CF$_3$ at the exocyclic carbon-carbon double bond. These compounds are synthetically valuable and found recent attention for the construction of chiral triarylmethanes bearing all carbon quaternary stereocenters, whose structural motifs can be found across pharmaceuticals and bioactive natural products.[86] Unlike mono-substituted *p*QMs, these disubstituted derivatives possess tertiary reaction centers, raising questions about how electronic and steric factors affect their reactivity and whether their electrophilic reactivities can still be adequately described by the Mayr-Patz relationship. These aspects are explored in detail in Chapter 4.

The second part of this thesis is dedicated to *o*QMs, which are synthetically highly versatile electrophiles. Their applications included (4+n) ring-forming reactions, bio-orthogonal ligation and biomolecule functionalization.[23] Improved understanding of the reactivity of synthetically and biologically useful *o*QMs will be important for a more targeted optimization of reaction conditions.

26

_____

Stabilized *o*QMs have been known since JURD,[31] and sesamol-based *o*QMs are the most commonly used synthetic subclass of *o*QMs. Nevertheless, there is no detailed synthetic basis for generating these valuable *o*QMs with various substituents on the aryl ring and with heterocyclic systems, not to mention the lack of spectroscopic characterization. Chapters 5 and 6 describe the syntheses of a series of stable sesamol-derived *o*QMs bearing a range of aryl and heteroaryl substituents, along with a detailed analysis of their electrophilic reactivities, investigated and rationalized from reactions with C-centered reference nucleophiles. Their reactivities are contextualized by comparisons to other electrophile classes, and supported by further physical organic methodology and quantum chemical analyses to enable reactivity prediction. Chapter 6 further explores the application of this *o*QM series in an enantioselective transformation with allenoates. The influence of substitution patterns on reaction yields and enantioselectivity is examined and discussed.

Since the Mayr-Patz equation is limited to polar reactions involving a single σ-bond formation in the rate-determining step, it does not apply to multibonding processes such as concerted cycloadditions. Significant deviations between experimental rate constants and rate constants calculated by the Mayr-Patz equation, as seen for example for 1,3-dipolar cycloadditions of diazomethanes, can serve as a mechanistic indicator and may suggest a different, possibly concerted reaction mechanism.[15] Thus, the Mayr-Patz equation could also be seen as a kind of diagnostic tool for probing reaction mechanisms. Given that *o*QMs are known to participate in a variety of [4+2] cycloaddition reactions, it was also intended to investigate their reactivity toward different dienophiles. A detailed description and mechanistic insights on the [4+2] cycloaddition reactions of *o*QMs and nucleophilic enamines as well as other dienophiles such as enol ethers, are given in Chapter 7.

Overall, the objective of the reactivity data developed in this thesis is to support the use of both *para*- and *ortho*-QMs as practical electrophiles in organic synthesis. They are intended to serve as a reference framework for comparing QMs to other classes of electrophiles, for predicting the reactivity of yet unknown derivatives and for guiding the design of new reactions and reaction partners. Furthermore, some of the QMs studied herein may serve as new standard electrophiles for future applications of the Mayr-Patz equation in nucleophile characterization.

_____

2.5. References

[1]   G. N. Lewis, *J. Am. Chem. Soc.* **1916**, *38*, 762.

[2]   J. N. Brönsted, *Recl. Trav. Chim. Pays-Bas* **1923**, *42*, 718.

[3]   C. K. Ingold, *Chem. Rev.* **1934**, *15*, 225.

[4]   C. G. Swain, C. B. Scott, *J. Am. Chem. Soc.* **1953**, *75*, 141.

[5]   J. O. Edwards, *J. Am. Chem. Soc.* **1954**, *76*, 1540.

[6]   J. F. Bunnett, *Annu. Rev. Phys. Chem.* **1963**, *14*, 271.

[7]   A. J. Parker, *Chem. Rev.* **1969**, *69*, 1.

[8]   C. D. Ritchie, *Acc. Chem. Res.* **1972**, *5*, 348.

[9]   C. D. Ritchie, *Can. J. Chem.* **1986**, *64*, 2239.

[10]   a) H. Mayr, M. Patz, *Angew. Chem. Int. Ed. Engl.* **1994**, *33*, 938; *Angew. Chem.* **1994**, *106*, 990; b) C. L. Perrin, I. Agranat, A. Bagno, S. E. Braslavsky, P. A. Fernandes, J.-F. Gal, G. C. Lloyd-Jones, H. Mayr, J. R. Murdoch, N. S. Nudelman, L. Radom, Z. Rappaport, M.-F. Ruasse, H.-U. Siehl, Y. Takeuchi, T. T. Tidwell, E. Uggerud, I. H. Williams *Pure Appl. Chem.* **2022**, *94*, 353.

[11]   a) H. Mayr, A. R. Ofial, *J. Phys. Org. Chem.* **2008**, *21*, 584; b) H. Mayr, A. R. Ofial, *Pure Appl. Chem.* **2005**, *77*, 1807; c) H. Mayr, *Tetrahedron* **2015**, *71*, 5095.

[12]   Reactivity parameters *E*, *N* and s_N can be retrieved at https://www.cup.lmu.de/oc/mayr/reaktionsdatenbank2/, which is a freely accessible website (accessed on 28/06/2025)

[13]   H. Mayr, B. Kempf, A. R. Ofial, *Acc. Chem. Res.* **2003**, *36*, 66.

[14]   T. B. Phan, M. Breugst, H. Mayr, *Angew. Chem. Int. Ed.* **2006**, *45*, 3869; *Angew. Chem.* **2006**, *118*, 3954.

[15]   a) H. Jangra, Q. Chen, E. Fuks, I. Zenz, P. Mayer, A. R. Ofial, H. Zipse, H. Mayr, *J. Am. Chem. Soc.* **2018**, *140*, 16758.

[16]   T. Schirmeister, C. Schmuck, P. R. Wich, *Beyer/Walter Organische Chemie*, Hirzel Verlag, Stuttgart, **2016**.

[17]   a) A. Michael, *J. Prakt. Chem.* **1887**, *35*, 349; b) T. Tokoroyama, *Eur. J. Org. Chem.* **2010**, *2010*, 2009.

[18]   a) Y. Zhang, W. Wang, *Catal. Sci. Technol.* **2012**, *2*, 42; b) A. N. Reznikov, Y. N. Klimochkin, *Synthesis* **2020**, *52*, 781.

[19]   a) D. Enders, A. Saint-Dizier, M.-I. Lannou, A. Lenzen, *Eur. J. Org. Chem.* **2006**, *2006*, 29; b) P. R. Krishna, A. Sreeshailam, R. Srinivas, *Tetrahedron* **2009**, *65*, 9657; c) R. S. Mamatha Jyothi, M. P. Sripathi, P. Thirupathi, *Curr. Org. Chem.* **2022**, *26*, 1264; d) P. Wadhwa, A. Kharbanda, A. Sharma, *Asian J. Org. Chem.* **2018**, *7*, 634.

[20]   a) C. F. Nising, S. Bräse, *Chem. Soc. Rev.* **2008**, *37*, 1218; b) C. Hui, F. Pu, J. Xu, *Chem. Eur. J.* **2017**, *23*, 4023.

_____

[21]   N. Halland, T. Hansen, K. A. Jørgensen, *Angew. Chem. Int. Ed.* **2003**, *42*, 4955.

[22]   B. D. Mather, K. Viswanathan, K. M. Miller, T. E. Long, *Prog. Polym. Sci.* **2006**, *31*, 487.

[23]   S. E. Rokita, *Quinone Methides*, Wiley, Hoboken, (NJ), **2009**.

[24]   L. Caruana, M. Fochi, L. Bernardi, *Molecules* **2015**, *20*, 11733.

[25]   M. M. Toteva, J. P. Richard, *Adv. Phys. Org. Chem.* **2011**, *45*, 39.

[26]   T. H. Zincke, *Justus Liebigs Ann. Chem.* **1902**, *320*, 145.

[27]   A. Bistrzycki, C. Herbst, *Ber. Dtsch. Chem. Ges.* **1903**, *36*, 2333.

[28]   A. Baeyer, V. Villiger, *Ber. Dtsch. Chem. Ges.* **1903**, *36*, 2774.

[29]   K. Fries, K. Kann, *Justus Liebigs Ann. Chem.* **1907**, *353*, 335.

[30]   P. D. Gardner, H. Sarrafizadeh, R. L. Brandon, *J. Am. Chem. Soc.* **1959**, *81*, 5515.

[31]   L. Jurd, *Tetrahedron* **1977**, *33*, 163.

[32]   a) R. W. van de Water, T. R. Pettus, *Tetrahedron* **2002**, *58*, 5367; b) C. G. S. Lima, F. P. Pauli, D. C. S. Costa, A. S. de Souza, L. S. M. Forezi, V. F. Ferreira, F. de Da Carvalho Silva, *Eur. J. Org. Chem.* **2020**, *2020*, 2650.

[33]   Y. Gong, K. Kato, *Synlett* **2002**, *2002*, 431.

[34]   a) M.-W. Chen, L.-L. Cao, Z.-S. Ye, G.-F. Jiang, Y.-G. Zhou, *Chem. Commun.* **2013**, *49*, 1660; b) K. Zielke, M. Waser, *Org. Lett.* **2018**, *20*, 768.

[35]   C. D. Bray, *Org. Biomol. Chem.* **2008**, *6*, 2815.

[36]   K. Chiba, T. Hirano, Y. Kitano, M. Tada, *Chem. Commun.* **1999**, 691.

[37]   Y. L. Mao, V. Boekelheide, *Proc. Nat. Acad. Sci. USA* **1980**, *77*, 1732.

[38]   a) H. Miyazaki, K. Honda, M. Asami, S. Inoue, *J. Org. Chem.* **1999**, *64*, 9507; b) H. Miyazaki, Y. Honda, K. Honda, S. Inoue, *Tetrahedron Lett.* **2000**, *41*, 2643.

[39]   a) P. Batsomboon, W. Phakhodee, S. Ruchirawat, P. Ploypradith, *J. Org. Chem.* **2009**, *74*, 4009; b) K. Akkarasereenon, K. Tangdenpaisal, S. Ruchirawat, P. Ploypradith, *Org. Biomol. Chem.* **2020**, *18*, 8854.

[40]   a) D. A. Bolon, *J. Org. Chem.* **1970**, *35*, 715; b) D. Osipov, V. Osyanin, Y. Klimochkin, *Synlett* **2012**, *23*, 917; c) D. Liao, H. Li, X. Lei, *Org. Lett.* **2012**, *14*, 18.

[41]   F. M. Dean, M. O. A. Orabi, *J. Chem. Soc., Perkin Trans. 1* **1982**, 2617.

[42]   a) M. Yato, T. Ohwada, K. Shudo, *J. Am. Chem. Soc.* **1990**, *112*, 5341; b) Z. Goldschmidt, S. Levinger, H. E. Gottlieb, *Tetrahedron Lett.* **1994**, *35*, 7273.

[43]   a) H. Heaney, J. M. Jablonski, *Chem. Commun. (London)* **1968**, 1139; b) H. Heaney, J. M. Jablonski, C. T. McCarty, *J. Chem. Soc., Perkin Trans. 1* **1972**, 2903.

[44]   N. Fixler, H. Salez, M. Demeunynck, J. Lhomme, *J. Chem. Soc., Perkin Trans. 1* **1995**, 1649.

[45]   H.-J. Hansen, *Helv. Chim. Acta* **1977**, *60*, 2007.

_____

[46]   a) B. Büyükkıdan, S. Bilgiç, O. Bilgiç, *Synth. Commun.* **2001**, *31*, 1263; b) M. von Strandtmann, M. P. Cohen, J. Shavel, *Tetrahedron Lett.* **1965**, *6*, 3103.

[47]   W. A. Sheppard, *J. Org. Chem.* **1968**, *33*, 3297.

[48]   a) L. Diao, C. Yang, P. Wan, *J. Am. Chem. Soc.* **1995**, *117*, 5369; b) P. Wan, B. Barker, L. Diao, M. Fischer, Y. Shi, C. Yang, *Can. J. Chem.* **1996**, *74*, 465; c) Y. Chiang, A. J. Kresge, Y. Zhu, *J. Am. Chem. Soc.* **2002**, *124*, 717; d) Y. Chiang, A. J. Kresge, Y. Zhu, *J. Am. Chem. Soc.* **2000**, *122*, 9854.

[49]   Y. Chiang, A. J. Kresge, Y. Zhu, *J. Am. Chem. Soc.* **2001**, *123*, 8089.

[50]   J.-P. Lumb, K. C. Choong, D. Trauner, *J. Am. Chem. Soc.* **2008**, 130, 9230.

[51]   D. Richter, N. Hampel, T. Singer, A. R. Ofial, H. Mayr, *Eur. J. Org. Chem.* **2009**, *2009*, 3203.

[52]   B. Koutek, L. Pavličková, M. Souček, *Synth. Commun.* **1976**, *6*, 305.

[53]   S. Evans, P. Nesvadba, S. Allenbach (Ciba-Geigy AG), EP0744392, **1996**.

[54]   P. Nesvadba, *Synth. Commun.* **2000**, *30*, 2825.

[55]   T. R. Kasturi, S. K. Jayaram, J. A. Sattigeri, P. V.P. Pragnacharyulu, T. N. Guru Row, Renuka K, K. Venkatesan, N. Shahina Begum, N. Munirathinam, *Tetrahedron* **1993**, *49*, 7145.

[56]   L. J. Filar, S. Winstein, *Tetrahedron Letters* **1960**, *1*, 9.

[57]   V. V. Ershov, A. A. Volod'kin, G. D. Ostapets-Sveshnikova, *Russ. Chem. Bull.* **1966**, *15*, 888.

[58]   a) Y. Chiang, A. J. Kresge, Y. Zhu, *J. Am. Chem. Soc.* **2002**, *124*, 6349; b) J. A. Chang, A. J. Kresge, H.-Q. Zhan, Y. Zhu, *J. Phys. Org. Chem.* **2004**, *17*, 579.

[59]   a) J.-Y. Wang, W.-J. Hao, S.-J. Tu, B. Jiang, *Org. Chem. Front.* **2020**, *7*, 1743; b) W.-J. Bai, J. G. David, Z.-G. Feng, M. G. Weaver, K.-L. Wu, T. R. R. Pettus, *Acc. Chem. Res.* **2014**, *47*, 3655.

[60]   W. Boerjan, J. Ralph, M. Baucher, *Annu. Rev. Plant Biol.* **2003**, *54*, 519.

[61]   Y. Wang, M. Chantreau, R. Sibout, S. Hawkins, *Front. Plant Sci.* **2013**, *4*, 220.

[62]   X. Zhu, T. Akiyama, T. Yokoyama, Y. Matsumoto, *J. Agric. Food Chem.* **2019**, *67*, 2139.

[63]   a) G. J. Leary, *Wood Sci. Technol.* **1980**, *14*, 21; b) T. Warinowski, S. Koutaniemi, A. Kärkönen, I. Sundberg, M. Toikka, L. K. Simola, I. Kilpeläinen, T. H. Teeri, *Front. Plant Sci.* **2016**, *7*, 1523.

[64]   S. M. Kupchan, A. Karim, C. Marcks, *J. Am. Chem. Soc.* **1968**, *90*, 5923.

[65]   a) J. Shi, J. Li, Z. Xu, L. Chen, R. Luo, C. Zhang, F. Gao, J. Zhang, C. Fu, *Front. Pharmacol.* **2020**, *11*, 558741; b) J. Sun, Z. Tian, J. Wu, J. Li, Q. Wang, S. Huang, M. Wang, *Drug Des. Devel. Ther.* **2024**, *18*, 1673; c) Y. Zhu, Y. Meng, J. Zhang, R. Liu, S. Shen, L. Gu, Y.-K. Wong, A. Ma, X. Chai, Y. Zhang et al., *Int. J. Biol. Sci.* **2024**, *20*, 5510.

[66]   a) Y. Uchihara, K. Tago, H. Taguchi, Y. Narukawa, F. Kiuchi, H. Tamura, M. Funakoshi-Tago, *Biochem. Pharmacol.* **2018**, *154*, 357; b) T. Bakhsh, N. M. Alyami, *Heliyon* **2024**, *10*, e34044.

[67]   a) E. Modica, R. Zanaletti, M. Freccero, M. Mella, *J. Org. Chem.* **2001**, *66*, 41; b) P. Pande, J. Shearer, J. Yang, W. A. Greenberg, S. E. Rokita, *J. Am. Chem. Soc.* **1999**, *121*, 6773.

[68]   S. Boridy, P. U. Le, K. Petrecca, D. Maysinger, *Cell Death Dis.* **2014**, *5*, e1216.

_____

[69]   S. T. Crooke, W. T. Bradner, *Cancer Treat. Rev.* **1976**, *3*, 121.

[70]   J. Verweij, H. M. Pinedo, *Anti-Cancer Drugs* **1990**, *1*, 5.

[71]   a) M. Tomasz, *Chemistry & Biology* **1995**, *2*, 575; b) L. Brulikova, J. Hlavac, P. Hradil, *Curr. Med. Chem.* **2012**, *19*, 364.

[72]   K. Ali, P. Mishra, A. Kumar, D. N. Reddy, S. Chowdhury, G. Panda, *Chem. Commun.* **2022**, *58*, 6160.

[73]   O. L. Chapman, M. R. Engel, J. P. Springer, J. C. Clardy, *J. Am. Chem. Soc.* **1971**, *93*, 6696.

[74]   J.-P. Lumb, D. Trauner, *Org. Lett.* **2005**, *7*, 5865.

[75]   a) V. A. Osyanin, A. V. Lukashenko, D. V. Osipov, *Russ. Chem. Rev.* **2021**, *90*, 324; b) D. V. Osipov, V. A. Osyanin, Y. N. Klimochkin, *Russ. Chem. Rev.* **2017**, *86*, 625.

[76]   Q. Hou, X. Liu, L. Chen, R. Cao, S. Yue, L. Zhu, B. Xiong, *Curr. Org. Chem.* **2025**, *29*, 1221.

[77]   C.-C. Chen, J.-S. Huang, T.-H. Wang, C.-H. Kuo, C.-J. Wang, S.-H. Wang, Y.-L. Leu, *Int. J. Mol. Sci.* **2017**, *18*, 2655.

[78]   C. Gharui, C. Parida, S. C. Pan, *J. Org. Chem.* **2021**, *86*, 13071.

[79]   L. Cui, D. Lv, Y. Wang, Z. Fan, Z. Li, Z. Zhou, *J. Org. Chem.* **2018**, *83*, 4221.

[80]   A. L. Sisson, D. Ekinci, A. Lendlein, *Polymer* **2013**, *54*, 4333.

[81]   H. Lv, W.-Q. Jia, L.-H. Sun, S. Ye, *Angew. Chem. Int. Ed.* **2013**, *52*, 8607.

[82]   X. Liu, Y. Ren, L. Zhu, T. Li, W. Xu, Y. Liu, K.-W. Tang, B. Xiong, *Tetrahedron* **2023**, *148*, 133655.

[83]   A. D. Woolhouse, *Aust. J. Chem.* **1977**, *30*, 1145.

[84]   M. M. Toteva, M. Moran, T. L. Amyes, J. P. Richard, *J. Am. Chem. Soc.* **2003**, *125*, 8814.

[85]   R. Lucius, R. Loos, H. Mayr, *Angew. Chem. Int. Ed.* **2002**, *41*, 91; *Angew. Chem.* **2002**, *114*, 97.

[86]   a) Z. Wang, Y. Zhu, X. Pan, G. Wang, L. Liu, *Angew. Chem. Int. Ed.* **2020**, *59*, 3053; b) X. Liu, C. Zhao, R. Zhu, L. Liu, *Angew. Chem. Int. Ed.* **2021**, *60*, 18499; *Angew. Chem.* **2021**, *133*, 18647.

Chapter 3. Reactivity of *δ*-Functionalized *Para*-Quinone Methides in Nucleophilic Addition Reactions

Author contributions

All experimental work was performed by C. Gross; A. Eitzinger carried out the quantum chemical calculations. P. Mayer performed the crystallographic analysis and visualization. The manuscript was written jointly by A. R. Ofial and C. Gross and with contributions from all authors.

Copyright

Parts of the supporting information are shown in section 3.2. A complete version of the electronic supporting information is accessible under the following link:

https://doi.org/10.1002/chem.202501224

The raw data of kinetic measurements that support the findings of this study are openly available in Open Data LMU under the following link:

https://doi.org/10.5282/ubm/data.582

3.1. Copies of Manuscript

Reactivity of δ-Functionalized *Para*-Quinone Methides in Nucleophilic Addition Reactions

Christoph Gross,[a] Andreas Eitzinger,[a, b] Peter Mayer,[a] and Armin R. Ofial*[a]

The electrophilic reactivities of *para*-quinone methides (*p*QMs) with functional groups (FG) at the exocyclic polarized carbon–carbon double bond were determined by photometrically monitoring the kinetics of their reactions with carbanions in dimethyl sulfoxide (DMSO) at 20 °C. The experimental second-order rate constants k_2 were evaluated by the Mayr-Patz equation, that is, the linear free energy relationship lg $k_2 = s_N(N + E)$, which was leveraged to determine the electrophilicity descriptors E of the *p*QMs. These electrophilicity parameters E were subsequently used to successfully predict the scope of the *p*QM reactions with C-, H-, N-, O-, and S-centered nucleophiles. Moreover, the electrophilicity parameters E correlate linearly with a linear combination of quantum-chemically calculated methyl anion affinities (MAAs) and buried volumes (%V_{bur}). While MAA values mainly reflect the thermodynamic driving force of the carbon–carbon bond formation, %V_{bur} values take account of the variable steric effects of substituents at the electrophilic δ-position of the *p*QMs. Knowledge of MAA and %V_{bur} thus enables chemists to tailor novel *p*QMs with predictable reactivity properties.

1. Introduction

Para-quinone methides (*p*QMs) are a subclass of cyclic Michael acceptors, in which an exocyclic methylene group is in conjugation with an α,β-unsaturated ketone.[1] This combination of functionalities results in a strong polarization of the exocyclic π-bond and a high reactivity toward nucleophiles at the δ-position (Scheme 1a).[2] Besides the significant role of *p*QMs in biological processes[3–5] they are frequently utilized in synthetic transformations where *p*QMs undergo 1,6-conjugate nucleophilic additions[6–9] or a multitude of ring-forming reactions.[10–13]

Owing to their relevance as vinylogous Michael acceptors, several attempts were made to characterize their electrophilicity, in particular by pH-dependent kinetic measurements in aqueous solution.[14–18] Furthermore, δ-aryl-substituted *p*QMs (**1** with FG = aryl, such as **1g** in Scheme 1b) resemble structural analogues of benzhydrylium ions and were, therefore, used by H. Mayr and coworkers as reference electrophiles to extend their comprehensive reactivity scales toward highly reactive nucleophiles.[19–21]

[a] C. Gross, Dr. A. Eitzinger, Dr. P. Mayer, Dr. A. R. Ofial
Department Chemie, Ludwig-Maximilians-Universität München,
Butenandtstr. 5–13, 81377 München, Germany
E-mail: ofial@lmu.de

[b] Dr. A. Eitzinger
Institute of Organic Chemistry, Johannes Kepler University Linz, Altenberger
Straße 69, 4040 Linz, Austria

The Mayr reactivity scales are based on the linear free energy relationship in Equation (1), that uses three parameters to calculate the second-order rate constant k_2 of a given electrophile-nucleophile reaction at 20 °C.[22–25]

$$\lg k_2 = s_N (N + E) \tag{1}$$

Nucleophiles are characterized by two solvent-dependent parameters, s_N and N. The reactivity of electrophiles is described by a single electrophilicity parameter E. So far, Equation (1) has been utilized to characterize the reactivity of > 1300 nucleophiles and 350 electrophiles, including aryl-substituted *ortho*- and *para*-quinone methides.[26]

Though syntheses and spectroscopic characterization of simple δ-functional group-substituted *para*-quinone methides (δ-FG-*p*QMs) **1** (Scheme 1) have been reported since the 1960s,[27–30] systematic reactivity studies of these versatile electrophiles with synthetically relevant nucleophiles in organic solvents are still scarce.[18,27,31,32]

This lack of knowledge is currently retarding a more comprehensive exploitation of the synthetic potential of δ-FG-*p*QMs and motivated us to quantify their electrophilicity by studying the kinetics of their reactions with carbanions **2** as reference nucleophiles. The experimentally determined rate constants k_2 of these model reactions provide the fundament for embedding δ-FG-*p*QMs **1** in Mayr's reactivity scales. The location of δ-FG-*p*QMs **1** in the electrophilicity scale will then provide a powerful tool to enhance the synthetic space of these electrophiles by the straightforward identification of novel nucleophilic reaction partners. Additionally, we will show that DFT calculations can be efficiently used to reliably predict the electrophilicities of further δ-FG-*p*QM derivatives.

Scheme 1. a) Nucleophiles attack *δ*-functionalized *para*-quinone methides (*δ*-FG-*p*QMs **1**) at the polarized exocyclic *π*-bond. b) Structures of *δ*-FG-*p*QM electrophiles and reference nucleophiles used in this work (counterion: K⁺ or K⁺/18-crown-6). Nucleophilicity parameters *N* (and *s*ₙ) refer to reactivities in DMSO; refs. [20,26].

2. Results and Discussion

2.1. Product Studies

First, we studied the products of the reactions between *p*QMs **1** and the potassium salts of the carbanions **2** that we selected as potential reference nucleophiles for the kinetic measurements. To do so, we generated the parent *δ*-FG-*p*QM **1a** (FG = H) by oxidation of 3,5-di-*tert*-butyl-4-hydroxytoluene (BHT) with silver(I) oxide in tetrachloromethane as originally reported by Winstein.[27,30] The NMR spectroscopic analysis showed that BHT was quantitatively converted into the *p*QM **1a** within 20 minutes under Winstein's conditions.[33] After filtration from solids, the thus obtained CCl₄ solution of **1a** was mixed with a DMSO solution of potassium diethyl malonate (**2j**). These reaction conditions did not furnish simple Michael adducts, however, but a mixture of the spirocyclopropane **3** and the bis-spiro cyclopentane **4**. After aqueous workup and separation by chromatography, **3** and **4** were isolated in yields of 31% and 51%, respectively (Scheme 2a). Analysis of **3** and **4** by single crystal X-ray diffraction (scXRD) confirmed the structural assignments (Figure 1a,b),[34] which were derived from the NMR spectra for both reaction products. We rationalized the formation of both **3** and **4** by initial Michael additions followed by ring-forming reactions involving radical intermediates.[35,36] The ring systems in the solid-state structures of both **3** and **4** are characterized by one C—C bond which is significantly longer than the average of the other C—C bond lengths in the same ring. In the three-membered ring of **3**, d(C1-C3) = 1.5711(13) Å is longer than d(C1-C2) = 1.4913(13) Å or d(C2-C3) = 1.5217(13) Å.[34] Even more obvious, d(C1-C2) = 1.6044(17) Å in the cyclopentane ring of **4**
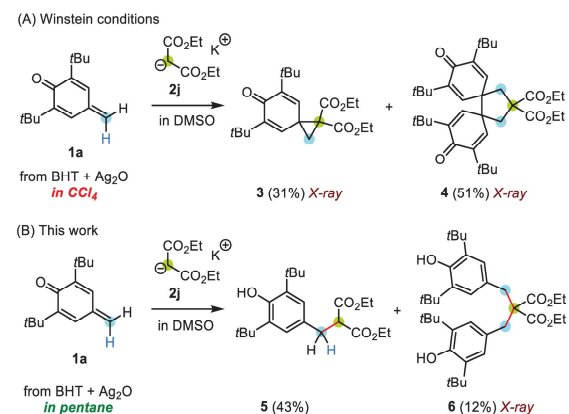
deviates from the lengths of the other C—C bonds in the same ring, which are in a narrow range from 1.5479(19) to 1.5552(19) Å.[34]

A screening of conditions for the generation of *p*QM **1a** by oxidation of BHT with silver(I) oxide identified pentane as a solvent, which made it possible to carry out the Michael reaction of **1a** and **2j** without competing intramolecular radical cyclizations. As shown in Scheme 2b, the 1:1 Michael adduct **5** as well as the 2:1 Michael adduct **6** were isolated (Figure 1c).[36] Thus, polar reactions of the parent **1a** with nucleophiles could be carried out without being disturbed by electron transfer reactions, presumably induced by traces of oxidizing metal ions.

A rapid fading of the colored *p*QMs **1**[33,37] was observed when they were mixed with the carbanions **2** (counterion: K⁺) in DMSO or *n*-pentane/DMSO solvent mixtures. The reaction mixtures were worked up and purified by chromatography to isolate the Michael adducts in unoptimized yields of 60–98% (Scheme 3). For example, *p*QM **1a** (FG = H) and **1e** (FG = Me) reacted with carbanions **2** to furnish after aqueous workup in good yields the simple 1,6-addition products **7–11**, which were spectroscopically characterized. In CDCl₃ solution, **9** was characterized as a 1:1 keto-enol mixture. In crystalline state, however, the scXRD analysis of **9** (Scheme 3d) showed exclusively the enol form of the 1,3-dicarbonyl groups of the dimedone moiety.

Also, the reactions of *p*QM **1c** (FG = CN) with deprotonated Meldrum's acid **2a** as well as with the malononitrile-derived carbanion **2h** generated the Michael adducts **12** and **13**, respectively, in decent yields of 79% and 86%. In agreement with the structural data for **7**, NMR spectroscopic data and scXRD analysis of **12** (Scheme 3e) showed the bis-lactone structure of the Meldrum's acid moiety. Indications for the alternative enol forms were not found. Phenol **13** carries three adjacent nitrile groups in the side chain at the 4-position (Scheme 3b,f). The analogous reaction of *p*QM **1d** (FG = CO₂Me) with the diethyl malonate-derived nucleophile **2j** yielded a 1,6-addition product with three ester groups at the side chain of the phenol **14** (Scheme 3c).

Scheme 2. Reactions of **1a** with the nucleophile **2j**: depending on the solvent used to preform *p*QM **1a** either a) cyclic products **3** and **4** from Michael addition/oxidative radical cyclization sequences or b) Michael adducts **5** and **6** were isolated (conditions: 1 hour, r.t.).

Chem. Eur. J. **2025**, *31*, e202501224 (2 of 9)

© 2025 The Author(s). Chemistry – A European Journal published by Wiley-VCH GmbH
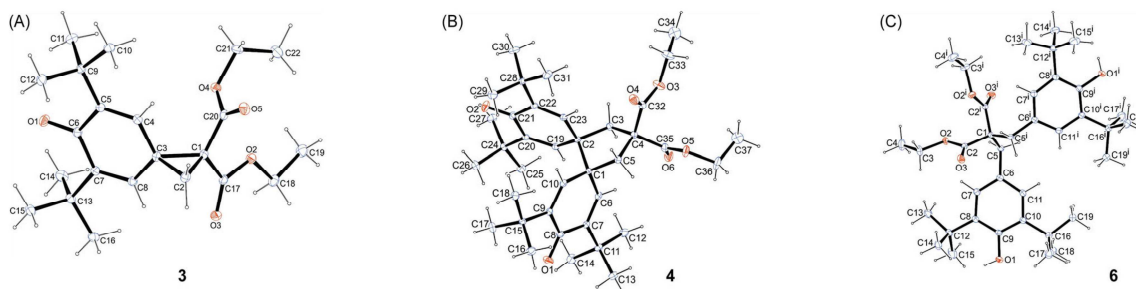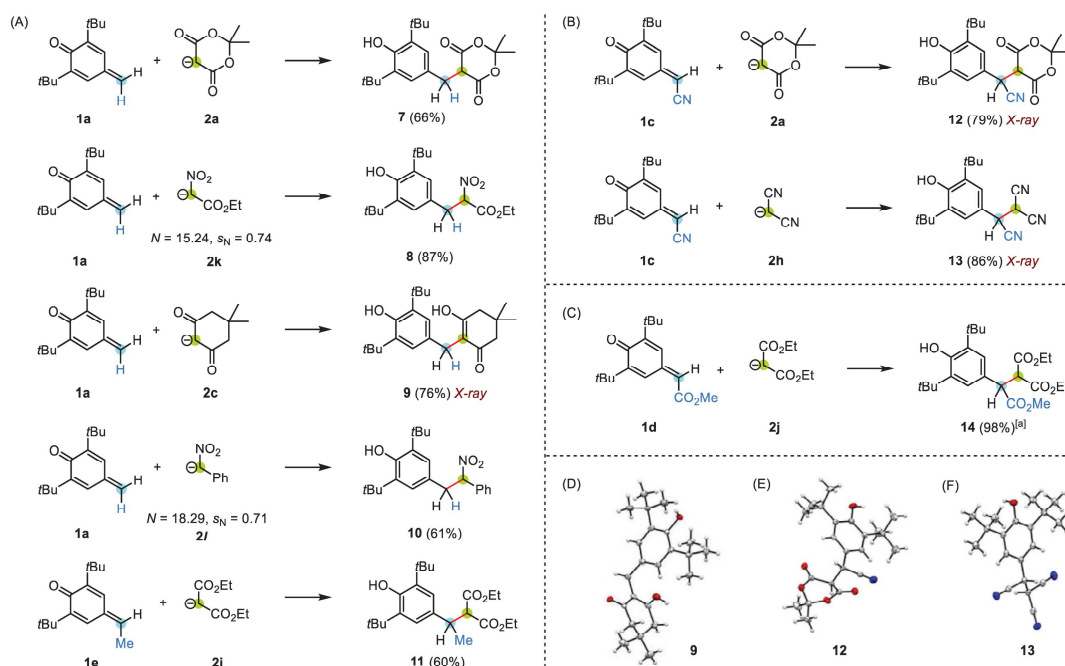
34

Figure 1. Crystalline products from the reactions of the *p*QM **1a** with potassium diethyl malonate (**2j**): scXRD structures of a) the cyclopropane **3**, b) the cyclopentane **4**, and c) the double Michael adduct **6**. Thermal ellipsoids are shown on the 25% probability level (at 173 K).[34]


Scheme 3. Michael additions of carbanionic nucleophiles **2** (counterion: K⁺) to *δ*-substituted *p*QMs **1a** and **1e** (a), **1c** (b), and **1d** (c) in DMSO or pentane/DMSO mixtures (1 hour at r.t.). The quinone methides **1** were generated from the corresponding phenols by oxidation with silver(I) oxide in *n*-pentane.[33] Yields refer to isolated products after aqueous workup. Single crystal structures with thermal ellipsoids on the 50% probability level (at 173 K) are shown for **9** (d), **12** (e), and **13** (f).[34] [a] Owing to a high degree of disorder in crystalline **14** only low-quality scXRD data were obtained.[33,34]

Scheme 4 illustrates that reactions of the *δ*-methoxy-*p*QM **1f** with carbanions took another course. Additions of the C-nucleophiles **2e** and **2j** to **1f** were accompanied by subsequent methanol eliminations to give the benzylidene pentan-2,4-dione **15** and the benzylidene malonate **16**, respectively. Nevertheless, formation of both **15** and **16** is rationalized by an initial *σ*-bond formation through an electrophile-nucleophile combination. The similar Brønsted basicities of the phenolate oxygen (pK_a = 16.8 for 2,6-di-*tert*-butylphenol in DMSO) and the acceptor-stabilized carbanions which emerge from the acetylacetone or malonate part of the adducts (pK_a = 15.1 for 2-methylacetylacetone; pK_a = 18.0 for dimethyl 2-methylmalonate in DMSO)[38] facilitate a subsequent proton shift from the CH acid to the phenolate oxygen to give carbanions, which then eliminate methoxide ions

to furnish the isolated benzylidenes **15** and **16**, respectively. An analogous course was described by Tsuri and colleagues for the reaction of **1f** with *α*-lithiated *N*-ethyl-*γ*-sultam, which gave the corresponding benzylidene compound considered as a drug candidate for the treatment of arthritis.[39]

2.2. Kinetics

The product studies showed that formation of all isolated products can be rationalized by electrophile-nucleophile combinations of **1** and **2**, in which one new *σ*-bond is formed in the first step of the reaction. Thus, a crucial prerequisite for the application of the Mayr-Patz equation (Equation (1)) was fulfilled and
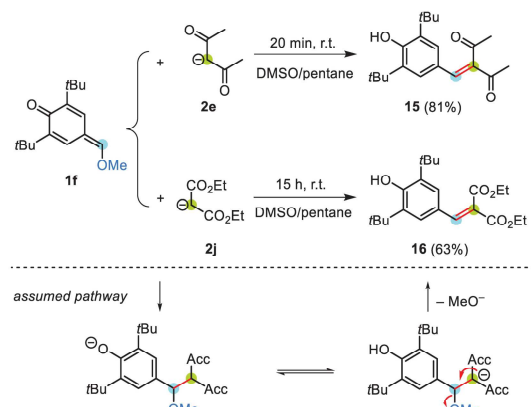
Scheme 4. The δ-methoxy-substituted *p*QM **1f** reacted with the carbanions **2e** and **2j** (counterion: K⁺) in an addition-elimination sequence to form **15** and **16**, respectively. Yields refer to isolated products after aqueous workup.
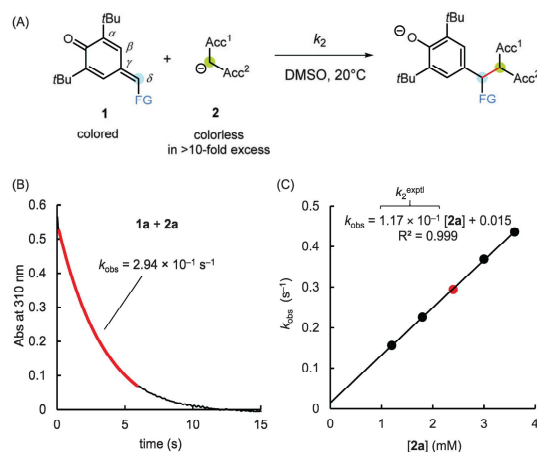

Figure 2. a) Carbon–carbon bond-forming reaction of an electrophilic *p*QM **1** with a C-centered nucleophile **2** in DMSO at 20 °C. b) The time-dependent decay of the absorbance of **1a** ([**1a**]$_0$ = 2.50 × 10⁻⁵ M) at 310 nm in the course of the reaction with **2a** ([**2a**]$_0$ = 2.40 × 10⁻³ M) was used to determine the first-order rate constant k_{obs} (s⁻¹). c) The slope of the linear correlation of k_{obs} with [**2a**] corresponds to the second-order rate constant k_2^{exp} (M⁻¹ s⁻¹) for the **1a** + **2a** addition reaction.

Table 1. Experimental and calculated second-order rate constants k_2 of the reactions of *p*QMs **1** with the reference nucleophiles **2** (DMSO, 20 °C).				
δ-FG-*p*QM	2	k_2^{exptl} [M⁻¹ s⁻¹]	$k_2^{Eq.(1)}$ [a] [M⁻¹ s⁻¹]	$k_2^{exptl}/k_2^{Eq.(1)}$
1a (FG = H)	2a	1.17 × 10²	2.27 × 10²	0.51
$E = -11.17$	2b	1.73 × 10³	7.16 × 10²	2.4
	2c	6.78 × 10³	8.45 × 10³	0.80
1b (FG = CF₃)	2f	7.92 × 10⁴ [b]	1.11 × 10⁵	0.71
$E = -11.68$ [b]	2h	1.03 × 10⁵ [b]	1.40 × 10⁵	0.74
	2i	2.73 × 10⁵ [b]	2.09 × 10⁵	1.3
	2j	5.38 × 10⁵ [b]	3.56 × 10⁵	1.5
1c (FG = CN)	2a	2.29 × 10¹	5.57 × 10¹	0.41
$E = -11.88$	2c	4.98 × 10³	2.40 × 10³	2.1
	2d	2.68 × 10³	4.24 × 10³	0.63
	2h	8.90 × 10⁴	1.03 × 10⁵	0.87
	2i	3.71 × 10⁵	1.53 × 10⁵	2.4
1d (FG = CO₂Me)	2c	2.22 × 10³	1.91 × 10³	1.2
$E = -12.01$	2e	9.55 × 10³	1.29 × 10⁴	0.74
	2g	7.58 × 10⁴	5.00 × 10⁴	1.5
	2h	2.53 × 10⁴	8.40 × 10⁴	0.30
	2i	1.04 × 10⁵	1.26 × 10⁵	0.83
	2j	6.68 × 10⁵	2.17 × 10⁵	3.1
1e (FG = Me)	2c	2.73 × 10²	9.87 × 10¹	2.8
$E = -13.68$	2g	3.52 × 10³	3.52 × 10³	1.0
	2h	4.55 × 10³	6.39 × 10³	0.71
	2i	5.05 × 10³	9.55 × 10³	0.53
	2j	1.48 × 10⁴	1.78 × 10⁴	0.83
1f (FG = OMe)	2e	4.85 × 10¹	7.15 × 10¹	0.68
$E = -15.10$	2g	4.29 × 10²	3.69 × 10²	1.2
	2h	1.04 × 10³	7.15 × 10²	1.5
	2j	1.89 × 10³	2.13 × 10³	0.89
1g (FG = Ph)	2c	2.63	3.40	0.77
$E = -15.58$	2e	3.26 × 10¹	3.19 × 10¹	1.0
	2g	1.93 × 10²	1.72 × 10²	1.1
	2h	2.70 × 10²	3.41 × 10²	0.79
	2i	5.56 × 10²	5.09 × 10²	1.1
	2j	1.37 × 10³	1.04 × 10³	1.3

[a] The second-order rate constants $k_2^{Eq.(1)}$ were calculated by using Equation (1), reported nucleophile-specific parameters N and s_N (from ref. [26]) as well as the electrophilicity parameter E of the *p*QMs **1** (this work). [b] From ref. [32].

we, therefore, set out to characterize the electrophilicity of the δ-FG-*p*QMs **1** by kinetic methods.

Figure 2 exemplifies the general procedure for determining the kinetics of the **1** + **2** reactions. The kinetics of the reactions of *p*QMs **1** with carbanions **2** in DMSO at 20 °C were monitored with stopped-flow and conventional UV-Vis spectroscopy by following the decay of the absorbance of the colored *p*QMs **1**. Initial concentrations of the colorless carbanions **2** were at least 10-fold higher than the initial concentrations of the *p*QMs **1** to fulfill pseudo first-order reaction conditions (Figure 2a). Thus, first-order rate constants k_{obs} (s⁻¹) were determined by least squares fitting of the mono-exponential decay function $A_t = A_0 \exp(-k_{obs}t) + C$ to the time-dependent absorbances A_t during the reaction of **1** with **2** (Figure 2b). The second-order rate constants k_2^{exptl} (M⁻¹ s⁻¹) were then calculated as the slopes of the linear correlations of k_{obs} with the carbanion concentrations, as exemplified in Figure 2c. Table 1 lists the second-order rate constants k_2 of all investigated electrophile-nucleophile combinations (see Supporting Information and ref. [40] for details of the kinetic measurements).

2.3. Correlation Analysis

To determine the Mayr electrophilicity descriptors E of the δ-functionalized *p*QMs **1** we used the second-order rate constants
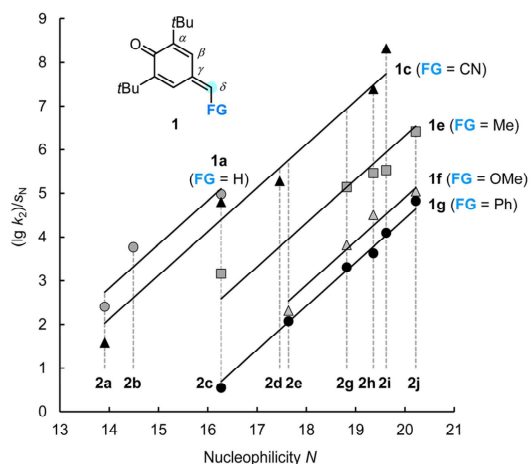
Figure 3. Plot of $(\lg k_2)/s_N$ for the reactions of the *p*QMs **1a**, **1c**, and **1e**−**1g** with the reference nucleophiles **2** against the nucleophilicity parameters N of **2** (DMSO, 20 °C). The slopes of the correlation lines were enforced to unity as required by Equation (1). The correlation for **1d** is shown in Figure S4 (Supporting Information).

k_2^{exptl} (Table 1) and the previously reported nucleophile-specific reactivity parameters (N and s_N) of the reference nucleophiles **2** (see Scheme 1). A least-squares analysis to minimize Δ^2 as defined in Equation (2)[21] by adjusting E as the only variable gave the electrophilicity E for each *p*QM **1**.

$$\Delta^2 = \Sigma\left(\lg k_2^{\text{exptl}} - s_N\left(N+E\right)\right)^2 \qquad (2)$$

The ratios $k_2^{\text{exptl}}/k_2^{\text{Eq.(1)}}$, which are listed in the 5$^{\text{th}}$ column of Table 1, show that using Equation (1) and the reported N and s_N parameters along with the electrophilicities E determined in this work, results in a deviation of $k_2^{\text{Eq.(1)}}$ from k_2^{exptl} lower than a factor of 3.3. For practical applications in organic synthesis (see below), this error margin is of sufficient precision, in particular if one considers that both electrophilicity (E) and nucleophilicity (N) scales currently cover 40 logarithmic orders of magnitude.[26] Usually, an accuracy of 1 kcal mol^{-1} (= 4.18 kJ mol^{-1}) is targeted in high-level quantum-chemical calculations for polar reactions in solution.[41] It is noteworthy, therefore, that the Gibbs energies of activation ($\Delta G^{\ddagger}$) calculated by using the three-parameter Equation (1) agree within ± 2.9 kJ mol^{-1} with the experimentally determined energetic barriers for the electrophile-nucleophile additions in Table 1.

Figure 3 visualizes the results of the kinetic data evaluation by Equation (1) and illustrates that the experimentally determined second-order rate constants ($\lg k_2^{\text{exptl}}$)/s_N correlate linearly with the nucleophilicity parameters N of the C-centered nucleophiles **2**. The slopes of these lines are enforced to unity, as required by Equation (1), and their intercepts with the abscissa [that is, ($\lg k_2^{\text{exptl}}$)/$s_N = 0$] correspond to $E = -N$.

On the basis of the Mayr E parameters, we compared the reactivity of the δ-FG-*p*QMs **1** with those of analogously substituted phenylogous *p*QMs. Figure 4 highlights that the electrophilicity of the simpler δ-FG-*p*QMs **1** is generally 1 to 4 orders of magnitude higher than that of the δ-aryl-substituted *p*QMs.
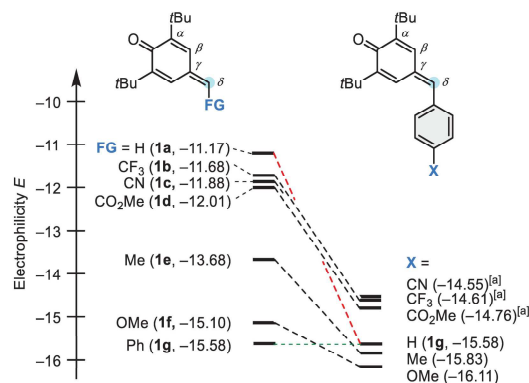

Figure 4. Comparison of the electrophilicities E of δ-FG-*p*QMs **1** with those of phenylogous *p*QMs. [a] The E values for X = CN, CF$_3$, and CO$_2$Me were extrapolated by a Hammett correlation with data from ref. [21].

The electronic substituent effects are obviously much stronger if the functional group is directly bound to the electrophilic center than being attached at a more remote position of the phenyl ring. For methyl- and methoxy-substituted *p*QMs **1e** and **1f**, moderate increases in electrophilic reactivity by two and one orders of magnitude, respectively, are observed. The *p*QMs **1c** and **1d** carrying electron-withdrawing groups, as well as the previously characterized δ-trifluoromethylated **1b**[32] are by roughly three units on the E scale more reactive than analogously aryl-substituted *p*QMs.

Additionally, the position of *p*QM **1a** in Figure 4 is interesting, as it outperformed the δ-methoxy-*p*QM **1f** by four orders of magnitude on the E scale. Moreover, **1a** is an even stronger electrophile than the δ-acceptor-substituted *p*QMs **1b** (FG = CF$_3$), **1c** (FG = CN), and **1d** (FG = CO$_2$Me). The sequence of δ-FG-*p*QMs **1** in Figure 4 clearly demonstrates, therefore, that electronic effects cannot be the only decisive factors that determine the reactivity of these electrophiles. In order to develop a model that reliably predicts the reactivity of δ-FG-*p*QMs **1** further dimensions have to be considered, as will be discussed below in the section on quantum-chemical calculations.

2.4. Scope of *p*QM Reactions with Further Types of Nucleophiles

After quantifying the reactivity of δ-FG-*p*QMs **1** by their Mayr electrophilicities E, these reactivity descriptors can now be used to rationalize reported reactions and to predict new reactions. Figure 5 shows a combination of electrophilicity and nucleophilicity scales, in which nucleophiles and electrophiles located on the same horizontal level ($E + N = 0$) combine with rate constants of $k \approx 1$ M^{-1} s^{-1} at 20 °C, corresponding to half-reaction times of 10 seconds for 0.1 M solutions. The δ-FG-*p*QMs **1** are located in a reactivity range of $-11.1 < E < -15.6$. It can, therefore, be predicted that the δ-FG-*p*QMs **1** form products easily with nucleophiles that exceed a nucleophilicity of $N > 7$ to 10.

It is in accord with these predictions that reactions of *p*QMs **1** with diazomethane ($N/s_N = 10.48/0.78$),[42] sulfonium ylides[43]
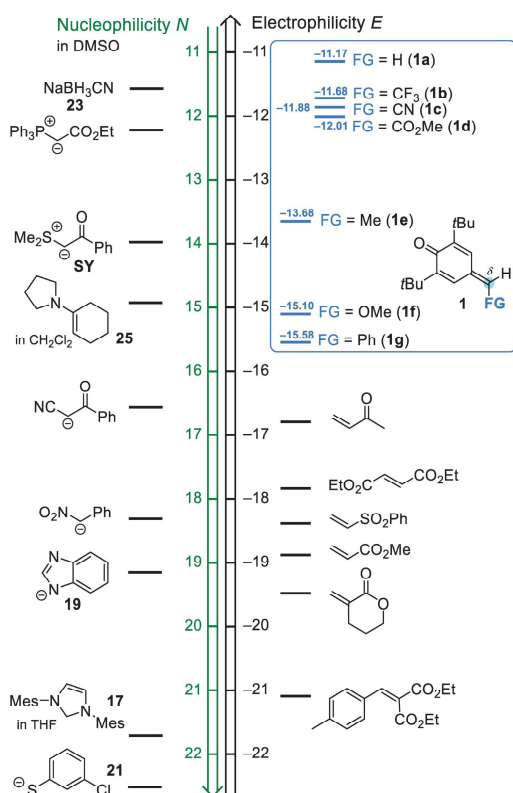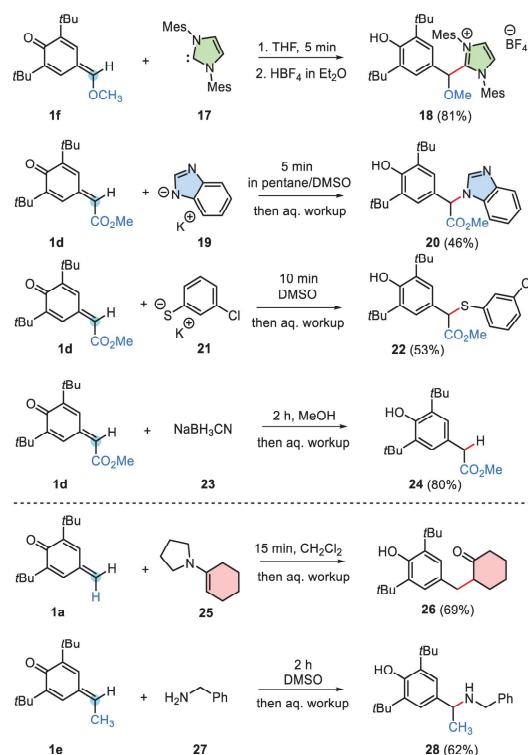
37

Figure 5. The δ-FG-*p*QMs **1** studied in this work and further Michael acceptors are ranked according to their electrophilicity parameters *E* in the right-hand part of the combined reactivity scales for nucleophiles (left-hand side) and electrophiles.[26]

Scheme 5. Extending the scope of reactions between δ-FG-*p*QMs **1** and carbon- or heteroatom-centered nucleophiles.

(for example, **SY** with $N/s_N = 13.95/0.69$), the anion of α-bromo-malonate[44] ($N/s_N = 18.19/0.74$ for α-chloro malonate), deprotonated α-bromo Meldrum's acid[45] ($N/s_N = 13.91/0.86$ for the parent **2a**), phosphorus nucleophiles,[46] such as triphenylphosphine ($N/s_N = 14.33/0.65$ in CH$_2$Cl$_2$) and trimethyl phosphite ($N/s_N = 9.04/0.70$ in MeOH/MeCN), have been reported in the literature.[26]

On a more quantitative basis, the unexpectedly high electrophilicity *E* of **1a** is corroborated by reported first-order rate constants for the hydrolysis[31] and methanolysis[27] of **1a**. Table 2 shows that using the solvent nucleophilicity parameters N_1 (and s_N) for 50/50 (v/v) water/acetonitrile and methanol[47] along with $E(\mathbf{1a}) = -11.17$ from this work in Equation (1) gives calculated rate constants, which agree within one order of magnitude with the experimentally determined first-order rate constants ($k^{\text{exptl}}/k^{\text{Eq.(1)}} = 4.2$ for hydrolysis; $k^{\text{exptl}}/k^{\text{Eq.(1)}} = 0.20$ for methanolysis). In addition, also the reactivity of **1a** toward hydroxide ions,[31,48] that is, a negatively charged O-nucleophile, is excellently reflected by the Mayr reactivity parameters *E*, *N*, and s_N in Equation (1) (entry 3 in Table 2).

To enhance the scope of nucleophilic reaction partners for the δ-FG-*p*QMs **1**, we explored further carbon- or heteroatom-centered nucleophiles of different reactivity in the range from $N = 11$ to $N = 22$ (Scheme 5).

The reactions of *p*QMs **1d** and **1f** with strong nucleophiles such as the N-heterocyclic carbene IMes (**17**, $N/s_N = 21.72/0.45$ in THF),[49] the anion of benzimidazole **19** ($N/s_N = 19.13/0.55$ in DMSO),[50] or the thiophenolate **21** ($N/s_N = 22.50/0.78$ in DMSO)[51] gave rapidly the Michael adducts **18**, **20**, and **22**, respectively. Also, the enamine **25** ($N/s_N = 14.91/0.86$)[26] and the primary amine **27** ($N/s_N = 15.28/0.65$)[26] reacted with *p*QMs **1** within short times to give after aqueous workup the ketone **26** and the secondary amine **28**, respectively. Due to the relatively high reactivity of δ-FG-*p*QMs **1**, which are significantly more reactive than typical Michael acceptors such as methyl vinyl ketone, methyl acrylate, or exo-methylene δ-valerolactone (Figure 5), it was also possible to observe product formations from rather weak nucleophiles, such as the mild hydride donor sodium cyanoborohydride **23** ($N/s_N = 11.52/0.67$).[52] It can therefore be concluded that the characterized electrophilicities *E* of δ-FG-*p*QMs **1** have proven useful to select in an informed way novel nucleophilic reaction partners for the *p*QMs **1**.

2.5. Quantum-Chemical Calculations

We used quantum-chemical calculations to unravel the seemingly unsystematic δ-FG effects on the electrophilicity of *p*QMs

38

Table 2. Comparison of reported and predicted rate constants for reactions of O-nucleophiles with the *p*QM **1a** ($E = -11.17$).

Entry	Nucleophile	k^{exptl} [a]	N (s_N)	$k^{Eq.(1)}$ [b]	$k^{exptl}/k^{Eq.(1)}$
1	50W50AN[c]	1.5×10^{-5} s^{-1} [d]	5.05 (0.89)[e]	3.6×10^{-6} s^{-1}	4.2[f]
2	MeOH	9.4×10^{-5} s^{-1} [g]	7.54 (0.92)[e]	4.6×10^{-4} s^{-1}	0.20[f]
3	HO$^-$ (in 50W50AN[c])	0.18 M^{-1} s^{-1} [d]	10.19 (0.62)[h]	0.25 M^{-1} s^{-1}	0.72[f]

[a] Experimentally determined first order (s^{-1}) or second order rate constants (M^{-1} s^{-1}) at 25 °C.
[b] First-order (s^{-1}) or second-order rate constants (M^{-1} s^{-1}) at 20 °C as predicted by Equation (1) from E, N, and s_N.
[c] 50W50AN = 50/50 (v/v) water/acetonitrile.
[d] At 25 °C, from ref. [31].
[e] Reactivity parameters N_1 and s_N as reported in ref. [47].
[f] We considered the temperature difference, that is, 25 °C in the experiments and 20 °C as standard in Equation (1), to be negligible for this comparison.
[g] At 25 °C, from ref. [27].
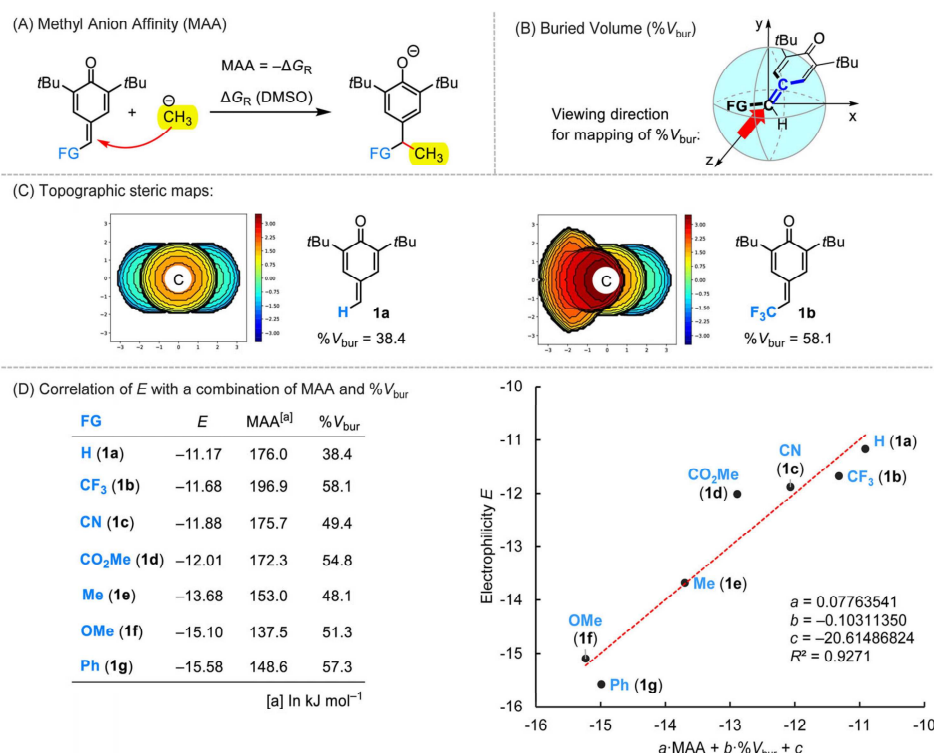[h] Reactivity parameters N and s_N as reported in ref. [48].

Figure 6. a) Definition reaction for the quantum-chemical calculation of MAAs of *p*QMs **1** at the SMD(DMSO)/B3LYP/6–311++G(3df,2pd)//B3LYP/6–31G(d,p) level of theory. b) Definition of the viewing direction for the determination of buried volumes (%V_{bur}). c) Topographic steric maps for **1a** and **1b** indicate the variable steric demand at the electrophilic position in *δ*-FG-*p*QMs **1**. d) The electrophilicity E of **1** correlates with a linear combination of MAA (in kJ mol^{-1}) and %V_{bur}.

1. Previously, the linear correlation of Mayr electrophilicities E with methyl anion affinities (MAAs)[53–55] was shown to enable the prediction of electrophilic reactivities of typical Michael acceptors, including a series of *δ*-aryl-*p*QMs and *ortho*-quinone methides when involving the continuum solvation model (SMD) in the MAA calculations.[56,57] Analogously, we calculated[58,59] the MAAs as the Gibbs reaction energies ΔG_R for the 1,6-Michael addition of a methyl anion to the *δ*-FG-*p*QMs **1a–1g** at the SMD(DMSO)[60]/B3LYP/6–311++G(3df,2pd)//B3LYP/6–31G(d,p) level of theory[61–63] (Figure 6a).

The calculated MAAs (in kJ mol^{-1}) are tabulated in Figure 6d along with the electrophilicity parameters E of the *δ*-FG-*p*QMs **1**. Attempts to establish a linear correlation of Mayr E with the MAAs of the *p*QMs **1** led, however, only to a relationship of inferior quality ($R^2 = 0.7725$).[33] This weak correlation deviates from previous results for a total of 52 Michael acceptors whose electrophilicities E were strongly correlated with MAA ($R^2 = 0.8890$).[57] Already the entries for the *δ*-FG-*p*QMs **1a–1c** indicate that the experimentally determined reactivities (Mayr E), which differ by less than one order of magnitude,

do not follow the trend of the thermodynamic driving force for the carbon–carbon bond formation that is reflected by the quantum-chemically calculated MAAs, which differ by more than 20 kJ mol^{-1} for **1a–1c**.

Obviously, the steric demand of the δ-FG at the *p*QMs **1** significantly affects their reactivity. We, therefore, used the optimized geometries from the quantum-chemical MAA calculations as input data to assess buried volumes (%V_{bur}, Figure 6b,c), from which we expected that they are a useful measure of steric effects at the reaction centers of the δ-FG-*p*QMs **1**.[64–66] Comparison of the %V_{bur} of **1a** with that of **1b** shows that the change from a δ-H- to a δ-(trifluoromethyl)-substituted *p*QM enhances the buried volume from 38% to 58%, which counteracts the Lewis acidity (MAA) that is significantly higher for **1b** than for **1a** (Figure 6d).

Thus, electronic and steric effects as expressed by MAA and %V_{bur} allow the qualitative interpretation of the electrophilic reactivity ordering of δ-FG-*p*QMs **1**. Also, quantitative predictions become possible though we have to admit that the use of only two parameters might be an oversimplification. Yet, experimentally determined electrophilicity parameters *E* for the 2,6-di-*tert*.-butyl-substituted *p*QMs showed an excellent linear relationship ($R^2 = 0.9271$) with a linear combination of MAAs and %V_{bur}. The graph in Figure 6d will, therefore, also be significantly helpful for predicting the reactivity of further δ-FG-*p*QMs, for which kinetic data are currently not available.

3. Conclusion

In summary, we quantified the Mayr electrophilicity parameters *E* of δ-functional group substituted *para*-quinone methides through following the kinetics of their reactions with carbanions as reference nucleophiles in DMSO. Product studies support that simple electrophile-nucleophile reactions gave rise to the photometrically observed decay of the absorbance of the quinone methides. We demonstrate that embedding and locating δ-FG-*p*QMs in Mayr's reactivity scales facilitates the informed selection of novel nucleophilic reaction partners. Thus, the data from this work will make it possible to systematically enhance the synthetic scope of δ-FG-*p*QMs toward currently unseen electrophile-nucleophile combinations.

Variation of FG within the series of δ-FG-*p*QMs gave rise, however, to a relative reactivity ordering that could not be predicted straightforwardly. Counterintuitively, the simple 2,6-di-*tert*.-butyl quinone methide **1a** (FG = H) was found to be a stronger electrophile than structurally analogous quinone methides with electron-withdrawing groups at the electrophilic center (δ-position). Quantum-chemically calculated methyl anion affinities and buried volumes (%V_{bur}) were, therefore, used to rationalize the relative reactivities of the studied δ-FG-*p*QMs. We show that the electrophilicities *E* of δ-FG-*p*QMs correlate linearly with a linear combination of methyl anion affinities and buried volumes (%V_{bur}). Thus, we established a simple relationship that will support the tailored development of additional novel *p*QMs with predictable properties.

4. Experimental Section

Chemicals: Supporting Information contains procedures for the preparation of δ-FG-*p*QMs **1** and the details for the reactions of **1** with anionic and neutral nucleophiles, which led to the isolated products **3–16**, **18**, **20**, **22**, **24**, **26**, and **28**.[34]

Kinetics: The kinetics of the reactions of the δ-FG-*p*QMs **1** with the (reference) nucleophiles **2** in DMSO at 20 °C were followed by using conventional photometric or UV-Vis stopped-flow techniques. Details of the kinetic experiments are given in the Supporting Information and in ref. [40].

Quantum-Chemical Calculations: Details are reported in the Supporting Information.

Supporting Information

The authors have cited additional references within the Supporting Information.[67–80]

Conflict of Interest

The authors declare no conflict of interest.

Data Availability Statement

The raw data of kinetic measurements that support the findings of this study are openly available in Open Data LMU at DOI: 10.5282/ubm/data.582, ref. [40]. Further data available in article supplementary information.

Keywords: buried volumes · electrophilicity · kinetics · linear free energy relationships · quinone methides

[1] S. E. Rokita, Ed., *Quinone Methides*, Wiley, Hoboken (NJ), **2009**.
[2] M. Freccero, *Mini-Rev. Org. Chem.* **2004**, *1*, 403.
[3] J. Ralph, P. F. Schatz, F. Lu, H. Kim, T. Akiyama, S. F. Nelsen, in *Quinone Methides* (Ed.: S. E. Rokita), Wiley **2009**, Hoboken (NJ), Chap. 12, p. 385.

[4] J. Liu, R. Cheng, N. Van Eps, N. Wang, T. Morizumi, W.-L. Ou, P. C. Klauser, S. Rozovsky, O. P. Ernst, L. Wang, *J. Am. Chem. Soc.* **2020**, *142*, 17057.

[5] K. Ali, P. Mishra, A. Kumar, D. N. Reddy, S. Chowdhury, G. Panda, *Chem. Commun.* **2022**, *58*, 6160.

[6] A. Parra, M. Tortosa, *ChemCatChem* **2015**, *7*, 1524.

[7] L. Caruana, M. Fochi, L. Bernardi, *Molecules* **2015**, *20*, 11733.

[8] J.-Y. Wang, W.-J. Hao, S.-J. Tu, B. Jiang, *Chem. Front.* **2020**, *7*, 1743.

[9] C. G. S. Lima, F. P. Pauli, D. C. S. Costa, A. S. de Souza, L. S. M. Forezi, V. F. Ferreira, F. de Carvalho da Silva, *Eur. J. Org. Chem.* **2020**, *2020*, 2650.

[10] A. D. Woolhouse, *Aust. J. Chem.* **1977**, *30*, 1145.

[11] G. Singh, R. Pandey, Y. A. Pankhade, S. Fatma, R. V. Anand, *Chem. Rec.* **2021**, *21*, 4150.

[12] X. Liu, Y. Ren, L. Zhu, T. Li, W. Xu, Y. Liu, K.-W. Tang, B. Xiong, *Tetrahedron* **2023**, *148*, 133655.

[13] J. Jose, A. Yadav, C. B. Tripathi, *Chem. Commun.* **2024**, *60*, 11315.

[14] L. Diao, C. Yang, P. Wan, *J. Am. Chem. Soc.* **1995**, *117*, 5369.

[15] L. Diao, P. Wan, *Can. J. Chem.* **2008**, *86*, 105.

[16] Y. Chiang, A. J. Kresge, Y. Zhu, *J. Am. Chem. Soc.* **2002**, *124*, 6349.

[17] M. M. Toteva, M. Moran, T. L. Amyes, J. P. Richard, *J. Am. Chem. Soc.* **2003**, *125*, 8814.

[18] M. M. Toteva, J. P. Richard, *Adv. Phys. Org. Chem.* **2011**, *45*, 39.

[19] R. Lucius, H. Mayr, *Angew. Chem. Int. Ed.* **2000**, *39*, 1995.

[20] R. Lucius, R. Loos, H. Mayr, *Angew. Chem. Int. Ed.* **2002**, *41*, 91.

[21] D. Richter, N. Hampel, T. Singer, A. R. Ofial, H. Mayr, *Eur. J. Org. Chem.* **2009**, *2009*, 3203.

[22] H. Mayr, M. Patz, *Angew. Chem. Int. Ed. Engl.* **1994**, *33*, 938.

[23] H. Mayr, T. Bug, M. F. Gotta, N. Hering, B. Irrgang, B. Janker, B. Kempf, R. Loos, A. R. Ofial, G. Remennikov, H. Schimmel, *J. Am. Chem. Soc.* **2001**, *123*, 9500.

[24] H. Mayr, A. R. Ofial, *Pure Appl. Chem.* **2005**, *77*, 1807.

[25] H. Mayr, *Tetrahedron* **2015**, *71*, 5095.

[26] Reactivity parameters *E*, *N*, and *s*$_N$ can be retrieved at, https://www.cup.lmu.de/oc/mayr/reaktionsdatenbank2/, which is a freely accessible website (accessed: Mar 2025).

[27] L. J. Filar, S. Winstein, *Tetrahedron Lett.* **1960**, *1*, 9.

[28] V. V. Ershov, A. A. Volod'kin, G. D. Ostapets-Sveshnikova, *Russ. Chem. Bull.* **1966**, *15*, 888.

[29] A. A. Volod'kin, V. V. Ershov, G. D. Ostapets-Sveshnikova, *Russ. Chem. Bull.* **1969**, *18*, 580.

[30] L. K. Dyall, S. Winstein, *J. Am. Chem. Soc.* **1972**, *94*, 2196.

[31] M. Gulsrud Willcockson, M. M. Toteva, V. J. Stella, *J. Pharm. Sci.* **2013**, *102*, 3579.

[32] M. Winter, R. Schütz, A. Eitzinger, A. R. Ofial, M. Waser, *Eur. J. Org. Chem.* **2020**, *2020*, 3812.

[33] See Supporting Information for details.

[34] Deposition Numbers CCDC 2431023 (for **3**), CCDC 2431024 (for **4**), CCDC 2431025 (for **6**), CCDC 2431026 (for **9**), CCDC 2432306 (for **12**), CCDC 2431027 (for **13**), and CCDC 2431028 (for **14**) contain the supplementary crystallographic data for this paper. These data are provided free of charge by the joint Cambridge Crystallographic Data Centre and Fachinformationszentrum Karlsruhe Access Structures service.

[35] K. Nakatuji, M. Oda, M. Kozaki, Y. Morimoto, K. Okada, *Chem. Lett.* **1998**, *27*, 845.

[36] The 2:1 Michael adduct **6** underwent quantitative cyclization to give **4** (yield: 94%) when treated with silver(I) oxide in a CCl₄/DMSO mixture.[33]

[37] L. I. Kudinova, A. A. Volod'kin, V. V. Ershov, T. I. Prokof'eva, *Russ. Chem. Bull.* **1978**, *27*, 1313.

[38] Brønsted acidities are from: https://organicchemistrydata.org/hansreich/resources/pka/ (accessed: Mar 2025).

[39] M. Inagaki, N. Haga, M. Kobayashi, N. Ohta, S. Kamata, T. Tsuri, *J. Org. Chem.* **2002**, *67*, 125.

[40] The raw data of kinetic measurements that support the findings of this study are openly available in Open Data LMU at https://doi.org/10.5282/ubm/data.582.

[41] M. Vahl, J. Proppe, *Phys. Chem. Chem. Phys.* **2023**, *25*, 2717.

[42] G. A. Nikiforov, B. D. Sviridov, A. A. Volod'kin, V. V. Ershov, *Russ. Chem. Bull.* **1971**, *20*, 778.

[43] Z. Yuan, X. Fang, X. Li, J. Wu, H. Yao, A. Lin, *J. Org. Chem.* **2015**, *80*, 11123.

[44] K. Gai, X. Fang, X. Li, J. Xu, X. Wu, A. Lin, H. Yao, *Chem. Commun.* **2015**, *51*, 15831.

[45] T. Li, D. Yan, C. Cui, X. Song, J. Chang, *Org. Chem. Front.* **2020**, *7*, 2682.

[46] V. T. Kolesnikov, Yu. A. Kopel'tsiv, A. A. Kudryavtsev, Yu. G. Shermolovich, *Zh. Obshch. Khim.* **1983**, *53*, 1265.

[47] S. Minegishi, S. Kobayashi, H. Mayr, *J. Am. Chem. Soc.* **2004**, *126*, 5174.

[48] S. Minegishi, H. Mayr, *J. Am. Chem. Soc.* **2003**, *125*, 286.

[49] B. Maji, M. Breugst, H. Mayr, *Angew. Chem. Int. Ed.* **2011**, *50*, 6915.

[50] M. Breugst, F. Corral Bautista, H. Mayr, *Chem. Eur. J.* **2012**, *18*, 127.

[51] P. M. Jüstel, C. D. Pignot, A. R. Ofial, *J. Org. Chem.* **2021**, *86*, 5965.

[52] D. Richter, H. Mayr, *Angew. Chem. Int. Ed.* **2009**, *48*, 1958.

[53] H. Mayr, M. Patz, M. F. Gotta, A. R. Ofial, *Pure Appl. Chem.* **1998**, *70*, 1993.

[54] G. M. Böttger, R. Fröhlich, E.-U. Würthwein, *Eur. J. Org. Chem.* **2000**, *2000*, 1589.

[55] A. Mood, M. Tavakoli, E. Gutman, D. Kadish, P. Baldi, D. L. Van Vranken, *J. Org. Chem.* **2020**, *85*, 4096.

[56] D. S. Allgäuer, H. Jangra, H. Asahara, Z. Li, Q. Chen, H. Zipse, A. R. Ofial, H. Mayr, *J. Am. Chem. Soc.* **2017**, *139*, 13318.

[57] C. Gross, A. Eitzinger, N. Hampel, P. Mayer, A. R. Ofial, *Chem. Eur. J.* **2025**, *31*, e202403785.

[58] *Schrödinger Release 2021–4: MacroModel*, Schrödinger, LLC, New York, NY, **2021**.

[59] Gaussian 16, Revision B.01, M. J. Frisch, G. W. Trucks, H. B. Schlegel, G. E. Scuseria, M. A. Robb, J. R. Cheeseman, G. Scalmani, V. Barone, G. A. Petersson, H. Nakatsuji, X. Li, M. Caricato, A. V. Marenich, J. Bloino, B. G. Janesko, R. Gomperts, B. Mennucci, H. P. Hratchian, J. V. Ortiz, A. F. Izmaylov, J. L. Sonnenberg, D. Williams-Young, F. Ding, F. Lipparini, F. Egidi, J. Goings, B. Peng, A. Petrone, T. Henderson, D. Ranasinghe, et al. Gaussian, Inc., Wallingford CT, **2016**.

[60] A. V. Marenich, C. J. Cramer, D. G. Truhlar, *J. Phys. Chem. B* **2009**, *113*, 6378.

[61] A. D. Becke, *J. Chem. Phys.* **1993**, *98*, 5648.

[62] R. Ditchfield, W. Hehre, J. A. Pople, *J. Chem. Phys.* **1971**, *54*, 724.

[63] R. Krishnan, J. S. Binkley, R. Seeger, J. A. Pople, *J. Chem. Phys.* **1980**, *72*, 650.

[64] L. Falivene, R. Credendino, A. Poater, A. Petta, L. Serra, R. Oliva, V. Scarano, L. Cavallo, *Organometallics* **2016**, *35*, 2286.

[65] L. Falivene, Z. Cao, A. Petta, L. Serra, A. Poater, R. Oliva, V. Scarano, L. Cavallo, *Nat. Chem.* **2019**, *11*, 872.

[66] Buried volumes (%*V*$_{bur}$) in this work were determined by using the *SambVca 2.1* web application: https://www.aocdweb.com/OMtools/sambvca2.1/ (accessed: Mar 2025).

[67] P. Nesvadba, *Synth. Commun.* **2000**, *30*, 2825.

[68] A. Ali, R. Jajoria, H. K. Harit, R. P. Singh, *J. Org. Chem.* **2022**, *87*, 5213.

[69] S. Evans, P. Nesvabda, S. Allenbach, (Ciba-Geigy AG), "A new one-pot process for the preparation of 7-aryl-2,6-disubstituted quinone methides" EP0744392, **1996**.

[70] V. Reddy, R. V. Anand, *Org. Lett.* **2015**, *17*, 3390.

[71] J. Ruiz Aranzaes, M.-C. Daniel, D. Astruc, *Can. J. Chem.* **2006**, *84*, 288.

[72] CrysAlis^{Pro}, Rigaku Oxford Diffraction, Tokyo, Japan, **2023**.

[73] O. V. Dolomanov, L. J. Bourhis, R. J. Gildea, J. A. K. Howard, H. Puschmann, *J. Appl. Cryst.* **2009**, *42*, 339.

[74] C. B. Huebschle, G. M. Sheldrick, B. Dittrich, *J. Appl. Cryst.* **2011**, *44*, 1281.

[75] L. J. Farrugia, *J. Appl. Cryst.* **2012**, *45*, 849.

[76] SAINT, Bruker AXS Inc., Madison, Wisconsin, USA, **2012**.

[77] SADABS, G. M. Sheldrick, University of Göttingen, Germany, **1996**.

[78] G. M. Sheldrick, *Acta Crystallogr.* **2015**, *A71*, 3.

[79] G. Knizia, *J. Chem. Theory Comput.* **2013**, *9*, 4834.

[80] F. Weigend, R. Ahlrichs, *Phys. Chem. Chem. Phys.* **2005**, *7*, 3297.

3.2. Supporting Information

3.2.1. Synthesis of *para*-Quinone Methides (*p*QMs)

2,6-Di-*tert*-butyl-4-methylenecyclohexa-2,5-dien-1-one (1a) was synthesized by oxidation of 3,5-di*tert*-butyl-4-hydroxytoluene (BHT) as described in ref. [1] but with slight modifications. For NMR analysis the oxidation was performed in two ways:

(a)   In a dry N_2-atmosphere, BHT (20.4 mg, 0.093mmol) was stirred with Ag_2O (300 mg, 1.30 mmol) in $CDCl_3$ (2 mL) or CCl_4 (2 mL) under the exclusion of light for 20 min. Then solids were filtered off (0.2 μm PTFE filter) before NMR spectroscopic analysis of the filtrate.

(b)   BHT (21.6 mg, 0.098 mmol) was stirred with Ag_2O (300 mg, 1.30 mmol) in *n*-pentane (2 mL) under the exclusion of light for 20 min under N_2-atmosphere. Then solids were filtered off (0.2 μm PTFE filter). The thus generated pentane solution of *p*QM **1a** (1 mL) was mixed with DMSO-$d6$ (1 mL). The *n*-pentane was evaporated under vacuum. The *p*QM **1a** remained dissolved in DMSO-d_6 and was used without further purification for NMR spectroscopic analysis.

1a (CG446_CDCl3)
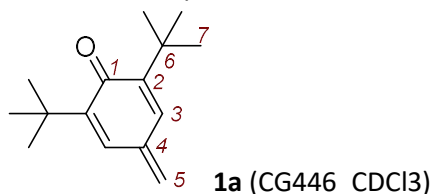
¹H NMR (400 MHz, $CDCl_3$): δ 6.94 (s, 2 H, 3-H), 5.77 (s, 2 H, 5-H), 1.28 ppm (s, 18 H, 7-H).

¹³C{¹H} NMR (101 MHz, $CDCl_3$): δ 186.5, 148.7, 139.0, 132.8, 128.3, 35.1, 29.6 ppm.

¹H NMR (400 MHz, DMSO-d_6): δ 7.12 (s, 2 H, 3-H), 6.09 (s, 2 H, 5-H), 1.23 ppm (s, 18 H, 7-H).

¹³C{¹H} NMR (101 MHz, DMSO-d_6): δ 185.8 (C_q, C=O), 147.3, 137.9, 133.2, 131.8, 34.7, 29.2 ppm.

¹H NMR (400 MHz, CCl_4):[1] δ 6.76 (s, 2 H), 5.58 (s, 2 H), 1.19 ppm (s, 18 H).

¹³C{¹H} NMR (101 MHz, CCl_4):[1] δ 185.4, 149.0, 139.4, 132.2, 126.8, 35.4, 29.9 ppm.

HRMS (EI): *m/z* calcd for $C_{15}H_{22}O^{•+}$ [M$^{•+}$]: 218.1665; found: 218.1663.

For photometric experiments, *p*QM **1a** was generated under the exclusion of light by stirring BHT (18.6 mg, 0.084 mmol) with Ag_2O (100 mg, 0.432 mmol) in *n*-pentane (3 mL) for 20 minutes. Then, solids were removed by filtration (0.2 μm PTFE filter) and an aliquot of the solution (0.5 mL) was mixed with DMSO (1.0 mL). The *n*-pentane was evaporated under vacuum. The *p*QM **1a** remained dissolved in DMSO. The thus prepared stock solution of **1a** in DMSO was used for kinetic experiments and for determining the extinction coefficient of **1a**. According to the NMR analysis in (b), *p*QM **1a** formed quantitatively from the BHT. Consequently, the molar amount of **1a** used in photometric experiments was calculated assuming a complete conversion of BHT to *p*QM **1a**.

(1) For NMR spectroscopic analysis in CCl_4, a capillary tube filled with $CDCl_3$ was added into the NMR tube to ensure proper shimming. Chemical shifts of NMR resonances were calibrated according to the residual solvent signal of $CDCl_3$.

2-(3,5-Di-*tert*-butyl-4-oxocyclohexa-2,5-dien-1-ylidene)acetonitrile (1c) was synthesized according to ref. [2]. NMR spectroscopic data in CDCl$_3$ agree with those described in ref. [2].


1c (CG067)
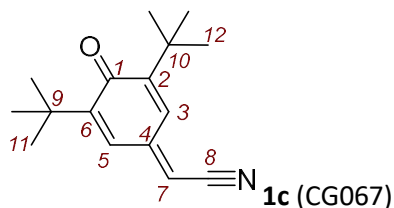
^{1}H NMR (400 MHz, CDCl$_3$): *δ* 7.32 (d, *J* = 2.5 Hz, 1 H, 5-H), 6.85 (d, *J* = 2.5 Hz, 1 H, 3-H), 5.66 (s, 1 H, 7-H), 1.31 (s, 9 H, 11-H), 1.28 ppm (s, 9 H, 12-H).

^{13}C{^{1}H} NMR (101 MHz, CDCl$_3$): *δ* 186.1 (C$_q$, C-1), 152.8 (C$_q$, C-6), 152.1 (C$_q$, C-2), 147.5 (C$_q$, C-4), 130.6 (CH, C-3), 127.3 (CH, C-5), 116.4 (C-8), 103.6 (CH, C-7), 35.9 (C$_q$, C-9), 35.7 (C$_q$, C-10), 29.6 (CH$_3$, C-11), 29.5 ppm (CH$_3$, C-12).

HRMS (EI): *m/z* calcd for C$_{16}$H$_{21}$NO$^{•+}$ [M$^{•+}$]: 243.1618; found: 243.1618.

IR (neat, ATR): $\tilde{v}$ 2959, 2207, 1630, 1617, 1582, 1363, 1253, 1084, 914, 879, 817, 743 cm^{-1}.

Methyl 2-(3,5-di-*tert*-butyl-4-oxocyclohexa-2,5-dien-1-ylidene)acetate (1d) was synthesized according to ref. [2]. NMR spectroscopic data in CDCl$_3$ agree with those described in ref. [2].

1d (CG475)
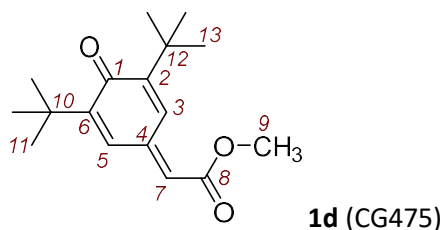
^{1}H NMR (400 MHz, CDCl$_3$): *δ* 8.30 (d, *J* = 3.1 Hz, 1 H), 6.78 (d, *J* = 2.4 Hz, 1 H), 6.14 (s, 1 H, 7-H), 3.81 (s, 3 H, 9-H), 1.30 (s, 9 H), 1.28 ppm (s, 9 H).

^{13}C{^{1}H} NMR (101 MHz, CDCl$_3$): *δ* 186.8 (C$_q$, C-1), 166.4, 151.6, 151.4, 142.8, 133.6, 127.2, 125.1, 52.0, 35.8, 35.4, 29.7, 29.6 ppm.

HRMS (EI): *m/z* calcd for C$_{17}$H$_{24}$O$_3^{•+}$ [M$^{•+}$]: 276.1720; found: 276.1718.

IR (neat, ATR): $\tilde{v}$ 2953, 1706, 1627, 1431, 1278, 1240, 1171, 1013, 932, 921, 860, 821 cm^{-1}.

2,6-Di-tert-butyl-4-ethylidenecyclohexa-2,5-dien-1-one (1e) was synthesized according to ref. [3]. NMR spectroscopic data in CDCl$_3$ agree with those described in ref. [3].
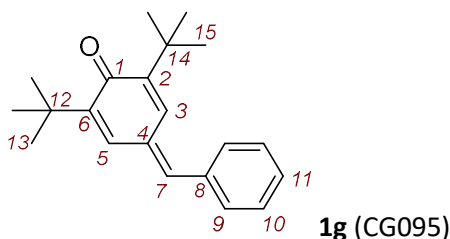

1e (TR01)
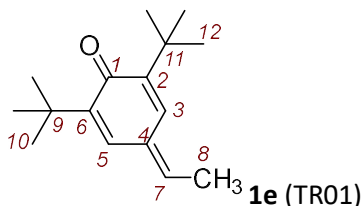
^{1}H NMR (600 MHz, CDCl$_3$): *δ* 7.30 (d, *J* = 2.5 Hz, 1 H), 6.84 (d, *J* = 2.6 Hz, 1 H), 6.41 (q, *J* = 7.7 Hz, 1 H, 7-H), 2.12 (d, *J* = 7.6 Hz, 3 H, 8-H), 1.31 (s, 9 H), 1.28 ppm (s, 9 H).

^{13}C{^{1}H} NMR (151 MHz, CDCl$_3$): *δ* 186.9 (C$_q$, C-1), 148.2 (C$_q$), 146.4 (C$_q$), 142.8 (CH, C-7), 135.1 (CH), 132.8 (C$_q$, C-4), 125.9 (CH), 35.5 (C$_q$), 34.9 (C$_q$), 29.60 (CH$_3$), 29.56 (CH$_3$), 15.2 ppm (CH$_3$, C-8).

HRMS (EI): *m/z* calcd for C$_{16}$H$_{24}$O$^{•+}$ [M$^{•+}$]: 232.1822; found: 232.1823.

IR (neat, ATR): $\tilde{v}$ 2950, 1613, 1586, 1572, 1452, 1434, 1358, 1250, 902, 883, 815, 746 cm^{-1}.

2,6-Di-*tert*-butyl-4-(methoxymethylene)cyclohexa-2,5-dien-1-one (1f) was synthesized according to ref. [4]. NMR spectroscopic data in CDCl$_3$ agree with those described in ref. [4].

1f (CG476_CDCl3)
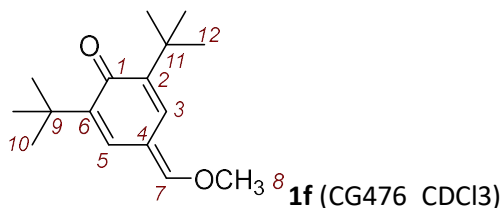
^{1}H NMR (600 MHz, CDCl$_3$): *δ* 7.39 (d, *J* = 3.2 Hz, 1 H), 6.88 (s, 1 H, 7-H), 6.82 (d, *J* = 2.4 Hz, 1 H), 3.98 (s, 3 H, 7-OCH$_3$), 1.30 (s, 9 H), 1.28 ppm (s, 9 H).

^{13}C{^{1}H} NMR (151 MHz, CDCl$_3$): *δ* 186.2 (C$_q$, C-1), 159.4 (CH, C-7), 147.3 (C$_q$), 145.6 (C$_q$), 131.1 (CH), 124.0 (CH), 114.6 (C$_q$, C-4), 62.4 (CH$_3$, 7-OCH$_3$), 35.4 (C$_q$), 35.0 (C$_q$), 29.6 (CH$_3$), 29.5 ppm (CH$_3$).

HRMS (EI): *m/z* calcd for C$_{16}$H$_{24}$O$_2$$^{•+}$ [M$^{•+}$]: 248.1771; found: 248.1772.

IR (neat, ATR): $\tilde{v}$ 2951, 1635, 1552, 1357, 1254, 1151, 1018, 987, 948, 915, 883, 818 cm^{-1}.

4-Benzylidene-2,6-di-*tert*-butylcyclohexa-2,5-dien-1-one (1g) was synthesized analogously to a reported procedure for aryl substituted *p*QMs.[5] NMR spectroscopic data in CDCl$_3$ agree with those described in ref. [6].

1g (CG095)

^{1}H NMR (400 MHz, CDCl$_3$): *δ* 7.53 (d, *J* = 3.3 Hz, 1 H), 7.49–7.35 (m, 5 H, 9-H, 10-H, and 11-H), 7.20 (s, 1 H, 7-H), 7.02 (d, *J* = 2.6 Hz, 1 H), 1.34 (s, 9 H), 1.31 ppm (s, 9 H).

^{13}C{^{1}H} NMR (101 MHz, CDCl$_3$): *δ* 186.7, 149.5, 147.9, 142.7, 136.1, 135.3, 132.1, 130.5, 129.2, 128.9, 127.9, 35.6, 35.2, 29.68, 29.65 ppm.

HRMS (EI): *m/z* calcd for C$_{21}$H$_{26}$O$^{•+}$ [M$^{•+}$]: 294.1979; found: 294.1976.

3.2.2. Products of Reactions of *p*QMs with C-Nucleophiles

General Procedure 1 (GP1) for Reactions of *p*QMs **1** with C-Nucleophiles **2**

A solution of nucleophile **2** (1.0 to 1.3 equiv.) in DMSO-*d*$_6$ (1.0 mmol) was transferred to the quinone methide **1** in a standard GC vial. The reaction solution was mixed using a sonicator. Then the reaction mixture was left for up to 4 h, depending on the nucleophile used. The mixture was quenched with saturated ammonium chloride solution (1 mL), diluted with water (5 mL) and extracted with diethyl ether (4 × 10 mL). The combined organic phases were washed with water (4 × 10 mL) and dried over MgSO$_4$. The solvent was removed under reduced pressure and the crude residue was either purified by silica gel chromatography or recrystallized to afford the reaction product.

Reactions of *p*QM 1a and Carbanion 2j

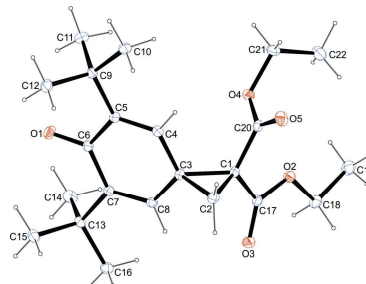**(A) Isolation of cyclized products 3 and 4 from the reaction in CCl$_4$/DMSO solution** (CG536)

2,6-Di-*tert*-butyl-4-methylphenol (BHT) (60.0 mg, 0.272 mmol) was dissolved in CCl$_4$ (2 mL) and Ag$_2$O (315 mg, 1.36 mmol) was added. The mixture was stirred for 20 min at room temperature under the exclusion of light. Solids were removed by filtration (0.2 μm PTFE filter) and a DMSO solution of **2j** (59.4 mg, 0.300 mmol in 10 mL) was added. The mixture was stirred for 1 h at room temperature under nitrogen atmosphere. The reaction was quenched with sat. NH$_4$Cl solution (5 mL), diluted with water (5 mL), and extracted with diethyl ether (4 × 10 mL). The combined organic phases were washed with water (4 × 10 mL) and dried over MgSO$_4$. After filtration, the solvent was removed under reduced pressure yielding a residue that was purified by preparative TLC (silica gel, eluent: *n*-pentane:EtOAc 97:3) to isolate **3** (31.5 mg, 31%) as a colorless solid (m.p. 95 °C) and **4** (41.0 mg, 51%) as a colorless solid (m.p. 187 °C).

(B) Isolation of Michael adducts 5 and 6 from the reaction in *n*-pentane/DMSO solution (CG536_4)

2,6-Di-*tert*-butyl-4-methylphenol (BHT) (65.0 mg, 0.295 mmol) was dissolved in *n*-pentane (2 mL) and Ag$_2$O (335 mg, 1.45 mmol) was added. The mixture was stirred for 20 min at room temperature under the exclusion of light. Solids were removed by filtration (0.2 μm PTFE filter) and a DMSO solution of **2j** (66.0 mg, 0.333 mmol in 10 mL) was added. The mixture was stirred for 1 h at room temperature under nitrogen atmosphere. The reaction was quenched with sat. NH$_4$Cl solution (5 mL), diluted with water (5 mL) and extracted with diethyl ether (4 × 10 mL). The combined organic phases were washed with water (4 × 10 mL) and dried over MgSO$_4$. After filtration, the solvent was removed under reduced pressure yielding a residue that was purified by preparative TLC (silica gel, *n*-pentane:EtOAc 95:5) to give **5** (48.0 mg, 43%) as a white solid (m.p. 156°C) and **6** (10.4 mg, 12%) as a white solid (m.p. 162°C).

(C) Conversion of 6 to 4 under the conditions of reaction (A) (CG646)

The 2,2-alkylated diethyl malonate **6** (20.0 mg, 0.034 mmol) was dissolved in CCl$_4$ (2 mL) and silver(I) oxide (78 mg, 0.34 mmol) was added. The mixture was stirred for 20 min at room temperature under the exclusion of light. Solids were removed by filtration (0.2 μm PTFE filter) and DMSO (5 mL) was added. The mixture was stirred for 2 h at room temperature under nitrogen atmosphere. The reaction was quenched with sat. NH$_4$Cl solution (5 mL), diluted with water (5 mL), and extracted with diethyl ether (4 × 10 mL). The combined organic phases were washed with water (4 × 10 mL) and dried over MgSO$_4$. After filtration, the solvent was removed under reduced pressure to give the cyclic **4** (19.0 mg, 94%) as a colorless solid, which was analyzed by ^{1}H NMR spectroscopy (Figure S1).

Figure S1: ^{1}H NMR spectrum of **4** in CDCl$_3$ (400 MHz) CG646

Diethyl 5,7-di-*tert*-butyl-6-oxospiro[2.5]octa-4,7-diene-1,1-dicarboxylate (3)

3 (CG536_1F20-29)   br006
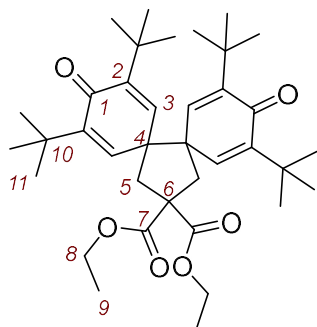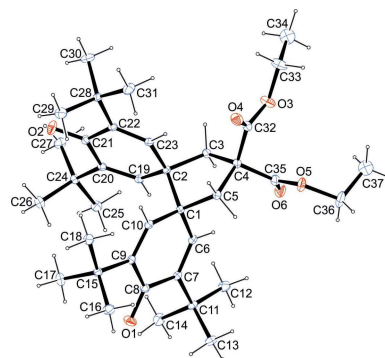
R_f (*n*-pentane/EtOAc 97:3, silica, UV) = 0.40.

^{1}H NMR (400 MHz, CDCl$_3$): *δ* 6.37 (s, 2 H, 3-H), 4.31–4.19 (m, 4 H, 8-H), 2.29 (s, 2 H, 5-H), 1.30 (t, *J* = 7.1 Hz, 6 H, 9-H), 1.22 ppm (s, 18 H, 11-H).

^{13}C{^{1}H} NMR (101 MHz, CDCl$_3$): *δ* 185.7 (C$_q$, C-1), 167.1 (C$_q$, C-7), 150.3 (C$_q$, C-2), 137.0 (CH, C-3), 62.5 (CH$_2$, C-8), 45.0 (C$_q$, C-6), 36.2 (C$_q$, C-4), 35.4 (C$_q$, C-10), 29.4 (CH$_3$, C-11), 27.7 (CH$_2$, C-5), 14.3 ppm (CH$_3$, C-9).

HRMS (pos. ESI): *m/z* calcd for C$_{22}$H$_{32}$NaO$_5{}^+$ [M + Na$^+$]: 399.2142; found: 399.2161.

IR (neat, ATR): $\tilde{v}$ 2958, 1729, 1652, 1632, 1459, 1371, 1310, 1265, 1210, 1107, 1022, 1002 cm^{-1}.

Diethyl 2,4,9,11-tetra-*tert*-butyl-3,10-dioxodispiro[5.0.5^7.3^6]pentadeca-1,4,8,11-tetraene-14,14-dicarboxylate (4)

46

4 (CG536_1F10-16)   br007

R_f (*n*-pentane/EtOAc 97:3, silica, UV) = 0.45.

^{1}H NMR (400 MHz, CDCl$_3$): *δ* 6.46 (s, 4 H, 3-H), 4.28 (q, *J* = 7.1 Hz, 4 H, 8-H), 2.79 (s, 4 H, 5-H), 1.29 (t, *J* = 7.1 Hz, 6 H, 9-H), 1.15 ppm (s, 36 H, 11-H).

^{13}C{^{1}H} NMR (101 MHz, CDCl$_3$): *δ* 185.9 (C$_q$, C-1), 172.2 (C$_q$, C-7), 148.8 (C$_q$, C-2), 139.9 (CH, C-3), 62.5 (CH$_2$, C-8), 59.7 (C$_q$, C-6), 56.6 (C$_q$, C-4), 43.8 (CH$_2$, C-5), 35.1 (C$_q$, C-10), 29.6 (CH$_3$, C-11), 14.2 ppm (CH$_3$, C-9).

HRMS (EI): *m/z* calcd for C$_{37}$H$_{54}$O$_6$$^{•+}$ [M$^{•+}$]: 594.3915; found: 594.3911.
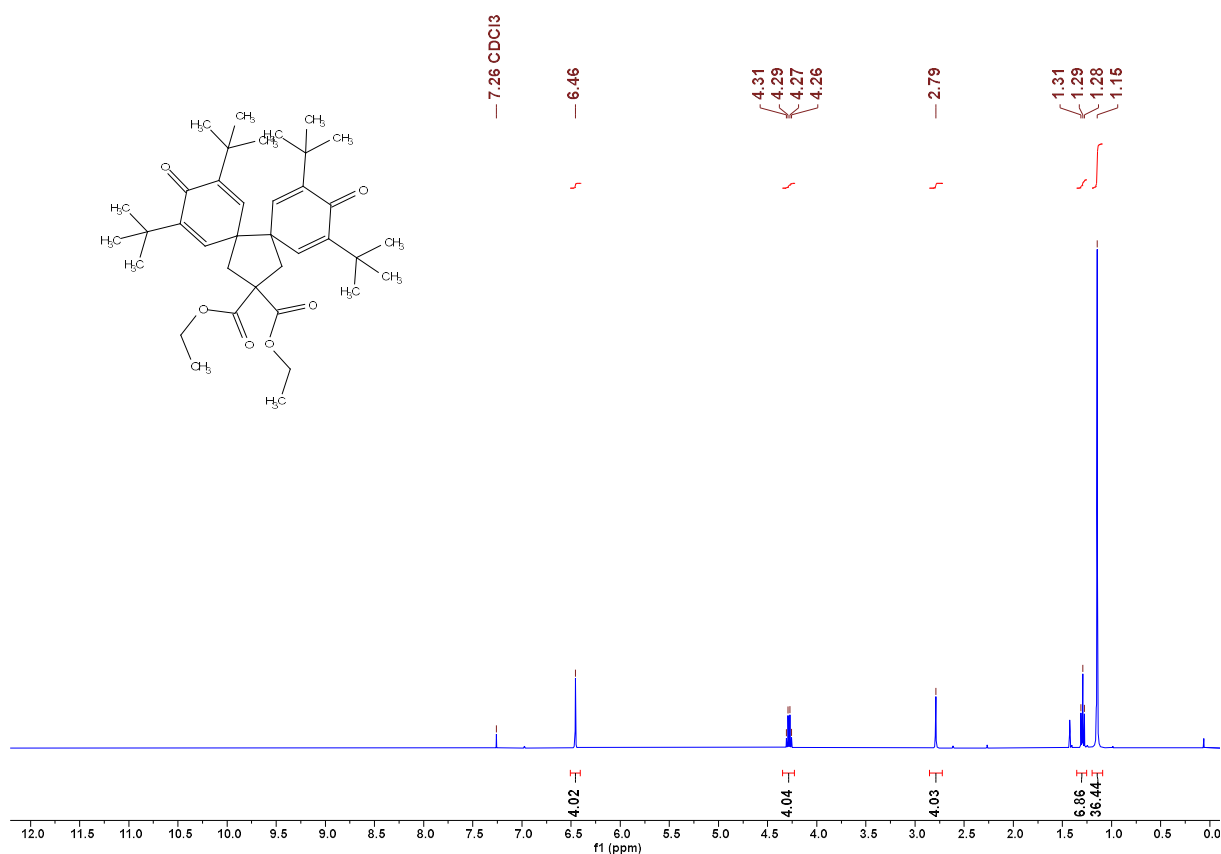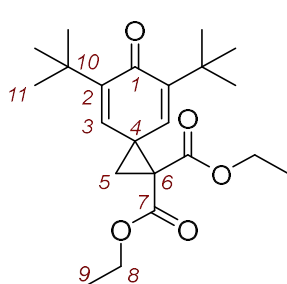
IR (neat, ATR): $\tilde{v}$ 2956, 1728, 1660, 1641, 1459, 1368, 1255, 1181, 1161, 1097, 1075, 881 cm^{-1}.

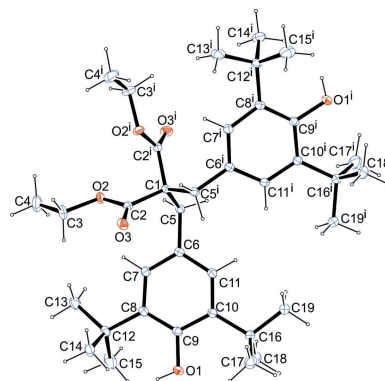**Diethyl 2-(3,5-di-*tert*-butyl-4-hydroxybenzyl)malonate (5)**
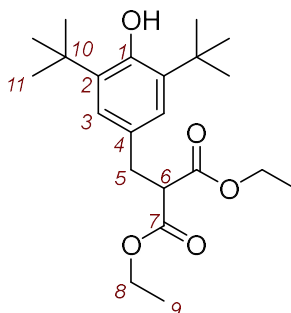
5 (CG536_4_2)

^{1}H NMR (600 MHz, CDCl$_3$): *δ* 6.98 (s, 2 H, 3-H), 5.09 (s, 1 H, 1-OH), 4.16 (q, *J* = 7.1 Hz, 4 H, 8-H), 3.61 (t, *J* = 7.8 Hz, 1 H, 6-H), 3.14 (d, *J* = 7.9 Hz, 2 H, 5-H), 1.42 (s, 18 H, 11-H), 1.21 ppm (t, *J* = 7.1 Hz, 6 H, 9-H).

^{13}C{^{1}H} NMR (151 MHz, CDCl$_3$): *δ* 169.1 (C$_q$, C-7), 152.5 (C$_q$, C-1), 135.8 (C$_q$, C-2), 128.4 (C$_q$, C-4), 125.3 (CH, C-3), 61.3 (CH$_2$, C-8), 54.2 (CH, C-6), 34.7 (CH$_2$, C-5), 34.3 (C$_q$, C-10), 30.3 (CH$_3$, C-11), 14.0 ppm (CH$_3$, C-9).

HRMS (EI): *m/z* calcd for C$_{22}$H$_{34}$O$_5$$^{•+}$ [M$^{•+}$]: 378.2401; found: 378.2401.

IR (neat, ATR): $\tilde{v}$ 3641, 2957, 1728, 1435, 1368, 1232, 1214, 1146, 1119, 1034, 865, 770 cm^{-1}.

Diethyl 2,2-bis(3,5-di-*tert*-butyl-4-hydroxybenzyl)malonate (6)

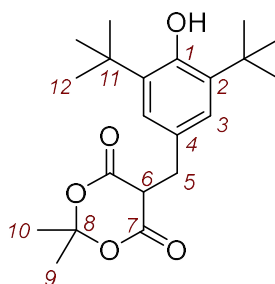**6** (CG536_4_1)   bv303

¹H NMR (600 MHz, CDCl₃): δ 7.02 (s, 4 H, 3-H), 5.09 (s, 2 H, 1-OH), 4.03 (q, *J* = 7.1 Hz, 4 H, 8-H), 3.17 (s, 4 H, 5-H), 1.41 (s, 36 H, 11-H), 1.10 ppm (t, *J* = 7.2 Hz, 6 H, 9-H).

¹³C{¹H} NMR (151 MHz, CDCl₃): δ 171.3 (C$_q$, C-7), 152.7 (C$_q$, C-1), 135.5 (C$_q$, C-2), 127.3 (C$_q$, C-4), 126.8 (CH, C-3), 61.1 (CH₂, C-8), 60.8 (C$_q$, C-6), 39.1 (CH₂, C-5), 34.4 (C$_q$, C-10), 30.5 (CH₃, C-11), 14.0 ppm (CH₃, C-9).

HRMS (pos. ESI): *m/z* calcd for C₃₇H₅₇O₆⁺ [M + H⁺]: 597.4150; found: 597.4139.

IR (neat, ATR): ṽ 3587, 2954, 1728, 1434, 1305, 1232, 1195, 1141, 1065, 982, 884, 771 cm⁻¹.

5-(3,5-Di-*tert*-butyl-4-hydroxybenzyl)-2,2-dimethyl-1,3-dioxane-4,6-dione (7)

7 (CG542)

BHT (64.0 mg, 0.29 mmol) was dissolved in *n*-pentane (2 mL) and Ag₂O (337 mg, 1.45 mmol) was added. The mixture was stirred for 20 min at room temperature under the exclusion of light. Solids were removed by filtration (0.2 μm PTFE Filter) and a DMSO solution of **2a** (61.9 mg, 0.34 mmol in 10 mL) was added. The mixture was stirred for 1 h at room temperature under nitrogen atmosphere. The reaction was quenched with aq. sat. NH₄Cl solution (5 mL), diluted with water (5 mL) and extracted with diethyl ether (4 × 10 mL). The combined organic phases were washed with water (4 × 10 mL) and dried over MgSO₄. The solvent was removed under reduced pressure yielding a crude product that was purified by preparative TLC (silica gel, *n*-pentane:EtOAc 9:1→8:2→7:3) to give **7** as a white solid (69.0 mg, 66%); m.p. 175 °C.
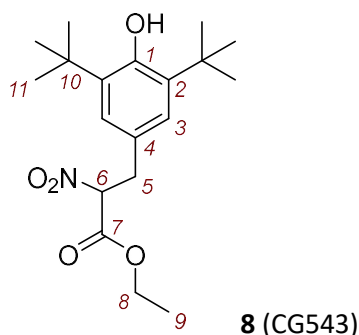
R$_f$ (*n*-pentane/EtOAc 9:1, silica, UV) = 0.15.

¹H NMR (400 MHz, CDCl₃): δ 7.10 (s, 2 H, 3-H), 5.15 (s, 1 H, 1-OH), 3.72 (t, *J* = 4.7 Hz, 1 H, 6-H), 3.43 (d, *J* = 4.8 Hz, 2 H, 5-H), 1.70 (s, 3 H, 9-H or 10-H), 1.41 (s, 18 H, 12-H), 1.28 ppm (s, 3 H, 9-H or 10-H).

¹³C{¹H} NMR (101 MHz, CDCl₃): δ 165.9 (C$_q$, C-7), 153.1 (C$_q$, C-1), 136.3 (C$_q$, C-2), 127.8 (C$_q$, C-4), 126.6 (CH, C-3), 105.4 (C$_q$, C-8), 48.6 (CH, C-6), 34.4 (C$_q$, C-11), 32.9 (CH₂, C-5), 30.4 (CH₃, C-12), 28.6 (CH₃, C-9 or C-10), 27.7 ppm (CH₃, C-9 or C-10).

HRMS (EI): *m/z* calcd for C₂₁H₃₀O₅•⁺ [M•⁺]: 362.2088; found: 362.2090.

IR (neat, ATR): ṽ 3638, 2957, 1744, 1435, 1393, 1344, 1281, 1200, 1088, 1016, 948, 909, 730 cm⁻¹.

Ethyl 3-(3,5-di-*tert*-butyl-4-hydroxyphenyl)-2-nitropropanoate (8)

8 (CG543)

BHT (66.1 mg, 0.30 mmol) was dissolved in *n*-pentane (2 mL) and Ag_2O (348 mg, 1.50 mmol) was added. The mixture was stirred for 20 min at room temperature under the exclusion of light. Solids were removed by filtration (0.2 μm PTFE Filter) and DMSO solution of **2k** was added [generated by mixing KO*t*Bu (37.0 mg, 0.33 mmol) and ethyl 2-nitroacetate (45.9 mg, 0.34 mmol) in 10 mL DMSO]. The mixture was vigorously stirred for 1 h at room temperature under nitrogen atmosphere. The reaction was quenched with aq. sat. NH_4Cl solution (5 mL), diluted with water (5 mL) and extracted with diethyl ether (4 × 10 mL). The combined organic phases were washed with water (4 × 10 mL) and dried over $MgSO_4$. The solvent was removed under reduced pressure to furnish a residue that was purified by preparative TLC (silica gel, *n*-pentane:EtOAc 95:5→9:1) to give **8** as a white solid (92.0 mg, 87%); m.p. 67 °C.
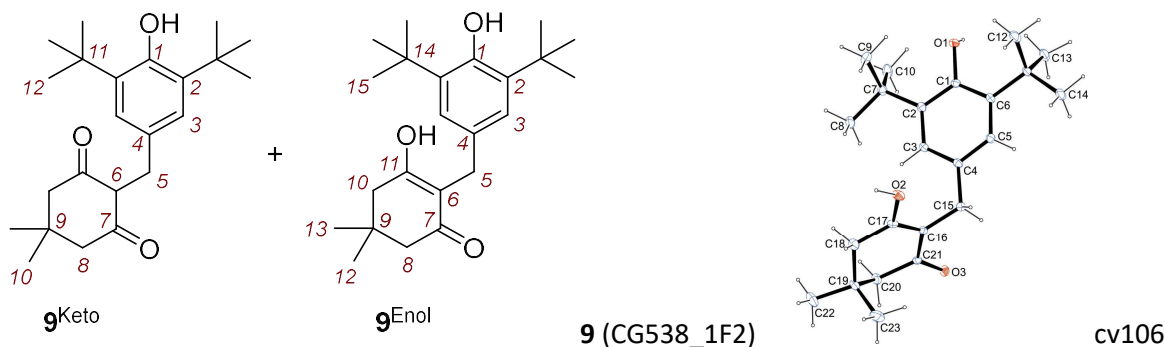
R_f (*n*-pentane/EtOAc 95:5, silica, UV) = 0.40.

[1H] NMR (600 MHz, $CDCl_3$): δ 6.97 (s, 2 H, 3-H), 5.30 (dd, *J* = 9.5, 5.8 Hz, 1 H, 6-H), 5.18 (s, 1 H, 1-OH), 4.29–4.25 (m, 2 H, 8-H), 3.48 (dd, *J* = 14.7, 9.5 Hz, 1 H, 5-H[a]), 3.39 (d, *J* = 14.7, 5.9 Hz, 1 H, 5-H[b]), 1.41 (s, 18 H, 11-H), 1.27 ppm (t, *J* = 7.1 Hz, 3 H, 9-H).

^{13}C{^{1}H} NMR (151 MHz, $CDCl_3$): δ 164.5 (C_q, C-7), 153.4 (C_q, C-1), 136.5 (C_q, C-2), 125.6 (CH, C-3), 124.8 (C_q, C-4), 89.7 (CH, C-6), 63.2 (CH_2, C-8), 36.4 (CH_2, C-5), 34.4 (C_q, C-10), 30.3 (CH_3, C-11), 14.0 ppm (CH_3, C-9).

HRMS (EI): *m/z* calcd for $C_{19}H_{29}NO_5^{•+}$ [M$^{•+}$]: 351.2040; found: 351.2038.

IR (neat, ATR): ṽ 3627, 2957, 1746, 1566, 1434, 1368, 1317, 1270, 1211, 1147, 1117, 1028 cm^{-1}.

2-(3,5-Di-*tert*-butyl-4-hydroxybenzyl)-3-hydroxy-5,5-dimethylcyclohex-2-en-1-one (9) CG538_1F2

9^{Keto} +   **9**^{Enol} **9** (CG538_1F2)   cv106

BHT (62.0 mg, 0.28 mmol) was dissolved in *n*-pentane (2 mL) and Ag_2O (326 mg, 1.41 mmol) was added. The mixture was stirred for 20 min at room temperature under the exclusion of light. Solids were removed by filtration (0.2 μm PTFE Filter) and a DMSO solution of **2c** (55.2 mg, 0.31 mmol in 10

mL) was added. The mixture was stirred for 1 h at room temperature under nitrogen atmosphere. Then, the reaction was quenched with aq. sat. NH₄Cl solution (5 mL), diluted with water (5 mL) and extracted with diethyl ether (4 × 10 mL). The combined organic phases were washed with water (4 × 10 mL) and dried over MgSO₄. The solvent was removed under reduced pressure yielding a residue that was purified by preparative TLC (silica gel, *n*-pentane:EtOAc 95:5→9:1→6:4) to give **9** as a white solid (77.0 mg, 0.21 mmol, 76%); m.p. 202 °C.

According to the integrals in the ^{1}H NMR spectrum, **9** was analyzed as a 46/54 mixture of keto and enol tautomers in CDCl₃.

^{1}H NMR (400 MHz, CDCl₃): δ = 7.04 (s, 2 H, 3-H^{Keto}), 7.00 (s, 2 H, 3-H^{Enol}), 5.81 (s, 1 H, 11-OH^{Enol}), 5.10 (s, 1 H, 1-OH^{Enol}), 5.07 (s, 1 H, 1-OH^{Keto}), 3.61 (s, 2 H, 5-H^{Enol}), 3.56 (t, *J* = 5.6 Hz, 1 H, 6-H^{Keto}), 3.10 (d, *J* = 5.7 Hz, 2 H, 5-H^{Keto}), 2.65 (d, *J* = 13.4 Hz, 2 H, 8-H^{Keto}), 2.42 (d, *J* = 12.9 Hz, 2 H, 8-H^{Keto}), 2.33 (s, 2 H, 10-H^{Enol}), 2.30 (s, 2 H, 8-H^{Enol}), 1.41 (s, 18 H, 12-H^{Keto}), 1.40 (s, 18 H, 15-H^{Enol}), 1.15 (s, 3 H, CH₃^{Enol}), 1.10 (s, 6 H, 10-H^{Keto}), 0.82 ppm (s, 3 H, CH₃^{Enol}).

^{13}C{^{1}H} NMR (101 MHz, CDCl₃): δ = 204.1 (C=O, C-7^{Keto}), 198.0 (C=O, C-7^{Enol}), 169.9 (C$_q$, C-11^{Enol}), 152.7, 152.3, 136.6, 135.8, 130.8, 129.2, 126.2, 124.9, 114.0, 69.6 (CH, C-6^{Keto}), 54.7, 50.6, 42.8, 34.5, 34.4, 32.1, 31.1, 30.4 (CH₃, C-12^{Keto}), 30.4 (CH₃, C-15^{Enol}), 30.4 (CH₃), 28.5 (CH₃), 28.2 (CH₂, C-5^{Keto}), 27.4 (CH₂, C-5^{Enol}), 26.5 ppm (CH₃).

HRMS (pos. ESI): *m/z* calcd for C₂₃H₃₄NaO₃$^+$ [M + Na$^+$]: 381.2400; found: 381.2407.

IR (neat, ATR): $\tilde{v}$ 3397, 2957, 1562, 1423, 1390, 1316, 1260, 1196, 1149, 1036, 1019, 766 cm^{-1}.

2,6-Di-*tert*-butyl-4-(2-nitro-2-phenylethyl)phenol (10)

10 (CG654)

BHT (51.5 mg, 0.234 mmol) was dissolved in *n*-pentane (2 mL) and Ag₂O (271 mg, 1.17 mmol) was added. The mixture was stirred for 20 min under the exclusion of light at room temperature. Solids were removed by filtration (0.2 μm PTFE Filter) and **2j** was added [generated in situ by mixing KO*t*Bu (31.5 mg, 0.281 mmol) and phenylnitromethane (49.7 mg, 0.362 mmol) in 5 mL DMSO]. The mixture was vigorously stirred for 1 h at room temperature under nitrogen atmosphere. The reaction was quenched with aq. sat. NH₄Cl solution (5 mL), diluted with water (5 mL) and extracted with diethyl ether (4 × 10 mL). The combined organic phases were washed with water (4 × 10 mL) and dried over MgSO₄. The solvent was removed under reduced pressure yielding a residue that was purified by preparative TLC (silica gel, *n*-pentane:EtOAc 97:3) to give **10** as an white solid (51.0 mg, 61%); m.p. 107 °C.
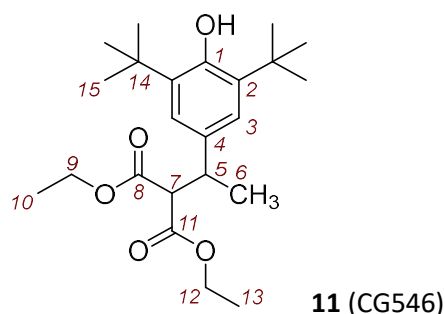
R$_f$ (*n*-pentane/EtOAc 97:3, silica, UV) = 0.50.

^{1}H NMR (400 MHz, CDCl₃): δ 7.50–7.47 (m, 2 H, 8-H), 7.42–7.39 (m, 3 H, 9-H and 10-H), 6.86 (s, 2 H, 3-H), 5.61 (dd, *J* = 8.7, 6.3 Hz, 1 H, 6-H), 5.12 (s, 1 H, 1-OH), 3.69 (dd, *J* = 14.3, 8.7 Hz, 1 H, 5-H^a), 3.28 (dd, *J* = 14.3, 6.4 Hz, 1 H, 5-H^b), 1.38 ppm (s, 18 H, 12-H).

^{13}C{^{1}H} NMR (101 MHz, CDCl$_3$): δ 153.1 (C$_q$, C-1), 136.3 (C$_q$, C-2), 134.8 (C$_q$, C-7), 129.9 (CH, C-10), 129.1 (CH, C-9), 128.0 (CH, C-8), 126.1 (C$_q$, C-4), 125.7 (CH, C-3), 93.0 (CH, C-6), 40.5 (CH$_2$, C-5), 34.4 (C$_q$, C-11), 30.4 ppm (CH$_3$, C-12).

HRMS (EI): *m/z* calcd for C$_{22}$H$_{29}$NO$_3$$^{\bullet+}$ [M$^{\bullet+}$]: 355.2142; found: 355.2142.
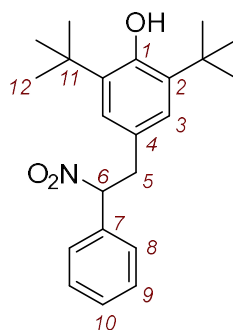
IR (neat, ATR): $\tilde{\nu}$ 3624, 2956, 1549, 1433, 1367, 1231, 1211, 1142, 1117, 873, 790, 767, 723, 694 cm^{-1}.

Diethyl 2-(1-(3,5-di-*tert*-butyl-4-hydroxyphenyl)ethyl)malonate (11) was synthesized according to GP1 (aqueous workup after 30 min) from the *p*QM **1e** (15.0 mg, 0.065 mmol) and **2j** (13.4 mg, 0.068 mmol) and yielding a residue that was purified by preparative TLC (silica gel, *n*-pentane:EtOAc 97:3) to give **11** as a colorless oil (15.3 mg, 60%).

11 (CG546)

R_f (*n*-pentane/EtOAc 97:3, silica, UV) = 0.15.

^{1}H NMR (600 MHz, CDCl$_3$): δ 6.99 (s, 2 H, 3-H), 5.07 (s, 1 H, 1-OH), 4.25–4.21 (m, 2 H, 9-H or 12-H), 3.90–3.85 (m, 2 H, 9-H or 12-H), 3.53 (d, *J* = 10.7 Hz, 1 H, 7-H), 3.47–3.41 (m, 1 H, 5-H), 1.41 (s, 18 H, 15-H), 1.31 (d, *J* = 6.7 Hz, 3 H, 6-H), 1.29 (t, *J* = 7.2 Hz, 3 H, 10-H or 13-H), 0.91 ppm (t, *J* = 7.1 Hz, 3 H, 10-H or 13-H).
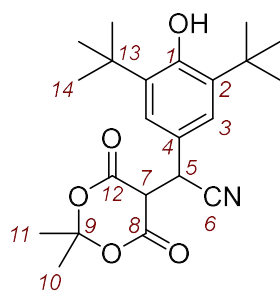
^{13}C{^{1}H} NMR (151 MHz, CDCl$_3$): δ 168.8 (C$_q$, C-8 or C-11), 168.4 (C$_q$, C-8 or C-11), 152.6 (C$_q$, C-1), 135.7 (C$_q$, C-2), 133.5 (C$_q$, C-4), 124.1 (CH, C-3), 61.5 (CH$_2$, C-9 or C-12), 61.1 (CH$_2$, C-9 or C-12), 60.0 (CH, C-7), 40.5 (CH, C-5), 34.5 (C$_q$, C-14), 30.4 (CH$_3$, C-15), 20.5 (CH$_3$, C-6), 14.3 (CH$_3$, C-10 or C-13), 13.9 ppm (CH$_3$, C-10 or C-13).

HRMS (EI): *m/z* calcd for C$_{23}$H$_{36}$O$_5$$^{\bullet+}$ [M$^{\bullet+}$]: 392.2557; found: 392.2556.
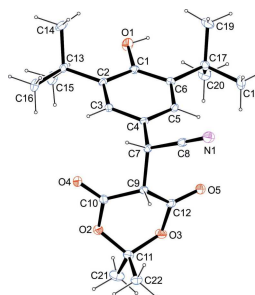
IR (neat, ATR): $\tilde{\nu}$ 3643, 2958, 1753, 1728, 1435, 1367, 1234, 1176, 1151, 1120, 1029, 880, 770 cm^{-1}.

2-(3,5-di-tert-butyl-4-hydroxyphenyl)-2-(2,2-dimethyl-4,6-dioxo-1,3-dioxan-5-yl)acetonitrile (12)

The *p*QM **1c** (15.2 mg, 0.062 mmol) was dissolved in *n*-pentane (2 mL) under nitrogen atmosphere and mixed with a DMSO solution of **2a** (14.8 mg, 0.081 mmol in 2 mL). The mixture was vigorously stirred for 20 min at room temperature under nitrogen atmosphere. Then, the reaction was quenched with 2 M hydrochloric acid (5 mL), diluted with water (5 mL) and extracted with diethyl ether (4 × 10 mL). The combined organic phases were washed with water (4 × 10 mL) and dried over MgSO$_4$. The solvent was removed under reduced pressure yielding a residue that was recrystallized from *n*-pentane/CH$_2$Cl$_2$ to give **12** as colorless crystals (19.0 mg, 79%); m.p. >130 °C (dec.).
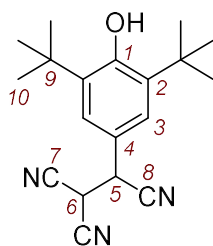
12 (CG651_1)   dv077

¹H NMR (400 MHz, acetonitrile-*d₃*): δ 7.32 (s, 2 H, 3-H), 5.60 (s, 1 H, 1-H), 4.95 (d, *J* = 2.8 Hz, 1 H, 5-H), 4.56 (d, *J* = 3.0 Hz, 1 H, 7-H), 1.78 (s, 3 H), 1.58 (s, 3 H), 1.40 ppm (s, 18 H, 14-H).

¹³C{¹H} NMR (101 MHz, acetonitrile-*d₃*): δ 164.2 (C=O), 163.8 (C=O), 154.9 (C_q, C-1), 138.4 (C_q, C-2), 126.7 (CH, C-3), 124.0 (C_q, C-4), 119.7 (C-N, C-6), 107.3 (C_q, C-9), 51.4 (CH, C-7), 35.3 (C_q, C-13), 34.7 (CH, C-5), 30.4 (CH_3, C-14), 28.6 (CH_3,9-CH_3), 26.9 ppm (CH_3, 9-CH_3).

HRMS (pos. ESI): *m/z* calcd for $C_{22}H_{29}NNaO_5^+$ [M + Na⁺]: 410.1938; found: 410.1932.

IR (neat, ATR): $\tilde{v}$ 3633, 2958, 2865, 2251, 1785, 1748, 1436, 1395, 1387, 1334, 1323, 1292, 1292, 1270, 1200, 1159, 1080, 1059, 1019, 994, 923, 900, 877, 860, 774, 735 cm⁻¹.

2-(3,5-Di-*tert*-butyl-4-hydroxyphenyl)ethane-1,1,2-tricarbonitrile (13)

13 (CG553)   br015

The *p*QM **1c** (15.0 mg, 0.062 mmol) was dissolved in *n*-pentane (2 mL) under nitrogen atmosphere and mixed with a DMSO solution of **2h** (7.1 mg, 0.068 mmol in 2 mL). The mixture was vigorously stirred for 30 min at room temperature. The reaction was quenched with aq. sat. NH₄Cl solution (2 mL), diluted with water (5 mL) and extracted with diethyl ether (3 × 10 mL). The combined organic phases were washed with water (3 × 10 mL) and dried over MgSO₄. The solvent was removed under reduced pressure yielding a residue that was purified by preparative TLC (silica gel, *n*-pentane:EtOAc 9:1) to give product **13** as an off-white solid (16.5 mg, 86%); m.p. 188 °C.

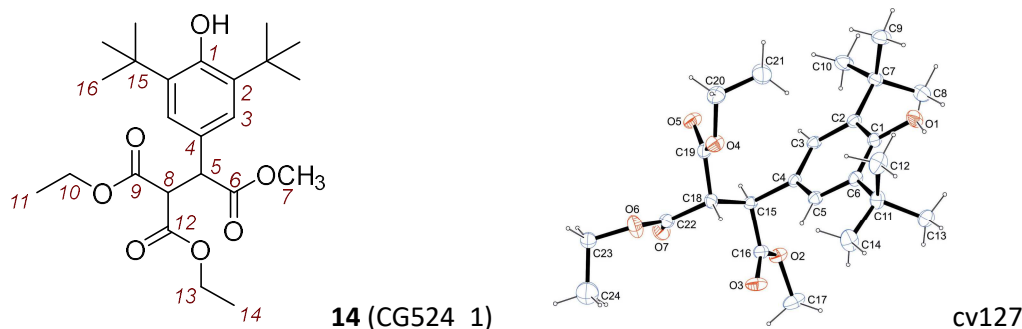*R*f (*n*-pentane/EtOAc 9:1, silica, UV) = 0.50.

¹H NMR (400 MHz, CDCl₃): δ 7.26 (s, 2 H, 3-H, superimposed by residual CHCl₃), 5.52 (s, 1 H, 1-OH), 4.38 (d, *J* = 5.6 Hz, 1 H, 5-H), 4.17 (d, *J* = 5.6 Hz, 1 H, 6-H), 1.46 ppm (s, 18 H, 10-H).

¹³C{¹H} NMR (101 MHz, CDCl₃): δ 156.0 (C_q, C-1), 137.7 (C_q, C-2), 125.1 (CH, C-3), 118.9 (C_q, C-4), 115.4 (C_q, C-8), 109.7 (C_q, C-7), 39.3 (CH, C-5), 34.7 (C_q, C-9), 30.2 (CH, C-6), 30.2 ppm (CH_3, C-10).

HRMS (EI): *m/z* calcd for $C_{19}H_{23}N_3O^{•+}$ [M•⁺]: 309.1836; found: 309.1836.

IR (neat, ATR): $\tilde{v}$ 3628, 2959, 2360, 2258, 1435, 1240, 1157, 1123, 909, 884, 733 cm⁻¹.

1,1-Diethyl 2-methyl 2-(3,5-di-*tert*-butyl-4-hydroxyphenyl)ethane-1,1,2-tricarboxylate (14) was synthesized according to GP1 (aqueous workup after 30 min) from **1d** (7.3 mg, 0.026 mmol) and **2j** (5.5 mg, 0.028 mmol) and yielding **14** as a white solid (11.1 mg, 98%); m.p. 77 °C.
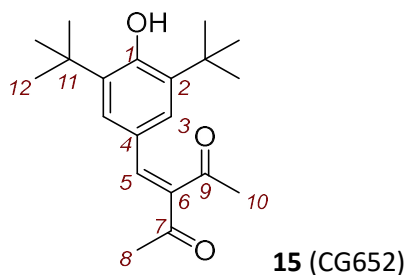

14 (CG524_1) cv127

¹H NMR (600 MHz, CDCl₃): δ 7.04 (s, 2 H, 3-H), 5.18 (s, 1 H, 1-OH), 4.24–4.15 (m, 4 H, 5-H, 8-H and 13-H), 3.93–3.84 (m, 2 H, 10-H), 3.68 (s, 3 H, 7-H), 1.40 (s, 18 H, 16-H), 1.27 (t, *J* = 7.2 Hz, 3 H, 11-H or 14-H), 0.89 ppm (t, *J* = 7.1 Hz, 3 H, 11-H or 14-H).

¹³C{¹H} NMR (151 MHz, CDCl₃): δ 173.0 (C$_q$, C-6), 168.2 (C$_q$, C-9 or C-12), 167.5 (C$_q$, C-9 or C-12), 153.7 (C$_q$, C-1), 136.1 (C$_q$, C-2), 125.3 (C$_q$, C-4), 125.2 (CH, C-3), 62.0 (CH₂, C-10 or C-13), 61.4 (CH₂, C-10 or C-13), 55.9 (CH, C-8), 52.6 (CH₃, C-7), 50.6 (CH, C-5), 34.5 (C$_q$, C-15), 30.3 (CH₃, C-16), 14.1 (CH₃, C-11 or C-14), 13.9 ppm (CH₃, C-11 or C-14).

HRMS (pos. ESI): *m/z* calcd for $C_{24}H_{36}NaO_7^+$ [M + Na⁺]: 459.2353; found: 459.2354.

IR (neat, ATR): $\tilde{v}$ 3602, 2957, 1731, 1435, 1368, 1299, 1236, 1159, 1121, 1023 cm⁻¹.

3-(3,5-Di-*tert*-butyl-4-hydroxybenzylidene)pentane-2,4-dione (15)

15 (CG652)

The *p*QM **1f** (24.0 mg, 0.097 mmol) was dissolved in *n*-pentane (2 mL) under nitrogen atmosphere and mixed with a DMSO solution of **2e** (15.2 mg, 0.11 mmol in 2 mL). The mixture was vigorously stirred under nitrogen atmosphere for 20 min at room temperature. The reaction was quenched with aq. sat. NH₄Cl solution (5 mL), diluted with water (5 mL) and extracted with diethyl ether (4 × 10 mL). The combined organic phases were washed with water (4 × 10 mL) and dried over MgSO₄. The solvent was removed under reduced pressure yielding a residue that was purified by preparative TLC (silica gel, *n*-pentane:EtOAc 85:15) to give **15** as a white solid (25.0 mg, 81%); m.p. 124 °C.
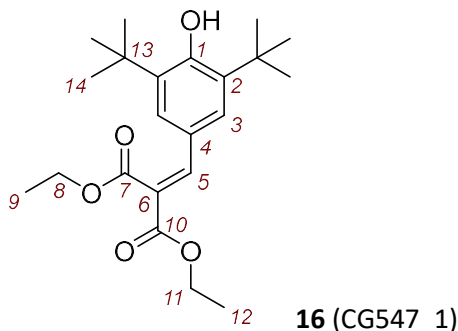
R$_f$ (*n*-pentane/EtOAc 85:15, silica, UV) = 0.60.

¹H NMR (600 MHz, CDCl₃): δ 7.41 (s, 1 H, 5-H), 7.24 (s, 2 H, 3-H), 5.63 (s, 1 H, 1-OH), 2.41 (s, 3 H, 8-H or 10-H), 2.35 (s, 3 H, 8-H or 10-H), 1.42 ppm (s, 18 H, 12-H).

¹³C{¹H} NMR (151 MHz, CDCl₃): δ 206.7 (C$_q$, C-7 or C-9), 196.8 (C$_q$, C-7 or C-9), 156.7 (C$_q$, C-1), 141.5 (CH, C-5), 139.9 (C$_q$, C-6), 136.6 (C$_q$, C-2), 128.0 (CH, C-3), 124.1 (C$_q$, C-4), 34.6 (C$_q$, C-11), 31.8 (CH₃, C-8 or C-10), 30.2 (CH₃, C-12), 26.5 ppm (CH₃, C-8 or C-10).

HRMS (EI): *m/z* calcd for $C_{20}H_{28}O_3^{\bullet+}$ [M$^{\bullet+}$]: 316.2033; found: 316.2015.

IR (neat, ATR): $\tilde{v}$ 3573, 2957, 1701, 1640, 1607, 1592, 1428, 1381, 1262, 1212, 1174, 1115, 918 cm^{-1}.

Diethyl 2-(3,5-di-*tert*-butyl-4-hydroxybenzylidene)malonate (16)

16 (CG547_1)

The *p*QM **1f** (22.8 mg, 0.092 mmol) was dissolved in *n*-pentane (2 mL) under nitrogen atmosphere and mixed with a DMSO solution of **2j** (20.0 mg, 0.10 mmol in 2 mL). The mixture was vigorously stirred for 15 h at room temperature under nitrogen atmosphere. The reaction was quenched with aq. sat. NH$_4$Cl solution (5 mL), diluted with water (5 mL) and extracted with diethyl ether (4 × 10 mL). The combined organic phases were washed with water (4 × 10 mL) and dried over MgSO$_4$. The solvent was removed under reduced pressure yielding a residue that was purified by preparative TLC (silica gel, *n*-pentane:EtOAc 97:3) to give **16** as a white solid (22.0 mg, 63%); m.p. 112 °C.
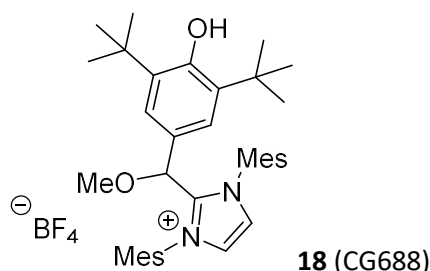
R$_f$ (*n*-pentane/EtOAc 97:3, silica, UV) = 0.15.

^{1}H NMR (400 MHz, CDCl$_3$): *δ* 7.65 (s, 1 H, 5-H), 7.34 (s, 2 H, 3-H), 5.57 (s, 1 H, 1-OH), 4.36 (q, *J* = 7.1 Hz, 2 H, 8-H or 11-H), 4.29 (q, *J* = 7.1 Hz, 2 H, 8-H or 11-H), 1.42 (s, 18 H, 14-H), 1.32 ppm (t, *J* = 7.1 Hz, 6 H, 9-H and 12-H).

^{13}C{^{1}H} NMR (101 MHz, CDCl$_3$): *δ* 167.7 (C$_q$, C-7 or C-10), 164.9 (C$_q$, C-7 or C-10), 156.6 (C$_q$, C-1), 143.2 (CH, C-5), 136.4 (C$_q$, C-2), 127.7 (CH, C-3), 124.3 (C$_q$, C-4), 122.7 (C$_q$, C-6), 61.7 (CH$_2$, C-8 or C-10), 61.4 (CH$_2$, C-8 or C-10), 34.5 (C$_q$, C-13), 30.3 (CH$_3$, C-14), 14.3 (CH$_3$, C-9 or C12), 14.2 ppm (CH$_3$, C-9 or C12).

HRMS (EI): *m/z* calcd for [C$_{22}$H$_{32}$O$_5$]$^{\bullet+}$ [M$^{\bullet+}$]: 376.2244; found: 379.2244.

IR (neat, ATR): $\tilde{v}$ 3594, 2952, 1722, 1688, 1622, 1430, 1384, 1259, 1207, 1141, 1067, 765 cm^{-1}.

3.2.3. Products of Reactions of *p*QMs with Further Classes of Nucleophiles

2-((3,5-Di-*tert*-butyl-4-hydroxyphenyl)(methoxy)methyl)-1,3-dimesityl-1*H*-imidazol-3-ium tetra-fluoroborate (18)
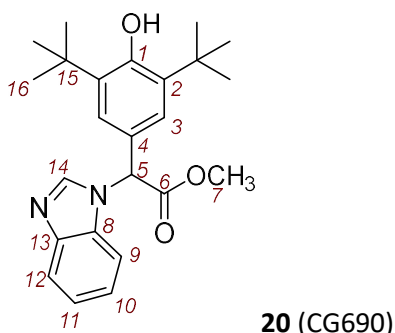

18 (CG688)

The *p*QM **1f** (18.0 mg, 0.073 mmol) and the *N*-heterocyclic carbene **17** (21.0 mg, 0.069 mmol) were dissolved in dry THF (5mL) under nitrogen atmosphere. The reaction mixture was stirred for 5 min at room temperature under nitrogen atmosphere. Then, the reaction was quenched with ethereal HBF$_4$ (10 μL, 11.1 mg, 0.069 mmol). The solvent was removed under reduced pressure. Subsequently, the crude material was dissolved in a minimum volume of DCM/Et$_2$O (ratio 1:4) and precipitated by addition of *n*-pentane to yield **18** as a white solid (36.0 mg, 81%); m.p. 199 °C.

^{1}H NMR (600 MHz, CDCl$_3$): δ 7.64 (s, 2 H), 7.09 (s, 2 H), 6.91 (s, 2 H), 6.41 (s, 2 H), 5.26 (s, 1 H), 5.02 (s, 1 H), 3.13 (s, 3 H, OMe), 2.36 (s, 6 H, 2 × CH$_3$), 2.19 (s, 6 H, 2 × CH$_3$), 1.73 (s, 6 H, 2 × CH$_3$), 1.24 ppm (s, 18 H, 2 × C(CH$_3$)$_3$).

^{13}C{^{1}H} NMR (151 MHz, CDCl$_3$): δ 154.7 (C$_q$), 143.7 (C$_q$), 141.8 (C$_q$), 136.5 (C$_q$), 135.1 (C$_q$), 135.0 (C$_q$), 130.3 (C$_q$), 130.1 (CH), 130.0 (CH), 125.9 (CH), 123.1 (CH), 121.1 (C$_q$), 74.9 (CH), 58.5 (OCH$_3$), 34.2 (C$_q$), 29.8 (CH$_3$), 21.3 (CH$_3$), 17.8 (CH$_3$), 16.9 ppm (CH$_3$).

HRMS (pos. ESI): *m/z* calcd for C$_{37}$H$_{49}$N$_2$O$_2^+$ [M − BF$_4^-$]: 553.3789; found: 553.3779.

IR (neat, ATR): ṽ 3532, 2964, 1503, 1432, 1230, 1196, 1098, 1049, 1035, 983, 851, 782, 774 cm^{-1}.

Methyl 2-(1*H*-benzo[*d*]imidazol-1-yl)-2-(3,5-di-*tert*-butyl-4-hydroxyphenyl)acetate (20)

20 (CG690)

The *p*QM **1d** (20.0 mg, 0.072 mmol) was dissolved in *n*-pentane (2 mL) under nitrogen atmosphere and **19** [generated by mixing KO*t*Bu (8.5 mg, 0.076 mmol) with benzimidazole (10.3 mg, 0.087 mmol) in 2 mL DMSO] was added to the *p*QM solution. The reaction mixture was vigorously stirred for 5 min at room temperature under nitrogen atmosphere. The reaction was quenched with aq. sat. NH$_4$Cl solution (2 mL), diluted with water (5 mL) and extracted with diethyl ether (4 × 10 mL). The combined organic phases were washed with water (4 × 10 mL) and dried over MgSO$_4$. The solvent was removed under reduced pressure yielding a residue that was purified by preparative TLC (silica gel, *n*-pentane:EtOAc:NEt$_3$ 50:48:2) to give **20** as a colorless solid (13.0 mg, 46%); m.p. 182 °C.

R_f (*n*-pentane/EtOAc/NEt$_3$ 50:48:2, silica, UV) = 0.55.

¹H NMR (600 MHz, CDCl$_3$): *δ* 7.83–7.81 (m, 2 H, 14-H, 12-H), 7.37–7.35 (m, 1 H, 9-H), 7.33–7.29 (m, 2 H, 10-H, 11-H), 7.22 (s, 2 H, 3-H), 6.04 (s, 1 H, 5-H), 5.45 (s, 1 H, 1-OH), 3.82 (s, 3 H, 7-H), 1.42 ppm (s, 18 H, 16-H).

¹³C{¹H} NMR (151 MHz, CDCl$_3$): *δ* 169.8 (C$_q$, C-6), 155.1 (C$_q$, C-1), 143.9 (C$_q$, C-13), 142.4 (CH, C-14), 137.2 (C$_q$, C-2), 134.0 (C$_q$, C-8), 125.4 (CH, C-3), 123.3 (CH, C-11), 123.2 (C$_q$, C-4), 122.7 (CH, C-10), 120.7 (CH, C-12), 109.5 (CH, C-9), 62.1 (CH, C-5), 53.2 (CH$_3$, C-7), 34.6 (C$_q$, C-15), 30.2 ppm (CH$_3$, C-16).

HRMS (EI): *m/z* calcd for C$_{24}$H$_{30}$N$_2$O$_3$$^{•+}$ [M$^{•+}$]: 394.2251; found: 394.2253.

IR (neat, ATR): $\tilde{\nu}$ 3625, 2955, 1748, 1484, 1457, 1434, 1281, 1200, 1173, 1009, 909, 766, 738 cm^{-1}.

Methyl 2-((3-chlorophenyl)thio)-2-(3,5-di-*tert*-butyl-4-hydroxyphenyl)acetate (22)

22 (CG693F2)
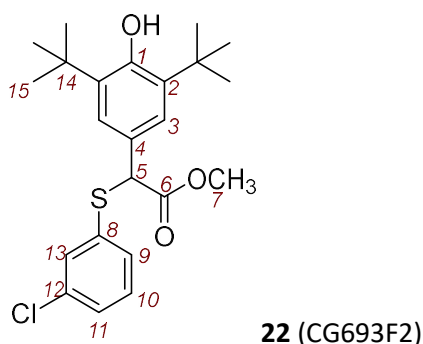
The *p*QM **1d** (20.0 mg, 0.072 mmol) was dissolved in DMSO (0.5 mL) under nitrogen atmosphere and **21** [generated by mixing KO*t*Bu (8.5 mg, 0.076 mmol) with 3-chlorothiophenol (18.8 mg, 0.130 mmol) in 0.5 ml DMSO] was added to the *p*QM solution. The reaction mixture was stirred for 10 min at room temperature under nitrogen atmosphere. The reaction was quenched with aq. sat. NH$_4$Cl solution (2 mL), diluted with water (5 mL) and extracted with diethyl ether (4 × 10 mL). The combined organic phases were washed with water (4 × 10 mL) and dried over MgSO$_4$. The solvent was removed under reduced pressure yielding a residue that was purified by preparative TLC (silica gel, *n*-pentane:EtOAc 97:3) to give the thioether **22** as a colorless oil (16.0 mg, 53%).

R_f (*n*-pentane/EtOAc 97:3, silica, UV) = 0.65.

¹H NMR (600 MHz, CDCl$_3$): *δ* 7.29–7.29 (m, 1 H, 10-H), 7.24–7.17 (m, 3 H, 9-H, 11-H and 13-H), 7.16–7.15 (m, 2 H, 3-H), 5.26 (s, 1 H, 1-OH), 4.87 (s, 1 H, 5-H), 3.70 (s, 3 H, 7-H), 1.41 ppm (s, 18 H, 15-H).

¹³C{¹H} NMR (151 MHz, CDCl$_3$): *δ* 171.2 (C$_q$, C-6), 154.1 (C$_q$, C-1), 136.3 (C$_q$, C-2), 136.1 (C$_q$, C-8), 134.5 (C$_q$, C-12), 132.4 (CH, C-10), 130.8 (CH), 130.0 (CH), 128.0 (CH), 125.5 (CH, C-3), 125.4 (C$_q$, C-4), 56.0 (CH, C-5), 52.8 (CH$_3$, C-7), 34.5 (C$_q$, C-14), 30.3 ppm (CH$_3$, C-15).

HRMS (EI): *m/z* calcd for C$_{23}$H$_{29}$ClO$_3$S$^{•+}$ [M$^{•+}$]: 420.1520; found: 420.1511.

IR (neat, ATR): $\tilde{\nu}$ 3634, 2955, 1737, 1576, 1564, 1461, 1433, 1238, 1210, 1149, 1121, 779, 681 cm^{-1}.

Methyl 2-(3,5-di-*tert*-butyl-4-hydroxyphenyl)acetate (24)

24 (CG699)
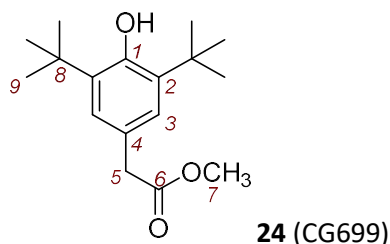
The *p*QM **1d** (25.0 mg, 0.090 mmol) was dissolved in methanol (2 mL) under nitrogen atmosphere and sodium cyanoborohydride **23** (12.5 mg, 0.199 mmol) was added portionwise over 10 min at room temperature. The mixture was stirred for 2 h at room temperature. The reaction was quenched by addition of aq. sat. ammonium chloride solution (2 mL), diluted with water (5 mL) and extracted with diethyl ether (3 × 10 mL). The combined organic phases were washed with water (3 × 10 mL) and dried over MgSO$_4$. The solvent was removed under reduced pressure yielding a residue that was purified by preparative TLC (silica gel, *n*-pentane:EtOAc 98:2) to give product **24** as a white solid (20.0 mg, 80%); m.p. 85 °C.

R$_f$ (*n*-pentane/EtOAc 98:2, silica, UV) = 0.35.

^{1}H NMR (600 MHz, CDCl$_3$): δ 7.08 (s, 2 H, 3-H), 5.15 (s, 1 H, 1-OH), 3.70 (s, 3 H, 7-H), 3.54 (s, 2 H, 5-H), 1.44 ppm (s, 18 H, 9-H).

^{13}C{^{1}H} NMR (151 MHz, CDCl$_3$): δ 172.9 (C$_q$, C-6), 153.0 (C$_q$, C-1), 136.1 (C$_q$, C-2), 126.0 (CH, C-3), 124.7 (C$_q$, C-4), 52.1 (CH$_3$, C-7), 41.1 (CH$_2$, C-5), 34.4 (C$_q$, C-8), 30.4 ppm (CH$_3$, C-9).

HRMS (EI): *m/z* calcd for C$_{17}$H$_{26}$O$_3$$^{•+}$ [M$^{•+}$]: 278.1876; found: 278.1874.

IR (neat, ATR): ṽ 3630, 2954, 1735, 1434, 1361, 1316, 1234, 1156, 1121, 1016 cm^{-1}.

2-(3,5-Di-*tert*-butyl-4-hydroxybenzyl)cyclohexan-1-one (26)

26 (CG695_DMSO)

BHT (33.0 mg, 0.150 mmol) was dissolved in *n*-pentane (2 mL) and Ag$_2$O (174 mg, 0.750 mmol) was added. The mixture was stirred for 20 min at room temperature under the exclusion of light. Solids were removed by filtration (0.2 µm PTFE Filter) and a dichloromethane solution of enamine **25** (22.7 mg, 0.150 mmol in 2 mL) was added. The mixture was stirred for 15 min at room temperature under nitrogen atmosphere. The reaction was quenched with hydrochloric acid (2 M, 2 mL), diluted with water (5 mL) and extracted with dichloromethane (3 × 10 mL). The combined organic phases were washed with aq. sat. NaHCO$_3$ solution (10 mL) and water (10 mL) and dried over MgSO$_4$. The solvent was removed under reduced pressure yielding a residue that was purified by preparative TLC (silica gel, *n*-pentane:EtOAc 97:3) to give **26** as a light yellow oil (33.0 mg, 69%).

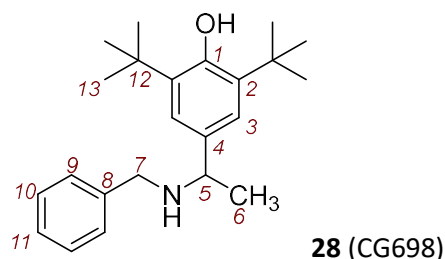*R*$_f$ (*n*-pentane/EtOAc 97:3, silica, UV) = 0.50.

_____

^{1}H NMR (400 MHz, DMSO-d_6): δ 6.86 (s, 2 H, 3-H), 6.67 (s, 1 H, 1-OH), 2.96 (dd, J = 13.9, 5.1 Hz, 1 H, 5-H^a), 2.57–2.53 (m, 1 H, 6-H), 2.45–2.33 (m, 1 H), 2.27–2.23 (m, 1 H), 2.23–2.17 (m, 1 H, 5-H^b), 1.98–1.89 (m, 2 H), 1.78–1.69 (m, 1 H), 1.63–1.51 (m, 2 H), 1.35 (s, 18 H, 13-H), 1.30–1.19 ppm (m, 1 H).

^{13}C{^{1}H} NMR (101 MHz, DMSO-d_6): δ 211.9 (C$_q$, C-7), 151.8 (C$_q$, C-1), 138.9 (C$_q$, C-2), 131.0 (C$_q$, C-4), 125.0 (CH, C-3), 51.6 (CH, C-6), 41.4 (CH$_2$), 35.0 (CH$_2$, C-5), 34.4 (C$_q$, C-12), 32.9 (CH$_2$), 30.4 (CH$_3$, C-13), 27.5(CH$_2$), 24.2 ppm (CH$_2$).

HRMS (EI): *m/z* calcd for C$_{21}$H$_{32}$O$_2^{\bullet+}$ [M$^{\bullet+}$]: 316.2397; found: 316.2394.

IR (neat, ATR): $\tilde{v}$ 3642, 2950, 2863, 1706, 1434, 1360, 1313, 1233, 1153, 1122, 883, 768 cm^{-1}.

4-(1-(Benzylamino)ethyl)-2,6-di-*tert*-butylphenol (28)

28 (CG698)

The *p*QM **1e** (29.0 mg, 0.12 mmol) was dissolved in DMSO (4 mL) under nitrogen atmosphere and a DMSO solution of benzylamine **27** (17.4 mg, 0.16 mmol in 1 mL) was added. The reaction mixture was stirred for 2 h at room temperature. The reaction was quenched by addition of water (10 mL) and extracted with diethyl ether (4 × 10 mL). The combined organic phases were washed with water (4 × 10 mL) and dried over MgSO$_4$. The solvent was removed under reduced pressure yielding a residue that was purified by preparative TLC (silica gel, *n*-pentane:EtOAc:NEt$_3$ 96:3:1) to give product **28** as a colorless oil (25.0 mg, 61%).

R$_f$ (*n*-pentane/EtOAc/NEt$_3$ 96:3:1, silica, UV) = 0.40.

^{1}H NMR (400 MHz, CD$_2$Cl$_2$): δ 7.31–7.30 (m, 4 H, 9-H and 10-H), 7.26–7.20 (m, 1 H, 11-H), 7.15 (s, 2 H, 3-H), 5.13 (s, 1 H, 1-OH), 3.72 (q, J = 6.6 Hz, 1 H, 5-H), 3.65 (d, J = 13.1 Hz, 1 H, 7-H^a), 3.60 (d, J = 13.1 Hz, 1 H, 7-H^b), 1.45 (s, 18 H, 13-H), 1.32 ppm (d, J = 6.6 Hz, 3 H, 6-H).

^{13}C{^{1}H} NMR (101 MHz, CD$_2$Cl$_2$): δ 152.9 (C$_q$, C-1), 141.7 (C$_q$, C-8), 136.7 (C$_q$, C-4), 136.2 (C$_q$, C-2), 128.61 (CH, C-9), 128.58 (CH, C-10), 127.0 (CH, C-11), 123.6 (CH, C-3), 58.1 (CH, C-5), 52.1 (CH$_2$, C-7), 34.7 (C$_q$, C-12), 30.6 (CH$_3$, C-13), 24.8 ppm (CH$_3$, C-6).
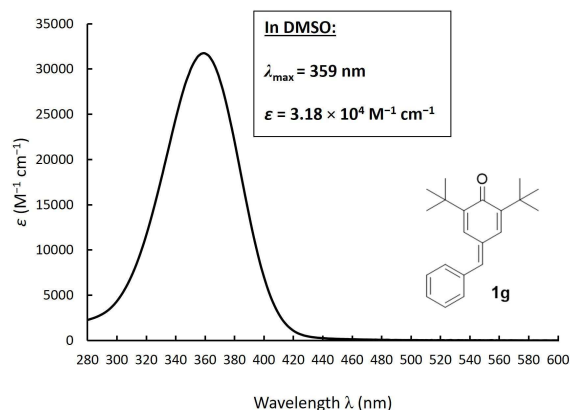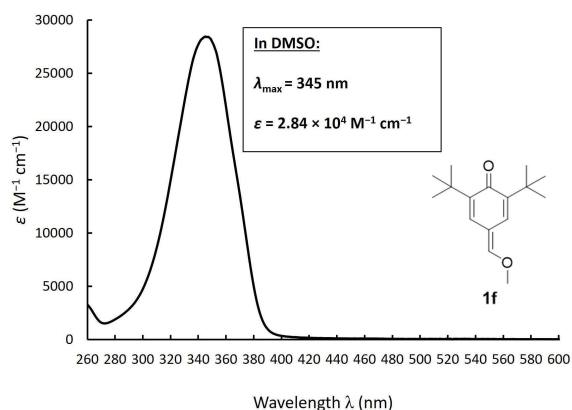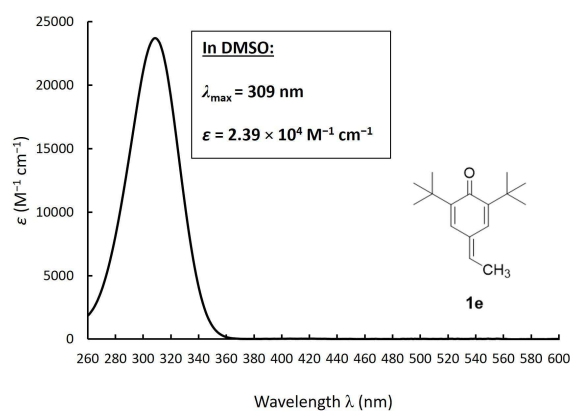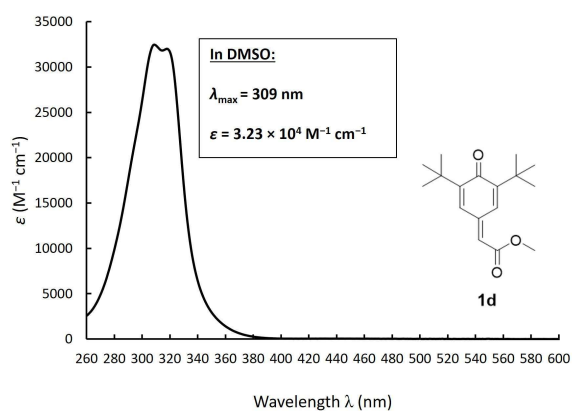
HRMS (pos. ESI): *m/z* calcd for C$_{23}$H$_{34}$NO$^+$ [M + H$^+$]: 340.2635; found: 340.2634.

3.2.4. UV/Vis Spectra and Molar Absorption Coefficients of *p*QMs

A solution of the quinone methide (3 mg *p*QM per mL DMSO) was added stepwise to a known volume of DMSO. The absorbances *A* of the *p*QM solutions were detected by using a *J&M* TIDAS diode array spectrophotometer (connected to a Hellma quartz probe with a path length *d* = 0.5 cm).

Molar absorption coefficients ε (M^{-1} cm^{-1}) were determined from the slopes of linear correlations of absorbance with *p*QM concentrations by assuming the validity of the Beer-Lambert law [Equation (S1)].

$$\lg (I_0/I) = A = \varepsilon \, d \, c \qquad \text{(S1)}$$
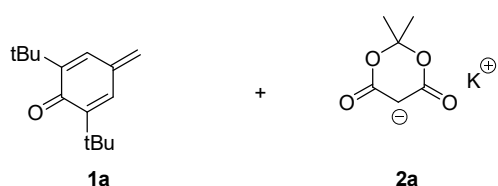

59

3.2.5. Kinetics of the Reactions of *p*QMs with Carbanions

Kinetic measurements were performed by using UV/Vis photometry on AppliedPhotophysics SX.20 stopped-flow instruments as well as on a conventional J&M TIDAS diode array spectrophotometer, which was controlled by TIDASDAQ3 (v3) software and connected to a Hellma 661.502-QX quartz Suprasil immersion probe (light path d = 5 mm) via fiber optic cables and standard SMA connectors. The temperature (20.0 ± 0.2 °C) was maintained constant by using circulating bath cryostats.

All solutions were prepared by using dry DMSO (ThermoScientific, DMSO 99.7+%, extra dry, over molecular sieve, AcroSeal) and kept under an atmosphere of dry nitrogen. The kinetic measurements for each *p*QM/nucleophile combination **1** + **2** were performed with or without added 18-crown-6 ether (18-c-6) and in some cases with addition of the corresponding CH-acid (**2**-H).
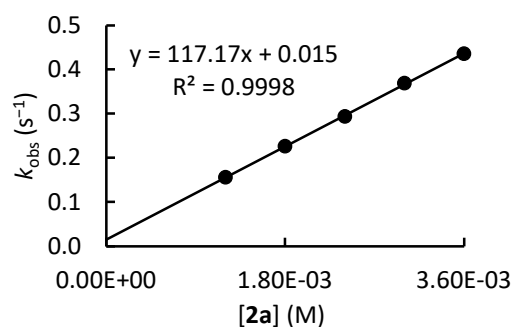
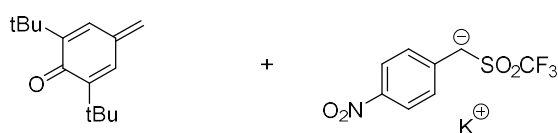**1a** + **2a** in DMSO (stopped-flow method, detection at 310 nm) CG544

[**1a**]$_0$ (M)	[**2a**]$_0^{[a]}$ (M)	[18-c-6]$_0$ (M)	k_{obs} (s^{-1})
2.50×10^{-5}	1.20×10^{-3}		1.56×10^{-1}
2.50×10^{-5}	1.80×10^{-3}	1.98×10^{-3}	2.26×10^{-1}
2.50×10^{-5}	2.40×10^{-3}		2.94×10^{-1}
2.50×10^{-5}	3.00×10^{-3}	3.30×10^{-3}	3.69×10^{-1}
2.50×10^{-5}	3.60×10^{-3}		4.36×10^{-1}

[a] Additionally, the reaction mixtures contained an equimolar amount of the corresponding CH-acid (**2**-H).

$$k_2 = (1.17 \pm 0.01) \times 10^2 \text{ M}^{-1} \text{ s}^{-1}$$
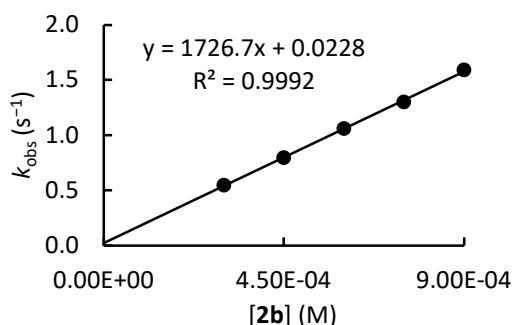
1a + **2b** in DMSO (stopped-flow method, detection at 320 nm) CG708

[**1a**]$_0$ (M)	[**2b**]$_0$ (M)	[18-c-6]$_0$ (M)	k_{obs} (s^{-1})
5.50×10^{-5}	3.00×10^{-4}		5.46×10^{-1}
5.50×10^{-5}	4.50×10^{-4}	4.95×10^{-4}	7.98×10^{-1}
5.50×10^{-5}	6.00×10^{-4}		1.06
5.50×10^{-5}	7.50×10^{-4}	8.25×10^{-4}	1.30
5.50×10^{-5}	9.00×10^{-4}		1.59

$$k_2 = (1.73 \pm 0.03) \times 10^3 \text{ M}^{-1} \text{ s}^{-1}$$

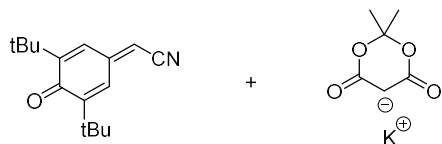**1a** + **2c** in DMSO (stopped-flow method, detection at 310 nm) CG541

$[\mathbf{1a}]_0$ (M)	$[\mathbf{2c}]_0^{[a]}$ (M)	$[18\text{-c-}6]_0$ (M)	k_{obs} (s^{-1})
2.18×10^{-5}	6.00×10^{-4}		5.79
2.18×10^{-5}	9.00×10^{-4}	9.90×10^{-4}	7.91
2.18×10^{-5}	1.20×10^{-3}		9.92
2.18×10^{-5}	1.50×10^{-3}	1.65×10^{-3}	11.9

[a] Additionally, the reaction mixtures contained an equimolar amount of the corresponding CH-acid (**2**-H).

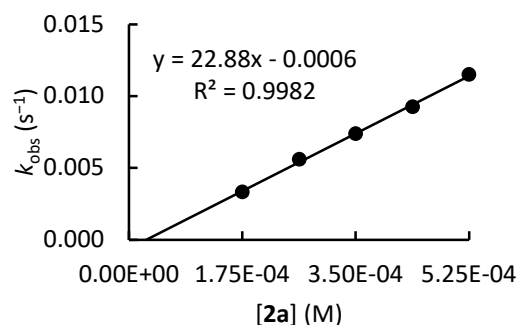$$k_2 = (6.78 \pm 0.08) \times 10^3 \text{ M}^{-1} \text{ s}^{-1}$$

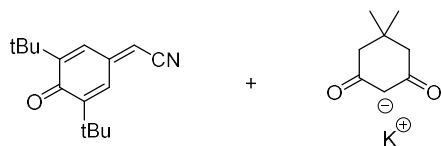**1c** + **2a** in DMSO (stopped-flow method, detection at 318 nm) CG081

$[\mathbf{1c}]_0$ (M)	$[\mathbf{2a}]_0^{[a]}$ (M)	$[18\text{-c-}6]_0$ (M)	k_{obs} (s^{-1})
1.90×10^{-5}	1.75×10^{-4}		3.32×10^{-3}
1.90×10^{-5}	2.63×10^{-4}	2.89×10^{-4}	5.59×10^{-3}
1.90×10^{-5}	3.50×10^{-4}		7.39×10^{-3}
1.90×10^{-5}	4.38×10^{-4}	4.82×10^{-4}	9.25×10^{-3}
1.90×10^{-5}	5.25×10^{-4}		1.15×10^{-2}

$$k_2 = (2.29 \pm 0.06) \times 10^1 \text{ M}^{-1} \text{ s}^{-1}$$

1c + **2c** in DMSO (stopped-flow method, detection at 318 nm) CG071

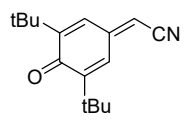| $[\mathbf{1c}]_0$ (M)	$[\mathbf{2c}]_0^{[a]}$ (M)	$[18\text{-c-}6]_0$ (M)	k_{obs} (s^{-1})
1.90×10^{-5}	1.75×10^{-4}		8.97×10^{-1}
1.90×10^{-5}	2.63×10^{-4}	2.89×10^{-4}	1.34
1.90×10^{-5}	3.50×10^{-4}		1.76
1.90×10^{-5}	4.38×10^{-4}	4.82×10^{-4}	2.19
1.90×10^{-5}	5.25×10^{-4}		2.65

[a] Additionally, the reaction mixtures contained an equimolar amount of the corresponding CH-acid (**2**-H).

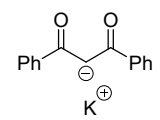$$k_2 = (4.98 \pm 0.04) \times 10^3 \text{ M}^{-1} \text{ s}^{-1}$$

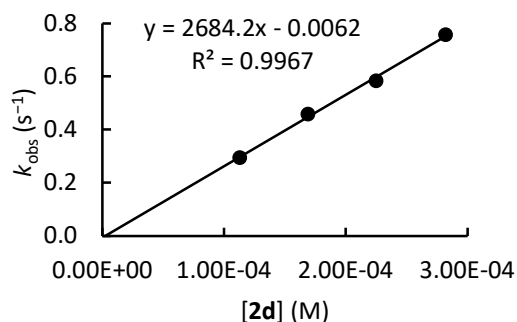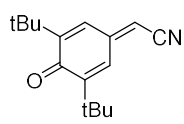**1c** + **2d** in DMSO (stopped-flow method, detection at 318 nm) CG083

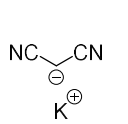| $[\mathbf{1c}]_0$ (M)	$[\mathbf{2d}]_0$ (M)	$[\text{18-c-6}]_0$ (M)	k_{obs} (s^{-1})
1.13×10^{-5}	1.13×10^{-4}		2.95×10^{-1}
1.13×10^{-5}	1.69×10^{-4}	1.86×10^{-4}	4.58×10^{-1}
1.13×10^{-5}	2.25×10^{-4}		5.83×10^{-1}
1.13×10^{-5}	2.82×10^{-4}	3.10×10^{-4}	7.57×10^{-1}

$$k_2 = (2.68 \pm 0.11) \times 10^3 \text{ M}^{-1}\text{ s}^{-1}$$

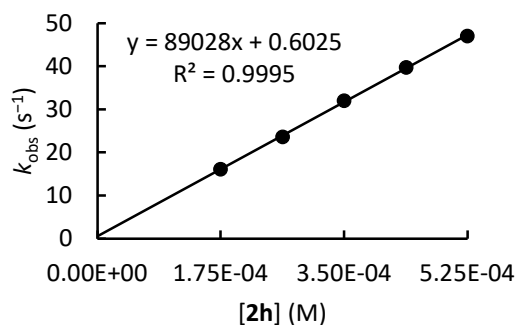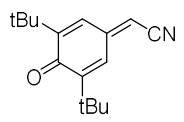**1c** + **2h** in DMSO (stopped-flow method, detection at 318 nm) CG074

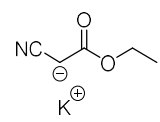| $[\mathbf{1c}]_0$ (M)	$[\mathbf{2h}]_0$ (M)	$[\text{18-c-6}]_0$ (M)	k_{obs} (s^{-1})
1.75×10^{-5}	1.75×10^{-4}		1.62×10^{1}
1.75×10^{-5}	2.63×10^{-4}	2.89×10^{-4}	2.37×10^{1}
1.75×10^{-5}	3.50×10^{-4}		3.21×10^{1}
1.75×10^{-5}	4.38×10^{-4}	4.82×10^{-4}	3.98×10^{1}
1.75×10^{-5}	5.25×10^{-4}		4.71×10^{1}

$$k_2 = (8.90 \pm 0.12) \times 10^4 \text{ M}^{-1}\text{ s}^{-1}$$

1c + **2i** in DMSO (stopped-flow method, detection at 318 nm) CG186
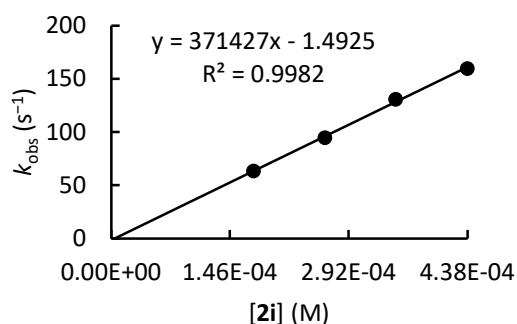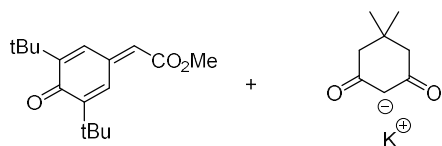

$[\mathbf{1c}]_0$ (M)	$[\mathbf{2i}]_0{}^{[a]}$ (M)	$[\text{18-c-6}]_0$ (M)	k_{obs} (s^{-1})
2.03×10^{-5}	1.75×10^{-4}		6.36×10^{1}
2.03×10^{-5}	2.63×10^{-4}	2.89×10^{-4}	9.48×10^{1}
2.03×10^{-5}	3.50×10^{-4}		1.31×10^{2}
2.03×10^{-5}	4.38×10^{-4}	4.82×10^{-4}	1.60×10^{2}

[a] Additionally, the reaction mixtures contained an equimolar amount of the corresponding CH-acid (**2**-H).

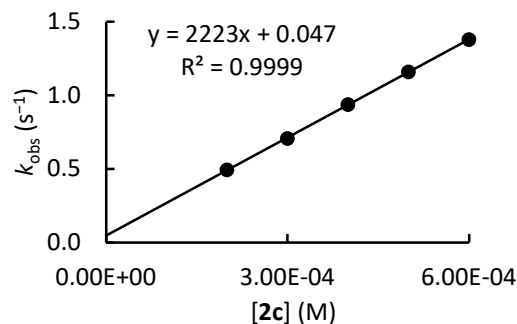$$k_2 = (3.71 \pm 0.11) \times 10^5 \text{ M}^{-1}\text{ s}^{-1}$$

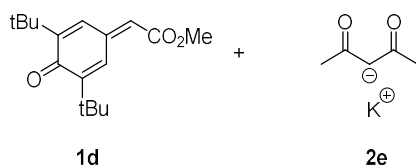**1d** + **2c** in DMSO (stopped-flow method, detection at 309 nm) CG534

$[1d]_0$ (M)	$[2c]_0^{[a]}$ (M)	$[18\text{-c-}6]_0$ (M)	k_{obs} (s^{-1})
2.22×10^{-5}	2.00×10^{-4}		4.95×10^{-1}
2.22×10^{-5}	3.00×10^{-4}	3.30×10^{-4}	7.07×10^{-1}
2.22×10^{-5}	4.00×10^{-4}		9.39×10^{-1}
2.22×10^{-5}	5.00×10^{-4}	5.50×10^{-4}	1.16
2.22×10^{-5}	6.00×10^{-4}		1.38

[a] Additionally, the reaction mixtures contained an equimolar amount of the corresponding CH-acid (**2**-H).

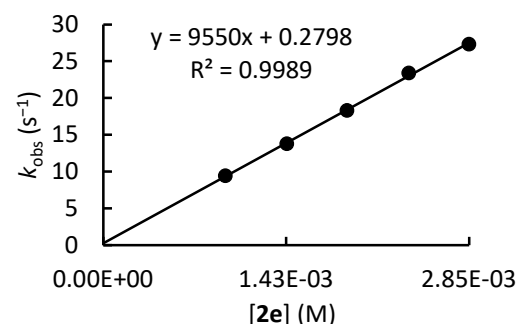$$k_2 = (2.22 \pm 0.02) \times 10^3 \text{ M}^{-1} \text{ s}^{-1}$$

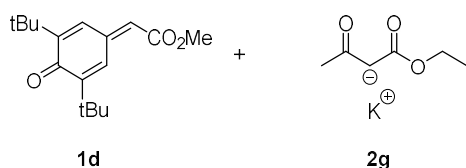**1d** + **2e** in DMSO (stopped-flow method, detection at 340 nm) CG533

$[1d]_0$ (M)	$[2e]_0^{[a]}$ (M)	$[18\text{-c-}6]_0$ (M)	k_{obs} (s^{-1})
9.78×10^{-5}	9.50×10^{-4}		9.42
9.78×10^{-5}	1.43×10^{-3}	1.57×10^{-3}	1.38×10^1
9.78×10^{-5}	1.90×10^{-3}		1.83×10^1
9.78×10^{-5}	2.38×10^{-3}	2.61×10^{-3}	2.34×10^1
9.78×10^{-5}	2.85×10^{-3}		2.73×10^1

[a] Additionally, the reaction mixtures contained an equimolar amount of the corresponding CH-acid (**2**-H).

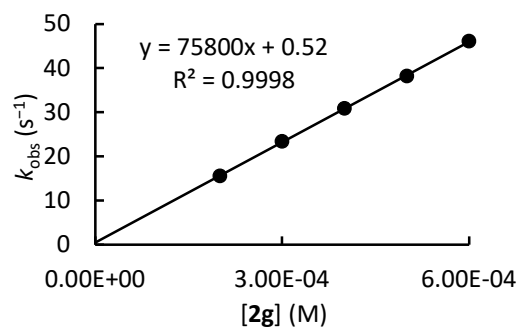$$k_2 = (9.55 \pm 0.18) \times 10^3 \text{ M}^{-1} \text{ s}^{-1}$$

1d + **2g** in DMSO (stopped-flow method, detection at 309 nm) CG531

$[1d]_0$ (M)	$[2g]_0^{[a]}$ (M)	$[18\text{-c-}6]_0$ (M)	k_{obs} (s^{-1})
1.54×10^{-5}	2.00×10^{-4}		1.56×10^1
1.54×10^{-5}	3.00×10^{-4}	3.30×10^{-4}	2.34×10^1
1.54×10^{-5}	4.00×10^{-4}		3.09×10^1
1.54×10^{-5}	5.00×10^{-4}	5.50×10^{-4}	3.82×10^1
1.54×10^{-5}	6.00×10^{-4}		4.61×10^1

[a] Additionally, the reaction mixtures contained an equimolar amount of the corresponding CH-acid (**2**-H).

$$k_2 = (7.58 \pm 0.05) \times 10^4 \text{ M}^{-1} \text{ s}^{-1}$$

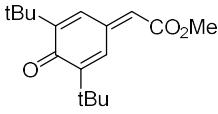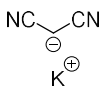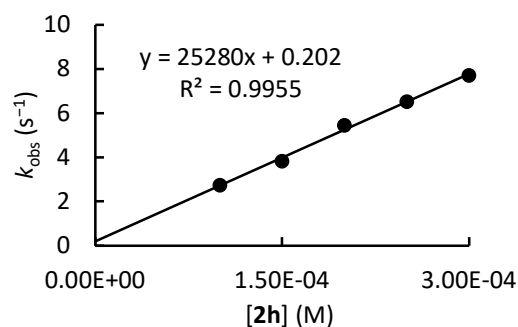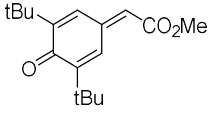**1d** + **2h** in DMSO (stopped-flow method, detection at 309 nm) CG530

[**1d**]$_0$ (M)	[**2h**]$_0$ (M)	[18-c-6]$_0$ (M)	k_{obs} (s^{-1})
1.70×10^{-5}	1.00×10^{-4}		2.75
1.70×10^{-5}	1.50×10^{-4}	1.65×10^{-4}	3.83
1.70×10^{-5}	2.00×10^{-4}		5.46
1.70×10^{-5}	2.50×10^{-4}	2.75×10^{-4}	6.53
1.70×10^{-5}	3.00×10^{-4}		7.72

$$k_2 = (2.53 \pm 0.10) \times 10^4 \text{ M}^{-1} \text{ s}^{-1}$$

1d + **2i** in DMSO (stopped-flow method, detection at 309 nm) CG532

[**1d**]$_0$ (M)	[**2i**]$_0$[a] (M)	[18-c-6]$_0$ (M)	k_{obs} (s^{-1})
1.75×10^{-5}	1.00×10^{-4}		1.06×10^1
1.75×10^{-5}	1.50×10^{-4}	1.65×10^{-4}	1.59×10^1
1.75×10^{-5}	2.00×10^{-4}		2.13×10^1
1.75×10^{-5}	2.50×10^{-4}	2.75×10^{-4}	2.60×10^1
1.75×10^{-5}	3.00×10^{-4}		3.16×10^1

[a] Additionally, the reaction mixtures contained an equimolar amount of the corresponding CH-acid (**2**-H).
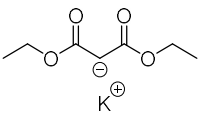
$$k_2 = (1.04 \pm 0.01) \times 10^5 \text{ M}^{-1} \text{ s}^{-1}$$

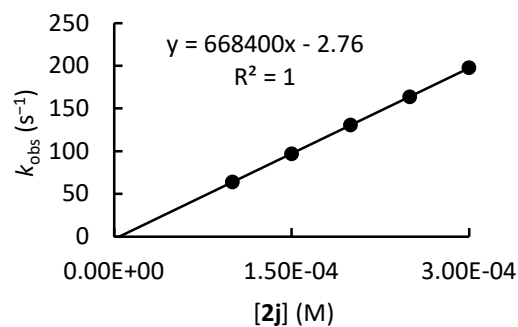**1d** + **2j** in DMSO (stopped-flow method, detection at 309 nm) CG523_1

[**1d**]$_0$ (M)	[**2j**]$_0$ (M)	[18-c-6]$_0$ (M)	k_{obs} (s^{-1})
1.38×10^{-5}	1.00×10^{-4}		6.42×10^1
1.38×10^{-5}	1.50×10^{-4}	1.65×10^{-4}	9.74×10^1
1.38×10^{-5}	2.00×10^{-4}		1.31×10^2
1.38×10^{-5}	2.50×10^{-4}	2.75×10^{-4}	1.64×10^2
1.38×10^{-5}	3.00×10^{-4}		1.98×10^2

$$k_2 = (6.68 \pm 0.02) \times 10^5 \text{ M}^{-1} \text{ s}^{-1}$$

1e+ **2c** in DMSO (stopped-flow method, detection at 310 nm) CG445_1

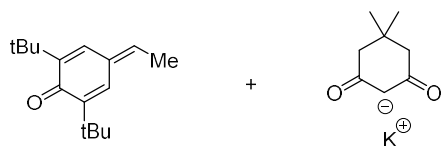| $[\textbf{1e}]_0$ (M)	$[\textbf{2c}]_0^{[a]}$ (M)	$[\text{18-c-6}]_0$ (M)	k_{obs} (s^{-1})
2.18×10^{-5}	3.00×10^{-4}		9.45×10^{-2}
2.18×10^{-5}	4.50×10^{-4}	4.95×10^{-4}	1.41×10^{-1}
2.18×10^{-5}	6.00×10^{-4}		1.79×10^{-1}
2.18×10^{-5}	7.50×10^{-4}	8.25×10^{-4}	2.22×10^{-1}
2.18×10^{-5}	9.00×10^{-4}		2.59×10^{-1}

[a] Additionally, the reaction mixtures contained an equimolar amount of the corresponding CH-acid (**2**-H).

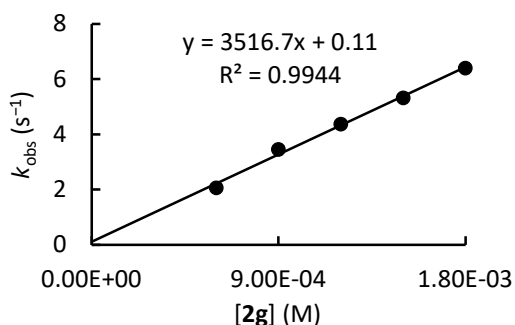$$k_2 = (2.73 \pm 0.06) \times 10^2 \text{ M}^{-1} \text{ s}^{-1}$$

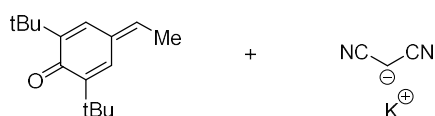**1e** + **2g** in DMSO (stopped-flow method, detection at 320 nm) CG444

$[\textbf{1e}]_0$ (M)	$[\textbf{2g}]_0$ (M)	$[\text{18-c-6}]_0$ (M)	k_{obs} (s^{-1})
1.97×10^{-5}	6.00×10^{-4}		2.07
1.97×10^{-5}	9.00×10^{-4}	9.90×10^{-4}	3.46
1.97×10^{-5}	1.20×10^{-3}		4.38
1.97×10^{-5}	1.50×10^{-3}	1.65×10^{-3}	5.33
1.97×10^{-5}	1.80×10^{-3}		6.41

$$k_2 = (3.52 \pm 0.15) \times 10^3 \text{ M}^{-1} \text{ s}^{-1}$$

1e + **2h** in DMSO (stopped-flow method, detection at 320 nm) CG441

$[\textbf{1e}]_0$ (M)	$[\textbf{2h}]_0$ (M)	$[\text{18-c-6}]_0$ (M)	k_{obs} (s^{-1})
1.97×10^{-5}	3.00×10^{-4}		1.59
1.97×10^{-5}	4.50×10^{-4}	4.95×10^{-4}	2.24
1.97×10^{-5}	6.00×10^{-4}		3.00
1.97×10^{-5}	7.50×10^{-4}	8.25×10^{-4}	3.70
1.97×10^{-5}	9.00×10^{-4}		4.27

$$k_2 = (4.55 \pm 0.12) \times 10^3 \text{ M}^{-1} \text{ s}^{-1}$$

1e + **2i** in DMSO (stopped-flow method, detection at 320 nm) CG443

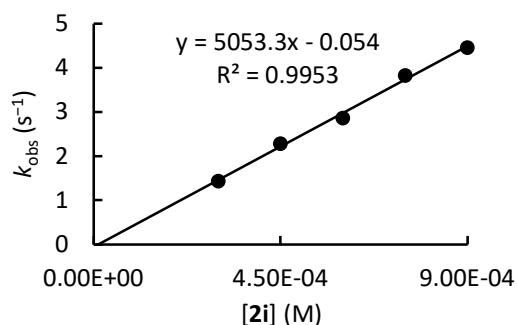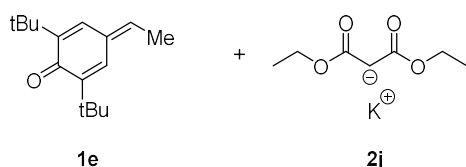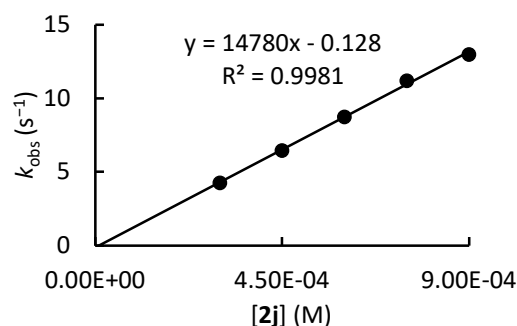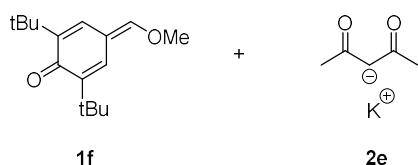| [**1e**]$_0$ (M)	[**2i**]$_0$ (M)	[18-c-6]$_0$ (M)	k_{obs} (s^{-1})
1.97×10^{-5}	3.00×10^{-4}		1.44
1.97×10^{-5}	4.50×10^{-4}	4.95×10^{-4}	2.29
1.97×10^{-5}	6.00×10^{-4}		2.87
1.97×10^{-5}	7.50×10^{-4}	8.25×10^{-4}	3.83
1.97×10^{-5}	9.00×10^{-4}		4.46

$$k_2 = (5.05 \pm 0.20) \times 10^3 \text{ M}^{-1}\text{ s}^{-1}$$

1e + **2j** in DMSO (stopped-flow method, detection at 320 nm) CG442

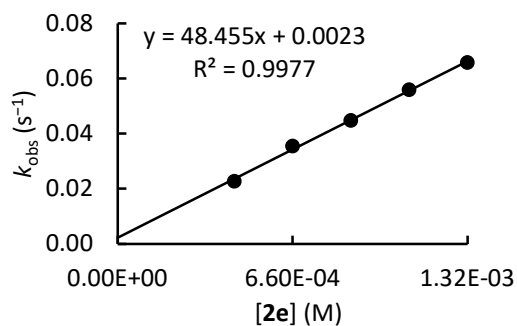| [**1e**]$_0$ (M)	[**2j**]$_0$ (M)	[18-c-6]$_0$ (M)	k_{obs} (s^{-1})
1.97×10^{-5}	3.00×10^{-4}		4.28
1.97×10^{-5}	4.50×10^{-4}	4.95×10^{-4}	6.47
1.97×10^{-5}	6.00×10^{-4}		8.75
1.97×10^{-5}	7.50×10^{-4}	8.25×10^{-4}	1.12×10^1
1.97×10^{-5}	9.00×10^{-4}		1.30×10^1

$$k_2 = (1.48 \pm 0.04) \times 10^4 \text{ M}^{-1}\text{ s}^{-1}$$

1f + **2e** in DMSO (stopped-flow method, detection at 345 nm) CG529

[**1f**]$_0$ (M)	[**2e**]$_0^{[a]}$ (M)	[18-c-6]$_0$ (M)	k_{obs} (s^{-1})
1.80×10^{-5}	4.40×10^{-4}		2.27×10^{-2}
1.80×10^{-5}	6.60×10^{-4}	7.26×10^{-4}	3.55×10^{-2}
1.80×10^{-5}	8.80×10^{-4}		4.48×10^{-2}
1.80×10^{-5}	1.10×10^{-3}	1.21×10^{-3}	5.59×10^{-2}
1.80×10^{-5}	1.32×10^{-3}		6.58×10^{-2}

[a] Additionally, the reaction mixtures contained an equimolar amount of the corresponding CH-acid (**2**-H).

$$k_2 = (4.85 \pm 0.14) \times 10^1 \text{ M}^{-1}\text{ s}^{-1}$$

1f + **2g** in DMSO (stopped-flow method, detection at 345 nm) CG528

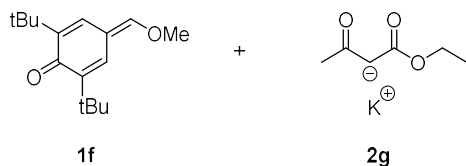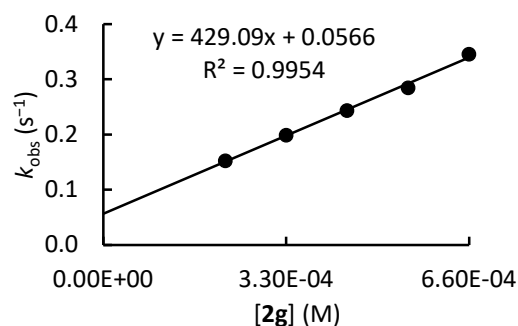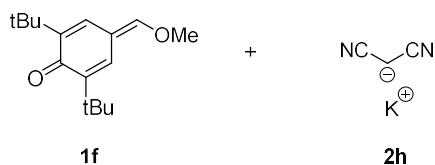| [**1f**]$_0$ (M)	[**2g**]$_0$ (M)	[18-c-6]$_0$ (M)	k_{obs} (s^{-1})
1.97×10^{-5}	2.20×10^{-4}		1.53×10^{-1}
1.97×10^{-5}	3.30×10^{-4}	3.63×10^{-4}	1.99×10^{-1}
1.97×10^{-5}	4.40×10^{-4}		2.44×10^{-1}
1.97×10^{-5}	5.50×10^{-4}	6.05×10^{-4}	2.85×10^{-1}
1.97×10^{-5}	6.60×10^{-4}		3.46×10^{-1}

$k_2 = (4.29 \pm 0.17) \times 10^2$ M^{-1} s^{-1}

1f + **2h** in DMSO (stopped-flow method, detection at 345 nm) CG527

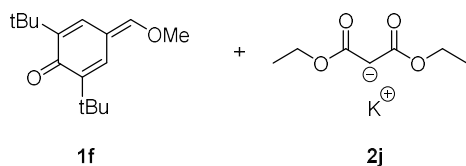| [**1f**]$_0$ (M)	[**2h**]$_0$ (M)	[18-c-6]$_0$ (M)	k_{obs} (s^{-1})
2.04×10^{-5}	2.20×10^{-4}		2.28×10^{-1}
2.04×10^{-5}	3.30×10^{-4}	3.63×10^{-4}	3.45×10^{-1}
2.04×10^{-5}	4.40×10^{-4}		4.49×10^{-1}
2.04×10^{-5}	5.50×10^{-4}	6.05×10^{-4}	5.77×10^{-1}
2.04×10^{-5}	6.60×10^{-4}		6.86×10^{-1}

$k_2 = (1.04 \pm 0.02) \times 10^3$ M^{-1} s^{-1}

1f + **2j** in DMSO (stopped-flow method, detection at 345 nm) CG526

[**1f**]$_0$ (M)	[**2j**]$_0$ (M)	[18-c-6]$_0$ (M)	k_{obs} (s^{-1})
2.08×10^{-5}	2.20×10^{-4}		4.31×10^{-1}
2.08×10^{-5}	3.30×10^{-4}	3.63×10^{-4}	6.72×10^{-1}
2.08×10^{-5}	4.40×10^{-4}		8.55×10^{-1}
2.08×10^{-5}	5.50×10^{-4}	6.05×10^{-4}	1.09
2.08×10^{-5}	6.60×10^{-4}		1.26

$k_2 = (1.89 \pm 0.06) \times 10^3$ M^{-1} s^{-1}

_____

1g + 2c in DMSO (conventional photometry, detection at 359 nm) CG116

$[1g]_0$ (M)	$[2c]_0^{[a]}$ (M)	$[18\text{-}c\text{-}6]_0$ (M)	k_{obs} (s^{-1})
3.82×10^{-5}	3.80×10^{-4}		1.15×10^{-3}
3.65×10^{-5}	5.50×10^{-4}	6.04×10^{-4}	1.51×10^{-3}
3.68×10^{-5}	7.40×10^{-4}		2.06×10^{-3}
3.58×10^{-5}	9.00×10^{-4}		2.50×10^{-3}

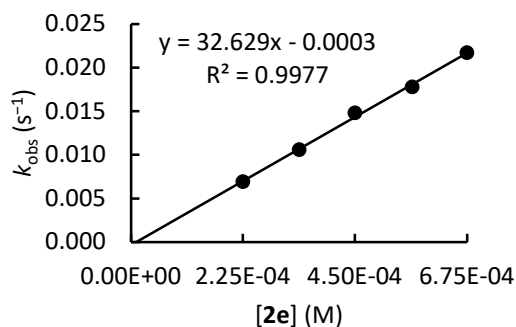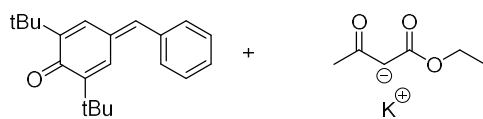[a] Additionally, the reaction mixtures contained an equimolar amount of the corresponding CH-acid (**2**-H).

$$k_2 = (2.63 \pm 0.12)\ M^{-1}\ s^{-1}$$

1g + 2e in DMSO (stopped-flow method, detection at 359 nm) CG115

$[1g]_0$ (M)	$[2e]_0^{[a]}$ (M)	$[18\text{-}c\text{-}6]_0$ (M)	k_{obs} (s^{-1})
2.20×10^{-5}	2.25×10^{-4}		6.91×10^{-3}
2.20×10^{-5}	3.38×10^{-4}	3.72×10^{-4}	1.06×10^{-2}
2.20×10^{-5}	4.50×10^{-4}		1.48×10^{-2}
2.20×10^{-5}	5.65×10^{-4}	6.20×10^{-4}	1.78×10^{-2}
2.20×10^{-5}	6.75×10^{-4}		2.17×10^{-2}

[a] Additionally, the reaction mixtures contained an equimolar amount of the corresponding CH-acid (**2**-H).
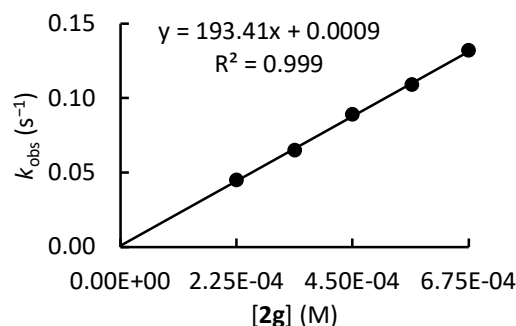
$$k_2 = (3.26 \pm 0.09) \times 10^1\ M^{-1}\ s^{-1}$$

1g + 2g in DMSO (stopped-flow method, detection at 359 nm) CG113

$[1g]_0$ (M)	$[2g]_0^{[a]}$ (M)	$[18\text{-}c\text{-}6]_0$ (M)	k_{obs} (s^{-1})
1.54×10^{-5}	2.25×10^{-4}		4.50×10^{-2}
1.54×10^{-5}	3.38×10^{-4}	3.72×10^{-4}	6.54×10^{-2}
1.54×10^{-5}	4.50×10^{-4}		8.98×10^{-2}
1.54×10^{-5}	5.65×10^{-4}	6.20×10^{-4}	1.09×10^{-1}
1.54×10^{-5}	6.75×10^{-4}		1.32×10^{-1}

[a] Additionally, the reaction mixtures contained an equimolar amount of the corresponding CH-acid (**2**-H).

$$k_2 = (1.93 \pm 0.04) \times 10^2\ M^{-1}\ s^{-1}$$

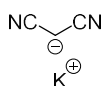**1g** + **2h** in DMSO (stopped-flow method, detection at 359 nm) CG109

[**1g**]$_0$ (M)	[**2h**]$_0^{[a]}$ (M)	[18-c-6]$_0$ (M)	k_{obs} (s^{-1})
1.79×10^{-5}	2.25×10^{-4}		5.65×10^{-2}
1.79×10^{-5}	3.38×10^{-4}	3.72×10^{-4}	7.99×10^{-2}
1.79×10^{-5}	4.50×10^{-4}		1.13×10^{-1}
1.79×10^{-5}	6.75×10^{-4}		1.76×10^{-1}

[a] Additionally, the reaction mixtures contained an equimolar amount of the corresponding CH-acid (**2**-H).

$$k_2 = (2.70 \pm 0.11) \times 10^2 \text{ M}^{-1} \text{ s}^{-1}$$

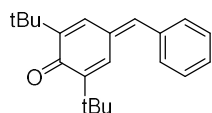**1g** + **2i** in DMSO (stopped-flow method, detection at 359 nm) CG111

[**1g**]$_0$ (M)	[**2i**]$_0^{[a]}$ (M)	[18-c-6]$_0$ (M)	k_{obs} (s^{-1})
1.82×10^{-5}	2.25×10^{-4}		1.24×10^{-1}
1.82×10^{-5}	3.38×10^{-4}	3.72×10^{-4}	1.80×10^{-1}
1.82×10^{-5}	4.50×10^{-4}		2.49×10^{-1}
1.82×10^{-5}	5.65×10^{-4}	6.20×10^{-4}	3.01×10^{-1}
1.82×10^{-5}	6.75×10^{-4}		3.77×10^{-1}

[a] Additionally, the reaction mixtures contained an equimolar amount of the corresponding CH-acid (**2**-H).

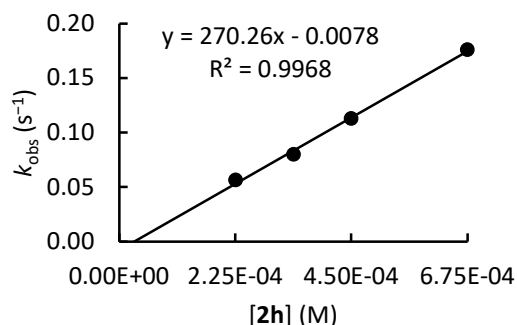$$k_2 = (5.56 \pm 0.20) \times 10^2 \text{ M}^{-1} \text{ s}^{-1}$$

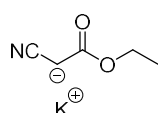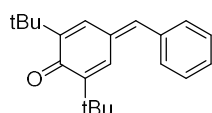**1g** + **2j** in DMSO (stopped-flow method, detection at 359 nm) CG112

[**1g**]$_0$ (M)	[**2j**]$_0^{[a]}$ (M)	[18-c-6]$_0$ (M)	k_{obs} (s^{-1})
1.73×10^{-5}	2.25×10^{-4}		3.51×10^{-1}
1.73×10^{-5}	3.38×10^{-4}	3.72×10^{-4}	4.87×10^{-1}
1.73×10^{-5}	4.50×10^{-4}		6.62×10^{-1}
1.73×10^{-5}	5.65×10^{-4}	6.20×10^{-4}	8.03×10^{-1}
1.73×10^{-5}	6.75×10^{-4}		9.67×10^{-1}

[a] Additionally, the reaction mixtures contained an equimolar amount of the corresponding CH-acid (**2**-H).

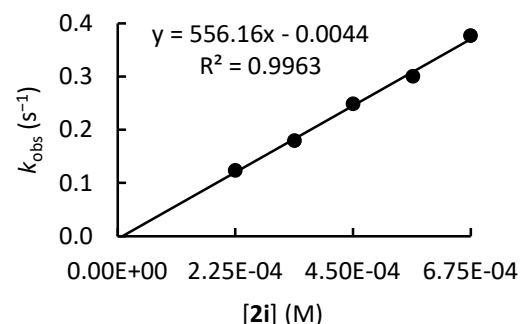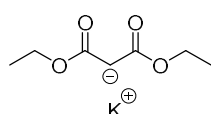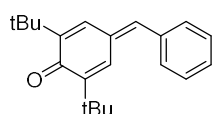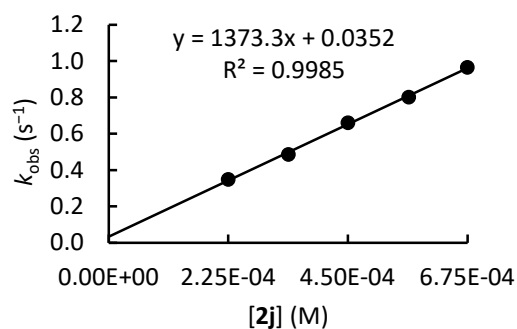$$k_2 = (1.37 \pm 0.03) \times 10^3 \text{ M}^{-1} \text{ s}^{-1}$$

3.2.6. Single Crystal X-Ray Structure Determination

Diethyl 5,7-di-*tert*-butyl-6-oxospiro[2.5]octa-4,7-diene-1,1-dicarboxylate (3)

(br006/CCDC 2431023, CG536_1F20-29)

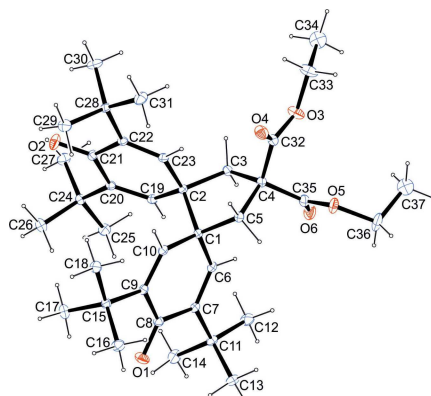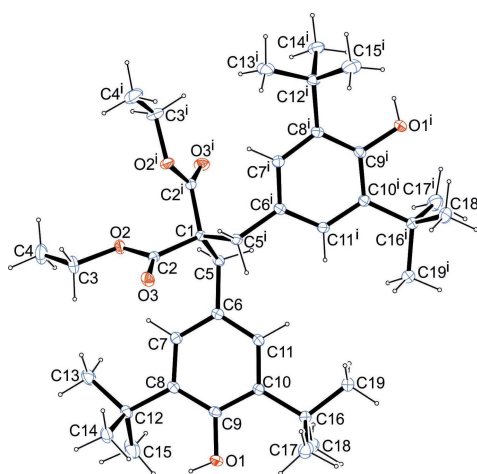|	
net formula	$C_{22}H_{32}O_5$
M_r/g mol^{-1}	376.47
crystal size/mm	0.180 × 0.140 × 0.090
T/K	100.00(10)
radiation	CuKα
diffractometer	'XtaLAB Synergy R, HyPix-Arc 150'
crystal system	monoclinic
space group	'P 1 21/c 1'
a/Å	15.68849(14)
b/Å	10.57193(8)
c/Å	12.90346(12)
α/°	90
β/°	99.1414(8)
γ/°	90
V/Å^3	2112.96(3)
Z	4
calc. density/g cm^{-3}	1.183
μ/mm^{-1}	0.666
absorption correction	multi-scan
transmission factor range	0.86773–1.00000
refls. measured	22888
R_{int}	0.0141
mean $\sigma(I)/I$	0.0111
θ range	2.853–75.555
observed refls.	4012
x, y (weighting scheme)	0.0410, 0.6133
hydrogen refinement	constr
Flack parameter	?
refls in refinement	4325
parameters	253
restraints	0
$R(F_{obs})$	0.0322
$R_w(F^2)$	0.0853
S	1.050
shift/error$_{max}$	0.001
max electron density/e Å^{-3}	0.294
min electron density/e Å^{-3}	−0.171

Diethyl 2,4,9,11-tetra-*tert*-butyl-3,10-dioxodispiro[5.0.5^7.3^6]pentadeca-1,4,8,11-tetraene-14,14-dicarboxylate (4)
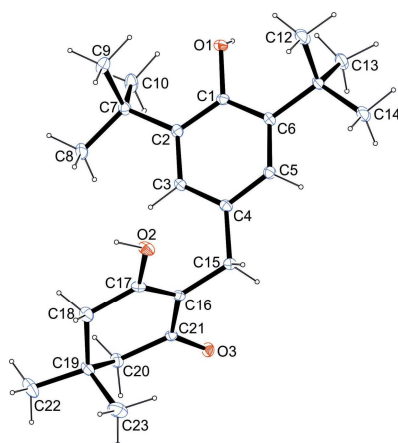

(br007/CCDC 2431024, CG536_1F10-16)

net formula	$C_{37}H_{54}O_6$
M_r/g mol^{-1}	594.80
crystal size/mm	0.150 × 0.120 × 0.080
T/K	100(2)
radiation	CuKα
diffractometer	'XtaLAB Synergy R, HyPix-Arc 150'
crystal system	monoclinic
space group	'P 2$_1$/c'
a/Å	9.63184(5)
b/Å	19.83515(9)
c/Å	18.85208(9)
α/°	90
β/°	90.3018(4)
γ/°	90
V/Å^3	3601.62(3)
Z	4
calc. density/g cm^{-3}	1.097
μ/mm^{-1}	0.576
absorption correction	multi-scan
transmission factor range	0.88082–1.00000
refls. measured	43861
R_{int}	0.0151
mean σ(I)/I	0.0082
θ range	2.2274–75.6685
observed refls.	7005
x, y (weighting scheme)	0.0766, 1.9217
hydrogen refinement	constr
Flack parameter	?
refls in refinement	7441
parameters	411
restraints	0
$R(F_{obs})$	0.0553
$R_w(F^2)$	0.1539
S	1.076
shift/error$_{max}$	0.001
max electron density/e Å^{-3}	0.590
min electron density/e Å^{-3}	−0.624

The disorder of two side chains has been described by split models. Split atoms have been refined partly isotropically (anisotropic refinement create new split suggestion).

_____

Diethyl 2,2-bis(3,5-di-*tert*-butyl-4-hydroxybenzyl)malonate (6)
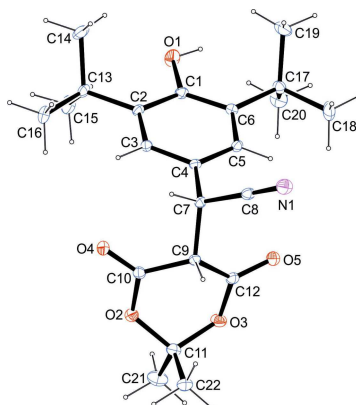

(bv303/CCDC 2431025, CG536_4_1)

net formula	$C_{37}H_{56}O_6$
M_r/g mol^{-1}	596.81
crystal size/mm	0.160 × 0.150 × 0.120
T/K	173.(2)
radiation	MoKα
diffractometer	'Bruker D8 Venture TXS'
crystal system	monoclinic
space group	'C 1 2/c 1'
a/Å	19.8525(4)
b/Å	13.4348(3)
c/Å	14.2279(3)
α/°	90
β/°	110.8130(10)
γ/°	90
V/Å^3	3547.16(13)
Z	4
calc. density/g cm^{-3}	1.118
μ/mm^{-1}	0.074
absorption correction	Multi-Scan
transmission factor range	0.96–0.99
refls. measured	30935
R_{int}	0.0392
mean $\sigma(I)/I$	0.0237
θ range	3.032–27.101
observed refls.	3233
x, y (weighting scheme)	0.0447, 2.9421
hydrogen refinement	mixed
Flack parameter	?
refls in refinement	3909
parameters	206
restraints	0
$R(F_{obs})$	0.0418
$R_w(F^2)$	0.1125
S	1.045
shift/error$_{max}$	0.001
max electron density/e Å^{-3}	0.256
min electron density/e Å^{-3}	−0.183

2-(3,5-Di-*tert*-butyl-4-hydroxybenzyl)-3-hydroxy-5,5-dimethylcyclohex-2-en-1-one (9)

(cv106/CCDC 2431026, CG538_2)

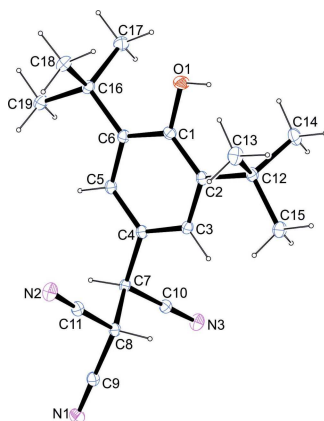|	
net formula	$C_{23}H_{34}O_3$
M_r/g mol^{-1}	358.50
crystal size/mm	0.110 × 0.020 × 0.020
T/K	173.(2)
radiation	MoKα
diffractometer	'Bruker D8 Venture TXS'
crystal system	orthorhombic
space group	'P n a 21'
a/Å	13.3840(8)
b/Å	17.7258(11)
c/Å	8.9518(5)
α/°	90
β/°	90
γ/°	90
V/Å^3	2123.7(2)
Z	4
calc. density/g cm^{-3}	1.121
μ/mm^{-1}	0.072
absorption correction	Multi-Scan
transmission factor range	0.96–1.00
refls. measured	34319
R_{int}	0.0734
mean $\sigma(I)/I$	0.0388
θ range	3.044–25.350
observed refls.	3599
x, y (weighting scheme)	0.0411, 0.3076
hydrogen refinement	mixed
Flack parameter	0.5
refls in refinement	3839
parameters	251
restraints	1
$R(F_{obs})$	0.0361
$R_w(F^2)$	0.0860
S	1.086
shift/error$_{max}$	0.001
max electron density/e Å^{-3}	0.134
min electron density/e Å^{-3}	−0.149

The structure has been refined as a 2-component perfect inversion twin.

2-(3,5-di-tert-butyl-4-hydroxyphenyl)-2-(2,2-dimethyl-4,6-dioxo-1,3-dioxan-5-yl)acetonitrile (12)
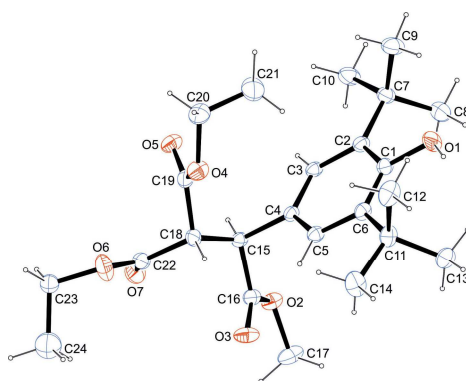

(dv077/CCDC 2432306, CG651_1)

net formula	$C_{22}H_{29}NO_5$
M_r/g mol^{-1}	387.46
crystal size/mm	0.110 × 0.080 × 0.040
T/K	173.(2)
radiation	MoKα
diffractometer	'Bruker D8 Venture TXS'
crystal system	triclinic
space group	'P -1'
a/Å	9.9324(8)
b/Å	10.1092(9)
c/Å	11.4597(9)
α/°	70.997(3)
β/°	74.677(3)
γ/°	89.897(3)
V/Å^3	1044.78(15)
Z	2
calc. density/g cm^{-3}	1.232
μ/mm^{-1}	0.087
absorption correction	Multi-Scan
transmission factor range	0.92–1.00
refls. measured	18053
R_{int}	0.0471
mean σ(I)/I	0.0437
θ range	3.275–27.483
observed refls.	4014
x, y (weighting scheme)	0.0383, 0.7441
hydrogen refinement	constr
Flack parameter	?
refls in refinement	4745
parameters	262
restraints	3
$R(F_{obs})$	0.0501
$R_w(F^2)$	0.1276
S	1.053
shift/error$_{max}$	0.001
max electron density/e Å^{-3}	0.376
min electron density/e Å^{-3}	−0.226

Free refinement of the H1 leads to a too short O1-H1 bond.

_____

2-(3,5-Di-*tert*-butyl-4-hydroxyphenyl)ethane-1,1,2-tricarbonitrile (13)

(br015/CCDC 2431027, CG553)

net formula	$C_{19}H_{23}N_3O$
M_r/g mol^{-1}	309.40
crystal size/mm	0.16 × 0.09 × 0.08
T/K	100(2)
radiation	CuKα
diffractometer	'XtaLAB Synergy R, HyPix-Arc 150'
crystal system	triclinic
space group	'P -1'
a/Å	5.94490(10)
b/Å	9.27980(10)
c/Å	16.32000(10)
α/°	93.5500(10)
β/°	95.9450(10)
γ/°	93.8890(10)
V/Å^3	891.270(19)
Z	2
calc. density/g cm^{-3}	1.153
μ/mm^{-1}	0.571
absorption correction	multi-scan
transmission factor range	0.96944–1.00000
refls. measured	30400
R_{int}	0.0227
mean σ(I)/I	0.0130
θ range	2.729–75.325
observed refls.	3258
x, y (weighting scheme)	0.0453, 0.1892
hydrogen refinement	constr
Flack parameter	_refine_ls_abs_structure_Flack
refls in refinement	3578
parameters	216
restraints	2
$R(F_{obs})$	0.0336
$R_w(F^2)$	0.0931
S	1.095
shift/error$_{max}$	0.001
max electron density/e Å^{-3}	0.242
min electron density/e Å^{-3}	−0.160

1,1-Diethyl 2-methyl 2-(3,5-di-*tert*-butyl-4-hydroxyphenyl)ethane-1,1,2-tricarboxylate (14)

(cv127/CCDC 2431028, CG524)

net formula	$C_{24}H_{36}O_7$
M_r/g mol^{-1}	436.53
crystal size/mm	0.130 × 0.090 × 0.070
T/K	173.(2)
radiation	MoKα
diffractometer	'Bruker D8 Venture TXS'
crystal system	triclinic
space group	'P -1'
a/Å	13.2864(6)
b/Å	15.0339(7)
c/Å	15.1617(7)
$α$/°	67.8270(10)
$β$/°	65.0750(10)
$γ$/°	85.373(2)
V/Å^3	2532.2(2)
Z	4
calc. density/g cm^{-3}	1.145
$μ$/mm^{-1}	0.083
absorption correction	Multi-Scan
transmission factor range	0.94–0.99
refls. measured	41669
R_{int}	0.0374
mean σ(I)/I	0.0318
θ range	2.574–25.350
observed refls.	6857
x, y (weighting scheme)	0.0354, 4.2812
hydrogen refinement	constr
Flack parameter	?
refls in refinement	9251
parameters	584
restraints	4
$R(F_{obs})$	0.0776
$R_w(F^2)$	0.1834
S	1.087
shift/error$_{max}$	0.001
max electron density/e Å^{-3}	0.445
min electron density/e Å^{-3}	−0.571

The asymmetric unit contains two formula units, whereas only one of the molecules are shown. One of the molecules shows only a disorder of an ethyl group. The other molecule is almost completely disordered. The disorders have been described by split models. Disordered atoms have been refined isotropically.

76

3.3. References

[1]   L. K. Dyall, S. Winstein, *J. Am. Chem. Soc.* **1972**, *94*, 2196.

[2]   P. Nesvadba, *Synth. Commun.* **2000**, *30*, 2825.

[3]   A. Ali, R. Jajoria, H. K. Harit, R. P. Singh, *J. Org. Chem.* **2022**, *87*, 5213.

[4]   M. Inagaki, N. Haga, M. Kobayashi, N. Ohta, S. Kamata, T. Tsuri, *J. Org. Chem.* **2002**, *67*, 125.

[5]   S. Evans, P. Nesvabda, S. Allenbach (Ciba-Geigy AG), EP 744392, **1996**.

[6]   V. Reddy, R. V. Anand, *Org. Lett.* **2015**, *17*, 3390.

Chapter 4. Electrophilic Reactivities of δ-Disubstituted *para*-Quinone Methides – A Limitation to the Mayr-Patz Equation
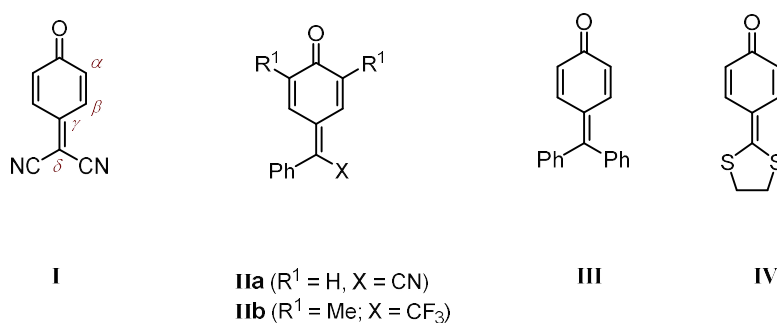
Contributions

All experimental work was performed by Christoph Gross and Jannik Roth under the supervision of Christoph Gross. Dr. Peter Mayer performed the X-ray crystallographic analysis and visualization.

4.1. Introduction

Simple *para*-quinone methides (*p*QMs) that carry no substituents next to the carbonyl oxygen are well-known transient species.[1] They readily undergo polymerization and cannot be isolated under standard conditions.[2] In order to suppress decomposition via polymerization, it is a common strategy to introduce bulky substituents, such as *tert*-butyl groups at the 2,6-positions.[3] This structural modification affords stable and isolable *para*-quinone methides, which are frequently used in diverse synthetic transformations.[4]

An alternative strategy involves the introduction of electron-withdrawing substituents, such as nitrile, ester or acyl groups, and electron-donating substituents, such as alkylthio, as well as ligands like phenyl groups at the exocyclic carbon-carbon double bond *(δ-position)* to mitigate its polymerizability.[5] This approach was successfully applied to the highly reactive and transient quinone dimethane[6] and can also be used on *para*-quinone methides without having bulky substituents at the 2,6-positions. For example (Scheme 1), *p*QMs such as 7,7-di(cyano)benzoquinone methide **I** [7], 7-cyano-7-(phenyl) benzoquinone methide **IIa**[8], 2,6-dimethyl-7-trifluoromethyl-7-(phenyl)benzoquinone methide **IIb**[9], 7,7-di(phenyl)benzoquinone methide **III**[10], 4-(1′,3′-dithiolan-2′-ylidene)-2,5-cyclohexadien-1-one **IV**[11] and further derivatives have been successfully synthesized and isolated in crystalline form.[12]

Scheme 1. Overview of stable and isolable *para*-quinone methides with electron-withdrawing and/or electron-donating substituents at the quinone methide's exocyclic double bond.

Addition reactions to these *δ*-disubstituted *p*QMs have been investigated in several cases. Among others, J. A. HYATT reported about reactions of *p*QM **I** with phenol, *N,N*-dimethylaniline, a [4+2] cycloaddition with cyclopentadiene and the formal addition of hydrogen.[7] The group of L. LIU explored the asymmetric synthesis of triarylmethane derivatives from *p*QMs **IIa** and **IIb**, using heteroarenes, phenols and *β*-ketoesters to construct all-carbon quaternary stereocenters, which are valuable motifs for medicinal applications.[9, 13, 14, 15] They further analyzed addition reactions of *p*QM **IIa** with anilines and secondary amines.[16]

Despite their increasing use as precursors for various transformations in organic synthesis, detailed information about their electrophilic reactivities is still lacking.

This chapter describes how these *δ*-disubstituted *p*QMs in particular *p*QMs **IIa** and **IIb** react with anionic acceptor-substituted nucleophiles. Known reactivity parameters N (and s_N) of carbanionic nucleophiles shall be used to determine the electrophilic reactivity parameters E of the *p*QMs in DMSO by applying the Mayr-Patz equation lg $k_2 = s_N(N + E)$ (Figure 1).[17]
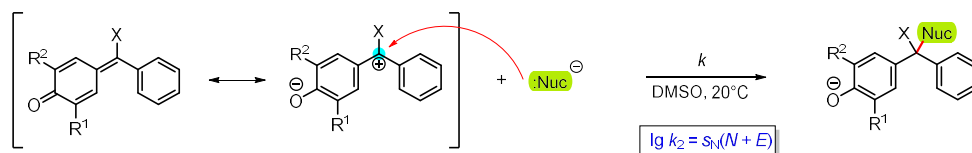
Figure 1. Carbon-carbon bond-forming reaction between δ-disubstituted *p*QMs and carbanionic reference nucleophiles.

Substituents on the exocyclic double bond as well as on the phenyl ring remote to the electrophilic center will be systematically varied to investigate electronic and steric effects. Finally, the electrophilic reactivities will be compared with those of previously characterized δ-aryl *p*QMs, and the validity of the derived electrophilicity parameters will be further evaluated through reactions and kinetic investigations with heteroatom-centered nucleophiles such as primary amines and thiophenolates (Figure 2).
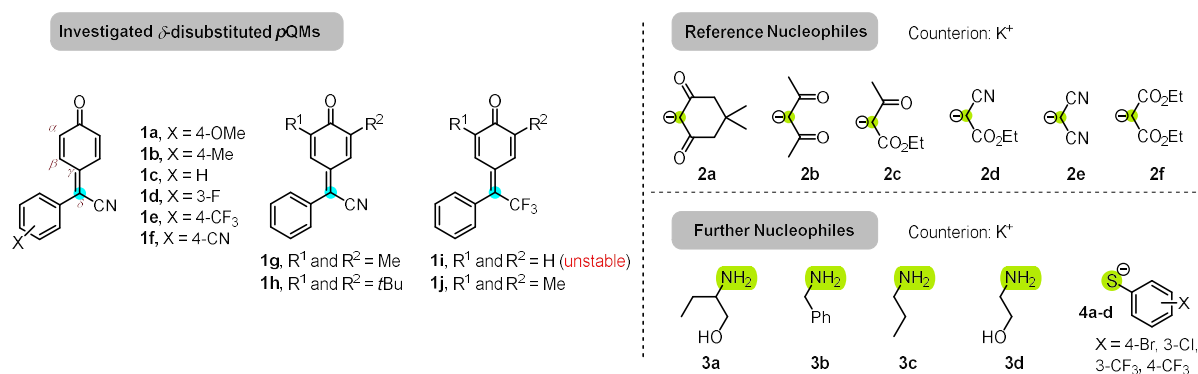

Figure 2. Overview of investigated δ-disubstituted *p*QMs (**1a-1j**), c-centered reference nucleophiles and heteroatom nucleophiles used.
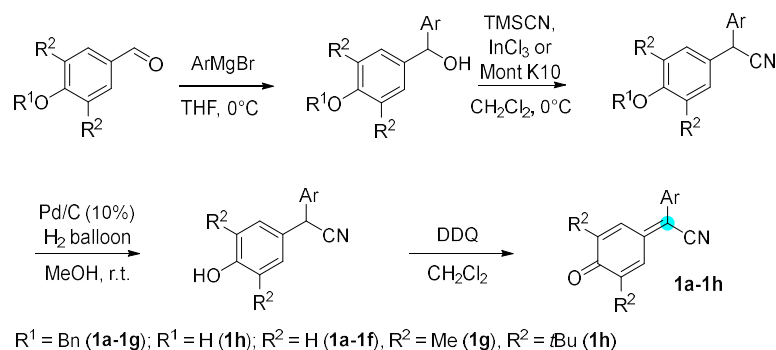
4.2. Results and discussion

Preparation of δ-disubstituted *p*QMs.

The δ-cyano δ-aryl substituted *p*QMs (CN *p*QMs) **1a-1e** and **1g** were prepared according to a four-step synthetic procedure as described by Liu and co-workers (Figure 3A).[14] The remaining CN *p*QMs **1f** and **1h** were synthesized in a similar manner to the previously described method, but with additional modifications (see experimental part for detailed information, section 4.4.3).

δ-Trifluoromethyl-δ-aryl disubstituted *p*QMs (CF$_3$ *p*QMs) are formally accessed by TsOH catalyzed condensation of the α-(trifluoromethyl)benzyl alcohol with the corresponding phenol as described in literature.[9] Despite repeated trials and optimized reaction conditions, this process did not lead to the formation of the desired CF$_3$ *p*QMs. Instead, the CF$_3$ *p*QMs **1i-1j** were obtained by a four-step synthesis starting from a Grignard reaction of the 4-bromoanisole derivatives with α,α,α-trifluoro acetophenone (Step **A**) This was followed by deoxygenation of the tertiary alcohol (Step **B**) and a BBr$_3$-catalysed deprotection of the anisyl residue (Step **C**). Finally, the phenols obtained were oxidized to the CF$_3$ *p*QMs by DDQ in dichloromethane (Step **D**) (Figure 3B). CF$_3$ *p*QM **1i** could be isolated in small quantities, but decomposed when it was dissolved in DMSO. Further information on the synthesis and analytic data of CF$_3$ *p*QMs are summarized in the experimental part, section 4.4.4.
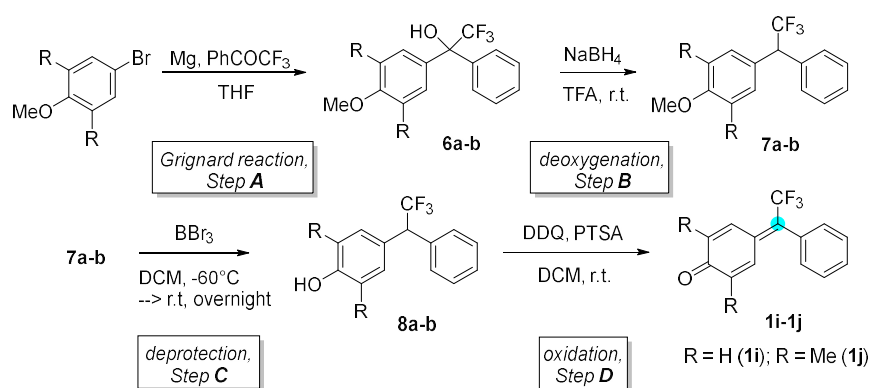
Figure 3. Overview of synthetic procedures to access (A) the CN *p*QMs **1a-1h** and (B) the CF$_3$ *p*QMs **1i-1j**. For the synthesis of CN *p*QM **1f** the Mont K10 was used, while CN *p*QM **1h** was synthesized without the deprotection step.

Product studies of *p*QMs with carbanionic reference nucleophiles.

Prior to the kinetic measurements, product studies were conducted to determine where the nucleophile attacks the electrophile and how many new σ-bonds are involved in the product formation. This information is relevant for the subsequent kinetic studies as the Mayr-Patz equation is only applicable when the rate-determining step involves the formation of a single new σ-bond. Ensuring that this criterion is met allows for a meaningful interpretation of the reactivity parameters derived from kinetic data.

The reactions between *p*QMs **1** and carbanions **2** (up to 1.3 equiv.) were carried out in dry DMSO at room temperature (+23°C) and followed by an aqueous work-up in most cases (Figure 4). The products were characterized by spectroscopic methods (NMR, MS, IR) and isolated after purification (flash chromatography) in moderate to good yields of 31-95% (Figure 4). Although an ambident reactivity for *δ*-disubstituted *p*QMs seems to be possible due to the electron-withdrawing CN- and CF$_3$-substituents that enable nucleophilic attack at the carbonyl carbon or at the cyclohexadiene moiety, the exocyclic double bond of the *p*QMs was always identified as the most electrophilic position based on the observed reaction products (for further information on individual product synthesis, see the experimental part, section 4.4.5).

9af (57%); X = CN, R^1 = H, R^2 = 4-OMe
9ef (54%); X = CN, R^1 = H, R^2 = 4-CF$_3$
9hf (56%); X = CN, R^1 = tBu, R^2 = H
9jf (90%); X = CF$_3$, R^1 = Me, R^2 = H

9ad (81%); X = CN, R^1 = H, R^2 = 4-OMe
9jd (91%); X = CF$_3$, R^1 = Me, R^2 = H

9ab (95%); X = CN, R^1 = H, R^2 = 4-OMe
9hb (31%); X = CN, R^1 = tBu, R^2 = H
9jb (60%); X = CF$_3$, R^1 = Me, R^2 = H

9ac (80%, d.r. = 51:49); X = CN, R^1 = H, R^2 = 4-OMe
9hc (29%, d.r. = 55:45); X = CN, R^1 = tBu, R^2 = H
9jc (44%, d.r. = 51:49); X = CF$_3$, R^1 = Me, R^2 = H

9ja (87%)

9aa

without aqueous workup,
directly analyzed by NMR spectroscopy

Reaction time: 4h for **9jf** and **9jd**, 15h for **9jc**, 24h for **9jb** and 72h for **9ja**
Reaction time: 30 min for all other products

Figure 4. Michael adducts formed from reactions between *δ*-disubstituted *p*QMs **1** and carbanionic reference nucleophiles **2** in dry DMSO at room temperature. Yields and diastereomer ratio refer to isolated **9** after flash chromatography.

Kinetic methodology.

The *p*QMs **1** (CN *p*QMs and CF$_3$ *p*QMs) are colorful compounds which absorb light in the visible region (λ_{max} = 304 nm - 420 nm) with molar extinction coefficients ε of 17400 − 28400 M^{-1} cm^{-1} (see experimental part for individual ε determination, section 4.4.7.). Consequently, the rates of the reactions of *p*QMs **1** with carbanionic reference nucleophiles **2** can easily be monitored by UV/Vis photometry (Figure 5A). DMSO was used as solvent for the kinetic measurements, as it efficiently dissociates salts of carbanions, especially those with potassium ions as counterions, due to its high relative dielectric constant (ε_r = 49 at 20 °C).[18] Depending on the speed of the reaction, either stopped-flow (fast reactions) or conventional UV/Vis spectroscopy (slow reactions) was employed. The kinetics were monitored by following the decay of the colored *p*QMs at their absorbance maxima λ_{max}. The colorless carbanions were used in concentrations at least ten times higher than those of the *p*QMs. This allowed to measure the kinetics under pseudo first-order reaction conditions. Consequently, first-order rate constants k_{obs} (s^{-1}) were derived by least squares fitting of the mono-exponential decay function $A = A_0 \exp(-k_{obs} t) + C$ to the experimental absorbances A_t of the colored *p*QMs (Figure 5B). For each electrophile-nucleophile couple a minimum of four different carbanion concentrations was used and the k_{obs} value for each concentration was determined at 20°C. The four to five kinetic measurements usually comprised two in which 18-crown-6 was additionally added to complex the potassium ions, and to check for potential attractive K$^+$/*p*QM interactions which would possibly increase the reactivity of the electrophile. Plotting the k_{obs} values against the concentrations of the nucleophiles led to linear correlations with only small intercepts, where the slope represents the

second-order rate constant k_2 of the bimolecular reaction (Figure 5C). The same kinetic methodology was also employed for kinetic experiments of *δ*-substituted *p*QMs with substituted thiophenolates and primary amines. The second-order rate constants k_2 of all investigated electrophile-nucleophile combinations are listed in Tables 1 and 2.
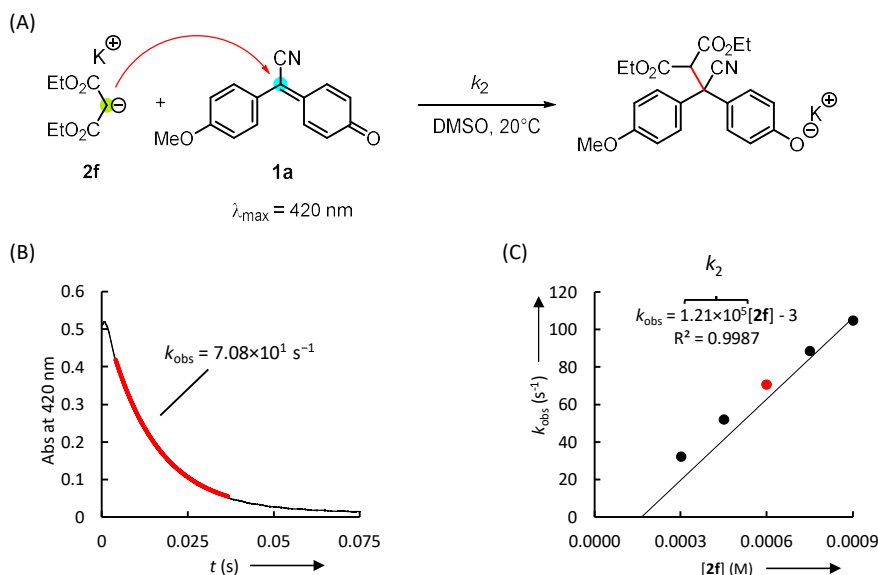

Figure 5. (A) Rate-determining addition reaction of carbanionic nucleophile **2f** to CN *p*QM **1a** in DMSO at 20°C; (B) Time-dependent decay of the absorbance of the colored CN *p*QM at 420 nm and observed first-order rate constant k_{obs}; (C) Linear correlation of experimentally determined first-order rate constants k_{obs} with concentrations of **2f**, the slope represents the second-order rate constant k_2.

Correlation analysis.

Normally, according to the Mayr-Patz equation (1), the experimentally determined second-order rate constants k_2 are combined with the reported reactivity parameters N (s_N) of the carbanionic nucleophiles **2** to calculate the electrophilicity parameters of the *p*QMs.

$$\lg k_2 = s_N(N + E) \qquad (1)$$

A least squares analysis is performed in which the sum of the deviations Δ^2 between the calculated $\lg k_2^{eq1}$ and the experimental rate constants $\lg k_2^{exp}$ is minimized according to equation (2).

$$\Delta^2 = \Sigma(\lg k_2^{exp} - \lg k_2^{eq1})^2 \qquad (2)$$

However, such an analysis does not lead to an adequate quantification of the electrophilic reactivities of the *δ*-disubstituted *p*QMs in this case. These electrophiles are best described by the extended Mayr-Patz equation (3) which comprises two electrophilicity parameters E (and s_E).[19]

$$\lg k_2 = s_E s_N(N + E) \qquad (3)$$

The logarithmic rate constants k_2^{exp} divided by s_N correlate linearly with the known nucleophilicity parameters N of the carbanionic reference nucleophiles (Figure 6). The intercept of the correlations represents $E \times s_E$ and the slope the s_E parameter. The electrophilicity parameter E is determined by dividing the y-axis intercept by the s_E value. The E (and s_E) parameters of all investigated *δ*-disubstituted *p*QMs are summarized in Table 1 (right column).

_____

Table 1. Experimentally determined second-order rate constants k_2^{exp} for the reactions of δ-disubstituted *p*QMs **1** with carbanionic reference nucleophiles **2a**-**2f** in DMSO at 20°C.

*p*QMs	k_2^{exp} (M^{-1} s^{-1})						E (s_E)
	2a[b] $N = 16.27$ $s_N = 0.77$	**2b**[b] $N = 17.64$ $s_N = 0.73$	**2c**[b] $N = 18.82$ $s_N = 0.69$	**2d**[b] $N = 19.36$ $s_N = 0.67$	**2e**[b] $N = 19.62$ $s_N = 0.62$	**2f**[b] $N = 20.22$ $s_N = 0.65$	
1a	3.09×10^1	5.26×10^2	8.43×10^3	3.42×10^4	n.d.	1.21×10^5	−15.08 (1.53)
1b	5.45×10^1	9.13×10^2	1.23×10^4	5.76×10^4	n.d.	2.08×10^5	−14.85 (1.54)
1c	6.53×10^1	1.20×10^3	1.87×10^4	7.06×10^4	n.d.	3.12×10^5	−14.86 (1.57)
1d	1.68×10^2	2.62×10^3	4.40×10^4	1.26×10^5	1.84×10^5	n.d.	−14.41 (1.53)
1e	3.02×10^2	5.28×10^3	8.88×10^4	2.16×10^5	n.d.	n.d.	−14.30 (1.55)
1f	4.89×10^2	6.58×10^3	1.10×10^5	2.55×10^5	3.97×10^5	n.d.	−14.03 (1.49)
1g	n.d.	1.38×10^1	2.02×10^2	n.d.	1.28×10^3	4.40×10^3	−16.64 (1.57)
1h	n.d.	2.70	5.82×10^1	$3.97 \times 10^{2[a]}$	3.23×10^2	1.04×10^3	−17.22 (1.57)
1j	3.70×10^{-3}	1.09×10^{-1}	2.80	$3.78 \times 10^{2[a]}$	$1.59 \times 10^{2[a]}$	8.93×10^1	−18.35 (1.57)

[a] outlier, second-order rate constant was excluded from E (s_E) parameter determinations.

[b] Nucleophilicity parameters N (and s_N) of carbanionic reference nucleophiles **2** taken from ref. [20].

CN *p*QMs **1a**-**1f** have s_E values of 1.49 to 1.57 and the electrophilicity parameters E are in a very narrow reactivity range of only one order of magnitude. It becomes evident that both electron-donating and electron-withdrawing substituents attached to the aryl group in meta and para positions have little influence on the electrophilic reactivity. CN *p*QMs **1g**-**1h**, on the other hand, have s_E values of 1.57 but are significantly less electrophilic than *p*QM **1c**, which can be explained by hyperconjugative effects of the auxiliary alkyl groups located in the 2,6 positions. The CF$_3$ *p*QM **1j** is the least electrophilic species and is 1.5 orders of magnitude less reactive than the similarly substituted CN *p*QM **1g**. For both CN *p*QMs and CF$_3$ *p*QMs, their electrophilic reactivity is largely directed by the two functional groups (-CN and -CF$_3$) directly located at the reactive center. Both functional groups are electron-withdrawing and exert similar electronic effects on the reaction center when considering Hammett substituent constants (σ$^+$ (CN) = 0.66, σ$^+$ (CF$_3$) = 0.61).[21] However, they can also act as π-electron donors, with the CN group ($\Sigma q\pi$ = –262) being a significantly stronger donor than the CF$_3$ group ($\Sigma q\pi$ = –29), based on $\Sigma q\pi$ values (from STO-3G calculations using optimized C–X bond lengths for substituents in alkyl, allylic and benzylic carbenium ions, established as $\Sigma q\pi$ without units).[22] Accordingly, the CN group would be expected to better stabilize the electrophilic center and thus result in lower reactivity of the corresponding *p*QM compared to its CF$_3$ analog. Contrary to this expectation, the observed reactivity follows the opposite trend. Therefore, this reactivity order cannot be explained solely by electronic effects. In addition to electronic influences, steric effects of the two functional groups appear to play

a decisive role. The CF₃ group (sp³-hybridised) is considerably more sterically demanding than the small, linearly aligned nitrile group (sp-hybridised).[23] This pronounced steric bulk of the CF₃ substituent evidently prevails the electronic effects and is the major factor that defines the electrophilic reactivity of the *p*QM **1j**.
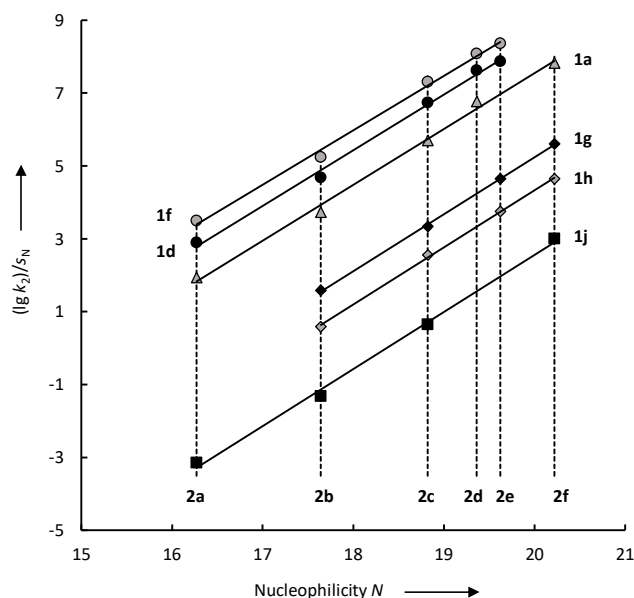

Figure 6. Linear correlations of (lg k_2)/s_N for the reactions of δ-disubstituted *p*QMs **1a, 1d, 1f-1h** and **1j** with carbanionic reference nucleophiles **2a-2f** against the nucleophilicity parameters *N* of **2a-2f** (DMSO, 20 °C). For all correlations, slopes s_E > 1 are observed. Correlations of CN *p*QMs **1b**-**1c** and **1e** are shown in the experimental part.

It should also be mentioned that s_E parameters are rather uncommon and are rarely observed for electrophiles. The Mayr-Patz equation (s_E = 1) is only valid for addition reactions in which only one new σ-bond is formed in the rate-determining step. For S$_N$2-type reactions (e.g. ring opening reactions of cyclopropanes[24] or the solvolysis of the S-methyldibenzothiophenium ion[25]), values of s_E < 1 have been observed. This can be rationalized by the fact that the rate-determining step in such reactions typically involves the concerted making and breaking of σ bonds, meaning that two σ bonds are affected simultaneously in these reaction processes.

In contrast, reactions with s_E > 1 have so far only been observed for nucleophilic additions of primary and secondary amines to acylating agents[26] and of carbanions to *ortho*- or *para*-substituted *N*-methyl pyridinium salts.[27] In both examples, the nucleophile attacks an sp²-hybridised carbon center. One proposed hypothesis for s_E > 1 in such systems is that these reactions proceed via an addition-elimination mechanism, during which one σ bond is formed while another is cleaved. This scenario likewise involves two σ bonds being altered in the transition state thereby violating the precondition for the successful application of the Mayr-Patz equation (1). In the case of δ-disubstituted *p*QMs only one new sigma bond is formed in the rate-determining step. Consequently, these *p*QMs should, in principle, be well described by the Mayr-Patz equation (1). However, it has been shown that equation (1) should not be applied to reactions involving sterically demanding reagents such as tritylium ions. The latter are very sensitive to variation in the steric demand of the nucleophile and can only be reliably described by equation (1) when reacting with small nucleophiles such as hydride donors or simple n-nucleophiles (e.g. amines).[28]

Similar to tritylium ions, δ-disubstituted *p*QMs possess a tertiary carbon atom as their reactive center, resulting in steric environments at the electrophilic position that differ significantly from those of established reference electrophiles (e.g., benzhydrylium ions and previously characterized δ-aryl *p*QMs).[20, 29] Variable steric effects seem to be particularly important for the CF$_3$ *p*QM as smaller anions such as malononitrile and ethyl cyanoacetate react considerably faster with this electrophile compared to other acceptor-substituted carbanions. Thus, the corresponding experimental second-order rate constants were excluded from the determination of the electrophilicity parameters E (and s_E) for the CF$_3$ *p*QM.

The origin of $s_E > 1$ for the δ-disubstituted *p*QMs remains unclear at the moment. However, one possible explanation could be steric effects caused by the additional functional group introduced at the exocyclic double bond. Alternatively, a significant contribution of deformation energy in the transition states of the reactions involving CN- and CF$_3$- substituted *p*QMs with carbanions may play a role. Quantum chemical calculations could eventually provide a more comprehensive understanding of these reactivity phenomena.

Nonetheless, the logarithm of the experimental second-order rate constants k_2 exhibit an excellent linear correlation with the Hammett σ constants of the substituents on the phenyl ring remote from the electrophilic center of the CN *p*QMs **1a**-**1f** (Figure 7A). This correlation will enable straightforward predictions of reaction rates for further, yet unknown CN *p*QMs. The one-electron reduction potentials of CN *p*QMs were determined via cyclic voltammetry (CV) measurements in MeCN (further information on the CV measurements and CV diagrams are shown in the experimental part, section 4.4.2 and 4.4.8). Since the redox processes were reversible, it was possible to determine true half-wave potentials $E_{1/2}$. Plotting lg k_2 against $E_{1/2}$ for the CN *p*QMs **1a**-**1f** revealed a strong linear correlation between these two parameters (Figure 7B), further supporting the electronic nature of the observed reactivity trends.
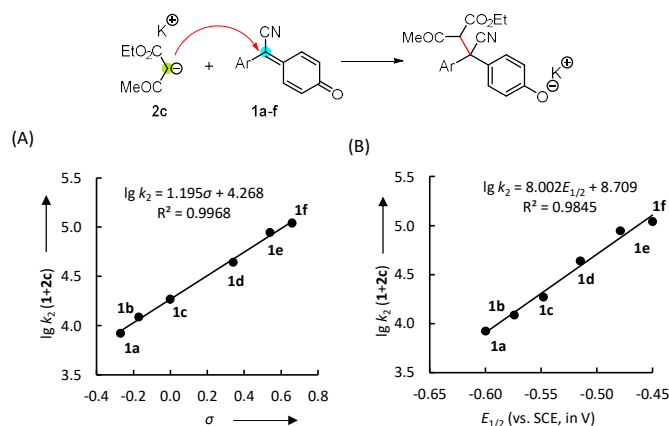
Figure 7. Linear correlations for the logarithm of experimental rate constants k_2 of reactions of **1**+**2c** vs. (A) Hammett substituent constants and (B) experimentally determined half-wave reduction potentials $E_{1/2}$ of CN *p*QMs.

Reactivity of δ-disubstituted *p*QMs in comparison to other Michael acceptors.

First of all, it would be worth comparing the immanent reactivities of the analyzed CN- and CF$_3$ -*p*QMs with those of previously studied aryl-substituted *p*QMs. However, drawing a direct comparison is rather challenging as they usually exhibit slightly different substitution patterns. For instance, the substituents at the 2,6-positions may be identical, but then the substituents attached to the aryl residue remote from the electrophilic center differ, or vice versa.

_____

The only exception is the CN *p*QM **1h** and the δ-aryl *p*QM discussed in Chapter 3, which differ solely by the presence of the nitrile group attached to the exocyclic double bond. A direct comparison of their reactivities can be drawn here, whereby comparing the electrophilicity parameters *E* directly with each other would be misleading as this would disregard the significant effect of the s_E parameter to the reactivity of the CN *p*QM **1h**. Therefore, it is more appropriate to compare the logarithmic second-order rate constants lg k_2 for reactions of these two *p*QMs with a single nucleophile or a series of nucleophiles. Accordingly, lg k_2 values of the CN *p*QM **1h** and the corresponding δ-aryl *p*QM **A** (without nitril group) were compared for reactions with the bis-acceptor substituted carbanions **2b**-**2c**, **2e**-**2f** (Figure 8).
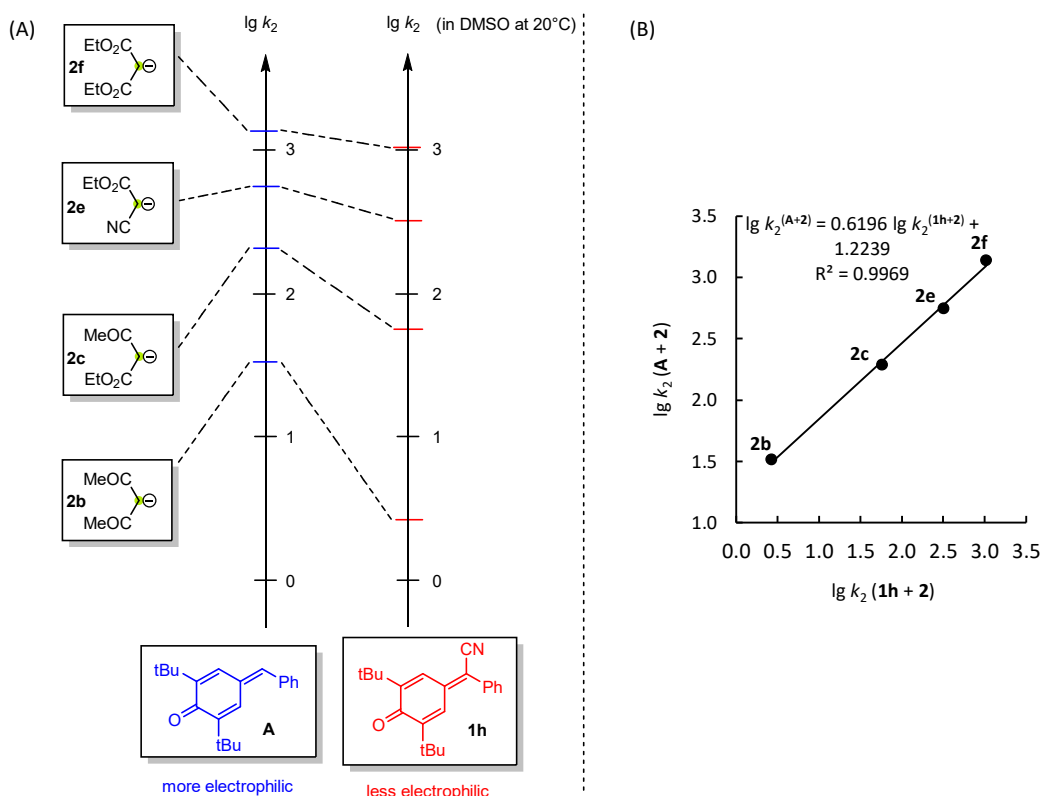
Figure 8. (A) Comparing the logarithm of second order rate constants k_2 for reactions of CN *p*QM **1h** and δ-aryl *p*QM **A** (without nitril group) with carbanions **2b**-**2c** and **2e**-**2f** in DMSO at 20°C. (B) Linear correlation of lg k_2 values for the reactions of *p*QM **A** with carbanions **2** versus the corresponding lg k_2 values for the reactions of CN *p*QM **1h** with the same nucleophiles.

Surprisingly, it was found that the δ-aryl *p*QM **A** is more reactive than the CN *p*QM **1h**, despite the fact that an electron-withdrawing substituent such as a nitrile group is expected to increase the electrophilicity at the electrophilic center. The difference between the lg k_2 values for a given nucleophile decreases with increasing reactivity of the carbanion (Figure 8A). This trend can be attributed to $s_E > 1$. The reduced reactivity of CN *p*QM **1h** compared to its nitrile-free analog **A** may be the result of steric hindrance near the electrophilic center introduced by the CN substituent.

Interestingly, the lg k_2 values for the reactions of δ-aryl *p*QM **A** and CN *p*QM **1h** with the carbanionic nucleophiles **2** show an excellent linear correlation (Figure 8B). This strong correlation implies that, once rate constants for one of the two *p*QMs with further carbanions are known, the corresponding values for the other can be reliably extrapolated.

In order to place the reactivity of CN and CF$_3$ *p*QMs in a greater context, the lg k_2 values for their reactions with carbanion **2c** were additionally compared with those of other Michael acceptors (Figure 9).
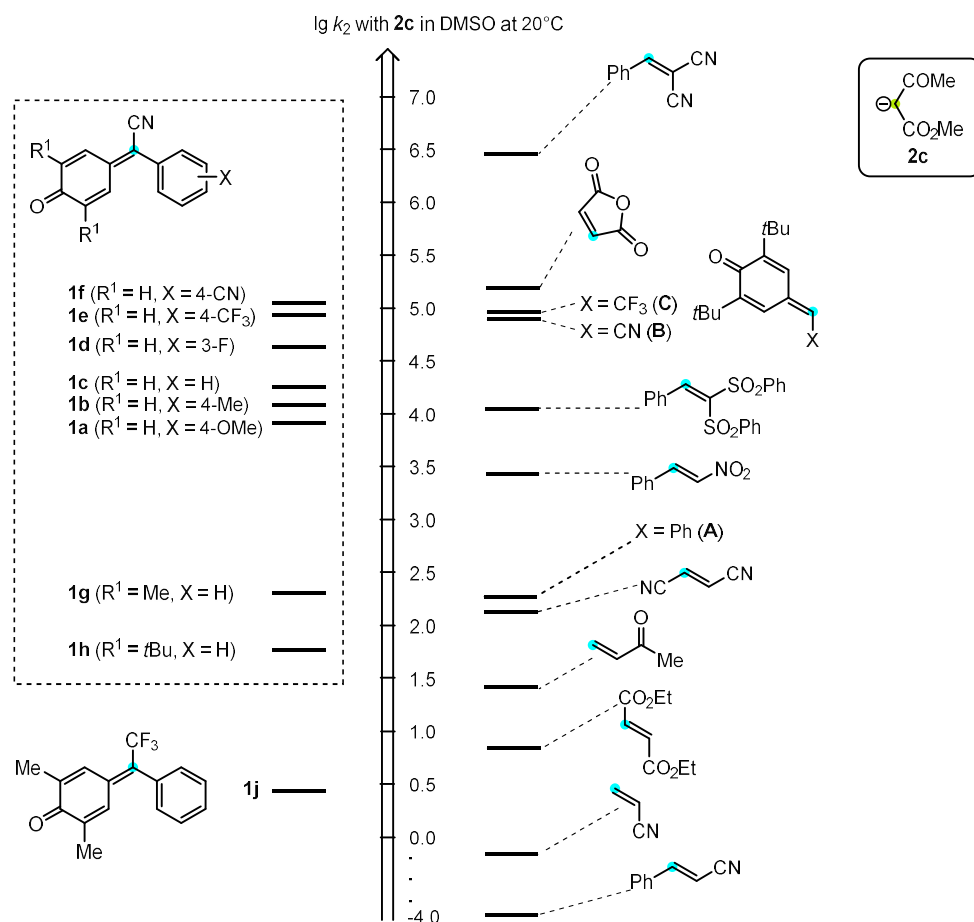
Figure 9. Comparison of the logarithm of experimental second-order rate constants k_2 for reactions of CN- and CF$_3$-*p*QMs with carbanion **2c** and calculated lg k_2 of further Michael acceptors in DMSO at 20°C; Reactivity parameters *E*, *N* and s_N for calculating the corresponding lg k_2 values were taken from ref. [30].

CN *p*QMs **1a**-**1f** span only a narrow reactivity range of around one order of magnitude, despite different substituents on the phenyl ring remote from the reactive center. Their lg k_2 values are comparable to that of maleic anhydride, simple *δ*-functionalized *p*QMs bearing CN, CF$_3$ groups (assigned as **B** and **C** for the context of this chapter) and a bissulfonyl ethylene derivative. However, they are significantly less reactive than benzylidene malononitrile.

Changing the substitution at the 2,6-positions from a small hydrogen atom to methyl and *tert*-butyl groups leads to a substantial decrease in reactivity for CN *p*QMs **1g-1h**, reducing their lg k_2 values by nearly two orders of magnitude. Their reactivity is located in a range covered by compounds such as fumaronitrile and methyl vinyl ketone. The CF$_3$ *p*QM **1j** is the least electrophilic compound studied and exhibits a reactivity between that of diethyl fumarate and acrylonitrile. Compared to its CN analog **1g**, it is approximately two orders of magnitude less reactive.

Interestingly, the simple *p*QMs **B** and **C** are nearly identical in reactivity, although the trend in their lg k_2 values is marginally reversed compared to the aryl-substituted analogs. It is suggested that steric effects are less pronounced in the absence of an additional bulky aryl group thus allowing electronic effects to dominate and compensate for minor steric effects. Furthermore, introducing an aryl group

lowers the reactivity by a significant three orders of magnitude when comparing CN *p*QM **1h** with the simple CN-functionalized *p*QM **B** without aryl group. This effect has also been observed for other Michael acceptors such as ethyl acrylates and cyclic enones, where substitution at the *β*-position with an additional methyl or phenyl group can lead to a drop in reactivity of up to seven orders of magnitude.[31] The observed reactivity trends align well with the underlying structural features of the *p*QMs and underscore the significant impact of both electronic and steric factors on their electrophilic reactivity.

Reactions of *δ*-disubstituted *p*QMs with heteroatom-centered nucleophiles.

Additionally, to assess the value of the quantified electrophilicity parameters E (and s_E) from the reactions of the *δ*-disubstituted *p*QMs with anionic reference nucleophiles **2**, reaction products and rate constants of CN *p*QMs with heteroatom-centered nucleophiles were investigated. Product studies of CN *p*QMs were performed with pyrrolidine, sodium borohydride, sodium methanethiolate and ethanol (Figure 10). According to the rule of thumb that product-forming electrophile nucleophile combinations require a minimum of lg $k_2 > -5$, it is expected that CN *p*QM **1a** (E = -15.08, s_E = 1.53) reacts quickly with strong nucleophiles like pyrrolidine (N = 18.58, s_N = 0.61 in MeCN[30]) and sodium borohydride (N = 14.74, s_N = 0.81 in DMSO[30]). As anticipated, the corresponding reaction products **10** and **11** were easily obtained after 3–4 hours. Though there are not yet nucleophilicity parameters N (and s_N) reported for sodium methanethiolate, it is expected that it has a comparable reactivity to that of thioacetate or thiophenolates, which have $N > 20$.[30] It can therefore be expected that its reaction with CN *p*QM **1a** is extremely fast, and the dialkyl sulfide **12** was obtained accordingly after just 30 min. In contrast, the reaction of CN *p*QM **1d** (E = -14.41, s_E = 1.53) with ethanol (N = 7.44, s_N = 0.90[30]) was anticipated to be extremely slow. As expected, the corresponding dialkyl ether **13** was formed only very slowly with an isolated yield of 71% after four weeks of reaction time, thereby further supporting the reliability of the determined electrophilicity parameters.
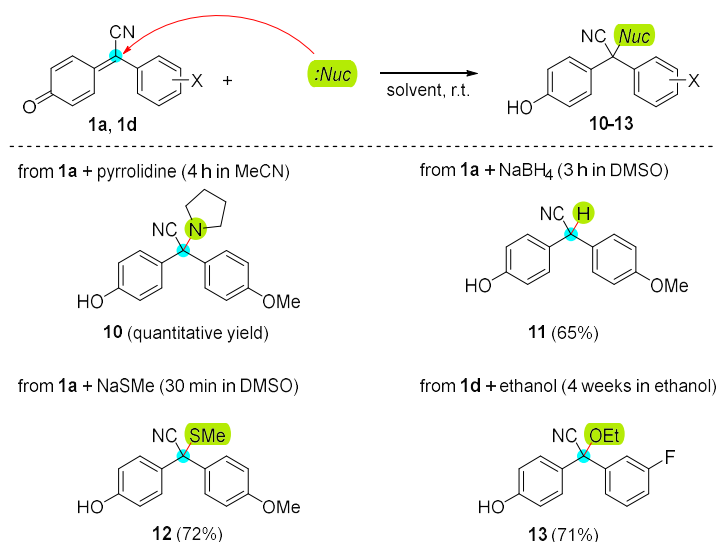
Figure 10. Isolated products from reactions of CN *p*QMs **1a** and **1d** with further H-, N-, O- and S-centered nucleophiles with known nucleophilicity parameters N (and s_N) except for sodium methanethiolate with expected reactivity of $N > 20$.

Furthermore, the kinetics of addition reactions of primary amines and thiophenolates to the CN *p*QMs **1e** and **1h** were investigated in DMSO at 20°C using UV/Vis spectroscopy by monitoring the decay of

the colored CN *p*QMs. Kinetic studies with amines **3** were conducted only for the more reactive CN *p*QM **1e**, while the thiophenolates **4**, which are very strong nucleophiles, were measured with the less reactive CN *p*QM **1h** to ensure that the reaction progress can still be monitored by the stopped-flow method. The determination of the corresponding second-order rate constants followed the previously described kinetic methodology used for reactions of CN *p*QMs with carbanionic reference nucleophiles **2**.

Table 2 summarizes all experimentally determined second-order rate constants k_2^{exp} as well as calculated rate constants k_2^{calc} by applying the extended Mayr-Patz equation (3) and the respective reactivity parameters of the electrophile and nucleophile. The rightmost column in Table 2 shows the ratio between calculated and experimental rate constants. For the reactions of CN *p*QM **1e** with primary amines **3**, the calculated ratio lies within a small error margin of up to a factor of 3. The reactions of CN *p*QM **1h** with thiophenolates **4** proceed somewhat slower than expected, but the deviations are still within an acceptable range. The corresponding rate constants were still predicted within approximately one order of magnitude and below a tolerable error factor of 100, which is generally considered as the predictive accuracy limit of the Mayr-Patz equation (1).

Table 2. Experimental and calculated second-order rate constants k_2 of the reactions of CN *p*QM **1e** with amines **3** and CN *p*QM **1h** with thiophenolates **4** in DMSO at 20°C.

Nucleophile + **1e**	N (s_N)[a]	k_2^{exp} (M^{-1} s^{-1})	k_2^{calc} (M^{-1} s^{-1})[b]	k_2^{calc}/k_2^{exp}
3a	14.39 (0.67)	8.12×10^{-1}	1.24	1.5
3b	15.28 (0.65)	1.21×10^{1}	9.71	0.8
3c	15.70 (0.64)	6.65×10^{1}	2.45×10^{1}	0.4
3d	16.07 (0.61)	2.78×10^{1}	4.72×10^{1}	1.7
Nucleophile + **1h**	N (s_N)[a]	k_2^{exp} (M^{-1} s^{-1})	k_2^{calc} (M^{-1} s^{-1})[c]	k_2^{calc}/k_2^{exp}
4a	21.30 (0.86)	1.02×10^{4}	3.23×10^{5}	32
4b	21.75 (0.86)	4.49×10^{4}	1.31×10^{6}	29
4c	22.50 (0.78)	7.88×10^{4}	2.92×10^{6}	37
4d	22.80 (0.78)	4.57×10^{5}	6.81×10^{6}	15

[a] Nucleophilicity parameters N (and s_N) in DMSO, taken from ref. [30].

[b] Calculated with Equation (3) and reactivity parameters (E = −14.30, s_E = 1.55) of CN *p*QM **1e** and N (s_N) of amines **3a**-**3d**.

[c] Calculated with Equation (3) and reactivity parameters (E = −17.22, s_E = 1.57) of CN *p*QM **1h** and N (s_N) of thiophenolates **4a**-**4d**.

In Figure 11 the experimental second-order rate constants k_2 of reactions of CN *p*QM **1e** and **1h** with amines **3** and thiophenolates **4** are visualized in plots of lg k_2/s_N against the nucleophilicity parameters N. The left plot shows two linear correlations for the CN *p*QM **1e**. The black correlation represents the previously discussed kinetics with the carbanionic reference nucleophiles, while the blue correlation

corresponds to reactions with primary amines **3**. Notably, the slope of the blue correlation is only slightly steeper than that of the carbanion correlation and the blue data points largely coincide with the carbanion trend line. This indicates very similar nucleophile-dependent reactivity and is consistent with the Mayr-Patz equation. The right plot of Figure 11 displays the data for reactions of CN *p*QM **1h** with thiophenolates **4**, shown as the orange correlation. The slope parameter is nearly identical to that of the carbanion correlation (black dots), while the thiophenolates are approximately one order of magnitude less reactive as expected.

Overall, the differences in slope across the three nucleophile classes are minimal. It is expected that the E and s_E parameters that define the electrophiles reactivity are mostly independent from the nucleophile used and this hypothesis is strongly supported by the obtained experimental results for carbanions, primary amines and thiophenolates. Whether this assumption also holds true for smaller and less sterically demanding nucleophiles, such as hydride donors, remains to be explored. Nevertheless, the relatively small deviations between experimental and calculated rate constants for reactions with amines and thiophenolates along with successful product studies involving further heteroatom-centered nucleophiles testify so far the high accuracy of the experimentally determined electrophilicity parameters of the *δ*-disubstituted *p*QMs. Furthermore, it demonstrates the applicability of the extended Mayr-Patz equation (3) to this class of electrophiles, and shows how the determined E and s_E parameters can now be used to semi-quantitatively predict reaction rates with additional classes of nucleophiles.
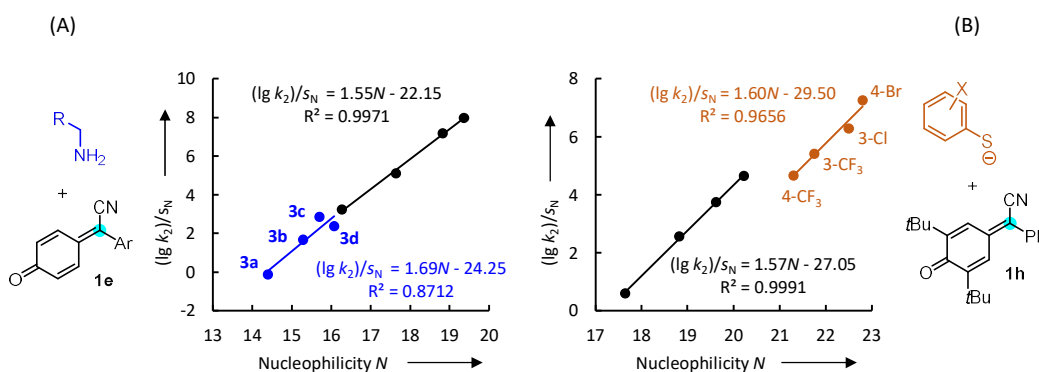
Figure 11. (A) Linear correlations of (lg k_2)/s_N against N for reactions of CN *p*QM **1e** with primary amines **3** (blue dots) and carbanionic reference nucleophiles (black dots) measured in DMSO at 20°C; (B) Linear correlations of (lg k_2)/s_N against N for reactions of CN *p*QM **1h** with substituted thiophenolates (orange dots) and carbanionic reference nucleophiles (black dots) measured in DMSO at 20°C.

4.3. Conclusion

In summary, the electrophilic reactivities of *δ*-CN- and *δ*-CF$_3$ *δ*-aryl disubstituted *para*-quinone methides (CN *p*QMs and CF$_3$ *p*QMs) were systematically investigated through reactions with carbanionic reference nucleophiles **2**. The experimentally determined second-order rate constants were used to derive their electrophile specific reactivity descriptors E. It turned out that these electrophiles need an additional s_E parameter to adequately describe their electrophilic reactivity according to the extended Mayr-Patz equation (3). Corresponding product studies confirmed that the exocyclic double bond is the most electrophilic site within these *p*QMs. While the origin of the observed $s_E > 1$ remains unclear, kinetic studies involving heteroatom-centered nucleophiles such as

primary amines **3** and thiophenolates **4** suggest that the s_E parameter is largely independent of the nucleophile class. Moreover, these additional kinetic studies further validated the obtained *E* (and s_E) parameters, as all the reaction rates were still predicted within approximately 1.5 orders of magnitude. The successful isolation of addition products from reactions with miscellaneous nucleophiles, such as pyrrolidine, further supports the accuracy of the determined reactivity parameters. It is therefore possible to semi-quantitatively predict rate constants for these *p*QMs with a broad range of nucleophile classes. In the future, the origin of $s_E > 1$ should be investigated in more detail. It would be useful to perform kinetic studies of these *p*QMs with a series of very small hydride donors with known *N* (and s_N) parameters. If these hydride donors have no significant impact on the s_E parameter, a steric contribution could be confidently ruled out. Additionally, it would be useful to perform quantum chemical calculations to get more insight into the transition states of these addition reactions and whether substantial deformation energy is involved that potentially contributes to the observed s_E parameters. Since most of the surveyed CN *p*QMs are free of bulky substituents in vicinity to the carbonyl group, it would further allow to activate the carbonyl group by Lewis acids, in order to systematically investigate the effects of Lewis acids on the reactivity of the *p*QMs in reactions with nucleophiles that typically show no reactivity against *p*QMs under standard conditions.

4.4. Experimental Section

4.4.1. Supplementary Figures
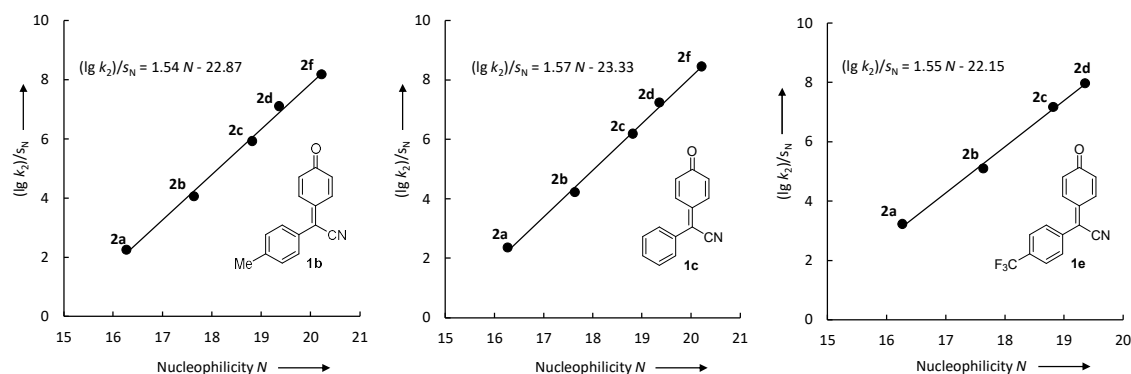
Figure 12. Linear correlations of (lg k_2)/s_N for the reactions of CN *p*QMs **1b-1c** and **1e** with carbanionic reference nucleophiles **2a-2f** against the nucleophilicity parameters *N* of **2a-2f** (DMSO, 20°C). *N* and s_N parameters for carbanions **2** were taken from ref. [20].

4.4.2. General

Commercial reagents and dry solvents (stored over molecular sieves) were used without further purification as purchased from Sigma-Aldrich or Acros Organics. THF was dried over sodium and distilled. For thin-layer chromatography, silica gel plates with F-254 fluorescence indicator (Merck) were used. Purification by flash column chromatography was performed using Merck silica gel 60 (0.040–0.063 mm) with freshly distilled solvents.

Melting points were acquired using Büchi Melting Point B-560 devices and are not corrected.

_____

Nuclear magnetic resonance (NMR) spectra were recorded on 400, 600, and 800 MHz spectrometers. NMR signals were assigned based on information from additional 2D NMR experiments (COSY, gHSQC, gHMBC). Residual solvent signals were used as internal reference (δ_H 7.26 ppm, δ_C 77.16 ppm for CDCl$_3$, δ_H 2.50 ppm, δ_C 39.52 ppm for d_6-DMSO).

Infrared (IR) spectra were recorded on a Perkin Elmer Spectrum BX-59343 instrument with a Smiths Detection DuraSamplIR II Diamond ATR sensor or a Bruker Tensor 27 FT-IR instrument with a "Platinum" Diamond ATR sensor for detection in the range 4500–600 cm^{-1} as a film for liquids or neat for solids.

High resolution (HRMS) mass spectra were recorded on a Finnigan MAT 90, a Finnigan MAT 95, a JEOL MStation JMS 700, a Thermo Finnigan LTQ FT Ultra Fourier Transform ion cyclotron resonance, a Q Exactive GC Orbitrap GC/MS or a Thermo Fisher Scientific LTQ Orbitrap XL. For ionization of the samples, either electron-impact ionization (EI) or electrospray ionization (ESI) was applied.

UV/Vis photometric measurements were carried out using a J&M TIDAS diode array spectrophotometer, which was controlled by TIDASDAQ3 (v3) software and connected to a Hellma 661.502-QX quartz Suprasil immersion probe (light path d = 5 mm) via fiber optic cables and standard SMA connectors.

The half-wave reduction potentials of *p*QMs ($E_{1/2}$) were determined in acetonitrile on a CH Instruments 630E electrochemical analyzer using a 2 mm diameter platinum working electrode, a platinum wire counter electrode and an Ag wire pseudo-reference electrode applying a scan rate of 0.1 V/s. Cyclic voltammetry measurements were performed in deaerated acetonitrile solutions containing 0.1 M tetra-*n*-butylammonium perchlorate, the CN *p*QMs **1** ($c \approx 1 \times 10^{-3}$ M), and ferrocene ($c = 7.5 \times 10^{-4}$ M) as an internal standard. The $E_{1/2}$(fc$^+$/fc in MeCN) = +0.382 V was used to calibrate E_p^{red} (**1** in MeCN) vs SCE.[32] The carbanionic reference nucleophiles **2a-2f** were isolated as potassium salts following literature known procedures.[33]

4.4.3. Preparation of δ-cyano *para*-Quinone Methides (CN *p*QMs)

CN *p*QMs **1a**-**1e**, **1g** and the unknown CN *p*QM species **1f** were synthesized in analogy to a literature procedure.[13, 14]

*p*QM **1h** was synthesized based on a literature procedure with some modifications.[13, 14]

4-((4-(benzyloxy)phenyl)(hydroxy)methyl)benzonitrile (5a)

Magnesium turnings (578 mg, 23.8 mmol) and two crystals of iodine were roasted under vacuum in a three necked round bottom flask for 5 min. Under N$_2$ atmosphere, 3 mL of anhydrous THF was added and 2-bromopropane (2.18 mL, 294 mg, 23.9 mmol) was added dropwise via a dropping funnel. The reaction mixture was heated shortly until initiation and then stirred at r.t. for 2 h. After cooling to 0°C, 4-iodobenzonitrile (2.18 g, 9.52 mmol) dissolved in 6 mL anhydrous THF dropwise via a dropping funnel and stirred for 2 h. 4-(benzyloxy)benzaldehyde (1.35 g, 6.35 mmol) was dissolved in 6 mL anhydrous THF and added dropwise to the reaction mixture via a dropping funnel and stirred for 2 h at 0°C. The reaction was quenched with 10 mL of sat. aq. NH$_4$Cl solution. The aqueous phase was extracted with 3×10 mL EtOAc. The combined organic phases were washed with 5 mL brine and dried over anhydrous MgSO$_4$. The solvent was removed under reduced pressure and the product was purified by flash

_____

column chromatography (silica gel, eluent: *n*-pentane:EtOAc = 8:2→7:3) to give **5a** (775 mg, 39%) as an off-white powder; m.p. 129°C.

5a (JR009)
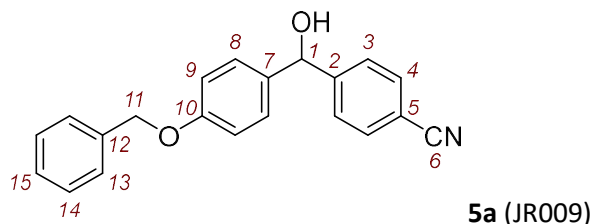
*R*_f (*n*-pentane/EtOAc = 8:2, silica, UV) = 0.15.

¹H NMR (600 MHz, CDCl₃): δ 7.62 (d, *J* = 8.5 Hz, 2 H, 4-H), 7.51 (d, *J* = 8.1 Hz, 2 H, 3-H), 7.43-7.30 (m, 5 H, 13-H, 14-H, 15-H), 7.24 (d, *J* = 8.5 Hz, 2 H, 8-H), 7.95 (d, *J* = 8.7 Hz, 2 H, 9-H), 5.83 (s, *J* = 3.0 Hz, 1 H, 1-H), 5.05 (s, 2 H, 11-H), 2.24 ppm (d, *J* = 3.3 Hz, 1 H, 1-OH).

¹³C{¹H} NMR (151 MHz, CDCl₃): δ 158.9 (C_q, C-10), 149.1 (C_q, C-2), 136.9 (C_q, C-12), 135.5 (C_q, C-7), 132.4 (CH, C-4), 128.8 (CH, C-14), 128.3 (CH, C-8), 128.2 (CH, C-15), 127.6 (CH, C-13), 127.0 (CH, C-3), 119.0 (C-N, C-6), 115.3 (CH, C-9), 111.2 (C_q, C-5), 75.4 (CH, C-1), 70.2 ppm (CH₂, C-11).

HRMS (EI): *m/z* calcd for C₂₁H₁₇NO₂•⁺ [M•⁺]: 315.1254; found: 315.1261.

IR (neat, ATR): ṽ 3522, 2918, 2880, 2227, 1607, 1510, 1237, 1171, 1015, 812, 740, 696 cm⁻¹.

4-((4-(benzyloxy)phenyl)(cyano)methyl)benzonitrile (5b)

Mont K-10 (50.0 mg) and trimethylsilanecarbonitrile (0.42 mL, 33.0 mg, 3.40 mmol) were added in a Schlenk tube and stirred vigorously. **5a** (514 mg, 1.63 mmol) was dissolved in 8 mL anhydrous CH₂Cl₂ and added dropwise (one drop every second) to the suspension via a syringe. The reaction mixture was stirred for 1 h at r.t.. After 2 h of stirring additional Mont K-10 (35.0 mg) was added. After 45 h the reaction mixture was filtered through a celite plug, the solvent was removed under reduced pressure and the product was purified by flash column chromatography (silica gel, eluent: *n*-pentane:EtOAc = 8:2) to give **5b** (158 mg, 30%) as a yellow oil.

5b (JR014)
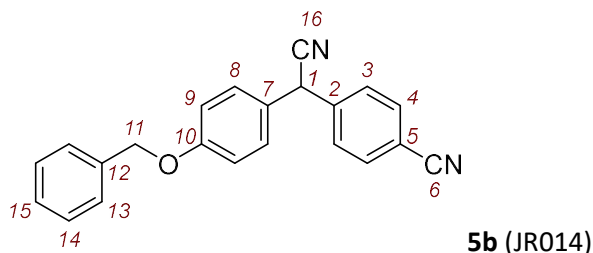
*R*_f (*n*-pentane/EtOAc = 8:2, silica, UV) = 0.45.

¹H NMR (600MHz, CDCl₃): δ 7.67 (d, *J* = 7.4 Hz, 2 H, 4-H), 7.47 (d, *J* = 8.2 Hz, 3 H, 3-H), 7.44-7.37 (m, 4 H, 13-H, 14-H), 7.34 (t, *J* = 6.9 Hz, 1 H, 15-H), 7.22 (d, *J* = 8.4 Hz, 2 H, 8-H), 6.99 (d, *J* = 8.7 Hz, 2 H, 9-H), 5.14 (s, 1 H, 1-H), 5.06 ppm (s, 2 H, 11-H).

¹³C{¹H} NMR (151MHz, CDCl₃): δ 159.2 (C_q, C-10), 141.4 (C_q, C-2), 136.5 (C_q, C-12), 133.1 (CH, C-4), 129.1 (CH, C-8), 128.8 (CH, C-14), 128.6 (CH, C-3), 128.3 (CH, C-15), 127.6 (CH, C-13), 126.8 (C_q, C-7), 118.9 (C-N, C-16), 118.2 (C-N, C-6), 115.9 (CH, C-9), 112.5 (C_q, C-5), 70.3 (CH₂, C-11), 41.9 ppm (CH, C-1).

_____

HRMS (EI): *m/z* calcd for $C_{22}H_{16}N_2O^{\bullet+}$ [M$^{\bullet+}$]: 324.1258; found: 324.1253.

IR (neat, ATR): $\tilde{v}$ 3033, 2928, 2228, 1608, 1509, 1453, 1244, 1177, 1020, 909, 826, 733, 695 cm^{-1}.

4-(cyano(4-hydroxyphenyl)methyl)-benzonitrile (5c)

5b (158 mg, 0.487 mmol) and Pd/C (5 wt.%, 62.0 mg) was added with 12 mL anhydrous MeOH to a Schlenk flask. A H$_2$ balloon was attached and the reaction mixture was stirred vigorously. After 28 h additional Pd/C (5 wt.%, 40.0 mg) was added and the H$_2$ balloon was refilled with hydrogen and reattached. After 45 h the reaction mixture was filtered through a celite plug, the solvent was removed under reduced pressure and the product was purified by flash column chromatography (silica gel, eluent: *n*-pentane:EtOAc = 7:3) to give **5c** (20 mg, 18%) as a yellow oil.

5c (JR017)
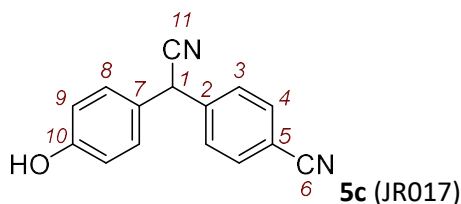
R_f (*n*-pentane/EtOAc = 7:3, silica, UV) = 0.40.

NMR spectra was not recorded for compound **5c** because it had to be used completely in the oxidation reaction to yield enough *p*-QM for kinetic analysis.

HRMS (EI): *m/z* calcd for $C_{15}H_{10}N_2O^{\bullet+}$ [M$^{\bullet+}$]: 234.0788; found: 234.0787.

IR (neat, ATR): $\tilde{v}$ 3033, 2928, 2228, 1608, 1509, 1453, 1244, 1177, 1020, 909, 826, 733, 695 cm^{-1}.

2,6-di-tert-butyl-4-(hydroxy(phenyl)methyl)phenol (5d)

5d (CG100_1)
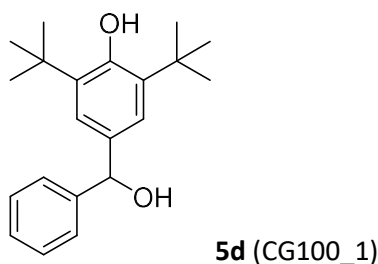
Magnesium turnings (258 mg, 10.7 mmol) were roasted under vacuum in a three necked round bottom flask for 5 min. Under N$_2$ atmosphere, 15 mL of anhydrous THF was added and 4-bromobenzene (1.08 mL, 10.2 mmol) was added dropwise via a dropping funnel. The reaction mixture was heated shortly until initiation and then stirred at r.t. for 1 h. 3,5-di-tert-butyl-4-hydroxybenzaldehyde (1.20 g, 5.12 mmol) was dissolved in 10 mL anhydrous THF and added dropwise to the reaction mixture via a dropping funnel under ice-cooling and stirred for 2 h at r.t.. The reaction was quenched with 10 mL of sat. aq. NH$_4$Cl solution. The aqueous phase was extracted with 3 × 10mL EtOAc. The combined organic phases were washed with 5 mL brine and dried over anhydrous MgSO$_4$. The solvent was removed under reduced pressure and the product was purified by flash column chromatography (silica gel, eluent: *n*-pentane:EtOAc = 9:1→8:2) to give **5d** (1.35 g, 85%) as an off-white powder (literature known compound ref. [34]).

NMR spectroscopic data in CDCl$_3$ agree with those described in ref. [34].

Chapter 4. Electrophilic Reactivities of *δ*-Disubstituted *para*-Quinone Methides – A Limitation to the Mayr-Patz Equation

_____

¹H NMR (600 MHz, CDCl₃): *δ* 7.42 (d, *J* = 6.6 Hz, 2 H), 7.35 (t, *J* = 7.7 Hz, 2 H), 7.27 (t, *J* = 7.3 Hz, 1 H), 7.18 (s, 2 H), 5.79 (d, *J* = 3.4 Hz, 1 H), 5.19 (s, 1 H), 2.15 (d, *J* = 3.4 Hz, 1 H), 1.42 ppm (s, 18 H).

¹³C{¹H} NMR (151 MHz, CDCl₃): *δ* 153.5, 144.2, 136.0, 134.7, 128.5, 127.4, 126.5, 123.8, 76.9, 34.5, 30.4 ppm.

2-(3,5-di-tert-butyl-4-hydroxyphenyl)-2-phenylacetonitrile (5e)

InCl₃ (92.0 mg, 0.416 mmol) and trimethylsilanecarbonitrile (0.68 mL, 0.540 g, 5.41 mmol) were added in a Schlenk tube and stirred at 0°C under nitrogen atmosphere. **5d** (1.30 g, 4.16 mmol) was dissolved in 10 mL anhydrous CH₂Cl₂ and added dropwise (one drop every second) to the suspension via a syringe. The reaction mixture was stirred for 1 h at r.t.. The reaction mixture was filtered through a celite plug, the solvent was removed under reduced pressure and the product was purified by flash column chromatography (silica gel, eluent: *n*-pentane:EtOAc = 96:4) to give **5e** (0.780 g, 58%) as a colorless oil (literature known compound: ref. [35]).

5e (CG103)
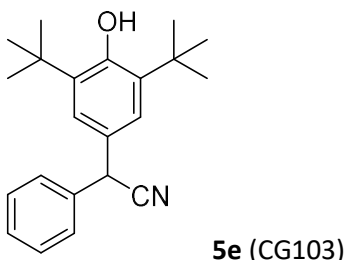
NMR spectroscopic data in CDCl₃ agree with those described in ref. [35].

¹H NMR (400 MHz, CDCl₃): *δ* 7.40 – 7.29 (m, 5 H), 7.11 (s, 2 H), 5.27 (s, 1 H), 5.08 (s, 1 H), 1.42 ppm (s, 18 H).

¹³C{¹H} NMR (101 MHz, CDCl₃): *δ* 153.8, 136.7, 136.5, 129.2, 128.1, 127.8, 126.6, 124.6, 120.5, 42.6, 34.5, 30.2 ppm.

2-(4-methoxyphenyl)-2-(4-oxocyclohexa-2,5-dien-1-ylidene)acetonitrile (1a) was prepared according to a literature procedure; m.p. 163°C.

1a (CG034)
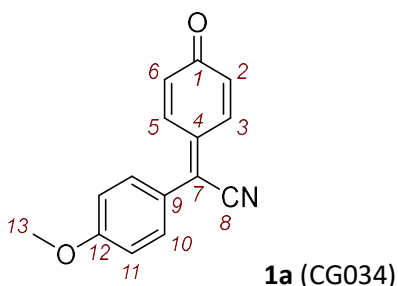
¹H NMR (400 MHz, CDCl₃): *δ* 7.82 (dd, *J* = 10.0, 2.7 Hz, 1 H, 5-H), 7.56 – 7.47 (m, 3 H, 3-H, 11-H), 7.04 (d, *J* = 8.9 Hz, 2 H, 10-H), 6.59 (dd, *J* = 10.0, 2.0 Hz, 1 H, 6-H), 6.49 (dd, *J* = 10.1, 1.9 Hz, 1 H, 2-H), 3.90 ppm (s, 3 H, 13-H).

¹³C{¹H} NMR (101 MHz, CDCl₃): δ 186.7 (C=O, C-1), 162.4 (C_q, C-12), 138.2 (C_q, C-4), 137.3 (CH, C-5), 134.8 (CH, C-3),132.7 (CH, C-11), 131.2 (CH, C-6), 131.1 (CH, C-2), 124.7 (C_q, C-9), 124.2 (C_q, C-7), 117.4 (C-N, C-8), 115.0 (CH, C-10), 55.8 ppm (CH₃, C-13).

HRMS (pos. ESI): *m/z* calcd for C₁₅H₁₂NO₂⁺ [M + H⁺]: 238.0833; found: 238.0866.

IR (neat, ATR) ṽ 1612, 1596, 1499, 1377, 1261, 1182, 1162, 1016, 858, 829 cm⁻¹.

2-(4-oxocyclohexa-2,5-dien-1-ylidene)-2-(p-tolyl)acetonitrile (1b) was prepared according to a literature procedure. NMR spectroscopic data in CDCl₃ agree with those described in ref. [14]; m.p. 116°C.

1b (CG024)
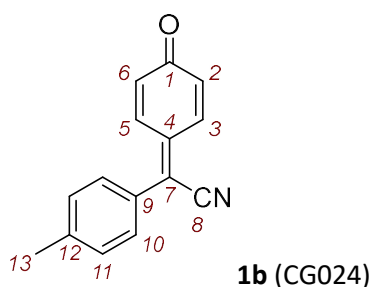
¹H NMR (400 MHz, CDCl₃): δ 7.83 (dd, *J* = 10.0, 2.7 Hz, 1 H, 5-H), 7.51 (dd, *J* = 10.1, 2.6 Hz, 1 H, 3-H), 7.43 (d, *J* = 8.3 Hz, 2 H, 10-H), 7.34 (d, *J* = 7.8 Hz, 2 H, 11-H), 6.60 (dd, *J* = 10.0, 2.0 Hz, 1 H, 6-H), 6.48 (dd, *J* = 10.1, 1.9 Hz, 1 H, 2-H), 2.45 ppm (s, 3 H, 13-H).

¹³C{¹H} NMR (101 MHz, CDCl₃): δ 186.7 (C=O, C-1), 142.4 (C_q, C-12), 139.2 (C_q, C-4), 137.2 (CH, C-5), 134.8 (CH, C-3), 131.3 (CH, C-6), 131.3 (CH, C-2), 130.7 (CH, C-10), 130.2 (CH, C-11), 129.4 (C_q, C-9), 124.4 (C_q, C-7), 117.3 (C-N, C-8), 21.7 ppm (CH₃, C-13).

HRMS (pos. ESI): *m/z* calcd for C₁₅H₁₂NO⁺ [M + H⁺]: 222.0913; found: 222.0916.

IR (neat, ATR): ṽ 1638, 1615, 1501, 1382, 1260, 1108, 1016, 862, 839, 817 cm⁻¹.

2-(4-oxocyclohexa-2,5-dien-1-ylidene)-2-phenylacetonitrile (1c) was prepared according to a literature procedure. NMR spectroscopic data in CDCl₃ agree with those described in ref. [14]; m.p. 122°C.

1c (CG021)
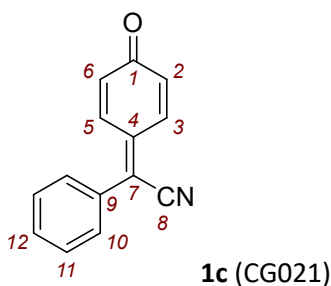
¹H NMR (400 MHz, CDCl₃): δ 7.85 (dd, *J* = 10.0, 2.7 Hz, 1 H, 5-H), 7.59 – 7.50 (m, 5 H, 10-H, 11-H, 12-H), 7.48 (dd, *J* = 10.1, 2.7 Hz, 1 H, 3-H), 6.62 (dd, *J* = 10.0, 1.9 Hz, 1 H, 6-H), 6.49 ppm (dd, *J* = 10.1, 2.0 Hz, 1 H, 2-H).

13C{1H} NMR (101 MHz, CDCl$_3$): *δ* 186.6 (C=O, C-1), 139.8 (C$_q$, C-4), 137.0 (CH, C-5), 134.6 (CH, C-3), 132.1 (C$_q$, C-9), 131.6 (CH, C-6), 131.5 (CH, C-2), 131.4 (CH, C-12), 130.6 (CH, C-11), 129.5 (CH, C-10), 124.1 (C$_q$, C-7), 117.2 ppm (C-N, C-8).

HRMS (pos. ESI): *m/z* calcd for C$_{14}$H$_{10}$NO$^+$ [M + H$^+$]: 208.0757; found: 208.0759.

IR (neat, ATR): *ṽ* 1624, 1609, 1514, 1262, 1173, 1110, 868, 849, 771, 761, 698 cm^{-1}.

2-(3-fluorophenyl)-2-(4-oxocyclohexa-2,5-dien-1-ylidene)acetonitrile (1d) was prepared according to a literature procedure. NMR spectroscopic data in CDCl$_3$ agree with those described in ref. [14]; m.p. 139°C.

1d (JR015)
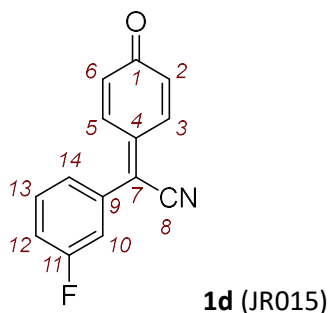
1H NMR (600MHz, CDCl$_3$): *δ* 7.83 (dd, *J* = 10.0 Hz, 2.6 Hz, 1 H, 5-H), 7.53 (td, *J* = 8.0 Hz, 5.6 Hz, 1 H, 13-H), 7.14 (dd, *J* = 10.1 Hz, 2.7 Hz, 1 H, 3-H), 7.31 (ddd, *J* = 7.8 Hz, 1.7 Hz, 0.9 Hz, 1 H, 14-H), 7.28-7.22 (m, 2 H, 10-H, 12-H), 6.63 (dd, *J* = 10.0 Hz, 1.9 Hz, 1 H, 6-H), 6.50 ppm (dd, *J* = 10.1 Hz, 1.9 Hz, 1 H, 2-H).

13C{1H} NMR (151MHz, CDCl$_3$): *δ* 186.4 (C=O, C-1), 162.9 (C-F, C-11, d, $^1J_{C,F}$ = 250.2 Hz), 140.6 (C$_q$, C-4), 136.8 (CH, C-5), 134.0 (CH, C-3), 133.8 (CH, C-13, d, $^3J_{C,F}$ = 7.9 Hz), 131.9 (CH, C-6), 131.9 (CH, C-2), 131.2 (C$_q$, C-9, d, $^3J_{C,F}$ = 8.4 Hz), 126.4 (CH, C-14, d, $^4J_{C,F}$ = 3.3 Hz), 122.2 (C$_q$, C-7, d, $^4J_{C,F}$ = 2.6 Hz), 118.5 (CH, C-12, d, $^2J_{C,F}$ = 21.1 Hz), 117.5 (CH, C-10, d, $^2J_{C,F}$ = 23.3 Hz), 116.9 ppm (C-N, C-8).

HRMS (EI): *m/z* calcd for C$_{14}$H$_8$FNO$^{•+}$ [M$^{•+}$]: 225.0585; found: 225.0583.

IR (neat, ATR): *ṽ* 2362, 1639, 1585, 1479, 1441, 1384, 1277, 1184, 1150, 1004, 861, 784, 691 cm^{-1}.

2-(4-oxocyclohexa-2,5-dien-1-ylidene)-2-(4-(trifluoromethyl)phenyl)acetonitrile (1e) was prepared according to a literature procedure. NMR spectroscopic data in CDCl$_3$ agree with those described in ref. [14]; m.p. 135°C.

1e (CG029)

Chapter 4. Electrophilic Reactivities of *δ*-Disubstituted *para*-Quinone Methides – A Limitation to the Mayr-Patz Equation

_____
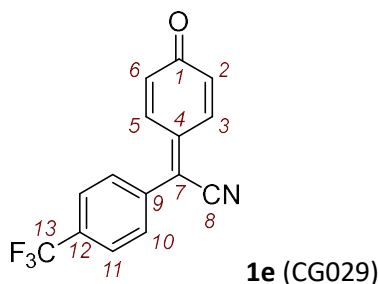
¹H NMR (400 MHz, CDCl₃): *δ* 7.88 – 7.77 (m, 3 H, 5-H, 11-H), 7.65 (d, *J* = 8.8, 0.8 Hz, 2 H, 10-H), 7.38 (dd, *J* = 10.1, 2.7 Hz, 1 H, 3-H), 6.65 (dd, *J* = 10.0, 1.9 Hz, 1 H, 6-H), 6.50 ppm (dd, *J* = 10.1, 2.0 Hz, 1 H, 2-H).

¹³C{¹H} NMR (101 MHz, CDCl₃): *δ* 186.3 (C=O, C-1), 141.1 (C$_q$, C-4), 136.6 (CH, C-5), 135.4 (C$_q$, C-9, q, $^5J_{C,F}$ = 1.4 Hz), 133.7 (CH, C-3), 133.1 (C$_q$, C-12, q, $^2J_{C,F}$ = 33.1 Hz), 132.2 (CH, C-6), 132.1 (CH, C-2), 130.9 (CH, C-10), 126.5 (CH, C-11, q, $^3J_{C,F}$ = 3.72 Hz), 123.5 (C-F, C-13, q, $^1J_{C,F}$ = 272.8 Hz), 121.8 (C$_q$, C-7), 116.8 ppm (C-N, C-8).

HRMS (pos. ESI): *m/z* calcd for C₁₅H₉F₃NO⁺ [M + H⁺]: 276.0631 found: 276.0633.

IR (neat, ATR): ṽ 1633, 1563, 1410, 1323, 1159, 1116, 1068, 1013, 850, 692 cm⁻¹.

4-(cyano(4-oxocyclohexa-2,5-dien-1-ylidene)methyl)benzonitrile (1f)

5c (21.6 mg, 0.092 mmol) was dissolved in 3 mL anhydrous CH₂Cl₂. DDQ (21.5 mg, 0.095 mmol) was added under stirring using argon as inert gas. After 2 h and 2.5 h additional DDQ (14.0 mg, 0.062 mmol) was added both times. After 3.5 h the reaction mixture was filtered through cotton, the solvent was removed under reduced pressure and the product was purified by flash column chromatography (silica gel, eluent: CH₂Cl₂:*n*-pentane:EtOAc = 50:47:3) to give **1f** (19.3 mg, 90%) as orange crystals; m.p. 193°C.

1f (JR019)
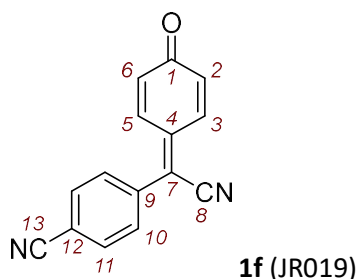
¹H NMR (600MHz, CDCl₃): *δ* 7.87-7.80 (m, 3 H, 11-H, 5-H), 7.65 (d, *J* = 8.4 Hz, 2 H, 10-H), 7.35 (dd, *J* = 10.1 Hz*,* 2.7 Hz, 1 H, 3-H), 6.65 (dd, *J* = 10.0 Hz*,* 1.9 Hz, 1 H, 6-H), 6.51 ppm (dd, *J* = 10.1 Hz*,* 1.9 Hz, 1 H, 2-H).

¹³C{¹H} NMR (151MHz, CDCl₃): *δ* 186.2 (C=O, C-1), 141.4 (C$_q$, C-4), 136.5 (CH, C-5), 136.1 (C$_q$, C-9), 133.4 (CH, C-3), 133.1 (CH, C-11), 132.3 (CH, C-6), 132.3 (CH, C-2), 131.1 (CH, C-10), 121.0 (C$_q$, C-12), 117.6 (C-N, C-13), 116.5 (C-N, C-8), 115.0 ppm (C$_q$, C-7).

HRMS (EI): *m/z* calcd for C₁₅H₈N₂O•⁺ [M•⁺]: 232.0631; found: 232.0629.

IR (neat, ATR): ṽ 3064, 2233, 2209, 1638, 1614, 1488, 1379, 1259, 1170, 1106, 1017, 857, 762 cm⁻¹.

2-(3,5-dimethyl-4-oxocyclohexa-2,5-dien-1-ylidene)-2-phenylacetonitrile **(1g)** was prepared according to a literature procedure. NMR spectroscopic data in CDCl₃ agree with those described in ref. [14]; m.p. 154°C.

1g (CG127)
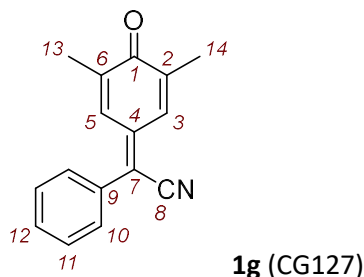
^{1}H NMR (400 MHz, CDCl$_3$): *δ* 7.61 (dd, *J* = 2.7, 1.5 Hz, 1 H, 5-H), 7.53 – 7.46 (m, 5 H, 9-H, 10-H, 11-H, 12-H), 7.21 (dd, *J* = 2.7, 1.5 Hz, 1 H, 3-H), 2.13 (d, *J* = 1.6 Hz, 3 H, 14-H), 2.02 ppm (d, *J* = 1.6 Hz, 3 H, 13-H).

^{13}C{^{1}H} NMR (101 MHz, CDCl$_3$): *δ* 187.1 (C=O, C-1), 140.6 (C$_q$, C-4), 139.8 (C$_q$, C-2), 139.8 (C$_q$, C6), 133.3 (CH, C-5), 132.6 (C$_q$, C-9), 130.7 (CH, C-3), 130.6 (CH, C-12), 130.5 (CH, C-10), 129.2 (CH, C-11), 120.0 (C$_q$, C-7), 117.9 (C-N, C-8), 16.9 (CH$_3$, C-13), 16.6 ppm (CH$_3$, C-14).

HRMS (EI): *m/z* calcd for C$_{16}$H$_{13}$NO$^{\bullet+}$ [M$^{\bullet+}$]: 235.0992; found: 235.0992.

IR (neat, ATR): $\tilde{v}$ 2918, 2211, 1615, 1575, 1447, 1372, 1192, 1031, 916, 871, 768, 697 cm^{-1}.

2-(3,5-di-tert-butyl-4-oxocyclohexa-2,5-dien-1-ylidene)-2-phenylacetonitrile (1h)

5e (0.780 g, 2.43 mmol) was dissolved in 10 mL anhydrous CH$_2$Cl$_2$. DDQ (0.610 g, 2.69 mmol) was added under stirring using nitrogen as inert gas. After 2 h the reaction mixture was filtered through cotton, the solvent was removed under reduced pressure and the product was purified by flash column chromatography (silica gel, eluent: *n*-pentane:EtOAc = 95:5) to give **1f** (525 mg, 67%) as red crystals; m.p. 110°C. Crystals suitable for single crystal X-Ray diffraction (scXRD) were obtained by recrystallisation from ethanol (literature known compound: ref. [36]).

1h (CG104)   zv313
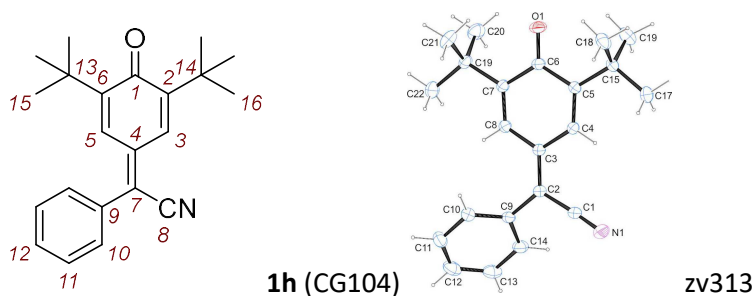
NMR spectroscopic data in CDCl$_3$ agree with those described in ref. [36].

^{1}H NMR (600 MHz, CDCl$_3$): *δ* 7.57 (d, *J* = 2.6 Hz, 1 H, 5-H), 7.54 – 7.46 (m, 5 H, 10-H, 11-H, 12-H), 7.22 (d, *J* = 2.6 Hz, 1 H, 3-H), 1.36 (s, 9 H, 16-H), 1.23 ppm (s, 9-H, 15-H).

^{13}C{^{1}H} NMR (151 MHz, CDCl$_3$): *δ* 186.5 (C=O, C-1), 151.9 (C$_q$, C-6), 151.6 (C$_q$, C-2), 141.1 (C$_q$, C-4), 132.8 (C$_q$, C-9), 130.5 (CH, C-12), 130.5 (CH, C-10), 129.9 (CH, C-5), 129.2 (CH, C-11), 127.4 (CH, C-3), 120.0 (C$_q$, C-7), 118.1 (C-N, C-8), 35.9 (C$_q$, C-14), 35.9 (C$_q$, C-13), 29.6 (CH$_3$, C-16), 29.6 ppm (CH$_3$, C-15).

HRMS (EI): *m/z* calcd for C$_{22}$H$_{25}$NO$^{\bullet+}$ [M$^{\bullet+}$]: 319.1936; found: 319.1933.

IR (neat, ATR): $\tilde{v}$ 2957, 1622, 1612, 1362, 1255, 1086, 911, 821, 762, 698 cm^{-1}.

4.4.4. Preparation of δ-trifluoromethyl *para*-Quinone Methides (CF$_3$ *p*QMs)
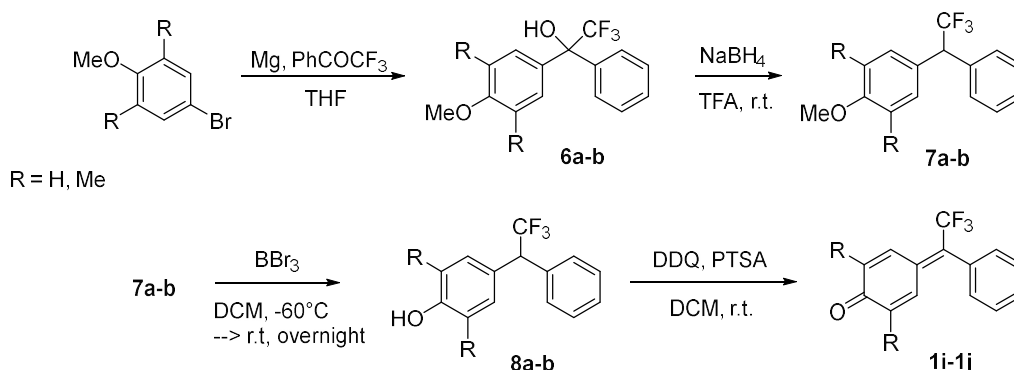
Scheme 2. Synthetic approach for δ-trifluoromethyl *para*-Quinone Methides (CF$_3$ *p*QMs).

2,2,2-trifluoro-1-(4-methoxyphenyl)-1-phenylethan-1-ol (6a)

In a flame-dried three necked flask equipped with reflux condenser and dropping funnel under nitrogen Magnesium turnings (0.239 g, 9.95 mmol) were stirred in dry THF (5 mL). The reaction vessel was heated until reflux and 1-bromo-4-methoxybenzene (1.77 g, 9.48 mmol) was added dropwise while the reaction was still heated. After almost full conversion of magnesium, 2,2,2-trifluoro-1-phenylethan-1-one (1.50 g, 8.61 mmol) was added dropwise under ice cooling. The reaction was stirred overnight at room temperature. The reaction was quenched by addition of sat. aq. NH$_4$Cl solution (15 mL). The aqueous phase was extracted with EtOAc (4 x 30 mL), the combined organic phases were washed with brine (2 x 15 mL), dried over MgSO$_4$ and filtered. The solvent was removed under reduced pressure and the crude product was purified by flash column chromatography (silica gel, eluent: *n*-hexane:CH$_2$Cl$_2$ = 9:1→1:1) to afford **6a** (1.60 g, 66%) as a colorless oil. (literature known compound: ref. [37]).

6a (CG151)
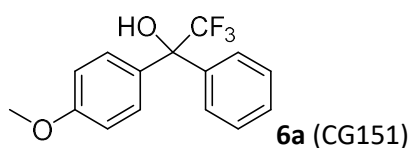
NMR spectroscopic data in CDCl$_3$ agree with those described in ref. [37].

^{1}H NMR (400 MHz, CDCl$_3$): δ 7.56 – 7.46 (m, 2 H), 7.45 – 7.31 (m, 5 H), 6.88 (d, *J* = 9.0 Hz, 2 H), 3.80 (s, 3 H), 2.90 ppm (s, 1 H).

^{13}C{^{1}H} NMR (101 MHz, CDCl$_3$): δ 159.7, 139.6, 131.6, 128.9 (q, $^3J_{C,F}$ = 1.8 Hz), 128.7, 128.3, 127.5 (q, $^3J_{C,F}$ = 1.8 Hz), 125.5 (q, $^1J_{C,F}$ = 286.1 Hz), 113.7, 79.3 (q, $^2J_{C,F}$ = 28.6 Hz), 55.4 ppm.

2,2,2-trifluoro-1-(4-methoxy-3,5-dimethylphenyl)-1-phenylethan-1-ol (6b)

In a flame-dried three necked flask equipped with reflux condenser and dropping funnel under nitrogen Magnesium turnings (0.372 g, 15.5 mmol) were stirred in dry THF (5 mL). The reaction vessel was heated until reflux and 5-bromo-2-methoxy-1,3-dimethylbenzene (3.01 g, 14.0 mmol) was added dropwise while the reaction was still heated. After almost full conversion of magnesium,

2,2,2-trifluoro-1-phenylethan-1-one (2.00 g, 11.5 mmol) was added dropwise under ice cooling. The reaction was stirred overnight at room temperature. The reaction was quenched by addition of sat. aq. NH$_4$Cl solution (15 mL). The aqueous phase was extracted with Et$_2$O (4 x 30 mL), the combined organic phases were washed with brine (2 x 15 mL), dried over MgSO$_4$ and filtered. The solvent was removed under reduced pressure and the crude product was purified by flash column chromatography (silica gel, eluent: *n*-pentane:EtOAc = 97:3→9:1) to afford **6b** (3.57 g, 77%) as a white solid.

6b (LD2)
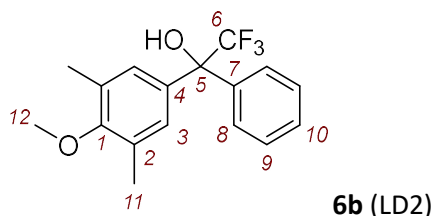
R_f (*n*-pentane/EtOAc 97:3, silica, UV) = 0.07.

^{1}H NMR (400 MHz, CDCl$_3$): δ 7.58 – 7.41 (m, 2 H, 8-H), 7.40 – 7.30 (m, 3 H, 9-H, 10-H), 7.09 (s, 2 H, 3-H), 3.71 (s, 3 H, 12-H), 3.17 (d, *J* = 4.6 Hz, 1 H, 5-H), 2.23 ppm (s, 6 H, 11-H).

^{13}C{^{1}H} NMR (101 MHz, CDCl$_3$): δ 156.9 (C$_q$, C-1), 139.6 (C$_q$, C-7), 134.9 (C$_q$, C-4), 130.8 (C$_q$, C-2), 128.6 (CH, C-10), 128.2 (CH, C-9), 128.0 (CH, C-3, q, $^4J_{C,F}$ = 1.8 Hz), 127.6 (CH, C-8, q, $^4J_{C,F}$ *J* = 1.7 Hz), 125.5 (C-F, C-6, q, $^1J_{C,F}$ = 286.5 Hz), 79.3 (C$_q$, C-5, q, $^2J_{C,F}$ = 28.4 Hz), 59.7 (CH$_3$, C-12), 16.4 (CH$_3$, C-11).

HRMS (EI): *m/z* calcd for C$_{14}$H$_9$F$_3$O$^{•+}$ [M$^{•+}$]: 310.1176; found: 310.1173.

IR (neat, ATR): $\tilde{v}$ 3353, 2950, 1452, 1265, 1180, 1164, 1139, 998, 877, 762, 725, 699 cm^{-1}.

1-methoxy-4-(2,2,2-trifluoro-1-phenylethyl)benzene (7a)

In a flame-dried flask under argon **6a** (0.700 g, 2.48 mmol) was dissolved in 6 mL CH$_2$Cl$_2$. BF$_3$·Et$_2$O (0.765 mL, 6.20 mmol) and triethyl silane (1.15 g, 9.91 mmol) were added at a temperature of -10°C and the reaction mixture was stirred for 20 h at r.t.. The reaction was quenched by addition of sat. aq. NaHCO$_3$ solution (15 mL). The aqueous phase was extracted with CH$_2$Cl$_2$ (4 x 10 mL), the combined organic phases were washed with brine (2 x 15 mL), dried over MgSO$_4$ and filtered. The solvent was removed under reduced pressure and the crude product was purified by flash column chromatography (silica gel, eluent: *n*-pentane:EtOAc = 95:5) to afford **7a** (0.480 g, 73%) as a colorless oil (literature known compound: ref. [38]).

7a (CG152_1)
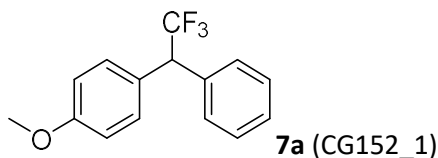
^{1}H NMR (400 MHz, CDCl$_3$): δ 7.41 – 7.27 (m, 7 H), 6.89 (d, *J* = 8.9 Hz, 2 H), 4.65 (q, *J* = 10.0 Hz, 1 H), 3.80 (s, 3 H).

^{13}C{^{1}H} NMR (101 MHz, CDCl$_3$): δ 159.3, 135.9 (d, *J* = 1.4 Hz), 130.4 (d, *J* = 1.5 Hz), 129.1 (q, *J* = 1.0 Hz), 128.8, 127.9, 127.6 (q, *J* = 1.8 Hz), 126.4 (d, $^1J_{C,F}$ = 280.2 Hz), 114.2, 55.4, 54.9 (q, $^2J_{C,F}$ = 27.5 Hz).

HRMS (EI): *m/z* calcd for C$_{15}$H$_{13}$F$_3$O$^{•+}$ [M$^{•+}$]: 266.0913; found: 266.0906.

2-methoxy-1,3-dimethyl-5-(2,2,2-trifluoro-1-phenylethyl)benzene (7b)

In a flame-dried flask under nitrogen **6b** (1.05 g, 3.22 mmol) was dissolved in TFA (15 mL) and stirred at r.t.. NaBH$_4$ (1.55 g, 41.0 mmol) was handled under Argon and added in small batches over 30 min. The reaction mixture was stirred for 2.5 h and was poured into H$_2$O (30 mL). The aqueous phase was extracted with Et$_2$O (4 x 30 mL), the combined organic phases were washed with brine (2 x 15 mL), dried over MgSO$_4$ and filtered. The solvent was removed under reduced pressure and the crude product was purified by flash column chromatography (silica gel, eluent: *n*-pentane:Et$_2$O = 95:5) to afford **7b** (0.99 g, quantitative yield) as a colorless liquid.

7b (LD3A)
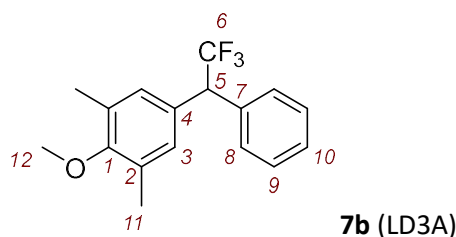
^{1}H NMR (400 MHz, CDCl$_3$): *δ* 7.45 − 7.28 (m, 5 H, 8-H, 9-H, 10-H), 7.02 (s, 2 H, 3-H), 4.69 − 4.50 (m, 1 H, 5-H), 3.73 (s, 3 H, 12-H), 2.28 ppm (s, 6 H, 11-H).

^{13}C{^{1}H} NMR (101 MHz, CDCl$_3$): *δ* 156.6 (C$_q$, C-1), 135.8 (C$_q$, C-7), 131.3 (C$_q$, C-4), 130.9 (C$_q$, C-2), 129.6 (CH, C-3), 129.2 (CH, C-10), 128.8 (CH, C-9), 128.0 (CH, C-8), 126.39 (C-F, C-6, q, $^1J_{C,F}$ = 279.7 Hz), 59.8 (CH$_3$, C-12), 55.2 (CH, C-5, q, $^2J_{C,F}$ = 27.4 Hz), 16.3 (CH$_3$, C-11) ppm.

HRMS (EI): *m/z* calcd for C$_{14}$H$_9$F$_3$O$^{•+}$ [M$^{•+}$]: 294.1226; found: 294.1225.

IR (film, ATR): $\tilde{v}$ 2932, 1789, 1485, 1257, 1223, 1140, 1103, 1012, 859, 708, 697, 659 cm^{-1}.

4-(2,2,2-trifluoro-1-phenylethyl)phenol (8a)

In a flame-dried flask under argon **7a** (0.225 g, 0.85 mmol) was dissolved in dry CH$_2$Cl$_2$ (5 mL). The mixture was cooled to -60 °C and BBr$_3$ (1.0 M in CH$_2$Cl$_2$, 0.93 mL, 0.93 mmol) was added *via* syringe. The reaction mixture was allowed to warm up to r.t. while it was stirred overnight. The reaction was quenched by addition of sat. aq. NaHCO$_3$ solution (15 mL). The aqueous phase was extracted with CH$_2$Cl$_2$ (4 x 10 mL), the combined organic phases were washed with brine (2 x 15 mL), dried over MgSO$_4$ and filtered. The solvent was removed under reduced pressure and the crude product was purified by flash column chromatography (silica gel, eluent: *n*-pentane:EtOAc = 95:5→9:1) to afford **8a** (0.198 g, 93%) as a yellowish oil (literature known compound: ref. [39]).

8a (CG153)
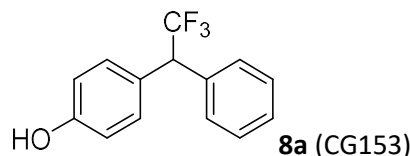
NMR spectroscopic data in CDCl$_3$ agree with those described in ref. [39].

^{1}H NMR (400 MHz, CDCl$_3$): *δ* 7.42 − 7.28 (m, 5 H), 7.24 (d, *J* = 8.8 Hz, 2 H), 6.81 (d, *J* = 8.8 Hz, 2 H), 5.04 (s, 1 H), 4.63 (q, *J* = 10.0 Hz, 1 H), 2.20 (s, 1 H).

^{13}C{^{1}H} NMR (101 MHz, CDCl$_3$): δ 155.3, 135.8 (q, *J* = 1.5 Hz), 130.6 (q, *J* = 1.1 Hz), 129.1 (q, *J* = 1.5 Hz), 128.8, 128.0, 127.8 (q, *J* = 1.7 Hz), 126.4 (q, $^1J_{C,F}$ = 280.6 Hz), 115.7, 54.8 (q, $^2J_{C,F}$ = 27.5 Hz).

HRMS (EI): *m/z* calcd for C$_{14}$H$_{11}$F$_3$O$^{•+}$ [M$^{•+}$]: 252.0757; found: 252.0756.

2,6-dimethyl-4-(2,2,2-trifluoro-1-phenylethyl)phenol (8b)

In a flame-dried flask under argon **7b** (0.447 g, 1.52 mmol) was dissolved in dry CH$_2$Cl$_2$ (5 mL). The mixture was cooled to -60 °C and BBr$_3$ (1.0 M in CH$_2$Cl$_2$, 1.98 mL, 1.98 mmol) was added *via* syringe. The reaction mixture was allowed to warm up to r.t. while it was stirred overnight. The reaction was quenched by addition of sat. aq. NaHCO$_3$ solution (15 mL). The aqueous phase was extracted with CH$_2$Cl$_2$ (4 x 10 mL), the combined organic phases were washed with brine (2 x 15 mL), dried over MgSO$_4$ and filtered. The solvent was removed under reduced pressure and the crude product was purified by flash column chromatography (silica gel, eluent: *n*-pentane:CH$_2$Cl$_2$ = 95:5) to afford **8b** (0.662 g, quantitative yield) as a yellowish oil (literature known compound: ref. [40]).

8b (LD4)
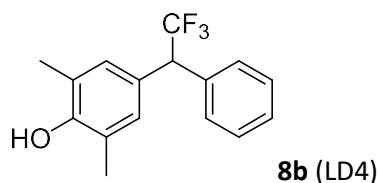
NMR spectroscopic data in CDCl$_3$ agree with those described in ref. [40].

R$_f$ (*n*-pentane/CH$_2$Cl$_2$ 95:5, silica, UV) = 0.15.
^{1}H NMR (400 MHz, CDCl$_3$): δ 7.42 – 7.27 (m, 5 H), 6.98 (s, 2 H), 4.64 – 4.59 (m, 1 H), 4.55 (q, *J* = 10.1 Hz, 1 H), 2.23 ppm (s, 6 H).
^{13}C{^{1}H} NMR (101 MHz, CDCl$_3$): δ 152.0, 136.1 (q, $J_{C,F}$ = 1.3 Hz), 129.4, 129.1, 128.8, 127.9, 127.1 (q, $J_{C,F}$ = 1.9 Hz), 126.5 (q, $^1J_{C,F}$ = 280.1 Hz), 123.4, 55.0 (q, $^2J_{C,F}$ = 27.4 Hz), 16.1 ppm.

HRMS (EI): *m/z* calcd for C$_{16}$H$_{13}$F$_3$O$^{•+}$ [M$^{•+}$]: 280.1070; found: 280.1070.

IR (neat, ATR): $\tilde{v}$ 3586, 2924, 1607, 1489, 1258, 1189, 1142, 1101, 857, 733, 696, 661 cm^{-1}.

4-(2,2,2-trifluoro-1-phenylethylidene)cyclohexa-2,5-dien-1-one (1i)

In a flame-dried flask under nitrogen **8a** (0.100 g, 0.396 mmol) was dissolved in dry CH$_2$Cl$_2$ (5 mL). DDQ (0.153 g, 0.674 mmol) and PTSA (0.0015 g, 0.00793 mmol) were added to the reaction mixture. The mixture was stirred until the TLC control showed almost full conversion. The reaction mixture was directly charged on a silica gel column (silica gel, eluent: *n*-pentane:CH$_2$Cl$_2$:EtOAc = 50:47:3) to afford **1i** (0.011 g, 11%) as a yellowish oil (unstable in DMSO solution).

1i (CG154_2)
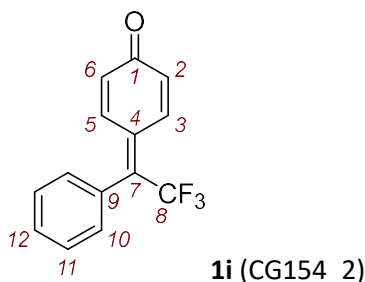
¹H NMR (400 MHz, CDCl₃): *δ* 7.80 (dt, *J* = 10.4, 2.1 Hz, 1 H, 5-H), 7.55 – 7.43 (m, 3 H, 10-H, 12-H), 7.28 (d, *J* = 5.3 Hz, 2 H, 11-H), 6.99 (dd, *J* = 10.2, 2.8 Hz, 1 H, 3-H), 6.53 (dd, *J* = 10.3, 2.7 Hz, 1 H, 6-H), 6.34 ppm (dd, *J* = 10.2, 2.2 Hz, 1 H, 2-H).

¹³C{¹H} NMR (101 MHz, CDCl₃): *δ* 186.5 (C=O, C-1), 141.4 (C$_q$, C-7, q, $^2J_{C,F}$ = 30.7 Hz), 137.6 (CH, C-3), 134.3 (CH, C-5, q, $^4J_{C,F}$ = 3.1 Hz), 134.0 (C$_q$, C-4, q, $^3J_{C,F}$ = 2.8 Hz), 132.2 (C$_q$, C-9, q, $^3J_{C,F}$ = 2.2 Hz), 131.2 (CH, C-6, q, $^5J_{C,F}$ = 0.8 Hz), 131.0 (CH, C-2, q, $^5J_{C,F}$ = 1.0 Hz), 130.1 (CH, C-11), 130.1 (CH, C-12), 128.7 (CH, C-10), 123.0 ppm (C-F, C-8, q, $^1J_{C,F}$ = 276.3 Hz).

¹⁹F NMR (377 MHz, CDCl₃): *δ* -53.69 ppm.

HRMS (EI): *m/z* calcd for C₁₄H₉F₃O•⁺ [M•⁺]: 250.0600; found: 250.0600.

IR (film, ATR) $\tilde{v}$ 1639, 1343, 1277, 1257, 1206, 1158, 1116, 937, 862, 726, 699, 654 cm⁻¹.

2,6-dimethyl-4-(2,2,2-trifluoro-1-phenylethylidene)cyclohexa-2,5-dien-1-one (1j)

In a flame-dried flask under nitrogen **8b** (0.101 g, 0.360 mmol) was dissolved in dry CH₂Cl₂ (5 mL). DDQ (0.091 g, 0.401 mmol) and PTSA (0.001 g, 0.00581 mmol) were added to the reaction mixture. The mixture was stirred until the TLC control showed almost full conversion. The reaction mixture was directly charged on a silica gel column (silica gel, eluent: *n*-pentane:CH₂Cl₂ = 9:1) to afford **1j** (0.064 g, 64 %) as a yellow solid (literature known compound: ref. [41]); m.p. 114°C.

1j (LD5)
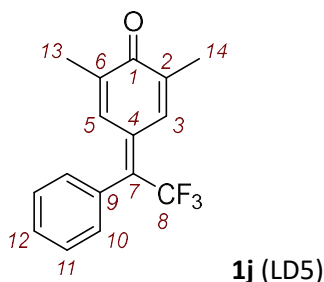
R$_f$ (*n*-pentane/CH₂Cl₂ 9:1, silica, UV) = 0.35.

¹H NMR (400 MHz, CDCl₃): *δ* 7.59 – 7.53 (m, 1 H, 5-H), 7.50 – 7.41 (m, 3 H, 11-H, 12-H), 7.30 – 7.20 (m, 2 H, 10-H), 6.75 – 6.65 (m, 1 H, 3-H), 2.15 – 2.05 (m, 3 H, 14-H), 1.90 ppm (s, 3 H, 13-H).

¹³C{¹H} NMR (101 MHz, CDCl₃): *δ* 187.1 (C=O, C-1), 138.8 (C$_q$, C-6), 138.6 (C$_q$, C-2), 137.6 (C$_q$, C-7, q, $^2J_{C,F}$ = 30.4 Hz), 134.5 (C$_q$, C-4, q, $^3J_{C,F}$ = 3.1 Hz), 133.49 (CH, C-3), 132.8 (C$_q$, C-9, q, $^3J_{C,F}$ = 2.3 Hz), 130.6 (CH, C-5, q, $^4J_{C,F}$ = 2.7 Hz), 130.3 (CH, C-10), 129.5 (CH, C-12), 128.5 (CH, C-11), 123.4 (C-F, C-8, q, $^1J_{C,F}$ = 275.9 Hz), 17.1 (CH₃, C-14), 16.6 ppm (CH₃, C-13).

¹⁹F NMR (377 MHz, CDCl₃): *δ* -52.83 ppm.

HRMS (EI): m/z calcd for C₁₆H₁₃F₃O•⁺ [M•⁺]: 278.0913; found: 278.0913.

IR (neat, ATR): $\tilde{v}$ 1624, 1441, 1374, 1265, 1221, 1160, 1120, 908, 835, 703, 668, 675 cm⁻¹.

4.4.5. Products of Reactions of *p*QMs with C-Nucleophiles

General Procedure (*GP1*):

A solution of the nucleophile (1.0 to 1.3 equiv.) in d_6-DMSO (1.0 mL) was mixed with *p*QM **1** in a standard GC vial by sonication. Then, the reaction mixture was left for up to 72 h at room temperature (23 °C). Subsequently, the mixture was quenched with sat. aq. ammonium chloride solution (1 mL), diluted with water (5 mL) and extracted with diethyl ether (4 × 10 mL). The combined organic phases were washed with water (4 × 10 mL) and dried over MgSO$_4$. The solvent was removed under reduced pressure at the rotary evaporator. The residue was further purified by chromatography and characterized by spectroscopic methods.

potassium(I)1-(cyano(4-hydroxyphenyl)(4-methoxyphenyl)methyl)-4,4-dimethyl-2,6-dioxo-cyclohexan-1-ide (9aa) was prepared by mixing of **1a** (7.8 mg, 0.033 mmol) and **2a** (5.9 mg, 0.043 mmol) in d_6-DMSO (0.8 mL). The reaction mixture was directly analysed by NMR spectroscopy.

9aa (CG060_3)
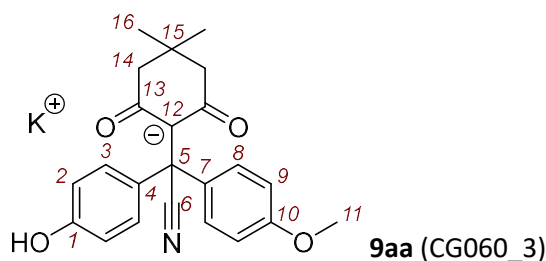
¹H NMR (400 MHz, d_6-DMSO): δ 9.33 (s, 1 H, 1-H), 7.05 (d, *J* = 8.8 Hz, 2 H, 8-H), 6.98 (d, *J* = 8.7 Hz, 2 H, 3-H), 6.67 (d, *J* = 9.0 Hz, 2 H, 9-H), 6.50 (d, *J* = 8.7 Hz, 2 H, 2-H), 3.67 (s, 3 H, 11-H), 1.87 (s, 4 H, 14-H), 0.93 ppm (s, 6 H, 16-H).

¹³C{¹H} NMR (101 MHz, d_6-DMSO): δ 185.6 (C=O, C-13), 156.9 (C$_q$, C-10), 155.2 (C$_q$, C-1), 137.6 (C$_q$, C-7), 134.8 (C$_q$, C-4), 128.6 (CH, C-3), 128.6 (CH, C-8), 125.6 (C-N, C-6), 113.9 (CH, C-2), 112.3 (CH, C-9), 107.6 (C$_q$, C-12), 54.9 (CH$_3$, C-11), 51.5 (CH$_2$, C-14), 49.7 (C$_q$, C-5), 30.8 (C$_q$, C-15), 28.9 ppm (CH$_3$, C-16).

HRMS (EI): *m/z* calcd for C$_{23}$H$_{23}$NO$_4$$^{•+}$ [M$^{•+}$]: 377.1622; found: 377.1617.

3-acetyl-2-(4-hydroxyphenyl)-2-(4-methoxyphenyl)-4-oxopentanenitrile (9ab) was prepared according to GP1 (aqueous workup after 30 min) from **1a** (7.8 mg, 0.033 mmol) and **2b** (5.9 mg, 0.043 mmol) to give **9ab** (10.6 mg, 95%) as a yellowish oil.
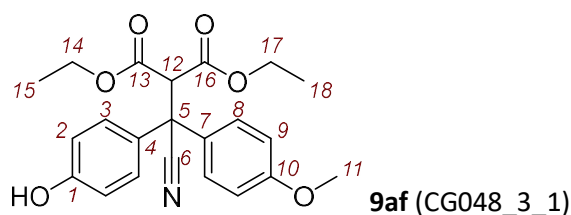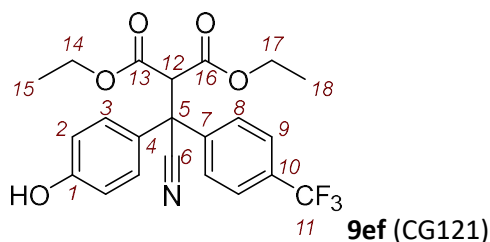

9ab (CG059_3)

¹H NMR (400 MHz, CDCl$_3$): δ 7.29 (d, *J* = 9.0 Hz, 2 H, 8-H), 7.20 (d, *J* = 8.9 Hz, 2 H, 3-H), 6.85 (d, *J* = 9.1 Hz, 2 H, 9-H), 6.79 (d, *J* = 8.9 Hz, 2 H, 2-H), 4.72 (s, 1 H, 12-H), 3.77 (s, 3 H, 11-H), 2.12 – 2.07 ppm (m, 6 H, 14-H, 16-H).

¹³C{¹H} NMR (101 MHz, CDCl$_3$): δ 200.7 (C=O, C-15), 200.6 (C=O, C-13), 159.4 (C$_q$, C-10), 156.7 (C$_q$, C-1), 130.5 (C$_q$, C-7), 129.6 (C$_q$, C-4), 128.1 (CH, C-3), 128.0 (CH, C-8), 121 (C-N, C-6), 116.3 (CH, C-2), 114.6 (CH, C-9), 74.2 (CH, C-12), 55.5 (CH$_3$, C-11), 50.1 (C$_q$, C-5), 31.0 (CH$_3$, C-16), 30.9 ppm (CH$_3$, C-14).

HRMS (EI): *m/z* calcd for $C_{20}H_{19}NO_4^{•+}$ [M$^{•+}$]: 337.1309; found: 337.1317.

IR (film, ATR): $\tilde{v}$ 3139, 2957, 2241, 1730, 1608, 1510, 1359, 1254, 1181, 1024, 829, 727 cm^{-1}.

ethyl 2-(cyano(4-hydroxyphenyl)(4-methoxyphenyl)methyl)-3-oxobutanoate (9ac) was prepared according to GP1 (aqueous workup after 30 min) from **1a** (7.8 mg, 0.033 mmol) and **2f** (7.2 mg, 0.043 mmol) to give **9af** (9.8 mg, 80%, mixture of diastereomers d.r. 51:49) as a colorless oil.

9ac (CG062)

¹H NMR (400 MHz, CDCl₃) *δ* 7.34 (d, *J* = 9.0 Hz, 2 H, 8-H^{minor}), 7.31 − 7.26 (m, 4 H, 3-H^{minor}, 8-H^{major}), 7.24 (d, *J* = 8.9 Hz, 2 H, 3-H^{major}), 6.86 (d, *J* = 4.1 Hz, 2 H, 2-H^{major}), 6.83 (d, *J* = 4.1 Hz, 2 H, 2-H^{minor}), 6.78 (d, *J* = 4.2 Hz, 2 H, 9-H^{major}), 6.76 (d, *J* = 4.1 Hz, 2 H, 9-H^{minor}), 5.15 (s, 2 H, 1-H$^{major/minor}$), 4.57 (s, 2 H, C-12$^{major/minor}$), 4.18 − 4.09 (m, 4 H, 16-H$^{major/minor}$), 3.78 (s, 3 H, 11-H^{major}), 3.77 (s, 3 H, 11-H^{minor}), 2.16 (s, 3 H, 14-H^{major}), 2.15 (s, 3 H, 14-H^{minor}), 1.17 − 1.11 ppm (m, 6 H, 14-H$^{major/minor}$).

¹³C{¹H} NMR (101 MHz, CDCl₃) *δ* 198.7 (C=O, C-13^{major}), 198.5 (C=O, C-13^{minor}), 165.9 (C=O, C-15^{minor}), 165.8 (C=O, C-15^{major}), 159.4 (C$_q$, C-10^{major}), 159.4 (C$_q$, C-10^{minor}), 155.6 (C$_q$, C-1$^{major/minor}$), 131.0 (C$_q$, C-8^{major}), 130.8 (C$_q$, C-8^{minor}), 130.6 (C$_q$, C-4^{major}), 130.4 (C$_q$, C-4^{minor}), 128.2 (CH, C-3^{major}), 128.1 (CH, C-3^{minor}), 128.0 (CH, C-8^{minor}), 127.9 (CH, C-8^{major}), 120.7 (C-N, C-6), 116.1 (CH, C-2^{major}), 116.0 (CH, C-2^{minor}), 114.6 (CH, C-9^{minor}), 114.4 (CH, C-9^{major}), 66.1 (CH, C-12^{major}), 66.1 (CH, C-12^{minor}), 62.5 (CH₂, C-16^{minor}), 62.5 (CH₂, C-16^{major}), 55.5 (CH₃, C-11^{minor}), 55.5 (CH₃, C-11^{major}), 50.1 (C$_q$, C-5$^{major/minor}$), 30.6 (CH₃, C-14$^{major/minor}$), 13.9 (CH₃, C-17$^{major/minor}$).

HRMS (EI): *m/z* calcd for $C_{21}H_{21}NO_5^{•+}$ [M$^{•+}$]: 367.1415; found: 367.1418.

IR (film, ATR): $\tilde{v}$ 3372, 2963, 2243, 1716, 1608, 1509, 1254, 1208, 1182, 1147, 1029, 829 cm^{-1}.

2-(4-hydroxyphenyl)-2-(4-methoxyphenyl)ethane-1,1,2-tricarbonitrile (9ad) was prepared according to GP1 (aqueous workup after 30 min) from **1a** (16.0 mg, 0.067 mmol) and **2d** (8.4 mg, 0.081 mmol) to give **9ad** (16.5 mg, 81%) as a yellowish oil.

9ad (CG049_3)

¹H NMR (400 MHz, CDCl₃): *δ* 7.37 (d, *J* = 9.1 Hz, 2 H, 8-H), 7.31 (d, *J* = 9.0 Hz, 2 H, 3-H), 6.97 (d, *J* = 9.1 Hz, 2 H, 9-H), 6.89 (d, *J* = 9.0 Hz, 2 H, 2-H), 5.66 (s, 1 H, 1-OH), 4.70 (s, 1 H, 12-H), 3.84 ppm (s, 3 H, 11-H).

^{13}C{^{1}H} NMR (101 MHz, CDCl$_3$): δ 160.9 (C$_q$, C-10), 157.3 (C$_q$, C-1), 128.8 (CH, C-3), 128.6 (CH, C-8), 125.9 (C$_q$, C-4), 125.7 (C$_q$, C-7), 118.2 (C-N, C-6), 116.7 (CH, C-2), 115.1 (CH, C-9), 109.9 (C-N, C-14), 109.9 (C-N, C-13), 55.7 (CH$_3$, C-11), 52.8 (C$_q$, C-5), 34.5 ppm (CH, C-12).

HRMS (neg. ESI): *m/z* calcd for C$_{18}$H$_{12}$N$_3$O$_2^-$ [M − H$^+$]: 302.0935; found: 302.0935.

IR (film, ATR): ṽ 3414, 2912, 2223, 1607, 1511, 1441, 1262, 1181, 1029, 827, 732, 702 cm^{-1}.

diethyl 2-(cyano(4-hydroxyphenyl)(4-methoxyphenyl)methyl)malonate (9af) was prepared according to GP1 (aqueous workup after 30 min) from **1a** (7.8 mg, 0.033 mmol) and **2f** (7.2 mg, 0.036 mmol). The crude product was purified by preparative TLC (silica gel, eluent: *n*-pentane:EtOAc = 1:1) to give **9af** (7.4 mg, 57%) as a colorless oil.

9af (CG048_3_1)

R$_f$ (*n*-pentane/EtOAc 1:1, silica, UV) = 0.80.

^{1}**H NMR** (600 MHz, CDCl$_3$): δ 7.34 (d, *J* = 8.5 Hz, 2 H, 8-H), 7.29 (d, *J* = 8.2 Hz, 2 H, 3-H), 6.85 (d, *J* = 8.8 Hz, 2 H, 9-H), 6.77 (d, *J* = 8.5 Hz, 2 H, 2-H), 5.09 (s, 1 H, 1-H), 4.45 (s, 1 H, 12-H), 4.17 – 4.08 (m, 4 H, 14-H, 17-H), 3.77 (s, 3 H, 11-H), 1.13 ppm (td, *J* = 7.1, 2.4 Hz, 6 H, 15-H, 18-H).

^{13}C{^{1}H} NMR (151 MHz, CDCl$_3$): δ 165.5 (C=O, C-13), 165.4 (C=O, C-16), 159.4 (C$_q$, C-10), 155.6 (C$_q$, C-1), 130.7 (C$_q$, C-4), 130.5 (C$_q$, C-7), 128.1 (CH, C-3), 127.9 (CH, C-8), 120.5 (C-N, C-6), 115.9 (CH, C-2), 114.4 (CH, C-9), 62.5 (CH$_2$, C-14), 62.4 (CH$_2$, C-17), 59.3 (CH, C-12), 55.5 (CH$_3$, C-11), 50.7 (C$_q$, C-5), 13.9 ppm (CH$_3$, C-15, C-18).

HRMS (pos. ESI): *m/z* calcd for C$_{22}$H$_{24}$NO$_6^+$ [M + H$^+$]: 396.1452; found: 396.1453.

IR (film, ATR): ṽ 3396, 2979, 2248, 1732, 1442, 1369, 1255, 1222, 1183, 1095, 1030, 829 cm^{-1}.

diethyl 2-(cyano(4-hydroxyphenyl)(4-(trifluoromethyl)phenyl)methyl)malonate (9ef) was prepared according to GP1 (aqueous workup after 30 min) from **1e** (10.0 mg, 0.036 mmol) and **2f** (8.6 mg, 0.044 mmol). The crude product was purified by preparative TLC (silica gel, eluent: *n*-pentane:EtOAc = 7:3) to give **9ef** (8.5 mg, 54%) as a yellowish oil.

9ef (CG121)

R$_f$ (*n*-pentane/EtOAc 7:3, silica, UV) = 0.75.

_____

^{1}H NMR (600 MHz, CDCl$_3$): δ 7.60 (m, 4 H, 8-H, 9-H), 7.30 (d, *J* = 8.8 Hz, 2 H, 3-H), 6.79 (d, *J* = 8.9 Hz, 2 H, 2-H), 5.31 (s, 1 H, 1-H), 4.53 (s, 1 H, 12-H), 4.20 – 4.07 (m, 4 H, 14-H, 17-H), 1.13 ppm (dt, *J* = 18.6, 7.2 Hz, 6 H, 15-H, 19-H).

^{13}C{^{1}H} NMR (151 MHz, CDCl$_3$): δ 165.2 (C=O, C-16), 165.2 (C=O, C-13), 156.0 (C$_q$, C-1), 142.6 (CH, C-8, q, $^4J_{C,F}$ = 1.3 Hz), 130.7 (C$_q$, C-10, q, $^2J_{C,F}$ = 32.9 Hz), 129.3 (C$_q$, C-4), 128.1 (CH, C-3), 127.1 (C$_q$, C-7), 126.1 (CH, C-9, q, $^3J_{C,F}$ = 3.7 Hz), 123.8 (C-F, C-11, q, $^1J_{C,F}$ = 272.3 Hz).119.8 (C-N, C-6), 116.2 (CH, C-2), 62.7 (CH$_2$, C-17), 62.7 (CH$_2$, C-14), 58.8 (CH, C-12), 51.3 (C$_q$, C-5), 13.9 (CH$_3$, C-18), 13.9 ppm (CH$_3$, C-15).

HRMS (EI): *m/z* calcd for C$_{22}$H$_{20}$F$_3$NO$_5$$^{•+}$ [M$^{•+}$]: 435.1289; found: 435.1289.

IR (film, ATR): ṽ 3422, 2983, 2248, 1732, 1513, 1322, 1222, 1166, 1124, 1070, 1016, 829 cm^{-1}.

3-acetyl-2-(3,5-di-tert-butyl-4-hydroxyphenyl)-4-oxo-2-phenylpentanenitrile (9hb) was prepared according to GP1 (aqueous workup after 30 min) from **1h** (19.9 mg, 0.063 mmol) and **2b** (10.9 mg, 0.079 mmol). The crude product was purified by preparative TLC (silica gel, eluent: *n*-pentane:EtOAc = 8:2) to give **9hb** (8.2 mg, 31%) as a colorless oil.

9hb (CG118_3)
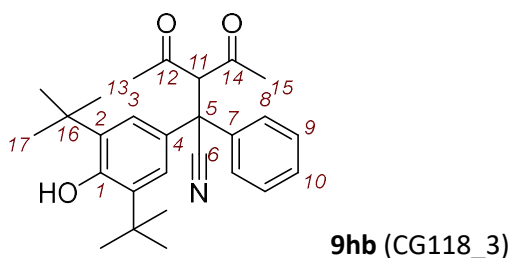
R$_f$ (*n*-pentane/EtOAc 8:2, silica, UV) = 0.50.

^{1}H NMR (400 MHz, CDCl$_3$): δ 7.46 – 7.39 (m, 2 H, 8-H), 7.39 – 7.28 (m, 3 H, 9-H, 10-H), 7.15 (s, 2 H, 3-H), 5.29 (s, 1 H, 1-H), 4.74 (s, 1 H, 11-H), 2.07 (s, 3 H, 15-H), 2.06 (s, 3 H, 13-H), 1.38 ppm (s, 18 H, 17-H).

^{13}C{^{1}H} NMR (101 MHz, CDCl$_3$): δ 200.7 (C=O, C-14), 200.5 (C=O, C-12), 153.8 (C$_q$, C-1), 138.7 (C$_q$, C-7), 136.7 (C$_q$, C-2), 129.3 (CH, C-9), 128.4 (CH, C-10; C$_q$, C-4), 126.8 (CH, C-8), 123.8 (CH, C-3), 120.9 (C-N, C-6), 74.4 (CH, C-11), 51.5 (C$_q$, C-5), 34.8 (C$_q$, C-16), 30.9 (CH$_3$, C-15), 30.9 (CH$_3$, C-13), 30.3 ppm (CH$_3$, C-17).

HRMS (EI): *m/z* calcd for C$_{27}$H$_{33}$NO$_3$$^{•+}$ [M$^{•+}$]: 419.2455; found: 419.2454.

IR (film, ATR): ṽ 3630, 2956, 2240, 1732, 1709, 1437, 1359, 1240, 1148, 911, 733, 699 cm^{-1}.

ethyl 2-(cyano(3,5-di-tert-butyl-4-hydroxyphenyl)(phenyl)methyl)-3-oxobutanoate (9hc) was prepared according to GP1 (aqueous workup after 30 min) from **1h** (20.0 mg, 0.063 mmol) and **2c** (12.6 mg, 0.075 mmol). The crude product was purified by preparative TLC (silica gel, eluent: *n*-pentane:EtOAc = 8:1) to give **9hc** (8.0 mg, 29%, mixture of diastereomers d.r. 55:45) as a colorless oil.

9hc (CG120_1)

R_f (n-pentane/EtOAc 8:1, silica, UV) = 0.50.

^{1}H NMR (600 MHz, CDCl$_3$) δ 7.48 – 7.41 (m, 2 H, 8-H), 7.37 – 7.32 (m, 2 H, 9-H), 7.30 – 7.26 (m, 1 H, 10-H), 7.22 – 7.15 (m, 2 H, 3-H), 5.28 – 5.22 (m, 1 H, 1-H), 4.63 – 4.60 (m, 1 H, 11-H), 4.16 – 4.04 (m, 2 H, 15-H), 2.15 – 2.07 (m, 3 H, 13-H), 1.40 – 1.36 (m, 18 H, 18-H), 1.09 ppm (t, *J* = 7.1 Hz, 3 H, 16-H).

^{13}C{^{1}H} NMR (151 MHz, CDCl$_3$) δ 198.8 (C=O, C-12^{minor}), 198.6 (C=O, C12^{major}), 166.0 (C=O, C-14^{major}), 165.9 (C=O, C-14^{minor}), 153.7 (C$_q$, C-1^{minor}), 153.6 (C$_q$, C-1^{major}), 139.0 (C$_q$, C-7^{minor}), 138.7 (C$_q$, C-7^{major}), 136.5 (C$_q$, C-2^{minor}), 136.3 (C$_q$, C-2^{major}), 129.1 (CH, C-9^{major}), 129.0 (CH, C-9^{minor}), 128.8 (C$_q$, C-4^{major}), 128.3 (C$_q$, C-4^{minor}), 128.2 (CH, C-10$^{major/minor}$), 126.7 (CH, C-8^{major}), 126.6 (CH, C-8^{minor}), 123.8 (CH, C-3^{minor}), 123.5 (CH, C-3^{major}), 120.6 (C-N, C-6^{minor}), 120.6 (C-N, C-6^{major}), 66.4 (CH, C-11^{major}), 66.0 (CH, C-11^{minor}), 62.3 (CH$_2$, C-15^{minor}), 62.3 (CH$_2$, C-15^{major}), 51.5 (C$_q$, C-5^{minor}), 51.4 (C$_q$, C-5^{major}), 34.7 (C$_q$, C-17^{minor}), 34.7 (C$_q$, C-17^{major}), 30.7 (CH$_3$, C-13^{minor}), 30.4 (CH$_3$, C-13^{major}), 30.3 (CH$_3$, C-18^{major}), 30.3 (CH$_3$, C-18^{minor}), 13.9 (CH$_3$, C-16^{major}), 13.9 ppm (CH$_3$, C-16^{minor}).

HRMS (EI): *m/z* calcd for C$_{28}$H$_{35}$NO$_4$$^{•+}$ [M$^{•+}$]: 449.2561; found: 449.2570.
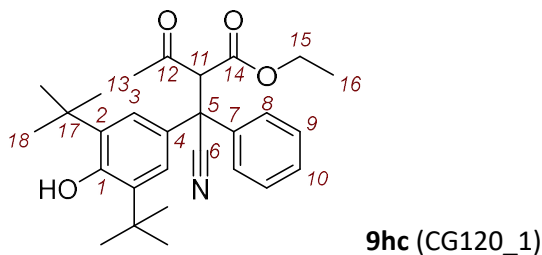
IR (neat, ATR): ṽ 3627, 2962, 2243, 1723, 1436, 1360, 1265, 1202, 1144, 1020, 732, 698 cm^{-1}.

diethyl 2-(cyano(3,5-di-tert-butyl-4-hydroxyphenyl)(phenyl)methyl)malonate (9hf) was prepared according to GP1 (aqueous workup after 30 min) from **1h** (19.7 mg, 0.062 mmol) and **2f** (14.1 mg, 0.071 mmol). The crude product was purified by preparative TLC (silica gel, eluent: *n*-pentane:EtOAc = 9:1) to give **9hf** (16.5 mg, 56%) as a colorless oil.

9hf (CG117)
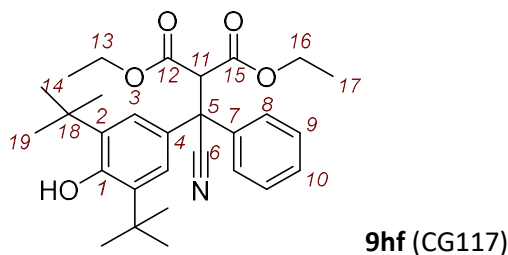
R_f (*n*-pentane/EtOAc 9:1, silica, UV) = 0.25.

^{1}H NMR (600 MHz, CDCl$_3$): δ 7.48 (d, *J* = 7.9 Hz, 2 H, 8-H), 7.34 (t, *J* = 7.8 Hz, 2 H, 9-H), 7.28 (d, *J* = 7.5 Hz, 1 H, 10-H), 7.22 (s, 2 H, 3-H), 5.23 (s, 1 H, 1-H), 4.51 (s, 1 H, 11-H), 4.16 – 4.03 (m, 4 H, 13-H, 16-H), 1.38 (s, 18 H, 19-H), 1.11 – 1.05 ppm (m, 6 H, 14-H, 17-H).

^{13}C{^{1}H} NMR (151 MHz, CDCl$_3$): δ 165.6 (C=O, C-15), 165.5 (C=O, C-12), 153.6 (C$_q$, C-1), 138.9 (C$_q$, C-7), 136.2 (C$_q$, C-2), 128.9 (CH, C-9), 128.5 (C$_q$, C-4), 128.1 (CH, C10), 126.6 (CH, C-8), 123.6 (CH, C-3), 120.5 (C-N, C-6), 62.3 (CH$_2$, C-16), 62.2 (CH$_2$, C-13), 59.4 (CH, C-11), 51.9 (C$_q$, C-5), 34.7 (C$_q$, C-18), 30.3 (CH$_3$, C-19), 13.9 (CH$_3$, C-17), 13.9 ppm (CH$_3$, C-14).

_____

HRMS (EI): *m/z* calcd for $C_{29}H_{37}NO_5^{\bullet+}$ [M$^{\bullet+}$]: 479.2667; found: 479.2665.

IR (film, ATR): $\tilde{v}$ 3627, 2960, 2243, 1737, 1436, 1367, 1314, 1218, 1151, 1036, 871, 697 cm^{-1}.

3-hydroxy-5,5-dimethyl-2-(2,2,2-trifluoro-1-(4-hydroxy-3,5-dimethylphenyl)-1-phenylethyl)cyclohex-2-en-1-one (9ja) was prepared according to GP1 (aqueous workup after 72 h) from **1j** (8.0 mg, 0.029 mmol) and **2a** (5.4 mg, 0.030 mmol). The crude product was purified by preparative TLC (silica gel, eluent: *n*-pentane:EtOAc:CH$_2$Cl$_2$ = 30:5:65) to give **9ja** (10.5 mg, 87%) as a white solid; m.p. 211°C.

9ja (CG182)
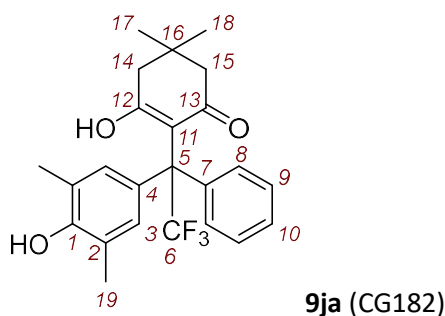
R_f (*n*-pentane/EtOAc/CH$_2$Cl$_2$ 30:5:65, silica, UV) = 0.50.

^{1}H NMR (600 MHz, CDCl$_3$): δ 7.38 – 7.31 (m, 3 H, 9-H, 10-H), 7.29 (d, *J* = 7.0 Hz, 2 H, 8-H), 6.89 (s, 2 H, 3-H), 5.69 (s, 1 H, 13-H), 4.80 (s, 1 H, 1-H), 2.42 – 2.32 (m, 4 H, 14-H, 15-H), 2.19 (s, 6 H, 19-H), 1.16 (s, 3 H, 18-H), 1.15 ppm (s, 3 H, 17-H).

^{13}C{^{1}H} NMR (151 MHz, CDCl$_3$): δ 196.2 (C=O, C-13), 171.7 (C$_q$, C-12), 152.7 (C$_q$, C-1), 138.1 (C$_q$, C-7), 129.2 (C$_q$, C-4), 129.1 (CH, C-3, q, $^4J_{C,F}$ = 2.1 Hz), 128.9 (CH, C-9), 128.5 (CH, C-8, q $^4J_{C,F}$ = 2.1 Hz), 128.2 (CH, C-10), 127.6 (C-F, C-6, q, $^1J_{C,F}$ = 288.3 Hz), 124.0 (C$_q$, C-2), 114.7 (C$_q$, C-11, q, $^3J_{C,F}$ = 1.2 Hz), 61.6 (C$_q$, C-5, q, $^2J_{C,F}$ = 26.1 Hz), 52.4 (CH$_2$, C-15), 45.0 (CH$_2$, C-14), 30.9 (C$_q$, C-16), 28.6 (CH$_3$, C-17), 28.1 (CH$_3$, C-18), 16.5 ppm (CH$_3$, C-19).

HRMS (pos. ESI): *m/z* calcd for $C_{24}H_{26}F_3O_3^+$ [M + H$^+$]: 419.1829; found: 419.1829.

IR (neat, ATR): $\tilde{v}$ 3510, 1562, 1491, 1377, 1311, 1210, 1142, 1128, 1025, 760, 717, 700 cm^{-1}.

3-(2,2,2-trifluoro-1-(4-hydroxy-3,5-dimethylphenyl)-1-phenylethyl)pentane-2,4-dione(9jb) was prepared according to GP1 (aqueous workup after 24 h) from **1j** (11.0 mg, 0.040 mmol) and **2b** (6.6 mg, 0.047 mmol). The crude product was purified by preparative TLC (silica gel, eluent: *n*-pentane:EtOAc:CH$_2$Cl$_2$ = 30:5:65) to give **9jb** (9.0 mg, 60%) as a colorless oil.

9jb (CG181)
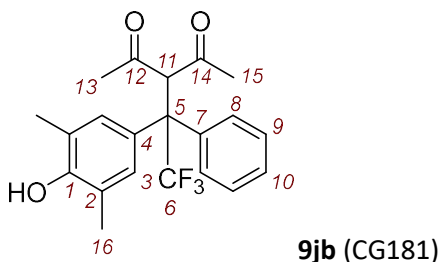
R_f (*n*-pentane/EtOAc/DCM 30:5:65, silica, UV) = 0.50.

1H NMR (600 MHz, CDCl$_3$): δ 7.40 (d, *J* = 8.3 Hz, 2 H, 8-H), 7.36 – 7.29 (m, 3 H, 9-H, 10-H), 6.97 (s, 2 H, 3-H), 5.04 (s, 1 H, 11-H), 4.71 (s, 1 H, 1-H), 2.20 (s, 6 H, 16-H), 2.03 (s, 3 H, 15-H), 2.02 ppm (s, 3 H, 13-H).

13C{1H} NMR (151 MHz, CDCl$_3$): δ 201.5 (C$_q$, C-14), 201.5 (C$_q$, C-12), 152.2 (C$_q$, C-1), 137.2 (C$_q$, C-7), 131.0 (CH, C-3, q, $^4J_{C,F}$ = 2.0 Hz), 130.7 (CH, C-8, q, $^4J_{C,F}$ = 1.8 Hz), 128.2 (CH, C-10, C$_q$, C-4), 127.8 (CH, C-9), 127.0 (C-F, C-6, q, $^1J_{C,F}$ = 285.8 Hz), 122.3 (Cq, C-2), 71.07 (CH, C-11), 61.0 (C$_q$, C-5, q, $^2J_{C,F}$ = 23.1 Hz), 31.9 (CH$_3$, C-15), 31.8 (CH$_3$, C-13), 16.3 ppm (CH$_3$, C-16).

19F NMR (377 MHz, CDCl$_3$): δ -63.74 ppm.

HRMS (neg. ESI): *m/z* calcd for C$_{21}$H$_{20}$F$_3$O$_3^-$ [M − H$^+$]: 377.1370; found: 377.1371.

IR (film, ATR): $\tilde{v}$ 3502, 2919, 1736, 1698, 1603, 1495, 1360, 1231, 1173, 1139, 718, 703 cm^{-1}.

ethyl 2-acetyl-4,4,4-trifluoro-3-(4-hydroxy-3,5-dimethylphenyl)-3-phenylbutanoate (9jc) was prepared according to GP1 (aqueous workup after 15 h) from **1j** (12.0 mg, 0.043 mmol) and **2a** (8.0 mg, 0.047 mmol). The crude product was purified by preparative TLC (silica gel, eluent: CH$_2$Cl$_2$: *n*-pentane = 2:1) to give **9ja** (7.8 mg, 44%, mixture of diastereomers, d.r. 51:49) as a colorless oil.

9jc (184)
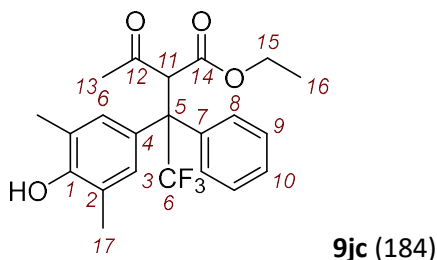
R_f (CH$_2$Cl$_2$/*n*-pentane 2:1, silica, UV) = 0.25.

1H NMR (400 MHz, CDCl$_3$): δ 7.49 (d, *J* = 8.8 Hz, 2 H, 8-H^{minor}), 7.38 (d, *J* = 7.2 Hz, 2 H, 8-H^{major}), 7.35 – 7.27 (m, 6 H, 9-H$^{major/minor}$, 10-H$^{major/minor}$), 7.03 (s, 2 H, 3-H^{major}), 6.94 (s, 2 H, 3-H^{minor}), 4.85 (s, 1 H, 11-H^{minor}), 4.83 (s, 1 H, 11-H^{major}), 4.70 (s, 1 H, 1-H^{minor}), 4.68 (s, 1 H, 1-H^{major}), 4.19 – 4.00 (m, 4 H, 15-H$^{major/minor}$), 2.21 (s, 6 H, 17-H^{major}), 2.19 (s, 6 H, 17-H^{minor}), 2.04 (s, 3 H, 13-H^{minor}), 2.03 (s, 3 H, 13-H^{major}), 1.23 – 1.09 (m, 6 H, 16-H$^{major/minor}$).

13C{1H} NMR (101 MHz, CDCl$_3$): δ 199.9 (C=O, C-12^{minor}), 199.8 (C=O, C-12^{major}), 167.1 (C=O, C-14^{major}), 166.9 (C=O, C-14^{minor}), 152.1 (C$_q$, C-1^{minor}), 152.0 (C$_q$, C-1^{major}), 137.7 (C$_q$, C-7^{minor}), 136.8 (C$_q$, C-7^{major}), 130.9 (CH, C-3^{major}, q, $^4J_{C,F}$ = 2.0 Hz), 130.8 (CH, C-3^{minor}, q, $^4J_{C,F}$ = 2.3 Hz), 130.7 (CH, C-8^{minor}, q, $^4J_{C,F}$ = 1.3 Hz), 130.5 (CH, C-8^{major}, q, $^4J_{C,F}$ = 1.7 Hz), 128.8 (C$_q$, C-4^{major}), 128.8 (C$_q$, C-4^{minor}), 128.1 (CH, C-10^{minor}), 128.1 (CH, C-10^{major}), 127.6 (CH, C-9^{minor}), 127.6 (CH, C-9^{major}), 126.9 (C-F, C-6^{minor}, q, $^1J_{C,F}$ = 286.3 Hz), 126.9 (C-F, C-6^{major} q, $^1J_{C,F}$ = 286.5 Hz), 122.1 (C$_q$, C-2^{minor}), 122.0 (C$_q$, C-2^{major}), 63.2 (CH, C-11^{major}), 62.9 (CH, C-11^{minor}), 61.9 (CH$_2$, C-15^{major}), 61.9 (CH$_2$, C-15^{minor}), 60.4 (C$_q$, C-5$^{major/minor}$, q, $^2J_{C,F}$ = 23.5 Hz), 31.2 (CH$_3$, C-13$^{major/minor}$), 16.3 (CH$_3$, C-17^{major}), 16.3 (CH$_3$, C-17^{minor}), 14.0 (CH$_3$, C-16^{minor}), 13.9 (CH$_3$, C-16^{major}).

19F NMR (377 MHz, CDCl$_3$): δ -63.87 (s, 3 F, 6-F^{major}), -64.08 ppm (s, 3 F, 6-F^{minor}).

HRMS (EI): *m/z* calcd for C$_{22}$H$_{23}$F$_3$O$_4^{\bullet+}$ [M$^{\bullet+}$]: 408.1543; found: 408.1543.

IR (neat, ATR): $\tilde{v}$ 3511, 2923, 1716, 1495, 1298, 1230, 1175, 1137, 1024, 909, 731, 701 cm^{-1}.

_____

2-(2,2,2-trifluoro-1-(4-hydroxy-3,5-dimethylphenyl)-1-phenylethyl)malononitrile (9jd) was prepared according to GP1 (aqueous workup after 4 h) from **1j** (12.0 mg, 0.043 mmol) and **2d** (4.9 mg, 0.047 mmol). The crude product was purified by preparative TLC (silica gel, eluent: *n*-pentane:EtOAc:CH$_2$Cl$_2$ = 30:5:65) to give **9jd** (13.4 mg, 91%) as a white solid; m.p. 177°C.

9jd (CG180_1)
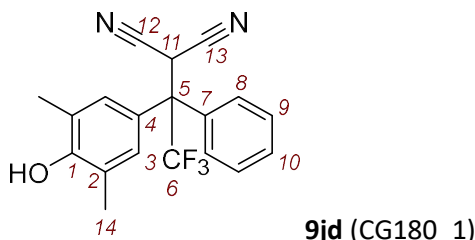
R_f (*n*-pentane/EtOAc/CH$_2$Cl$_2$ 30:5:65, silica, UV) = 0.60.

^{1}H NMR (600 MHz, CDCl$_3$): δ 7.50 – 7.40 (m, 5 H, 8-H, 9-H, 10-H), 6.97 (s, 2 H, 3-H), 4.86 (s, 1 H, 1-H), 4.77 (s, 1 H, 11-H), 2.24 ppm (s, 6 H, 14-H).

^{13}C{^{1}H} NMR (151 MHz, CDCl$_3$): δ 153.4 (C$_q$, C-1), 134.3 (C$_q$, C-7), 129.8 (CH, C-10), 129.4 (CH, C-3, q, $^4J_{C,F}$ = 1.7 Hz), 129.1 (CH, C-8, q, $^4J_{C,F}$ = 1.8 Hz), 129.0 (CH, C-9), 125.4 (C-F, C-6, q, $^1J_{C,F}$ = 286.5 Hz), 125.3 (C$_q$, C-4), 123.6 (C$_q$, C-2), 110.7 (C-N, C-13), 110.6 (C-N, C-12), 60.0 (C$_q$, C-5, q, $^2J_{C,F}$ = 24.9 Hz), 31.4 (CH, C-11, q, $^3J_{C,F}$ = 2.4 Hz), 16.3 ppm (CH$_3$, C-14).

^{19}F NMR (377 MHz, CDCl$_3$): δ -65.00 ppm.

HRMS (EI): *m*/z calcd for C$_{19}$H$_{15}$F$_3$N$_2$O$^{•+}$ [M$^{•+}$]: 344.1131; found: 344.1129.

IR (neat, ATR): ṽ 3485, 2887, 2262, 1492, 1238, 1202, 1139, 1027, 871, 742, 718, 701 cm^{-1}.

diethyl 2-(2,2,2-trifluoro-1-(4-hydroxy-3,5-dimethylphenyl)-1-phenylethyl)malonate (9jf) was prepared according to GP1 (aqueous workup after 4 h) from **1j** (12.0 mg, 0.043 mmol) and **2f** (9.4 mg, 0.047 mmol). The crude product was purified by preparative TLC (silica gel, eluent: *n*-pentane:EtOAc = 8:2) to give **9jf** (17.0 mg, 90%) as a colorless oil.

9jf (CG179)
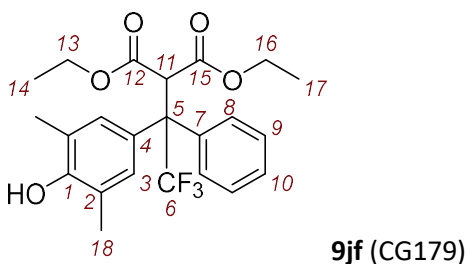
R_f (*n*-pentane/EtOAc 8:2, silica, UV) = 0.70.

^{1}H NMR (400 MHz, CDCl$_3$): δ 7.52 – 7.43 (m, 2 H, 8-H), 7.35 – 7.27 (m, 3 H, 9-H, 10-H), 7.00 (s, 2 H, 3-H), 4.74 (s, 1 H, 11-H), 4.69 (s, 1 H, 1-H), 4.14 – 3.95 (m, 4 H, 13-H, 16-H), 2.19 (s, 6 H, 18-H), 1.14 (t, *J* = 7.1 Hz, 3 H, 17-H), 1.09 ppm (t, *J* = 7.1 Hz, 3 H, 14-H).

^{13}C{^{1}H} NMR (101 MHz, CDCl$_3$): δ 166.5 (C=O, C-15), 166.5 (C=O, C-12), 152.0 (C$_q$, C-1), 137.4 (C$_q$, C-7), 130.6 (CH, C-3, q, $^4J_{C,F}$ = 1.7 Hz), 130.4 (CH, C-8, q, $^4J_{C,F}$ = 1.7 Hz), 128.6 (C$_q$, C-4), 128.0 (CH, C-10), 127.5 (CH, C-9), 126.8 (C-F, C-6, q, $^1J_{C,F}$ = 286.5 Hz), 122.0 (C$_q$, C-2), 61.9 (CH$_2$, C-16), 61.8 (CH$_2$, C-13), 60.1 (C$_q$, C-5, q, $^2J_{C,F}$ = 23.7 Hz), 57.0 (CH, C-11), 16.3 (CH$_3$, C-18), 13.9 (CH$_3$, C-17), 13.8 ppm (CH$_3$, C-14).

^{19}F NMR (377 MHz, CDCl$_3$): δ -63.76 ppm.

HRMS (EI): *m/z* calcd for $C_{23}H_{25}F_3O_5^{\bullet+}$ [M$^{\bullet+}$]: 438.1649; found: 438.1647.

IR (film, ATR): $\tilde{v}$ 3505, 2982, 1732, 1494, 1369, 1301, 1220, 1137, 1025, 870, 735, 700 cm^{-1}.

4.4.6. Products of δ-cyano *para*-Quinone Methides with other Nucleophiles (Heteroatoms)

2-(4-hydroxyphenyl)-2-(4-methoxyphenyl)-2-(pyrrolidin-1-yl)acetonitrile (10) was prepared by mixing of **1a** (11.5 mg, 0.049 mmol), and pyrrolidine (6.9 mg, 8.0 µL, 0.098 mmol) in 2 mL of d_3-acetonitrile under nitrogen atmosphere. After 4 h all volatiles were removed under reduced pressure and the residue **10** was analysed by NMR spectroscopy.

10 (CG192_1)
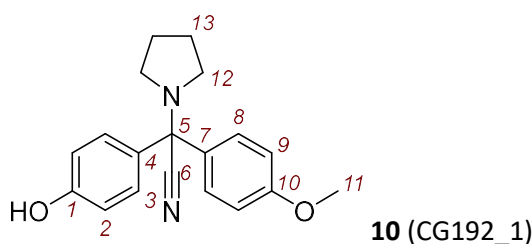
^{1}H NMR (400 MHz, CD$_3$CN): *δ* 7.54 (d, *J* = 8.9 Hz, 2 H, 8-H), 7.43 (d, *J* = 8.7 Hz, 2 H, 3-H), 6.88 (d, *J* = 8.9 Hz, 2 H, 9-H), 6.73 (d, *J* = 8.7 Hz, 2 H, 2-H), 6.23 (s, 1 H,1-H), 3.74 (s, 3 H, 11-H), 2.64 – 2.43 (m, 4 H, 12-H), 1.87 – 1.74 ppm (m, 4 H, 13-H).

^{13}C{^{1}H} NMR (101 MHz, CD$_3$CN): *δ* 160.3 (C$_q$, C-10), 158.9 (C$_q$, C-1), 134.6 (C$_q$, C-7), 132.6 (C$_q$, C-4), 128.1 (CH, C-3), 128.0 (CH, C-8), 119.1 (C-N, C-6), 116.6 (CH, C-2), 115.0 (CH, C-9), 75.0 (C$_q$, C-5), 56.0 (CH$_3$, C-11), 50.6 (CH$_2$, C-12), 24.4 ppm (CH$_2$, C-13).

HRMS (neg. ESI): *m/z* calcd for $C_{19}H_{19}N_2O_2^-$ [M − H$^+$]: 307.1452 found: 307.1452.

2-(4-hydroxyphenyl)-2-(4-methoxyphenyl)acetonitrile (11) was prepared according to GP1 (aqueous workup after 3 h) from **1a** (12.0 mg, 0.051 mmol) and NaBH$_4$ (2.1 mg, 0.056 mmol). The crude product was purified by preparative TLC (silica gel, eluent: *n*-pentane:EtOAc = 7:3) to give **11** (7.9 mg, 65%) as a colorless solid (literature known compound: ref. [13]); m.p. 179°C.

11 (CG198F1)
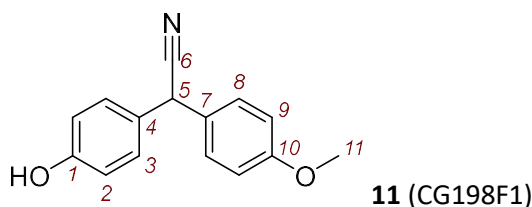
R$_f$ (*n*-pentane/EtOAc 7:3, silica, UV) = 0.60.
^{1}H NMR (400 MHz, CDCl$_3$): *δ* 7.23 (d, *J* = 8.4 Hz, 2 H, 8-H), 7.19 (d, *J* = 8.2 Hz, 2 H, 3-H), 6.89 (d, *J* = 8.9 Hz, 2 H, 9-H), 6.82 (d, *J* = 8.8 Hz, 2 H, 2-H), 5.04 (s, 1 H, 5-H), 4.83 (s, 1 H, 1-H), 3.80 ppm (s, 3 H, 11-H).

^{13}C{^{1}H} NMR (101 MHz, CDCl$_3$): *δ* 159.6 (C$_q$, C-10), 155.5 (C$_q$, C-1), 129.2 (CH, C-3), 129.0 (CH, C-8), 128.7 (C$_q$, C-4), 128.3 (C$_q$, C-7), 120.2 (C-N, C-6), 116.1 (CH, C-2), 114.7 (CH, C-9), 55.5 (CH$_3$, C-11), 41.2 ppm (CH, C-5).

HRMS (EI): *m/z* calcd for $C_{15}H_{13}O_2N^{\bullet+}$ [M$^{\bullet+}$]: 239.0941; found: 239.0941.

IR (neat, ATR): $\tilde{v}$ 3462, 2919, 2260, 1610, 1509, 1438, 1251, 1174, 1027, 815, 789, 761 cm^{-1}.

2-(4-hydroxyphenyl)-2-(4-methoxyphenyl)-2-(methylthio)acetonitrile (12) was prepared according to GP1 (aqueous workup after 30 min) from **1a** (14.0 mg, 0.059 mmol) and sodium methanethiolate (4.5 mg, 0.065 mmol). The crude product was purified by preparative TLC (silica gel, eluent: *n*-pentane:EtOAc = 7:3) to give **12** (12.1 mg, 72%) as a yellowish oil.

12 (CG191)
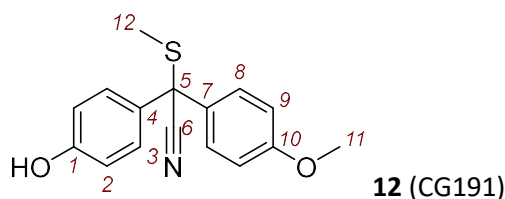
R_f (*n*-pentane/EtOAc 7:3, silica, UV) = 0.60.
^{1}H NMR (600 MHz, CDCl$_3$): δ 7.48 (d, *J* = 9.0 Hz, 2 H, 8-H), 7.43 (d, *J* = 8.9 Hz, 2 H, 3-H), 6.90 (d, *J* = 9.0 Hz, 2 H, 9-H), 6.83 (d, *J* = 8.9 Hz, 2 H, 2-H), 5.06 (s, 1 H, 1-H), 3.81 (s, 3 H, 11-H), 2.16 ppm (s, 3 H, 12-H).

^{13}C{^{1}H} NMR (151 MHz, CDCl$_3$): δ 159.8 (C$_q$, C-10), 155.9 (C$_q$, C-1), 129.6 (C$_q$, C-4), 129.3 (C$_q$, C-7), 129.2 (CH, C-3), 129.0 (CH, C-8), 120.3 (C-N, C-6), 115.8 (CH, C-2), 114.3 (CH, C-9), 55.5 (CH$_3$, C-11), 54.3 (C$_q$, C-5), 15.8 ppm (CH$_3$, C-12).

HRMS (neg. ESI): *m/z* calcd for $C_{16}H_{14}NO_2S^-$ [M − H$^+$]: 284.0750; found: 284.0752.

IR (film, ATR): $\tilde{v}$ 3385, 2917, 2235, 1606, 1506, 1439, 1252, 1174, 1116, 1032, 965, 830 cm^{-1}.

2-ethoxy-2-(3-fluorophenyl)-2-(4-hydroxyphenyl)acetonitrile (13) was prepared by dissolving **1d** (30.0 mg, 0.13 mmol) in 3 mL of ethanol. After four weeks almost full decolorization occurred. The solvent was removed under reduced pressure and the crude product was purified by preparative TLC (silica gel, eluent: *n*-pentane:EtOAc = 8:2) to give **13** (25 mg, 71%) as a yellowish oil.

13 (JR015EtOH)
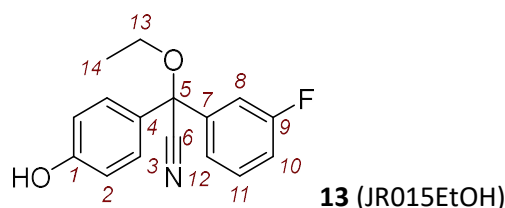
R_f (*n*-pentane/EtOAc 8:2, silica, UV) = 0.60.
^{1}H NMR (400 MHz, CDCl$_3$): δ 7.40 – 7.28 (m, 3 H, 3-H, 11-H), 7.28 – 7.23 (m, 1 H, 12-H), 7.20 (dt, *J* = 9.7, 2.2 Hz, 1 H, 8-H), 7.03 (td, *J* = 9.2, 3.1 Hz, 1 H, 10-H), 6.82 (d, *J* = 8.9 Hz, 2 H, 2-H), 5.27 (s, 1 H, 1-H), 3.69 – 3.44 (m, 2 H, 13-H), 1.30 ppm (t, *J* = 7.0 Hz, 3 H, 14-H).

^{13}C{^{1}H} NMR (101 MHz, CDCl$_3$): δ 163.0 (C-F, C-9, d, $^1J_{C,F}$ = 247.5 Hz), 156.5 (C$_q$, C-1), 142.2 (C$_q$, C-7, d, $^3J_{C,F}$ = 7.1 Hz), 130.9 (C$_q$, C-4), 130.4 (CH, C-11, d, $^3J_{C,F}$ = 8.2 Hz), 128.2 (CH, C-3), 122.3 (CH, C-12, d, $^4J_{C,F}$ = 3.1 Hz), 118.5 (C-N, C-6), 116.1 (CH, C-10, d, $^2J_{C,F}$ = 21.2 Hz), 115.8 (CH, C-2), 113.7 (CH, C-8, d, $^2J_{C,F}$ = 23.7 Hz), 80.9 (C$_q$, C-5, d, $^4J_{C,F}$ = 2.1 Hz), 62.7 (CH$_2$, C-13), 15.1 ppm (CH$_3$, C-14).

_____

HRMS (EI): *m/z* calcd for $C_{16}H_{14}FNO_2^{\bullet+}$ [$M^{\bullet+}$]: 271.1004; found: 271.1004.

IR (film, ATR): $\tilde{v}$ 3409, 2980, 2243, 1593, 1511, 1442, 1244, 1174, 1066, 811, 785, 692 cm^{-1}.

4.4.7. UV/Vis Spectra and Molar Absorption Coefficients of δ-substituted *p*QMs

A solution of the quinone methide (4-16 mM in dry DMSO) was added stepwise to a known volume of DMSO. The absorbances *A* of the *p*QM solutions were detected by using a *J&M* TIDAS diode array spectrophotometer (connected to a Hellma quartz probe with a path length *d* = 0.5 cm).

Molar absorption coefficients ε (M^{-1} cm^{-1}) were determined from the slopes of linear correlations of absorbance with *p*QM concentrations by assuming the validity of the Beer-Lambert law [Equation (S1)].

$$\lg (I_0/I) = A = \varepsilon\, d\, c \qquad\qquad (S1)$$

Solutions of CN *p*QM **1a** in DMSO: Concentration-dependent absorbance *A* at λ = 420 nm.

V (L)	[**1a**] (M)	Abs (420 nm)
0.02400	0	0.000
0.02402	8.77×10^{-6}	0.120
0.02404	1.75×10^{-5}	0.234
0.02406	2.63×10^{-5}	0.360
0.02408	3.50×10^{-5}	0.450
0.02410	4.37×10^{-5}	0.572
0.02412	5.24×10^{-5}	0.662
0.02414	6.11×10^{-5}	0.767
0.02416	6.98×10^{-5}	0.873
0.02418	7.84×10^{-5}	0.968
0.02420	8.71×10^{-5}	1.085
0.02422	9.57×10^{-5}	1.173

Abs = 12190[**1a**] + 0.0204
R^2 = 0.9991
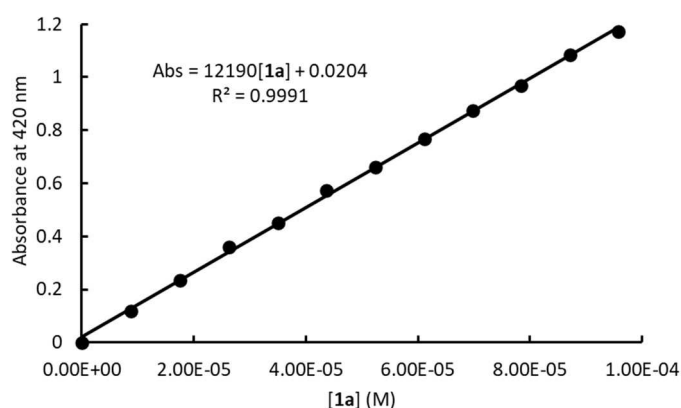
Concentration-dependent absorbance of CN *p*QM **1a** used to determine ε (at λ = 420 nm, *d* = 0.5 cm).

In DMSO:

λ_{max} = **420 nm**

ε = **2.44 × 10⁴ M⁻¹ cm⁻¹**

1a

Wavelength λ (nm)

_____
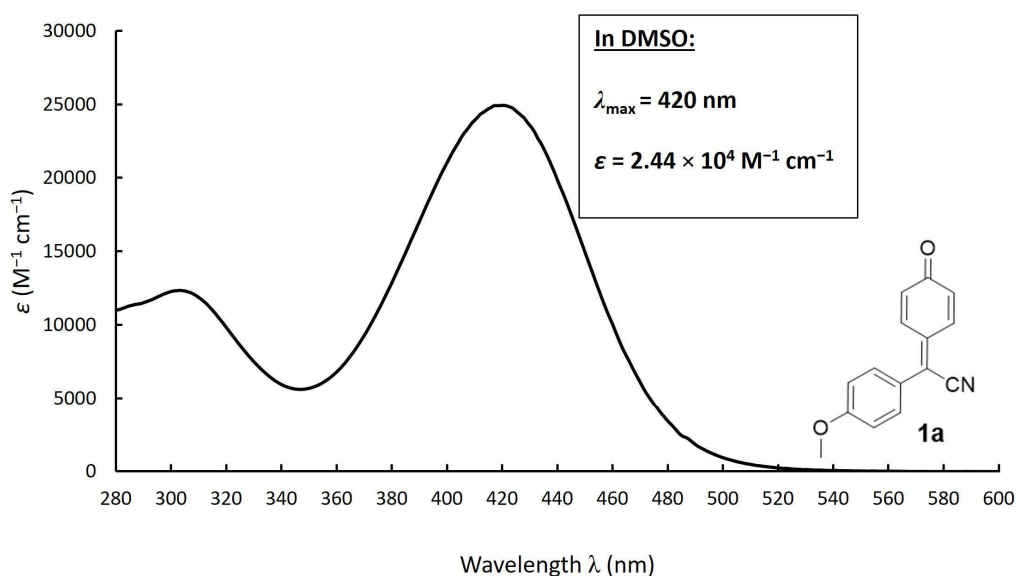
Solutions of CN *p*QM **1b** in DMSO: Concentration-dependent absorbance *A* at λ = 383 nm.

V (L)	[**1b**] (M)	Abs (383 nm)
0.02400	0	0.000
0.02402	1.13×10^{-5}	0.138
0.02404	2.26×10^{-5}	0.274
0.02406	3.38×10^{-5}	0.381
0.02408	4.50×10^{-5}	0.503
0.02410	5.63×10^{-5}	0.648
0.02412	6.75×10^{-5}	0.758
0.02414	7.86×10^{-5}	0.881
0.02416	8.98×10^{-5}	1.001
0.02418	1.01×10^{-4}	1.135
0.02420	1.12×10^{-4}	1.251

y = 11098[**1b**] + 0.0103
R^2 = 0.9996

Concentration-dependent absorbance of CN *p*QM **1b** used to determine ε (at λ = 383 nm, *d* = 0.5 cm).

In DMSO:

λ_{max} = **383 nm**

ε = **2.22×10^4 M^{-1} cm^{-1}**
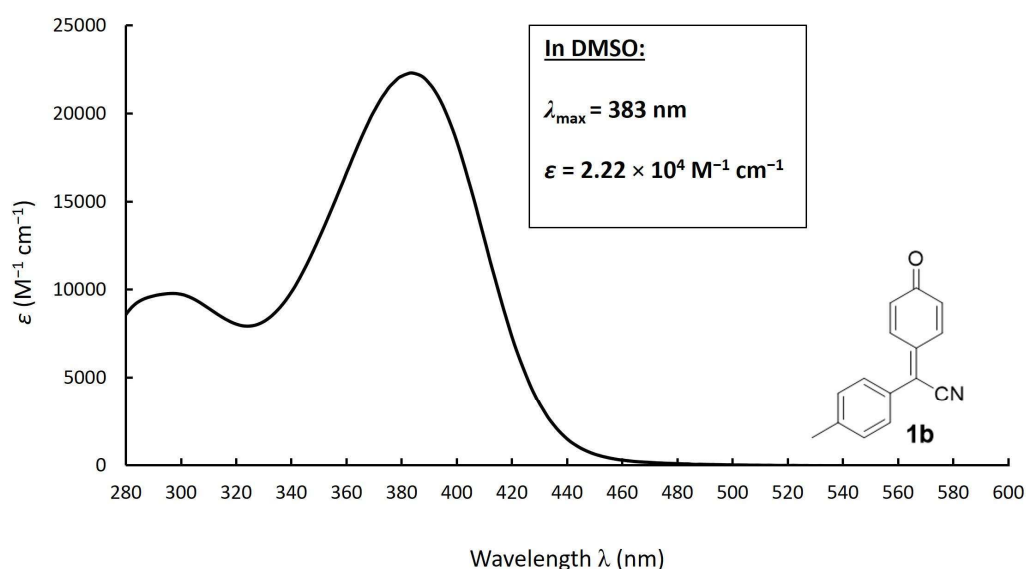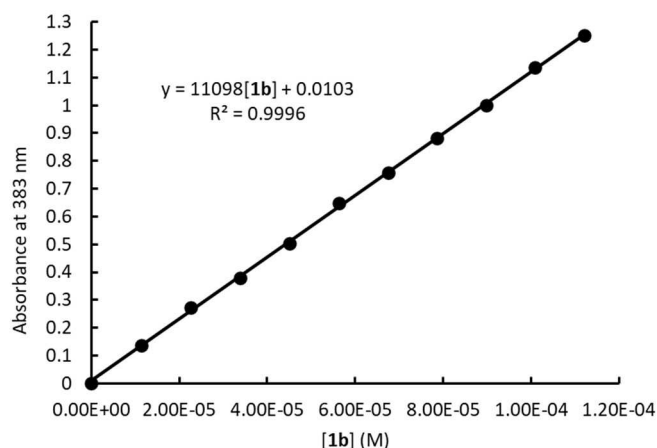
Solutions of CN *p*QM **1c** in DMSO: Concentration-dependent absorbance *A* at λ = 364 nm.

V (L)	[**1c**] (M)	Abs (364 nm)
0.02400	0	0.000
0.02410	1.50×10^{-5}	0.150
0.02420	2.99×10^{-5}	0.290
0.02430	4.47×10^{-5}	0.433
0.02440	5.93×10^{-5}	0.570
0.02450	7.39×10^{-5}	0.709
0.02460	8.83×10^{-5}	0.845
0.02470	1.03×10^{-4}	0.947
0.02480	1.17×10^{-4}	1.112
0.02490	1.31×10^{-4}	1.242
0.02500	1.45×10^{-4}	1.370

y = 9451[**1c**] + 0.0073
R^2 = 0.9999

Concentration-dependent absorbance of CN *p*QM **1c** used to determine ε (at λ = 364 nm, *d* = 0.5 cm).

In DMSO:

λ_{max} = 364 nm

ε = 1.89 × 10⁴ M⁻¹ cm⁻¹
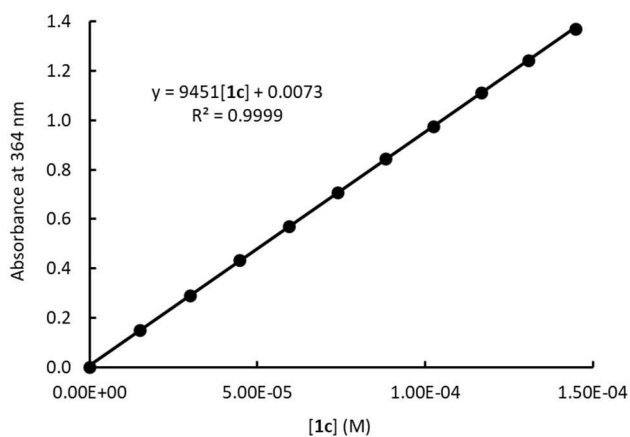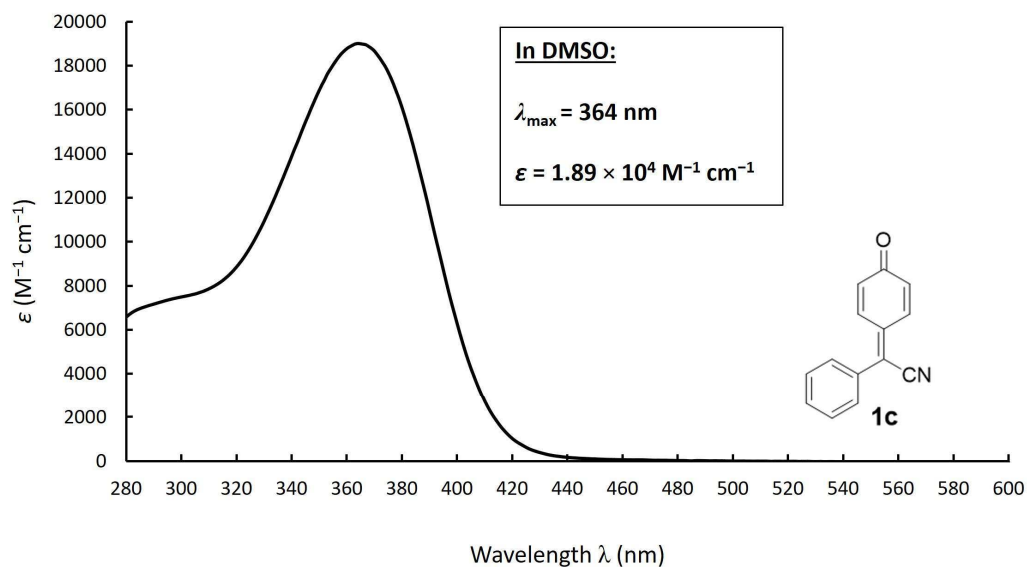
Solutions of CN *p*QM **1d** in DMSO: Concentration-dependent absorbance *A* at λ = 353 nm.

V	[1d]	Abs
(L)	(M)	(353 nm)
0.02400	0	0.000
0.02402	1.24 × 10⁻⁵	0.094
0.02404	2.47 × 10⁻⁵	0.221
0.02406	3.71 × 10⁻⁵	0.348
0.02408	4.94 × 10⁻⁵	0.471
0.02412	7.40 × 10⁻⁵	0.721
0.02414	8.63 × 10⁻⁵	0.852
0.02416	9.85 × 10⁻⁵	0.987
0.02418	1.11 × 10⁻⁴	1.102

y = 10135[**1d**] - 0.0225
R^2 = 0.9993
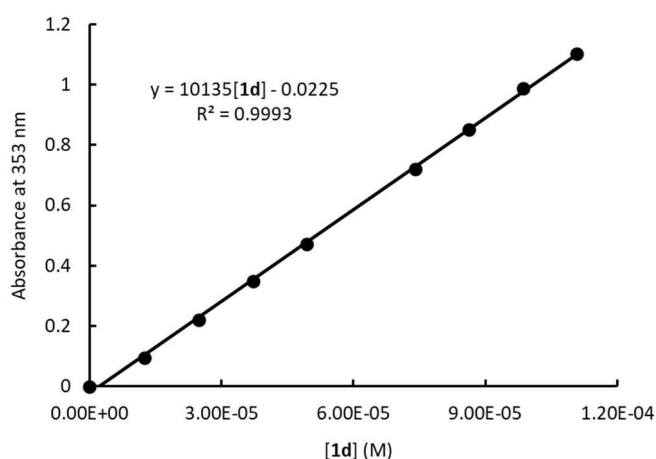
Concentration-dependent absorbance of CN *p*QM **1d** used to determine *ε* (at λ = 353 nm, *d* = 0.5 cm).

In DMSO:

λ_{max} = 353 nm

ε = 2.03 × 10⁴ M⁻¹ cm⁻¹

118

_____
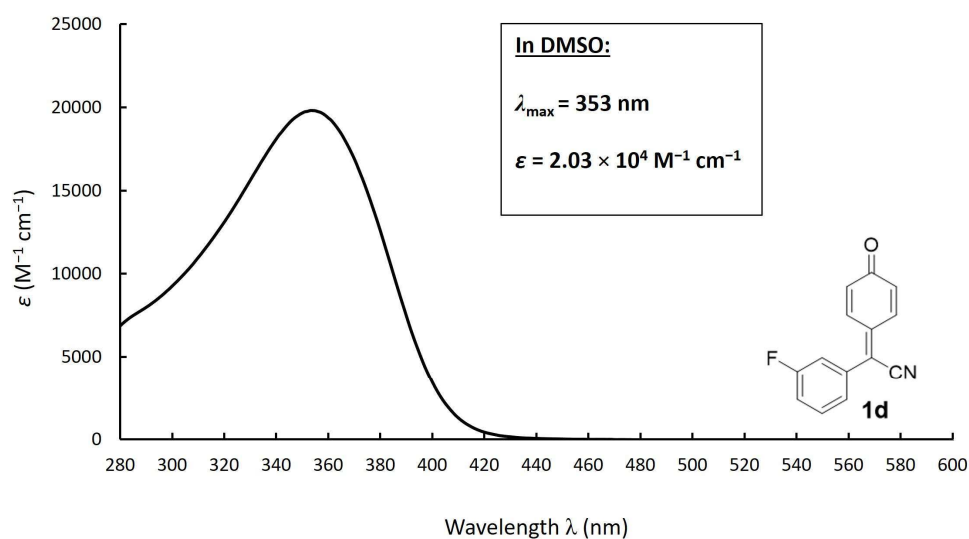
Solutions of CN *p*QM **1e** in DMSO: Concentration-dependent absorbance *A* at λ = 344 nm.

V (L)	[**1e**] (M)	Abs (344 nm)
0.02400	0	0.000
0.02402	7.26×10^{-6}	0.097
0.02404	1.45×10^{-5}	0.203
0.02406	2.17×10^{-5}	0.306
0.02408	2.90×10^{-5}	0.417
0.02410	3.62×10^{-5}	0.520
0.02412	4.34×10^{-5}	0.618
0.02414	5.06×10^{-5}	0.732
0.02416	5.77×10^{-5}	0.824
0.02418	6.49×10^{-5}	0.923
0.02420	7.21×10^{-5}	1.019
0.02422	7.92×10^{-5}	1.120
0.02424	8.63×10^{-5}	1.221

$y = 14191[\mathbf{1e}] + 0.0009$
$R^2 = 0.9998$
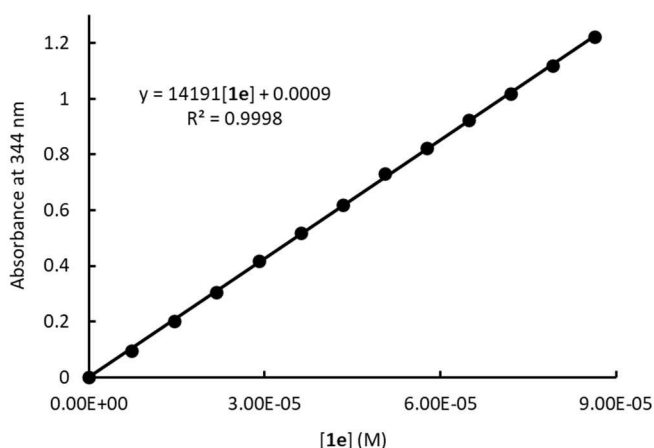
Concentration-dependent absorbance of CN *p*QM **1e** used to determine ε (at λ = 344 nm, *d* = 0.5 cm).

In DMSO:

λ_{max} = **344 nm**

$\varepsilon = 2.84 \times 10^4$ **M^{-1} cm^{-1}**
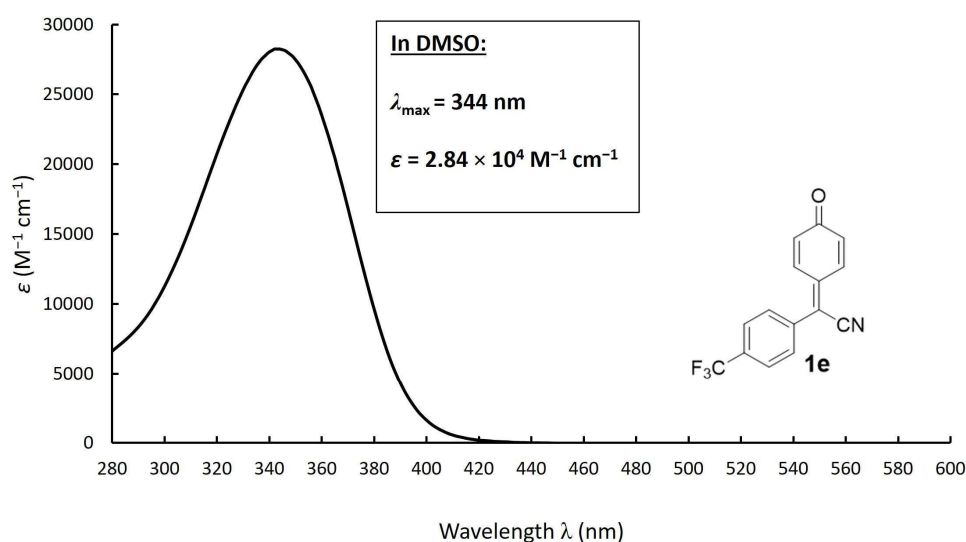
Solutions of CN *p*QM **1f** in DMSO: Concentration-dependent absorbance *A* at λ = 350 nm.

V (L)	[**1f**] (M)	Abs (350 nm)
0.02400	0	0.000
0.02402	1.00×10^{-5}	0.059
0.02404	2.01×10^{-5}	0.193
0.02406	3.01×10^{-5}	0.336
0.02408	4.01×10^{-5}	0.461
0.02410	5.00×10^{-5}	0.629
0.02412	6.00×10^{-5}	0.731
0.02414	6.99×10^{-5}	0.857
0.02416	7.98×10^{-5}	0.994
0.02418	8.98×10^{-5}	1.122
0.02420	9.96×10^{-5}	1.259

$y = 13012x - 0.0461$
$R^2 = 0.9977$
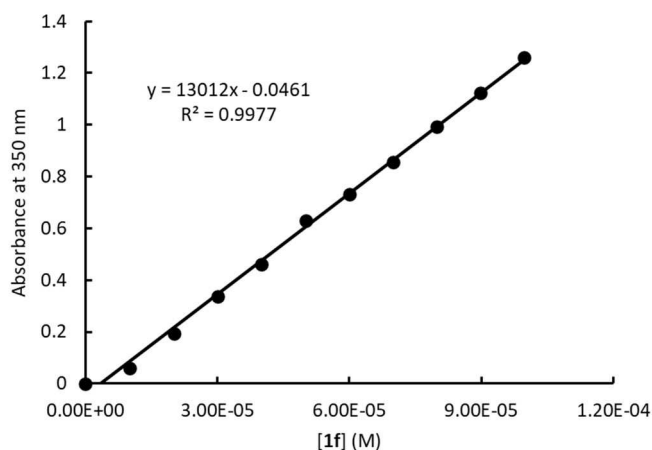
Concentration-dependent absorbance of CN *p*QM **1f** used to determine ε (at λ = 350 nm, *d* = 0.5 cm).

_____

In DMSO:

λ_{max} = 350 nm

$\varepsilon = 2.60 \times 10^4$ M^{-1} cm^{-1}
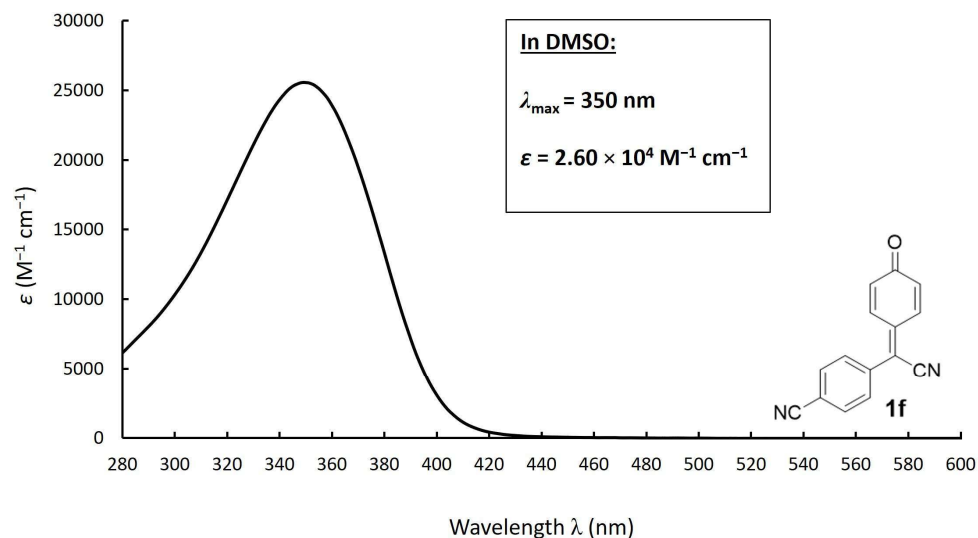
Solutions of CN *p*QM **1g** in DMSO: Concentration-dependent absorbance *A* at λ = 365 nm.

V (L)	[**1g**] (M)	Abs (365 nm)
0.02400	0	0.000
0.02402	1.38×10^{-5}	0.170
0.02404	2.76×10^{-5}	0.333
0.02406	4.13×10^{-5}	0.483
0.02408	5.51×10^{-5}	0.657
0.02410	6.88×10^{-5}	0.807
0.02412	8.25×10^{-5}	0.981
0.02414	9.61×10^{-5}	1.130
0.02416	1.10×10^{-4}	1.320

y = 11879[**1g**] + 0.0002
R² = 0.9996
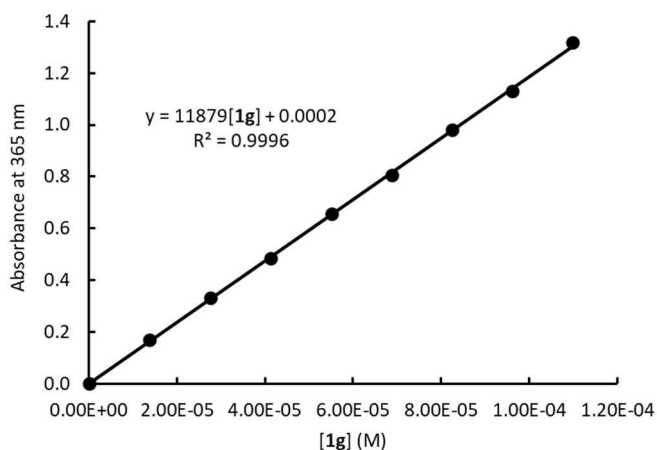
Concentration-dependent absorbance of CN *p*QM **1g** used to determine *ε* (at λ = 365 nm, *d* = 0.5 cm).

In DMSO:

λ_{max} = 365 nm

$\varepsilon = 2.38 \times 10^4$ M^{-1} cm^{-1}

120
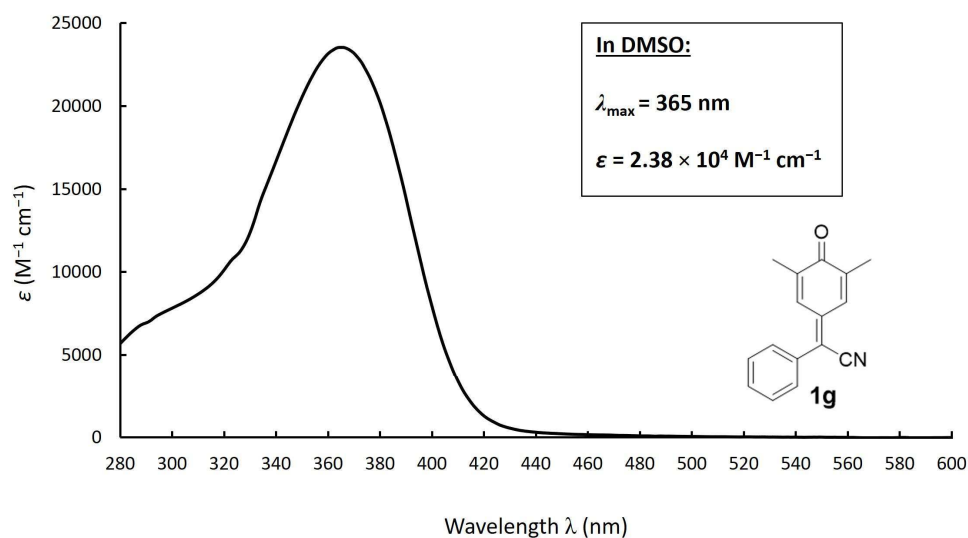
Solutions of CN *p*QM **1h** in DMSO: Concentration-dependent absorbance *A* at λ = 367 nm.

V	[**1h**]	Abs
(L)	(M)	(367 nm)
0.02400	0	0.000
0.02402	7.56×10^{-6}	0.080
0.02404	1.51×10^{-5}	0.200
0.02406	2.26×10^{-5}	0.303
0.02408	3.02×10^{-5}	0.405
0.02410	3.77×10^{-5}	0.511
0.02412	4.52×10^{-5}	0.608
0.02414	5.26×10^{-5}	0.710
0.02416	6.01×10^{-5}	0.807
0.02418	6.76×10^{-5}	0.910
0.02420	7.50×10^{-5}	1.021

y = 13648[**1h**] - 0.0082
R^2 = 0.9997
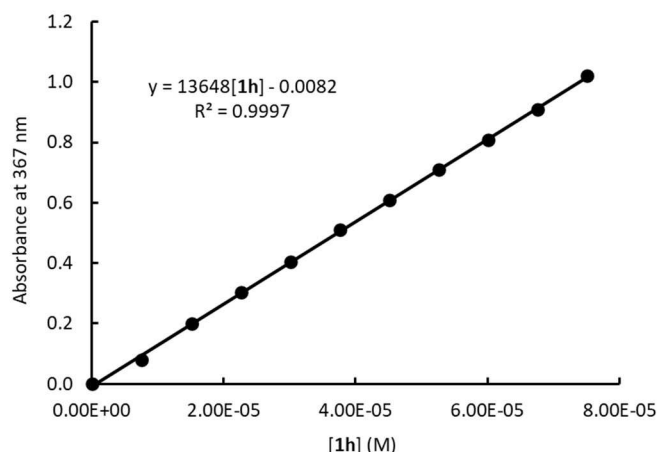
Concentration-dependent absorbance of CN *p*QM **1h** used to determine *ε* (at λ = 367 nm, *d* = 0.5 cm).

In DMSO:

λ_{max} = **367 nm**

ε = **2.73 × 10⁴ M⁻¹ cm⁻¹**
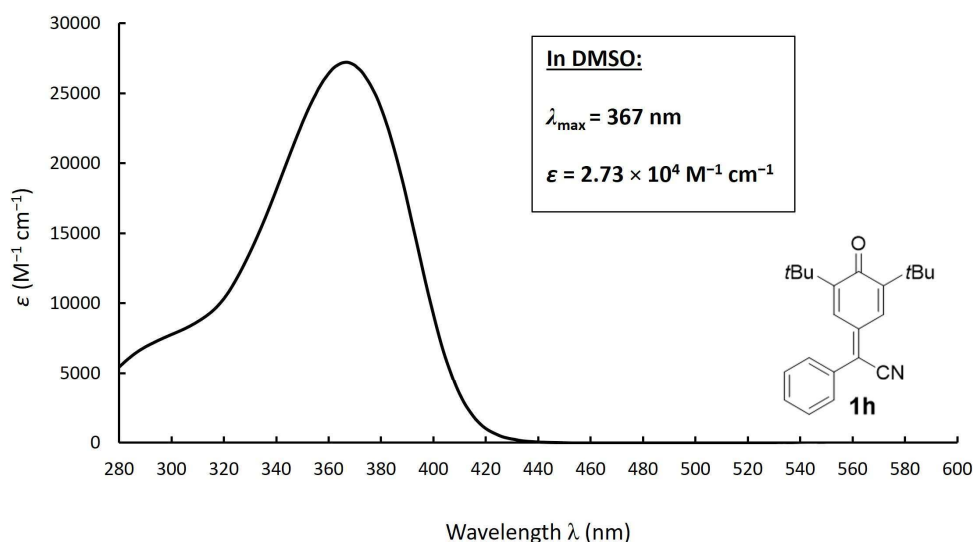
Solutions of CF₃ *p*QM **1j** in DMSO: Concentration-dependent absorbance *A* at λ = 304 nm.

V	[**1j**]	Abs
(L)	(M)	(304 nm)
0.02400	0	0.000
0.02402	1.12×10^{-5}	0.080
0.02412	6.70×10^{-5}	0.200
0.02417	9.48×10^{-5}	0.303
0.02419	1.06×10^{-4}	0.405
0.02421	1.17×10^{-4}	0.511
0.02423	1.28×10^{-4}	0.608
0.02425	1.39×10^{-4}	0.710

y = 8596.8[**1j**] - 0.0167
R^2 = 0.9989
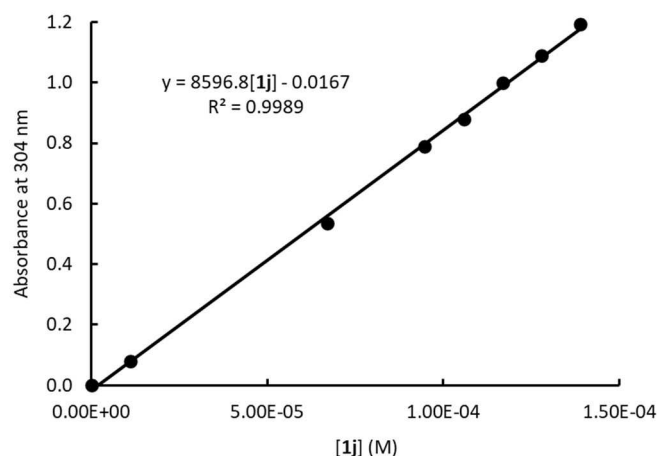
Concentration-dependent absorbance of CF₃ *p*QM **1j** used to determine *ε* (at λ = 304 nm, *d* = 0.5 cm).

In DMSO:

λ_{max} = 304 nm

$\varepsilon = 1.72 \times 10^4$ M^{-1} cm^{-1}
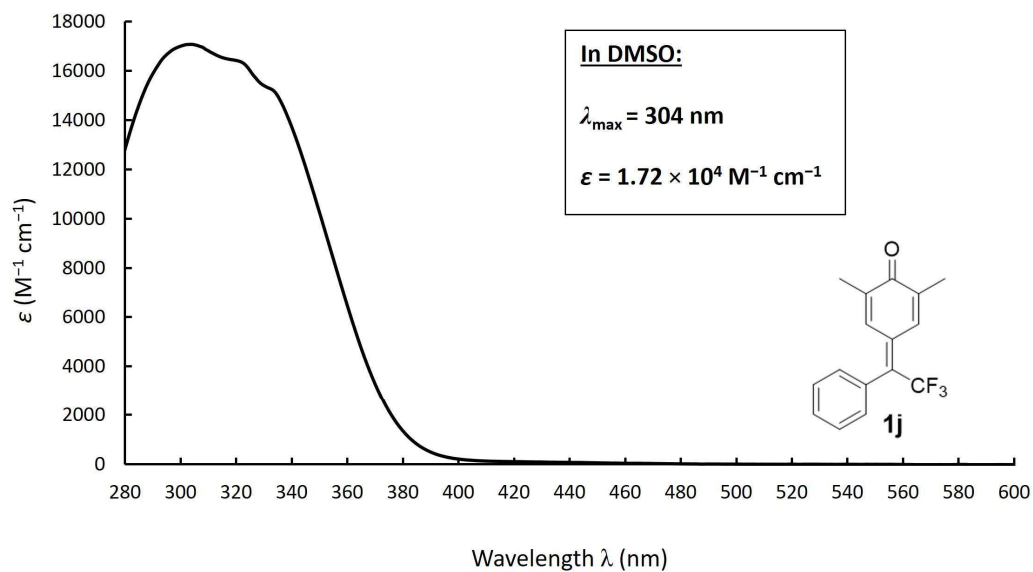
4.4.8. Cyclic Voltammetry-Redox Potentials of *δ*-cyano *para*-Quinone Methides
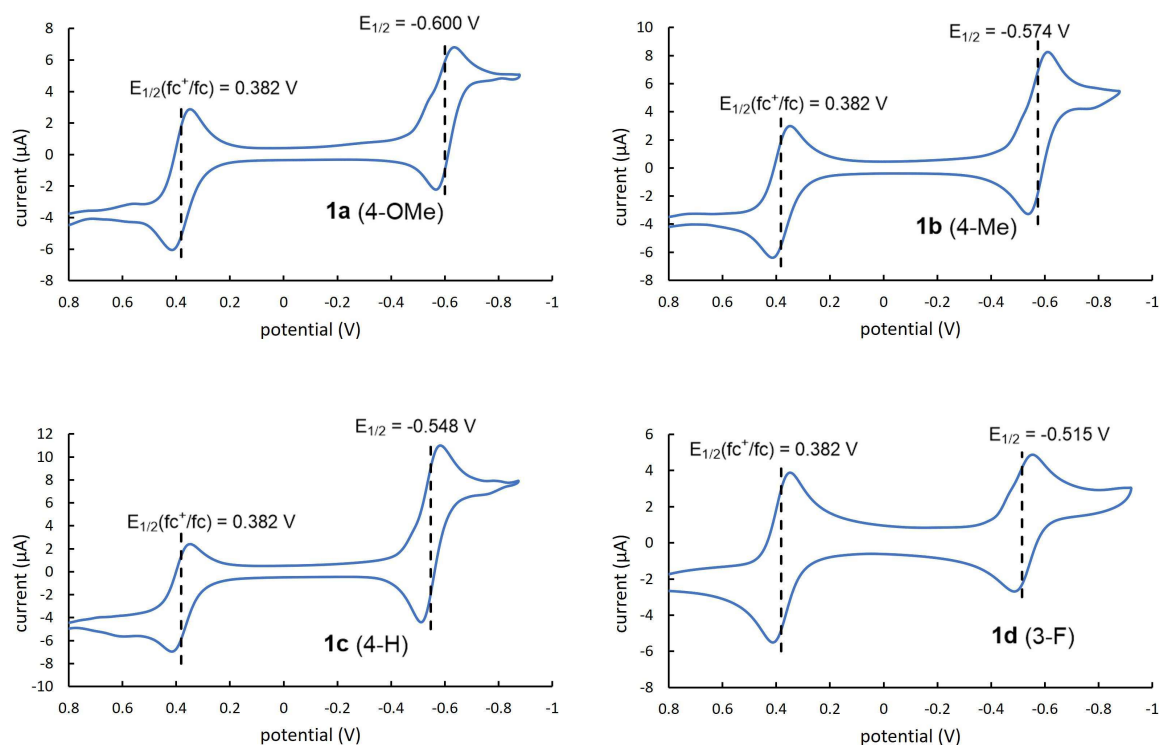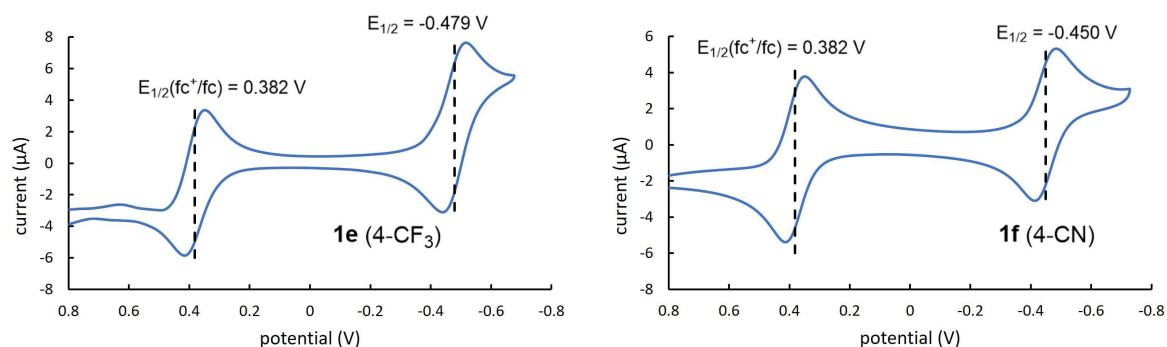
4.4.9. Single Crystal X-Ray Structure Determination

The X-ray intensity data of **1h** (zv313) were measured on a Bruker D8 Venture TXS system equipped with a multilayer mirror monochromator and a Mo Kα rotating anode X-ray tube (λ = 0.71073 Å). The frames were integrated with the Bruker SAINT software package.[42] Data were corrected for absorption effects using the Multi-Scan method (SADABS).[43] The structure was solved and refined using the Bruker SHELXTL Software Package.[44] All hydrogen atoms have been calculated in ideal geometry riding on their parent atoms. The figures have been drawn at the 50% ellipsoid probability level.[45]

2-(3,5-di-tert-butyl-4-oxocyclohexa-2,5-dien-1-ylidene)-2-phenylacetonitrile (1h)
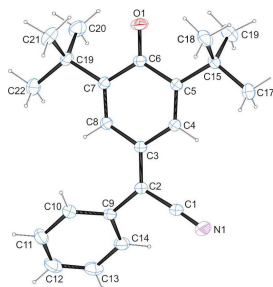
1h (zv313, CG104)

net formula	$C_{22}H_{25}NO$
M_r/g mol^{-1}	319.43
crystal size/mm	0.120 × 0.070 × 0.050
T/K	298.(2)
radiation	MoKα
diffractometer	'Bruker D8 Venture TXS'
crystal system	monoclinic
space group	'C 1 2/c 1'
a/Å	23.9479(15)
b/Å	10.4227(6)
c/Å	18.2166(11)
$α$/°	90
$β$/°	123.876(2)
$γ$/°	90
V/Å^3	3775.0(4)
Z	8
calc. density/g cm^{-3}	1.124
$μ$/mm^{-1}	0.068
absorption correction	Multi-Scan
transmission factor range	0.97–1.00
refls. measured	32636
R_{int}	0.0435
mean σ(I)/I	0.0247
θ range	2.302–27.102
observed refls.	3164
x, y (weighting scheme)	0.0554, 2.0852
hydrogen refinement	constr
Flack parameter	?
refls in refinement	4153
parameters	223
restraints	0
$R(F_{obs})$	0.0497
$R_w(F^2)$	0.1362
S	1.053
shift/error$_{max}$	0.001
max electron density/e Å^{-3}	0.221
min electron density/e Å^{-3}	−0.162

_____

4.4.10. Kinetics of the Reactions of *p*QMs with Carbanions

Kinetic measurements were performed by using UV/Vis photometry on AppliedPhotophysics SX.20 stopped-flow instruments as well as on a conventional J&M TIDAS diode array spectrophotometer, which was controlled by TIDASDAQ3 (v3) software and connected to a Hellma 661.502-QX quartz Suprasil immersion probe (light path d = 5 mm) via fiber optic cables and standard SMA connectors. The temperature (20.0 ± 0.2 °C) was maintained constant by using circulating bath cryostats. All solutions were prepared by using dry DMSO (ThermoScientific, DMSO 99.7+%, extra dry, over molecular sieve, AcroSeal) and kept under an atmosphere of dry nitrogen. The kinetic measurements for each *p*QM/nucleophile combination were performed with or without added 18-crown-6 ether (18-c-6) and in some cases with addition of the corresponding CH-acid (**2**-H).

1a + **2a** in DMSO (stopped-flow method, detection at 420 nm) CG039

[**1a**]$_0$ (M)	[**2a**]$_0$ (M)	[18-c-6]$_0$ (M)	k_{obs} (s^{-1})
2.42×10^{-5}	3.00×10^{-4}		9.43×10^{-3}
2.42×10^{-5}	4.50×10^{-4}	4.95×10^{-4}	1.35×10^{-2}
2.42×10^{-5}	6.00×10^{-4}		1.86×10^{-2}
2.42×10^{-5}	7.50×10^{-4}	8.25×10^{-4}	2.25×10^{-2}
2.42×10^{-5}	9.00×10^{-4}		2.81×10^{-2}

$$k_2 = 3.09 \times 10^1 \ M^{-1} \ s^{-1}$$
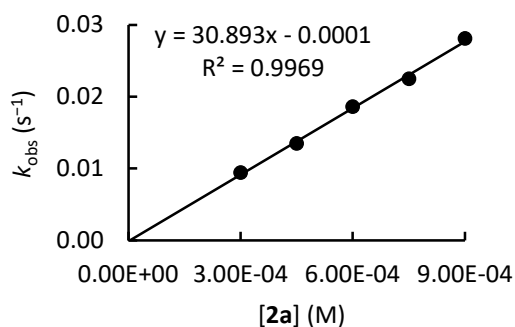
1a + **2b** in DMSO (stopped-flow method, detection at 420 nm) CG051
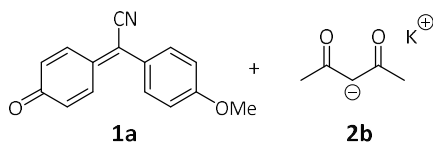
[**1a**]$_0$ (M)	[**2b**]$_0$ (M)	[18-c-6]$_0$ (M)	k_{obs} (s^{-1})
2.38×10^{-5}	3.00×10^{-4}		1.50×10^{-1}
2.38×10^{-5}	4.50×10^{-4}	4.95×10^{-4}	2.30×10^{-1}
2.38×10^{-5}	6.00×10^{-4}		3.06×10^{-1}
2.38×10^{-5}	7.50×10^{-4}	8.25×10^{-4}	3.89×10^{-1}
2.38×10^{-5}	9.00×10^{-4}		4.65×10^{-1}

$$k_2 = 5.26 \times 10^2 \ M^{-1} \ s^{-1}$$
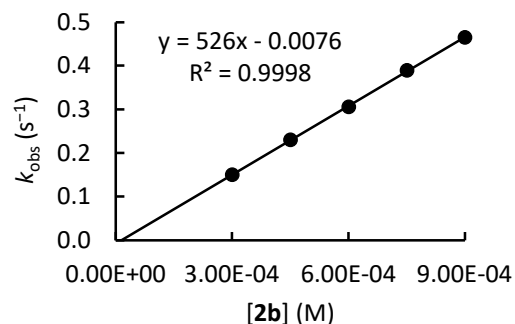
_____

1a + **2c** in DMSO (stopped-flow method, detection at 420 nm) CG047
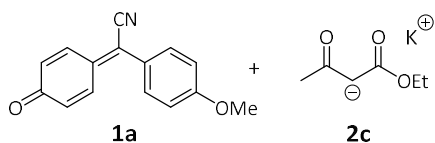
[**1a**]$_0$ (M)	[**2c**]$_0$ (M)	[18-c-6]$_0$ (M)	k_{obs} (s^{-1})
2.40×10^{-5}	3.00×10^{-4}		2.12
2.40×10^{-5}	4.50×10^{-4}	4.95×10^{-4}	3.57
2.40×10^{-5}	6.00×10^{-4}		4.81
2.40×10^{-5}	7.50×10^{-4}	8.25×10^{-4}	6.08
2.40×10^{-5}	9.00×10^{-4}		7.19

$$k_2 = 8.43 \times 10^3 \text{ M}^{-1} \text{ s}^{-1}$$
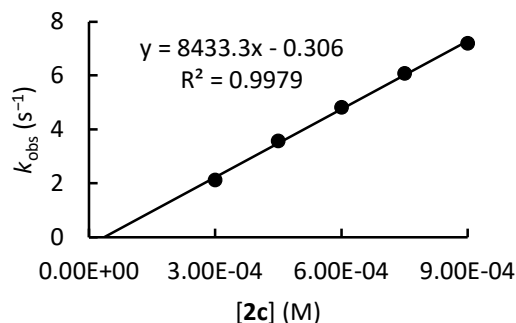
1a + **2d** in DMSO (stopped-flow method, detection at 420 nm) CG040
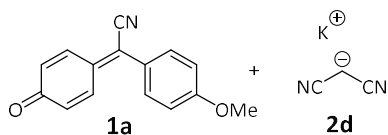
[**1a**]$_0$ (M)	[**2d**]$_0$ (M)	[18-c-6]$_0$ (M)	k_{obs} (s^{-1})
2.28×10^{-5}	3.00×10^{-4}		9.52
2.28×10^{-5}	4.50×10^{-4}	4.95×10^{-4}	1.48×10^1
2.28×10^{-5}	6.00×10^{-4}		2.02×10^1
2.28×10^{-5}	7.50×10^{-4}	8.25×10^{-4}	2.49×10^1
2.28×10^{-5}	9.00×10^{-4}		3.01×10^1

$$k_2 = 3.42 \times 10^4 \text{ M}^{-1} \text{ s}^{-1}$$
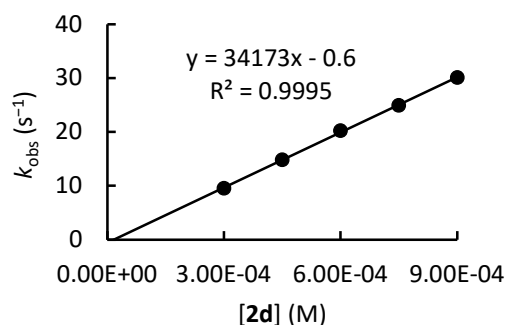
1a + **2f** in DMSO (stopped-flow method, detection at 420 nm) CG041
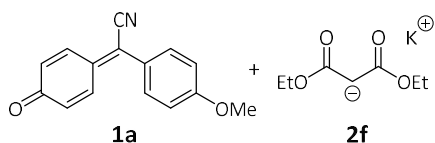
[**1a**]$_0$ (M)	[**2f**]$_0$ (M)	[18-c-6]$_0$ (M)	k_{obs} (s^{-1})
2.20×10^{-5}	3.00×10^{-4}		3.23×10^1
2.20×10^{-5}	4.50×10^{-4}	4.95×10^{-4}	5.21×10^1
2.20×10^{-5}	6.00×10^{-4}		7.08×10^1
2.20×10^{-5}	7.50×10^{-4}	8.25×10^{-4}	8.86×10^1
2.20×10^{-5}	9.00×10^{-4}		1.05×10^2

$$k_2 = 1.21 \times 10^5 \text{ M}^{-1} \text{ s}^{-1}$$
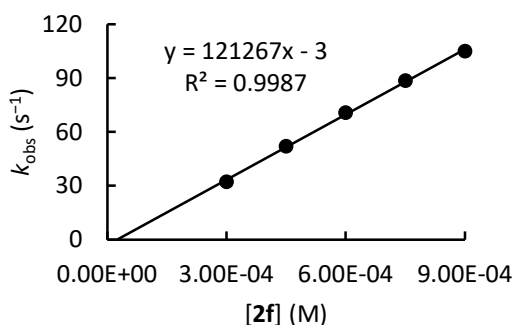
_____

1b + **2a** in DMSO (stopped-flow method, detection at 383 nm) CG078
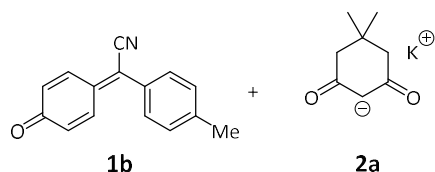
[**1b**]$_0$ (M)	[**2a**]$_0$ (M)	[18-c-6]$_0$ (M)	k_{obs} (s^{-1})
2.56×10^{-5}	2.50×10^{-4}		1.32×10^{-2}
2.56×10^{-5}	3.75×10^{-4}	4.13×10^{-4}	1.99×10^{-2}
2.56×10^{-5}	5.00×10^{-4}		2.65×10^{-2}
2.56×10^{-5}	6.25×10^{-4}	6.90×10^{-4}	3.30×10^{-2}
2.56×10^{-5}	7.50×10^{-4}		4.07×10^{-2}

$$k_2 = 5.45 \times 10^1 \text{ M}^{-1} \text{ s}^{-1}$$
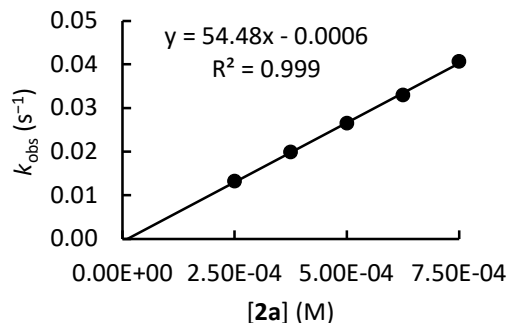
1b + **2b** in DMSO (stopped-flow method, detection at 383 nm) CG068
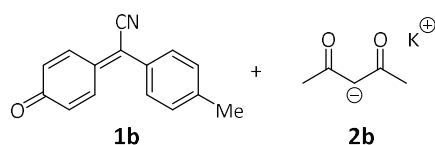
[**1b**]$_0$ (M)	[**2b**]$_0^{[a]}$ (M)	[18-c-6]$_0$ (M)	k_{obs} (s^{-1})
2.47×10^{-5}	2.50×10^{-4}		2.22×10^{-1}
2.47×10^{-5}	3.75×10^{-4}	4.13×10^{-4}	3.37×10^{-1}
2.47×10^{-5}	5.00×10^{-4}		4.50×10^{-1}
2.47×10^{-5}	6.25×10^{-4}	6.90×10^{-4}	5.60×10^{-1}
2.47×10^{-5}	7.50×10^{-4}		6.81×10^{-1}

[a] Additionally, the reaction mixtures contained an equimolar amount of the corresponding CH–acid (**2**-H).

$$k_2 = 9.13 \times 10^2 \text{ M}^{-1} \text{ s}^{-1}$$
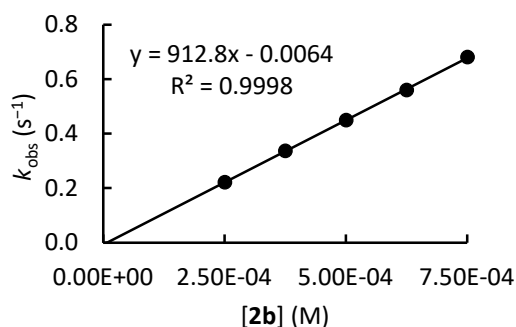
1b + **2c** in DMSO (stopped-flow method, detection at 383 nm) CG053
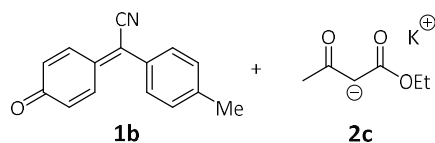
[**1b**]$_0$ (M)	[**2c**]$_0$ (M)	[18-c-6]$_0$ (M)	k_{obs} (s^{-1})
2.51×10^{-5}	3.00×10^{-4}		3.49
2.51×10^{-5}	4.50×10^{-4}	4.95×10^{-4}	5.55
2.51×10^{-5}	6.00×10^{-4}		7.39
2.51×10^{-5}	7.50×10^{-4}	8.25×10^{-4}	9.56
2.51×10^{-5}	9.00×10^{-4}		1.07×10^1

$$k_2 = 1.23 \times 10^4 \text{ M}^{-1} \text{ s}^{-1}$$
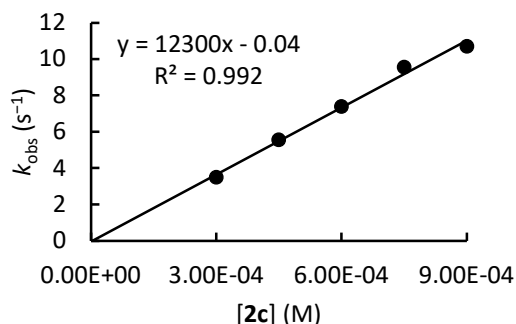
_____

1b + **2d** in DMSO (stopped-flow method, detection at 383 nm) CG026
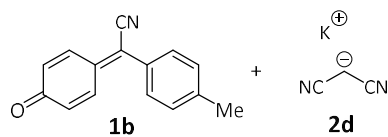
[**1b**]$_0$ (M)	[**2d**]$_0$ (M)	[18-c-6]$_0$ (M)	k_{obs} (s^{-1})
2.83×10^{-5}	2.5×10^{-4}		1.28×10^1
2.83×10^{-5}	3.75×10^{-4}	4.13×10^{-4}	1.98×10^1
2.83×10^{-5}	5.00×10^{-4}		2.69×10^1
2.83×10^{-5}	6.25×10^{-4}	6.90×10^{-4}	3.38×10^1
2.83×10^{-5}	7.50×10^{-4}		4.18×10^1

$$k_2 = 5.76 \times 10^4 \text{ M}^{-1} \text{ s}^{-1}$$
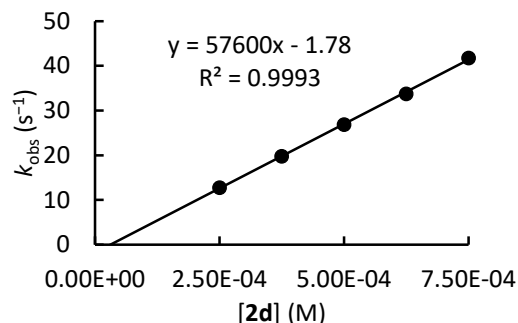
1b + **2f** in DMSO (stopped-flow method, detection at 383 nm) CG023
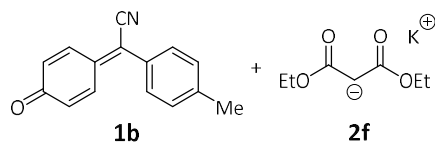
[**1b**]$_0$ (M)	[**2f**]$_0$ (M)	[18-c-6]$_0$ (M)	k_{obs} (s^{-1})
2.71×10^{-5}	7.5×10^{-4}		1.20×10^2
2.71×10^{-5}	1.13×10^{-3}	1.24×10^{-3}	1.74×10^2
2.71×10^{-5}	1.50×10^{-3}		2.48×10^2
2.71×10^{-5}	1.88×10^{-3}	2.07×10^{-3}	3.49×10^2
2.71×10^{-5}	2.25×10^{-3}		4.23×10^2

$$k_2 = 2.08 \times 10^5 \text{ M}^{-1} \text{ s}^{-1}$$
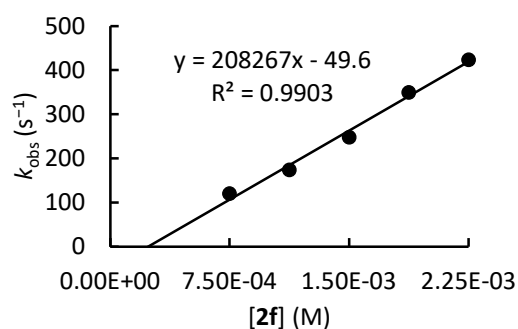
1c + **2a** in DMSO (stopped-flow method, detection at 365 nm) CG038
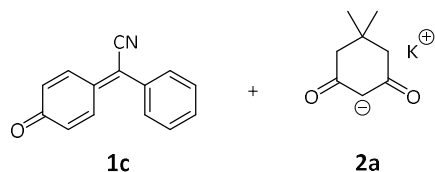
[**1c**]$_0$ (M)	[**2a**]$_0$ (M)	[18-c-6]$_0$ (M)	k_{obs} (s^{-1})
3.52×10^{-5}	3.00×10^{-4}		2.13×10^{-2}
3.52×10^{-5}	4.50×10^{-4}	4.95×10^{-4}	3.01×10^{-2}
3.52×10^{-5}	6.00×10^{-4}		4.07×10^{-2}
3.52×10^{-5}	7.50×10^{-4}	8.25×10^{-4}	4.92×10^{-2}
3.52×10^{-5}	9.00×10^{-4}		6.07×10^{-2}

$$k_2 = 6.53 \times 10^1 \text{ M}^{-1} \text{ s}^{-1}$$
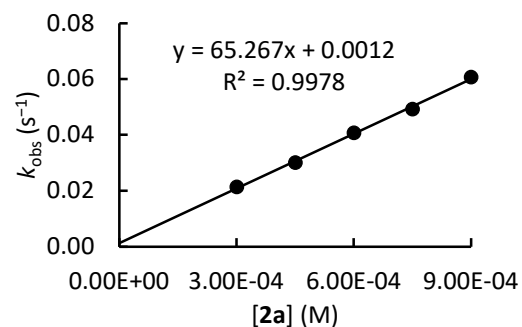
_____

1c + **2b** in DMSO (stopped-flow method, detection at 365 nm) CG050
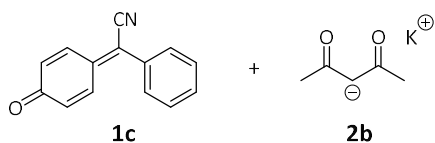
$[\mathbf{1c}]_0$ (M)	$[\mathbf{2b}]_0$ (M)	$[\text{18-c-6}]_0$ (M)	k_{obs} (s^{-1})
3.42×10^{-5}	3.00×10^{-4}		3.18×10^{-1}
3.42×10^{-5}	4.50×10^{-4}	4.95×10^{-4}	4.98×10^{-1}
3.42×10^{-5}	6.00×10^{-4}		6.71×10^{-1}
3.42×10^{-5}	7.50×10^{-4}	8.25×10^{-4}	8.63×10^{-1}
3.42×10^{-5}	9.00×10^{-4}		1.04

$$k_2 = 1.20 \times 10^3 \text{ M}^{-1}\text{ s}^{-1}$$
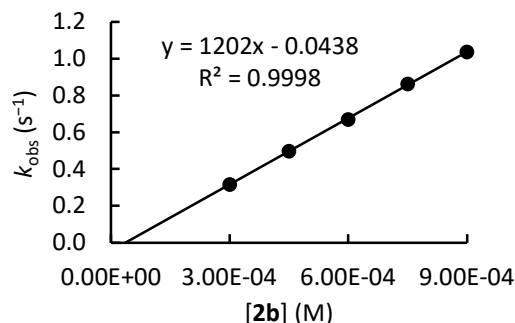
1c + **2c** in DMSO (stopped-flow method, detection at 365 nm) CG046
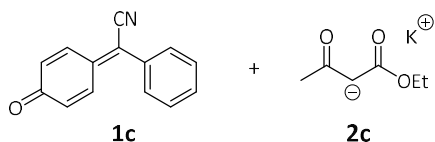
$[\mathbf{1c}]_0$ (M)	$[\mathbf{2c}]_0$ (M)	$[\text{18-c-6}]_0$ (M)	k_{obs} (s^{-1})
3.36×10^{-5}	3.00×10^{-4}		5.17
3.36×10^{-5}	4.50×10^{-4}	4.95×10^{-4}	8.12
3.36×10^{-5}	6.00×10^{-4}		1.08×10^1
3.36×10^{-5}	7.50×10^{-4}	8.25×10^{-4}	1.37×10^1
3.36×10^{-5}	9.00×10^{-4}		1.64×10^1

$$k_2 = 1.87 \times 10^4 \text{ M}^{-1}\text{ s}^{-1}$$
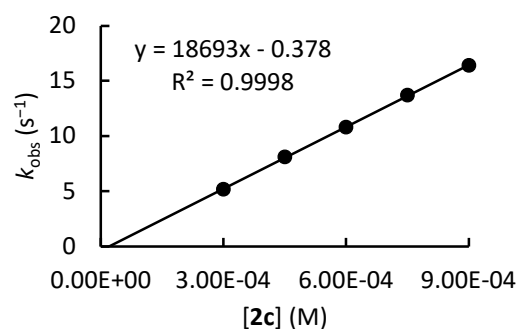
1c + **2d** in DMSO (stopped-flow method, detection at 365 nm) CG025
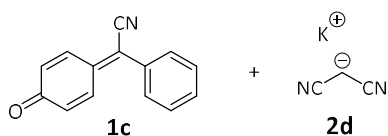
$[\mathbf{1c}]_0$ (M)	$[\mathbf{2d}]_0$ (M)	$[\text{18-c-6}]_0$ (M)	k_{obs} (s^{-1})
3.16×10^{-5}	2.50×10^{-4}		1.64×10^1
3.16×10^{-5}	3.75×10^{-4}	4.13×10^{-4}	2.47×10^1
3.16×10^{-5}	5.00×10^{-4}		3.33×10^1
3.16×10^{-5}	6.25×10^{-4}	6.90×10^{-4}	4.19×10^1
3.16×10^{-5}	7.50×10^{-4}		5.19×10^1

$$k_2 = 7.06 \times 10^4 \text{ M}^{-1}\text{ s}^{-1}$$
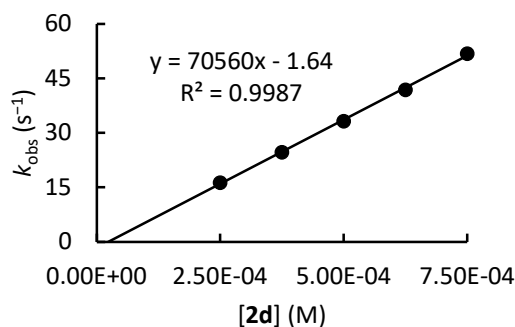
_____

1c + **2f** in DMSO (stopped-flow method, detection at 365 nm) CG022
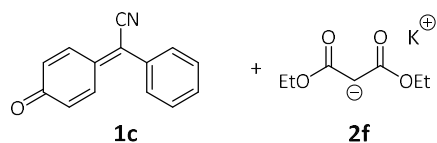
[**1c**]$_0$ (M)	[**2f**]$_0$ (M)	[18-c-6]$_0$ (M)	k_{obs} (s^{-1})
2.78×10^{-5}	7.50×10^{-4}		1.92×10^{2}
2.78×10^{-5}	1.13×10^{-4}	1.24×10^{-3}	3.07×10^{2}
2.78×10^{-5}	1.50×10^{-4}		4.16×10^{2}
2.78×10^{-5}	2.25×10^{-4}		6.60×10^{2}

$$k_2 = 3.12 \times 10^5 \ \text{M}^{-1} \ \text{s}^{-1}$$

Plot: $y = 311695x - 44.571$, $R^2 = 0.9994$
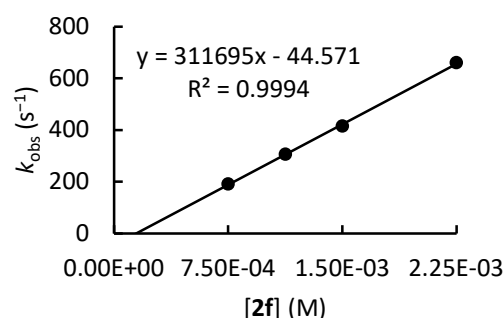
1d + **2a** in DMSO (stopped-flow method, detection at 353 nm) JR026
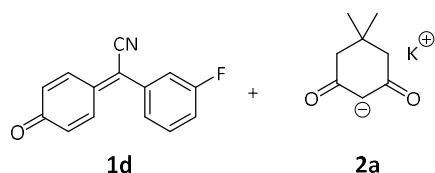
[**1d**]$_0$ (M)	[**2a**]$_0$ (M)	[18-c-6]$_0$ (M)	k_{obs} (s^{-1})
2.50×10^{-5}	2.50×10^{-4}		3.95×10^{-2}
2.50×10^{-5}	3.75×10^{-4}	4.13×10^{-4}	5.88×10^{-2}
2.50×10^{-5}	5.00×10^{-4}		8.01×10^{-2}
2.50×10^{-5}	6.25×10^{-4}	6.90×10^{-4}	9.94×10^{-2}
2.50×10^{-5}	7.50×10^{-4}		1.24×10^{-1}

$$k_2 = 1.68 \times 10^2 \ \text{M}^{-1} \ \text{s}^{-1}$$

Plot: $y = 167.68x - 0.0035$, $R^2 = 0.9981$
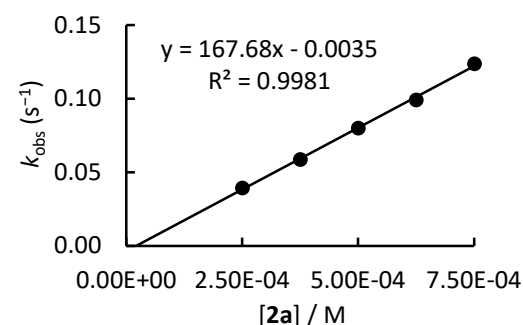
1d + **2b** in DMSO (stopped-flow method, detection at 353 nm) JR025
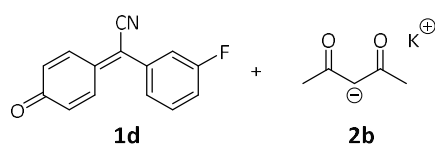
[**1d**]$_0$ (M)	[**2b**]$_0$ (M)	[18-c-6]$_0$ (M)	k_{obs} (s^{-1})
2.50×10^{-5}	2.50×10^{-4}		6.29×10^{-1}
2.50×10^{-5}	3.75×10^{-4}	4.13×10^{-4}	9.72×10^{-1}
2.50×10^{-5}	5.00×10^{-4}		1.29
2.50×10^{-5}	6.25×10^{-4}	6.90×10^{-4}	1.65
2.50×10^{-5}	7.50×10^{-4}		1.93

$$k_2 = 2.62 \times 10^3 \ \text{M}^{-1} \ \text{s}^{-1}$$
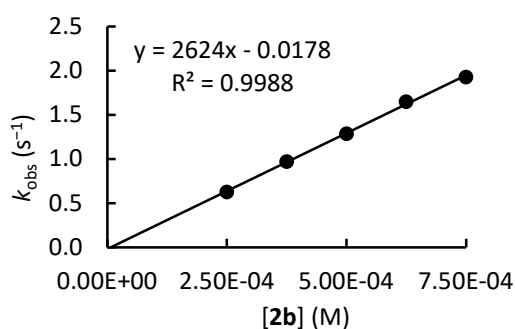
Plot: $y = 2624x - 0.0178$, $R^2 = 0.9988$

1d + **2c** in DMSO (stopped-flow method, detection at 353 nm) JR024
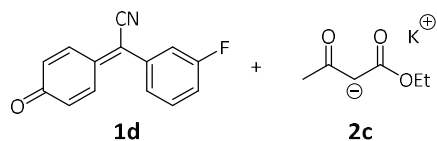
[**1d**]$_0$ (M)	[**2c**]$_0$ (M)	[18-c-6]$_0$ (M)	k_{obs} (s^{-1})
2.50×10^{-5}	2.50×10^{-4}		9.61
2.50×10^{-5}	3.75×10^{-4}	4.13×10^{-4}	1.53×10^1
2.50×10^{-5}	5.00×10^{-4}		2.05×10^1
2.50×10^{-5}	6.25×10^{-4}	6.90×10^{-4}	2.61×10^1
2.50×10^{-5}	7.50×10^{-4}		3.17×10^1

$$k_2 = 4.40 \times 10^4 \text{ M}^{-1} \text{ s}^{-1}$$

y = 43984x - 1.35
R² = 0.9998
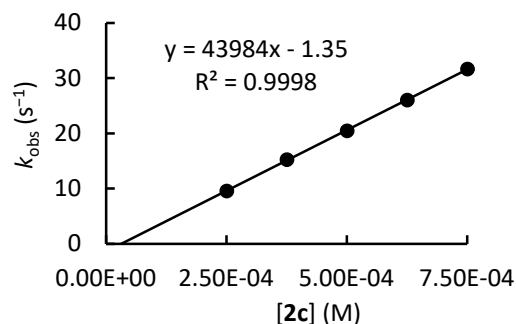
1d + **2d** in DMSO (stopped-flow method, detection at 353 nm) JR022
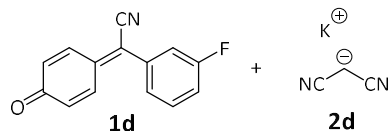
[**1d**]$_0$ (M)	[**2d**]$_0$ (M)	[18-c-6]$_0$ (M)	k_{obs} (s^{-1})
2.50×10^{-5}	2.50×10^{-4}		3.01×10^1
2.50×10^{-5}	3.75×10^{-4}	4.13×10^{-4}	4.57×10^1
2.50×10^{-5}	5.00×10^{-4}		6.02×10^1
2.50×10^{-5}	6.25×10^{-4}	6.90×10^{-4}	7.67×10^1
2.50×10^{-5}	7.50×10^{-4}		9.36×10^1

$$k_2 = 1.26 \times 10^5 \text{ M}^{-1} \text{ s}^{-1}$$

y = 126400x - 1.94
R² = 0.9992
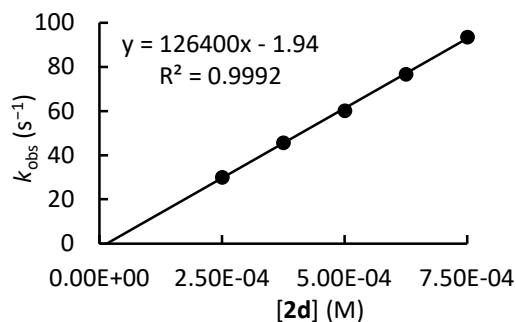
1d + **2e** in DMSO (stopped-flow method, detection at 353 nm) JR023
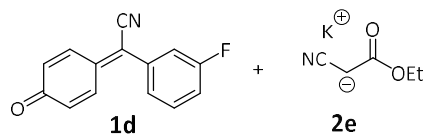
[**1d**]$_0$ (M)	[**2e**]$_0$ (M)	[18-c-6]$_0$ (M)	k_{obs} (s^{-1})
2.50×10^{-5}	2.50×10^{-4}		4.32×10^1
2.50×10^{-5}	3.75×10^{-4}	4.13×10^{-4}	6.40×10^1
2.50×10^{-5}	5.00×10^{-4}		8.91×10^1
2.50×10^{-5}	6.25×10^{-4}	6.90×10^{-4}	1.10×10^2
2.50×10^{-5}	7.50×10^{-4}		1.35×10^2

$$k_2 = 1.84 \times 10^5 \text{ M}^{-1} \text{ s}^{-1}$$
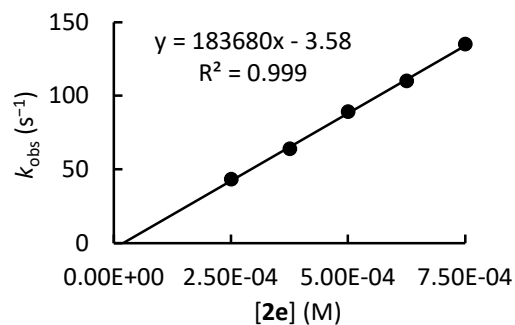
y = 183680x - 3.58
R² = 0.999

_____

1e + **2a** in DMSO (stopped-flow method, detection at 344 nm) CG055
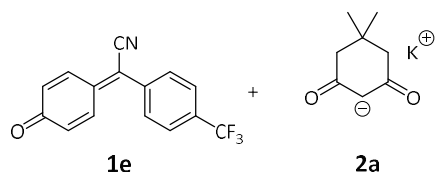
[**1e**]$_0$ (M)	[**2a**]$_0^{[a]}$ (M)	[18-c-6]$_0$ (M)	k_{obs} (s^{-1})
2.23×10^{-5}	3.00×10^{-4}		9.50×10^{-2}
2.23×10^{-5}	4.50×10^{-4}	4.95×10^{-4}	1.44×10^{-1}
2.23×10^{-5}	6.00×10^{-4}		1.88×10^{-1}
2.23×10^{-5}	7.50×10^{-4}	8.25×10^{-4}	2.37×10^{-1}
2.23×10^{-5}	9.00×10^{-4}		2.75×10^{-1}

[a] Additionally, the reaction mixtures contained an equimolar amount of the corresponding CH–acid (**2**-H).

$$k_2 = 3.02 \times 10^2 \text{ M}^{-1} \text{ s}^{-1}$$
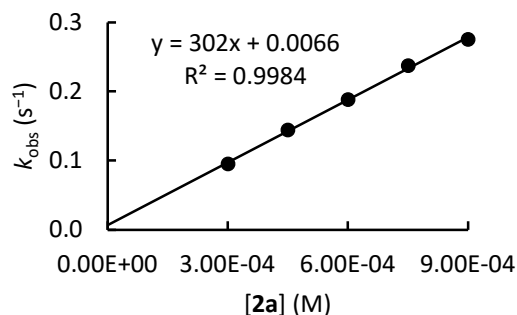
1e + **2b** in DMSO (stopped-flow method, detection at 344 nm) CG056
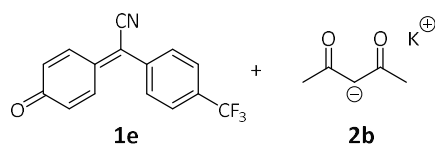
[**1e**]$_0$ (M)	[**2b**]$_0$ (M)	[18-c-6]$_0$ (M)	k_{obs} (s^{-1})
2.20×10^{-5}	1.50×10^{-4}		6.79×10^{-1}
2.20×10^{-5}	2.25×10^{-4}	2.48×10^{-4}	9.94×10^{-1}
2.20×10^{-5}	3.00×10^{-4}		1.45
2.20×10^{-5}	3.75×10^{-4}	4.13×10^{-4}	1.79
2.20×10^{-5}	4.50×10^{-4}		2.26

$$k_2 = 5.28 \times 10^3 \text{ M}^{-1} \text{ s}^{-1}$$
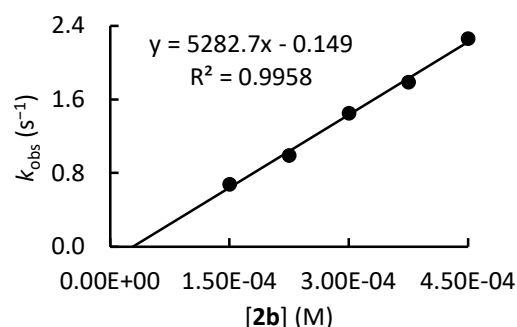
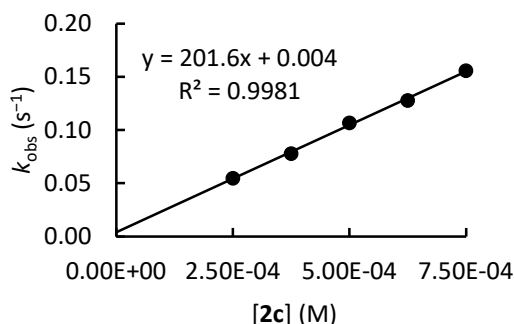**1e** + **2c** in DMSO (stopped-flow method, detection at 344 nm) CG052
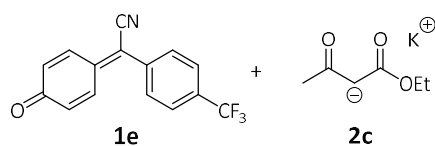
[**1e**]$_0$ (M)	[**2c**]$_0$ (M)	[18-c-6]$_0$ (M)	k_{obs} (s^{-1})
1.88×10^{-5}	3.00×10^{-4}		2.53×10^1
1.88×10^{-5}	4.50×10^{-4}	4.95×10^{-4}	3.91×10^1
1.88×10^{-5}	6.00×10^{-4}		5.22×10^1
1.88×10^{-5}	7.50×10^{-4}	8.25×10^{-4}	6.67×10^1
1.88×10^{-5}	9.00×10^{-4}		7.81×10^1

$$k_2 = 8.88 \times 10^4 \text{ M}^{-1} \text{ s}^{-1}$$
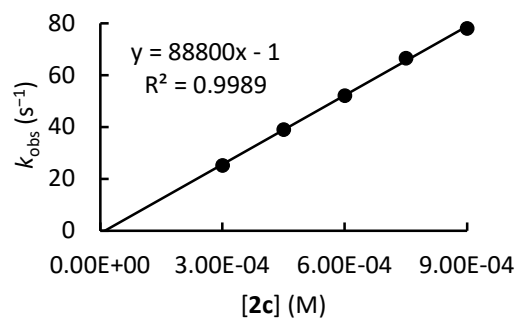
_____

1e + **2d** in DMSO (stopped-flow method, detection at 344 nm) CG030
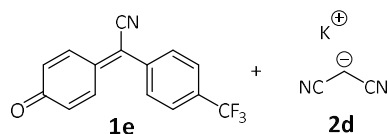
[**1e**]$_0$ (M)	[**2d**]$_0$ (M)	[18-c-6]$_0$ (M)	k_{obs} (s^{-1})
1.61×10^{-5}	2.50×10^{-4}		4.79×10^1
1.61×10^{-5}	3.75×10^{-4}	4.13×10^{-4}	7.17×10^1
1.61×10^{-5}	5.00×10^{-4}		1.04×10^2
1.61×10^{-5}	6.25×10^{-4}	6.90×10^{-4}	1.25×10^2
1.61×10^{-5}	7.50×10^{-4}		1.56×10^2

$$k_2 = 2.16 \times 10^5 \text{ M}^{-1}\text{ s}^{-1}$$

$y = 215600x - 6.88$
$R^2 = 0.9966$
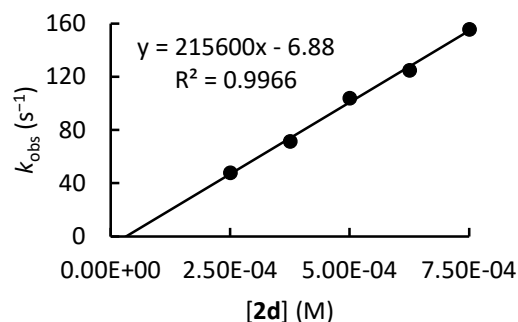
1f + **2a** in DMSO (stopped-flow method, detection at 350 nm) JR031
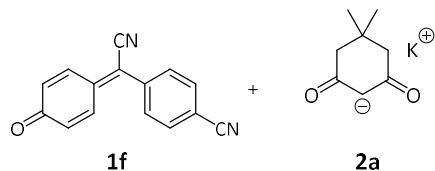
[**1f**]$_0$ (M)	[**2a**]$_0$ (M)	[18-c-6]$_0$ (M)	k_{obs} (s^{-1})
4.00×10^{-5}	4.00×10^{-4}		1.78×10^{-1}
4.00×10^{-5}	6.00×10^{-4}	6.60×10^{-4}	2.67×10^{-1}
4.00×10^{-5}	8.00×10^{-4}		3.79×10^{-1}
4.00×10^{-5}	1.00×10^{-3}	1.10×10^{-3}	4.74×10^{-1}
4.00×10^{-5}	1.20×10^{-3}		5.63×10^{-1}

$$k_2 = 4.89 \times 10^2 \text{ M}^{-1}\text{ s}^{-1}$$

$y = 488.5x - 0.0186$
$R^2 = 0.9985$
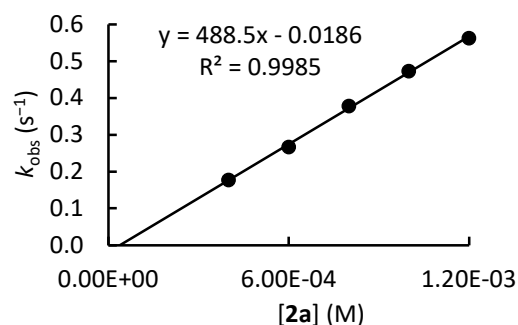
1f + **2b** in DMSO (stopped-flow method, detection at 350 nm) JR030
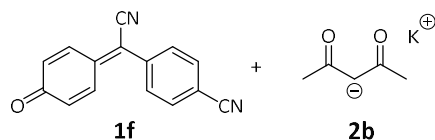
[**1f**]$_0$ (M)	[**2b**]$_0$ (M)	[18-c-6]$_0$ (M)	k_{obs} (s^{-1})
4.00×10^{-5}	4.00×10^{-4}		2.56
4.00×10^{-5}	6.00×10^{-4}	6.60×10^{-4}	4.05
4.00×10^{-5}	8.00×10^{-4}		5.09
4.00×10^{-5}	1.00×10^{-3}	1.10×10^{-3}	7.05
4.00×10^{-5}	1.20×10^{-3}		7.64

$$k_2 = 6.58 \times 10^3 \text{ M}^{-1}\text{ s}^{-1}$$
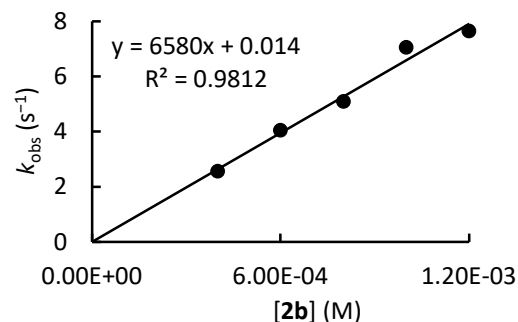
$y = 6580x + 0.014$
$R^2 = 0.9812$

_____

1f + **2c** in DMSO (stopped-flow method, detection at 350 nm) JR029
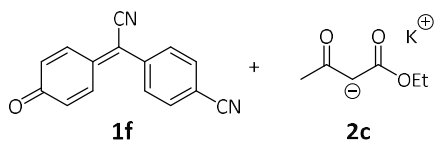
$[\mathbf{1f}]_0$ (M)	$[\mathbf{2c}]_0$ (M)	$[\text{18-c-6}]_0$ (M)	k_{obs} (s^{-1})
4.00×10^{-5}	4.00×10^{-4}		4.08×10^{1}
4.00×10^{-5}	6.00×10^{-4}	6.60×10^{-4}	6.60×10^{1}
4.00×10^{-5}	8.00×10^{-4}		8.67×10^{1}
4.00×10^{-5}	1.00×10^{-3}	1.10×10^{-3}	1.11×10^{2}
4.00×10^{-5}	1.20×10^{-3}		1.28×10^{2}

$$k_2 = 1.10 \times 10^5 \text{ M}^{-1} \text{ s}^{-1}$$
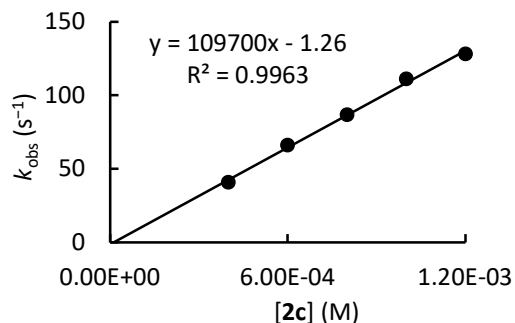
1f + **2d** in DMSO (stopped-flow method, detection at 350 nm) JR032
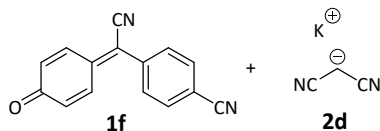
$[\mathbf{1f}]_0$ (M)	$[\mathbf{2d}]_0$ (M)	$[\text{18-c-6}]_0$ (M)	k_{obs} (s^{-1})
4.00×10^{-5}	4.00×10^{-4}		9.73×10^{1}
4.00×10^{-5}	6.00×10^{-4}	6.60×10^{-4}	1.40×10^{2}
4.00×10^{-5}	8.00×10^{-4}		2.04×10^{2}
4.00×10^{-5}	1.00×10^{-3}	1.10×10^{-3}	2.37×10^{2}
4.00×10^{-5}	1.20×10^{-3}		3.04×10^{2}

$$k_2 = 2.55 \times 10^5 \text{ M}^{-1} \text{ s}^{-1}$$
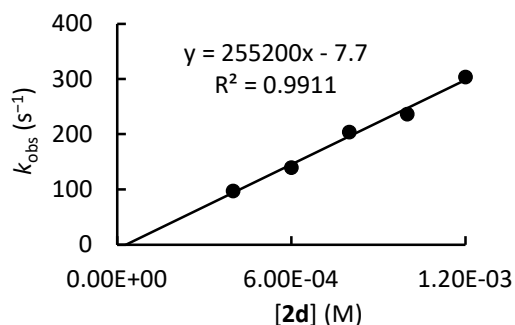
1f + **2e** in DMSO (stopped-flow method, detection at 350 nm) JR034
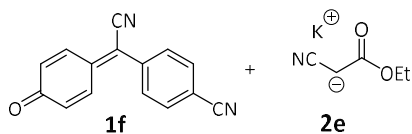
$[\mathbf{1f}]_0$ (M)	$[\mathbf{2e}]_0$ (M)	$[\text{18-c-6}]_0$ (M)	k_{obs} (s^{-1})
4.00×10^{-5}	4.00×10^{-4}		1.65×10^{2}
4.00×10^{-5}	6.00×10^{-4}	6.60×10^{-4}	2.39×10^{2}
4.00×10^{-5}	8.00×10^{-4}		3.29×10^{2}
4.00×10^{-5}	1.00×10^{-3}	1.10×10^{-3}	3.77×10^{2}
4.00×10^{-5}	1.20×10^{-3}		4.93×10^{2}

$$k_2 = 3.97 \times 10^5 \text{ M}^{-1} \text{ s}^{-1}$$

_____
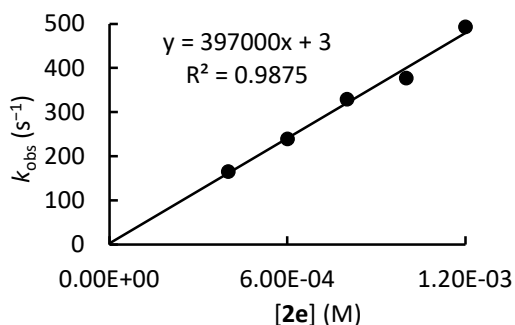
1g + **2b** in DMSO (stopped-flow method, detection at 365 nm) CG136
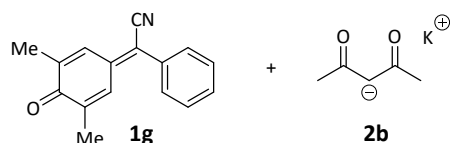
[**1g**]$_0$ (M)	[**2b**]$_0$ (M)	[18-c-6]$_0$ (M)	k_{obs} (s^{-1})
2.89×10^{-5}	2.50×10^{-4}		3.27×10^{-3}
2.89×10^{-5}	3.75×10^{-4}	4.13×10^{-4}	4.78×10^{-3}
2.89×10^{-5}	5.00×10^{-4}		6.57×10^{-3}
2.89×10^{-5}	6.25×10^{-4}	6.90×10^{-4}	7.97×10^{-3}
2.89×10^{-5}	7.50×10^{-4}		1.03×10^{-2}
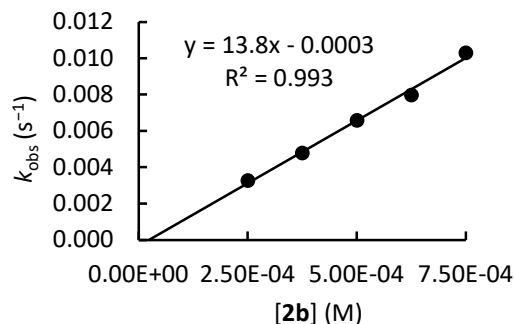
[a] Additionally, the reaction mixtures contained an equimolar amount of the corresponding CH–acid (**2**-H).

$$k_2 = 1.38 \times 10^1 \text{ M}^{-1} \text{ s}^{-1}$$

**1g** + **2c** in DMSO (stopped-flow method, detection at 365 nm) CG135
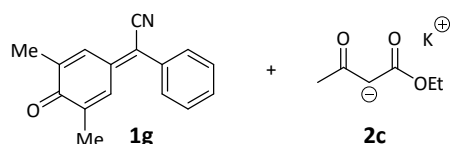
[**1g**]$_0$ (M)	[**2c**]$_0^{[a]}$ (M)	[18-c-6]$_0$ (M)	k_{obs} (s^{-1})
2.85×10^{-5}	2.50×10^{-4}		5.50×10^{-2}
2.85×10^{-5}	3.75×10^{-4}	4.13×10^{-4}	7.80×10^{-2}
2.85×10^{-5}	5.00×10^{-4}		1.07×10^{-1}
2.85×10^{-5}	6.25×10^{-4}	6.90×10^{-4}	1.28×10^{-1}
2.85×10^{-5}	7.50×10^{-4}		1.56×10^{-1}

[a] Additionally, the reaction mixtures contained an equimolar amount of the corresponding CH–acid (**2**-H).

$$k_2 = 2.02 \times 10^2 \text{ M}^{-1} \text{ s}^{-1}$$

1g + **2e** in DMSO (stopped-flow method, detection at 365 nm) CG134
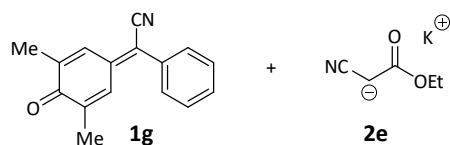
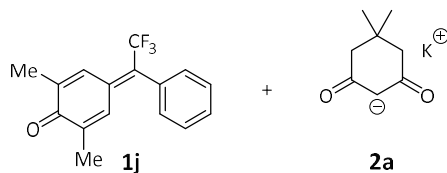| [**1g**]$_0$ (M)	[**2e**]$_0^{[a]}$ (M)	[18-c-6]$_0$ (M)	k_{obs} (s^{-1})
2.63×10^{-5}	2.50×10^{-4}		3.27×10^{-1}
2.63×10^{-5}	3.75×10^{-4}	4.13×10^{-4}	4.74×10^{-1}
2.63×10^{-5}	5.00×10^{-4}		6.50×10^{-1}
2.63×10^{-5}	6.25×10^{-4}	6.90×10^{-4}	7.88×10^{-1}
2.63×10^{-5}	7.50×10^{-4}		9.71×10^{-1}
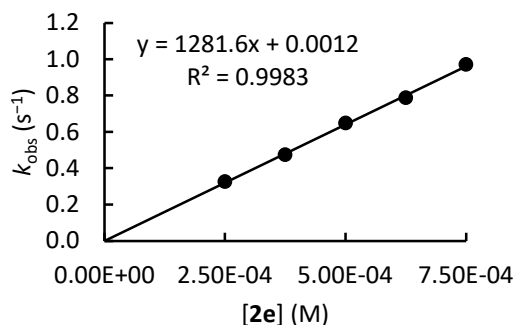
[a] Additionally, the reaction mixtures contained an equimolar amount of the corresponding CH–acid (**2**-H).

$$k_2 = 1.28 \times 10^3 \text{ M}^{-1} \text{ s}^{-1}$$

1g + **2f** in DMSO (stopped-flow method, detection at 365 nm) CG133
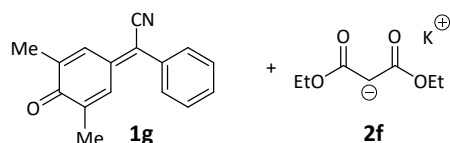
[**1g**]$_0$ (M)	[**2f**]$_0$[a] (M)	[18-c-6]$_0$ (M)	k_{obs} (s^{-1})
2.81 × 10^{-5}	2.50 × 10^{-4}		1.13
2.81 × 10^{-5}	3.75 × 10^{-4}	4.13 × 10^{-4}	1.65
2.81 × 10^{-5}	5.00 × 10^{-4}		2.26
2.81 × 10^{-5}	6.25 × 10^{-4}	6.90 × 10^{-4}	2.82
2.81 × 10^{-5}	7.50 × 10^{-4}		3.29

[a] Additionally, the reaction mixtures contained an equimolar amount of the corresponding CH–acid (**2**-H).

$$k_2 = 4.40 \times 10^3 \text{ M}^{-1} \text{ s}^{-1}$$
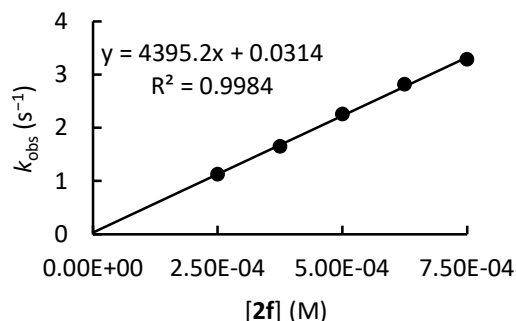
1h + **2b** in DMSO (conventional photometry, detection at 367 nm) CG114
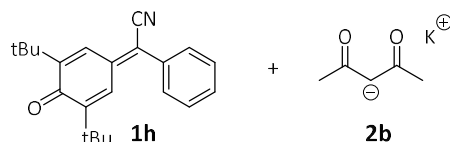
[**1h**]$_0$ (M)	[**2b**]$_0$[a] (M)	[18-c-6]$_0$ (M)	k_{obs} (s^{-1})
5.23 × 10^{-5}	5.23 × 10^{-4}		2.74 × 10^{-3}
4.87 × 10^{-5}	7.33 × 10^{-4}	8.04 × 10^{-4}	3.21 × 10^{-3}
5.09 × 10^{-5}	1.02 × 10^{-3}		4.15 × 10^{-3}
4.56 × 10^{-5}	1.14 × 10^{-3}	1.25 × 10^{-3}	4.35 × 10^{-3}
4.99 × 10^{-5}	1.50 × 10^{-3}		5.34 × 10^{-3}

[a] Additionally, the reaction mixtures contained an equimolar amount of the corresponding CH–acid (**2**-H).

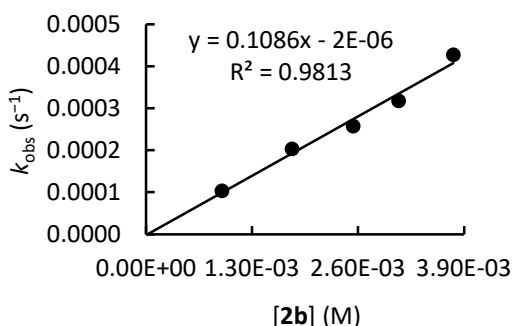$$k_2 = 2.70 \times 10^0 \text{ M}^{-1} \text{ s}^{-1}$$
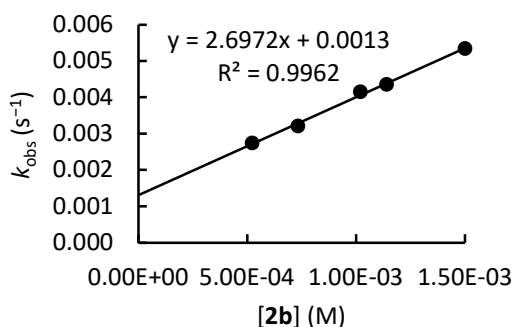
1h + **2c** in DMSO (stopped-flow method, detection at 367 nm) CG107_1
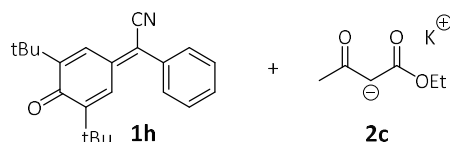
[**1h**]$_0$ (M)	[**2c**]$_0$[a] (M)	[18-c-6]$_0$ (M)	k_{obs} (s^{-1})
2.19 × 10^{-5}	2.25 × 10^{-4}		1.82 × 10^{-2}
2.19 × 10^{-5}	3.38 × 10^{-4}	3.72 × 10^{-4}	2.36 × 10^{-2}
2.19 × 10^{-5}	4.50 × 10^{-4}		3.15 × 10^{-2}
2.19 × 10^{-5}	5.65 × 10^{-4}	6.20 × 10^{-4}	3.64 × 10^{-2}
2.19 × 10^{-5}	6.75 × 10^{-4}		4.46 × 10^{-2}

[a] Additionally, the reaction mixtures contained an equimolar amount of the corresponding CH–acid (**2**-H).

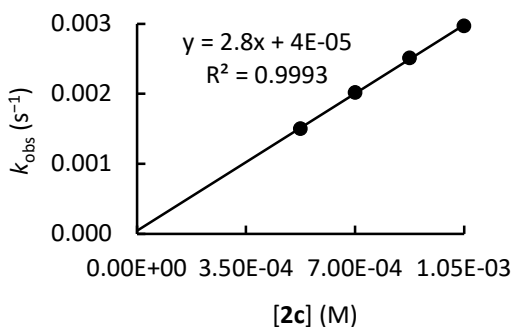$$k_2 = 5.82 \times 10^1 \text{ M}^{-1} \text{ s}^{-1}$$
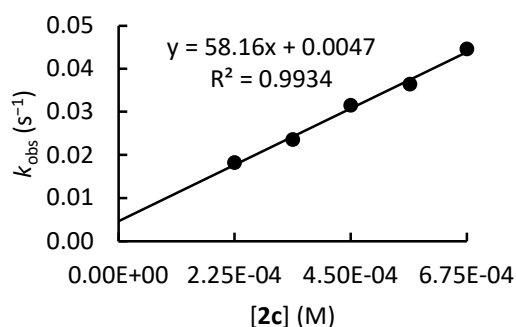
_____

1h + **2d** in DMSO (stopped-flow method, detection at 367 nm) CG106_1
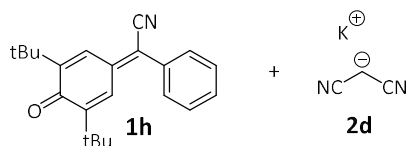
[**1h**]$_0$ (M)	[**2d**]$_0$[a] (M)	[18-c-6]$_0$ (M)	k_{obs}, (s^{-1})
2.21 × 10^{-5}	2.25 × 10^{-4}		8.55 × 10^{-2}
2.21 × 10^{-5}	3.38 × 10^{-4}	3.72 × 10^{-4}	1.25 × 10^{-1}
2.21 × 10^{-5}	4.50 × 10^{-4}		1.74 × 10^{-1}
2.21 × 10^{-5}	5.65 × 10^{-4}	6.20 × 10^{-4}	2.10 × 10^{-1}
2.21 × 10^{-5}	6.75 × 10^{-4}		2.67 × 10^{-1}

y = 396.65x - 0.0065
R² = 0.9942

[a] Additionally, the reaction mixtures contained an equimolar amount of the corresponding CH–acid (**2**-H).

$$k_2 = 3.97 \times 10^2 \ M^{-1} \ s^{-1}$$
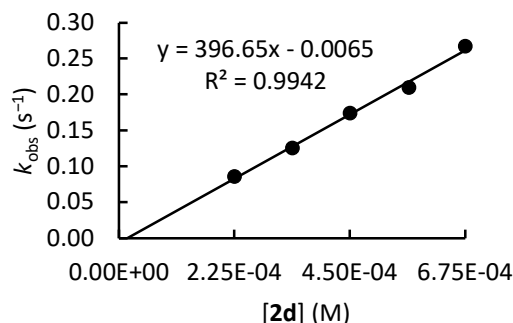
1h + **2e** in DMSO (stopped-flow method, detection at 367 nm) CG110
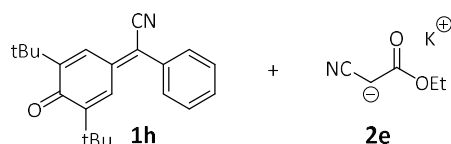
[**1h**]$_0$ (M)	[**2e**]$_0$ (M)	[18-c-6]$_0$ (M)	k_{obs} (s^{-1})
2.18 × 10^{-5}	2.25 × 10^{-4}		7.13 × 10^{-2}
2.18 × 10^{-5}	3.38 × 10^{-4}	3.72 × 10^{-4}	1.04 × 10^{-1}
2.18 × 10^{-5}	4.50 × 10^{-4}		1.45 × 10^{-1}
2.18 × 10^{-5}	5.65 × 10^{-4}	6.20 × 10^{-4}	1.75 × 10^{-1}
2.18 × 10^{-5}	6.75 × 10^{-4}		2.18 × 10^{-1}

y = 323.01x - 0.0028
R² = 0.9967

[a] Additionally, the reaction mixtures contained an equimolar amount of the corresponding CH–acid (**2**-H).

$$k_2 = 3.23 \times 10^2 \ M^{-1} \ s^{-1}$$
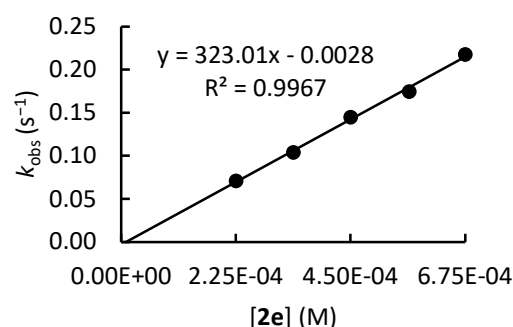
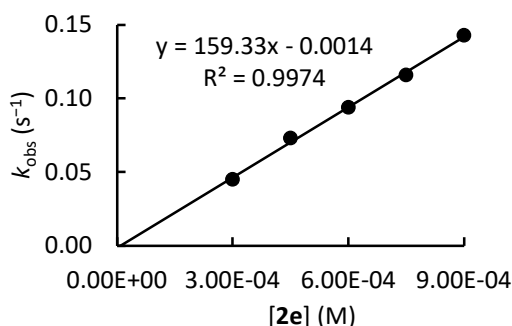**1h** + **2f** in DMSO (stopped-flow method, detection at 367 nm) CG105_1
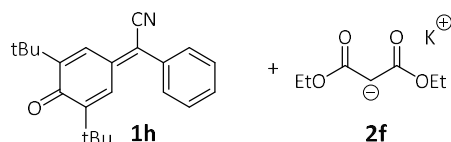
[**1h**]$_0$ (M)	[**2f**]$_0$[a] (M)	[18-c-6]$_0$ (M)	k_{obs} (s^{-1})
2.18 × 10^{-5}	2.25 × 10^{-4}		2.77 × 10^{-1}
2.18 × 10^{-5}	3.38 × 10^{-4}	3.72 × 10^{-4}	3.83 × 10^{-1}
2.18 × 10^{-5}	4.50 × 10^{-4}		5.16 × 10^{-1}
2.18 × 10^{-5}	5.65 × 10^{-4}	6.20 × 10^{-4}	6.20 × 10^{-1}
2.18 × 10^{-5}	6.75 × 10^{-4}		7.45 × 10^{-1}

y = 1040.2x + 0.0396
R² = 0.9985

[a] Additionally, the reaction mixtures contained an equimolar amount of the corresponding CH–acid (**2**-H).

$$k_2 = 1.04 \times 10^3 \ M^{-1} \ s^{-1}$$
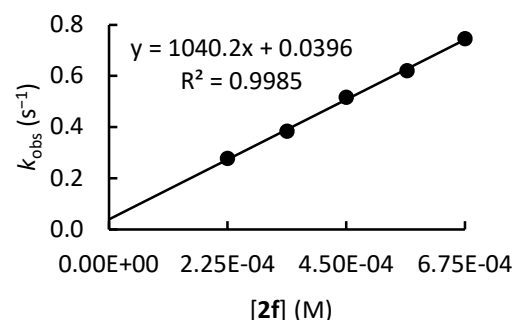
1j + **2a** in DMSO (conventional photometry, detection at 340 nm) CG177

| [**1j**]$_0$ (M)	[**2a**]$_0$[a] (M)	[18-c-6]$_0$ (M)	k_{obs} (s^{-1})
6.18×10^{-5}	1.85×10^{-3}	2.03×10^{-3}	1.19×10^{-5}
6.32×10^{-5}	2.53×10^{-3}		1.37×10^{-5}
6.45×10^{-5}	3.22×10^{-3}		1.68×10^{-5}
6.27×10^{-5}	3.76×10^{-3}		1.88×10^{-5}

[a] Additionally, the reaction mixtures contained an equimolar amount of the corresponding CH–acid (**2**-H).

$$k_2 = 3.70 \times 10^{-3} \text{ M}^{-1} \text{ s}^{-1}$$
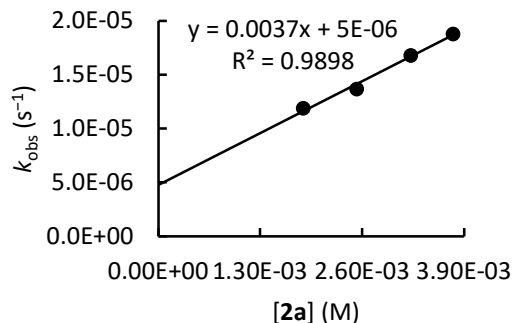
1j + **2b** in DMSO (conventional photometry, detection at 340 nm) CG175
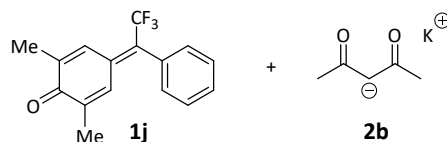
[**1j**]$_0$ (M)	[**2b**]$_0$[a] (M)	[18-c-6]$_0$ (M)	k_{obs} (s^{-1})
6.21×10^{-5}	9.31×10^{-4}	1.02×10^{-3}	1.03×10^{-4}
5.98×10^{-5}	1.79×10^{-3}	1.97×10^{-3}	2.03×10^{-4}
6.35×10^{-5}	2.54×10^{-3}		2.57×10^{-4}
6.20×10^{-5}	3.10×10^{-3}		3.17×10^{-4}
6.28×10^{-5}	3.77×10^{-3}		4.27×10^{-4}

[a] Additionally, the reaction mixtures contained an equimolar amount of the corresponding CH–acid (**2**-H).

$$k_2 = 1.09 \times 10^{-1} \text{ M}^{-1} \text{ s}^{-1}$$

1j + **2c** in DMSO (stopped-flow method, detection at 330 nm) CG174
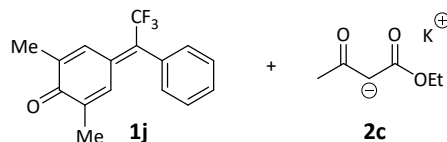
[**1j**]$_0$ (M)	[**2c**]$_0$[a] (M)	[18-c-6]$_0$ (M)	k_{obs} (s^{-1})
3.85×10^{-5}	5.25×10^{-4}	5.80×10^{-4}	1.50×10^{-3}
3.85×10^{-5}	7.00×10^{-4}		2.02×10^{-3}
3.85×10^{-5}	8.75×10^{-4}	9.65×10^{-4}	2.51×10^{-3}
3.85×10^{-5}	1.05×10^{-3}		2.97×10^{-3}

[a] Additionally, the reaction mixtures contained an equimolar amount of the corresponding CH–acid (**2**-H).

$$k_2 = 2.80 \times 10^0 \text{ M}^{-1} \text{ s}^{-1}$$

_____

1j + **2d** in DMSO (stopped–flow method, detection at 330 nm) CG173
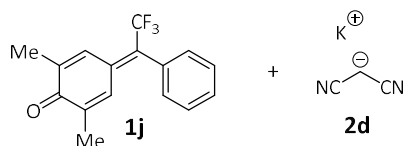
[**1j**]$_0$ (M)	[**2d**]$_0$[a] (M)	[18-c-6]$_0$ (M)	k_{obs} (s^{-1})
4.07×10^{-5}	3.50×10^{-4}		1.33×10^{-1}
4.07×10^{-5}	5.25×10^{-4}	5.80×10^{-4}	1.97×10^{-1}
4.07×10^{-5}	7.00×10^{-4}		2.65×10^{-1}
4.07×10^{-5}	8.75×10^{-4}	9.65×10^{-4}	3.28×10^{-1}
4.07×10^{-5}	1.05×10^{-4}		3.98×10^{-1}

[a] Additionally, the reaction mixtures contained an equimolar amount of the corresponding CH–acid (**2**-H).

$$k_2 = 3.78 \times 10^2 \text{ M}^{-1} \text{ s}^{-1}$$
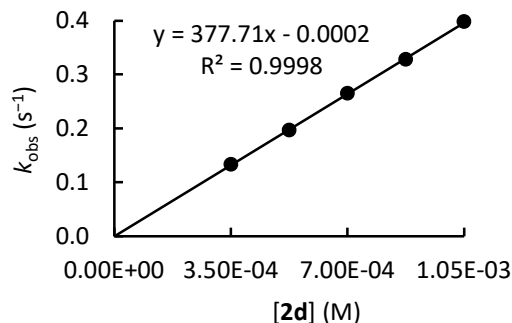
1j + **2e** in DMSO (stopped-flow method, detection at 304 nm) CG172
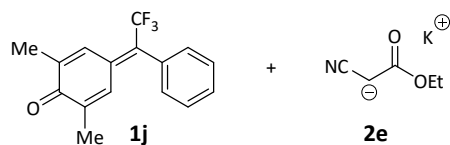
[**1j**]$_0$ (M)	[**2e**]$_0$[a] (M)	[18-c-6]$_0$ (M)	k_{obs} (s^{-1})
3.45×10^{-5}	3.00×10^{-4}		4.50×10^{-2}
3.45×10^{-5}	4.50×10^{-4}	4.95×10^{-4}	7.30×10^{-2}
3.45×10^{-5}	6.00×10^{-4}		9.40×10^{-2}
3.45×10^{-5}	7.50×10^{-4}	8.25×10^{-4}	1.16×10^{-1}
3.45×10^{-5}	9.00×10^{-4}		1.43×10^{-1}

[a] Additionally, the reaction mixtures contained an equimolar amount of the corresponding CH–acid (**2**-H).

$$k_2 = 1.59 \times 10^2 \text{ M}^{-1} \text{ s}^{-1}$$

1j + **2f** in DMSO (stopped-flow method, detection at 304 nm) CG171
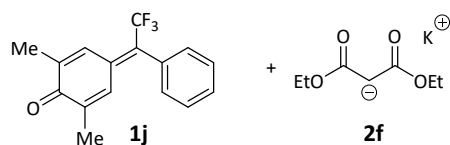
[**1j**]$_0$ (M)	[**2f**]$_0$[a] (M)	[18-c-6]$_0$ (M)	k_{obs} (s^{-1})
3.16×10^{-5}	3.00×10^{-4}		3.00×10^{-2}
3.16×10^{-5}	4.50×10^{-4}	4.95×10^{-4}	4.40×10^{-2}
3.16×10^{-5}	6.00×10^{-4}		5.70×10^{-2}
3.16×10^{-5}	7.50×10^{-4}	8.25×10^{-4}	7.20×10^{-2}
3.16×10^{-5}	9.00×10^{-4}		8.30×10^{-2}

[a] Additionally, the reaction mixtures contained an equimolar amount of the corresponding CH–acid (**2**-H).

$$k_2 = 8.93 \times 10^1 \text{ M}^{-1} \text{ s}^{-1}$$
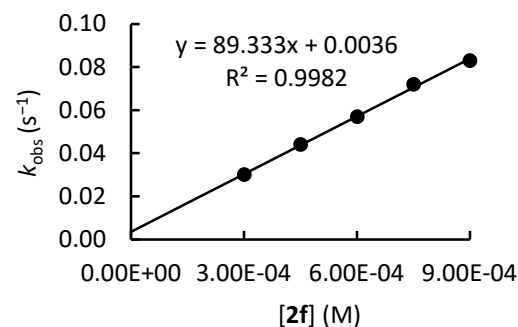
4.4.11. Kinetics of the Reactions of CN *p*QMs with Miscellaneous Nucleophiles

1e + **3a** in DMSO (conventional photometry, detection at 344 nm) CG540
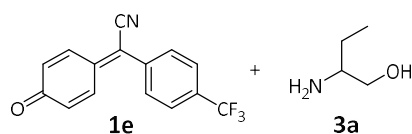
[**1e**]$_0$ (M)	[**3a**]$_0$ (M)	k_{obs} (s^{-1})
2.16×10^{-5}	5.72×10^{-4}	1.60×10^{-4}
2.13×10^{-5}	1.70×10^{-3}	9.07×10^{-4}
2.13×10^{-5}	2.27×10^{-3}	1.43×10^{-3}
2.09×10^{-5}	2.82×10^{-3}	2.01×10^{-3}

$$k_2 = 8.12 \times 10^{-1} \text{ M}^{-1} \text{ s}^{-1}$$
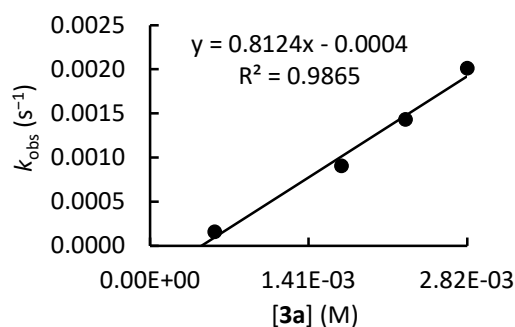
1e + **3b** in DMSO (stopped-flow method, detection at 344 nm) CG372
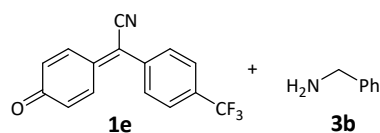
[**1e**]$_0$ (M)	[**3b**]$_0$ (M)	k_{obs} (s^{-1})
2.06×10^{-5}	6.00×10^{-4}	4.20×10^{-3}
2.06×10^{-5}	1.20×10^{-3}	1.07×10^{-2}
2.06×10^{-5}	1.80×10^{-3}	1.83×10^{-2}
2.06×10^{-5}	2.40×10^{-3}	2.59×10^{-2}

$$k_2 = 1.21 \times 10^1 \text{ M}^{-1} \text{ s}^{-1}$$
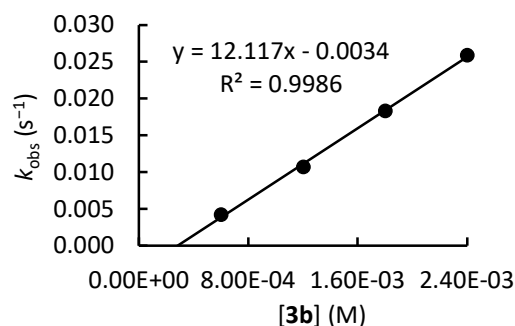
1e + **3c** in DMSO (stopped-flow method, detection at 344 nm) CG371
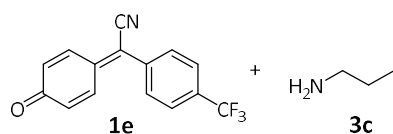
[**1e**]$_0$ (M)	[**3c**]$_0$ (M)	k_{obs} (s^{-1})
2.02×10^{-5}	6.00×10^{-4}	3.62×10^{-2}
2.02×10^{-5}	1.20×10^{-3}	7.72×10^{-2}
2.02×10^{-5}	1.80×10^{-3}	1.17×10^{-1}
2.02×10^{-5}	2.40×10^{-3}	1.56×10^{-1}

$$k_2 = 6.65 \times 10^1 \text{ M}^{-1} \text{ s}^{-1}$$
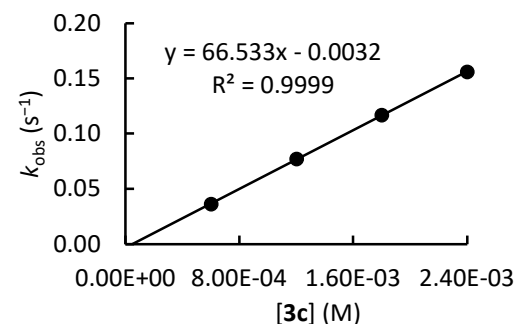
_____

1e + **3d** in DMSO (stopped-flow method, detection at 344 nm) CG370
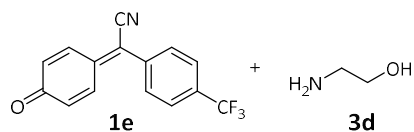
[**1e**]$_0$ (M)	[**3d**]$_0$ (M)	k_{obs} (s^{-1})
2.02×10^{-5}	6.00×10^{-4}	1.49×10^{-2}
2.02×10^{-5}	1.20×10^{-3}	3.10×10^{-2}
2.02×10^{-5}	1.80×10^{-3}	4.78×10^{-2}
2.02×10^{-5}	2.40×10^{-3}	6.49×10^{-2}

$$k_2 = 2.78 \times 10^1 \text{ M}^{-1}\text{ s}^{-1}$$
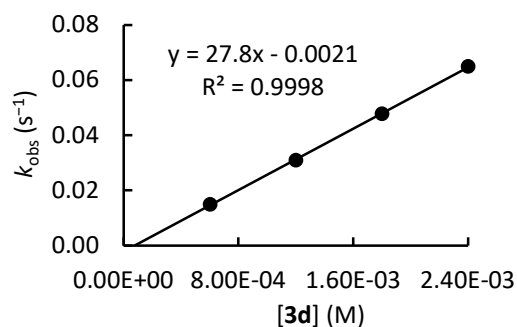
1h + **4a** in DMSO (stopped-flow method, detection at 367 nm) CG364
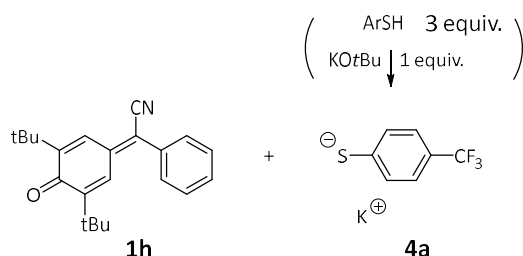
[**1h**]$_0$ (M)	[**4a**]$_0$ (M)	k_{obs} (s^{-1})
1.84×10^{-5}	6.25×10^{-4}	2.18
1.84×10^{-5}	9.40×10^{-4}	4.58
1.84×10^{-5}	1.25×10^{-3}	7.92
1.84×10^{-5}	1.57×10^{-3}	1.18×10^1

$$k_2 = 1.02 \times 10^4 \text{ M}^{-1}\text{ s}^{-1}$$
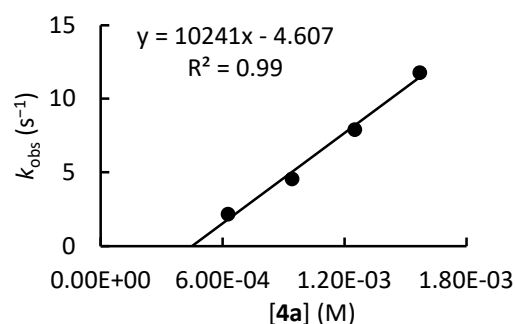
1h + **4b** in DMSO (stopped-flow method, detection at 367 nm) CG367
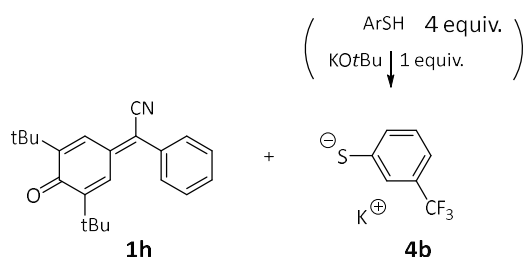
[**1h**]$_0$ (M)	[**4b**]$_0$ (M)	k_{obs} (s^{-1})
2.28×10^{-5}	6.25×10^{-4}	9.24
2.28×10^{-5}	9.40×10^{-4}	2.06×10^1
2.28×10^{-5}	1.25×10^{-3}	3.38×10^1
2.28×10^{-5}	1.57×10^{-3}	5.19×10^1

$$k_2 = 4.49 \times 10^4 \text{ M}^{-1}\text{ s}^{-1}$$
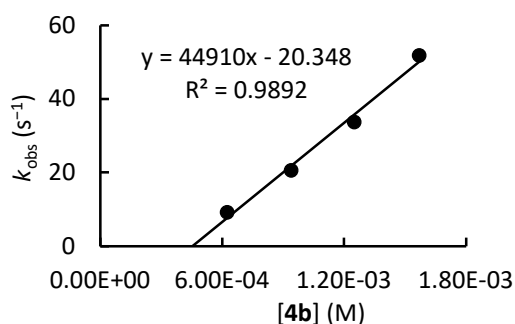
1h + **4c** in DMSO (stopped-flow method, detection at 367 nm) CG365
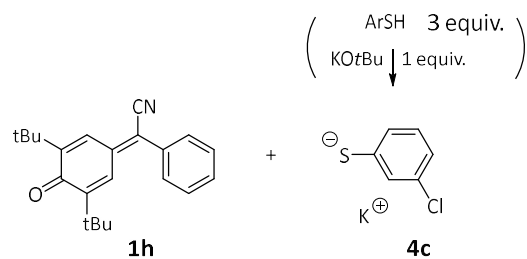
[**1h**]$_0$ (M)	[**4c**]$_0$ (M)	k_{obs} (s^{-1})
2.28×10^{-5}	6.25×10^{-4}	1.56×10^{1}
2.28×10^{-5}	9.40×10^{-4}	3.35×10^{1}
2.28×10^{-5}	1.25×10^{-3}	5.79×10^{1}
2.28×10^{-5}	1.57×10^{-3}	9.00×10^{1}

$k_2 = 7.88 \times 10^{4}$ M^{-1} s^{-1}
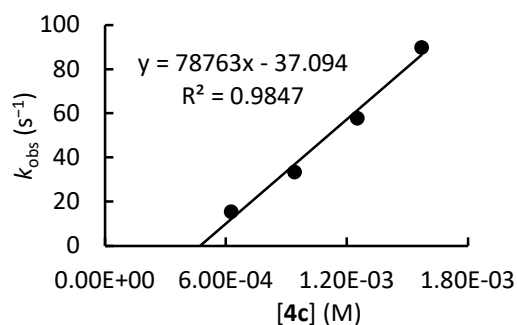
1h + **4d** in DMSO (stopped-flow method, detection at 367 nm) CG368
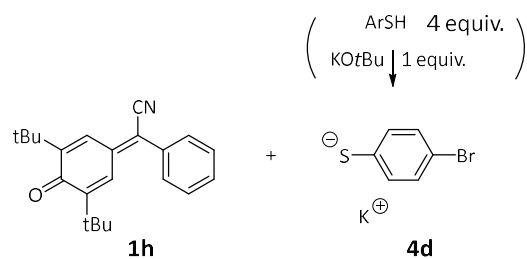
[**1h**]$_0$ (M)	[**4d**]$_0$ (M)	k_{obs} (s^{-1})
1.69×10^{-5}	6.25×10^{-4}	9.83×10^{1}
1.51×10^{-5}	9.40×10^{-4}	2.15×10^{2}
1.21×10^{-5}	1.25×10^{-3}	3.84×10^{2}

$k_2 = 4.57 \times 10^{5}$ M^{-1} s^{-1}
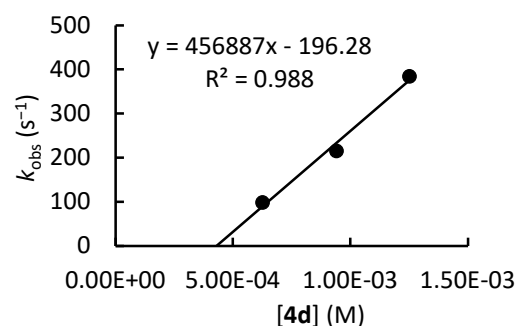
4.4.12. Copies of ^{1}H, ^{13}C, ^{19}F NMR spectra
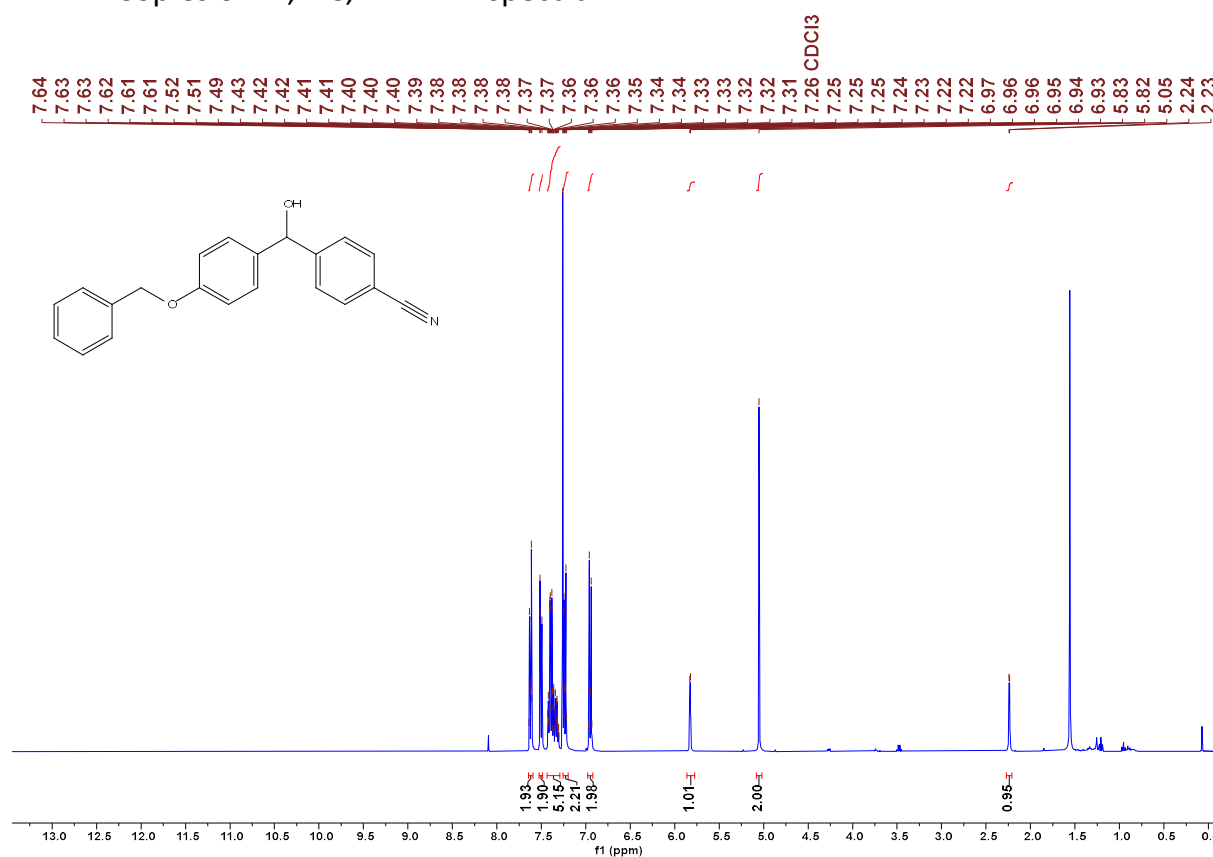
Figure 13. ^{1}H NMR spectrum of **5a** in CDCl$_3$ (600 MHz) JR009
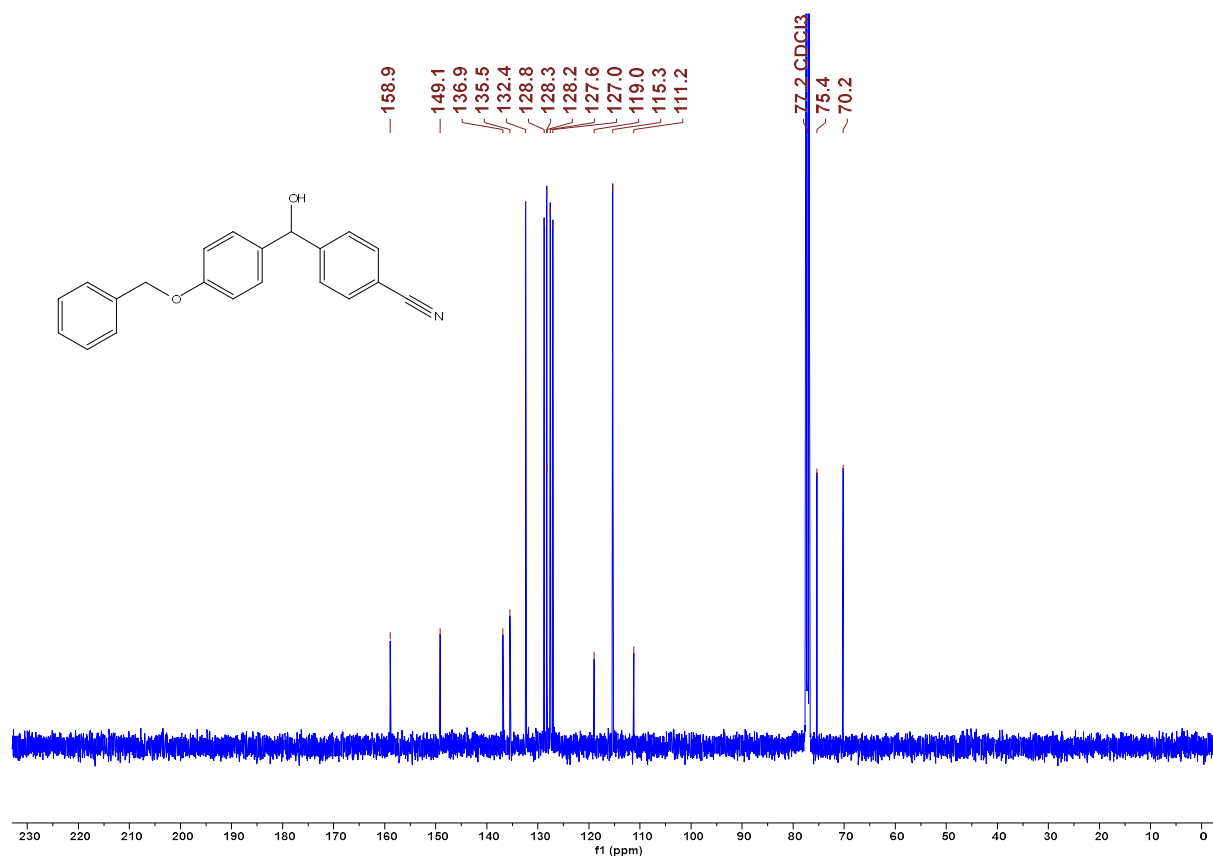
Figure 14. ^{13}C NMR spectrum of **5a** in CDCl$_3$ (151 MHz) JR009

143
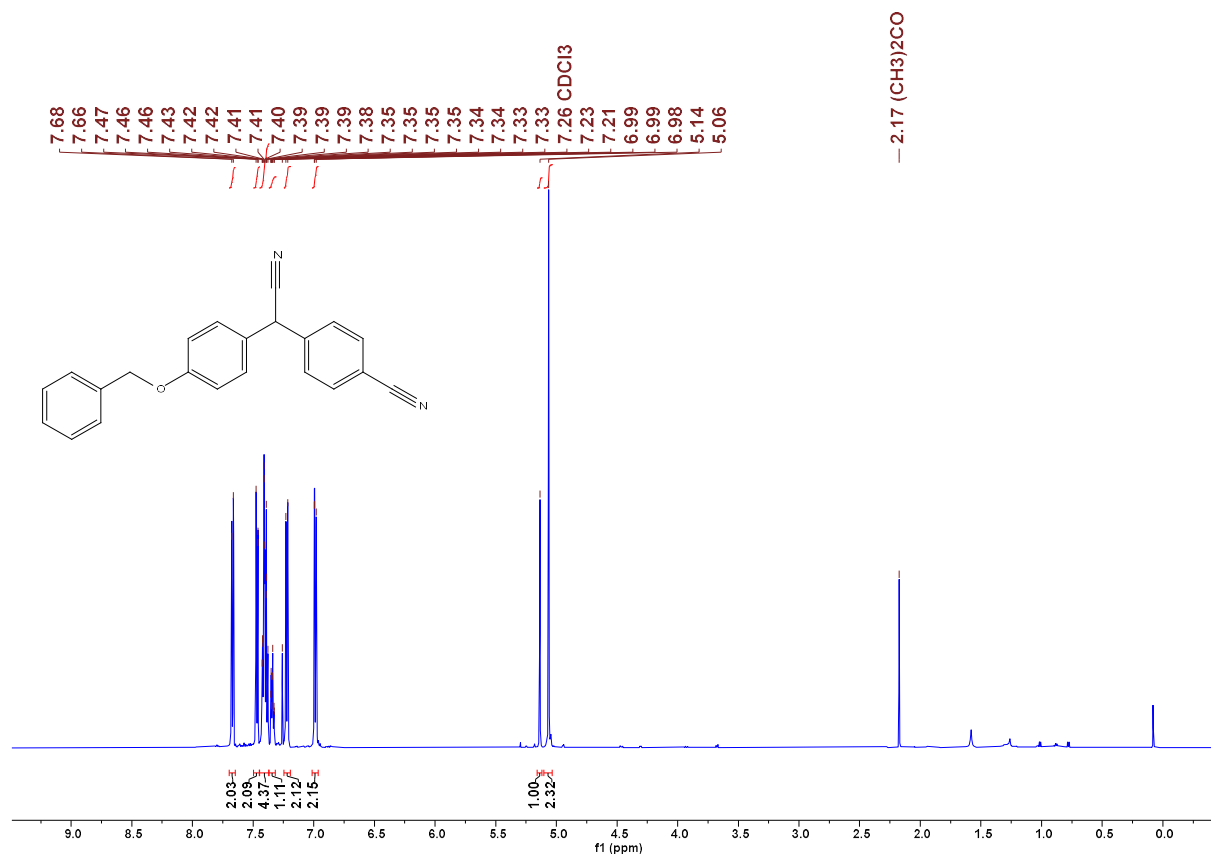
Figure 15. ^{1}H NMR spectrum of **5b** in CDCl$_3$ (600 MHz) JR014
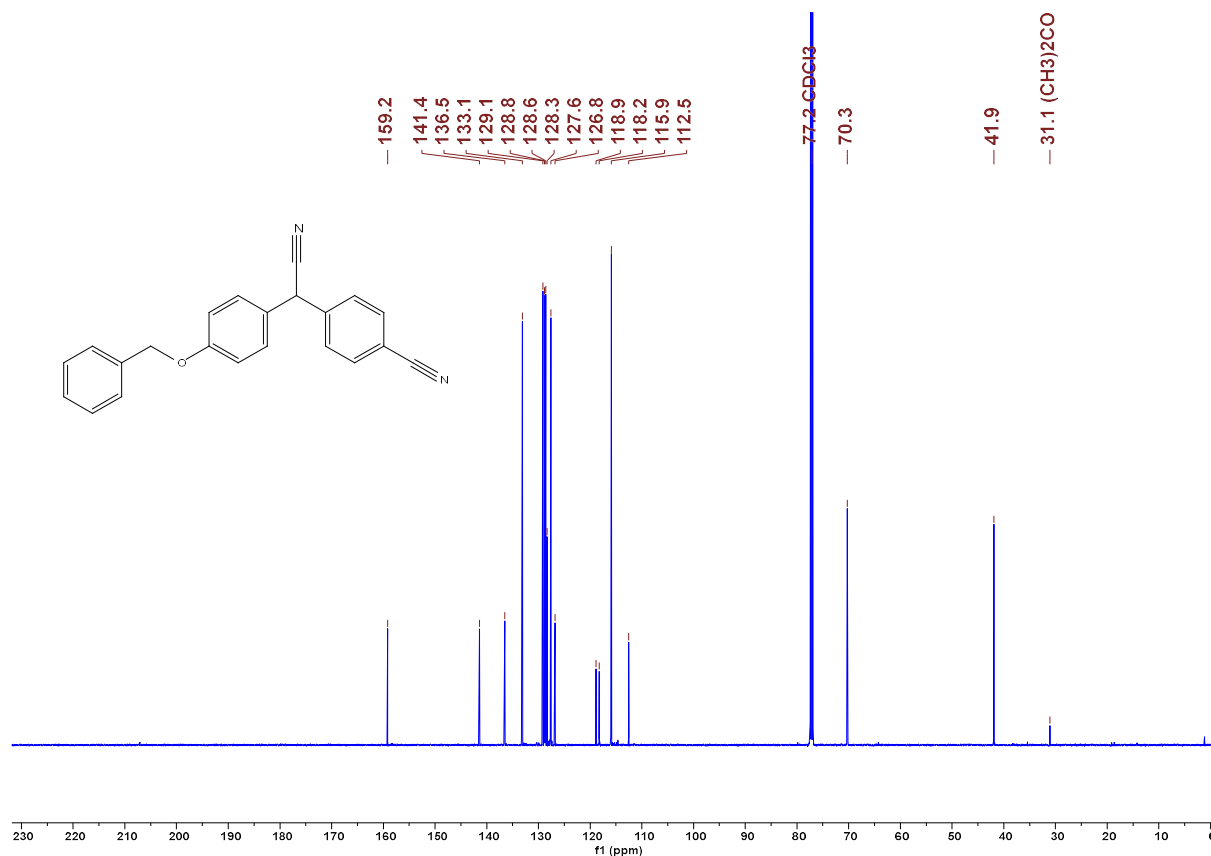
Figure 16. ^{13}C NMR spectrum of **5b** in CDCl$_3$ (151 MHz) JR014

Chapter 4. Electrophilic Reactivities of *δ*-Disubstituted *para*-Quinone Methides – A Limitation to the Mayr-Patz Equation

_____
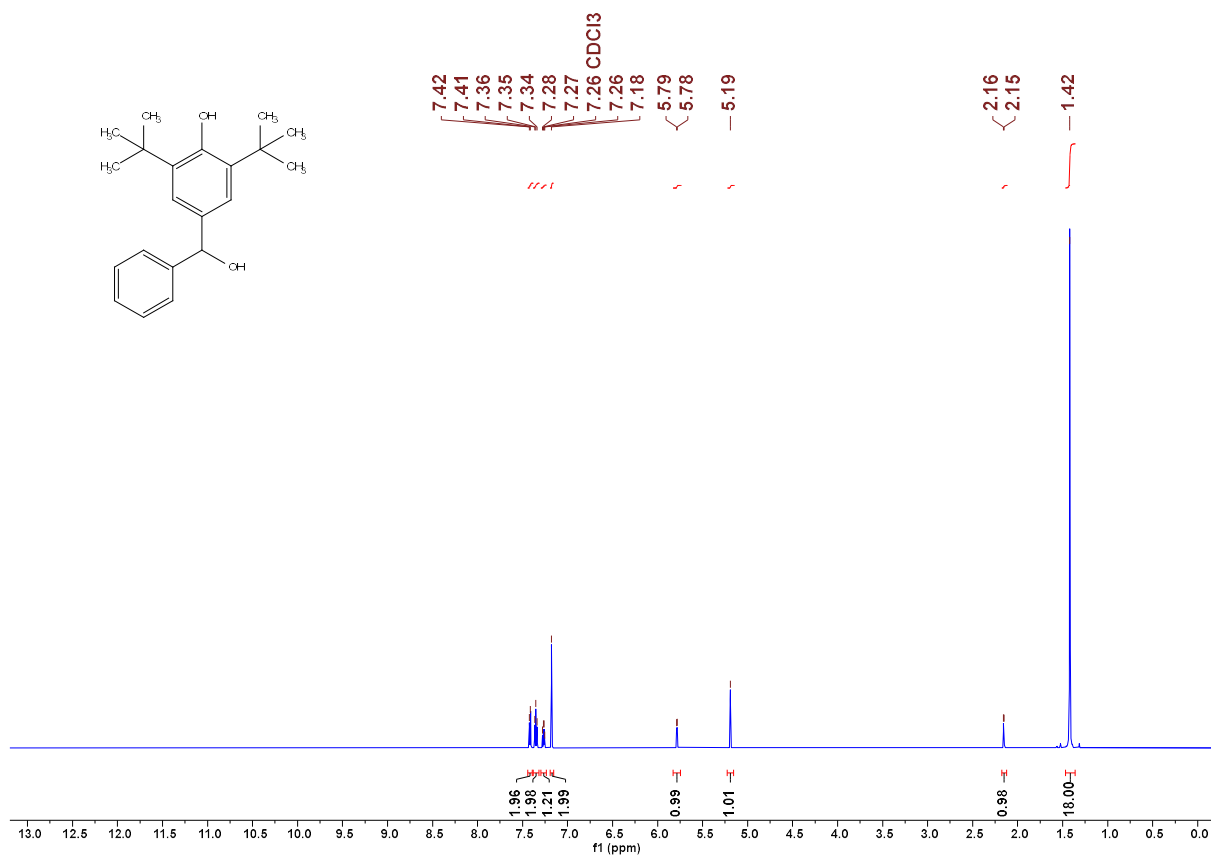
Figure 17. ¹H NMR spectrum of **5d** in CDCl₃ (400 MHz) CG100_1
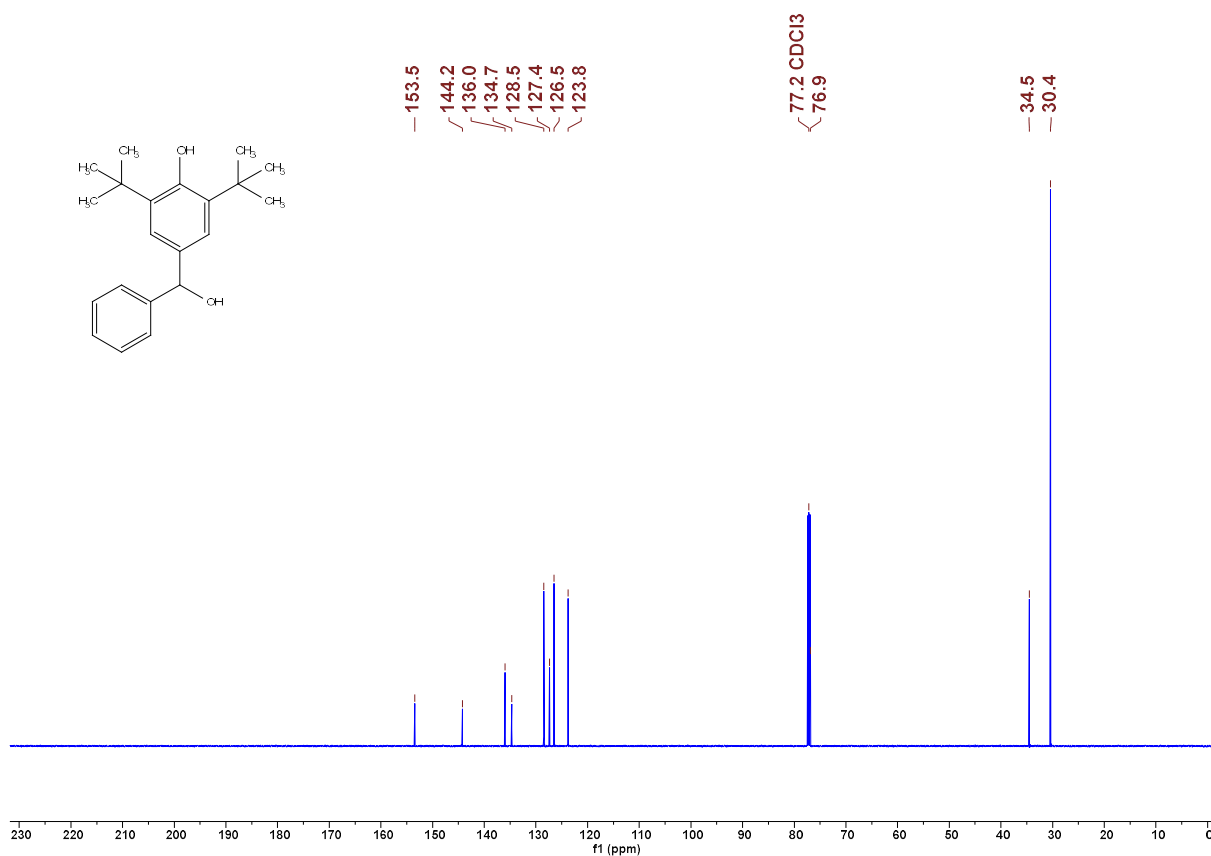
Figure 18. ¹³C NMR spectrum of **5d** in CDCl₃ (101 MHz) CG100_1
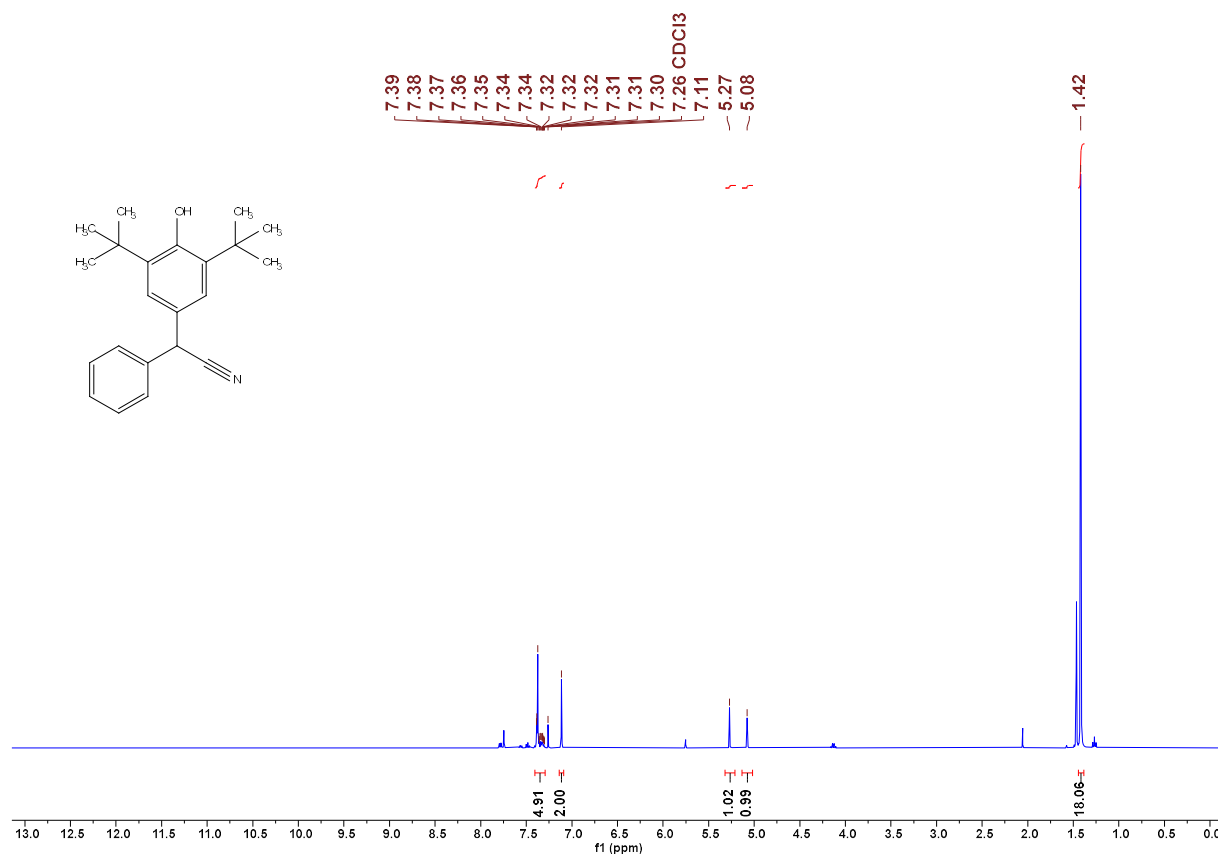
Figure 19. ^{1}H NMR spectrum of **5e** in CDCl₃ (400 MHz) CG103
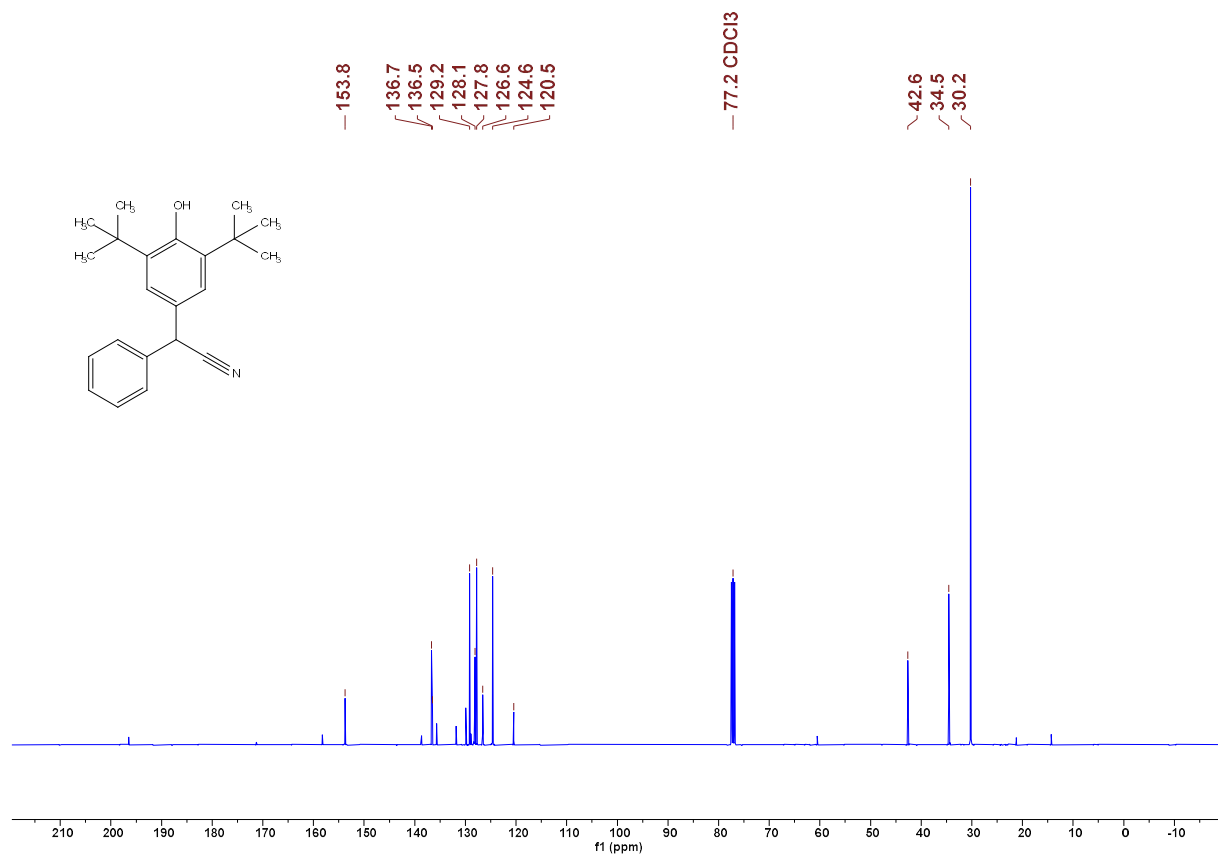
Figure 20. ^{13}C NMR spectrum of **5e** in CDCl₃ (101 MHz) CG103
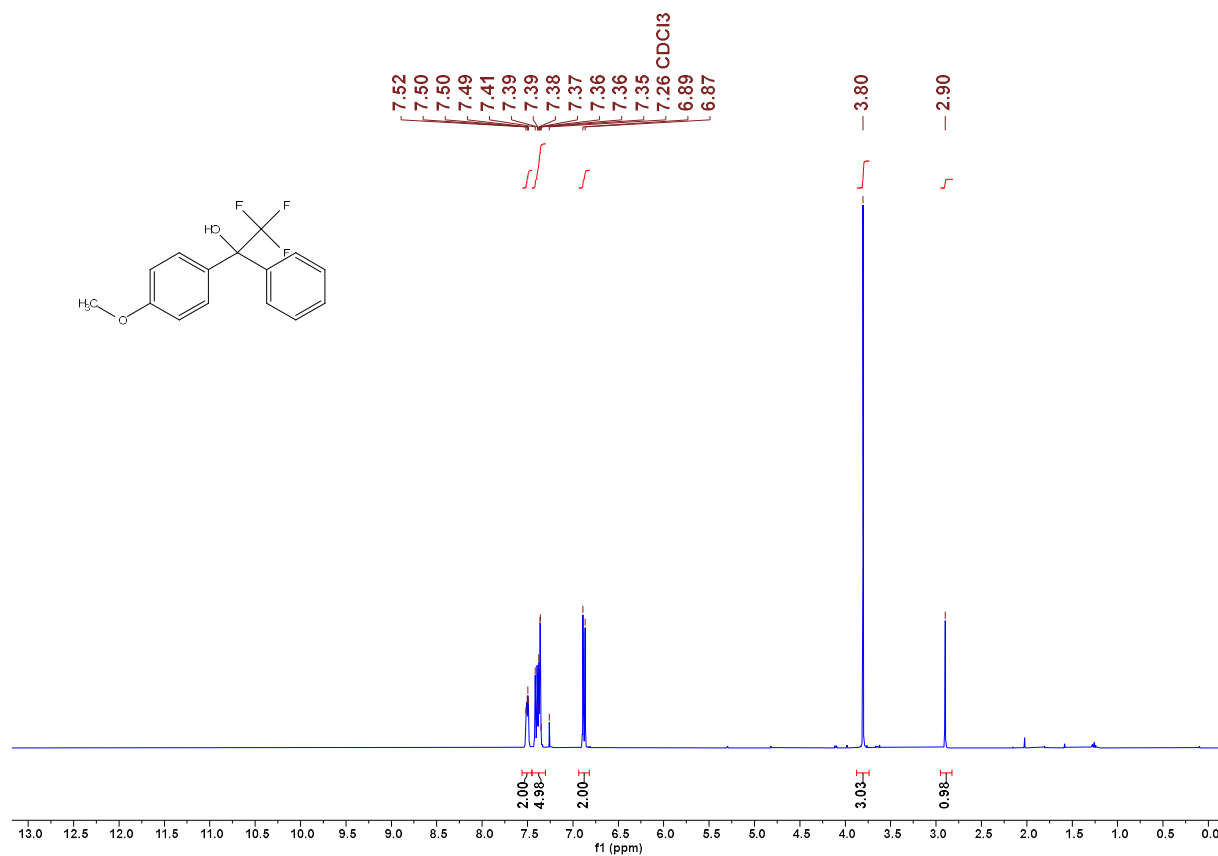
Figure 21. ^{1}H NMR spectrum of **6a** in CDCl$_3$ (400 MHz) CG151
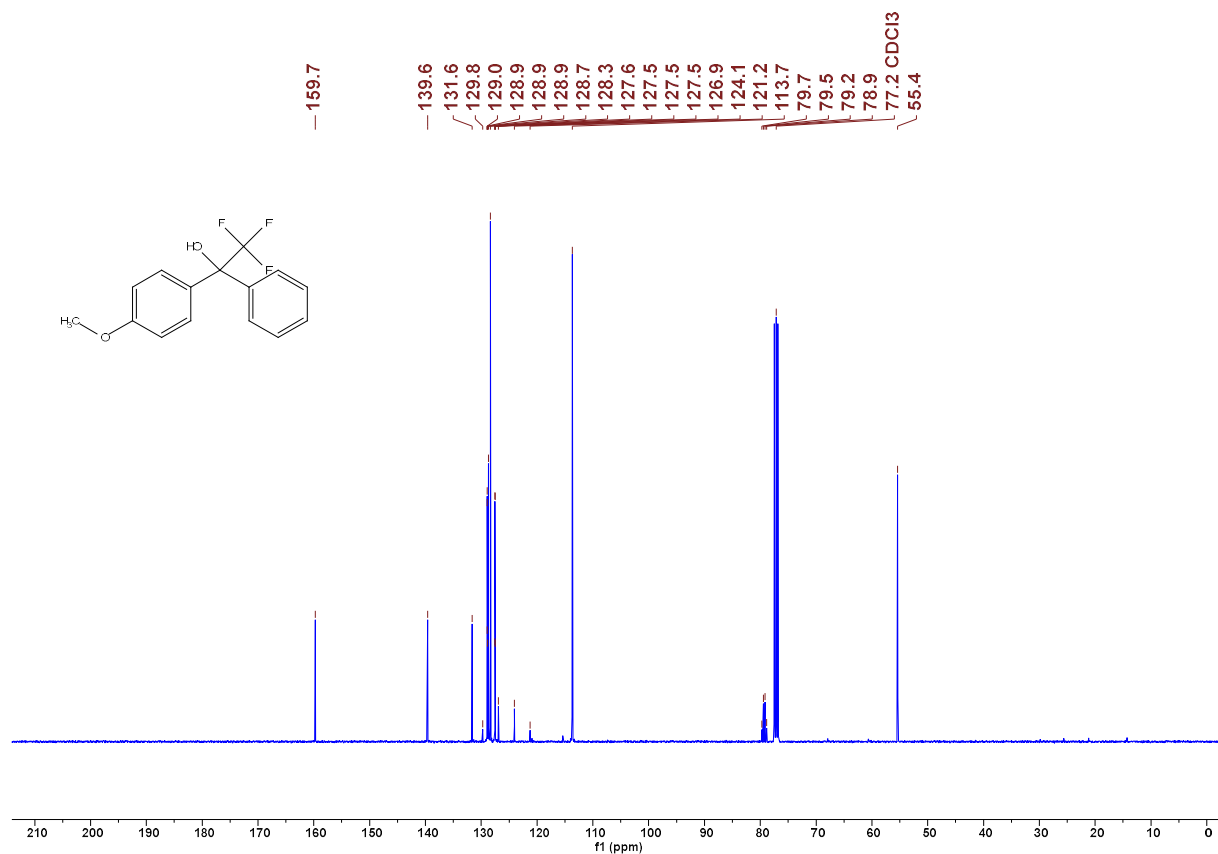
Figure 22. ^{13}C NMR spectrum of **6a** in CDCl$_3$ (101 MHz) CG151
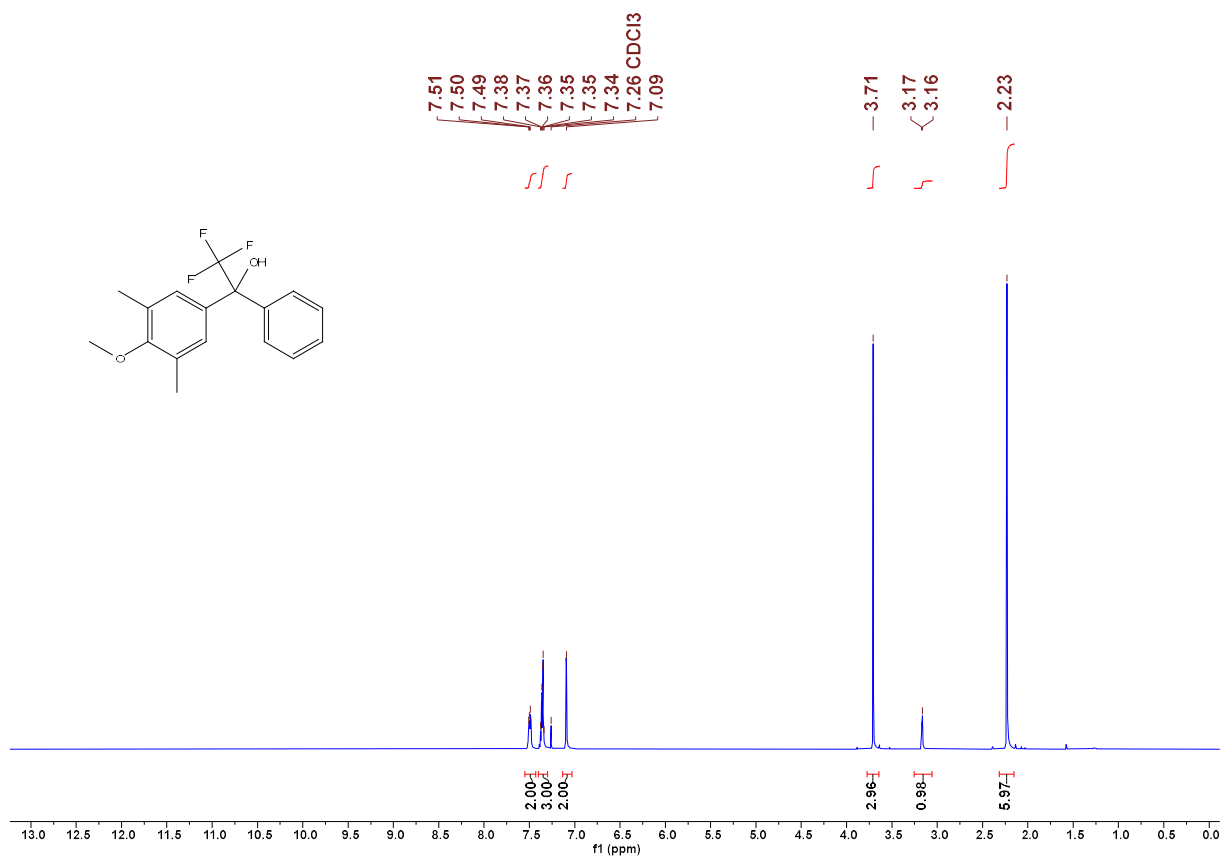
Figure 23. ^{1}H NMR spectrum of **6b** in CDCl$_3$ (400 MHz) LD2
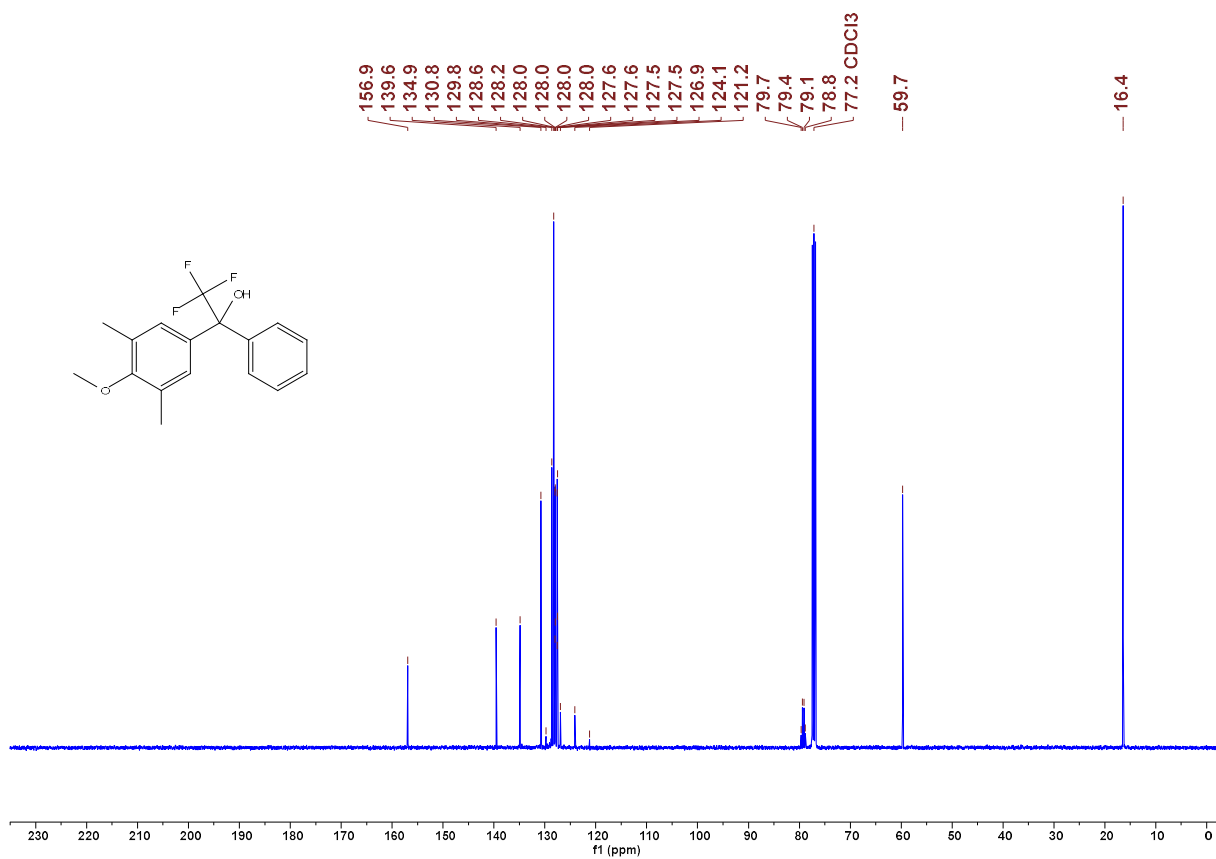
Figure 24. ^{13}C NMR spectrum of **6b** in CDCl$_3$ (101 MHz) LD2
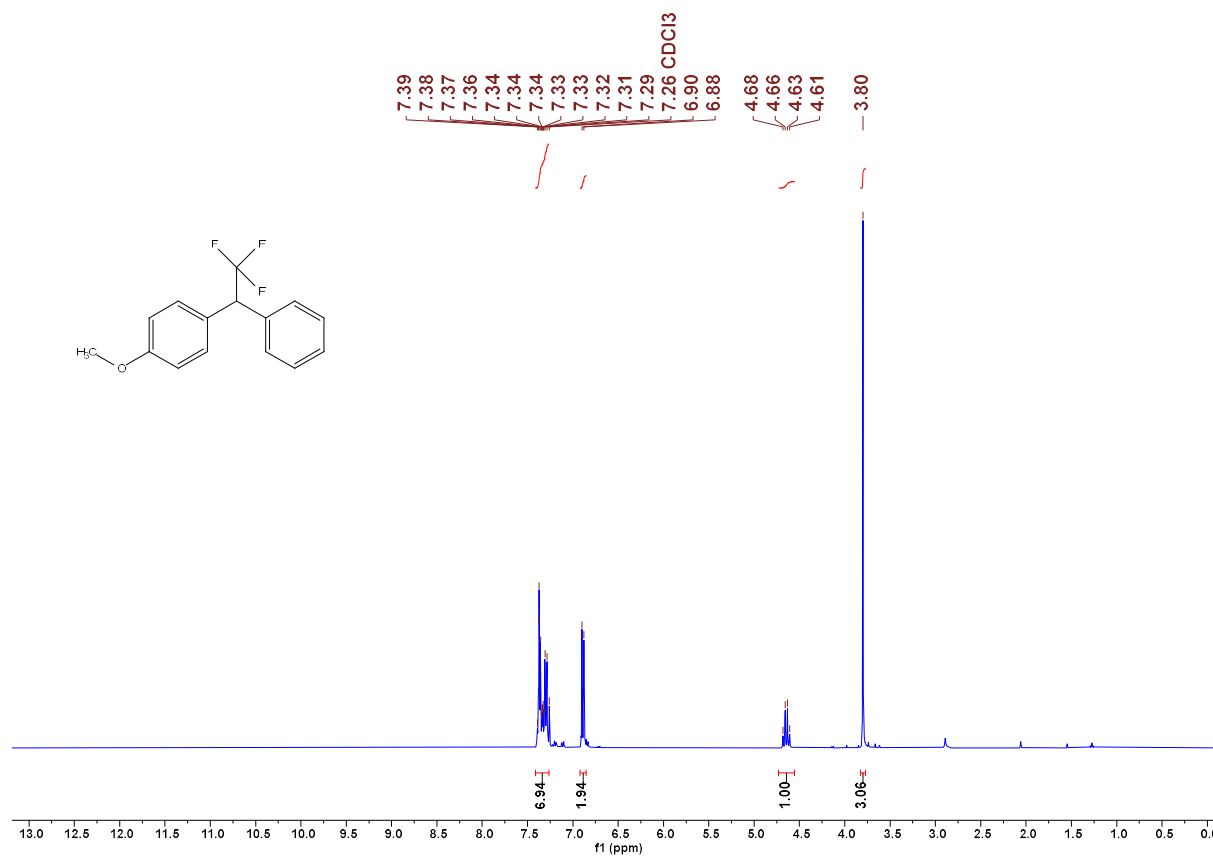
Figure 25. ^{1}H NMR spectrum of **7a** in CDCl₃ (400 MHz) CG152_1
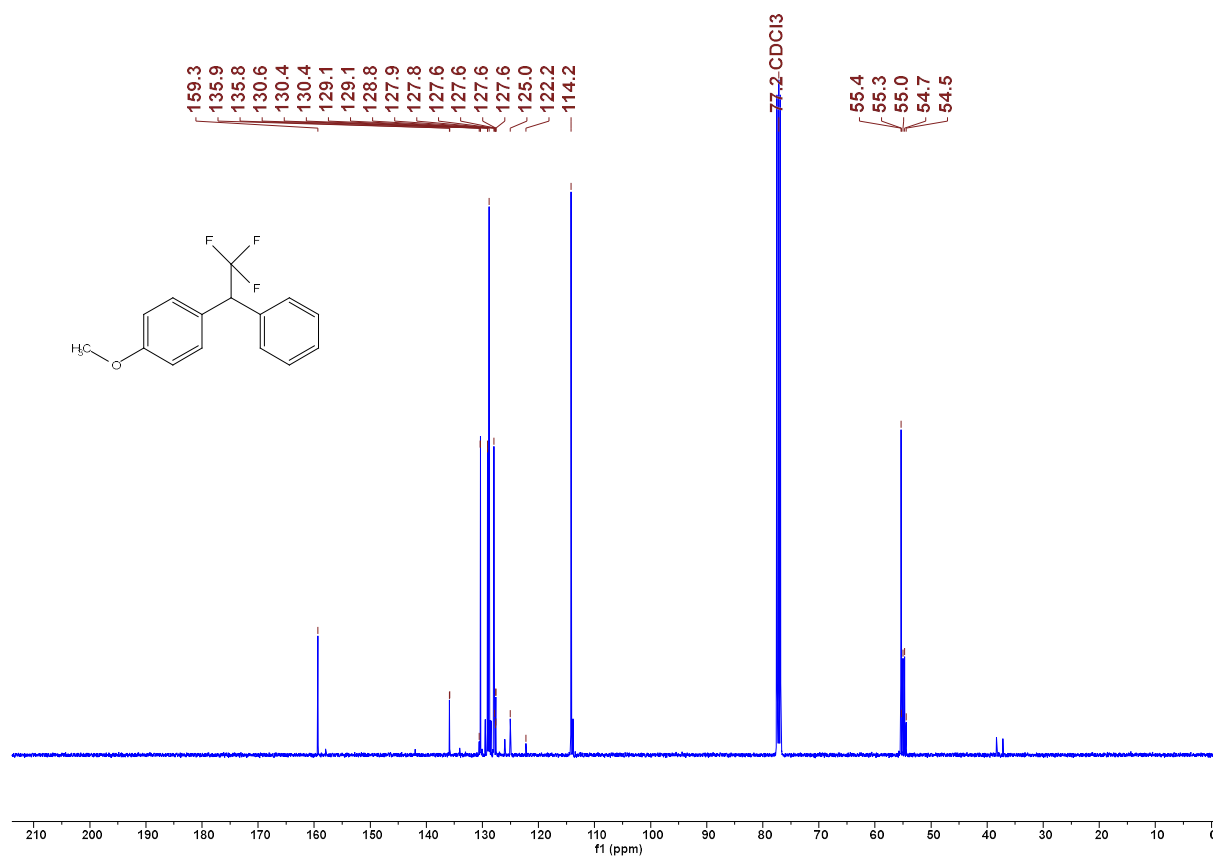
Figure 26. ^{13}C NMR spectrum of **7a** in CDCl₃ (101 MHz) CG152_1
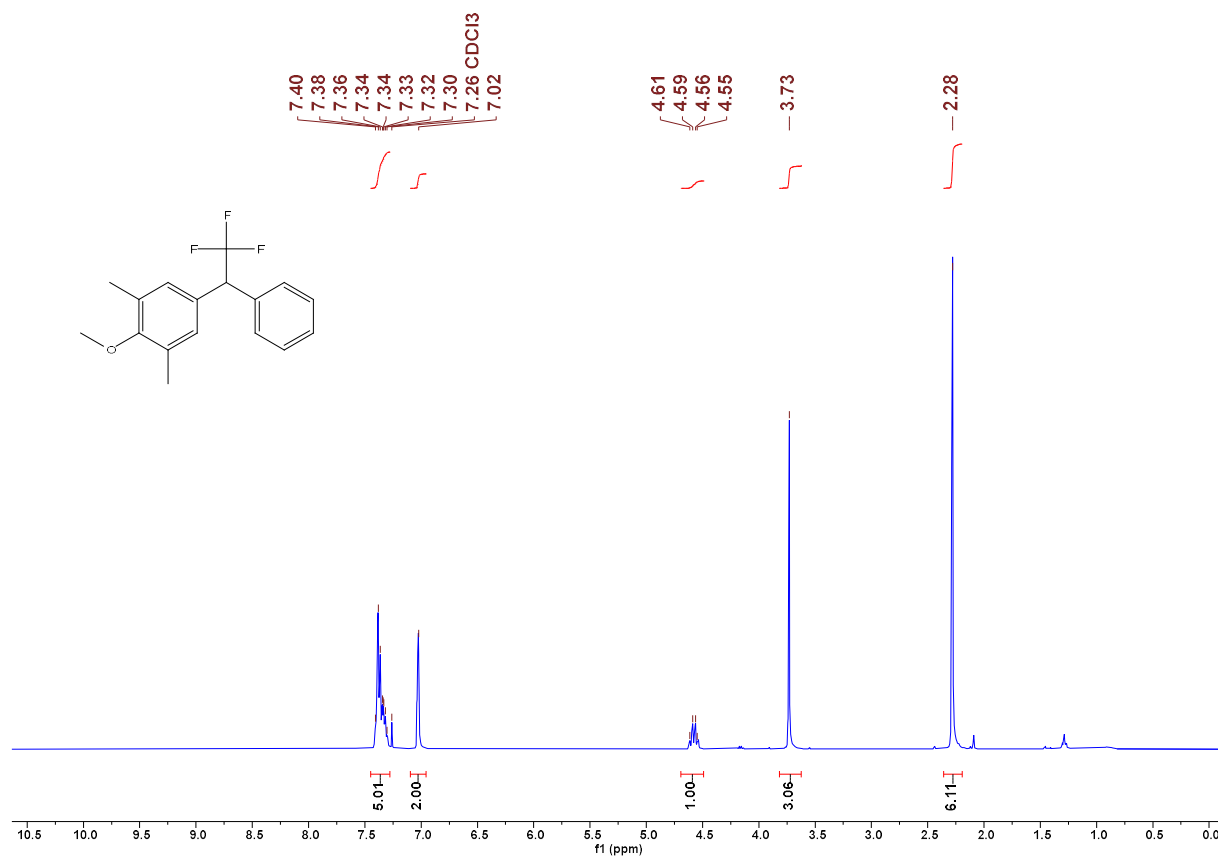
Figure 27. ^{1}H NMR spectrum of **7b** in CDCl$_3$ (400 MHz) LD3A
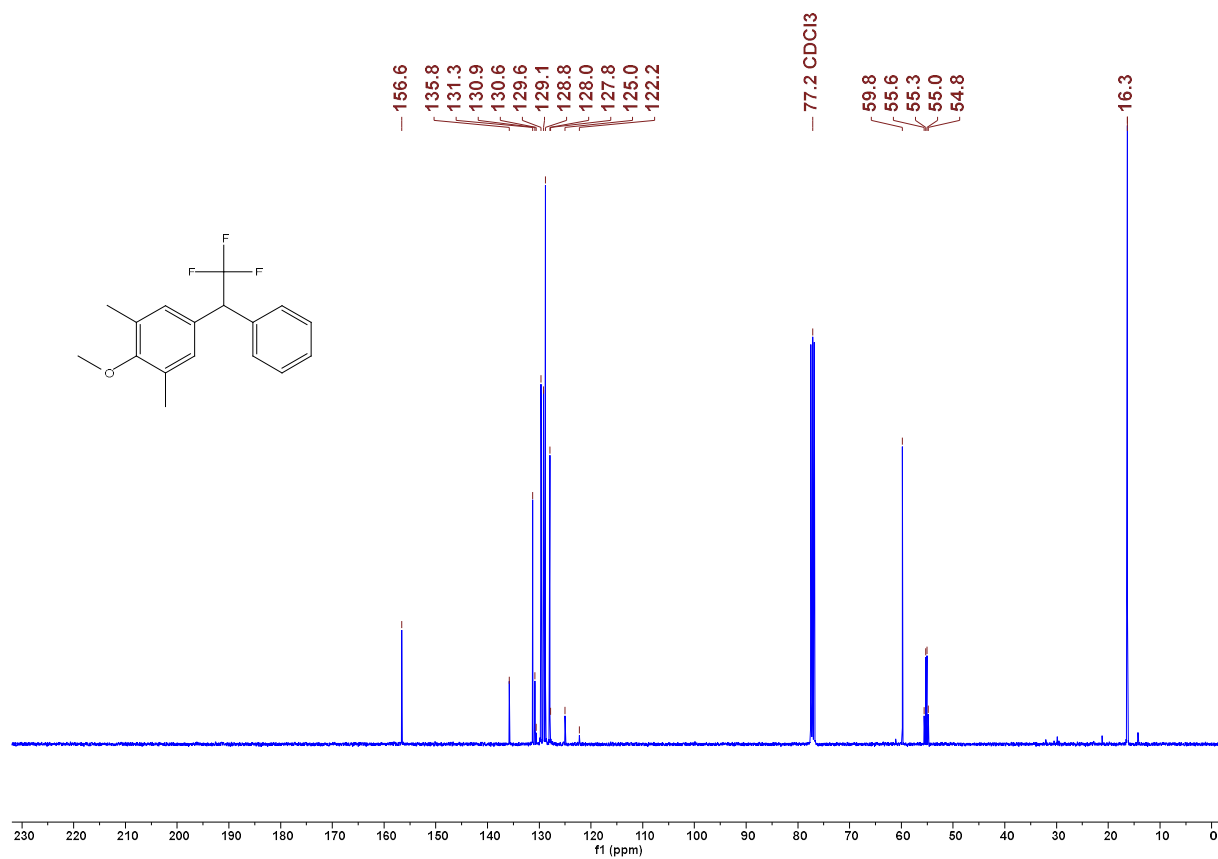
Figure 28. ^{13}C NMR spectrum of **7b** in CDCl$_3$ (101 MHz) LD3A

150
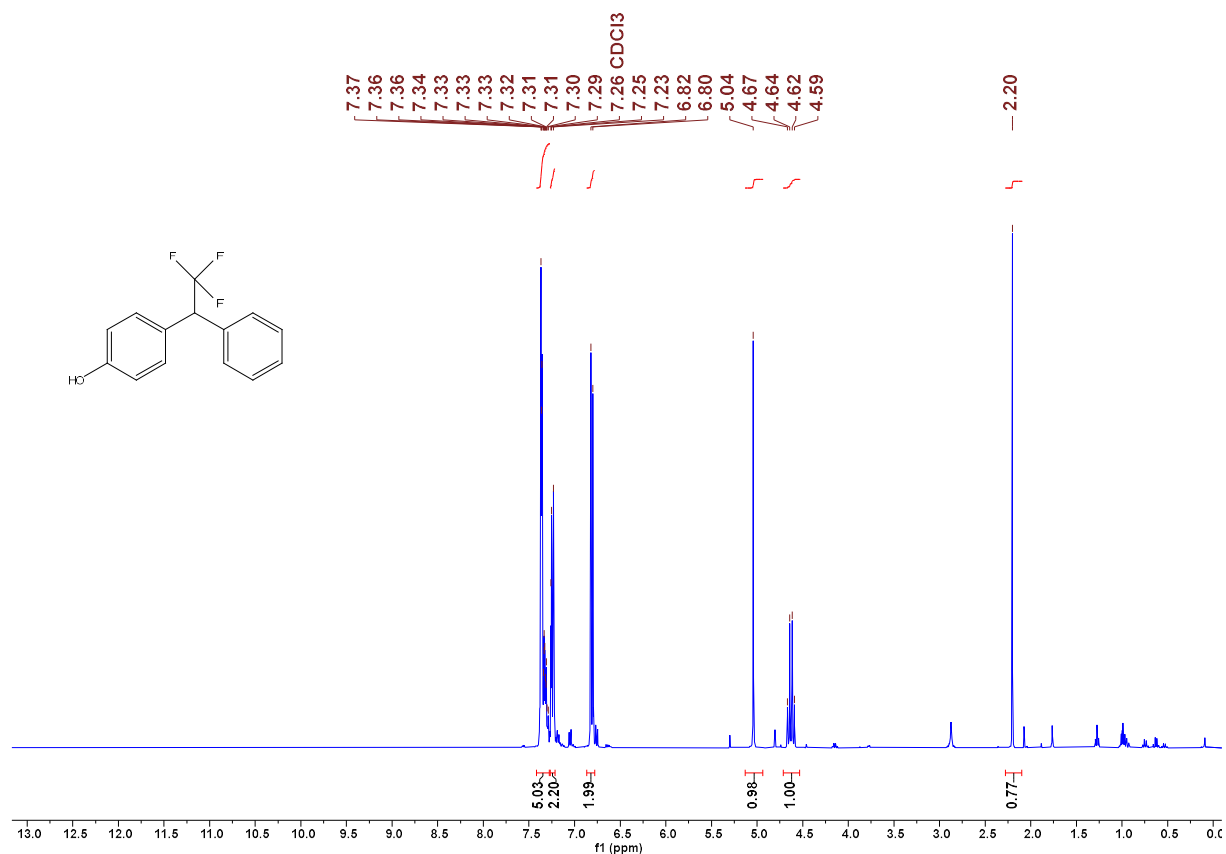
Figure 29. ^{1}H NMR spectrum of **8a** in CDCl$_3$ (400 MHz) CG153
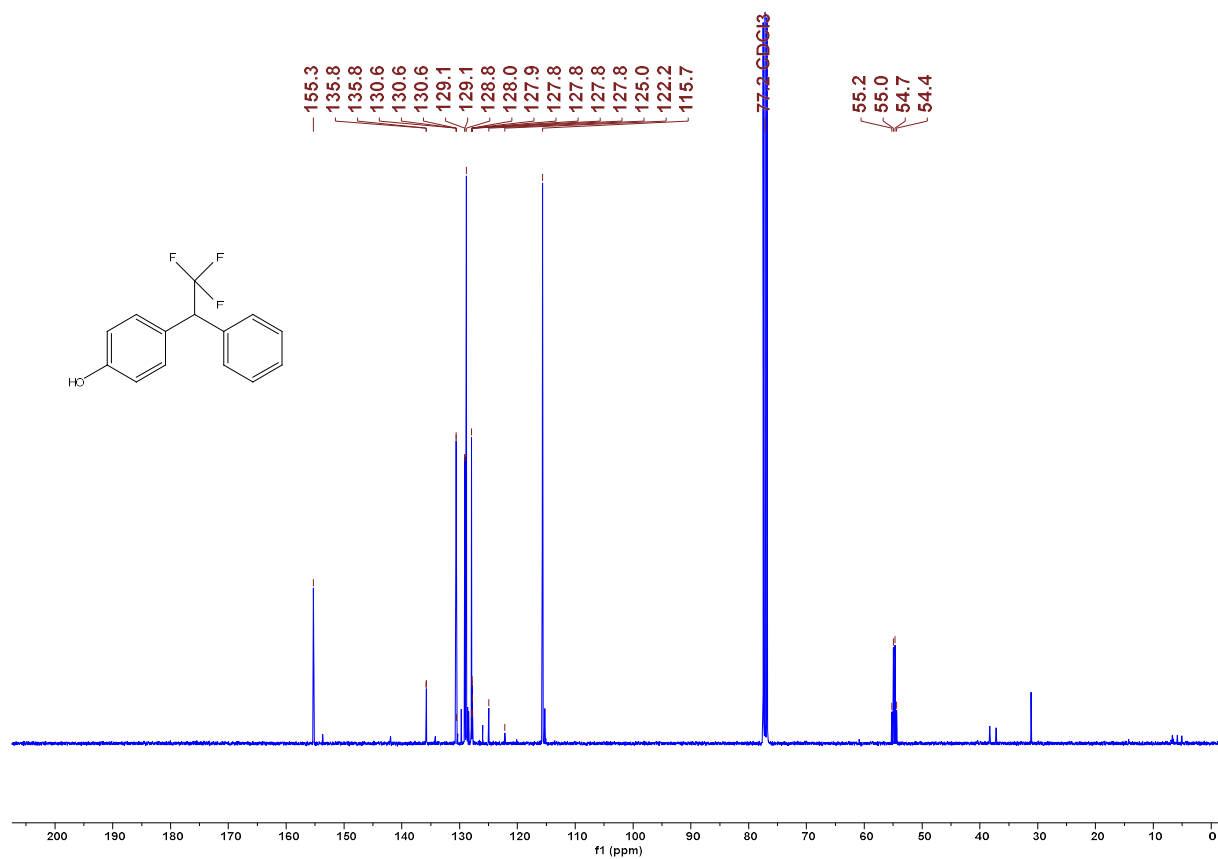
Figure 30. ^{13}C NMR spectrum of **8a** in CDCl$_3$ (101 MHz) CG153
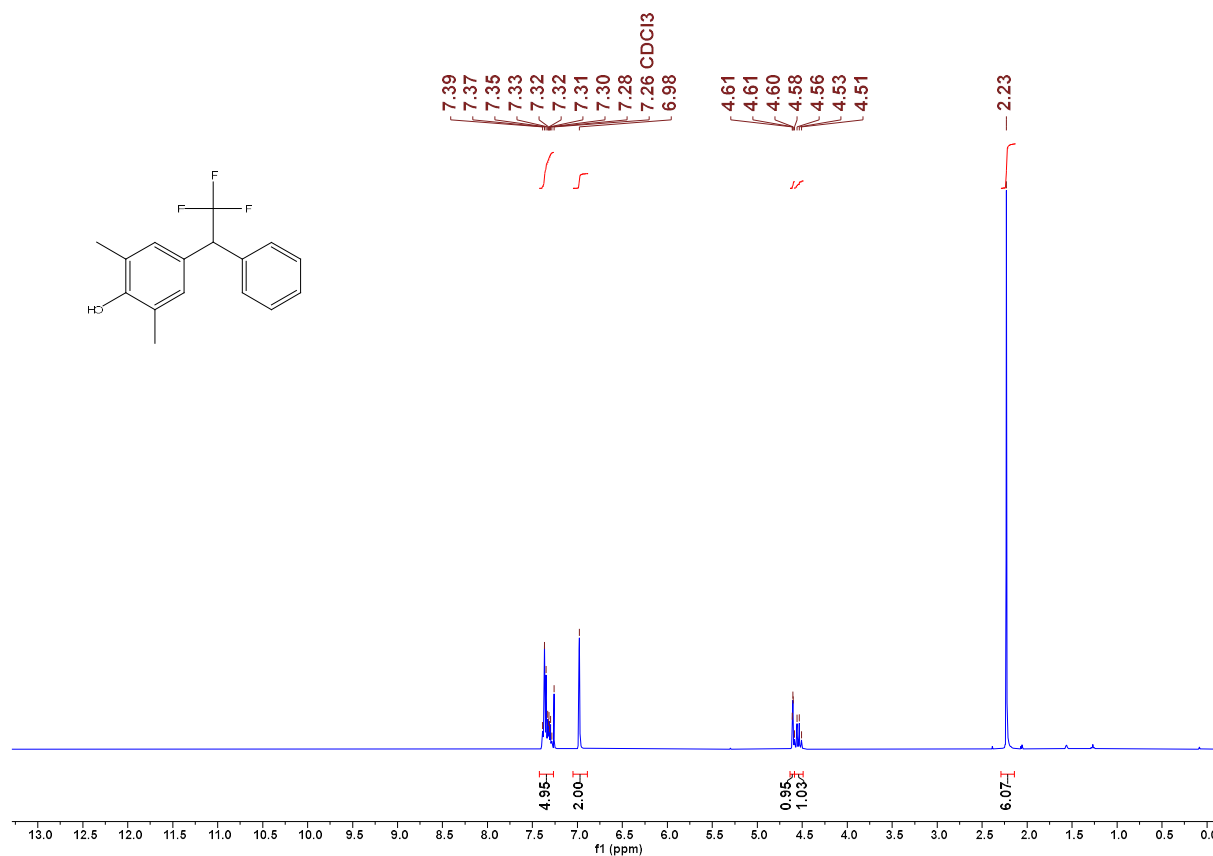
Figure 31. ^{1}H NMR spectrum of **8b** in CDCl$_3$ (400 MHz) LD4
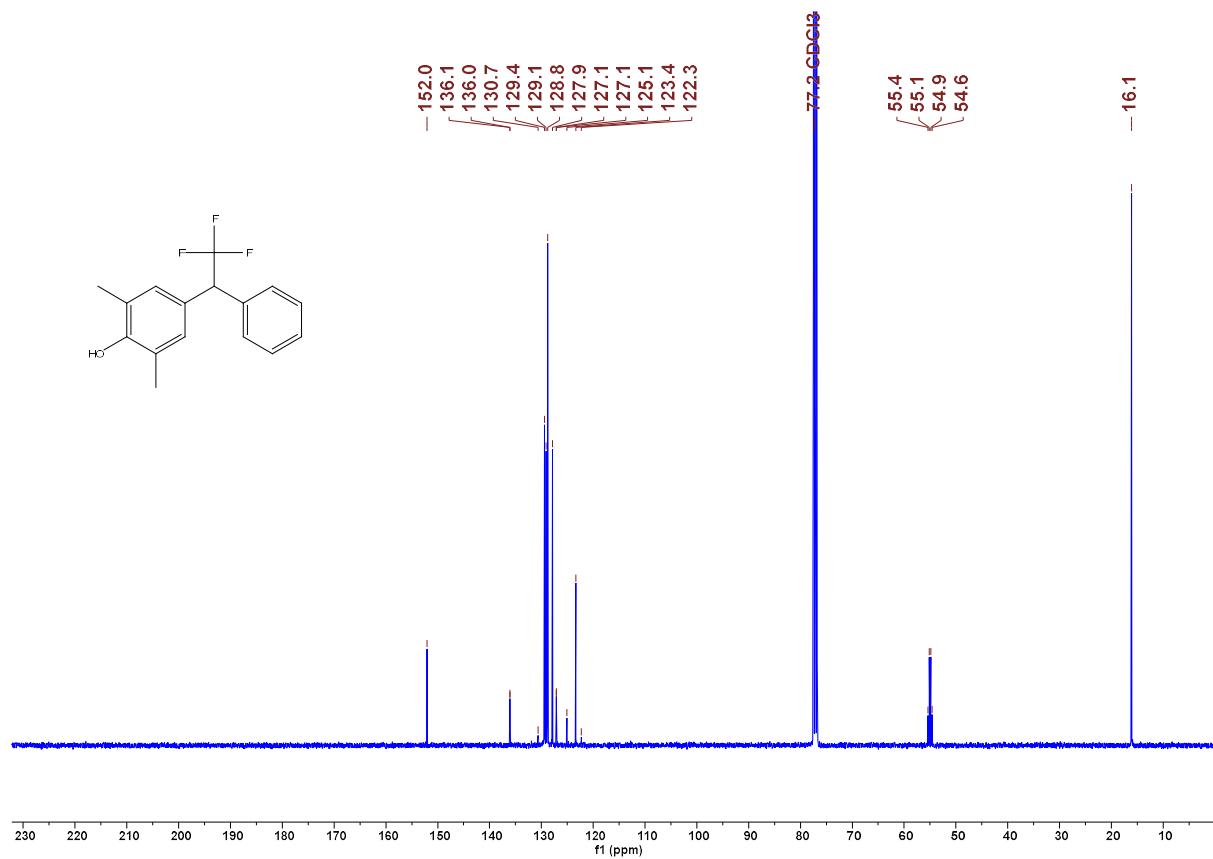
Figure 32. ^{13}C NMR spectrum of **8b** in CDCl$_3$ (101 MHz) LD4
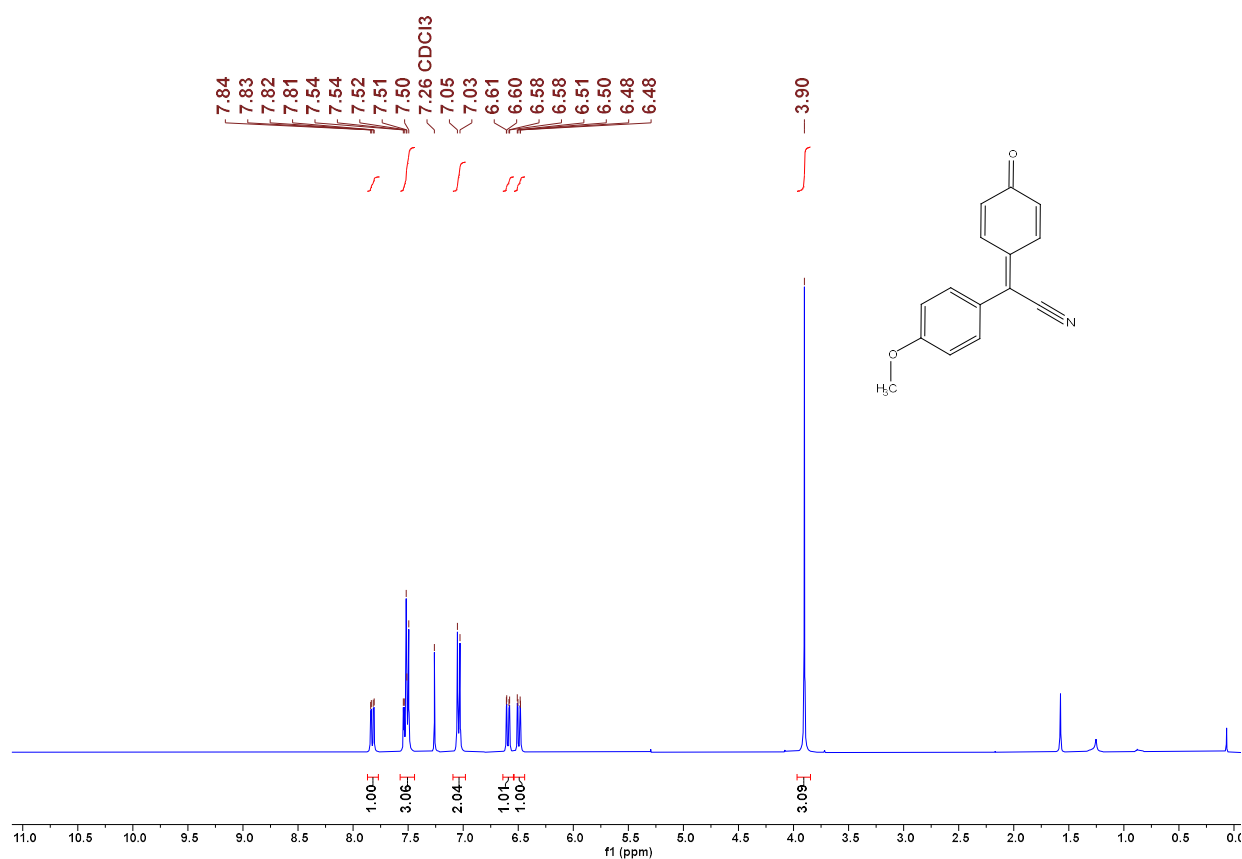
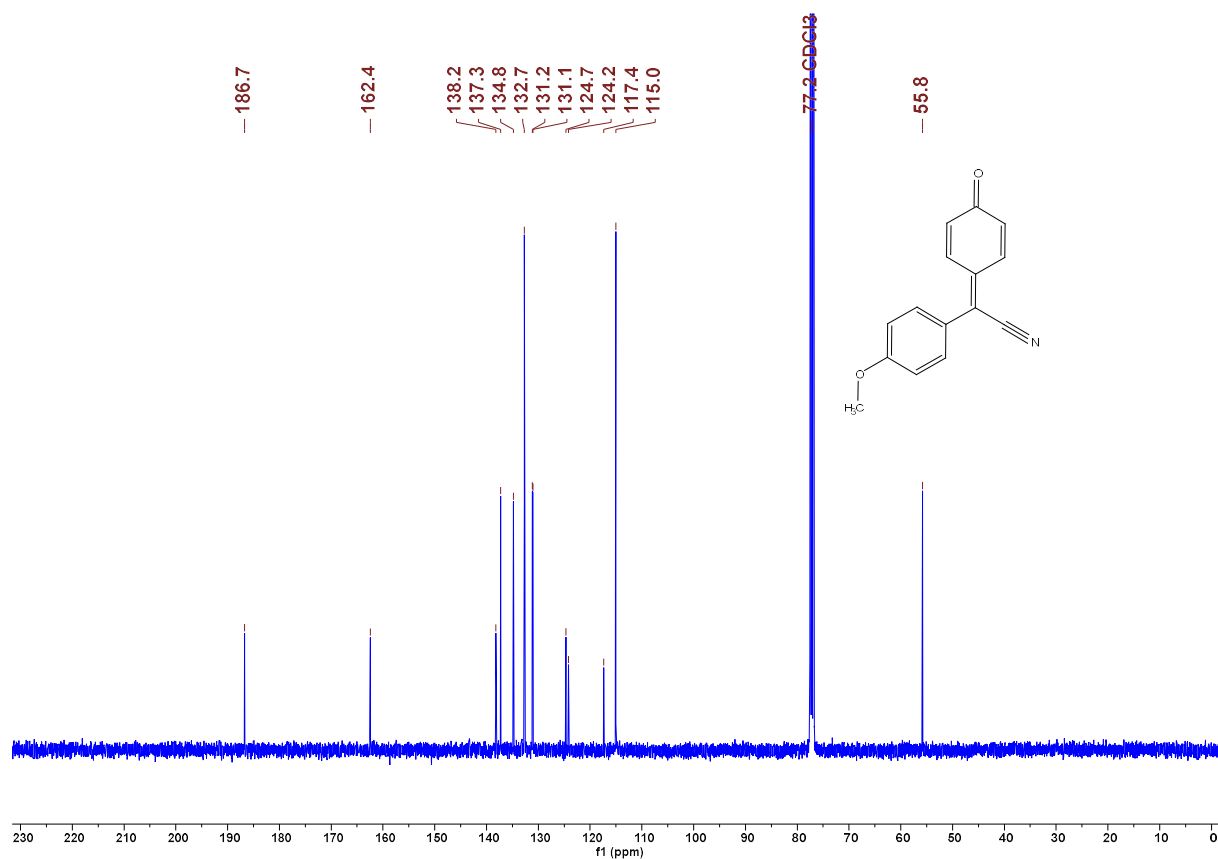**Figure 33.** ^{1}H NMR spectrum of **1a** in CDCl₃ (400 MHz) CG034

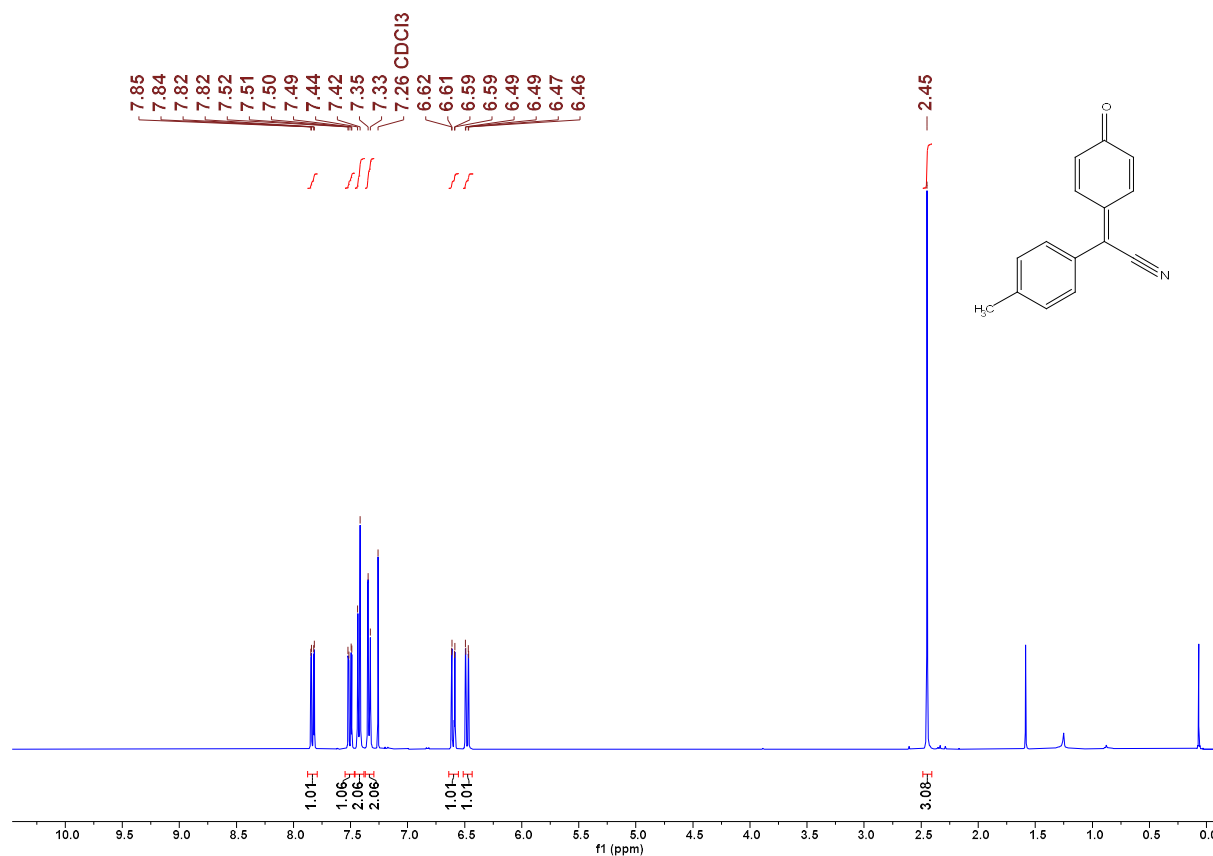**Figure 34.** ^{13}C NMR spectrum of **1a** in CDCl₃ (101 MHz) CG034
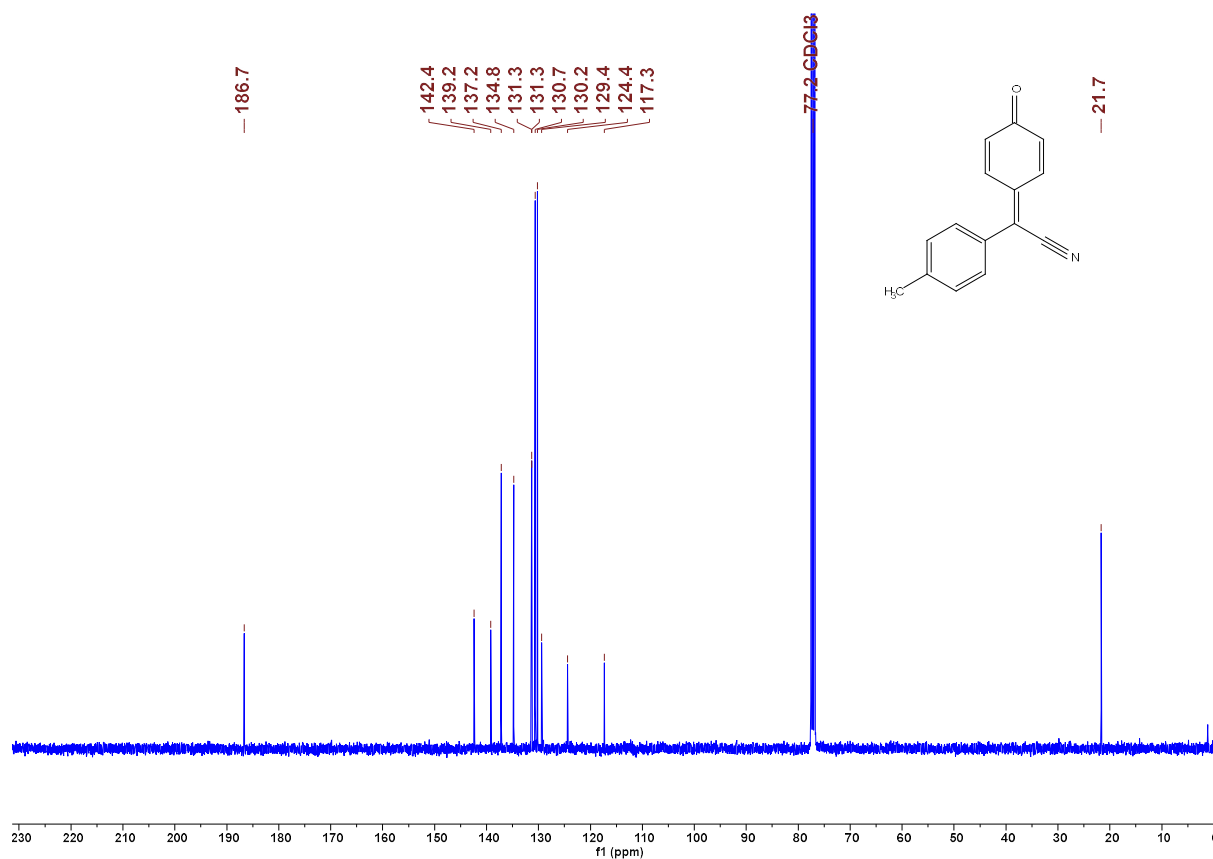
Figure 35. ^{1}H NMR spectrum of **1b** in CDCl$_3$ (400 MHz) CG024

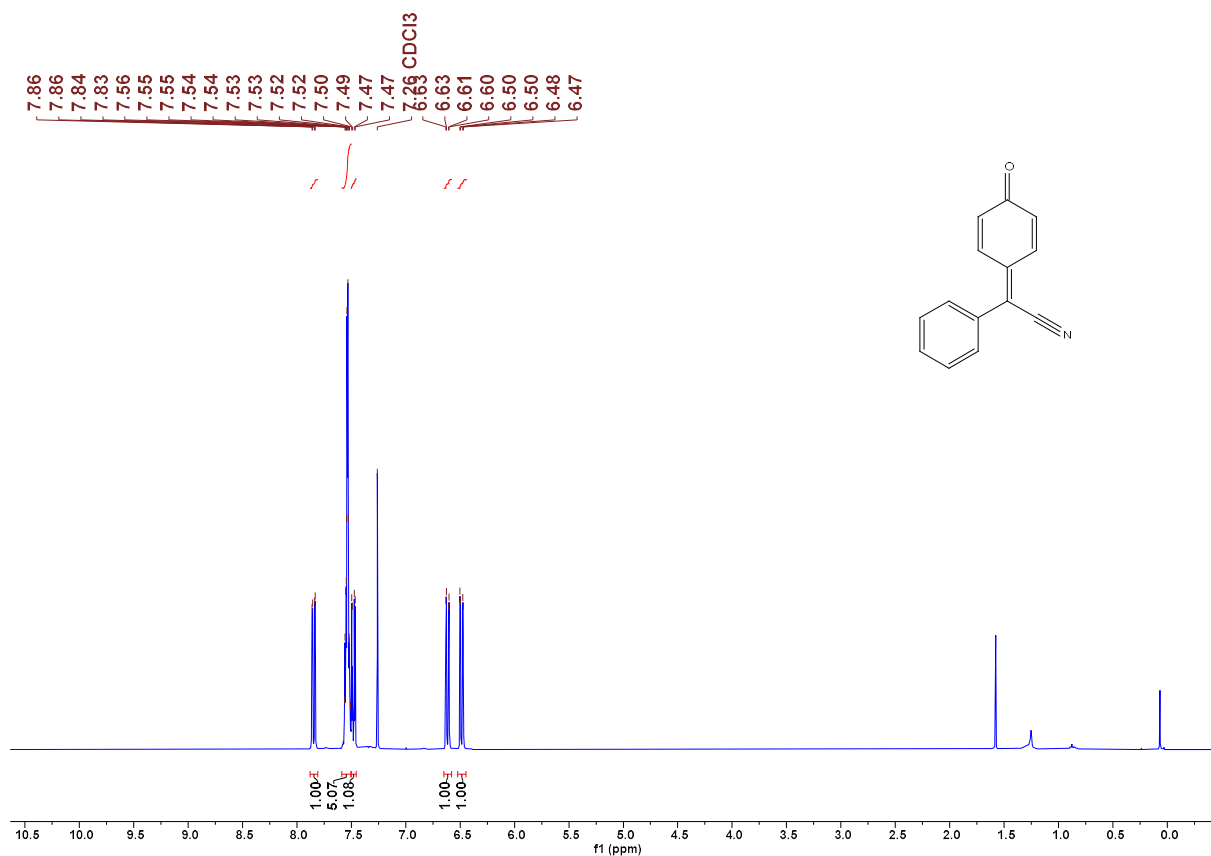**Figure 36.** ^{13}C NMR spectrum of **1b** in CDCl$_3$ (101 MHz) CG024
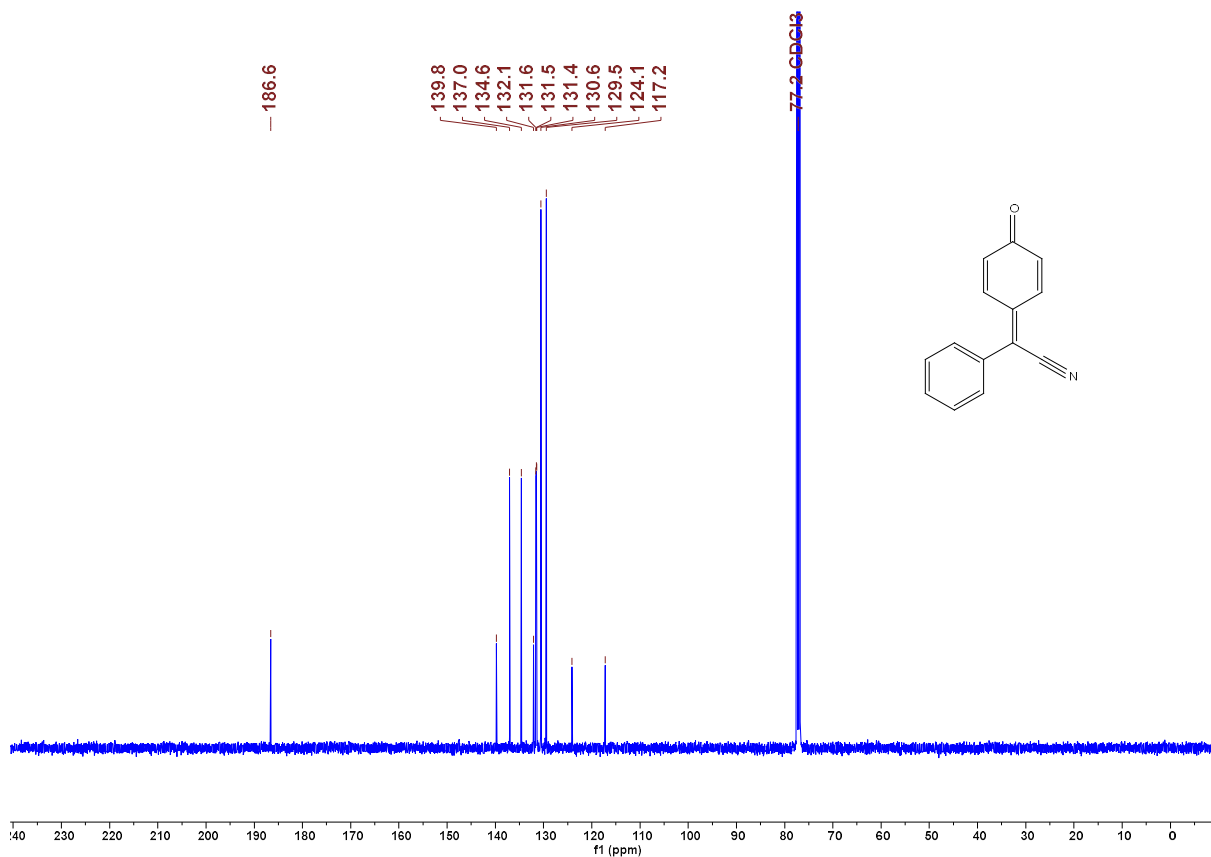
154

Figure 37. ^{1}H NMR spectrum of **1c** in CDCl$_3$ (400 MHz) CG021

Figure 38. ^{13}C NMR spectrum of **1c** in CDCl$_3$ (101 MHz) CG021

Figure 39. ^{1}H NMR spectrum of **1d** in CDCl$_3$ (600 MHz) JR015

Figure 40. ^{13}C NMR spectrum of **1d** in CDCl$_3$ (151 MHz) JR015
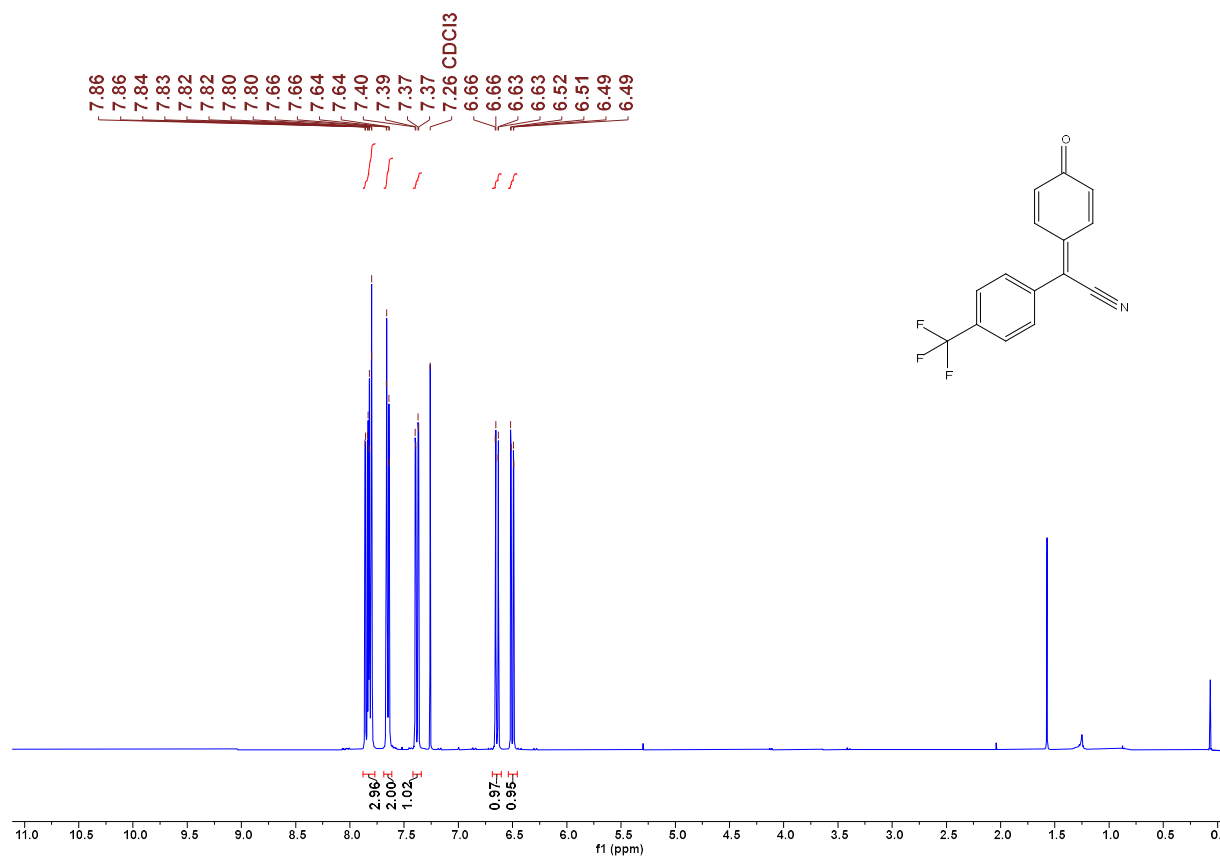
Figure 41. ^{1}H NMR spectrum of **1e** in CDCl$_3$ (400 MHz) CG029
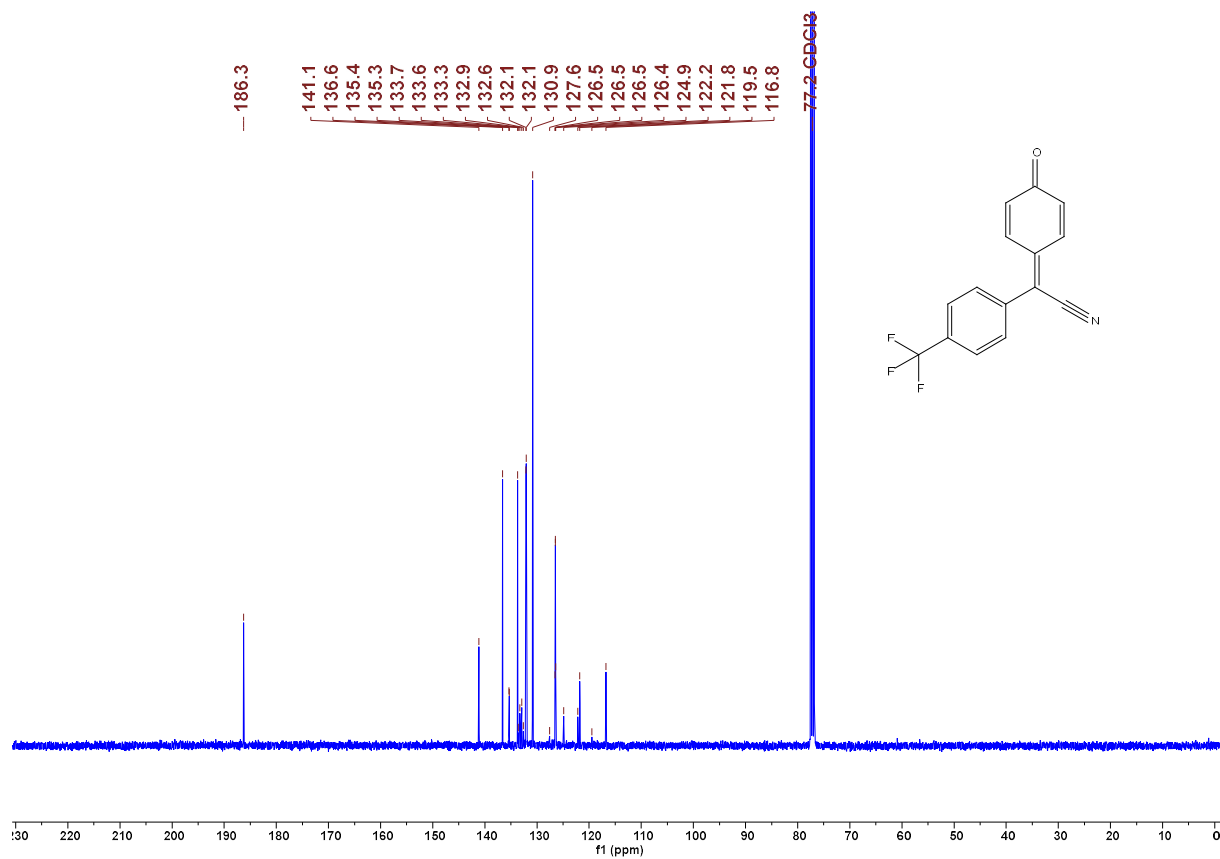
Figure 42. ^{13}C NMR spectrum of **1e** in CDCl$_3$ (101 MHz) CG029

157
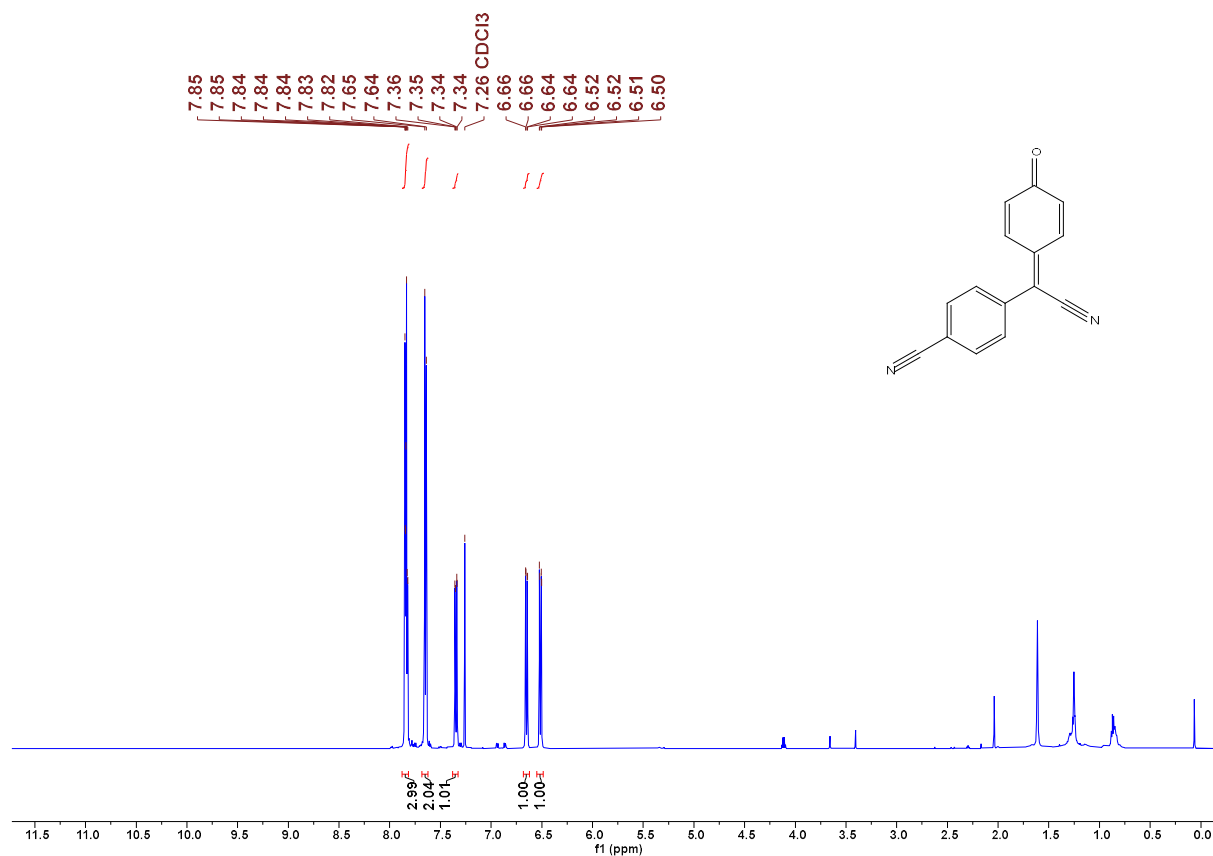
Figure 43. ^{1}H NMR spectrum of **1f** in CDCl$_3$ (600 MHz) JR019
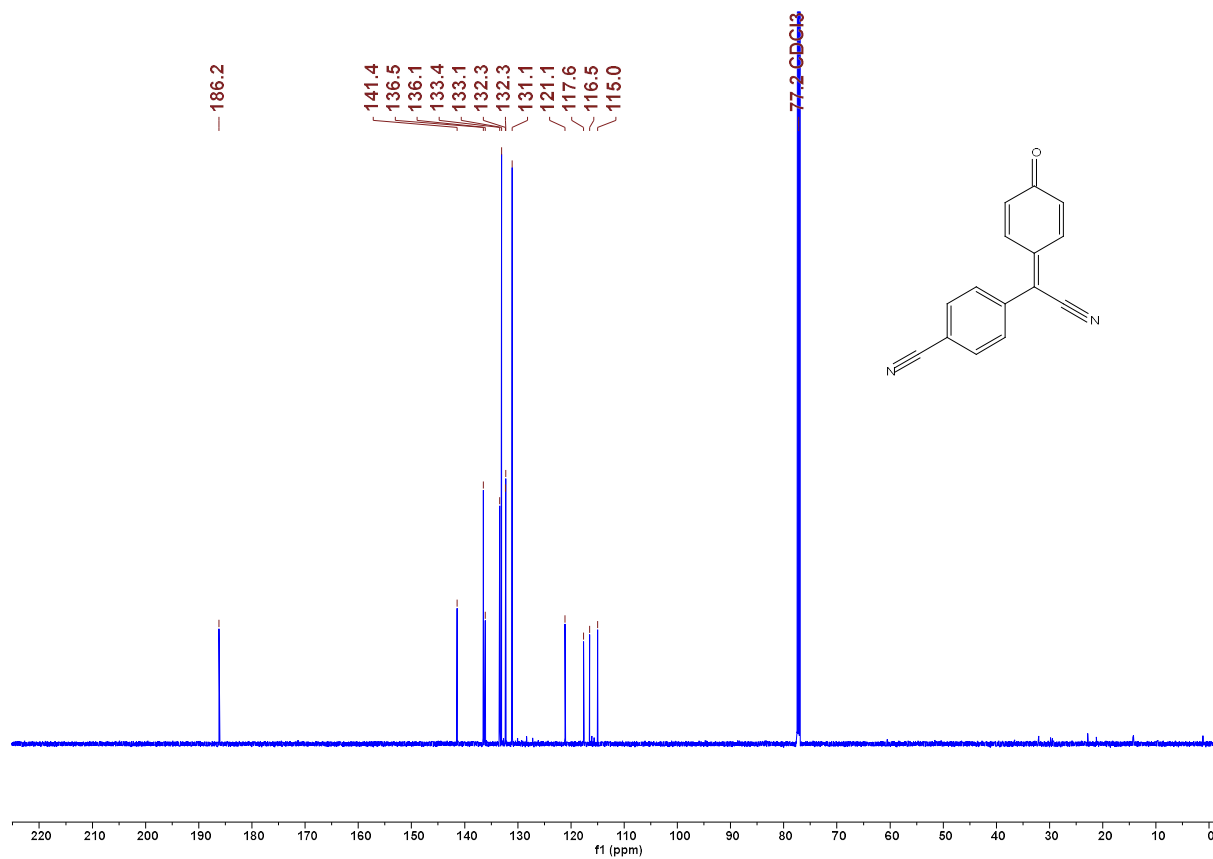
Figure 44. ^{13}C NMR spectrum of **1f** in CDCl$_3$ (151 MHz) JR019

158
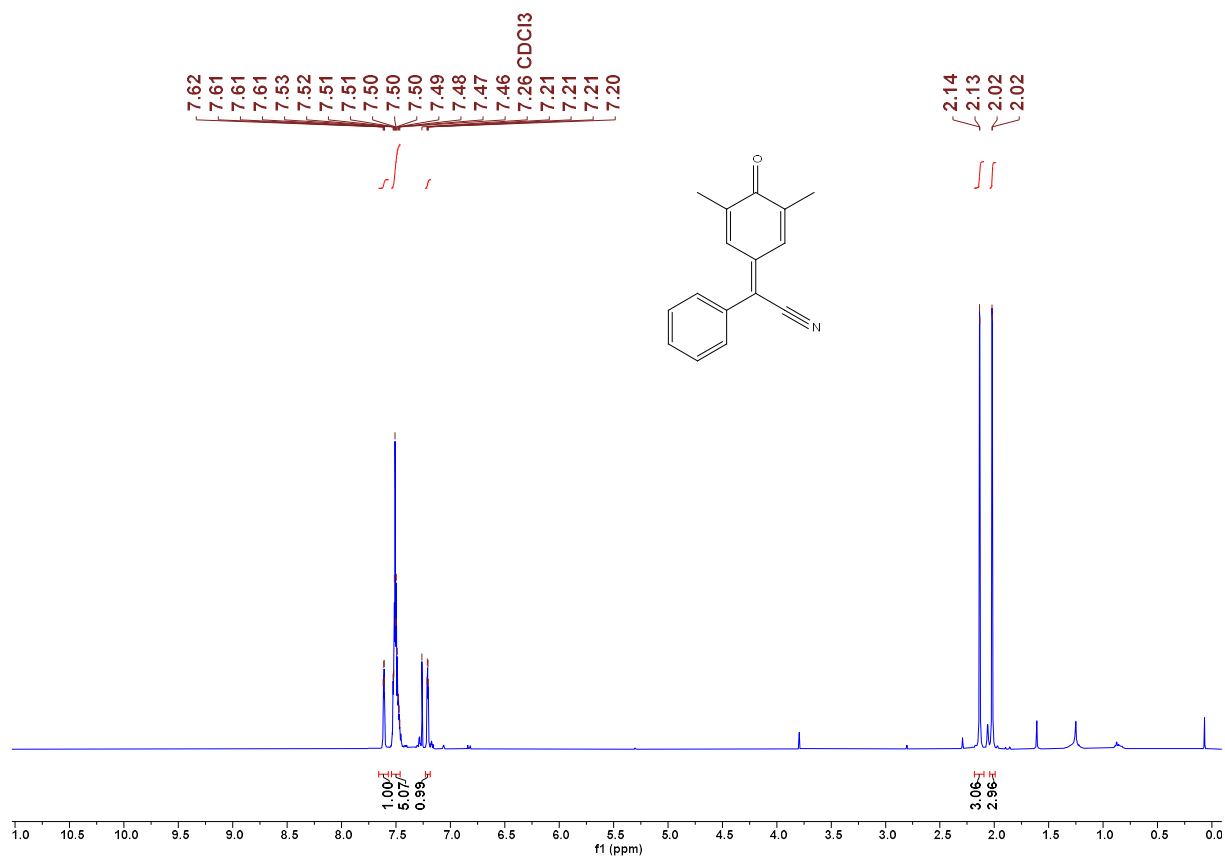
Figure 45. ^{1}H NMR spectrum of **1g** in CDCl$_3$ (400 MHz) CG127
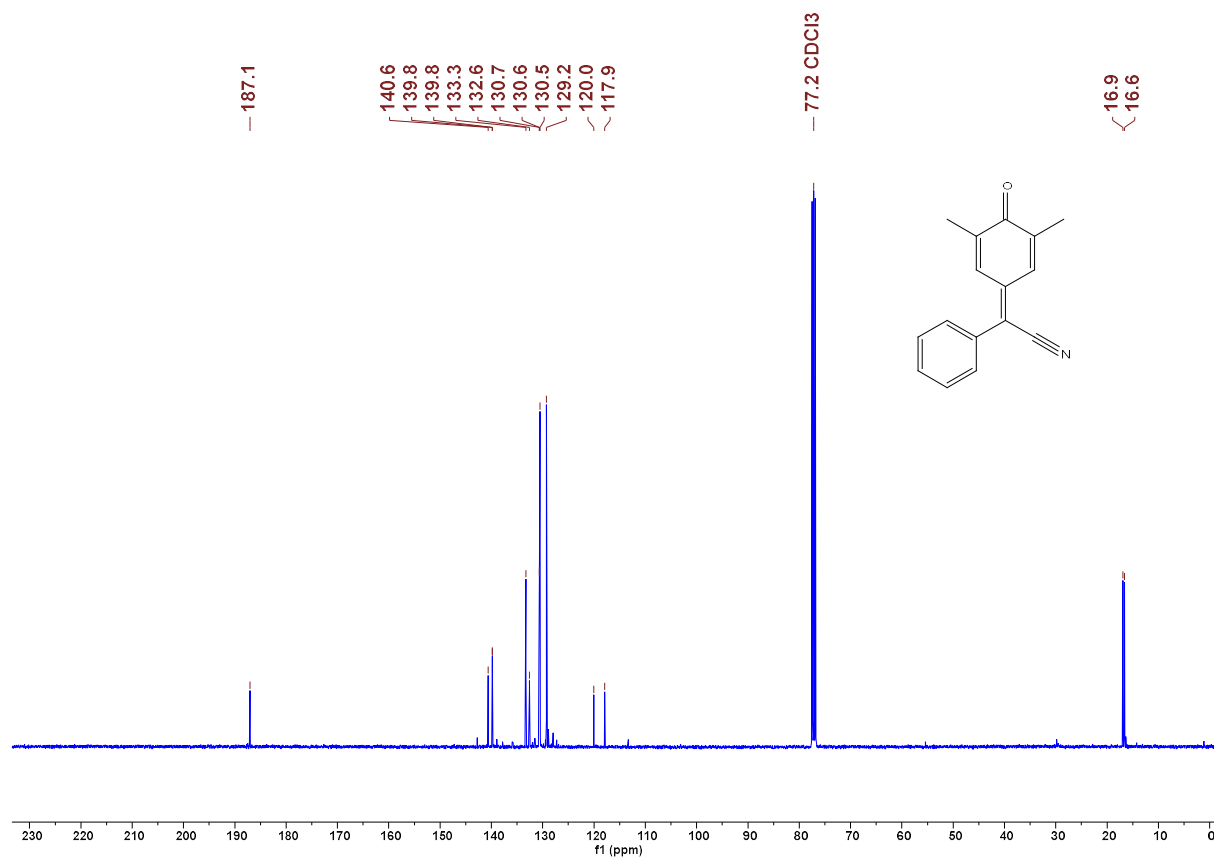
Figure 46. ^{13}C NMR spectrum of **1g** in CDCl$_3$ (101 MHz) CG127
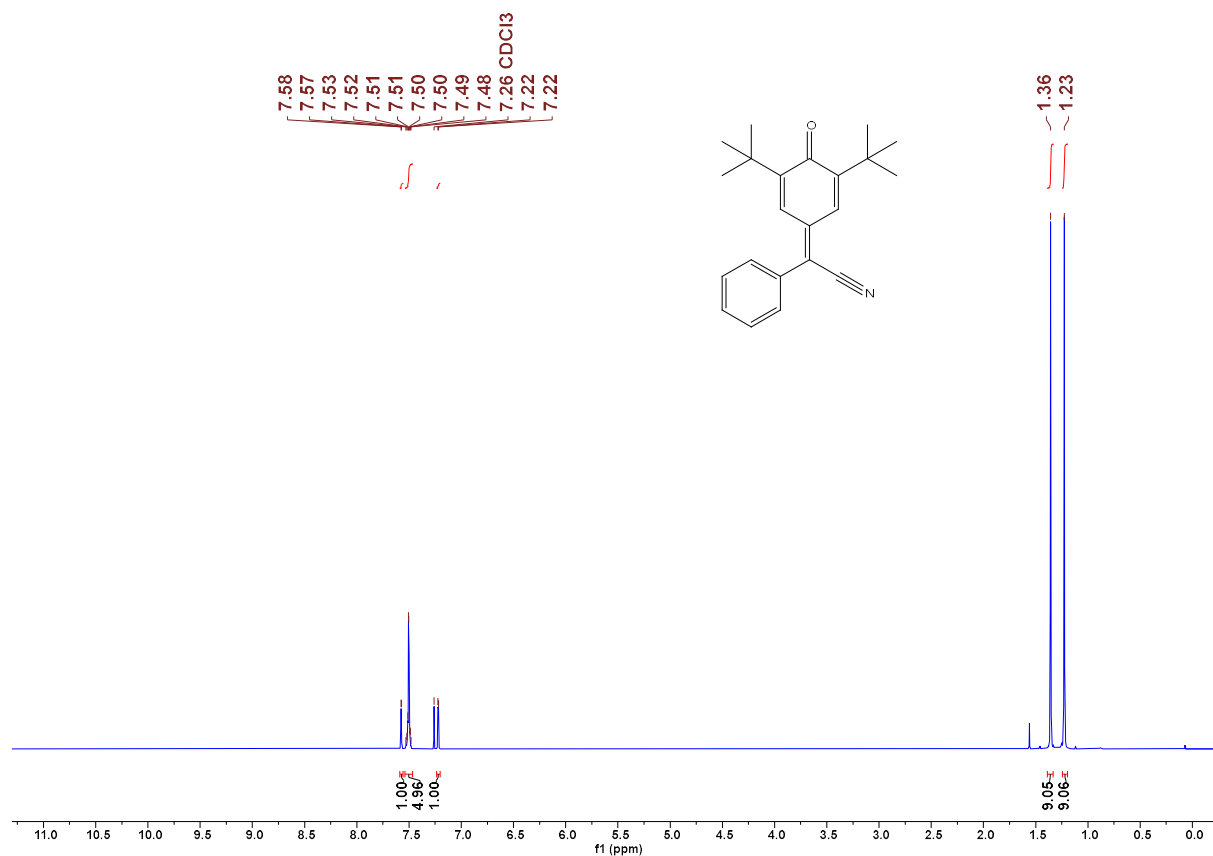
Figure 47. ^{1}H NMR spectrum of **1h** in CDCl₃ (600 MHz) CG104
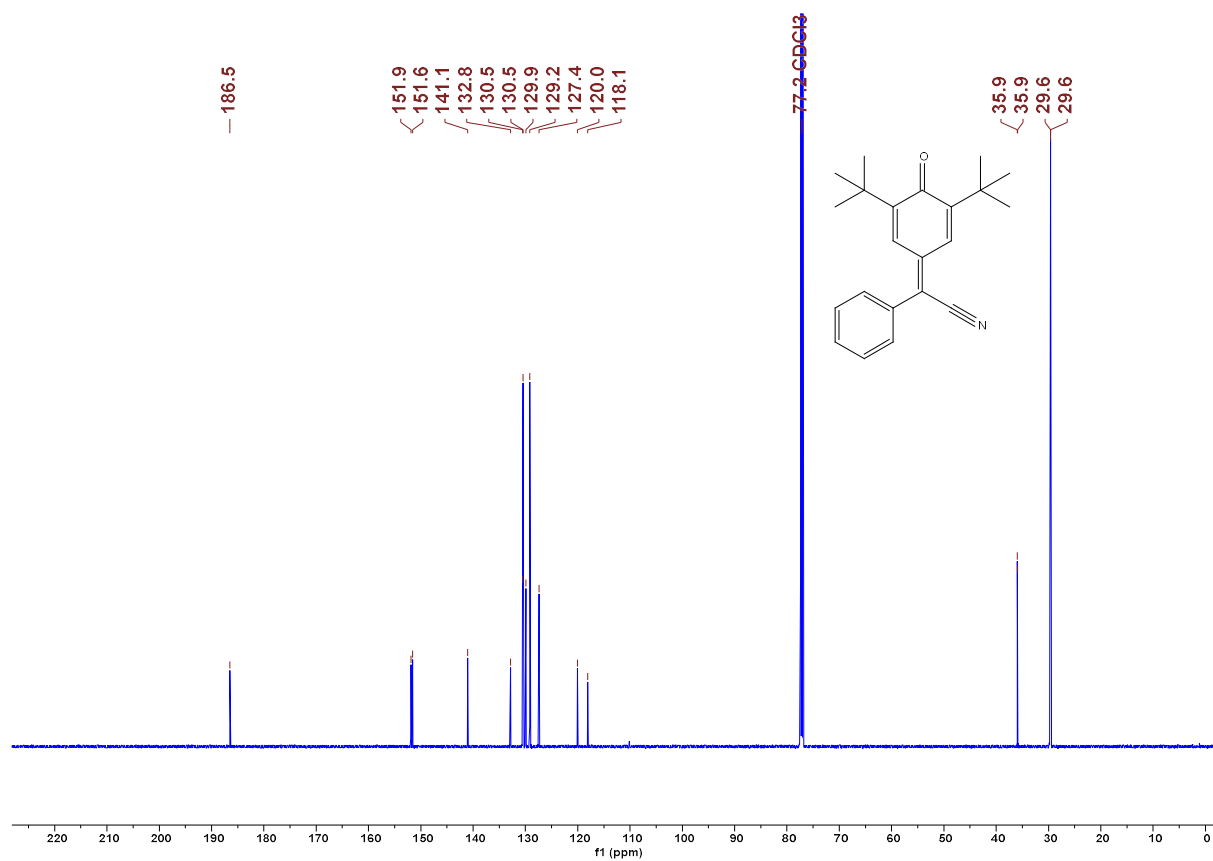
Figure 48. ^{13}C NMR spectrum of **1h** in CDCl₃ (151 MHz) CG104
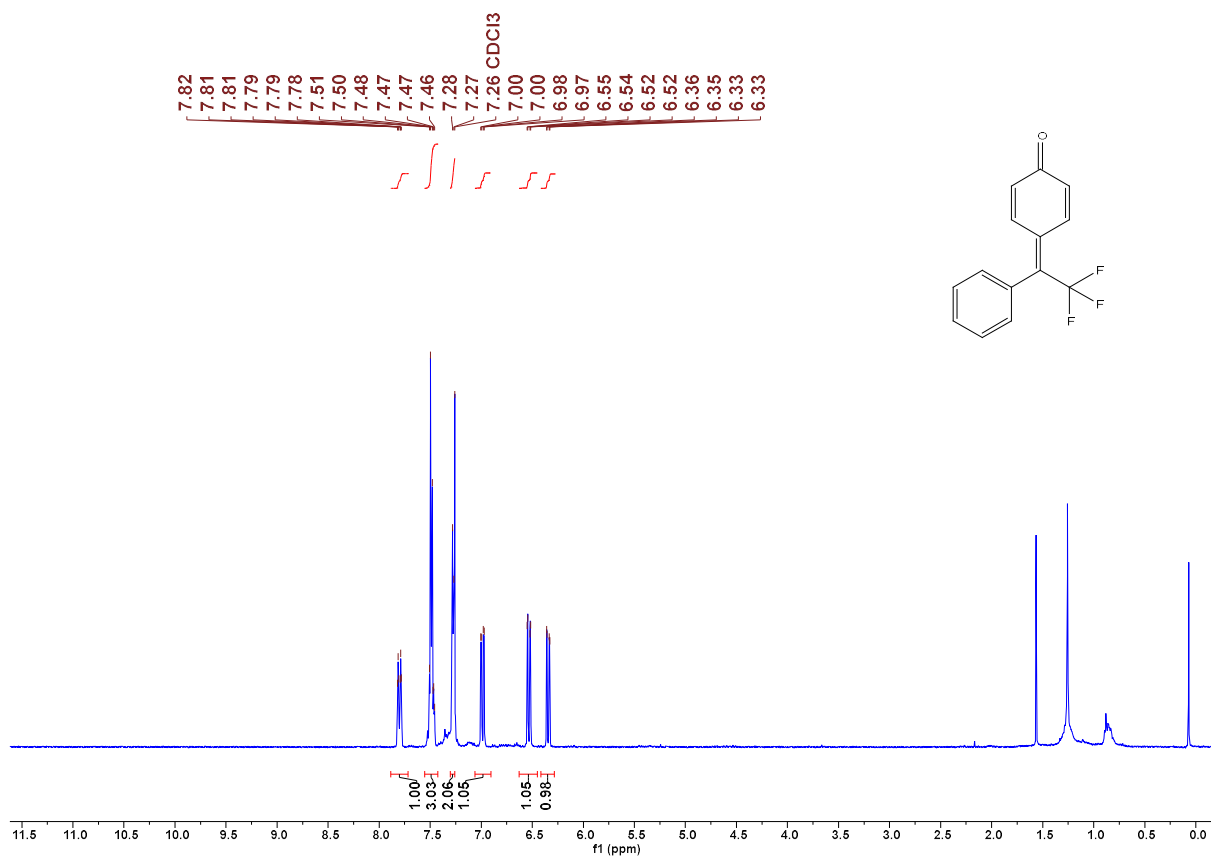
Figure 49. ^{1}H NMR spectrum of **1i** in CDCl$_3$ (400 MHz) CG154_2
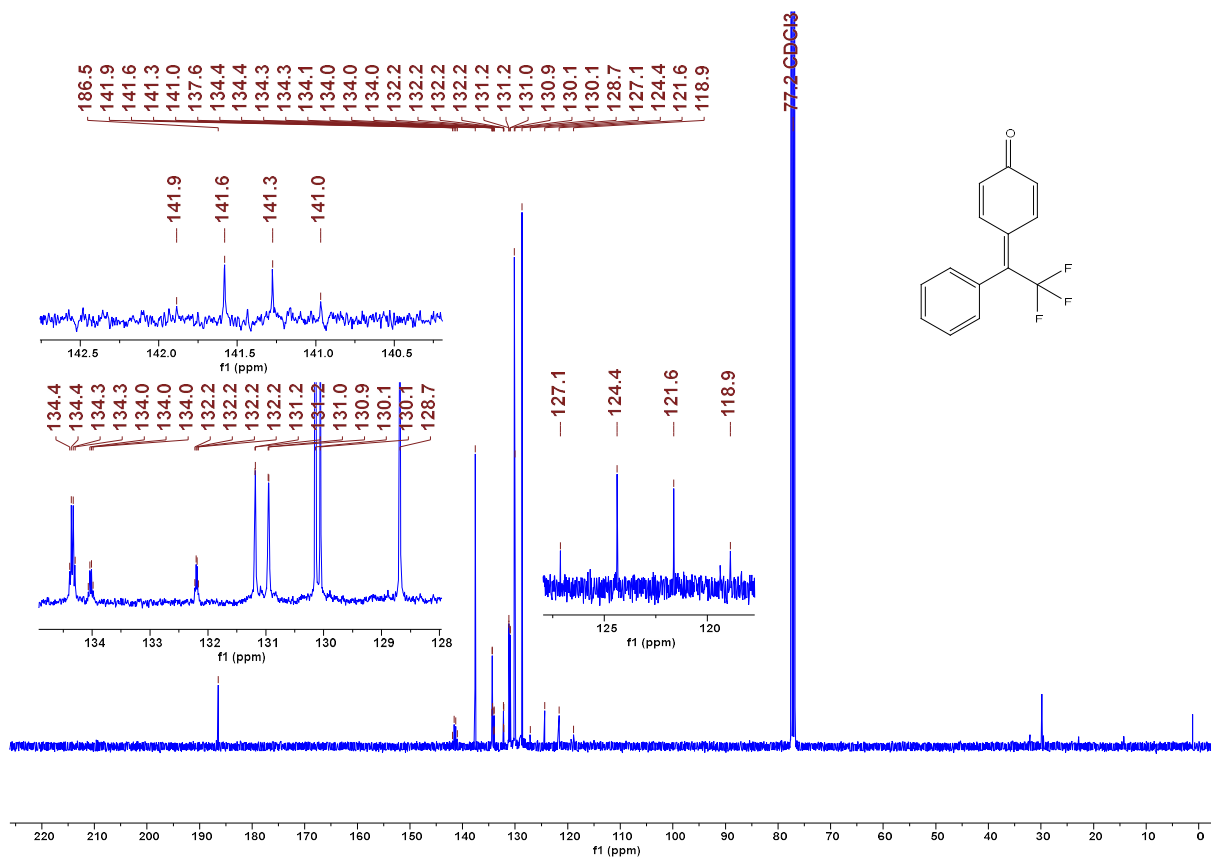
Figure 50. ^{13}C NMR spectrum of **1i** in CDCl$_3$ (101 MHz) CG154_2

_____
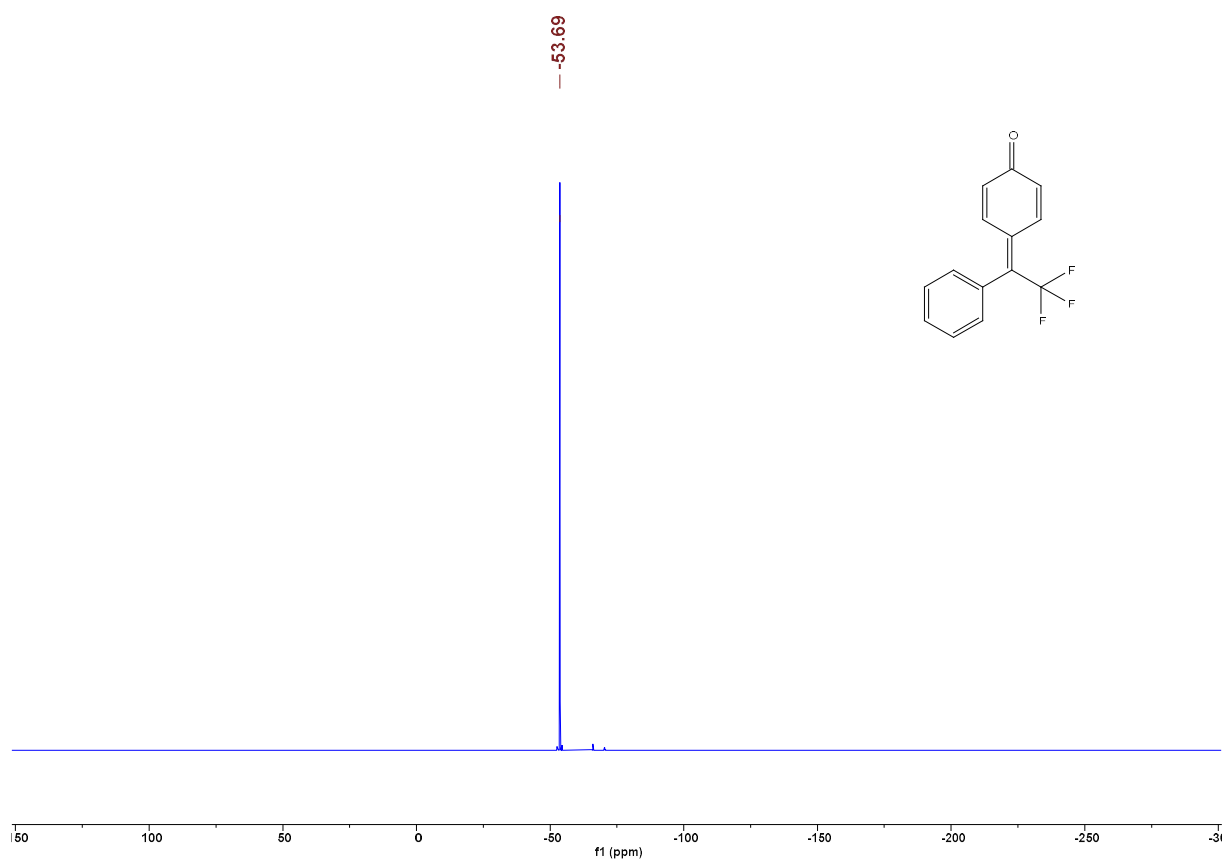
Figure 51. ^{19}F NMR spectrum of **1i** in CDCl$_3$ (377 MHz) CG154_2
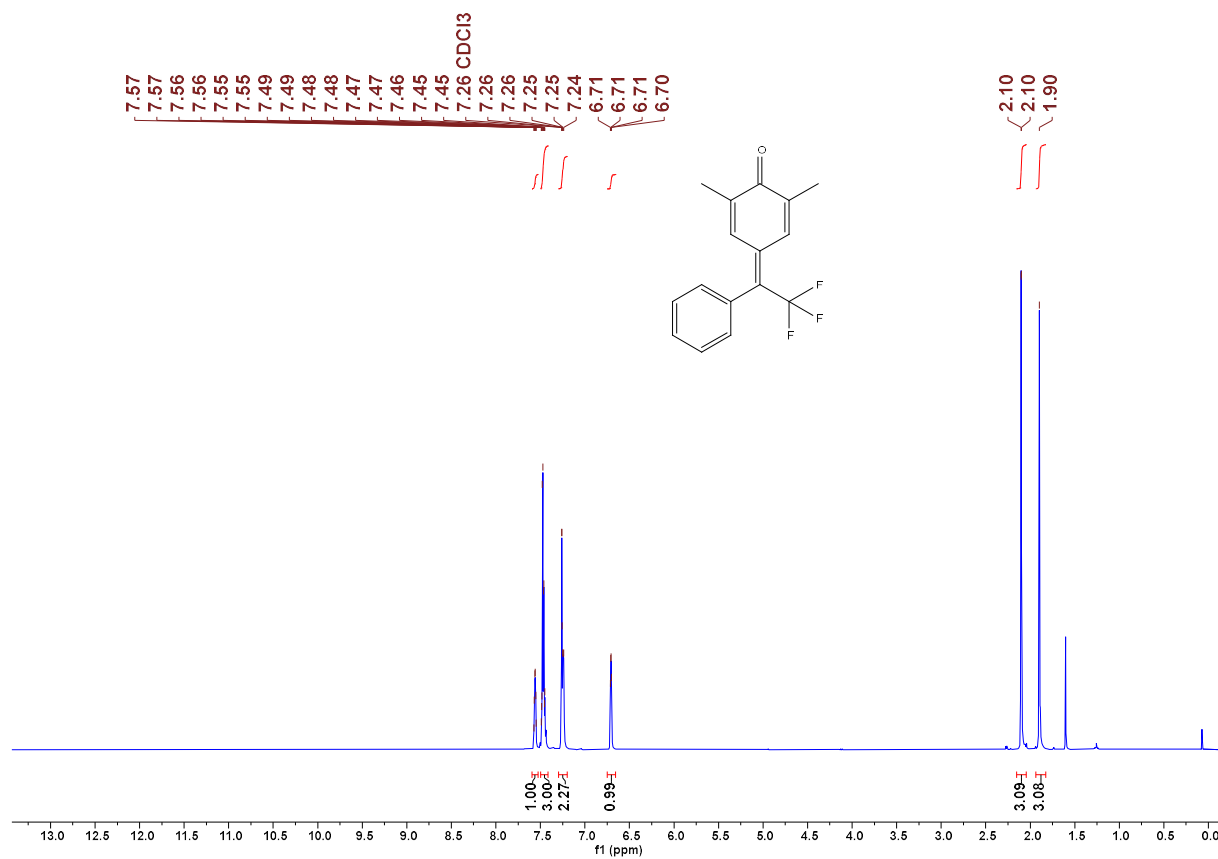
Figure 52. ^{1}H NMR spectrum of **1j** in CDCl$_3$ (400 MHz) LD5

Figure 53. ^{13}C NMR spectrum of **1j** in CDCl$_3$ (101 MHz) LD5

Figure 54. ^{19}F NMR spectrum of **1j** in CDCl$_3$ (377 MHz) LD5

Figure 55. ¹H NMR spectrum of **9aa** in DMSO-d₆ (400 MHz) CG060_3

Figure 56. ¹³C NMR spectrum of **9aa** in DMSO-d₆ (101 MHz) CG060_3
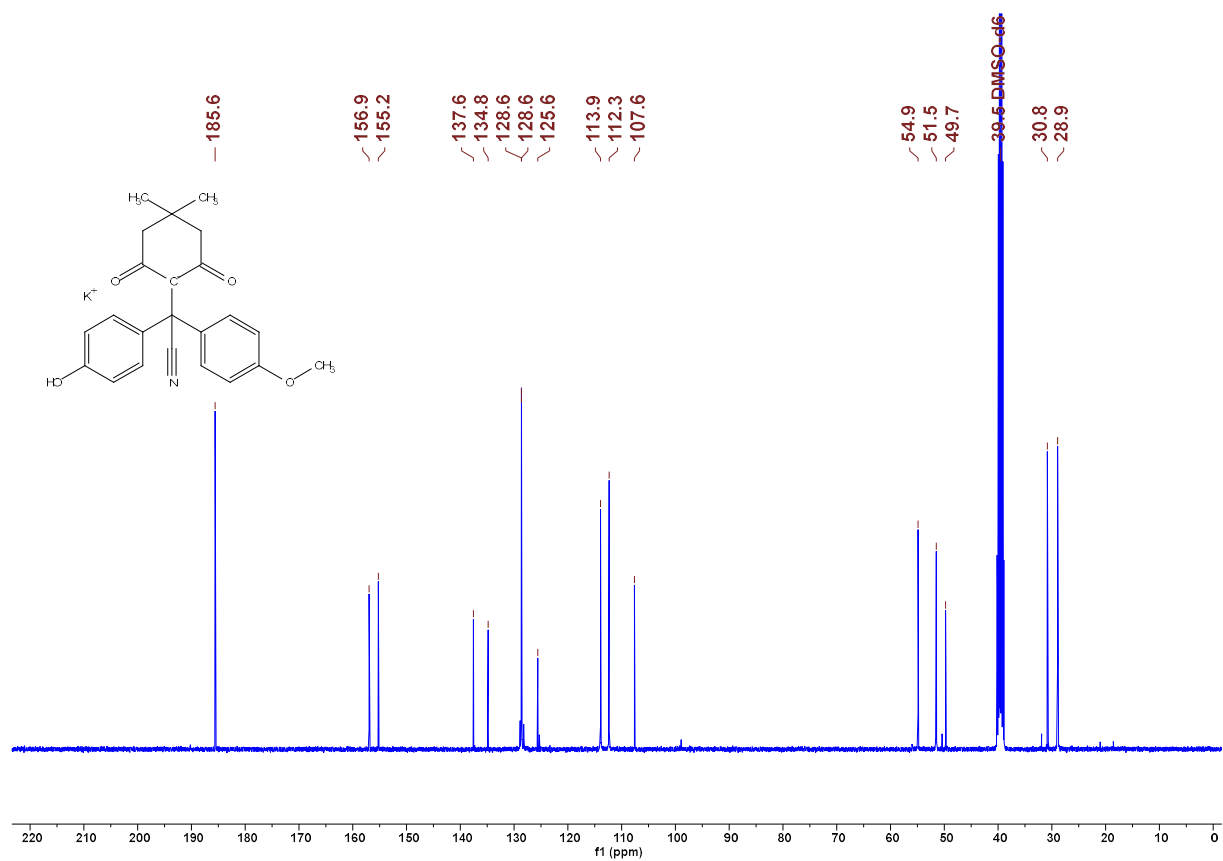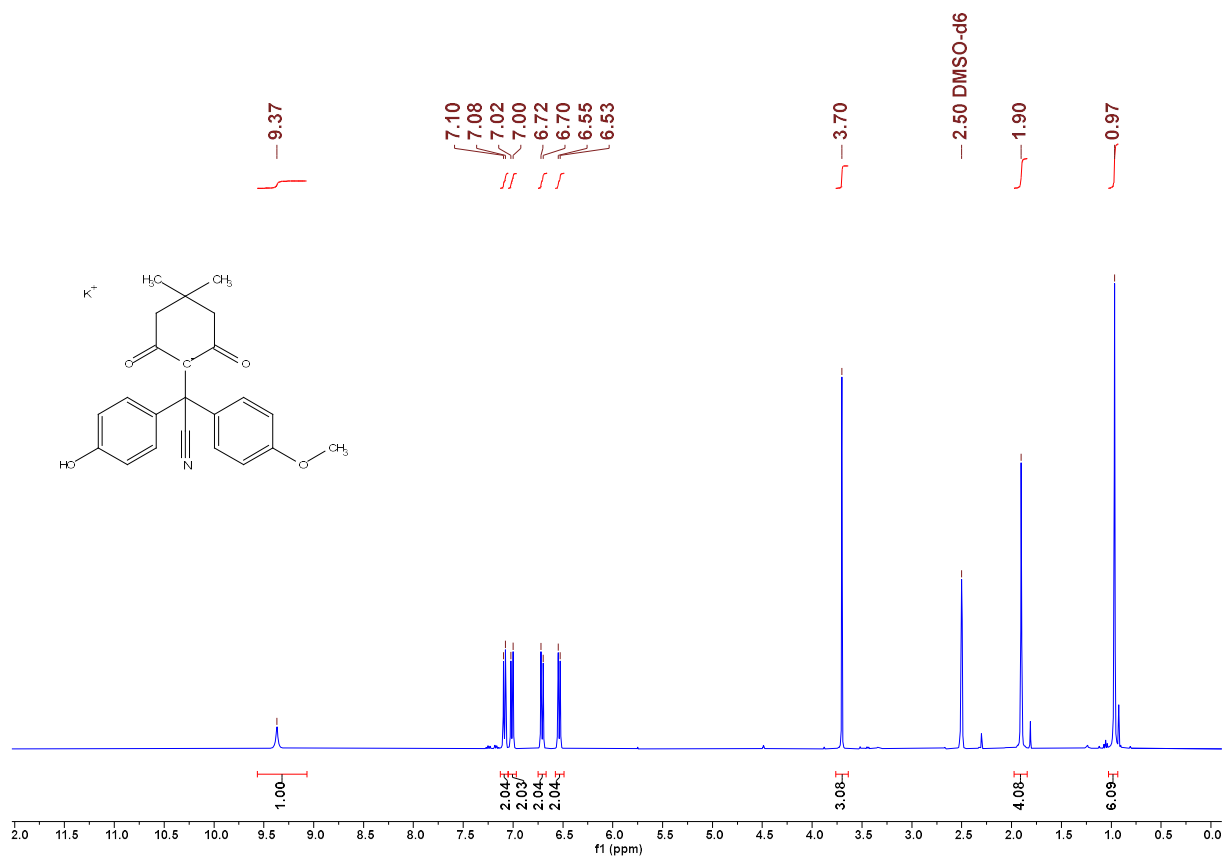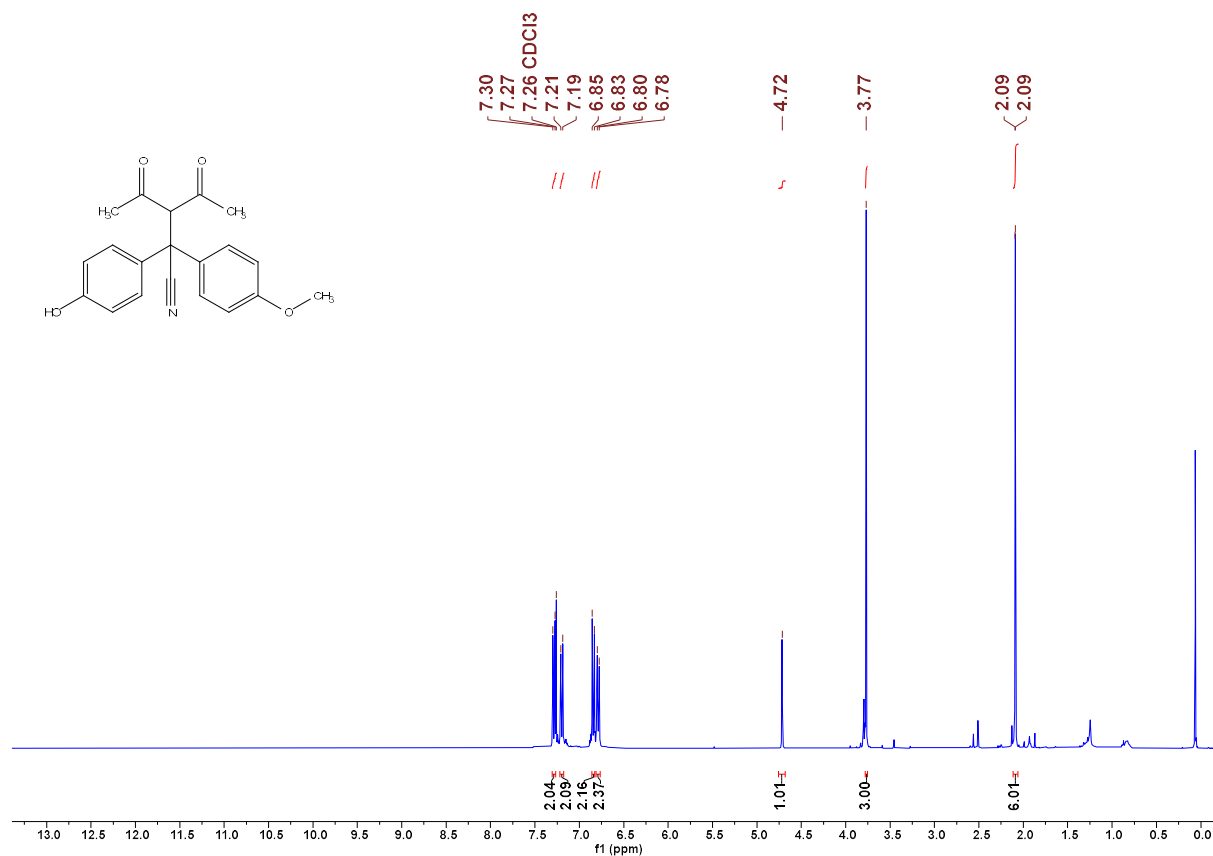
Figure 57. ^{1}H NMR spectrum of **9ab** in CDCl$_3$ (400 MHz) CG059_3
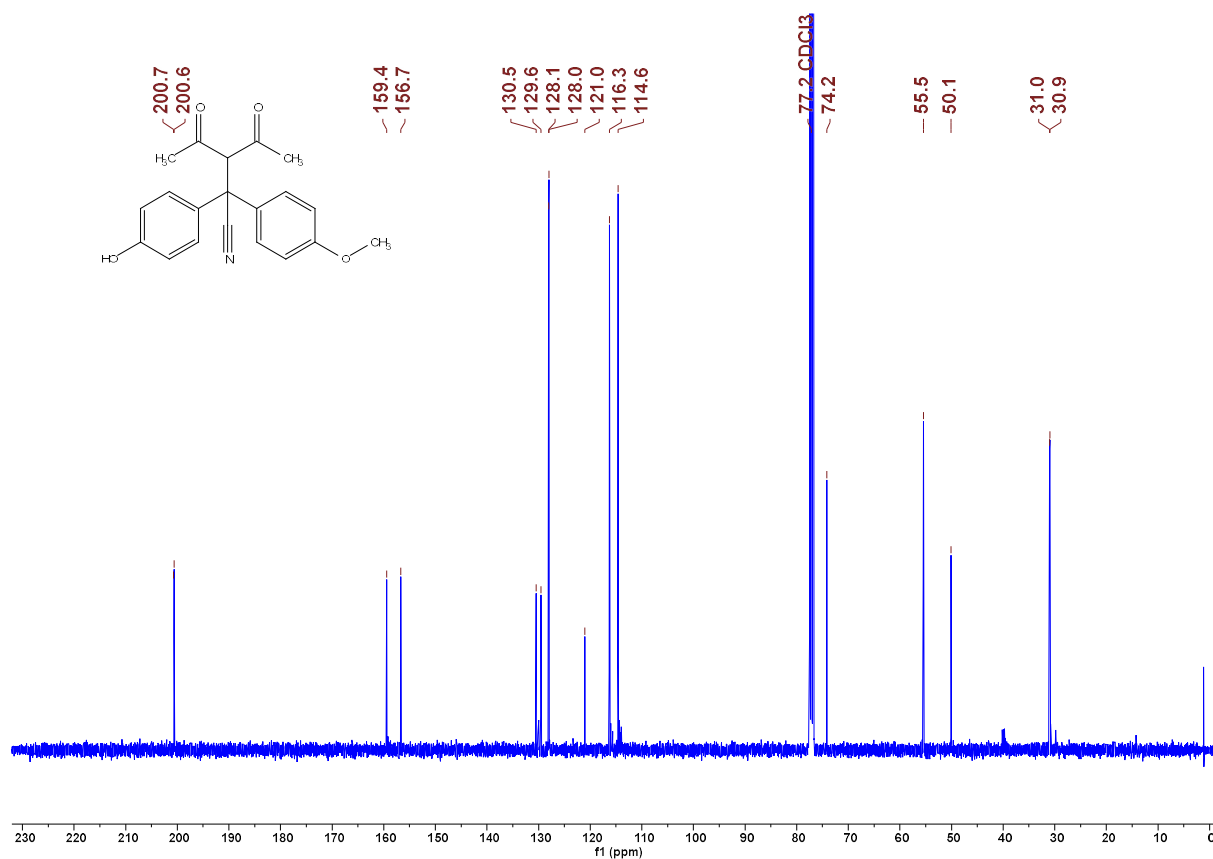
Figure 58. ^{13}C NMR spectrum of **9ab** in CDCl$_3$ (101 MHz) CG059_3

165
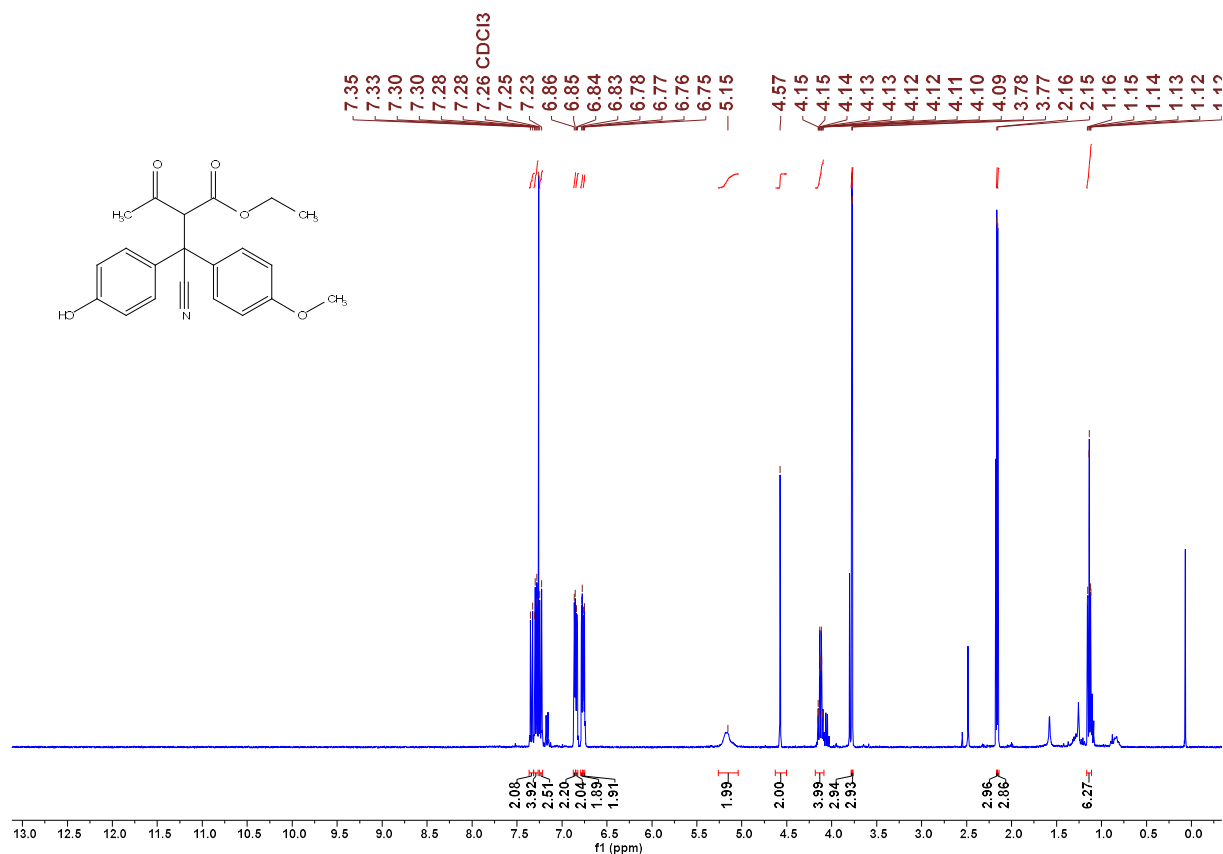
Figure 59. ^{1}H NMR spectrum of **9ac** in CDCl$_3$ (400 MHz) CG062
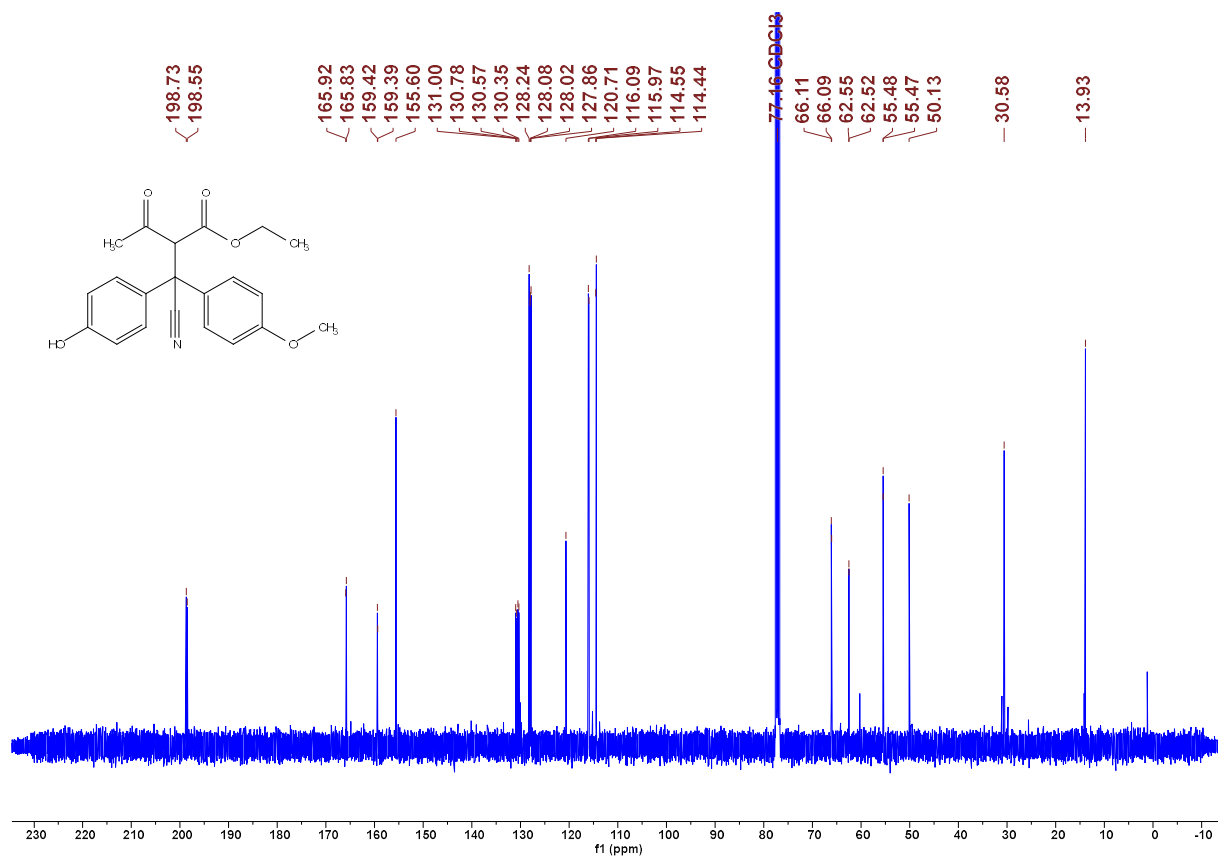
Figure 60. ^{13}C NMR spectrum of **9ac** in CDCl$_3$ (101 MHz) CG062

166
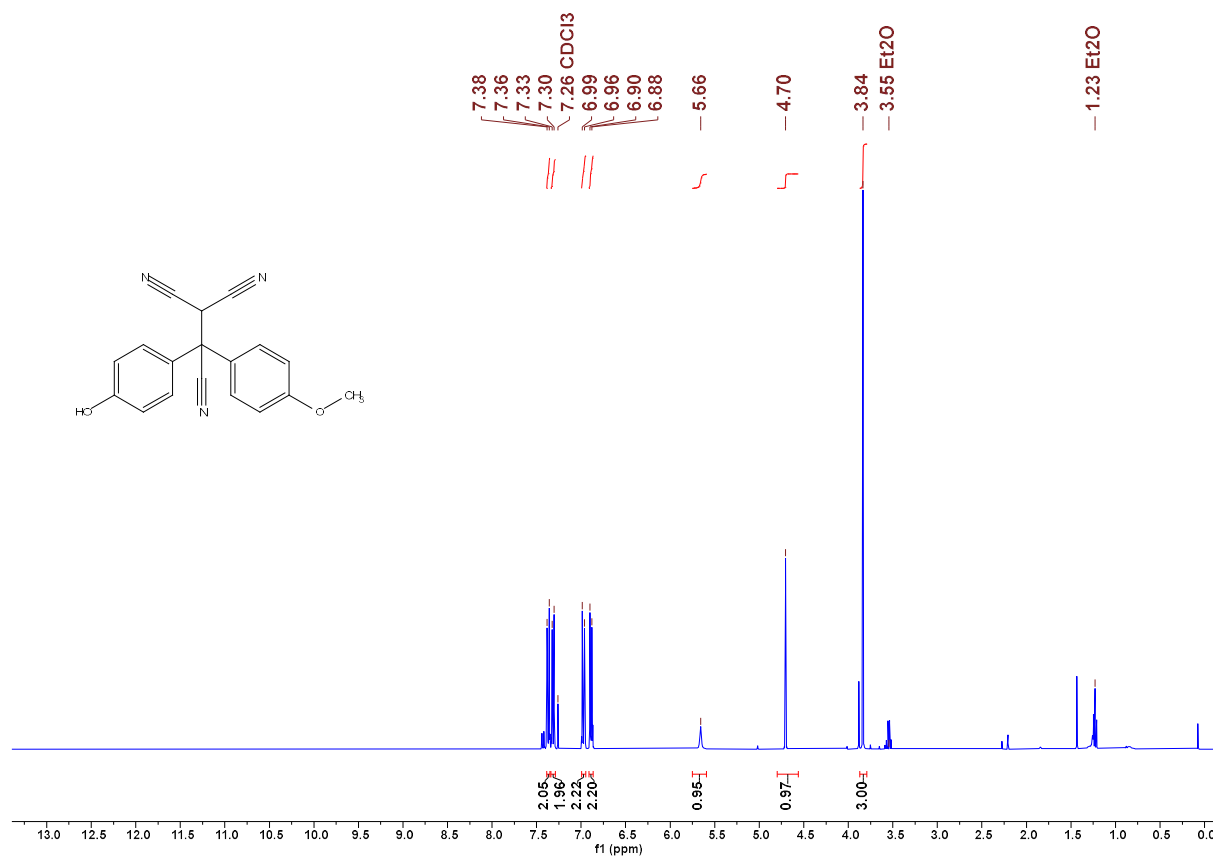
Figure 61. ^{1}H NMR spectrum of **9ad** in CDCl$_3$ (400 MHz) CG049_3
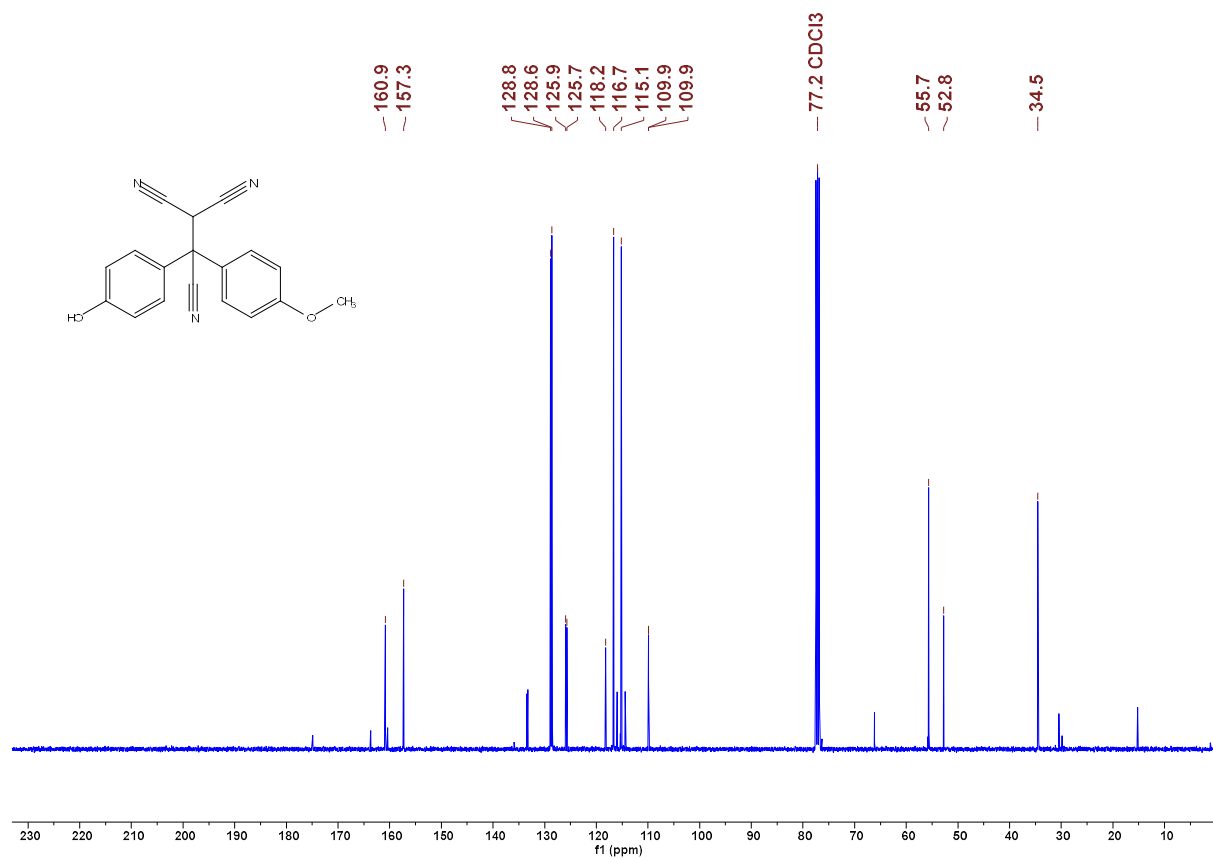
Figure 62. ^{13}C NMR spectrum of **9ad** in CDCl$_3$ (101 MHz) CG049_3
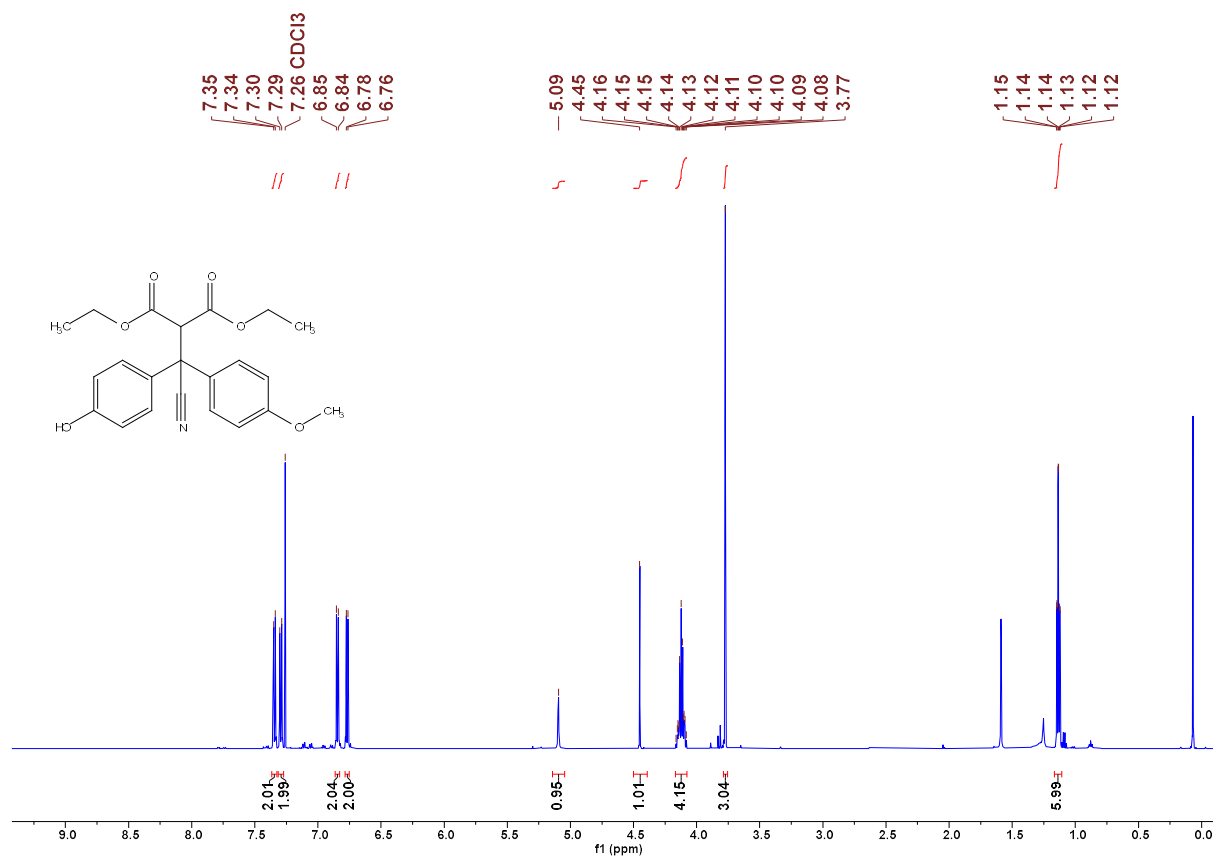
Figure 63. ^{1}H NMR spectrum of **9af** in CDCl$_3$ (600 MHz) CG048_3_1
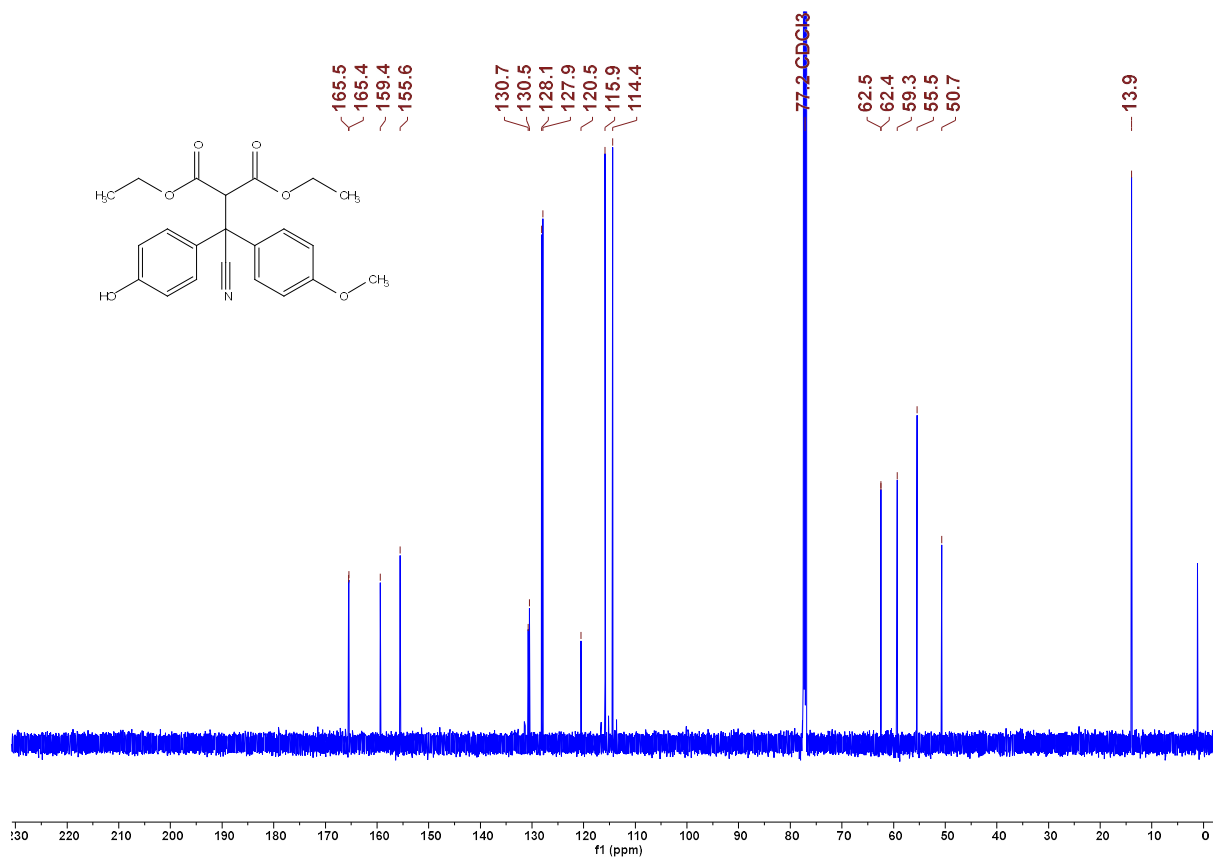
Figure 64. ^{13}C NMR spectrum of **9af** in CDCl$_3$ (151 MHz) CG048_3_1
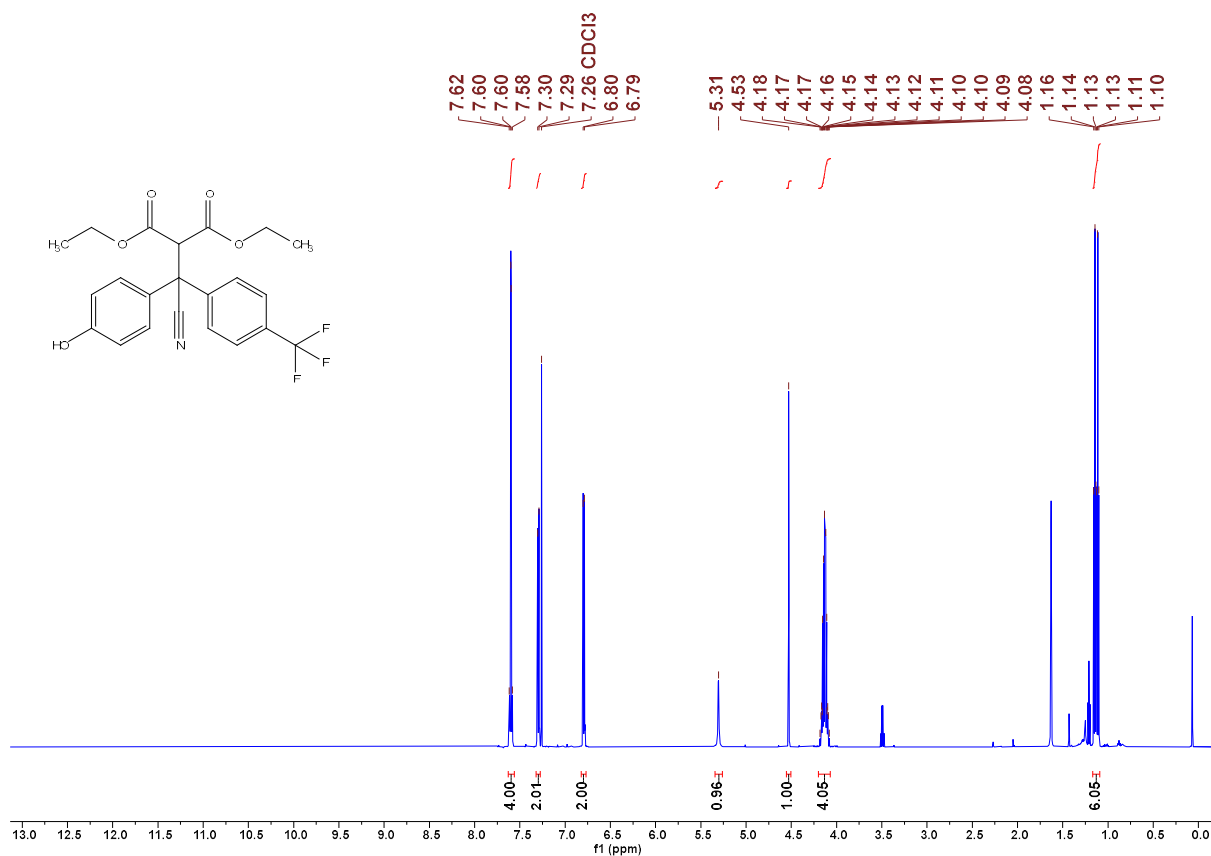
Figure 65. ^{1}H NMR spectrum of **9ef** in CDCl$_3$ (600 MHz) CG121_1
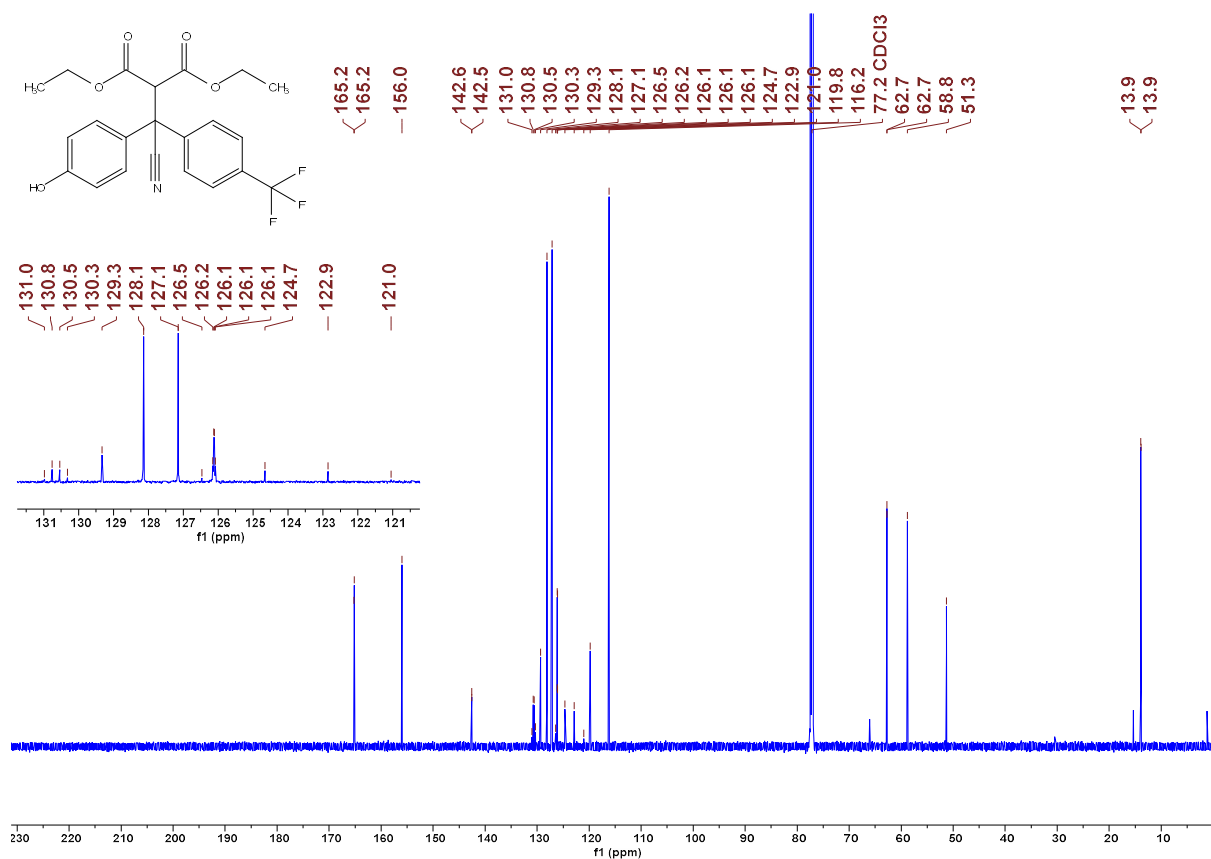
Figure 66. ^{13}C NMR spectrum of **9ef** in CDCl$_3$ (151 MHz) CG121_1
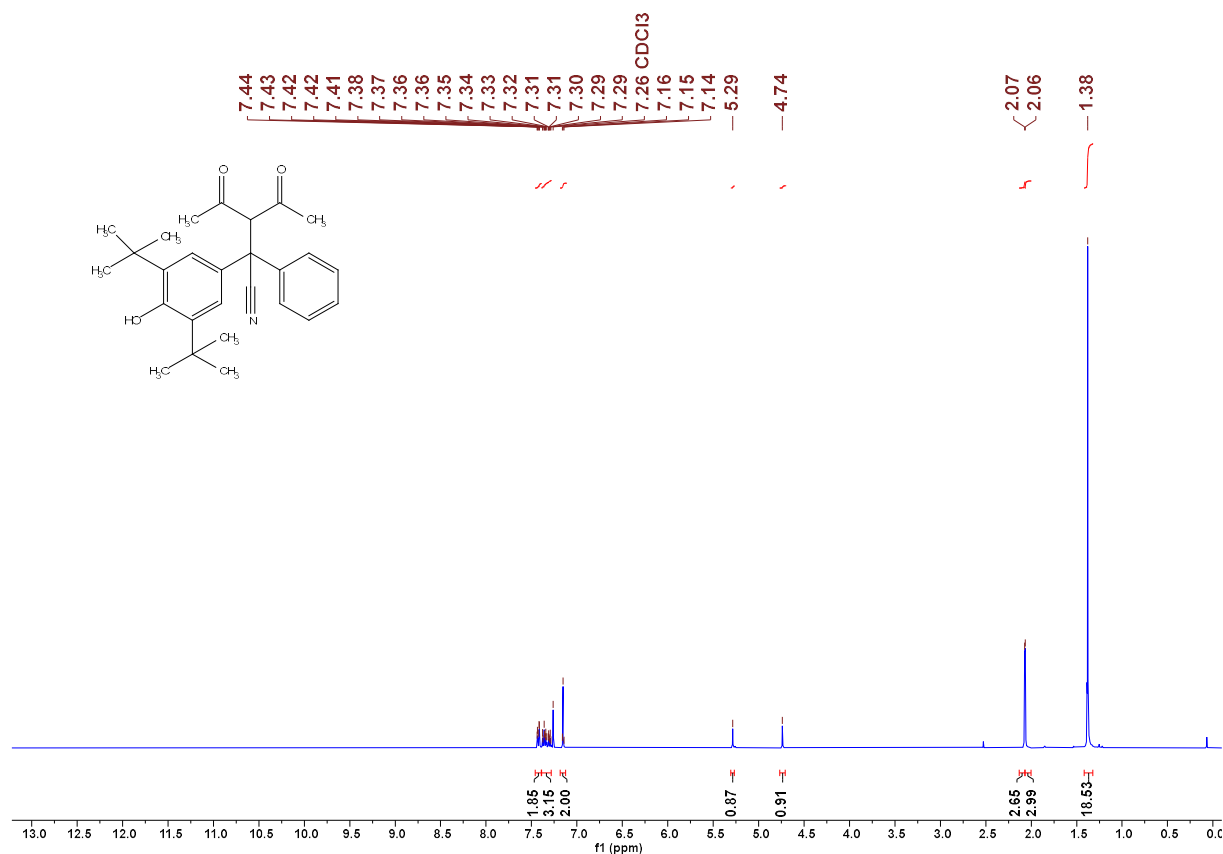
Figure 67. ^{1}H NMR spectrum of **9hb** in CDCl$_3$ (400 MHz) CG118_3
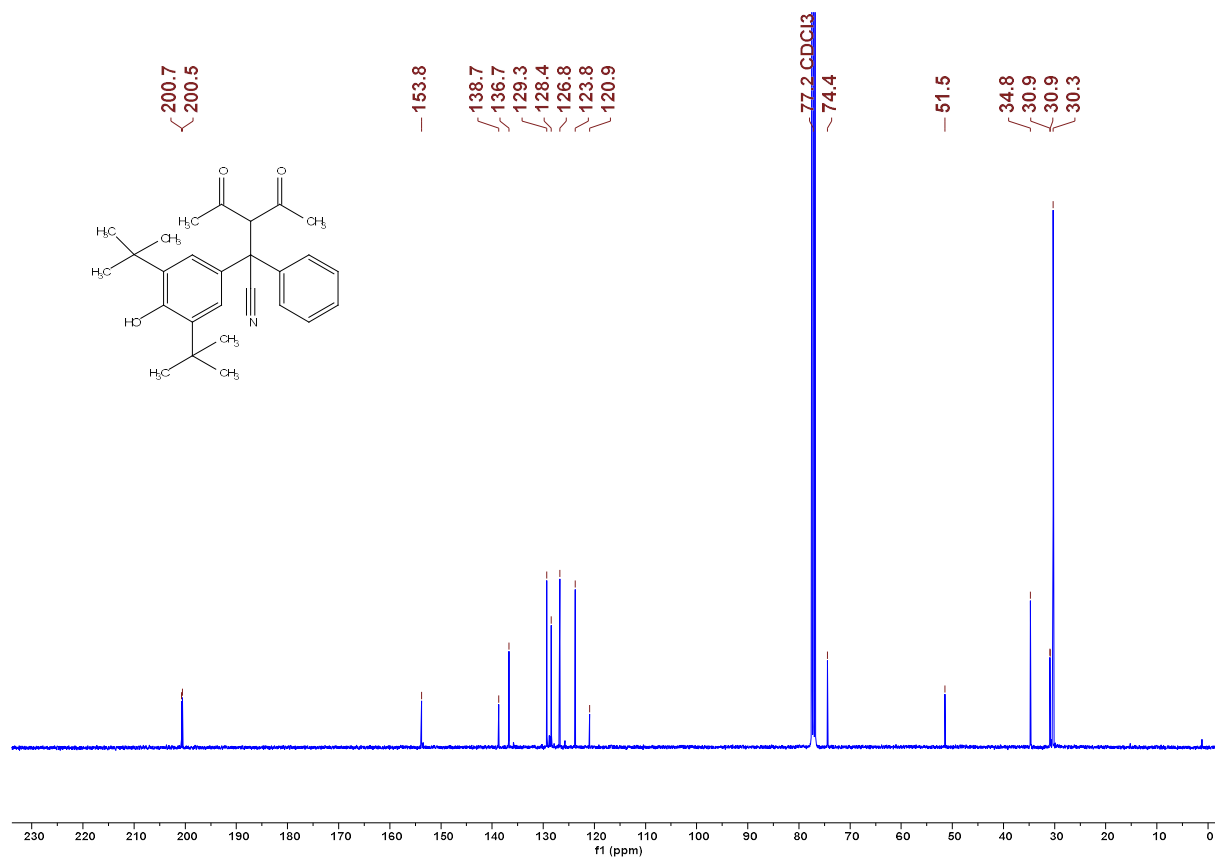
Figure 68. ^{13}C NMR spectrum of **9hb** in CDCl$_3$ (101 MHz) CG118_3

170
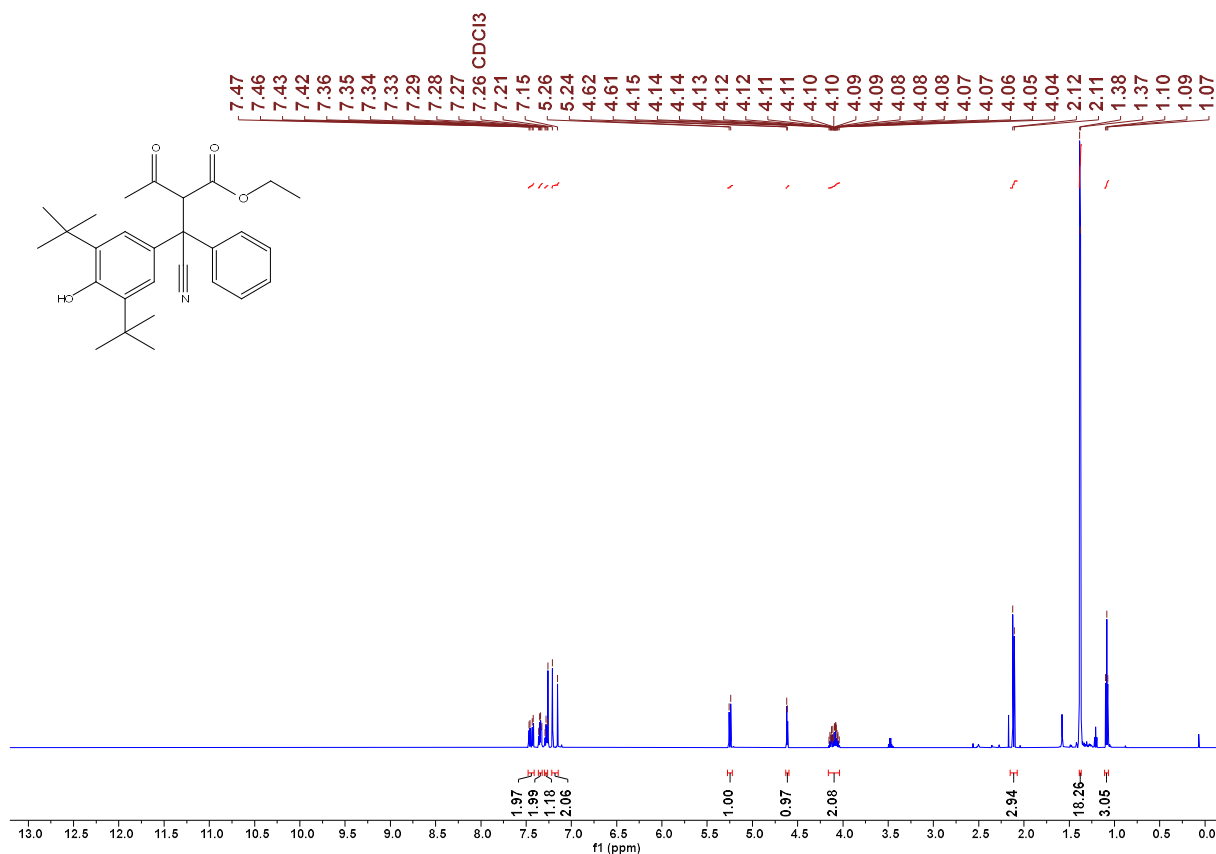
Figure 69. ^{1}H NMR spectrum of **9hc** in CDCl₃ (600 MHz) CG120_1
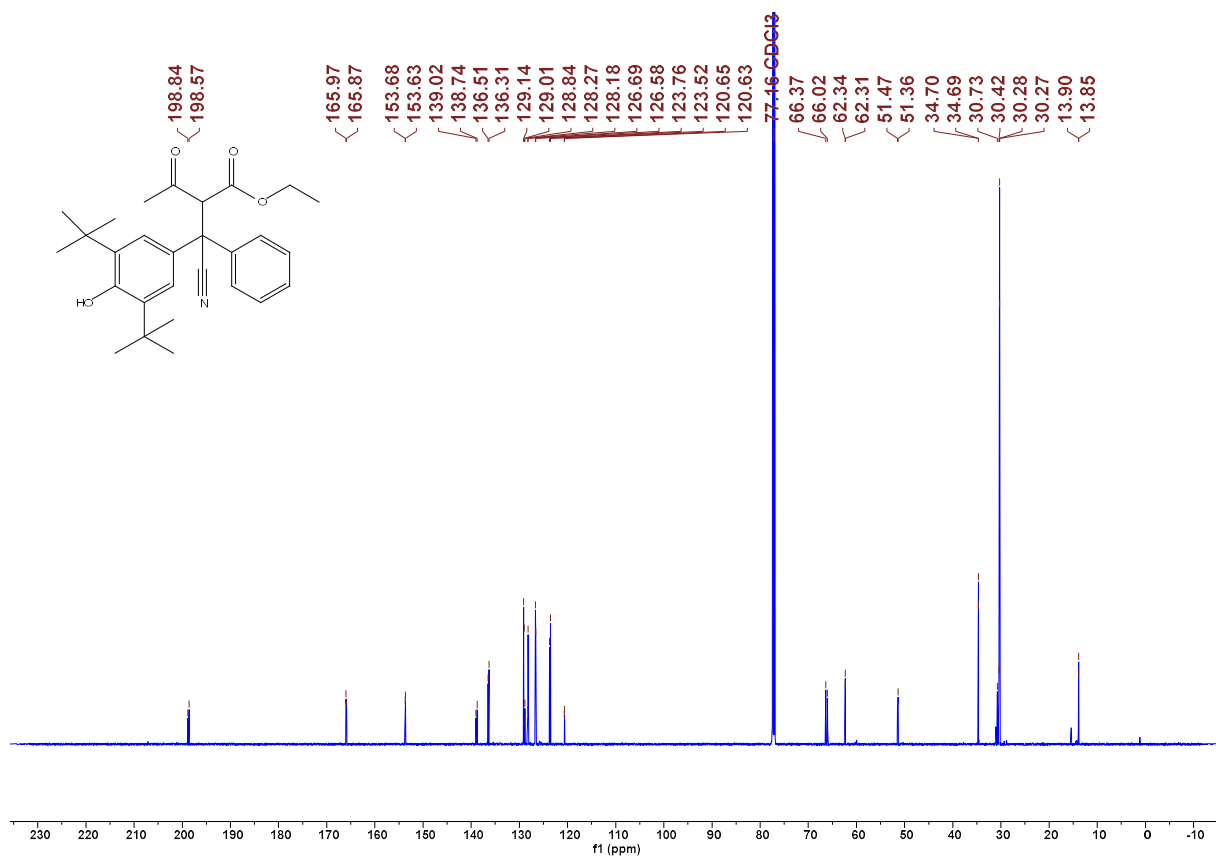
Figure 70. ^{13}C NMR spectrum of **9hc** in CDCl₃ (151 MHz) CG120_1
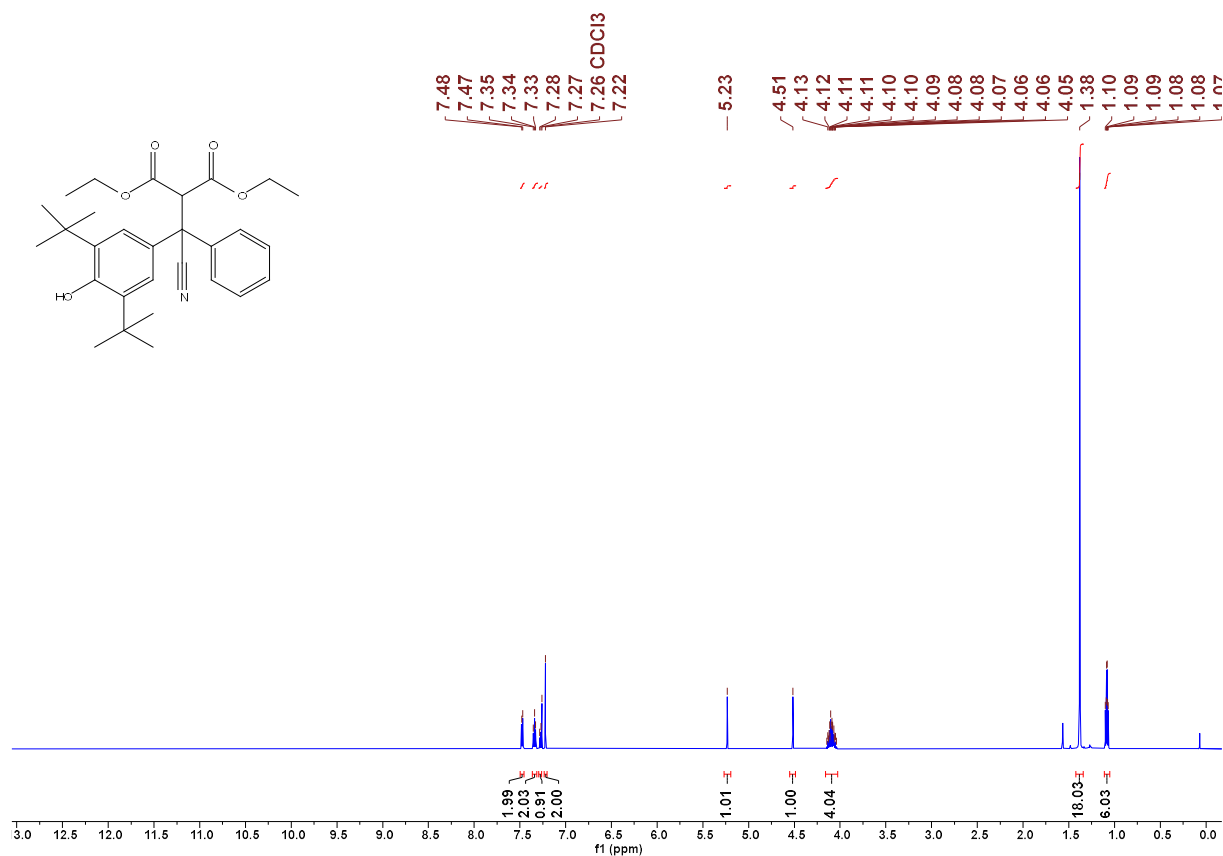
Figure 71. ^{1}H NMR spectrum of **9hf** in CDCl$_3$ (600 MHz) CG117
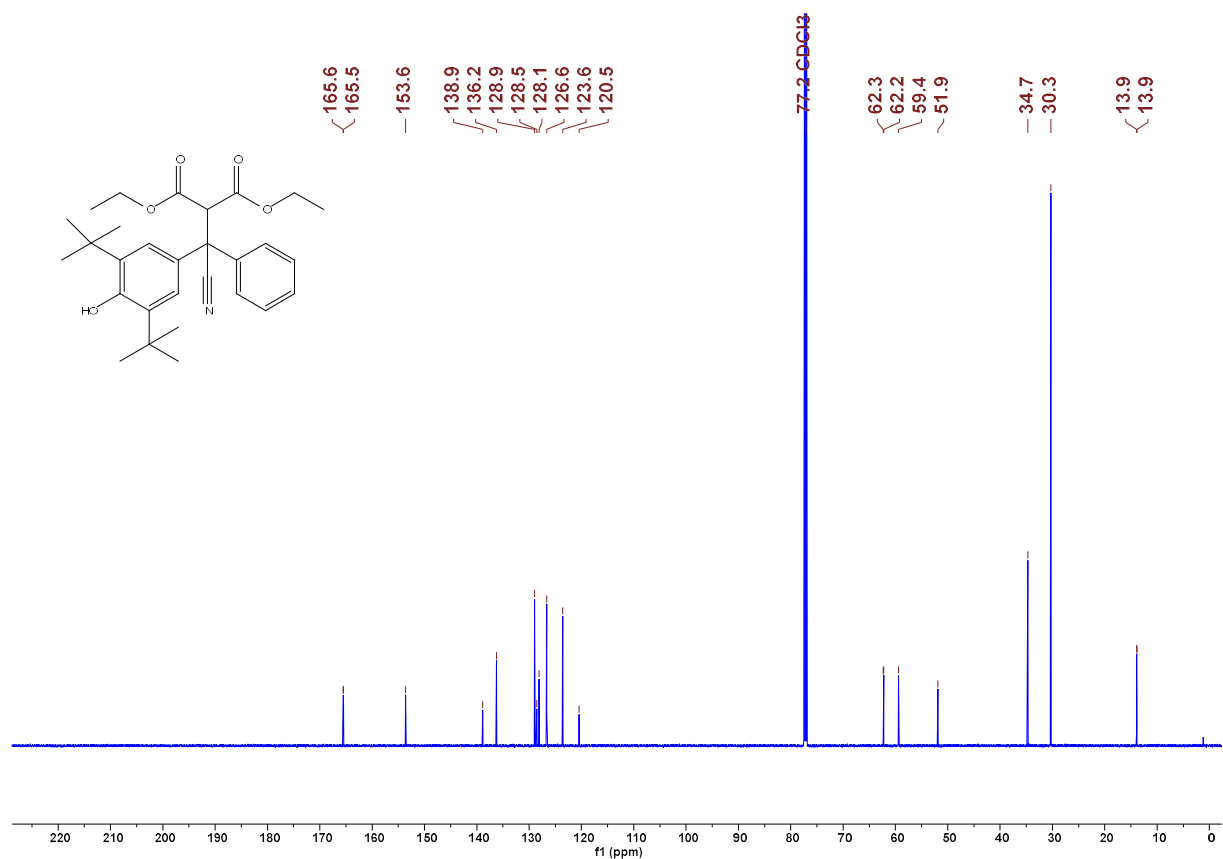
Figure 72. ^{13}C NMR spectrum of **9hf** in CDCl$_3$ (151 MHz) CG117_1
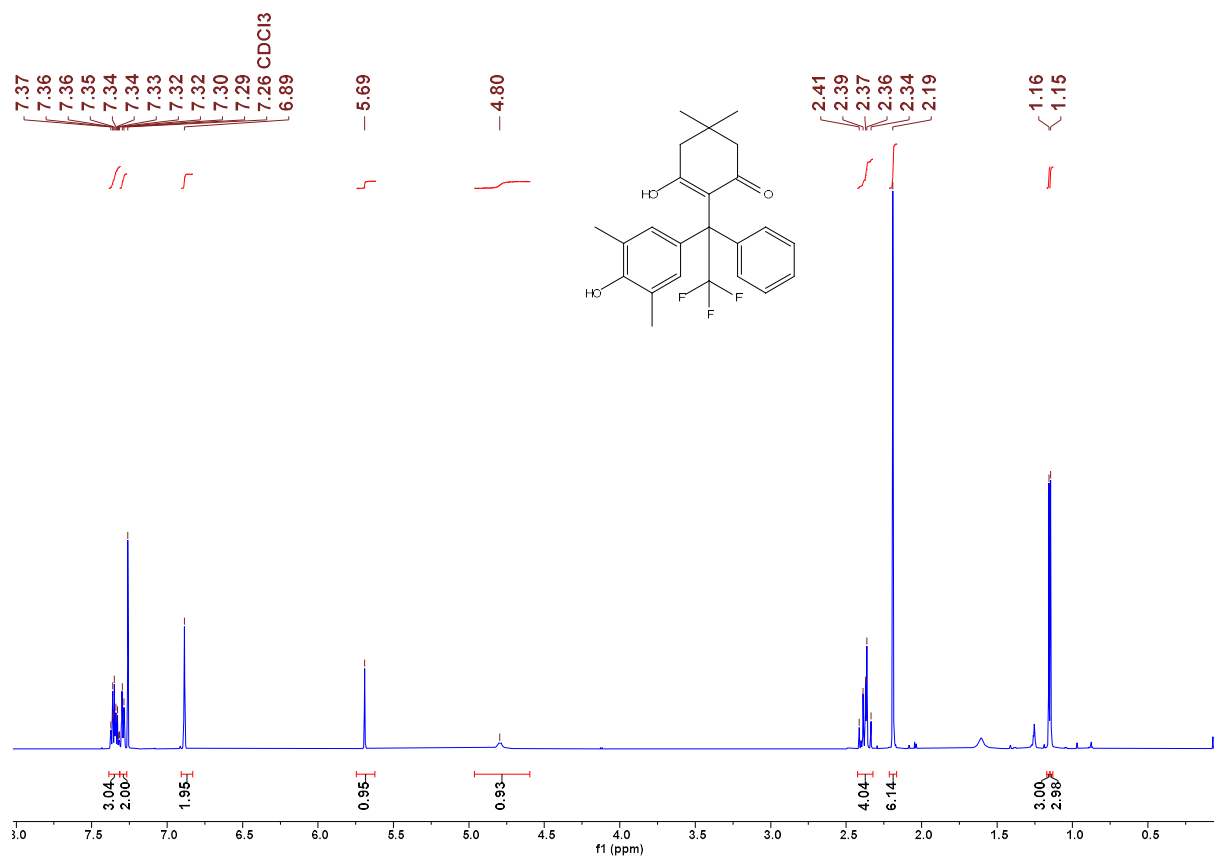
Figure 73. ^{1}H NMR spectrum of **9ja** in CDCl$_3$ (600 MHz) CG182
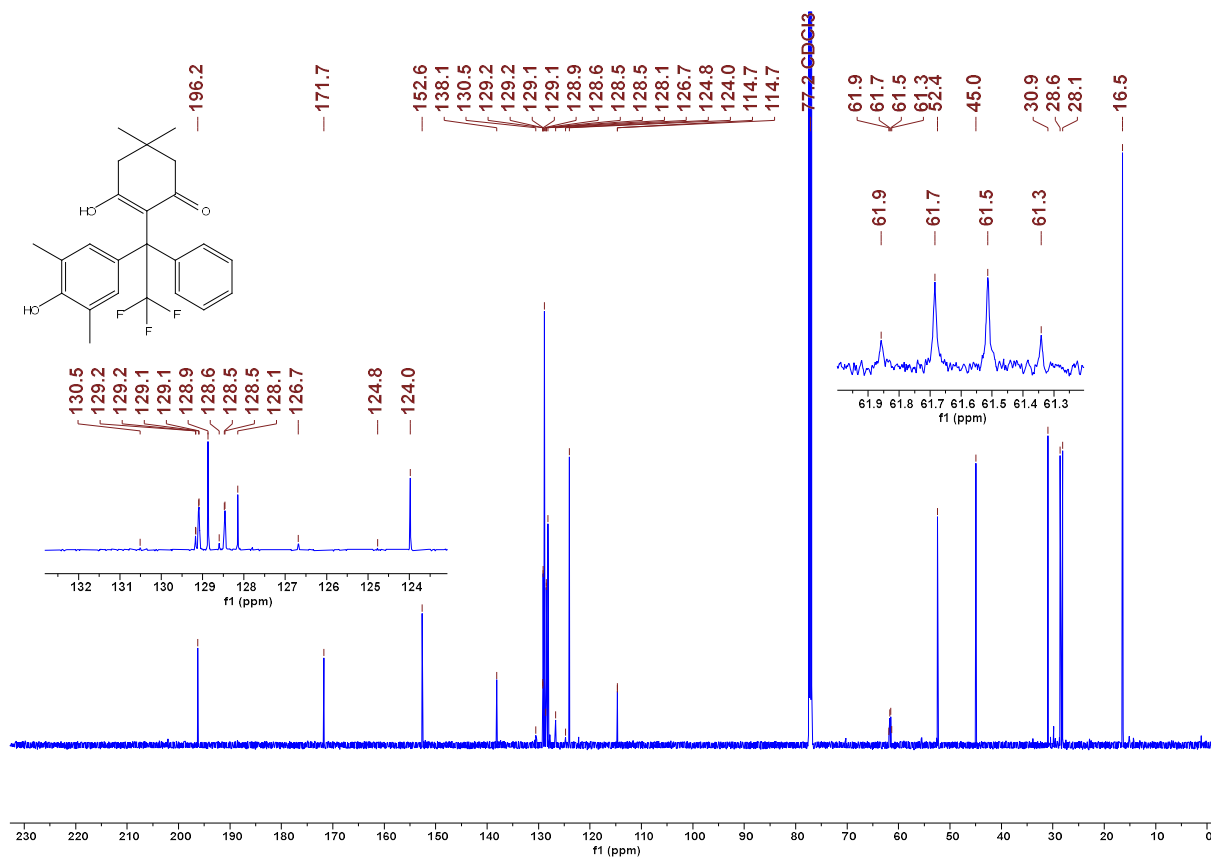
Figure 74. ^{13}C NMR spectrum of **9ja** in CDCl$_3$ (151 MHz) CG182
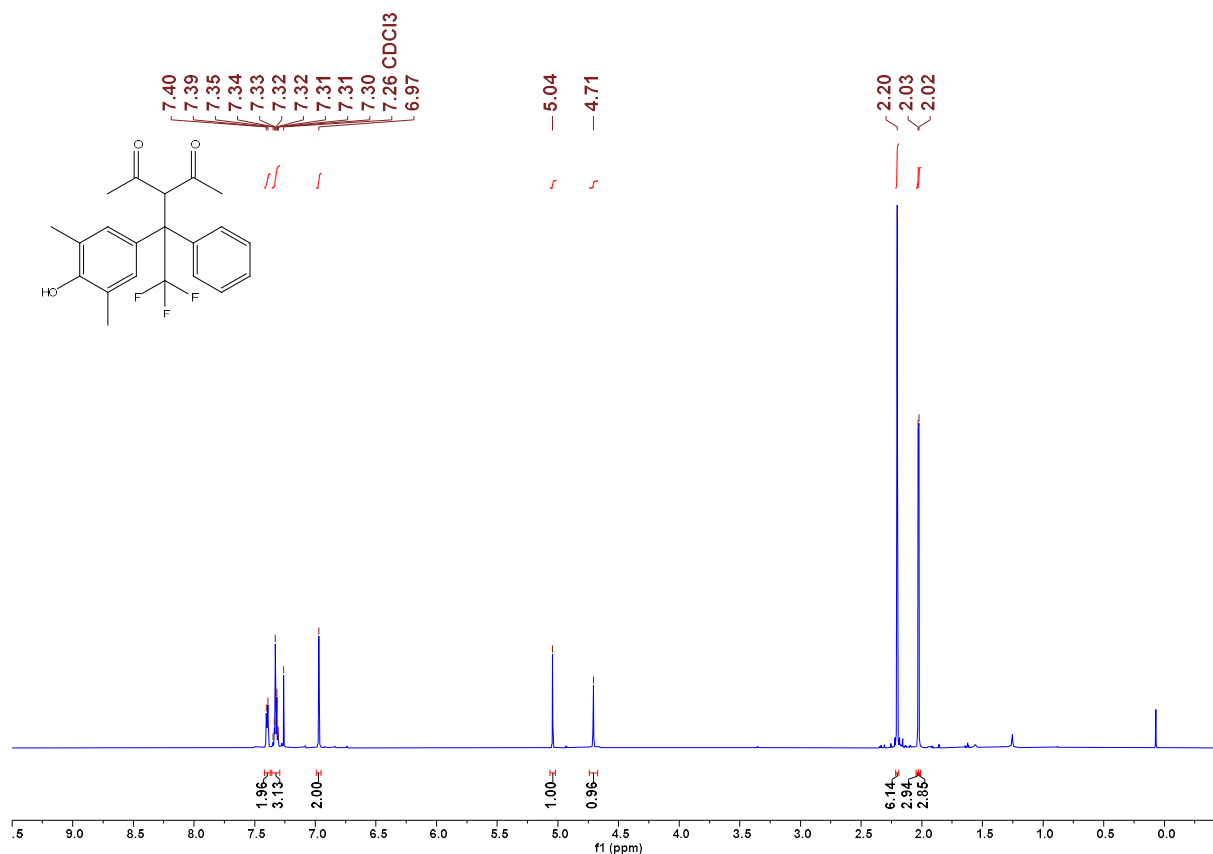
Figure 75. ^{1}H NMR spectrum of **9jb** in CDCl$_3$ (600 MHz) CG181
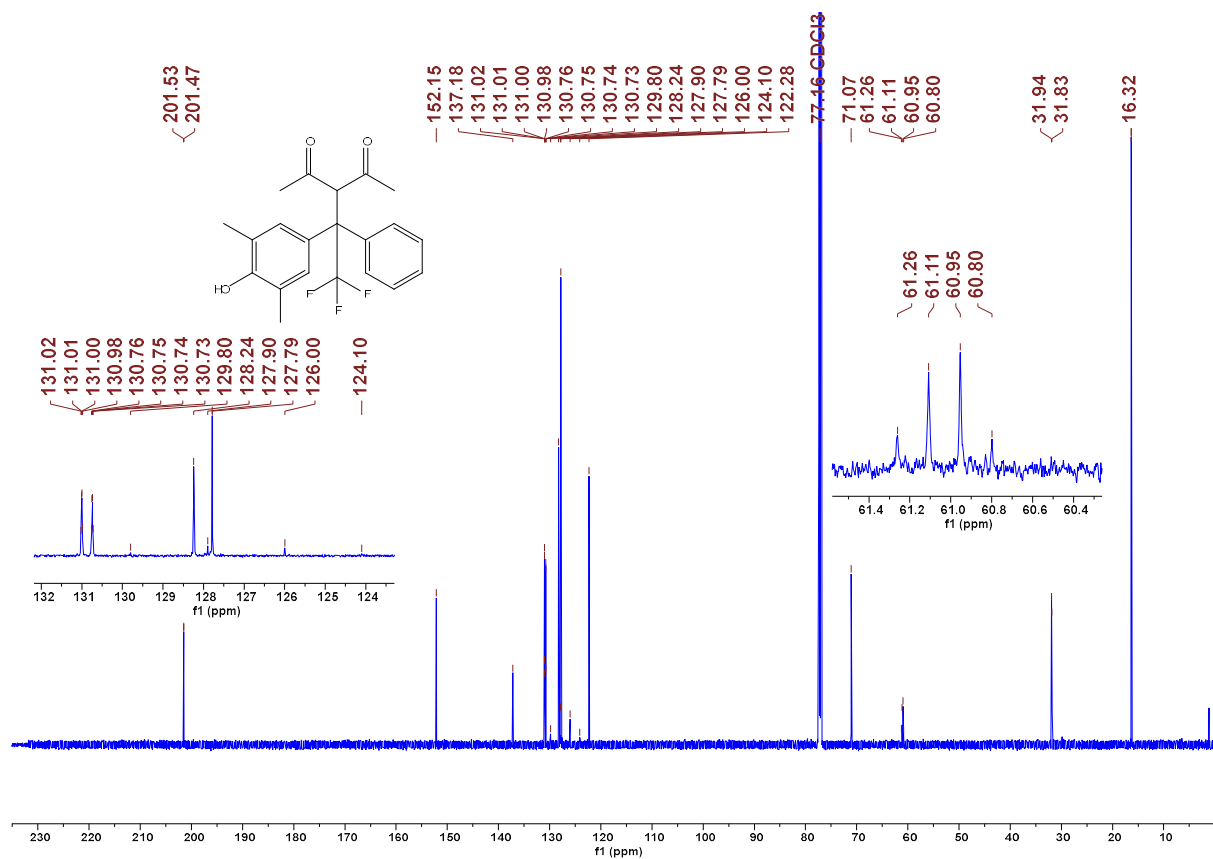
Figure 76. ^{13}C NMR spectrum of **9jb** in CDCl$_3$ (151 MHz) CG181

174
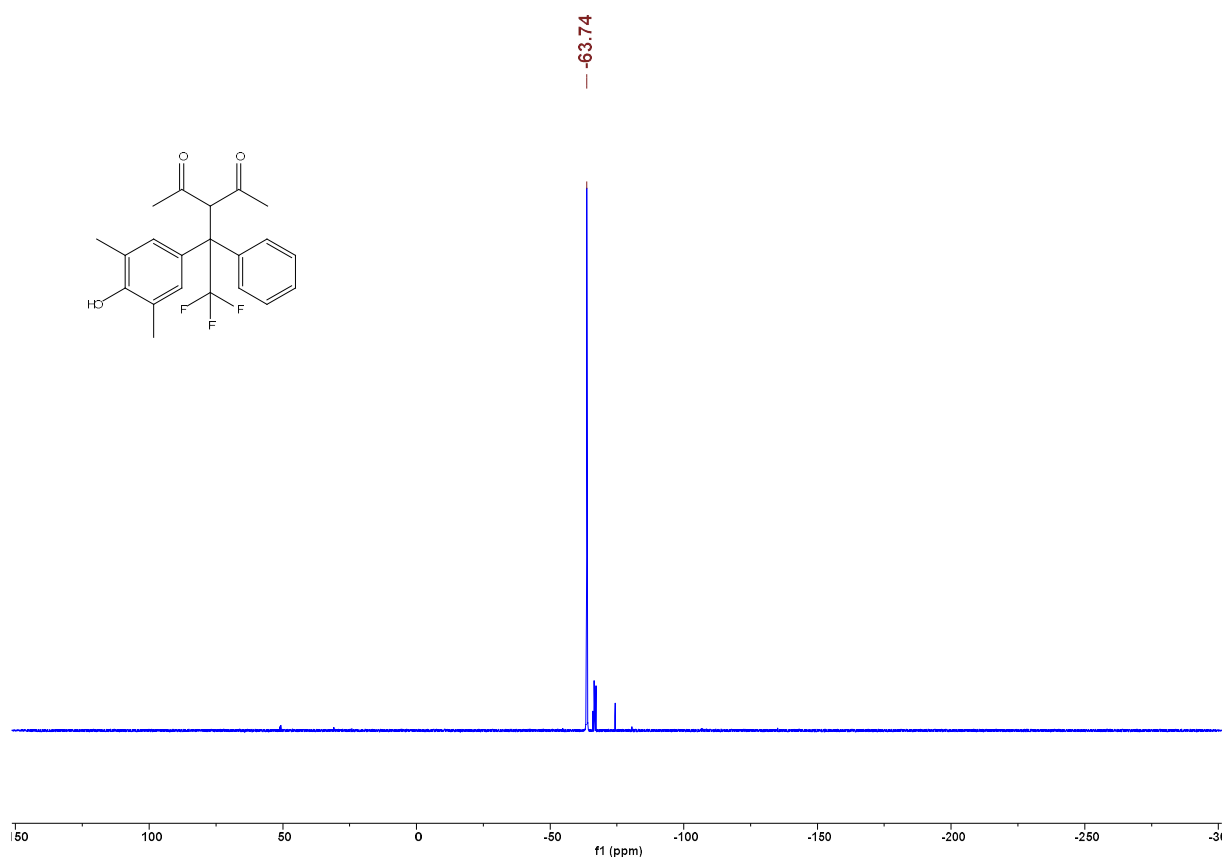
Figure 77. ^{19}F NMR spectrum of **9jb** in CDCl$_3$ (377 MHz) CG181
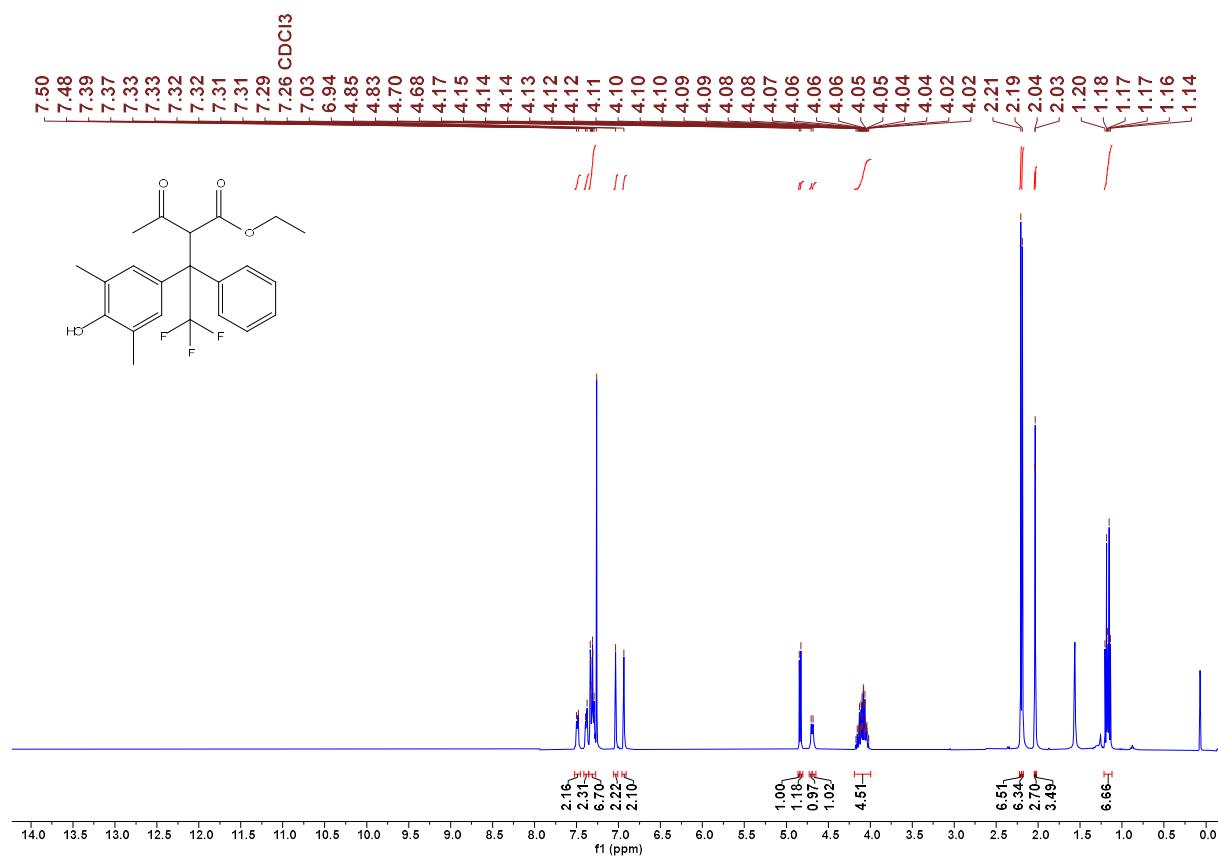
Figure 78. ^{1}H NMR spectrum of **9jc** in CDCl$_3$ (400 MHz) CG184

175
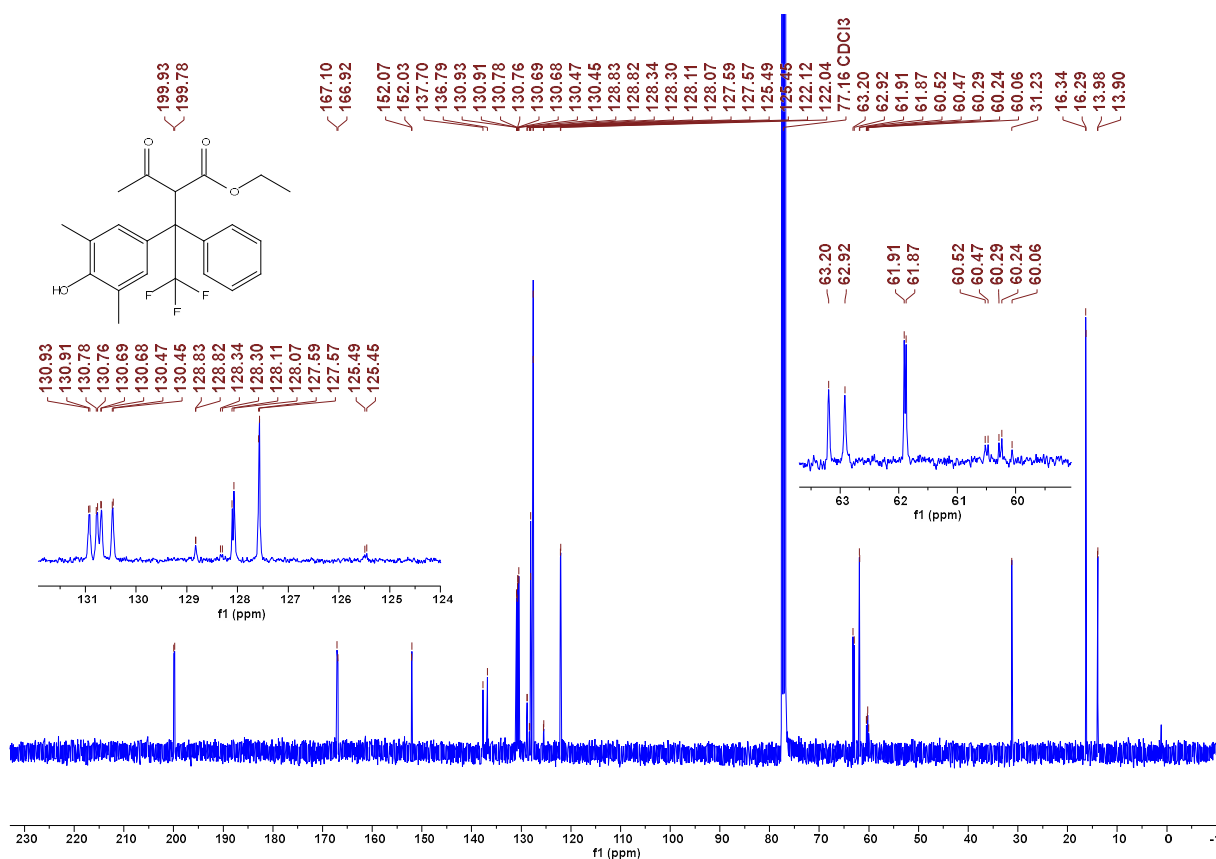
Figure 79. ^{13}C NMR spectrum of **9jc** in CDCl$_3$ (101 MHz) CG184
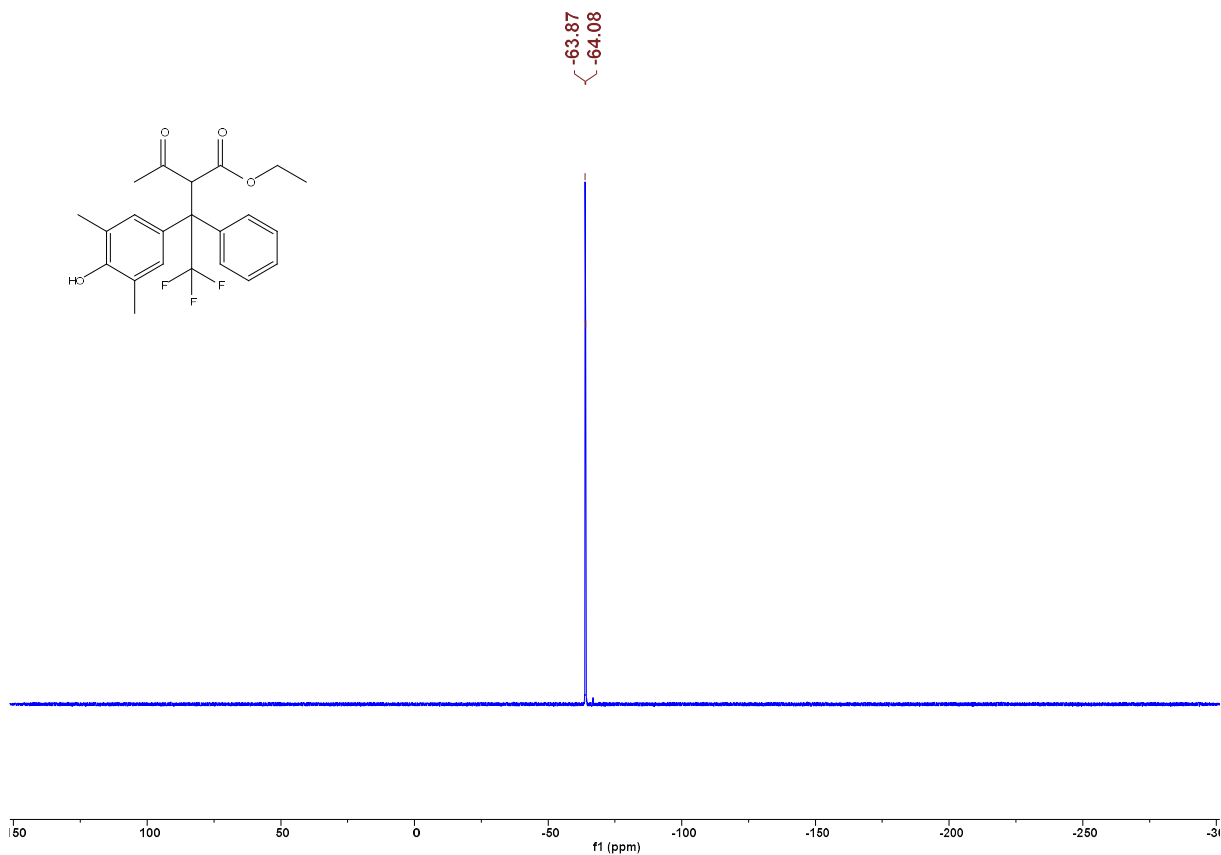
Figure 80. ^{19}F NMR spectrum of **9jc** in CDCl$_3$ (377 MHz) CG184

176
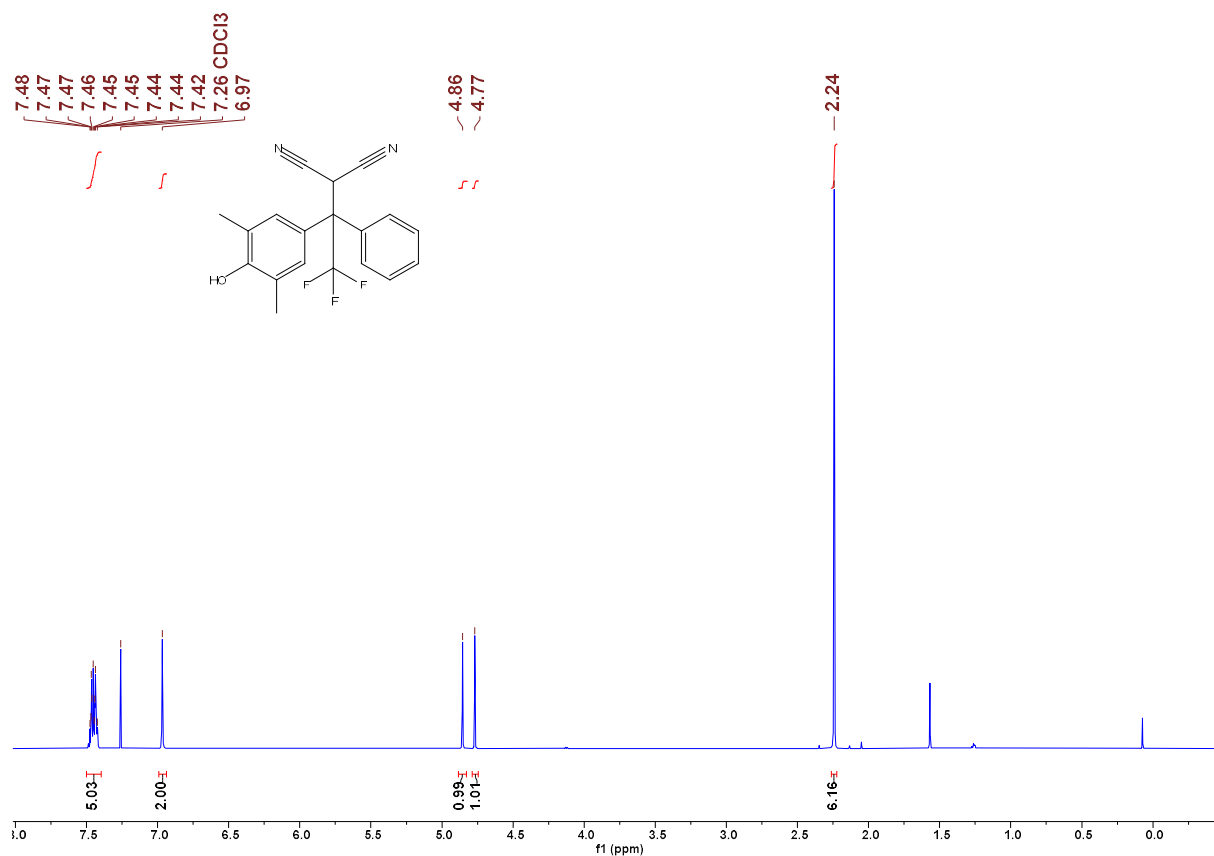
Figure 81. ^{1}H NMR spectrum of **9jd** in CDCl$_3$ (600 MHz) CG180_1
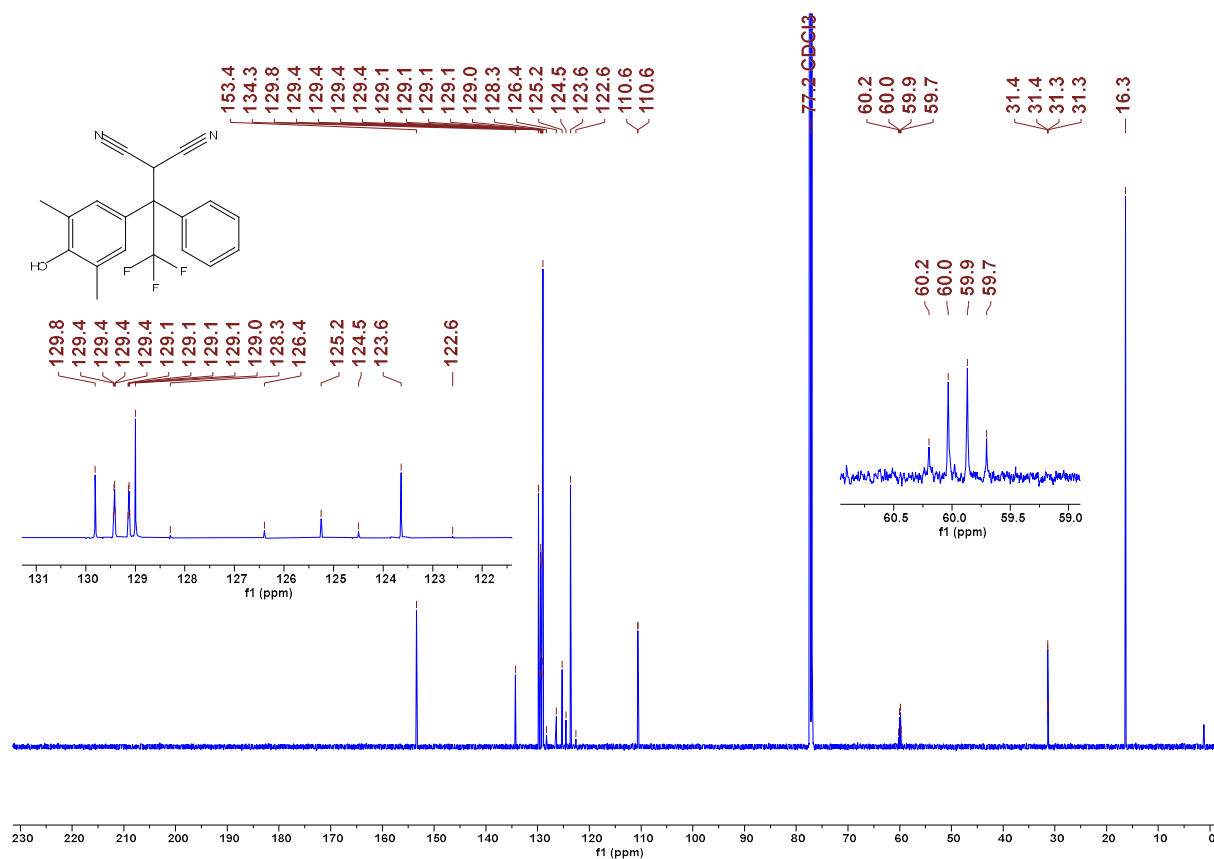
Figure 82. ^{13}C NMR spectrum of **9jd** in CDCl$_3$ (151 MHz) CG180_1

177
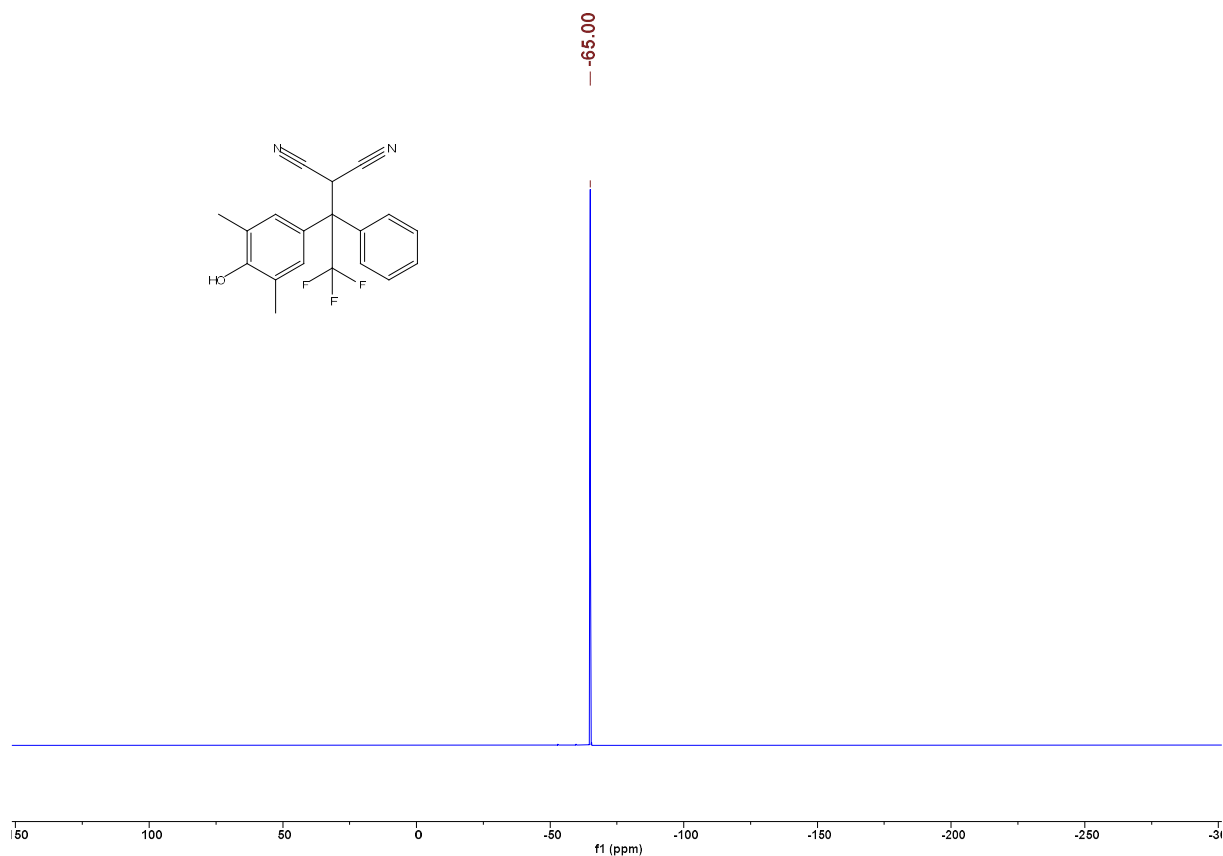
Figure 83. ^{19}F NMR spectrum of **9jd** in CDCl$_3$ (377 MHz) CG180_1
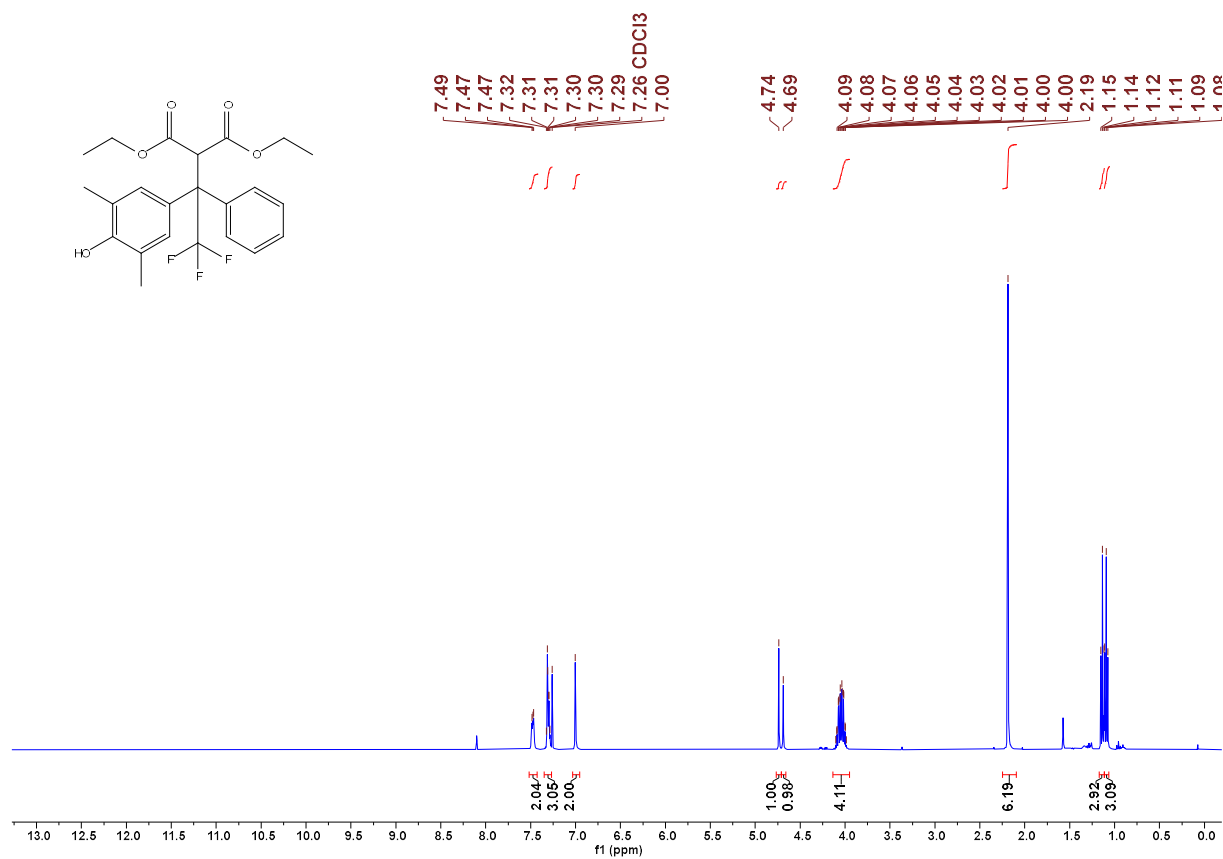
Figure 84. ^{1}H NMR spectrum of **9jf** in CDCl$_3$ (400 MHz) CG179
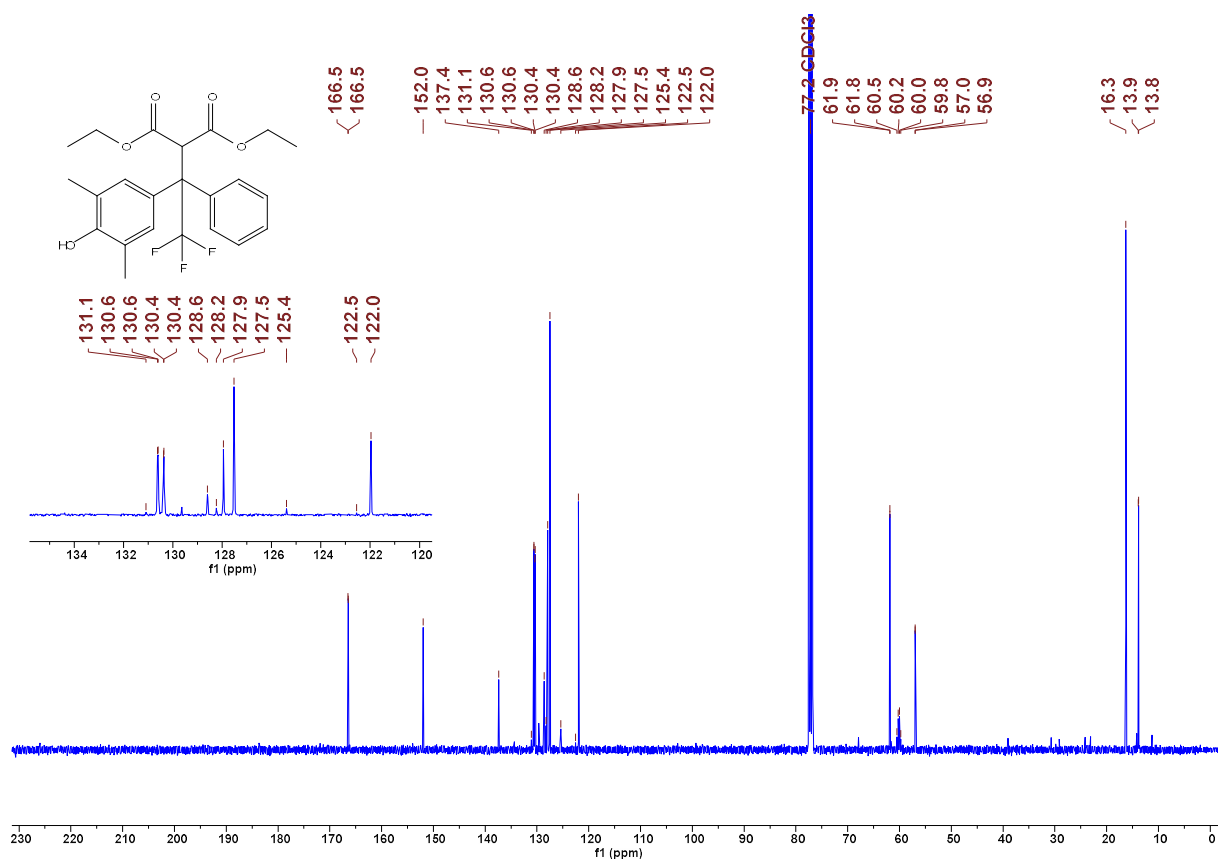
Figure 85. ^{13}C NMR spectrum of **9jf** in CDCl$_3$ (101 MHz) CG179
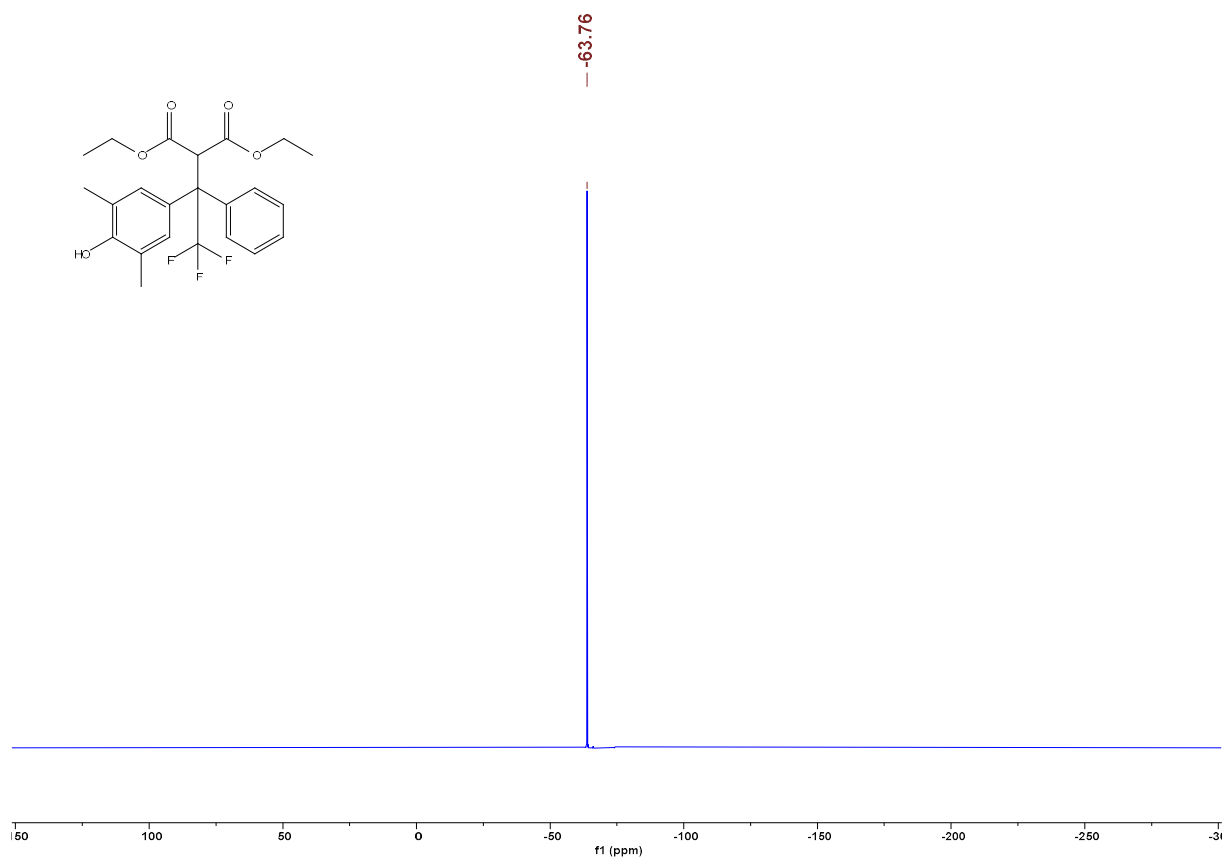
Figure 86. ^{19}F NMR spectrum of **9jf** in CDCl$_3$ (377 MHz) CG179

179
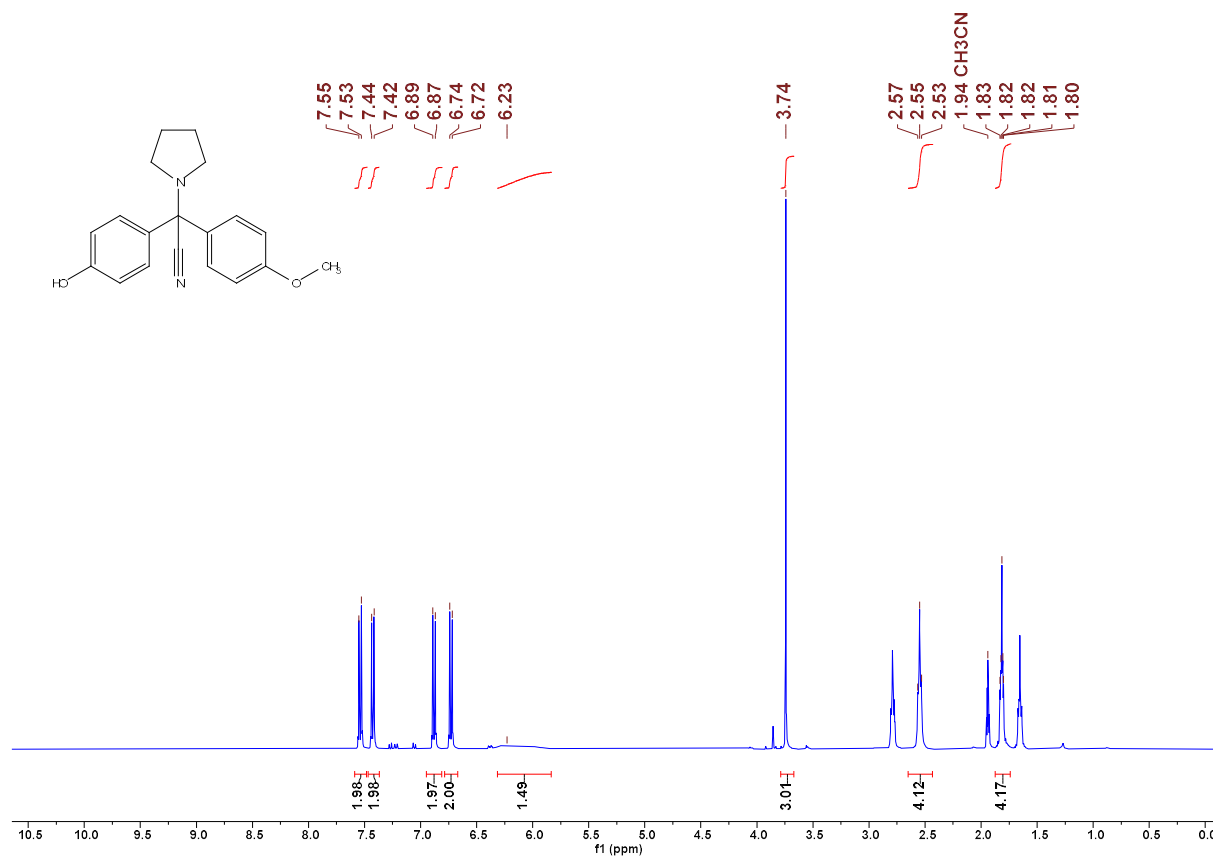
Figure 87. ¹H NMR spectrum of **10** in CDCl₃ (400 MHz) CG192_1
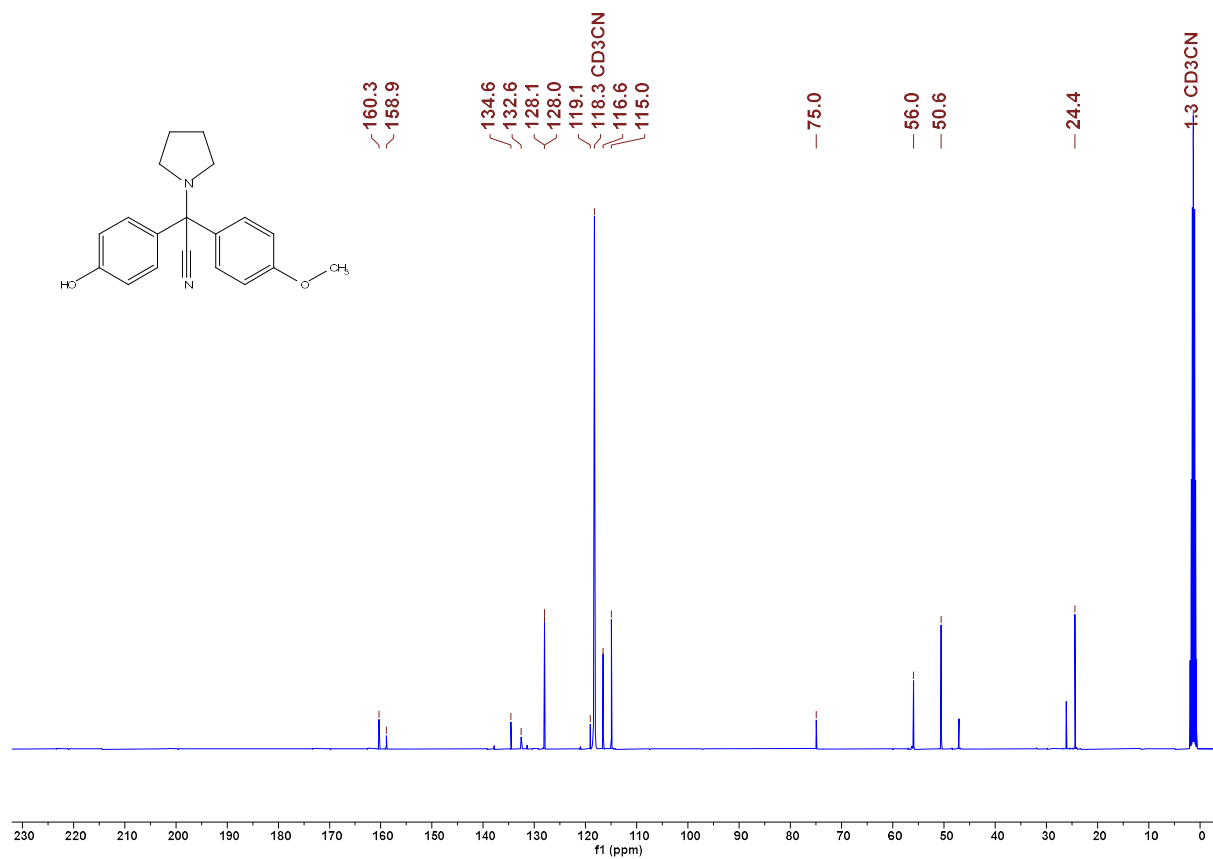
Figure 88. ¹³C NMR spectrum of **10** in CDCl₃ (101 MHz) CG192_1
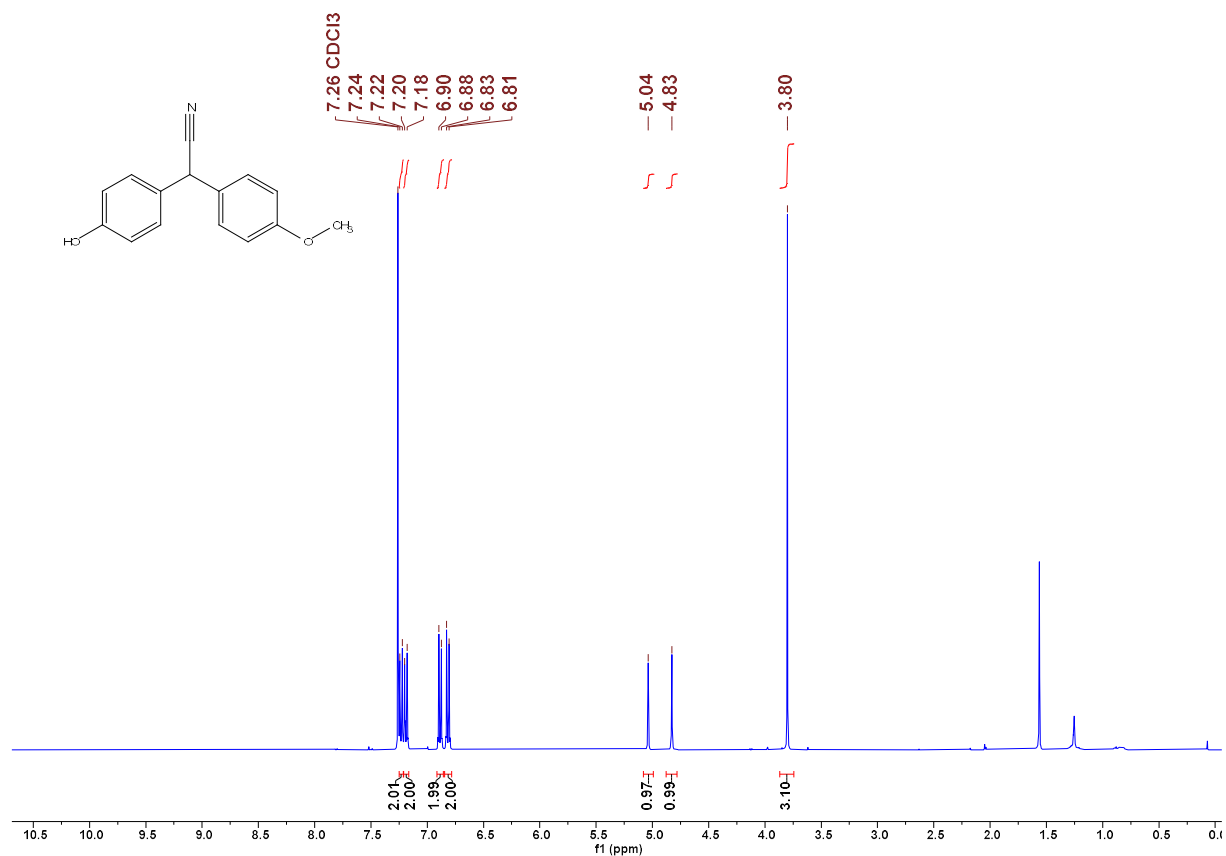
Figure 89. ^{1}H NMR spectrum of **11** in CDCl$_3$ (400 MHz) CG198F1
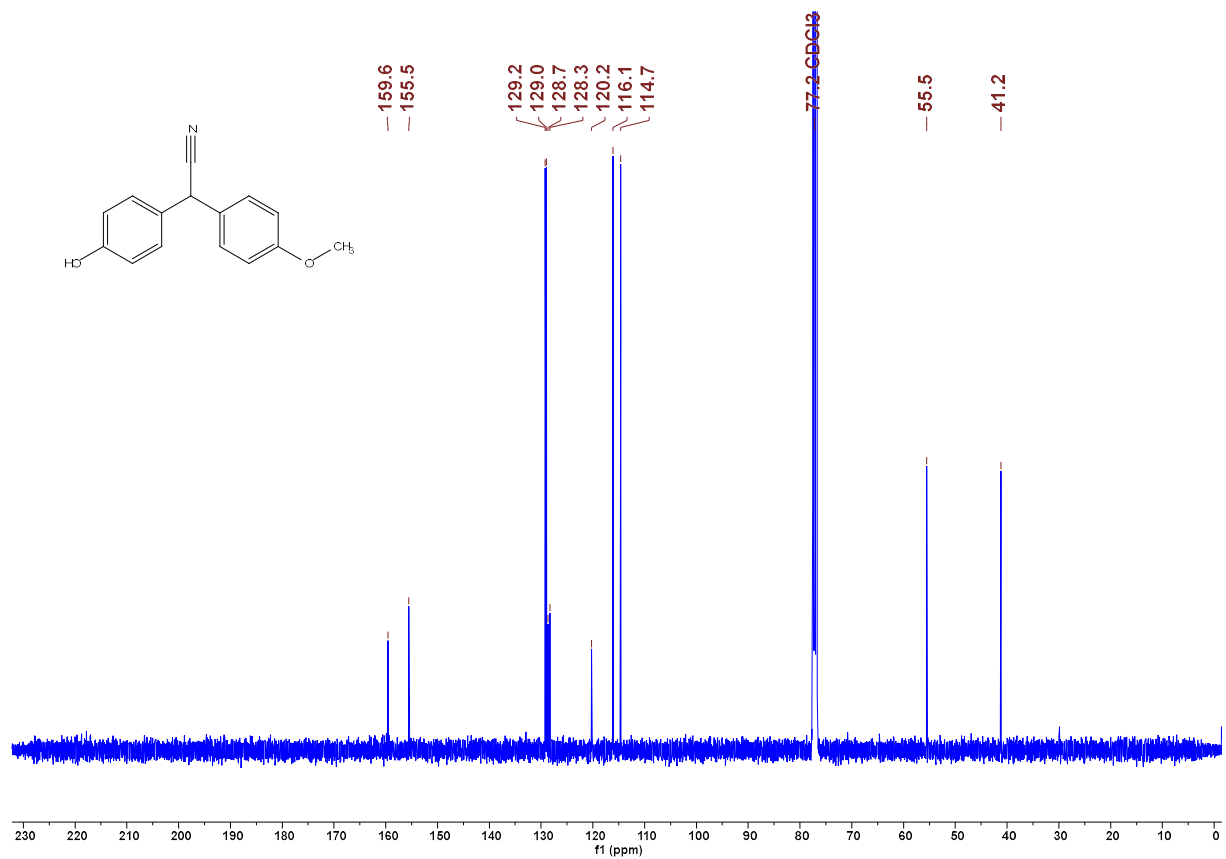
Figure 90. ^{13}C NMR spectrum of **11** in CDCl$_3$ (101 MHz) CG198F1
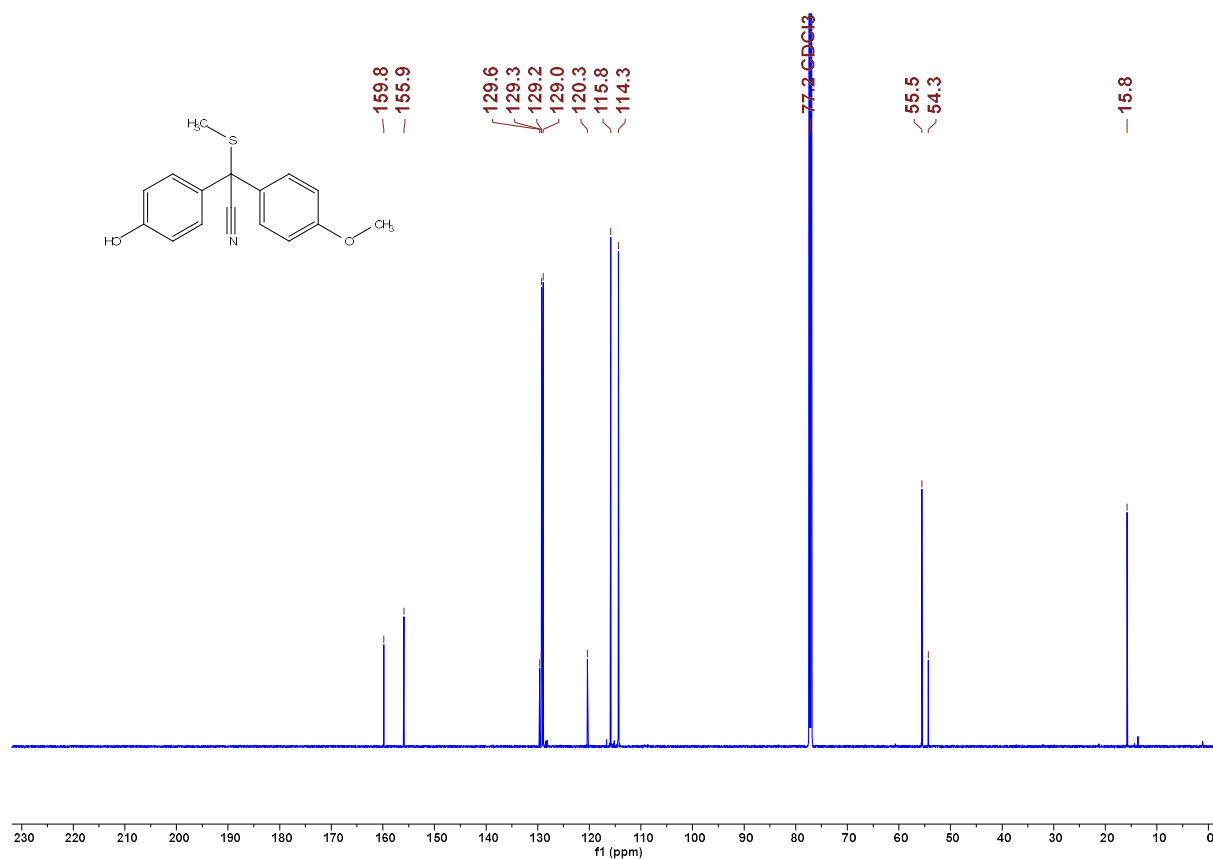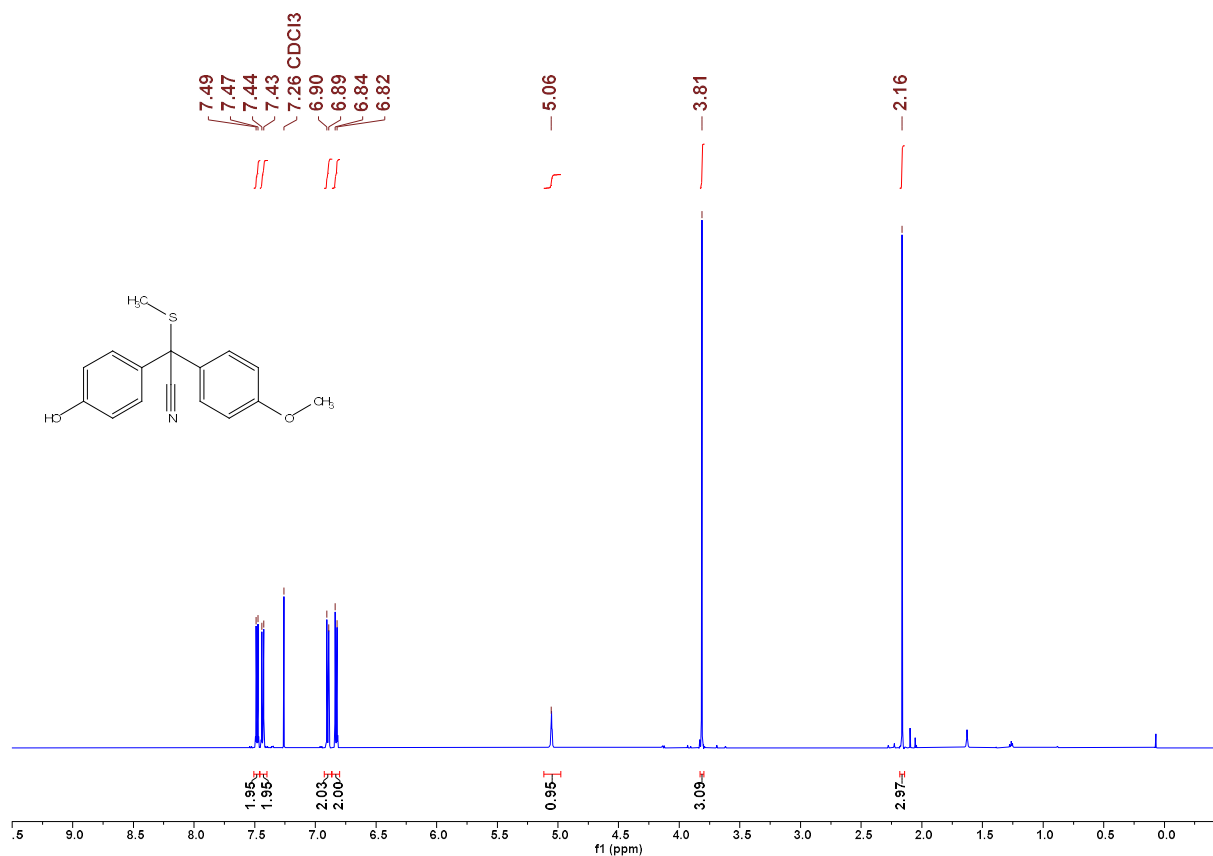
181

Figure 91. ^{1}H NMR spectrum of **12** in CDCl$_3$ (600 MHz) CG191

Figure 92. ^{13}C NMR spectrum of **12** in CDCl$_3$ (151 MHz) CG191
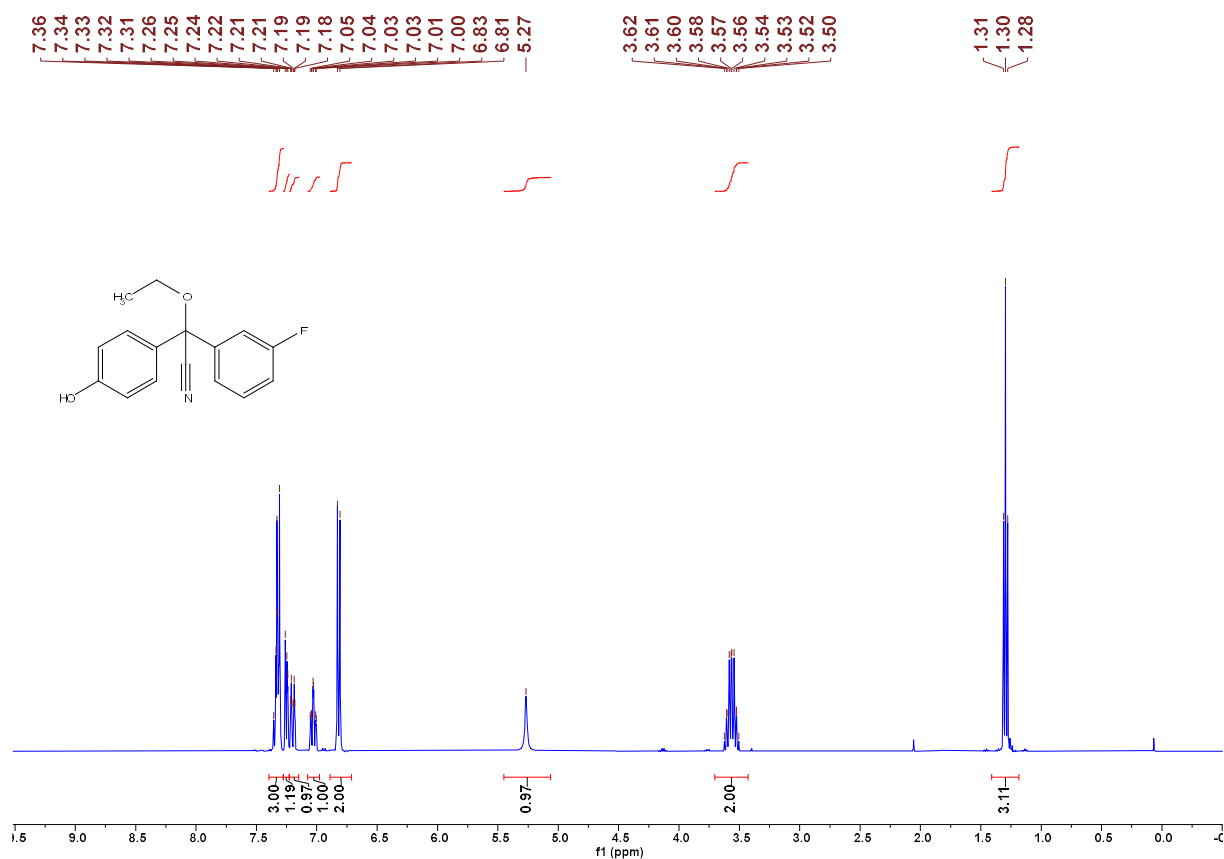
Figure 93. ^{1}H NMR spectrum of **13** in CDCl$_3$ (400 MHz) JR015EtOH
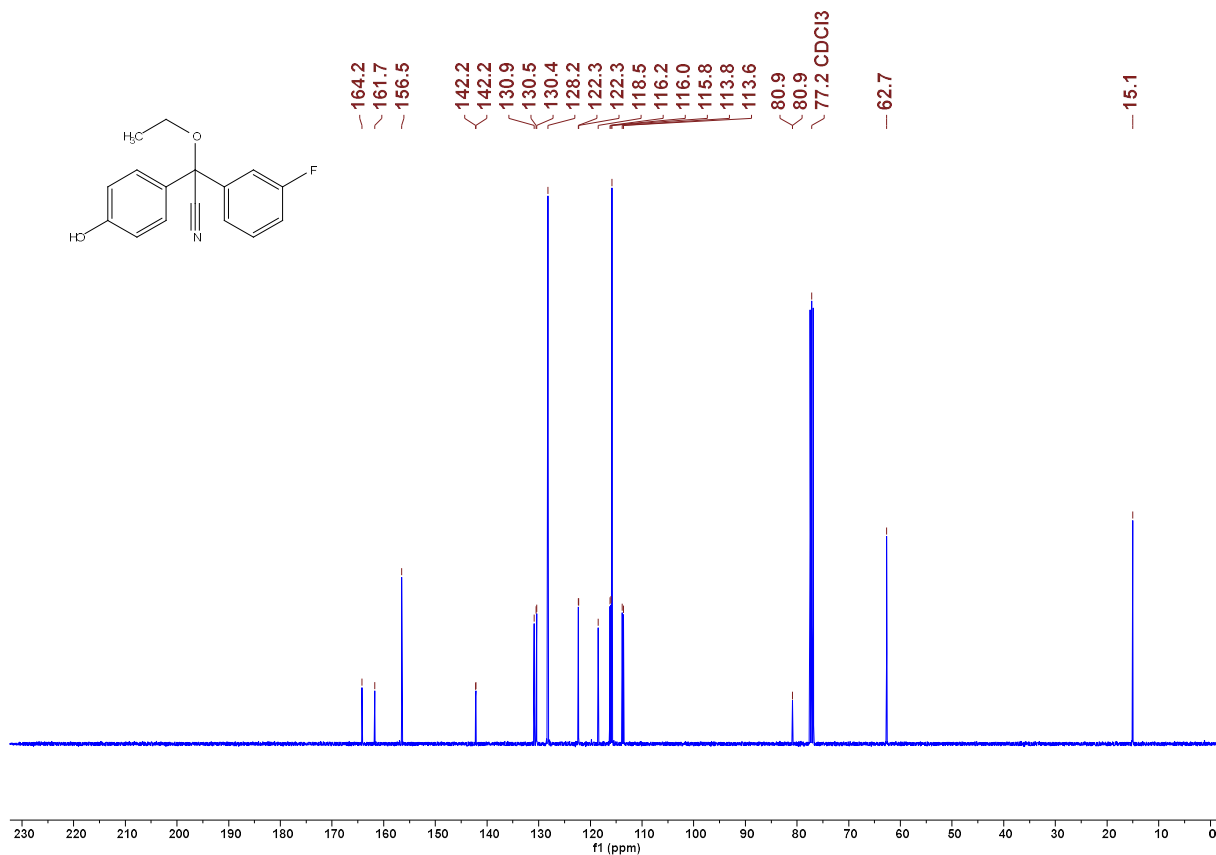
Figure 94. ^{13}C NMR spectrum of **13** in CDCl$_3$ (101 MHz) JR015EtOH

4.5. References

[1]   A. B. Turner, *Q. Rev., Chem. Soc.* **1964**, *18*, 347.

[2]   K. Auwers, *Ber. Dtsch. Chem. Ges.* **1903**, *36*, 1878.

[3]   V. V. Ershov, A. A. Volod'kin, G. D. Ostapets-Sveshnikova, *Russ. Chem. Bull.* **1966**, *15*, 888.

[4]   a) C. G. S. Lima, F. P. Pauli, D. C. S. Costa, A. S. de Souza, L. S. M. Forezi, V. F. Ferreira, F. de Da Carvalho Silva, *Eur. J. Org. Chem.* **2020**, *2020*, 2650; b) J.-Y. Wang, W.-J. Hao, S.-J. Tu, B. Jiang, *Org. Chem. Front.* **2020**, *7*, 1743; c) X. Liu, Y. Ren, L. Zhu, T. Li, W. Xu, Y. Liu, K.-W. Tang, B. Xiong, *Tetrahedron* **2023**, *148*, 133655.

[5]   T. Itoh, *Prog. Polym. Sci.* **2001**, *26*, 1019.

[6]   a) L. A. Errede, M. Szwarc, *Q. Rev., Chem. Soc.* **1958**, *12*, 301; b) D. S. Acker, W. R. Hertler, *J. Am. Chem. Soc.* **1962**, *84*, 3370; c) T. Itoh, H. Okuno, T. Hishida, A. Inokuchi, N. Kamei, T. Sato, M. Kubo, S. Iwatsuki, *Tetrahedron* **1997**, *53*, 15247.

[7]   J. A. Hyatt, *J. Org. Chem.* **1983**, *48*, 129.

[8]   T. Itoh, E. Nakanishi, M. Okayama, M. Kubo, *Macromolecules* **2000**, *33*, 269.

[9]   Y. Ma, J. Pang, X. Pan, S. Ma, X. Liu, L. Liu, *Synlett* **2020**, *31*, 1619.

[10]   a) A. Bistrzycki, C. Herbst, *Ber. Dtsch. Chem. Ges.* **1903**, *36*, 2333; b) A. Baeyer, V. Villiger, *Ber. Dtsch. Chem. Ges.* **1903**, *36*, 2774.

[11]   R. Gompper, R. R. Schmidt, E. Kutter, *Justus Liebigs Ann. Chem.* **1965**, *684*, 37.

[12]   T. Itoh, T. Wanibe, S. Iwatsuki, *J. Polym. Sci. A Polym. Chem.* **1996**, *34*, 963.

[13]   Z. Wang, Y. Zhu, X. Pan, G. Wang, L. Liu, *Angew. Chem. Int. Ed.* **2020**, *59*, 3053.

[14]   Y. Qi, F. Zhang, L. Wang, A. Feng, R. Zhu, S. Sun, W. Li, L. Liu, *Org. Biomol. Chem.* **2020**, *18*, 3522.

[15]   a) X. Liu, C. Zhao, R. Zhu, L. Liu, *Angew. Chem. Int. Ed.* **2021**, *60*, 18499; *Angew. Chem.* **2021**, *133*, 18647; b) Y. Zhu, H. Wang, G. Wang, Z. Wang, Z. Liu, L. Liu, *Org. Lett.* **2021**, *23*, 7248.

[16]   L. Wang, N. Wang, Y. Qi, S. Sun, X. Liu, W. Li, L. Liu, *Chin. J. Org. Chem.* **2020**, *40*, 3934.

[17]   a) H. Mayr, M. Patz, *Angew. Chem. Int. Ed. Engl.* **1994**, *33*, 938.; *Angew. Chem.* **1994**, *106*, 990.

[18]   C. Reichardt, T. Welton, *Solvents and solvent effects in organic chemistry*, Wiley-VCH, Weinheim, **2011**.

[19]   H. Mayr, *Tetrahedron* **2015**, *71*, 5095.

[20]   R. Lucius, R. Loos, H. Mayr, *Angew. Chem. Int. Ed.* **2002**, *41*, 91; *Angew. Chem.* **2002**, *114*, 97.

[21]   C. Hansch, A. Leo, R. W. Taft, *Chem. Rev.* **1991**, *91*, 165.

[22]   A. J. Fernandes, A. Panossian, B. Michelet, A. Martin-Mingot, F. R. Leroux, S. Thibaudeau, *Beilstein J. Org. Chem.* **2021**, *17*, 343.

[23]   T. Schirmeister, C. Schmuck, P. R. Wich, *Beyer/Walter Organische Chemie*, Hirzel Verlag, Stuttgart, **2016**.

[24]   a) P. M. Jüstel, A. Stan, C. D. Pignot, A. R. Ofial, *Chem. Eur. J.* **2021**, *27*, 15928; b) A. Eitzinger, A. R. Ofial, *Pure Appl. Chem.* **2023**, *95*, 389.

[25]   T. B. Phan, M. Breugst, H. Mayr, *Angew. Chem. Int. Ed.* **2006**, *45*, 3869; *Angew. Chem.* **2006**, *118*, 3954.

[26]   T. A. Nigst, H. Mayr, *Eur. J. Org. Chem.* **2013**, *2013*, 2155.

[27]   Hsu Jer-Ray (2025): *Reactivity Characterization of o/p-Substituted N-Methylpyridinium Salts*, Masterarbeit, Ludwig-Maximilians-Universität München, München, Deutschland.

[28]   a) S. Minegishi, H. Mayr, *J. Am. Chem. Soc.* **2003**, *125*, 286; b) A. R. Ofial, *Pure Appl. Chem.* **2015**, *87*, 341.

[29]   a) H. Mayr, T. Bug, M. F. Gotta, N. Hering, B. Irrgang, B. Janker, B. Kempf, R. Loos, A. R. Ofial, G. Remennikov, H. Schimmel, *J. Am. Chem. Soc.* **2001**, *123*, 9500.

[30]   Reactivity parameters *E*, *N* and s_N can be retrieved at https://www.cup.lmu.de/oc/mayr/reaktionsdatenbank2/, which is a freely accessible webpage.

[31]   a) D. S. Allgäuer, H. Jangra, H. Asahara, Z. Li, Q. Chen, H. Zipse, A. R. Ofial, H. Mayr, *J. Am. Chem. Soc.* **2017**, *139*, 13318; b) R. J. Mayer, P. W. A. Allihn, N. Hampel, P. Mayer, S. A. Sieber, A. R. Ofial, *Chem. Sci.* **2021**, *12*, 4850.

[32]   J. Ruiz Aranzaes, M.-C. Daniel, D. Astruc, *Can. J. Chem*., 2006, **84**, 288.

[33]   Lucius Roland (2001): *Kinetische Untersuchungen zur Nukleophilie stabilisierter Carbanionen*, Dissertation, Ludwig-Maximilians-Universität München, München, Deutschland. (https://doi.org/10.5282/edoc.257)

[34]   J. Li, K. Wang, J. Wu, H. Zhang, Y. Chen, Q. Liu, J. Xu, W. Yi, *Eur. J. Org. Chem.* **2022**, *2022*.

[35]   S. R. Shirsath, G. H. Shinde, A. C. Shaikh, M. Muthukrishnan, *J. Org. Chem.* **2018**, *83*, 12305.

[36]   Y. Chen, Z. Yu, Z. Jiang, J.-P. Tan, J.-H. Wu, Y. Lan, X. Ren, T. Wang, *ACS Catal.* **2021**, *11*, 14168.

[37]   D. van der Born, J. K. D. M. Herscheid, R. V. A. Orru, D. J. Vugts, *Chem. Commun.* **2013**, *49*, 4018.

[38]   S. G. Lee, Y. T. Park, *Bull. Korean Chem. Soc.* **2003**, *24*, 1241.

[39]   X. Pan, Z. Wang, L. Kan, Y. Mao, Y. Zhu, L. Liu, *Chem. Sci.* **2020**, *11*, 2414.

[40]   Q.-Y. Wu, G.-Z. Ao, F. Liu, *Org. Chem. Front.* **2018**, *5*, 2061.

[41]   Y. Ma, J. Pang, X. Pan, S. Ma, X. Liu, L. Liu, *Synlett* **2020**, *31*, 1619.

[42]   *SAINT*, Bruker AXS Inc., Madison, Wisconsin, USA, **2012**.

[43]   G. M. Sheldrick, *SADABS*, University of Göttingen (Germany), **1996**.

[44]   G. M. Sheldrick, *Acta Cryst.* **2015**, *A71*, 3.

[45]   L. J. Farrugia, *J. Appl. Cryst.*, **2012**, *45*, 849.

Chapter 5. Defining the Synthetic Scope of *ortho*-Quinone Methides by Quantifying Their Electrophilicity

Author Contributions

All experiments were performed by C. Gross and with synthetic support by N. Hampel. Crystallographic analysis and visualization was performed by P. Mayer. Quantum chemical investigations were performed, analyzed and visualized by A. Eitzinger. The manuscript was written jointly by A. R. Ofial and C. Gross and with contributions from all authors.

Copyright

Parts of the supporting information are shown in section 5.2. A complete version of the electronic supporting information (*ESI*) is accessible under the following link:

https://doi.org/10.1002/chem.202403785

The raw data of kinetic measurements that support the findings of this study are openly available in Open Data LMU under the following link:

https://doi.org/10.5282/ubm/data.542

5.1. Copies of Manuscript

Defining the Synthetic Scope of *ortho*-Quinone Methides by Quantifying their Electrophilicity

Christoph Gross,[a] Andreas Eitzinger,[a, b] Nathalie Hampel,[a] Peter Mayer,[a] and Armin R. Ofial*[a]

A series of aryl-substituted *ortho*-quinone methides (*o*QMs) was synthesised and structurally characterised. Kinetic studies of the nucleophilic additions of carbanions (reference nucleophiles) to *o*QMs were used to determine second-order rate constants k_2 for the carbon-carbon bond forming reactions (20 °C, DMSO) at the *o*QMs' exocyclic π-bond. Analysing the kinetic data by the linear free energy relationship $\lg k_2 = s_N(N+E)$ revealed the Mayr electrophilicities *E* of the *o*QMs. The electrophilicities *E* of *o*QMs correlate linearly with Hammett substituent constants and experimentally determined reduction potentials E_p^{red} as well as with quantum-chemically calculated methyl anion affinities (MAAs), which provides valuable tools for prediciting the reactivity of further types of *o*QMs. Embedding the *o*QMs in Mayr's reactivity scales enables to predict novel nucleophilic reaction partners for *o*QMs and can productively be used to prepare simple Michael adducts as well as 4+2 or 4+1 cyclisation products as demonstrated in this work by several novel reactions with neutral or negatively charged C-, N-, and S-nucleophiles.

Introduction

Cyclohexadienes with a carbonyl and an exo-methylene group in either 1,2- or 1,4-positions are called *ortho*- and *para*-quinone methides (*o*QMs and *p*QMs), respectively. Owing to the polarisation of the molecules, which could also be drawn as phenolate substituted carbenium ions (Figure 1), they are electrophiles that readily undergo reactions with a wide range of nucleophiles. Nucleophilic attack occurs at the exocyclic carbon atom of *p*QMs and generates 1,6-conjugate Michael adducts stabilised by the aromatisation of the cyclohexadiene moiety in the initial step of the reactions. Analogously, Michael additions to *o*QMs furnish the respective 1,4-conjugate adducts.[1,2]

While many *p*QMs were isolated and spectroscopically characterised, only few stable *o*QMs are known[3] and Pettus et al. entitled their 2002 review *"o-Quinone methides: intermediates underdeveloped and underutilized in organic synthesis"*.[4] Efforts to exploit novel paths to generate *o*QMs have been numerous since then. Based on the commonly accepted assumption that *o*QMs are highly reactive and transient species, it is an often used strategy that, once formed as reactive
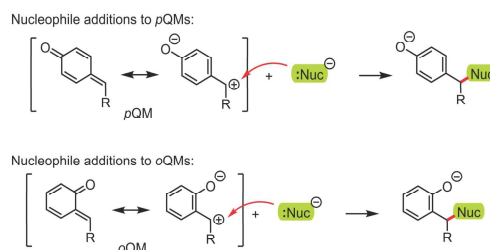
Figure 1. Polarisation of QMs and covalent bond-forming reactions with nucleophiles.

intermediates in solution, the *o*QMs are immediately trapped by reactions with nucleophiles or dienophiles.[5,6]

Depending on the location of additional functional groups in both the *o*QMs and the nucleophiles, a wide range of reaction sequences to construct complex (hetero)cyclic scaffolds is accessible. Cyclisation reactions via (4+3)-, (4+2)-, (4+1)-, (3+2)-, or (2+1)-modes are frequently used.[5,7,8] Control of emerging stereocenters in such ring-forming reactions can be attained by using chiral metal-based or metal-free (organo)catalysts.[5d,8c] The high reactivity of *o*QMs has furthermore been exploited in multicomponent reactions[9] as well as for bio-orthogonal ligations and biomolecule functionalisations.[5b,8,10]

Sophisticated synthetic strategies have made *o*QMs attractive building blocks in synthesis directed toward natural products[11] or substances with bioactivity.[8b] Understanding the reactivity of synthetically interesting and biologically relevant *o*QMs will be key for a more targeted optimisation of reaction conditions and a rational selection and design of tailored nucleophilic or Lewis-base catalysts for controlling the features of the complex QM-based product structures. Despite their

[a] C. Gross, A. Eitzinger, N. Hampel, P. Mayer, A. R. Ofial
Department Chemie, Ludwig-Maximilians-Universität München, Bute-nandtstr. 5–13, 81377 München, Germany
E-mail: ofial@lmu.de

[b] A. Eitzinger
Current address: Institute of Organic Chemistry, Johannes Kepler University Linz, Austria

Chem. Eur. J. **2025**, *31*, e202403785 (1 of 11)

© 2024 The Author(s). Chemistry - A European Journal published by Wiley-VCH GmbH

187

increasing utility in organic chemistry little quantitative information about their reactivity can be retrieved from literature.[2a,12–16] Kinetic studies on the reactivity of oQMs towards O-, N-, and S-centred nucleophiles in aqueous solution required special techniques, e.g. laser flash photolytic equipment, for the in situ generation of the oQMs from persistent precursors in solution.[13–17]

The currently most comprehensive data collection on the polar reactivity of organic electrophiles and nucleophiles to predict the efficiency of polar addition reactions in solution phase is based on the Mayr-Patz Equation (1).[18]

$$\lg k_2(20\,°C) = s_N(N + E)$$ (1)

In Equation (1), *E* represents the electrophilicity of the electrophile, and nucleophiles are characterised by two solvent-dependent parameters, s_N and *N*.[19] Equation (1) has successfully been applied to characterise the reactivity of >1300 nucleophiles and 350 electrophiles, including several *p*QMs.[20,21] By combining the three parameters *E*, *N*, and s_N in Equation (1), it is possible to calculate the second-order rate constant k_2 (at 20 °C) for a certain electrophile/nucleophile combination and predict if a certain reaction between an electrophile and a nucleophile will be fast enough to be successful. By extensive kinetic studies of the reactions of carbon-centred nucleophiles with sesamol-derived oQMs under standardised conditions (Scheme 1A) we aimed to provide, in this work, a fundamental quantitative understanding of the electrophilic reactivities of the synthetically most frequently used oQMs.

In this work, we report on the synthesis, isolation, and characterisation of oQMs **1**. With the oQMs in our hands, we studied the kinetics of their carbon-carbon bond-forming reactions with carbanions **2** (reference nucleophiles, structures shown in Scheme 1B) by stopped-flow and conventional photometric methods.

Evaluating the experimentally determined second-order rate constants $k_2(20\,°C)$ by Equation (1) enabled us to characterise the electrophilicities *E* of the oQMs, which were subsequently used to predict novel Michael additions and cyclisation reactions of oQMs. We, furthermore, show that reduction potentials E_p^{red} as well as quantum-chemically calculated methyl anion affinities (MAAs) are valuable tools for predicting the electrophilicity of oQMs.

Results and Discussion

Synthesis and Characterisation of Stable oQMs

The use of oQMs in organic synthesis has widely increased in the recent decade and most authors refer to the procedure originally reported by Jurd for preparing the sesamol-derived oQM **1b** (Scheme 2).[3a] Though several further oQMs with different substituents at the aryl ring have successfully been employed in synthesis, we were unable to identify publications that mentioned details of the applied procedures for the oQM synthesis. Consequently, there is a lack of detailed reports on reliable synthetic procedures which also comprises the currently non-existent spectroscopic characterisation of oQMs.

In a first step, we therefore set out to fill this gap by developing a general synthetic scheme for differently substituted oQMs and their precursors. Ideally, the scope of this synthetic scheme could comprise methods for the preparation of oQMs with both electron-donating and electron-withdrawing substituents and, thus, variability in their electrophilic reactivity.

General procedure 1 (GP1 in Scheme 2) starts with the deprotonation of sesamol by methyl magnesium iodide and the subsequent reaction of the sesamolate ion with benzoyl chlorides, as described by Zhou and colleagues.[22] GP1 was employed for preparing the substituted phenols **3a** and **3c–3i**. Reduction of the diarylmethanones **3a** and **3c–3i** to the

Scheme 1. (A) Bond-forming reaction between oQMs and anionic nucleophiles. (B) Structures of the electrophilic oQMs **1** and C-centred anionic reference nucleophiles used in this work (the electrophilic reaction centre is marked in blue, the nucleophilic reaction centre is marked in green, counterion: K⁺, nucleophile-specific reactivity parameters *N* and s_N from ref. [20b]).

Scheme 2. Preparation of stable and crystalline oQMs **1a–1h**. See Supporting Information for details (ani = *p*-methoxyphenyl, the lower-case letters indicate the identity of the aryl groups Ar as defined in Scheme 1).

188

diarylmethanes **4a** and **4c–4i** in GP2 was achieved (a) by base-mediated carbonate formation with methyl chloroformate and (b) subsequent addition of aq. sodium borohydride, as originally reported by Mitchell and colleagues.[23] Finally, Jurd's method,[3a] that is, the oxidation of the diarylmethanes **4** by silver(I) oxide yielded the *o*QMs **1a–1h** (GP3). Details of the individual procedures are given in the Supporting Information. The yields of isolated *o*QMs **1** were only low to moderate because the *o*QMs were crystallised directly from their reaction solutions. With regard to the intended kinetic studies with *o*QMs, we focussed on the purity of the isolated *o*QMs and did not further optimise the procedures for higher yields.

Oxidation of **4i**, which carries a perfluorophenyl group (Ar = C_6F_5), by silver(I) ions did not provide *o*QM **1i** but generated acetal **5** instead (yield: 76%) probably owing to a dimerisation of phenoxy radicals. The structural assignment for **5** was corroborated by single crystal X-ray diffraction (scXRD) analysis (Supporting Information).[24a] Thus, it could be confirmed that the mode of dimerisation differs from previously reported Diels-Alder like dimerisations[3a] or trimerisations of *o*QMs.[6b]

The eight isolated *o*QMs **1a–1h** were fully characterised by spectroscopic methods (Supporting Information). The *o*QMs are crystalline solids, with colours covering a spectrum from yellow to deep red. The X-ray crystal structure of **1b** at room temperature was determined in ref.[3b] In this work, crystals of suitable quality for analysis by scXRD at 173 K were obtained for the *o*QMs **1a**, **1b**, **1c** and **1h** (Figure 2).[24a] The scXRD analysis revealed that the dimethylamino-substituted *o*QM **1a** is almost planar in solid state (twist angle: 6.5°) whereas the aryl and the quinone π-systems in the methyl- and the nitro-substituted *o*QMs **1c** and **1h**, respectively, are twisted by 30.3° to 36.9°. Owing to the fact that the respective twist angles in **1b** are 33.9°/36.6° (29.3°/31.9° in ref.[3b]) the planar structure of **1a** seems to result from packing effects. Interestingly, the C—O bond length in the carbonyl groups remains unaffected (±0.1 pm) when changing from the electron-donating *p*-(dimethylamino)-substituent in **1a** to the strongly electron-accepting *p*-nitro-substituent at the aryl ring of *o*QM **1h**. Differently, the C1-C2 distance slightly varies depending on the substituent at the phenyl ring (Figure 2), which may indicate a sufficient dynamic range for reactivity studies within the series of the electrophilic *o*QMs **1a–1h**.

As illustrated by the photographs in Figure 3, the absorption maxima λ_{max} of DMSO solutions of **1a–1h** vary in the range from 417 (for **1f**) to 504 nm (for **1a**) (see Supporting Information for individual UV-Vis spectra). The series of absorption maxima correlates linearly with the quantum-chemically calculated chemical hardness η of the *o*QMs, which correspond to the HOMO-LUMO energy gaps according to $\eta = \varepsilon_{LUMO} - \varepsilon_{HOMO}$. This correlation holds for seven of the eight *o*QMs in this study ($R^2 = 0.9877$, $n = 7$, Supporting Information, Figure S1), but leaves the *p*-nitro derivative **1h** as an outlier, which was excluded when constructing the correlation line.

Electrophilicity *E* of *o*QMs

Reactions of *o*QMs with reference nucleophiles. After successful isolation and characterisation of the *o*QMs **1**, we next investigated the products of *o*QM reactions with the set of carbanions **2** that we intended to use as reference nucleophiles for the kinetic studies. To mimic the reaction conditions of the kinetic experiments as closely as possible, the electrophile-nucleophile reactions were conducted in DMSO at ambient temperature (23 ± 1 °C) without further optimisation.

As depicted in Scheme 3, the reactions of the 1,1-bis-acceptor stabilised carbanions **2** (counterion: K⁺) with the *o*QMs **1** generally gave (dihydro)chromenes **6**, which were isolated after aqueous workup in moderate to good yields and characterised by spectroscopic methods. Hence, the hemiacetals **6ba**, **6bb**, and **6bc** were obtained from reactions of the *o*QM **1b** with carbanions derived from dimedone (**2a**), acetyl acetone (**2b**), and ethyl acetoacetate (**2c**), respectively. The reaction of **1b** with **2a** was carried out at a 1 mmol scale and produced the tetracyclic **6ba** in a yield of 90%. Significantly, only one diastereomer (according to the NMR detection limit) of **6ba** was detected though **6ba** carries three stereocentres. Crystals of **6ba** obtained by the vapour diffusion method (pentane→dichloromethane at +4 °C) were suitable for analysis by scXRD[24a] and confirmed the structural assignment derived from the NMR spectra.

Reactions of the malononitrile anion **2d** with **1b** and **1d** furnished 2-amino-3-cyano-4*H*-chromenes **6bd**[6b] and **6dd**, respectively. In the reaction of **1b** with the ethyl cyanoacetate-derived anion **2e**, the ester group was more susceptible to ring closure by attack of the phenolate intermediate than the cyano group. Thus the addition of **2e** to **1b** finally gave the chroman-2-one **6be** with low diastereoselectivity and in a yield of 38%. The low yield of **6be** is explained by formation of a significant amount of the trapping product of the phenolate intermediate
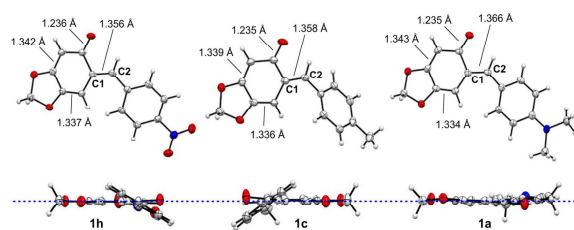

Figure 2. Single crystal X-ray structures of *o*QMs **1a**, **1c** and **1h**. Thermal ellipsoids are shown at the 25% probability level. Bottom: Side views of *o*QMs **1a**, **1c** and **1h**. The blue line indicates the plane through the quinone moieties.

Figure 3. Photos of DMSO solutions of *o*QMs **1a–1h**.

λ_{max} = 504   435   424   419   421   417   419   437 nm

Figure 4. (A) Carbon-carbon bond-forming reaction of an *o*QM **1** with an anionic nucleophile **2**. (B) Determination of the observed rate constant k_{obs} (s^{-1}) from the exponential decay of the *o*QM absorbance A at 437 nm versus time for the reaction between *o*QM **1 h** ($c_0 = 4.30 \times 10^{-5}$ M) and carbanion **2 d** ($c_0 = 1.50 \times 10^{-3}$ M, counterion: K$^+$). (C) The slope of the linear correlation of k_{obs} with [**2 d**] corresponds to the second-order rate constant k_2^{exp} (M^{-1} s^{-1}) for the **1 h + 2 d** addition reaction.

Scheme 3. Products isolated from the reactions *o*QMs **1** with the reference nucleophiles **2** (counterion: K$^+$; ani = *p*-methoxyphenyl, tol = *p*-tolyl, pcp = *p*-chlorophenyl).

A to form the simple Michael adduct **7 be** (isolated in a yield of 41%) after aqueous workup. Further benzochroman-2-ones were isolated with excellent diastereoselectivity from the reactions of the diethyl malonate-derived carbanion **2 f** with the *o*QMs **1 b** (yield: 75%), **1 c** (78%), **1 d** (48%), and **1 e** (75%).

To summarise, the origin of all isolated heterocyclic products **6** can be explained by conjugate addition of an anionic C-centred nucleophile at the exocyclic C—C double bond of the *o*QM, which generates adduct **A**. The reaction then continues towards the isolated heterocyclic products by an intramolecular attack of the phenolate oxygen at the most electrophilic carbon in one of the acceptor groups (rel. reactivity: keto C=O > ester C=O > C≡N), initially introduced to stabilise the carbanions.

Kinetics. The straightforward product formation observed for the reactions of the *o*QMs **1** with the nucleophiles **2** encouraged us to study the kinetics of these reactions in order to characterise the electrophilicity of the *o*QMs.

The general workflow of the kinetics experiments with *o*QMs is illustrated in Figure 4. The reactions of the coloured

*o*QMs **1** with carbanions **2** in DMSO at 20 °C yielded colourless solutions. The decay of the *o*QM absorption was used to photometrically monitor the kinetics of these carbon-carbon bond-forming reactions by stopped-flow or conventional UV/VIS spectrometers.[24b] To simplify the evaluation of the kinetic experiments, carbanion concentrations were chosen which exceeded those of the *o*QMs by at least a factor of ten. Hence, the kinetics were measured under pseudo-first-order reaction conditions. First-order rate constants k_{obs} (s^{-1}) were derived by least squares-fitting of the mono-exponential decay function $A_t = A_0 \exp(-k_{obs}t) + C$ to the time-dependent absorbances A_t.

The carbanions **2** can form ion pairs with the potassium counterions, which would reduce the nucleophilicity of the carbanions. On the other hand, attractive K$^+$/*o*QM interactions would possibly increase the reactivity of the electrophiles. Therefore, the four to five kinetic measurements for each **1 + 2** couple included two experiments, in which 18-crown-6 (18-c-6) was added (1.1 equiv. relative to [**2**]). The 18-crown-6 ether complexes potassium ions effectively with a complex stability constant of lg $K = 3.35$ in DMSO at 298 K.[24c] However, indiscriminately of whether the individual k_{obs} for a given **1 + 2** couple were determined from reaction mixtures with or without the crown ether additive, the plots of k_{obs} versus nucleophile concentrations, [**2**], gave linear correlations with only minor intercepts and slopes reflecting the second-order rate constants k_2 (M^{-1} s^{-1}). These observations, in agreement with previous reports on the kinetics of carbanion reactions with *p*QMs,[20a] show that at the low ion concentrations in DMSO used in the kinetic experiments of this work, the kinetics of *o*QM/carbanion combinations are not significantly affected by either ion pair formation or K$^+$/*o*QM complexation. The second-order rate constants k_2 derived for reactions of *o*QMs **1** with the reference nucleophiles **2** in DMSO at 20 °C are listed in Table 1. Details of the individual kinetic experiments are given in the Supporting Information.

Table 1. Experimentally determined second-order rate constants k_2^{exp} for the reactions of *o*QMs **1a–1h** with carbanions **2a–2f** (DMSO, 20 °C).

*o*QMs	k_2^{exp} ($M^{-1}s^{-1}$)						E
	2a	**2b**	**2c**	**2d**	**2e**	**2f**	
1a	1.13	1.84×10^1	4.44×10^1	5.55×10^2	4.13×10^2	1.38×10^2	−16.07
1b	3.85	8.00×10^1	2.00×10^2	1.92×10^3	1.36×10^3	8.53×10^2	−15.20
1c	5.72	1.60×10^2	4.60×10^2	2.94×10^3	2.75×10^3	1.21×10^3	−14.85
1d	1.35×10^1	2.77×10^2	8.06×10^2	3.82×10^3	4.57×10^3	2.85×10^3	−14.47
1e	2.55×10^1	5.34×10^2	1.67×10^3	7.78×10^3	1.16×10^4	8.31×10^3	−13.99
1f	2.99×10^1	6.21×10^2	1.83×10^3	6.34×10^3	8.43×10^3	8.10×10^3	−14.00
1g	5.26×10^1	1.19×10^3	4.01×10^3	1.22×10^4	2.18×10^4	1.88×10^4	−13.54
1h	9.69×10^1	2.27×10^3	7.63×10^3	2.07×10^4	3.51×10^4	4.38×10^4	−13.15

In accord with Equation (1), the experimentally determined second-order rate constants k_2 of the reactions of *o*QMs **1a–1h** with the anionic reference nucleophiles **2** were combined with reported N (and s_N) parameters of **2** to calculate the electrophilicities E of *o*QMs. For this, the sum of deviations Δ^2 between calculated lg $k_2^{Eq.(1)}$ [$-s_N(N+E)$] and experimental rate constants lg k_2^{exp} for reactions of a given *o*QM **1** with a series of reference nucleophiles **2** was minimised by the least-squares method according to Equation (2).

$$\Delta^2 = \Sigma(\text{lg } k_2^{exp} - \text{lg } k_2^{Eq.(1)})^2 \qquad (2)$$

The results of this procedure for calculating electrophilicities E can be visualised in plots of (lg k_2^{exp})/s_N vs. N, which are linear with a fixed unity slope as required by Equation (1). It should be noted that the reactivity parameters N (and s_N) of the carbanions **2** (reference nucleophiles) were calculated from the second-order rate constants of their addition reactions to *p*QMs and benzhydrylium ions (in DMSO at 20 °C).[20] Therefore, N (and s_N) reflect the one-bond nucleophilicities of the reference nucleophiles **2** and the linear (lg k_2^{exp})/s_N vs. N plots shown in Figures S2–S9 (Supporting Information) demonstrate that the kinetics of the carbanion/*o*QM reactions in this work correlate linearly with these one-bond nucleophilicities (N). In the 8×6 = 48 data array of *o*QM reactions with reference nucleophiles in Table 1, the maximum deviation between $k_2^{Eq.(1)}$ and k_2^{exp} is within a factor of 4 indicating a high confidence level of the determined electrophilicity parameters E of **1a–1h** (Table 1, right column) for predicting the rates of carbon-carbon bond-forming reactions with carbanionic nucleophiles.

Correlation Analysis

Figure 5 depicts the excellent linear correlation of electrophilicity E with the Hammett substituent constants σ for the substituents at the aromatic ring of the *o*QMs.[25] This correlation allows for a straightforward prediction of the Mayr E parameter for further aryl-substituted *o*QMs by considering the electronic effects at positions remote from the reaction centre.
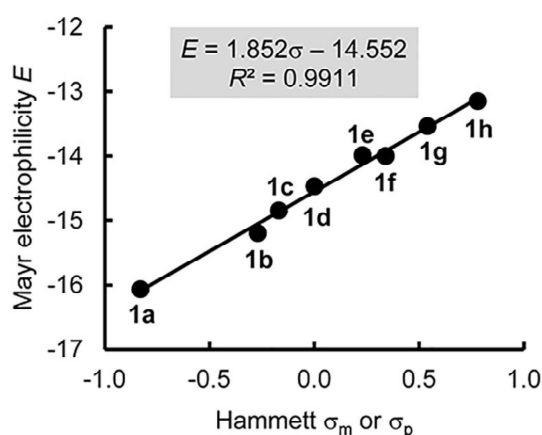
Figure 5. Linear correlation between Mayr electrophilicity E and Hammett substituent constants for **1a–1h** (with data from Supporting Information, Table S2).

The electronic effects of substituents at the aromatic ring in *o*QMs exactly mirror those in *para*-quinone methides (*p*QMs) as indicated by the unity slope of the linear relationship in Figure 6. However, when quinone methides with analogous substituents are compared, the *o*QMs are approx. by a factor of 10 more reactive towards nucleophiles than the analogous *p*QMs.

The kinetic studies provided insight in the electron-pair accepting abilities of *o*QMs in bond-forming reactions with anionic C-centred nucleophiles. We then aimed to supplement these data by one-electron reduction potentials, E^{red}. The cyclic voltammetry (CV) measurements for *o*QMs were performed in 0.1 M tetra-*n*-butyl ammonium perchlorate solutions of deaerated acetonitrile with a 2 mm diameter platinum working electrode, a platinum wire counter electrode and an Ag wire pseudo-reference electrode. A ferrocene solution was used as internal standard [$E_{1/2}$(fc$^+$/fc) = +0.382 V vs. SCE in MeCN].[26] Non-reversibility of the redox process accounts for the fact that only the peak potentials E_p^{red} of *o*QMs **1a–1h** could be determined as exemplified for the CVs of **1c** and **1f** in Figure 7 (all other CV diagrams are shown in the Supporting Information, Section 7). Plotting the Mayr electrophilicity E vs. the E_p^{red} of

$$E^{oQM} = 0.9999 E^{pQM} + 1.0687$$
$$R^2 = 0.9846$$
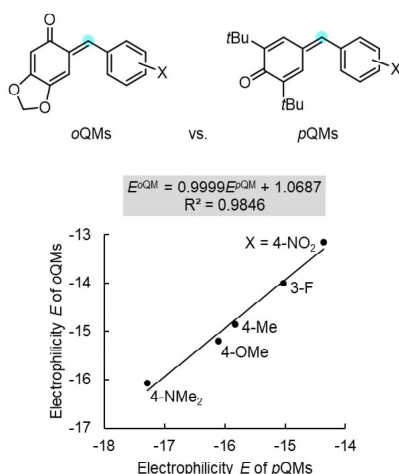
Figure 6. Correlation of the electrophilicities E of *o*QMs **1** with those of analogously ring-substituted *p*QMs (with data from Table 1 for *o*QMs and from refs. [20b, 21a] for *p*QMs).

*o*QMs **1a–1g** shows that these two properties of *o*QMs are strongly correlated (Figure 7C).

Table 2. Experimental (k_2^{exp}) and calculated ($k_2^{Eq.(1)}$) second-order rate constants for the reactions of the *o*QM **1b** ($E = -15.20$) with neutral or negatively charged C-, N- or S-centred nucleophiles in DMSO at 20 °C.

Nuc	$N\ (s_N)^{[a]}$	k_2^{exp} ($M^{-1} s^{-1}$)	$k_2^{Eq.(1)}$ ($M^{-1} s^{-1}$)	$k_2^{exp}/k_2^{Eq.(1)}$
8	18.67 (0.68)	2.59×10^2	2.29×10^2	1.1
9	14.48 (0.71)	4.37	3.08×10^{-1}	14
10	12.21 (0.62)	1.52×10^{-2}	1.40×10^{-2}	1.1
11	19.71 (0.86)	3.17×10^4	7.56×10^3	4.2
12a	17.19 (0.71)	4.40×10^2	2.59×10^1	17
12b	16.96 (0.67)	1.37×10^2	1.51×10^1	9.1
12c	15.70 (0.64)	2.03×10^1	2.09	9.7
12d	15.28 (0.65)	1.12×10^1	1.13	9.9
12e	14.39 (0.67)	3.26	2.87×10^{-1}	11
12f	12.15 (0.65)	1.42×10^{-1}	1.04×10^{-2}	14

[a] Nucleophile-specific reactivity parameters N and s_N were taken from ref. [32].

Applying the *o*QM Electrophilicity Parameters E

Comparing the reactivity of *o*QMs **1a–1h** with other classes of electrophilic compounds shows that *o*QMs are located in a reactivity range also covered by phenylvinyl ketone, *N*-methyl-maleimide or the 1,1-bissulfonyl-activated styrene (Figure 8). Consequently, *o*QMs are more reactive than many typically used Michael acceptors, such as benzylidene malonates,[27] acrylates,[28] or lactones with exocyclic methylene groups,[29] which have significantly more negative E parameters. Even the highly reactive ethenesulfonyl fluoride (ESF)[30] is only one order of magnitude more electrophilic than the most reactive *o*QM **1h** studied in this work.[31]

A precision of predicted second-order rate constants within two orders of magnitude is usually observed when Equation (1)

is applied to calculate the rates of electrophile-nucleophile combinations which do not belong to the set of reference reactions.[33] To assess the predictive power of the determined E parameters of *o*QMs we decided to extend the structural space of nucleophiles by studying the kinetics of the addition reactions of anionic or neutral C-, S-, or N-centred nucleophiles to *o*QM **1b** in DMSO.

The first entry in Table 2 shows the rate constants k_2^{exp} and $k_2^{Eq.(1)}$ for the reaction of **1b** with the carbanion **8** (counterion: K$^+$), which is structurally similar to the reference nucleophiles used to calibrate the electrophilicity of **1b**. For this electrophile-nucleophile combination, the calculated $k_2^{Eq.(1)}$ is within the experimental error margin of k_2^{exp} ($\pm 10\%$). This agreement suggests that the C–C bond formation is the rate-determining
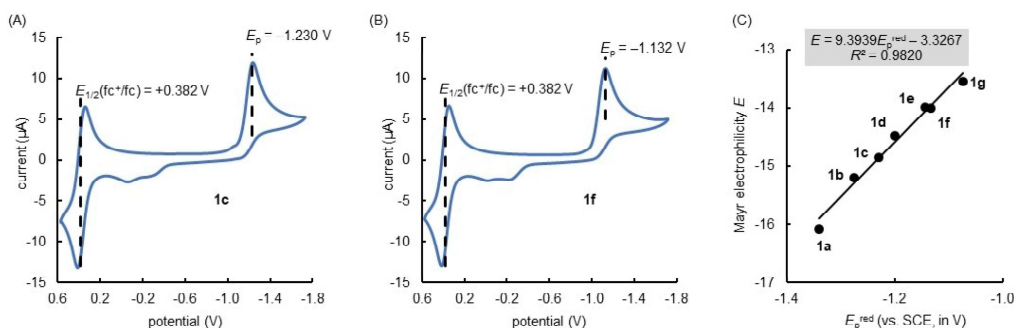
Figure 7. Cyclic voltammograms of (A) **1c** and (B) **1f** and (C) linear correlation of Mayr electrophilicity E with the reduction peak potentials E_p^{red} (V vs. SCE in acetonitrile) in the range of the *o*QMs from **1a** to **1g**.

Chem. Eur. J. **2025**, *31*, e202403785 (6 of 11)

© 2024 The Author(s). Chemistry - A European Journal published by Wiley-VCH GmbH

192

Figure 8. Embedding the *o*QMs **1** (blue background) on Mayr's electrophilicity scale. In combination with Mayr's nucleophilicity scale the location of **1** enables users to identify novel nucleophilic reaction partners for *o*QMs (see main text). Reactivity parameters E, N and s_N are from this work or ref. [32]. Nucleophile-specific reactivity parameters N (s_N) refer to DMSO if not mentioned otherwise. Electrophiles react with nucleophiles on the same horizontal level (that is, $E + N = 0$) with half reaction times of approx. 10 seconds for 0.1 molar solutions. At ambient temperature, electrophiles will react only sluggishly with nucleophiles (of $s_N = 0.66$) located more than seven to eight units below their own level.

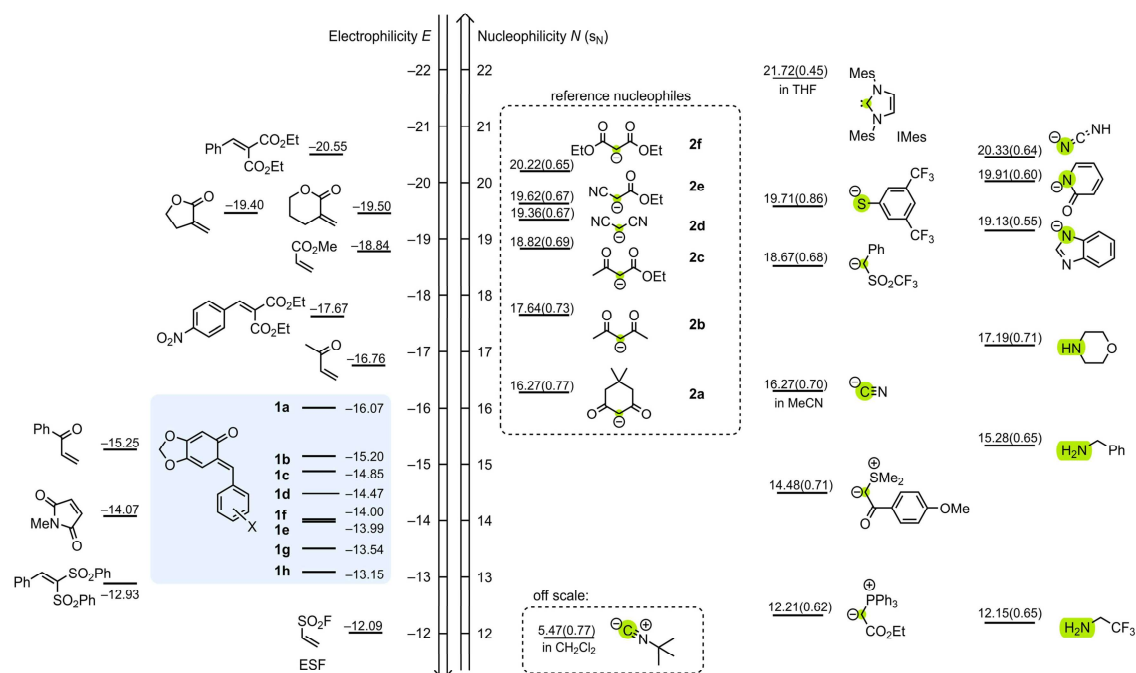step in the course of the $4 + 1$ cyclisation sequence towards the isolated 2,3-diaryl-substituted dihydrobenzofuran derivative **8′**, which is generated from the initial adduct through a fast subsequent intramolecular S_N2 reaction (Scheme 4A).

Furthermore, also the rate constants for the reactions of **1b** with the ylides **9** and **10** were still correctly predicted within roughly one order of magnitude (Table 2). Accordingly, we isolated diastereomerically pure dihydrobenzofuran **9′** in 96% yield from the reaction of **1b** with the sulfonium ylide **9** (Scheme 4B).[34] In perfect agreement with the predicted reaction kinetics also the phosphonium ylide **10** underwent an addition reaction to the exocyclic methylene group of **1b** and furnished after proton migration the ylide **10′** in 62% yield (Scheme 4C). The competing Wittig olefination at the carbonyl group of **1b** was not observed with **10** in DMSO.

The potassium thiophenolate **11** exemplifies the reaction of a sulphur nucleophile with **1b**. The experimental kinetics of the **11 + 1b** reaction proceeded four times faster than calculated by Equation (1) (Table 2). In agreement with the fast reaction kinetics, the thioether **11′** was isolated in 87% yield after 1 h reaction time at ambient temperature, aqueous workup and purification by column chromatography (Scheme 4D).

Deviations of up to a factor of 17 between k_2^{exp} and $k_2^{Eq.(1)}$ were observed for reactions of **1b** with primary and secondary amines **12a–12f** (Table 2). These reactions might benefit from an activating hydrogen-bonding interaction between the

carbonyl-group of the *o*QM **1b** and the nucleophiles' amino group. The product **12c′** of the reaction of **1b** with *n*-propylamine (**12c**) was isolated in 73% yield (Scheme 4E).

The marginal deviations of k_2^{exp} from $k_2^{Eq.(1)}$ in Table 2 and the reasonable products yields (Scheme 4) indicate that the electrophilicity parameters E of *o*QMs **1** calibrated against the carbanions **2a–2f** are well transferable and can, thus, be used to estimate the reactivity of *o*QMs also towards other classes of nucleophiles beyond those of the originally used reference nucleophiles. According to the rule of thumb that product-forming electrophile-nucleophile combinations at 20 °C require a minimum of $E + N > -5$ we tested further nucleophile/*o*QM couples.

The position of anionic, nitrogen-centred nucleophiles in the upper right corner of Figure 8 reveals that fast reactions with *o*QMs can be expected at ambient temperature. Hence, it was a save guess that *o*QM **1b** ($E = -15.20$) undergoes 1,4-additions with the cyanamide anion ($N = 20.33$, $s_N = 0.64$), the anion of 2-pyridone ($N = 19.91$, $s_N = 0.60$), or the deprotonated benzimidazole ($N = 19.13$, $s_N = 0.55$). Intramolecular trapping generates the isolated benzo[1,2-*e*][1,3]oxazin-6-amine **13** from **1b** and the cyanamide anion, whereas **14** and **15**, which were isolated after aqueous workup, resemble the direct Michael adducts of the anionic heterocycles and **1b** (Figure 9).

The highly reactive *N*-heterocyclic carbene IMes ($N = 21.72$, $s_N = 0.45$) generated adduct **16** with **1b** within a few minutes
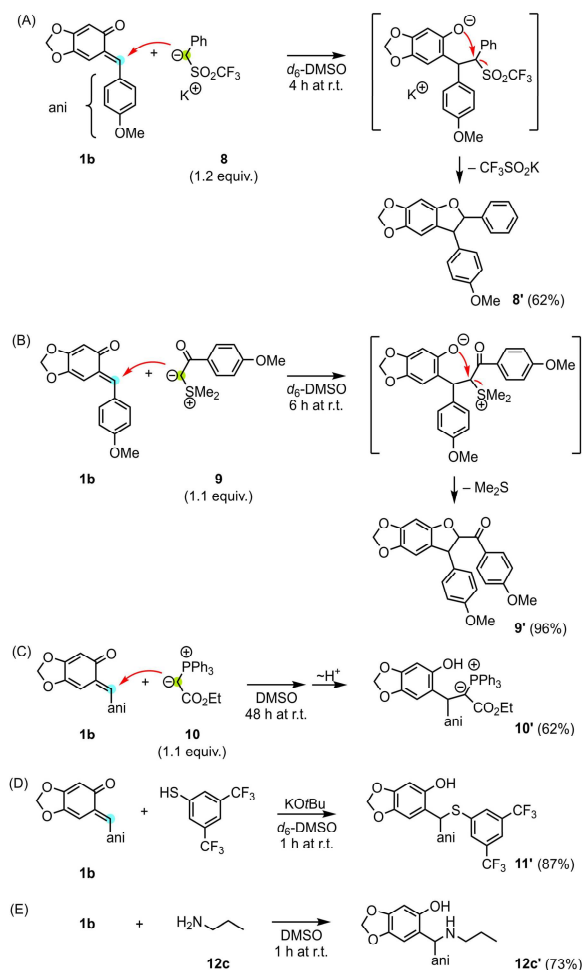
Scheme 4. Isolated products for kinetically studied reactions in Table 2. (A) Dihydrobenzofuran formation (**8′**) from the reaction of *o*QM **1b** with **8**. (B) Reaction of the *o*QM **1b** with **9** and subsequent ring-closure to yield **9′**. (C) Phosphonium ylide **10′** isolated from the reaction of **1b** with **10**. (D) Thioether **11′** isolated from the reaction of **1b** with **11** (generated from the thiophenol and potassium *tert*-butoxide). (E) Adduct **12 c′** from the reaction of *n*-propylamine **12 c** with *o*QM **1b**.

Figure 9. Isolated products from reactions of *o*QM **1b** with further N- and C-centred nucleophiles with known nucleophilicity parameters *N* (and s_N).

Quantum-Chemical Calculations

Quantum chemical calculations were performed to investigate the general electronic properties of *o*QMs. Additionally, we aimed to establish a method for the in silico prediction of *o*QM electrophilicities. The HOMO and LUMO energies ε_{HOMO} and ε_{LUMO} were determined from single point calculations at the SMD(DMSO)/B3LYP/6-311 + + G(3df,2pd)//B3LYP/6-31G(d,p) level of theory (Table 3).[35]

Figure 10 illustrates the LUMO of *o*QM **1b**, which is mostly located around the quinone moiety and the exocyclic double bond in line with the general regioselectivity in *o*QM reactions with nucleophiles.

It was previously shown that methyl anion affinities (MAAs) correlate linearly with the Mayr electrophilicities *E* of a set of 44 Michael acceptors (**M1–M44**, for structures see Supporting Information, Table S3).[28] By using a COSMO solvent model,[37] these correlations were subsequently extended by Van Vranken, Baldi and colleagues who demonstrated that MAA values are an effective tool to predict the electrophilic reactivity of neutral

and was isolated after acidic aqueous workup. The reaction of **1b** with sodium cyanide ($N/s_N = 16.27/0.70$ in acetontrile) is less spontaneous and requires one hour reaction time to yield the 2-amino 3-arylbenzofuran derivative **17** (yield: 54%). A sluggish adduct formation is predicted by Equation (1) for the reaction of **1b** with *tert*-butyl isocyanide, for which the nucleophilicity parameters $N/s_N = 5.47/0.77$ were calibrated based on the kinetics of its reactions with benzhydrylium ions in dichloromethane. Accordingly, we isolated the 2-aminobenzofuran **18** in a yield of 52% after a reaction time of 5 days at ambient temperature.

Table 3. Quantum-chemically calculated frontier orbital energies, global electrophilicities (ω) and methyl anion affinities (MAA) of *o*QMs (calculated at the SMD(DMSO)/B3LYP/6-311 + + G(3df,2pd)//B3LYP/6-31G(d,p) level of theory).

*o*QM	*E*	ε_{HOMO} (eV)	ε_{LUMO} (eV)	ω (eV)	MAA (kJ mol^{-1})
1a	−16.07	−4.883	−2.101	2.192	119.5
1b	−15.20	−5.295	−2.217	2.292	126.1
1c	−14.85	−5.448	−2.277	2.352	129.7
1d	−14.47	−5.520	−2.312	2.390	135.8
1e	−13.99	−5.554	−2.381	2.480	136.4
1f	−14.00	−5.583	−2.375	2.472	141.6
1	−13.54	−5.633	−2.444	2.557	142.9
1h	−13.15	−5.718	−2.827	3.158	147.0
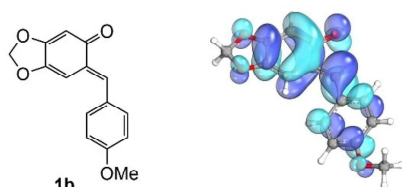
Figure 10. LUMO of *o*QM **1 b**, calculated at the SMD(DMSO)/B3LYP/6-311++G(3df,2pd)//B3LYP/6-31G(d,p) level of theory and visualised with IboView (ref. [36]).

and cationic electrophiles in a reactivity range of 50 orders of magnitude without performing additional kinetic experiments.[38]

We calculated the MAA of *o*QMs **1 a–1 h** as Gibbs reaction energies ($\Delta_r G°$) for the addition of the methyl anion to the *o*QMs **1** in DMSO as depicted in the definition reaction in the table head of Table 3. In order to consistently integrate the MAA data for *o*QMs **1** into our existing MAA collection for previously studied Michael acceptors, we used the same quantum-chemical method as in ref.[28], that is, calculations were carried out at the SMD(DMSO)/B3LYP/6-311++G-(3df,2pd)//B3LYP/6-31G(d,p) level of theory with DMSO-solvated gas-phase optimised structures. Interestingly, the *o*QMs **1 a–1 h** (Table 3) match the correlation line of the *E* vs. MAA relationship with little scatter (Figure 11). In consequence, the correlation coefficient R^2 of the *E* vs. MAA correlation improves from $R^2 = 0.8857$ $(n = 44)$[28] to $R^2 = 0.8890$ when data for the eight *o*QMs **1** are included ($n = 52$).

As seen in previous reports for other types of Michael acceptors,[28] Parr's global electrophilicity index ω,[39] which is ultimately derived from frontier molecular orbital energies ε_{HOMO} and ε_{LUMO} (Supporting Information, Section 12 and Table S4), is of low predictive power for *o*QM electrophilicities *E* ($R^2 = 0.6771$). Thus, Gibbs reaction energies for the carbon-carbon bond-formation of Michael acceptors with the simplest possible carbon nucleophile, the methyl anion, are suggested as the

method of choice for roughly predicting the electrophilic reactivity of further *o*QMs or other Michael acceptors within a correlation that currently covers 20 orders of magnitude on the *E* scale.

Conclusions

We synthesised a series of stable *o*QMs with substituent variation on the aryl moiety. Carbanions were used as reference nucleophiles and the kinetics of their reactions with *o*QMs in DMSO at 20 °C was determined by using stopped-flow and conventional photometry. Evaluation of the kinetic data according to the Mayr-Patz equation [Equation (1)] enabled us to characterise the *o*QMs' electrophilicity *E*, which correlate linearly with their Hammett substituent constants and reduction potentials E_p^{red}. Kinetic experiments and product studies with further carbon- and heteroatom-centred nucleophiles revealed the excellent predictive power of the experimentally determined electrophilicities *E*. Quantum-chemically calculated methyl anion affinities are suggested for estimating the reactivities of further *o*QMs of unseen structure.

In conclusion, the ready synthetic accessibility of *o*QMs, their unanticipated stability in crystalline form, and their versatile applications in simple Michael 1,4-additions or various Michael addition/heterocyclic ring-closure tandem reactions, which have become predictable through the determination of the *o*QMs' electrophilicities *E*, will advance the efficiency of their synthetic applications as well as their use as probes in biochemical studies. Furthermore, the structural motif of *o*QMs differs from those of previously calibrated electrophiles on the Mayr scale.[32] Hence, the *o*QMs expand the chemical space of characterised electrophiles and resemble a novel challenge for self-learning algorithms that use *E*, *N* (and s_N) for benchmarking. As a consequence of the structurally more diverse training set now available, we look forward to seeing high precision reactivity predictions generated by machine learning, efficient quantum-chemical methods, neural networks, or combinations thereof.[40–45] In our ongoing studies on the mechanism of reactions with coupled bond formations, we intend to use the *E* parameters for analysing [4 + 2]-cycloadditions of *o*QMs.

Supporting Information

The authors have cited additional references within the Supporting Information.[46–57]
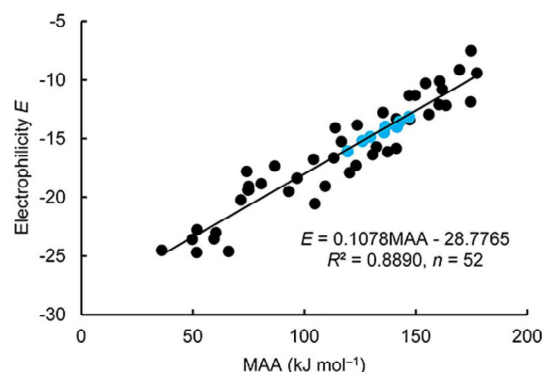
Acknowledgements

Figure 11. Linear correlation of electrophilicities *E* with MAAs for *o*QMs **1 a–1 h** (blue circles, this work, data from Table 3) and 44 further Michael acceptors (data from ref. [28], see Supporting Information, Table S3 for structures and reported *E* and MAA values of **M1–M44**).

195

Conflict of Interests

The authors declare no conflict of interest.

Data Availability Statement

The raw data of kinetic measurements that support the findings of this study are openly available in Open Data LMU at DOI: 10.5282/ubm/data.542, ref. [24b]. Further data available in article supplementary information.

[1] S. E. Rokita, Ed., *Quinone Methides*, Wiley, Hoboken (NJ) **2009**.

[2] Reviews: a) M. M. Toteva, J. P. Richard, *Adv. Phys. Org. Chem.* **2011**, *45*, 39–91; b) J.-Y. Wang, W.-J. Hao, S.-J. Tu, B. Jiang, *Org. Chem. Front.* **2020**, *7*, 1743–1778; c) C. G. S. Lima, F. P. Pauli, D. C. S. Costa, A. S. de Souza, L. S. M. Forezi, V. F. Ferreira, F. de Carvalho da Silva, *Eur. J. Org. Chem.* **2020**, *2020*, 2650–2692.

[3] a) L. Jurd, *Tetrahedron* **1977**, *33*, 163–168; b) A. Arduini, A. Pochini, R. Ungaro, P. Domiano, *J. Chem. Soc. Perkin Trans. 1* **1986**, 1391–1395; c) S. R. Angle, W. Yang, *J. Am. Chem. Soc.* **1990**, *112*, 4524–4528.

[4] R. W. Van De Water, T. R. R. Pettus, *Tetrahedron* **2002**, *58*, 5367–5405.

[5] Reviews: a) W.-J. Bai, J. G. David, Z.-G. Feng, M. G. Weaver, K.-L. Wu, T. R. R. Pettus, *Acc. Chem. Res.* **2014**, *47*, 3655–3664; b) Q. Li, T. Dong, X. Liu, X. Zhang, X. Yang, X. Lei, *Curr. Org. Chem.* **2014**, *18*, 86–92; c) M. S. Singh, A. Nagaraju, N. Anand, S. Chowdhury, *RSC Adv.* **2014**, *4*, 55924–55959; d) Z. Wang, J. Sun, *Synthesis* **2015**, *47*, 3629–3644; e) L. Caruana, M. Fochi, L. Bernardi, *Molecules* **2015**, *20*, 11733–11764; f) A. A. Jaworski, K. A. Scheidt, *J. Org. Chem.* **2016**, *81*, 10145–10153; g) V. A. Osyanin, A. V. Lukashenko, D. V. Osipov, *Russ. Chem. Rev.* **2021**, *90*, 324–373; h) B. J. Nachtsheim, *Nat. Chem.* **2020**, *12*, 326–328.

[6] Selected recent examples: a) X. He, R. Li, P. Y. Choy, M. Xie, J. Duan, Y. Tang, Y. Shang, F. Y. Kwong, *Commun. Chem.* **2021**, *4*, 42; b) M. Uyanik, K. Nishioka, R. Kondo, K. Ishihara, *Nat. Chem.* **2020**, *12*, 353–362.

[7] For selected examples: a) H. Lv, W. Q. Jia, L. H. Sun, S. Ye, *Angew. Chem. Int. Ed.* **2013**, *52*, 8607–8610; b) J. Izquierdo, A. Orue, K. A. Scheidt, *J. Am. Chem. Soc.* **2013**, *135*, 10634–10637; c) H. Lam, Z. Qureshi, M. Wegmann, M. Lautens, *Angew. Chem. Int. Ed.* **2018**, *57*, 16185–16189; d) M. Sun, C. Ma, S.-J. Zhou, S.-F. Lou, J. Xiao, Y. Jiao, F. Shi, *Angew. Chem. Int. Ed.* **2019**, *58*, 8703–8708; e) B. M. Trost, Z. Zuo, *Angew. Chem. Int. Ed.* **2020**, *59*, 1243–1247; f) A. Sunjela, H. J. Loui, C. Schneider, *Angew. Chem. Int. Ed.* **2020**, *59*, 5536–5540; g) Q. Tan, H. Yu, Y. Luo, F. Chang, X. Liu, Y. Zhou, X. Feng, *Chem. Commun.* **2021**, *57*, 3018–3021.

[8] a) D. V. Osipov, V. A. Osyanin, Y. N. Klimochkin, *Russ. Chem. Rev.* **2017**, *86*, 625–687; b) K. Ali, P. Mishra, A. Kumar, D. N. Reddy, S. Chowdhury, G. Panda, *Chem. Commun.* **2022**, *58*, 6160–6175; c) C. Dorsch, C. Schneider, *Synthesis* **2022**, *54*, 3125–3141.

[9] M. T. M. Martins, K. Rodrigues, F. Dias, R. Silva, M. de Moraes, M. F. V. da Silva, K. R. Lucio, K. D'Oliveira Góes, P. A. do Nascimento, A. S. S. da Silva, V. F. Ferreira, A. C. Cunha, *Chem. Rec.* **2022**, *22*, e202100251.

[10] a) C. Huang, S. E. Rokita, *Front. Chem. Sci. Eng.* **2016**, *10*, 213–221; b) C. Huang, Y. Liu, S. E. Rokita, *Signal Transduction Target. Ther.* **2016**, *1*, 16009; c) Y. Zhang, S. Liu, F. Guo, S. Qin, N. Zhou, Z. Liu, X. Fan, P. R. Chen, *J. Am. Chem. Soc.* **2024**, *146*, 15186–15197.

[11] a) N. J. Willis, C. D. Bray, *Chem. Eur. J.* **2012**, *18*, 9160–9173; b) B. Yang, S. Gao, *Chem. Soc. Rev.* **2018**, *47*, 7926–7953; c) C. D.-T. Nielsen, H. Abas,

A. C. Spivey, *Synthesis* **2018**, *50*, 4008–4018; d) T. N. Purdy, B. S. Moore, A. L. Lukowski, *J. Nat. Prod.* **2022**, *85*, 688–701.

[12] M. Freccero, F. Doria, in *Quinone Methides* (Ed: S. E. Rokita), Wiley, Hoboken (NJ) **2009**, Chapter 2, pp. 33–67.

[13] a) L. Diao, C. Yang, P. Wan, *J. Am. Chem. Soc.* **1995**, *117*, 5369–5370; b) P. Wan, B. Barker, L. Diao, M. Fischer, Y. Shi, C. Yang, *Can. J. Chem.* **1996**, *74*, 465–475; c) L. Diao, P. Wan, *Can. J. Chem.* **2008**, *86*, 105–118.

[14] a) Y. Chiang, A. J. Kresge, Y. Zhu, *J. Am. Chem. Soc.* **2000**, *122*, 9854–9855; b) Y. Chiang, A. J. Kresge, Y. Zhu, *J. Am. Chem. Soc.* **2001**, *123*, 8089–8094; c) Y. Chiang, A. J. Kresge, Y. Zhu, *J. Am. Chem. Soc.* **2002**, *124*, 717–722; d) Y. Chiang, A. J. Kresge, Y. Zhu, *J. Am. Chem. Soc.* **2002**, *124*, 6349–6356.

[15] M. Freccero, *Mini-Rev. Org. Chem.* **2004**, *1*, 403–415.

[16] E. Modica, R. Zanaletti, M. Freccero, M. Mella, *J. Org. Chem.* **2001**, *66*, 41–52.

[17] a) E. E. Weinert, R. Dondi, S. Colloredo-Meiz, K. N. Frankenfield, C. H. Mitchell, M. Freccero, S. E. Rokita, *J. Am. Chem. Soc.* **2006**, *128*, 11940–11947; b) J. Ma, M. Sekutor, D. Skalamera, N. Basaric, D. L. Phillips, *J. Org. Chem.* **2019**, *84*, 8630–8637.

[18] C. L. Perrin, I. Agranat, A. Bagno, S. E. Braslavsky, P. A. Fernandes, J.-F. Gal, G. C. Lloyd-Jones, H. Mayr, J. R. Murdoch, N. S. Nudelman, L. Radom, Z. Rappoport, M.-F. Ruasse, H.-U. Siehl, Y. Takeuchi, T. T. Tidwell, E. Uggerud, I. H. Williams, *Pure Appl. Chem.* **2022**, *94*, 353–534.

[19] a) H. Mayr, M. Patz, *Angew. Chem. Int. Ed.* **1994**, *33*, 938–957; b) H. Mayr, A. R. Ofial, *J. Phys. Org. Chem.* **2008**, *21*, 584–595; c) H. Mayr, *Tetrahedron* **2015**, *71*, 5095–5111.

[20] a) R. Lucius, H. Mayr, *Angew. Chem. Int. Ed.* **2000**, *39*, 1995–1997; b) R. Lucius, R. Loos, H. Mayr, *Angew. Chem. Int. Ed.* **2002**, *41*, 91–95.

[21] a) D. Richter, N. Hampel, T. Singer, A. R. Ofial, H. Mayr, *Eur. J. Org. Chem.* **2009**, *2009*, 3203–3211; b) M. Winter, R. Schütz, A. Eitzinger, A. R. Ofial, M. Waser, *Eur. J. Org. Chem.* **2020**, *2020*, 3812–3817.

[22] B. Wu, M.-W. Chen, Z.-S. Ye, C.-B. Yu, Y.-G. Zhou, *Adv. Synth. Catal.* **2014**, *356*, 383–387.

[23] D. Mitchell, C. W. Doecke, L. A. Hay, T. M. Koenig, D. D. Wirth, *Tetrahedron Lett.* **1995**, *36*, 5335–5338.

[24] a) Deposition Numbers CCDC 2386679 (for **1a**), CCDC 2386682 (for **1b**), CCDC 2386677 (for **1c**), CCDC 2386678 (for **1h**), CCDC 2386680 (for **5**), and CCDC 2386681 (for **6ba**) contain the supplementary crystallographic data for this paper. These data are provided free of charge by the joint Cambridge Crystallographic Data Centre and Fachinformationszentrum Karlsruhe Access Structures service; b) The raw data of kinetic measurements that support the findings of this study are openly available in Open Data LMU at DOI: 10.5282/ubm/data.542; c) P. Solov'ev, N. N. Strakhova, O. A. Raevsky, V. Rüdiger, H.-J. Schneider, *J. Org. Chem.* **1996**, *61*, 5221–5226.

[25] C. Hansch, A. Leo, R. W. Taft, *Chem. Rev.* **1991**, *91*, 165–195.

[26] J. Ruiz Aranzaes, M.-C. Daniel, D. Astruc, *Can. J. Chem.* **2006**, *84*, 288–299.

[27] O. Kaumanns, R. Lucius, H. Mayr, *Chem. Eur. J.* **2008**, *14*, 9675–9682.

[28] D. S. Allgäuer, H. Jangra, H. Asahara, Z. Li, Q. Chen, H. Zipse, A. R. Ofial, H. Mayr, *J. Am. Chem. Soc.* **2017**, *139*, 13318–13329.

[29] R. J. Mayer, P. W. A. Allihn, N. Hampel, P. Mayer, S. A. Sieber, A. R. Ofial, *Chem. Sci.* **2021**, *12*, 4850–4865.

[30] J. Dong, L. Krasnova, M. G. Finn, K. B. Sharpless, *Angew. Chem. Int. Ed.* **2014**, *53*, 9430–9448.

[31] Q. Chen, P. Mayer, H. Mayr, *Angew. Chem. Int. Ed.* **2016**, *55*, 12664–12667.

[32] Reactivity parameters *E*, *N*, and s_N can be retrieved at https://www.cup.lmu.de/oc/mayr/reaktionsdatenbank2/, which is a freely accessible website (accessed on 29/10/2024).

[33] H. Mayr, *Angew. Chem. Int. Ed.* **2011**, *50*, 3612–3618.

[34] Analogous reactions of oQMs with sulfonium ylides were reported in ref. [22].

[35] See Supporting Information for details of the quantum-chemical calculations.

[36] G. Knizia, *J. Chem. Theory Comput.* **2013**, *9*, 4834–4843.

[37] a) A. Klamt, G. Schüürmann, *J. Chem. Soc. Perkin Trans. 2* **1993**, 799–805; b) A. Klamt, *WIREs Comput. Mol. Sci.* **2011**, *1*, 699–709.

[38] a) A. Mood, M. Tavakoli, E. Gutman, D. Kadish, P. Baldi, D. L. Van Vranken, *J. Org. Chem.* **2020**, *85*, 4096–4102; b) M. Tavakoli, A. Mood, D. Van Vranken, P. Baldi, *J. Chem. Inf. Model.* **2022**, *62*, 2121–2132.

[39] a) R. G. Parr, L. Szentpaly, S. Liu, *J. Am. Chem. Soc.* **1999**, *121*, 1922–1924; b) L. R. Domingo, M. Rios-Gutierrez, P. Perez, *Molecules* **2016**, *21*, 748.

[40] S. A. Cuesta, M. Moreno, R. A. López, J. R. Mora, J. L. Paz, E. A. Márquez, *J. Chem. Inf. Model.* **2023**, *63*, 507–521.

[41] Y. Liu, Q. Yang, J. Cheng, L. Zhang, S. Luo, J.-P. Cheng, *ChemPhysChem* **2023**, *24*, e202300162.

[42] P. Bianchi, J. C. M. Monbaliu, *Angew. Chem. Int. Ed.* **2024**, *63*, e202311526.

[43] M. Vahl, J. Proppe, *Phys. Chem. Chem. Phys.* **2023**, *25*, 2717–2728.

[44] N. Ree, A. H. Göller, J. H. Jensen, *Digital Discovery* **2024**, *3*, 347–354.

[45] W. Nie, D. Liu, S. Li, H. Yu, Y. Fu, *J. Chem. Inf. Model.* **2022**, *62*, 4319–4328.

[46] M. J. Heravi, M. Daraie, *Monatsh. Chem.* **2014**, *145*, 1479–1482.

[47] *SAINT*, Bruker AXS Inc., Madison, Wisconsin, USA **2012**.

[48] G. M. Sheldrick, *SADABS*, University of Göttingen, Germany, **1996**.

[49] G. M. Sheldrick, *Acta Cryst.* **2015**, *A71*, 3–8.

[50] L. J. Farrugia, *J. Appl. Cryst.* **2012**, *45*, 849–854.

[51] A. D. Becke, *J. Chem. Phys.* **1993**, *98*, 5648–5652.

[52] R. Ditchfield, W. Hehre, J. A. Pople, *J. Chem. Phys.* **1971**, *54*, 724–728.

[53] R. Krishnan, J. S. Binkley, R. Seeger, J. A. Pople, *J. Chem. Phys.* **1980**, *72*, 650–654.

[54] A. V. Marenich, C. J. Cramer, D. G. Truhlar, *J. Phys. Chem. B* **2009**, *113*, 6378–6396.

[55] Z. Li, H. Jangra, Q. Chen, P. Mayer, A. R. Ofial, H. Zipse, H. Mayr, *J. Am. Chem. Soc.* **2018**, *140*, 5500–5515.

[56] *Schrödinger Release 2021–4: MacroModel*, Schrödinger, LLC, New York, NY **2021**.

[57] M. J. Frisch, G. W. Trucks, H. B. Schlegel, G. E. Scuseria, M. A. Robb, J. R. Cheeseman, G. Scalmani, V. Barone, G. A. Petersson, H. Nakatsuji, X. Li, M. Caricato, A. Marenich, J. Bloino, B. G. Janesko, R. Gomperts, B. Mennucci, H. P. Hratchian, J. V. Ortiz, A. F. Izmaylov, J. L. Sonnenberg, D. Williams-Young, F. Ding, F. Lipparini, F. Egidi, J. Goings, B. Peng, A. Petrone, T. Henderson, D. Ranasinghe, V. G. Zakrzewski, J. Gao, N. Rega, G. Zheng, W. Liang, M. Hada, M. Ehara, K. Toyota, R. Fukuda, J. Hasegawa, M. Ishida, T. Nakajima, Y. Honda, O. Kitao, H. Nakai, T. Vreven, K. Throssell, J. A. Montgomery, Jr., J. E. Peralta, F. Ogliaro, M. Bearpark, J. J. Heyd, E. Brothers, K. N. Kudin, V. N. Staroverov, T. Keith, R. Kobayashi, J. Normand, K. Raghavachari, A. Rendell, J. C. Burant, S. S. Iyengar, J. Tomasi, M. Cossi, J. M. Millam, M. Klene, C. Adamo, R. Cammi, J. W. Ochterski, R. L. Martin, K. Morokuma, O. Farkas, J. B. Foresman, D. J. Fox, *Gaussian 09, Revision D.01*, Gaussian, Inc., Wallingford CT **2016**.

_____

5.2. Supporting Information

5.2.1. Supplementary Figures

Electrophilicities of oQMs 1a–1h.

The slopes of the correlation lines in the Figs. S1–S8 are set to unity as required by Equation (1) and illustrate the results from least-square minimizations $\Delta^2 = (\lg\ k_2^{exp} - s_N(N + E))^2$ to calculate the electrophilicity E of the oQMs **1**. The least-squares minimizations used the experimental second-order rate constants k_2^{exp} in DMSO at 20 °C from Table 1 (Manuscript, section 5.1.) and the reported nucleophile-specific parameters N and s_N of the reference nucleophiles **2a–2f** from ref. [1] as input in an MS Excel spreadsheet. The E parameter was defined as an adjustable variable and optimized for the individual oQMs **1** by using the MS Excel Solver (GRG algorithm).

oQMs **1**
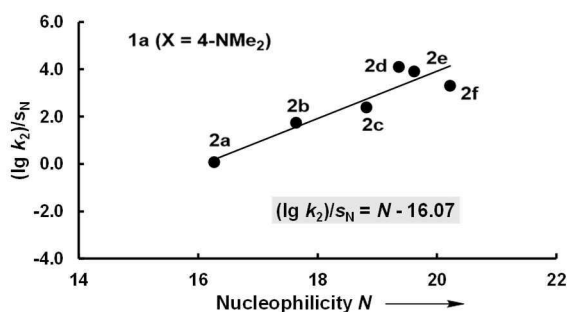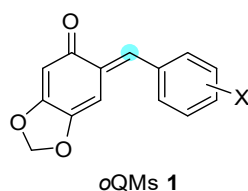
Fig. S1. Correlation of $(\lg k_2)/s_N$ vs. N for oQM **1a**.
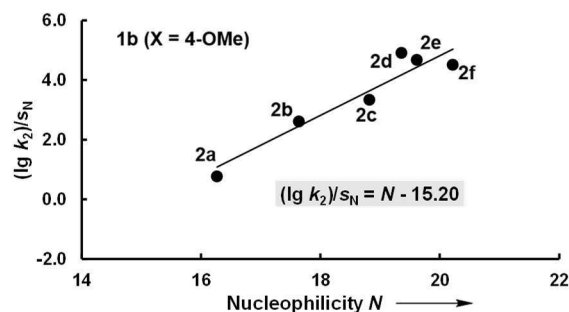
Fig. S2. Correlation of $(\lg k_2)/s_N$ vs. N for oQM **1b**.
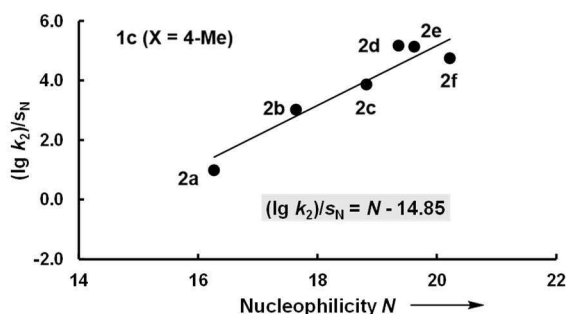
Fig. S3. Correlation of $(\lg k_2)/s_N$ vs. N for oQM **1c**.
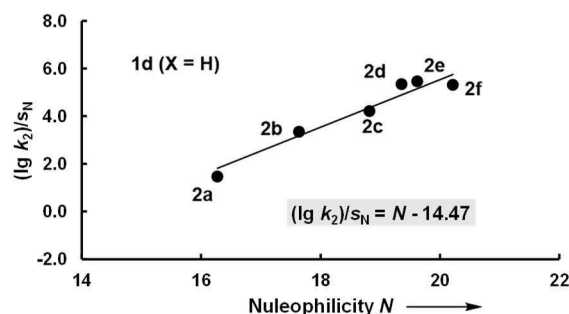
Fig. S4. Correlation of $(\lg k_2)/s_N$ vs. N for oQM **1d**.
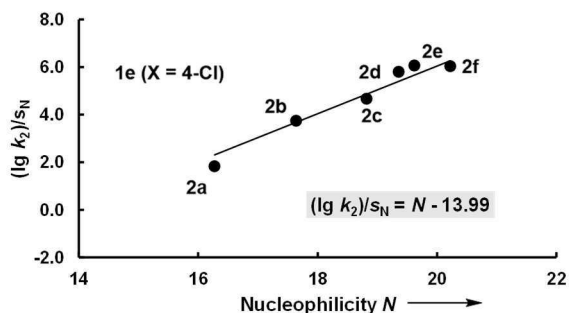
Fig. S5. Correlation of $(\lg k_2)/s_N$ vs. N for *o*QM **1e**.
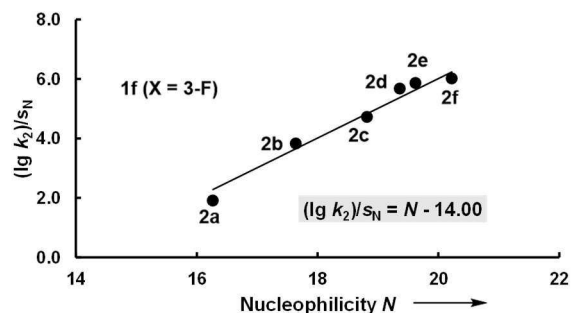
Fig. S6. Correlation of $(\lg k_2)/s_N$ vs. N for *o*QM **1f**.
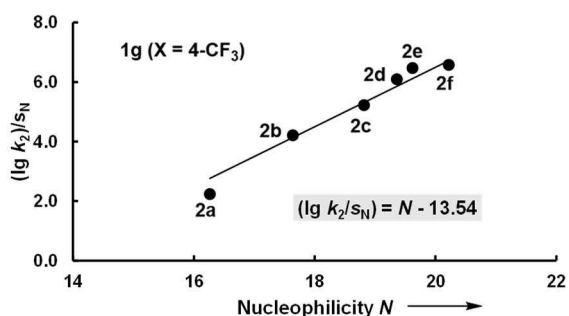
Fig. S7. Correlation of $(\lg k_2)/s_N$ vs. N for *o*QM **1g**.
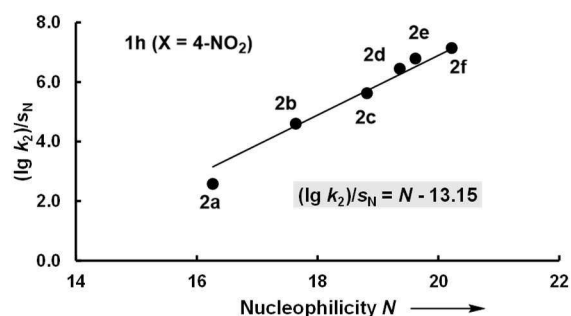
Fig. S8. Correlation of $(\lg k_2)/s_N$ vs. N for *o*QM **1h**.

Table S1. Electrophilicity parameters E (this work) and Hammett substituent constants σ from ref. [2] (used for the construction of Fig. 5 in the manuscript, section 5.1).

*o*QMs **1**
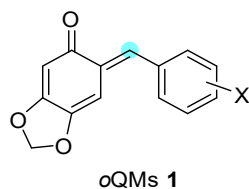
*o*QM	Substituent X	Electrophilicity E	Hammett σ
1a	4-N(CH$_3$)$_2$	−16.07	−0.83
1b	4-OCH$_3$	−15.20	−0.27
1c	4-CH$_3$	−14.85	−0.17
1d	H	−14.47	0
1e	4-Cl	−13.99	0.23
1f	3-F	−14.00	0.34
1g	4-CF$_3$	−13.54	0.54
1h	4-NO$_2$	−13.15	0.78

_____

5.2.2. Synthesis of *ortho*-Quinone Methides

Diaryl methanones **3a** and **3c–3i** were prepared by following *General Procedure 1 (GP1)*, which is rooted on a literature procedure.[3]

Phenols **4a-4i** were prepared from **3** according to *General Procedure 2 (GP2)*, which is based on a literature procedure.[4]

Ortho-quinone methides (*o*QMs) **1a–1h** were prepared by following *General Procedure 3 (GP3)* in analogy to a procedure that was initially reported for the synthesis of *o*QM **1b**.[5]
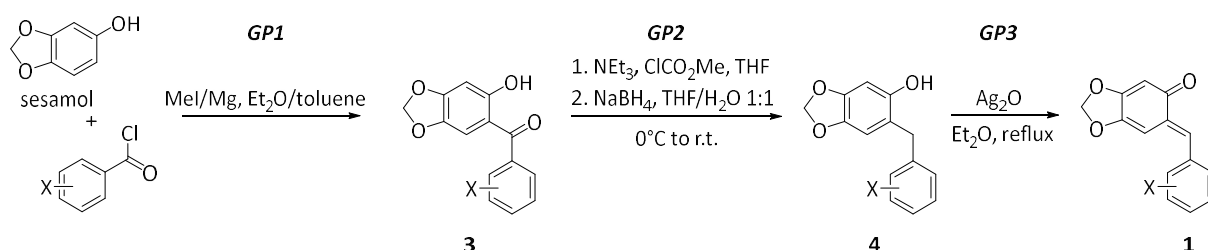
Synthesis of Diaryl Methanones 3

General Procedure (GP1)

Magnesium turnings were flame-dried in a three-necked flask under vacuum and flushed with dry nitrogen. Methyl iodide was added to a suspension of magnesium and diethyl ether (10 mL) under reflux and the mixture was stirred until complete reaction of the magnesium. Sesamol, dissolved in diethyl ether (5 mL), was added dropwise, and the reaction mixture was stirred for 2 h. The solvent was removed under vacuum and the residue was suspended in dry toluene (30 mL). Aryl chloride was dissolved in toluene (5 mL) and added dropwise at 0°C over a period of 20 min. The reaction mixture was stirred for 20 h at room temperature (approx. 23 °C). The mixture was quenched with aq. saturated NH$_4$Cl solution (20 mL) and extracted with ethyl acetate (4 × 30 mL). The combined organic phases were washed with brine (2 × 30 mL) and dried over MgSO$_4$. The solvent was removed under reduced pressure and the crude residue was purified by silica gel chromatography and crystallized from *n*-hexane/dichloromethane mixtures to afford the diaryl methanones **3**.

(4-(Dimethylamino)phenyl)(6-hydroxybenzo[*d*][1,3]dioxol-5-yl)methanone (3a) was prepared (*GP1*) from magnesium (0.42 g, 17.3 mmol), methyl iodide (4.11 g, 29.0 mmol), sesamol (1.60 g, 11.6 mmol), and 4-(dimethylamino)benzoyl chloride (2.13 g, 11.6 mmol, added portion by portion to the reaction mixture). Purification of the crude material by flash chromatography (silica gel, *n*-pentane:EtOAc:NEt$_3$ = 78:20:2) and crystallization (from *n*-hexane/CH$_2$Cl$_2$) gave **3a** (1.73 g, 52%) as yellow crystals; m.p. 188 °C.

3a (CG249_1)
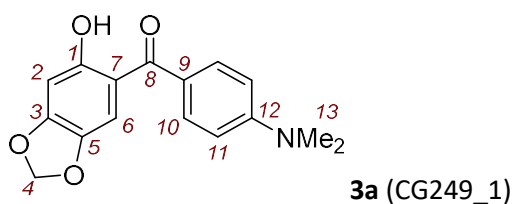
¹H NMR (400 MHz, CDCl$_3$): δ 13.03 (s, 1 H, 1-OH), 7.65 (d, *J* = 9.1 Hz, 2 H, 10-H), 7.10 (s, 1 H, 6-H), 6.71 (d, *J* = 9.1 Hz, 2 H, 11-H), 6.53 (s, 1 H, 2-H), 5.97 (s, 2-H, 4-H), 3.07 ppm (s, 6 H, 13-H).

_____

$^{13}C\{^1H\}$ **NMR** (101 MHz, CDCl$_3$): δ 197.8 (C$_q$, C-8), 162.4 (C$_q$, C-1), 153.5 (C$_q$, C-3), 153.0 (C$_q$, C-12), 134.0 (C$_q$, C-5), 131.8 (CH, C-10), 125.4 (C$_q$, C-9), 112.3 (C$_q$, C-7), 110.9 (CH, C-11), 110.3 (CH, C-6), 101.8 (CH$_2$, C-4), 99.0 (CH, C-2), 40.2 ppm (CH$_3$, C-13).

HRMS (EI): *m/z* calcd for C$_{16}$H$_{15}$NO$_4$$^{\bullet+}$ [M$^{\bullet+}$]: 285.0996; found: 285.1001.

IR (neat, ATR): $\tilde{\nu}$ 3095, 2907, 1626, 1598, 1577, 1480, 1419, 1332, 1246, 1182, 1036, 937, 832, 797, 776 cm^{-1}.

(6-Hydroxybenzo[*d*][1,3]dioxol-5-yl)(p-tolyl)methanone (3c) was prepared (*GP1*) from magnesium (0.396 g, 16.3 mmol), methyl iodide (3.85 g, 27.1 mmol), sesamol (1.50 g, 10.9 mmol), and 4-methylbenzoyl chloride (1.68 g, 10.9 mmol). Purification of the crude material by flash chromatography (silica gel, eluent: *n*-pentane:EtOAc = 9:1) furnished **3c** (1.17 g, 42%) as yellow crystals (literature known compound: ref. [3]); m.p. 106 °C.

3c (LL02/CG701)

R$_f$ (*n*-pentane/EtOAc 9:1, silica, UV) = 0.40.

^{1}**H NMR** (599 MHz, CDCl$_3$): δ 13.03 (s, 1 H), 7.54 (d, *J* = 8.2 Hz, 2 H), 7.29 (d, *J* = 7.8 Hz, 2 H), 6.98 (s, 1 H), 6.54 (s, 1 H), 5.98 (s, 2 H), 2.44 ppm (s, 3 H).

$^{13}C\{^1H\}$ **NMR** (151 MHz, CDCl$_3$): δ 199.6, 163.3, 154.5, 142.3, 140.3, 135.6, 129.2, 129.1, 111.9, 110.2, 102.0, 99.0, 21.7 ppm.

HRMS (EI): *m/z* calcd for C$_{15}$H$_{12}$O$_4$$^{\bullet+}$ [M$^{\bullet+}$]: 256.0730; found: 256.0729.
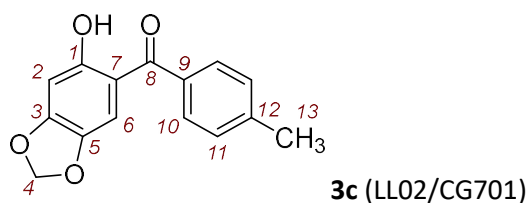
IR (neat, ATR): $\tilde{\nu}$ 2910, 1621, 1597, 1496, 1475, 1414, 1338, 1251, 1206, 1177, 1041, 935, 834, 789, 770 cm^{-1}.

(6-Hydroxybenzo[*d*][1,3]dioxol-5-yl)(phenyl)methanone (3d) was prepared (*GP1*) from magnesium (0.396 g, 16.3 mmol), methyl iodide (3.85 g, 27.1 mmol), sesamol (1.50 g, 10.9 mmol), and benzoyl chloride (1.53 g, 10.9 mmol). Purification of the crude material by flash chromatography (silica gel, eluent: *n*-pentane:EtOAc = 9:1) and crystallization (from *n*-hexane/CH$_2$Cl$_2$) yielded **3d** (1.39 g, 53%) as yellow crystals (literature known compound: ref. [3]); m.p. 120 °C.

3d (NG01/CG700)
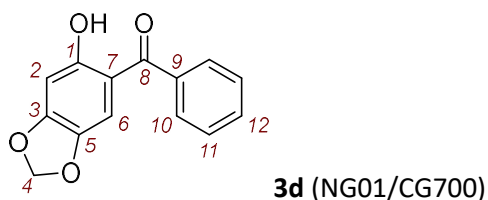
^{1}**H NMR** (600 MHz, CDCl$_3$): δ 13.01 (s, 1 H), 7.62 (d, *J* = 6.9 Hz, 2 H), 7.56 (t, *J* = 7.2 Hz, 1 H), 7.50–7.48 (m, 2 H), 6.94 (s, 1 H), 6.55 (s, 1 H), 5.98 ppm (s, 2 H).

$^{13}C\{^1H\}$ **NMR** (151 MHz, CDCl$_3$): δ 199.7, 163.5, 154.7, 140.4, 138.4, 131.6, 128.8, 128.5, 111.8, 110.1, 102.1, 99.0 ppm.

HRMS (EI): *m/z* calcd for $C_{14}H_{10}O_4^{\bullet+}$ [M$^{\bullet+}$]: 242.0574; found: 242.0574.

IR (neat, ATR): $\tilde{v}$ 2900, 1629, 1608, 1598, 1487, 1474, 1424, 1339, 1252, 1202, 1042, 935, 798, 748, 706, 696 cm^{-1}.

(4-Chlorophenyl)(6-hydroxybenzo[*d*][1,3]dioxol-5-yl)methanone (3e) was prepared (*GP1*) from magnesium (0.260 g, 10.7 mmol), methyl iodide (2.57 g, 18.1 mmol), sesamol (1.00 g, 7.24 mmol), and 4-chlorobenzoyl chloride (1.27 g, 7.26 mmol). Purification of the crude material by flash chromatography (silica gel, eluent: *n*-pentane:EtOAc = 9:1) and crystallization (from *n*-hexane/CH$_2$Cl$_2$) furnished **3e** (0.960 g, 48%) as yellow crystals; m.p. 122 °C.

3e (CG306)
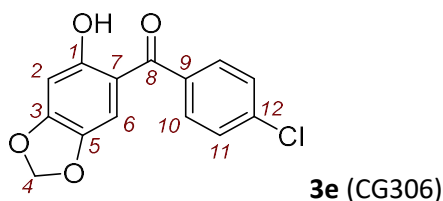
R_f (*n*-pentane/EtOAc = 9:1, silica, UV) = 0.60.

^{1}H NMR (600 MHz, CDCl$_3$): δ 12.89 (s, 1 H, 1-OH), 7.58 (d, *J* = 8.8 Hz, 2 H, 10-H), 7.47 (d, *J* = 8.8 Hz, 2 H, 11-H), 6.88 (s, 1 H, 6-H), 6.55 (s, 1 H, 2-H), 5.99 ppm (s, 2 H, 4-H).

^{13}C{^{1}H} NMR (151 MHz, CDCl$_3$): δ 198.3 (C$_q$, C-8), 163.6 (C$_q$, C-1), 154.9 (C$_q$, C-3), 140.5 (C$_q$, C-5), 138.0 (C$_q$, C-12), 136.6 (C$_q$, C-9), 130.3 (CH, C-10), 128.9 (CH, C-11), 111.5 (C$_q$, C-7), 109.6 (CH, C-6), 102.2 (CH$_2$, C-4), 99.1 ppm (CH, C-2).

HRMS (EI): *m/z* calcd for $C_{14}H_9{}^{35}ClO_4^{\bullet+}$ [M$^{\bullet+}$]: 276.0184; found: 276.0181.

IR (neat, ATR): $\tilde{v}$ 2919, 1617, 1584, 1479, 1392, 1324, 1267, 1193, 1178, 1137, 1090, 1043, 1013, 929, 881, 836, 774 cm^{-1}.

(3-Fluorophenyl)(6-hydroxybenzo[*d*][1,3]dioxol-5-yl)methanone (3f) was prepared (*GP1*) from magnesium (0.260 g, 10.7 mmol), methyl iodide (2.57 g, 18.1 mmol), sesamol (1.00 g, 7.24 mmol), and 3-fluorobenzoyl chloride (1.15 g, 7.25 mmol). Purification of the crude material by flash chromatography (silica gel, eluent: *n*-pentane:EtOAc = 9:1) and crystallization (from *n*-hexane/CH$_2$Cl$_2$) yielded **3f** (0.910 g, 48%) as yellow crystals; m.p. 123 °C.

3f (CG311)
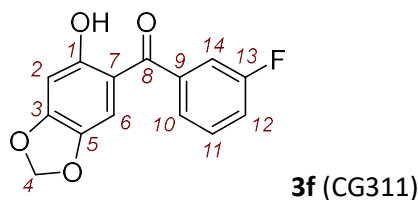
R_f (*n*-pentane/EtOAc = 9:1, silica, UV) = 0.50.

^{1}H NMR (400 MHz, CDCl$_3$): δ 12.85 (s, 1 H, 1-OH), 7.50–7.45 (m, 1 H, 11-H), 7.40–7.38 (m, 1 H, 10-H), 7.34–7.31 (m, 1 H, 14-H), 7.28–7.23 (m, 1 H, 12-H), 6.90 (s, 1 H, 6-H), 6.55 (s, 1 H, 2-H), 6.00 ppm (s, 2 H, 4-H).

^{13}C{^{1}H} NMR (101 MHz, CDCl$_3$): δ 198.0 (C$_q$, d, $^4J_{C,F}$ = 2.1 Hz, C-8), 163.7 (C$_q$, C-1), 162.6 (C$_q$, d, $^1J_{C,F}$ = 248.7 Hz, C-13), 155.1 (C$_q$, C-3), 140.6 (C$_q$, C-5), 140.3 (C$_q$, d, $^3J_{C,F}$ = 6.7 Hz, C-9), 130.3 (CH, d, $^3J_{C,F}$ = 7.9

Hz, C-11), 124.5 (CH, d, $^4J_{C,F}$ = 3.2 Hz, C-10), 118.6 (CH, d, $^2J_{C,F}$ = 21.3 Hz, C-12), 115.8 (CH, d, $^2J_{C,F}$ = 22.9 Hz, C-14), 111.5 (C$_q$, C-7), 109.7 (CH, C-6), 102.2 (CH$_2$, C-4), 99.1 ppm (CH, C-2).

HRMS (EI): *m/z* calcd for C$_{14}$H$_9$FO$_4$$^{\bullet+}$ [M$^{\bullet+}$]: 260.0479; found: 260.0475.

IR (neat, ATR): $\tilde{v}$ 3068, 1625, 1579, 1474, 1424, 1339, 1261, 1222, 1180, 928, 863, 809, 770, 690 cm^{-1}.

(6-Hydroxybenzo[*d*][1,3]dioxol-5-yl)(4-(trifluoromethyl)phenyl)methanone (3g) was prepared (*GP1*) from magnesium (0.260 g, 10.7 mmol), methyl iodide (2.57 g, 18.1 mmol), sesamol (1.00 g, 7.24 mmol), and 4-(trifluoromethyl)benzoyl chloride (1.51 g, 7.24 mmol). Purification of the crude material by flash chromatography (silica gel, eluent: *n*-pentane:EtOAc = 9:1) and crystallization (*n*-hexane/CH$_2$Cl$_2$) delivered **3g** (1.45 g, 65%) as yellow crystals; m.p. 118 °C.

3g (CG321)

R$_f$ (*n*-pentane/EtOAc = 9:1, silica, UV) = 0.60.

^{1}H NMR (400 MHz, CDCl$_3$): δ 12.85 (s, 1 H, 1-OH), 7.78–7.71 (m, 4 H, 10-H, 11-H), 6.81 (s, 1 H, 6-H), 6.56 (s, 1 H, 2-H), 6.00 ppm (s, 2 H, 4-H).

^{13}C{^{1}H} NMR (101 MHz, CDCl$_3$): δ 198.2 (C$_q$, C-8), 163.9 (C$_q$, C-1), 155.3 (C$_q$, C-3), 141.5 (C$_q$, , q, $^5J_{C,F}$ = 1.2 Hz, C-9), 140.7 (C$_q$, C-5), 133.1 (C$_q$, q, $^2J_{C,F}$ = 32.8 Hz, C-12), 129.0 (CH, C-10), 125.6 (CH, q, $^3J_{C,F}$ = 3.7 Hz, C-11), 123.8 (C$_q$, q, $^1J_{C,F}$ = 272.6 Hz, C-13), 111.4 (C$_q$, C-7), 109.4 (CH, C-6), 102.3 (CH$_2$, C-4), 99.2 ppm (CH, C-2).

HRMS (EI): *m/z* calcd for C$_{15}$H$_9$F$_3$O$_4$$^{\bullet+}$ [M$^{\bullet+}$]: 310.0447; found: 310.0445.
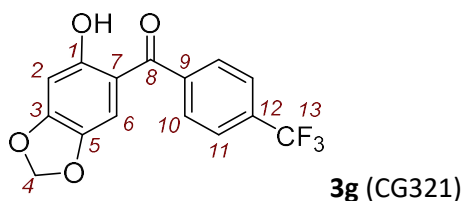
IR (neat, ATR): $\tilde{v}$ 2929, 1639, 1625, 1594, 1503, 1476, 1420, 1319, 1202, 1170, 1121, 1108, 1038, 933, 843, 796 cm^{-1}.

(6-Hydroxybenzo[*d*][1,3]dioxol-5-yl)(4-nitrophenyl)methanone (3h) was prepared (*GP1*) from magnesium (0.260 g, 10.7 mmol), methyl iodide (2.57 g, 18.1 mmol), sesamol (1.00 g, 7.24 mmol), and 4-nitrobenzoyl chloride (1.34 g, 7.22 mmol, directly added to the reaction mixture). Purification of the crude material by flash chromatography (silica gel, eluent: *n*-pentane:EtOAc = 8:2) and crystallization (from *n*-hexane/CH$_2$Cl$_2$) gave **3h** (0.850 g, 2.96 mmol, 41%) as orange crystals; m.p. 192 °C.

3h (CG317)
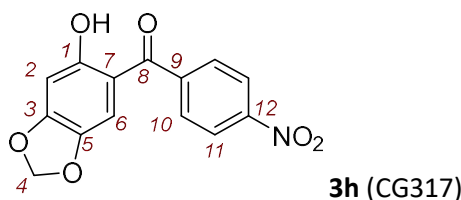
R$_f$ (*n*-pentane/EtOAc = 8:2, silica, UV) = 0.60.

^{1}H NMR (600 MHz, CDCl$_3$): δ 12.78 (s, 1 H, 1-OH), 8.36 (d, *J* = 8.8 Hz, 2 H, 11-H), 7.77 (d, *J* = 8.8 Hz, 2 H, 10-H), 6.75 (s, 1 H, 6-H), 6.57 (s, 1 H, 2-H), 6.01 ppm (s, 2 H, 4-H).

_____

^{13}C{^{1}H} NMR (151 MHz, CDCl$_3$): δ 197.3 (C=O, C-8), 164.1 (C$_q$, C-1), 155.7 (C$_q$, C-3), 149.4 (C$_q$, C-12), 143.8 (C$_q$, C-9), 140.9 (C$_q$, C-5), 129.6 (CH, C-10), 123.8 (CH, C-11), 111.2 (C$_q$, C-7), 109.0 (CH, C-6), 102.4 (CH$_2$, C-4), 99.3 ppm (CH, C-2).

HRMS (EI): *m/z* calcd for C$_{14}$H$_9$NO$_6$$^{\bullet+}$ [M$^{\bullet+}$]: 287.0424; found: 287.0425.

IR (neat, ATR): $\tilde{v}$ 3080, 1623, 1591, 1523, 1509, 1477, 1419, 1326, 1316, 1251, 1189, 1143, 1032, 927, 810, 698 cm^{-1}.

(6-Hydroxybenzo[*d*][1,3]dioxol-5-yl)(pentafluorophenyl)methanone (3i) was prepared (*GP1*) from magnesium (0.264 g, 10.9 mmol), methyl iodide (2.57 g, 18.1 mmol), sesamol (1.00 g, 7.24 mmol), and perfluorobenzoyl chloride (1.67 g, 7.24 mmol). Purification of the crude material by flash chromatography (silica gel, eluent: *n*-pentane:EtOAc = 9:1) and crystallization (*n*-hexane/CH$_2$Cl$_2$) yielded **3i** (1.37 g, 57%) as yellow crystals; m.p. 157 °C.

3i (CW02/LW02)

R_f (n-pentane/EtOAc 9:1, silica, UV) = 0.30.

^{1}H NMR (600 MHz, CDCl$_3$): δ 12.34 (s, 1 H, 1-OH), 6.55 (s, 1 H, 2-H), 6.54–6.53 (m, 1 H, 6-H), 6.02 ppm (s, 2 H, 4-H).

^{13}C{^{1}H} NMR (151 MHz, CDCl$_3$): δ 186.9 (C$_q$, C-8), 164.1 (C$_q$, C-1), 156.7 (C$_q$, C-3), 143.4 (C$_q$, dm, $^1J_{C,F}$ = 252 Hz, C-10), 142.6 (C$_q$, dm, $^1J_{C,F}$ = 258 Hz, C-12), 141.6 (C$_q$, C-5), 137.8 (C$_q$, dm, $^1J_{C,F}$ = 256 Hz), 113.3–112.9 (C$_q$, m, C-9), 112.8 (C$_q$, C-7), 107.8 (CH, C-6), 102.7 (CH$_2$, C-4), 99.0 ppm (CH, C-2).

^{19}F NMR (376 MHz, CDCl$_3$): δ −139.97 to −140.01 (m, 2 F, 10-F), −150.25 (tt, *J* = 20.7, 2.7 Hz, 1 F, 12-F), −159.33 to −159.49 ppm (m, 2 F, 11-F).

HRMS (EI): *m/z* calcd for C$_{14}$H$_5$F$_5$O$_4$$^{\bullet+}$ [M$^{\bullet+}$]: 332.0103; found: 332.0109.
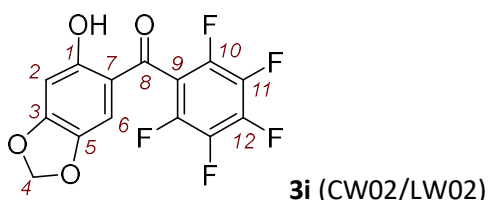
IR (neat, ATR): $\tilde{v}$ 2917, 1652, 1615, 1597, 1523, 1493, 1472, 1420, 1347, 1184, 1127, 1037, 987, 935, 854, 773, 723, 707 cm^{-1}.

Synthesis of Phenols 4

General Procedure (GP2)

In a flame-dried round-bottom flask under nitrogen diaryl methanones **3** were dissolved in dry THF. Triethylamine and methyl chloroformate were added and the reaction mixture was stirred for 1 h at 0°C.The mixture was filtered to remove precipitated triethylammonium chloride. Then the filtrate was reduced to half the volume by solvent evaporation at the rotary evaporator. The carbonate solution in THF was added to a mixture of NaBH$_4$ in water at 0°C, resulting in an approximately 1:1 mixture of THF/H$_2$O. The reaction mixture was stirred for 3 h at room temperature. The mixture was quenched with water (20 mL) and extracted with diethyl ether (4 × 30 mL). The combined organic phases were washed with brine (30 mL) and dried over MgSO$_4$. The solvent was removed under reduced pressure

at the rotary evaporator. The crude product was purified by chromatography on silica gel to afford the phenols **4**.

6-(4-(Dimethylamino)benzyl)benzo[*d*][1,3]dioxol-5-ol (4a) was prepared (analogous to *GP2*) from **3a** (1.02 g, 3.58 mmol), KO*t*Bu (1.20 g, 10.7 mmol), methyl chloroformate (0.98 g, 10.4 mmol) in THF (100 mL). After filtration, the solution was reduced to half of the volume by solvent evaporation at the rotary evaporator before sodium borohydride (1.35 g, 35.7 mmol in 50 mL water) was added. Purification of the crude material by flash chromatography (silica gel, eluent: *n*-pentane:EtOAc = 8:2) yielded **4a** (0.812 g, 84%) as an off-white solid; m.p. 102 °C.

4a (CG251_1)
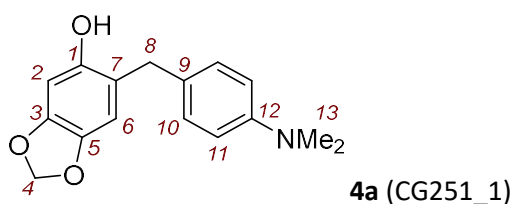
R_f (*n*-pentane/EtOAc = 8:2, silica, UV) = 0.30.

^{1}H NMR (600 MHz, CDCl$_3$): δ 7.08 (d, J = 8.8 Hz, 2 H, 10-H), 6.70 (d, J = 8.8 Hz, 2 H, 11-H), 6.61 (s, 1 H, 6-H), 6.40 (s, 1 H, 2-H), 5.88 (s, 2 H, 4-H), 4.57 (br s, 1 H, 1-OH), 3.80 (s, 2 H, 8-H), 2.92 ppm (s, 6 H, 13-H).

^{13}C{^{1}H} NMR (151 MHz, CDCl$_3$): δ 149.7 (C$_q$, C-12), 148.6 (C$_q$, C-1), 146.7 (C$_q$, C-3), 141.5 (C$_q$, C-5), 129.3 (CH, C-10), 127.2 (C$_q$, C-9), 119.4 (C$_q$, C-7), 113.4 (CH, C-11), 110.1 (CH, C-6), 101.1 (CH$_2$, C-4), 98.9 (CH, C-2), 40.9 (CH$_3$, C-13), 35.8 ppm (CH$_2$, C-8).

HRMS (EI): *m/z* calcd for C$_{16}$H$_{17}$NO$_3$$^{\bullet+}$ [M$^{\bullet+}$]: 271.1203; found: 271.1205.

IR (neat, ATR): $\tilde{\nu}$ 2885, 2799, 1613, 1518, 1503, 1480, 1441, 1343, 1288, 1163, 1035, 932, 854 cm^{-1}.

6-(4-Methoxybenzyl)benzo[*d*][1,3]dioxol-5-ol (4b) was prepared by following the procedure in ref. [5] Sesamol (2.68 g, 19.4 mmol), ascorbic acid (0.957 g, 5.43 mmol), and 4-methoxybenzyl alcohol (2.68 g, 19.4 mmol) were dissolved in 2% aq. citric acid (100 mL). The reaction mixture was stirred under reflux for 20 h. After cooling at room temperature, the reaction mixture was extracted with EtOAc (3 × 30 mL). The combined organic phases were washed with brine (30 mL), dried over MgSO$_4$, and the solvent was removed under reduced pressure. Purification of the crude material by flash chromatography (silica gel, eluent: *n*-pentane:EtOAc = 8:2) and crystallization (from *n*-hexane/DCM) furnished **4b** (3.93 g, 15.2 mmol, 78%) as colorless crystals; m.p. 109 °C (ref. [5], m.p. 110 °C).

4b (CG196)
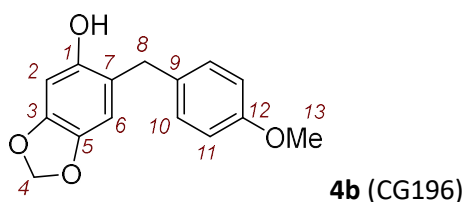
^{1}H NMR (400 MHz, CDCl$_3$): δ 7.13 (d, J = 8.9 Hz, 2 H), 6.84 (d, J = 8.8 Hz, 2 H), 6.59 (s, 1 H), 6.40 (s, 1 H), 5.88 (s, 2 H), 4.51 (s, 1 H), 3.83 (s, 2 H), 3.79 ppm (s, 3 H).

^{13}C{^{1}H} NMR (101 MHz, CDCl$_3$): δ 158.3, 148.3, 146.7, 141.6, 131.9, 129.6, 119.2, 114.3, 110.1, 101.1, 98.8, 55.4, 35.5 ppm.

HRMS (EI): *m/z* calcd for $C_{15}H_{14}O_4{}^{\bullet+}$ [$M^{\bullet+}$]: 258.0887; found: 258.0888.

6-(4-Methylbenzyl)benzo[*d*][1,3]dioxol-5-ol (4c) was prepared (*GP2*) from **3c** (1.17 g, 4.57 mmol), triethylamine (0.693 g, 6.85 mmol), methyl chloroformate (0.496 g, 5.25 mmol) in THF (40 mL). After filtration, the solution was reduced to half of the volume by solvent evaporation at the rotary evaporator before sodium borohydride (0.691 g, 18.3 mmol in 20 mL water) was added. Purification of the crude material by flash chromatography (silica gel, eluent: *n*-pentane:EtOAc = 9:1) furnished **4c** (0.985 g, 89%) as an off-white solid (literature known compound: ref. [3]); m.p. 69 °C.

4c (LL03/CG703)
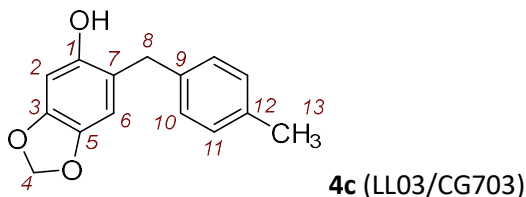
R_f (*n*-pentane/EtOAc = 9:1, silica, UV) = 0.24.

¹H NMR (400 MHz, CDCl₃): δ 7.11 (s, 4 H), 6.60 (s, 1 H), 6.40 (s, 1 H), 5.89 (s, 2 H), 4.39 (br s, 1 H), 3.85 (s, 2 H), 2.32 (s, 3 H) ppm.

¹³C{¹H} NMR (101 MHz, CDCl₃): δ 148.3, 146.7, 141.6, 136.7, 136.2, 129.6, 128.5, 119.0, 110.2, 101.1, 98.8, 36.1, 21.2 ppm.

HRMS (EI): *m/z* calcd for $C_{15}H_{14}O_3{}^{\bullet+}$ [$M^{\bullet+}$]: 242.0937; found: 242.0938.

IR (neat, ATR): ṽ 3213, 2891, 1501, 1483, 1456, 1433, 1182, 1148, 1035, 935, 909, 869, 850, 809, 759 cm⁻¹.

6-Benzylbenzo[*d*][1,3]dioxol-5-ol (4d) was prepared (*GP2*) from **3d** (1.39 g, 5.74 mmol), triethylamine (0.871 g, 8.61 mmol), methyl chloroformate (0.624 g, 6.60 mmol) in THF (40 mL). After filtration, the solution was reduced to half of the volume by solvent evaporation at the rotary evaporator before sodium borohydride (0.868 g, 23.0 mmol in 20 mL water) was added. Purification of the crude material by flash chromatography (silica gel, eluent: *n*-pentane:EtOAc = 19:1 → 8:2) yielded **4c** (1.18 g, 90%) as colorless solid (literature known compound: ref. [3]); m.p. 67 °C.

4d (CG255/CG702)
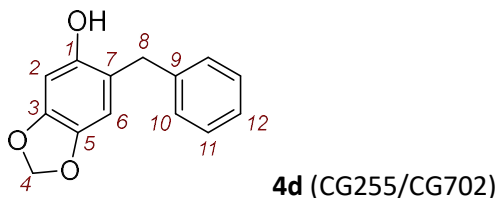
R_f (*n*-pentane/EtOAc = 9:1, silica, UV) = 0.58.

¹H NMR (600 MHz, CDCl₃): δ 7.31–7.29 (m, 2 H), 7.23–7.21 (m, 3 H), 6.60 (s, 1 H), 6.41 (s, 1 H), 5.89 (s, 2 H), 4.38 (s, 1 H), 3.90 ppm (s, 2 H).

¹³C{¹H} NMR (151 MHz, CDCl₃): δ 148.2, 146.8, 141.7, 140.0, 128.9, 128.6, 126.6, 118.9, 110.2, 101.2, 98.8, 36.3 ppm.

HRMS (EI): *m/z* calcd for $C_{14}H_{12}O_3{}^{\bullet+}$ [$M^{\bullet+}$]: 228.0781; found: 228.0782.

IR (neat, ATR): ṽ 3435, 2917, 1508, 1442, 1429, 1293, 1270, 1172, 1028, 934, 920, 903, 856, 819, 767, 735, 716, 696 cm⁻¹.

6-(4-Chlorobenzyl)benzo[*d*][1,3]dioxol-5-ol (4e) was prepared (*GP2*) from **3e** (0.940 g, 3.40 mmol), triethylamine (0.516 g, 5.10 mmol), methyl chloroformate (0.369 g, 3.91 mmol) in THF (40 mL). After filtration, the solution was reduced to half of the volume by solvent evaporation at the rotary evaporator before sodium borohydride (0.514 g, 13.6 mmol in 20 mL water) was added. Purification of the crude material by flash chromatography (silica gel, eluent: *n*-pentane:EtOAc = 9:1) gave **4e** (0.832 g, 93%) as a white solid; m.p. 105°C.

4e (CG308)
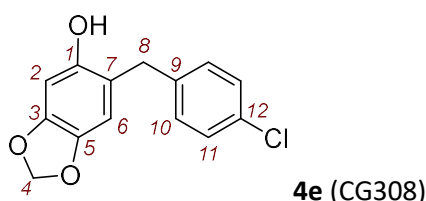
*R*f (*n*-pentane/EtOAc = 9:1, silica, UV) = 0.35.

¹H NMR (600 MHz, CDCl₃): δ 7.25 (d, *J* = 8.7 Hz, 2 H, 11-H), 7.14 (d, *J* = 8.7 Hz, 2 H, 10-H), 6.56 (s, 1 H, 6-H), 6.39 (s, 1 H, 2-H), 5.89 (s, 2 H, 4-H), 4.37 (s, 1 H, 1-OH), 3.85 ppm (s, 2 H, 8-H).

¹³C{¹H} NMR (151 MHz, CDCl₃): δ 148.0 (C_q, C-1), 146.8 (C_q, C-3), 141.8 (C_q, C-5), 138.8 (C_q, C-9), 132.2 (C_q, C-12), 130.0 (CH, C-10), 128.8 (CH, C-11), 118.6 (C_q, C-7), 110.1 (CH, C-6), 101.2 (CH₂, C-4), 98.7 (CH, C-2), 35.5 ppm (CH₂, C-8).

HRMS (EI): *m/z* calcd for C₁₄H₁₁³⁵ClO₃•⁺ [M•⁺]: 262.0391; found: 262.0389.

IR (neat, ATR): ṽ 3458, 2889, 1506, 1488, 1443, 1431, 1179, 1032, 1012, 917, 810, 782, 761 cm⁻¹.

6-(3-Fluorobenzyl)benzo[*d*][1,3]dioxol-5-ol (4f) was prepared (*GP2*) from **3f** (0.900 g, 3.46 mmol), triethylamine (0.525 g, 5.19 mmol), methyl chloroformate (0.376 g, 3.98 mmol) in THF (30 mL). After filtration, the solution was reduced to half of the volume by solvent evaporation at the rotary evaporator before sodium borohydride (0.523 g, 13.8 mmol in 15 mL water) was added. Purification of the crude material by flash chromatography (silica gel, eluent: *n*-pentane:EtOAc = 9:1) furnished **4f** (0.665 g, 78%) as a white solid (contaminated with traces of EtOAc).

4f (CG312

*R*f (*n*-pentane/EtOAc = 9:1, silica, UV) = 0.30.

¹H NMR (600 MHz, CDCl₃): δ 7.26–7.22 (m, 1 H, 11-H), 6.99 (d, *J* = 8.1 Hz, 1 H, 10-H), 6.91–6.88 (m, 2 H, 12-H, 14-H), 6.58 (s, 1 H, 6-H), 6.40 (s, 1 H, 2-H), 5.89 (s, 2H, 4-H), 4.50 (s, 1 H, 1-OH), 3.88 ppm (s, 2 H, 8-H).

¹³C{¹H} NMR (151 MHz, CDCl₃): δ 163.2 (C_q, d, ¹J_{C,F} = 245.8 Hz, C-13), 148.1 (C_q, C-1), 146.9 (C_q, C-3), 143.1 (C_q, d, ³J_{C,F} = 7.1 Hz. C-9), 141.7 (C_q, C-5), 130.1 (CH, d, ³J_{C,F} = 8.3 Hz, C-11), 124.2 (CH, d, ⁴J_{C,F} = 2.7

_____

Hz, C-10), 118.3 (C_q, C-7), 115.6 (CH, d, $^2J_{C,F}$ = 21.3 Hz, C-14), 113.3 (CH, d, $^2J_{C,F}$ = 21.1 Hz, C-12), 110.2 (CH, C-6), 101.2 (CH_2, C-4), 98.7 (CH, C-2), 35.8 ppm (CH_2, d, $^4J_{C,F}$ = 1.7 Hz, C-8).

HRMS (EI): *m/z* calcd for $C_{14}H_{11}FO_3^{\bullet+}$ [M$^{\bullet+}$]: 246.0687; found: 246.0683.

IR (neat, ATR): $\tilde{v}$ 3502, 3230, 2907, 1614, 1588, 1504, 1484, 1458, 1443, 1244, 1178, 1140, 1033, 929, 862, 753, 689 cm^{-1}.

6-(4-(Trifluoromethyl)benzyl)benzo[*d*][1,3]dioxol-5-ol (4g) was prepared (*GP2*) from **3g** (1.30 g, 4.19 mmol), triethylamine (0.636 g, 6.29 mmol), methyl chloroformate (0.455 g, 4.82 mmol) in THF (40 mL). After filtration, the solution was reduced to half of the volume by solvent evaporation at the rotary evaporator before sodium borohydride (0.634 g, 16.8 mmol in 20 mL water) was added. Purification of the crude material by flash chromatography (silica gel, eluent: *n*-pentane:EtOAc = 9:1) yielded **4g** (1.05 g, 85%) as a white solid; m.p. 110 °C.

4g (CG327)

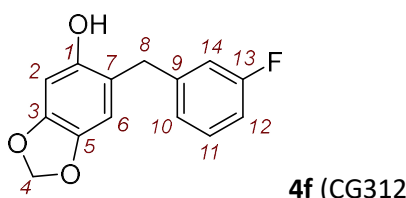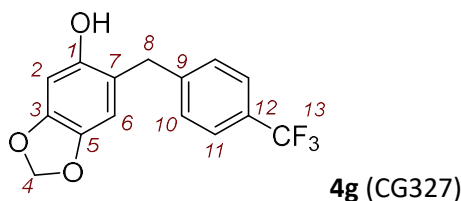R_f (*n*-pentane/EtOAc = 9:1, silica, UV) = 0.30.

¹H NMR (600 MHz, CDCl₃): δ 7.53 (d, *J* = 8.2 Hz, 2 H, 11-H), 7.32 (d, *J* = 7.9 Hz, 2 H, 10-H), 6.58 (s, 1 H, 6-H), 6.39 (s, 1 H, 2-H), 5.90 (s, 2 H, 4-H), 4.43 (s, 1 H, 1-OH), 3.94 ppm (s, 2 H, 8-H).

¹³C{¹H} NMR (151 MHz, CDCl₃): δ 147.9 (C_q, C-1), 146.9 (C_q, C-3), 144.8 (C_q, q, $^5J_{C,F}$ = 1.3 Hz, C-9), 141.8 (C_q, C-5), 129.0 (CH, C-10), 128.6 (C_q, q, $^2J_{C,F}$ = 32.4 Hz, C-12), 125.6 (CH, q, $^3J_{C,F}$ = 3.8 Hz, C-11), 124.4 (C_q, q, $^1J_{C,F}$ = 271.9 Hz, C-13), 118.2 (C_q, C-7), 110.2 (CH, C-6), 101.3 (CH_2, C-4), 98.6 (CH, C-2), 35.9 ppm (CH_2, C-8).

HRMS (EI): *m/z* calcd for $C_{15}H_{11}F_3O_3^{\bullet+}$ [M$^{\bullet+}$]: 296.0655; found: 296.0653.

IR (neat, ATR): $\tilde{v}$ 3471, 1617, 1512, 1494, 1446, 1427, 1328, 1184, 1156, 1101, 1068, 1034, 920, 818, 764 cm^{-1}.

6-(4-Nitrobenzyl)benzo[*d*][1,3]dioxol-5-ol (4h) was prepared (*GP2*) from **3h** (0.805 g, 2.80 mmol), triethylamine (0.425 g, 4.20 mmol), methyl chloroformate (0.305 g, 3.23 mmol) in THF (30 mL). After filtration, the solution was reduced to half of the volume by solvent evaporation at the rotary evaporator before sodium borohydride (0.424 g, 11.2 mmol in 15 mL water) was added. Purification of the crude material by flash chromatography (silica gel, eluent: *n*-pentane:EtOAc = 8:2) gave **4h** (0.630 g, 82%) as an orange solid; m.p. 156 °C.

4h (CG328 - but NMR spectra are named CG329!)
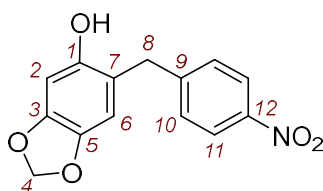
R_f (*n*-pentane/EtOAc = 8:2, silica, UV) = 0.30.

1H NMR (400 MHz, d_6-DMSO): δ 9.23 (s, 1 H, 1-OH), 8.12 (d, J = 8.9 Hz, 2 H, 11-H), 7.45 (d, J = 8.9 Hz, 2 H, 10-H), 6.74 (s, 1 H, 6-H), 6.45 (s, 1 H, 2-H), 5.87 (s, 2 H, 4-H), 3.90 ppm (s, 2 H, 8-H).

13C{1H} NMR (101 MHz, d_6-DMSO): δ 150.1 (C_q, C-12), 149.5 (C_q, C-1), 146.1 (C_q, C-3), 145.7 (C_q, C-9), 139.7 (C_q, C-5), 129.5 (CH, C-10), 123.4 (CH, C-11), 117.3 (C_q, C-7), 109.9 (CH, C-6), 100.6 (CH_2, C-4), 97.7 (CH, C-2), 35.0 ppm (CH_2, C-8).

HRMS (EI): *m/z* calcd for $C_{14}H_{11}NO_5^{\bullet+}$ [M$^{\bullet+}$]: 273.0632; found: 273.0634.

IR (neat, ATR): $\tilde{v}$ 3412, 2902, 1597, 1503, 1439, 1341, 1172, 1031, 925, 877, 860, 739, 699 cm^{-1}.

6-((Pentafluorophenyl)methyl)benzo[*d*][1,3]dioxol-5-ol (4i) was prepared (*GP2*) from **3i** (1.14 g, 3.43 mmol), triethylamine (0.533 g, 5.27 mmol), methyl chloroformate (0.382 g, 4.04 mmol) in THF (40 mL). After filtration, the solution was reduced to half of the volume by solvent evaporation at the rotary evaporator before sodium borohydride (0.531 g, 14.0 mmol in 20 mL water) was added. Purification of the crude material by flash chromatography (silica gel, eluent: *n*-pentane:EtOAc = 4:1) furnished **4i** (0.916 g, 2.89 mmol, 84%) as an off-white solid; m.p. 121 °C.

4i (LW03)
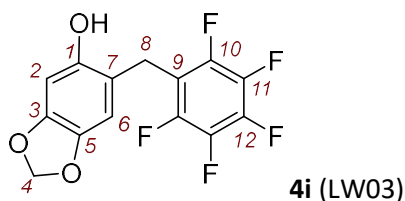
1H NMR (600 MHz, CDCl$_3$): δ 6.55 (s, 1 H, 6-H), 6.35 (s, 1 H, 2-H), 5.88 (s, 2 H, 4-H), 4.69 (br s, 1 H, 1-OH), 3.93 ppm (s, 2 H, 8-H).

13C{1H} NMR (151 MHz, CDCl$_3$): δ 147.8 (C_q, C-1), 147.1 (C_q, C-2), 145.3 (C_q, dm, $^1J_{C,F}$ = 246 Hz, C-10), 141.8 (C_q, C-5), 140.0 (C_q, dm, $^1J_{C,F}$ = 252.1 Hz, C-12), 137.6 (C_q, dm, $^1J_{C,F}$ = 250 Hz, C-11), 115.6 (C_q, C-7), 114.0 (C_q, td, $J_{C,F}$ = 18.5, 3.9 Hz, C-9), 109.4 (CH, br t, J = 1.6 Hz, C-6), 101.4 (CH_2, C-4), 98.5 (CH, C-2), 22.5 ppm (CH_2, C-8).

19F NMR (376 MHz, CDCl$_3$): δ −142.6 (dd, J = 21.8, 8.8 Hz, 2 F, 10-F), −157.3 (t, J = 20.8 Hz, 1 F, 12-F), −162.3 to −162.8 ppm (m, 2 F, 11-F).

HRMS (EI): *m/z* calcd for $C_{14}H_7F_5O_3^{\bullet+}$ [M$^{\bullet+}$]: 318.0310; found: 318.0311.

IR (neat, ATR): $\tilde{v}$ 3274, 2926, 1500, 1492, 1444, 1421, 1403, 1260, 1192, 1169, 1121, 1032, 994, 963, 930, 862, 825 cm^{-1}.

Synthesis of *o*QMs 1

General Procedure (GP3)

The phenols **3** were dissolved in dry diethyl ether under argon atmosphere and treated with silver(I) oxide. The reaction mixture was stirred at 42°C for 5 h. Then the mixture was filtered. The volume of the filtrate was reduced to one third of the original volume by solvent evaporation at the rotary evaporator. Crystals formed upon cooling the remaining solution in a freezer (−18 °C). The crystalline products were isolated by filtration.

_____

(*E*)-6-(4-(Dimethylamino)benzylidene)benzo[*d*][1,3]dioxol-5(6*H*)-one (1a) was prepared (*GP3*) from **4a** (0.800 g, 2.95 mmol) and silver(I) oxide (2.05 g, 8.85 mmol) in diethyl ether (80 mL). The reaction mixture was filtered, and the filtration residue was washed with acetone (100 mL). The combined organic phases were evaporated to dryness. The red residue was dissolved in acetone (30 mL). The volume of the acetone solution was reduced to ca. 10 mL by solvent evaporation at the rotary evaporator, which led to precipitation of *o*QM **1a** (0.352 g, 44%) as dark-red crystals; m.p. 124 °C.

1a (CG252)   cv086
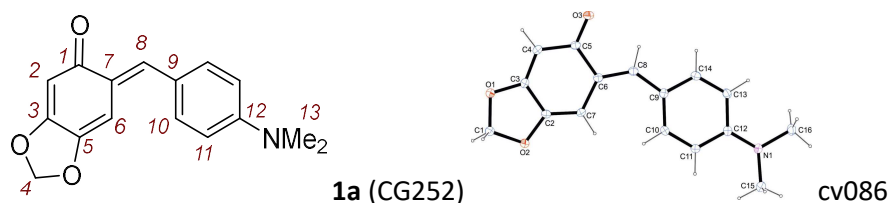
¹H NMR (400 MHz, d_6-DMSO): δ 7.62 (s, 1 H, 8-H), 7.56 (d, *J* = 9.1 Hz, 2 H, 10-H), 6.87 (s, 1 H, 6-H), 6.78 (d, *J* = 9.1 Hz, 2 H, 11-H), 6.03 (s, 2 H, 4-H), 5.90 (s, 1 H, 2-H), 3.03 ppm (s, 6 H, 13-H).

¹³C{¹H} NMR (101 MHz, d_6-DMSO): δ 183.7 (C_q, C-1), 160.8 (C_q, C-3), 151.4 (C_q, C-12), 145.0 (C_q, C-5), 141.9 (CH, C-8), 133.2 (CH, C-10), 125.8 (C_q, C-7), 122.2 (C_q, C-9), 112.1 (CH, C-11), 102.3 (CH_2, C-4), 100.8 (CH, C-2), 99.1 (CH, C-6), 39.6 ppm (CH_3, C-13).

HRMS (pos. ESI): *m/z* calcd for $C_{16}H_{16}NO_3^+$ [M + H]⁺: 270.1125; found: 270.1125.

IR (neat, ATR): $\tilde{\nu}$ = 2916, 1660, 1602, 1501, 1421, 1410, 1362, 1210, 1188, 1169, 1030, 952, 943, 811, 704 cm⁻¹.

(*E*)-6-(4-Methoxybenzylidene)benzo[*d*][1,3]dioxol-5(6*H*)-one (**1b**) was prepared (*GP3*) from **4b** (1.00 g, 3.87 mmol) and silver(I) oxide (2.24 g, 9.67 mmol) in diethyl ether (90 mL) to yield the *o*QM **1b** (0.410 g, 41%) as orange crystals (literature known compound: ref. [5]); m.p. 131 °C.

1b (CG197)
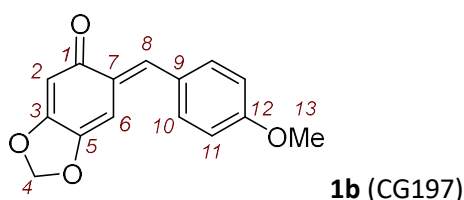
¹H NMR (400 MHz, CDCl₃): δ 7.89 (s, 1 H), 7.49 (d, *J* = 8.8 Hz, 2 H), 6.96 (d, *J* = 8.8 Hz, 2 H), 6.71 (s, 1 H), 5.97 (s, 1 H), 5.89 (s, 2 H), 3.86 ppm (s, 3 H).

¹³C{¹H} NMR (101 MHz, CDCl₃): δ 185.7, 161.5, 161.0, 146.2, 142.3, 132.6, 129.2, 128.3, 114.6, 102.0, 101.9, 99.4, 55.6 ppm.

¹H NMR (400 MHz, d_6-DMSO): δ 7.64 (s, 1 H), 7.62 (d, *J* = 8.9 Hz, 2 H), 7.04 (d, *J* = 8.9 Hz, 2 H), 6.77 (s, 1 H), 6.06 (s, 2 H), 5.94 (s, 1 H), 3.82 ppm (s, 3 H).

¹³C{¹H} NMR (101 MHz, d_6-DMSO): δ 184.1, 161.5, 160.6, 146.4, 140.1, 132.7, 128.4, 127.5, 114.6, 102.7, 100.6, 98.1, 55.4 ppm.

HRMS (pos. ESI): *m/z* calcd for $C_{15}H_{13}O_4^+$ [M + H]⁺: 257.0808; found: 257.0804.

IR (neat, ATR): $\tilde{\nu}$ 2929, 2841, 1619, 1598, 1540, 1507, 1410, 1361, 1251, 1218, 1201, 1176, 1023, 944, 827, 764 cm⁻¹.

(*E*)-6-(4-Methylbenzylidene)benzo[*d*][1,3]dioxol-5(6H)-one (1c) was prepared (*GP3*) from **4c** (0.980 g, 4.05 mmol) and silver(I) oxide (2.81 g, 12.1 mmol) in diethyl ether (90 mL) to yield the *o*QM **1c** (0.290 g, 30%) as orange crystals; m.p. 119 °C.

1c (LL05_DMSO/CG705)   zv536
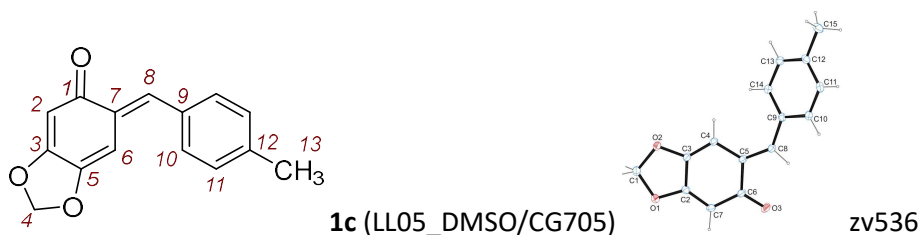
¹H NMR (400 MHz, d_6-DMSO): δ 7.64 (s, 1 H, 8-H), 7.51 (d, *J* = 8.3 Hz, 2 H, 10-H), 7.29 (d, *J* = 8.1 Hz, 2 H, 11-H), 6.72 (s, 1 H, 6-H), 6.07 (s, 2 H, 4-H), 5.95 (s, 1 H, 2-H), 2.35 ppm (s, 3 H, 13-H).

¹³C{¹H} NMR (101 MHz, d_6-DMSO): δ 184.1 (C_q, C-1), 161.6 (C_q, C-3), 146.7 (C_q, C-5), 140.0 (CH, C-8), 139.7 (C_q, C-12), 132.1 (C_q, C-9), 130.5 (CH, C-10), 129.6 (CH, C-11), 129.5 (C_q, C-7), 102.7 (CH_2, C-4), 100.5 (CH, C-2), 97.9 (CH, C-6), 21.0 ppm (CH_3, C-13).

IR (neat, ATR): $\tilde{v}$ 2907, 1661, 1620, 1537, 1503, 1422, 1362, 1225, 1179, 1036, 952, 853, 839, 812, 774 cm⁻¹.

HRMS (pos. ESI): *m/z* calcd for $C_{15}H_{13}O_3^+$ [M + H⁺]: 241.0859; found: 241.0855.

Elemental Analysis: Calcd (%) for $C_{15}H_{13}O_3$: C 74.99, H 5.03; found: C 74.83, H 4.92.

(*E*)-6-Benzylidenebenzo[*d*][1,3]dioxol-5(6*H*)-one (1d) was prepared (*GP3*) from **4d** (0.705 g, 3.09 mmol) and silver(I) oxide (2.15 g, 9.27 mmol) in diethyl ether (80 mL) to furnish the oQM **1d** (0.248 g, 36%) as yellow crystals; m.p. 77.0°C.

1d (CG259_1/CG704)
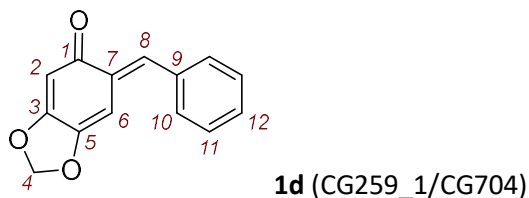
¹H NMR (600 MHz, d_6-DMSO): δ 7.68 (s, 1 H, 8-H), 7.60 (d, *J* = 7.3 Hz, 2 H, 10-H), 7.49–7.42 (m, 3 H, 11-H, 12-H), 6.70 (s, 1 H, 6-H), 6.08 (s, 2 H, 4-H), 5.97 ppm (s, 1 H, 2-H).

¹³C{¹H} NMR (101 MHz, d_6-DMSO): δ 184.2 (C_q, C-1), 161.8 (C_q, C-3), 147.0 (C_q, C-5), 139.7 (CH, C-8), 134.9 (C_q, C-9), 130.4 (CH, C-10), 130.1 (C_q, C-7), 129.5 (CH, C-12), 129.0 (CH, C-11), 102.8 (CH_2, C-4), 100.5 (CH, C-2), 97.7 (CH, C-6).

HRMS (pos. ESI): *m/z* calcd for $C_{14}H_{11}O_3^+$ [M + H⁺]: 227.0703; found: 227.0705.

IR (neat, ATR): $\tilde{v}$ 2928, 1627, 1572, 1550, 1490, 1445, 1411, 1359, 1222, 1197, 1112, 1023, 942, 829, 749, 692 cm⁻¹.

(*E*)-6-(4-Chlorobenzylidene)benzo[*d*][1,3]dioxol-5(6*H*)-one (1e) was prepared (*GP3*) from **4e** (0.560 g, 2.13 mmol) and silver(I) oxide (1.48 g, 6.39 mmol) in diethyl ether (50 mL) to yield the *o*QM **1e** (0.250 g, 45%) as yellow crystals; m.p. 150 °C.
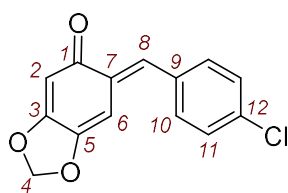
1e (CG309)

¹H NMR (400 MHz, d_6-DMSO): δ 7.64–7.62 (m, 3 H, 8-H, 10-H), 7.52 (d, *J* = 8.8 Hz, 2 H, 11-H), 6.68 (s, 1 H, 6-H), 6.08 (s, 2 H, 4-H), 5.97 ppm (s, 1 H, 2-H).

¹³C{¹H} NMR (101 MHz, d_6-DMSO): δ 184.0 (C_q, C-1), 161.8 (C_q, C-3), 147.3 (C_q, C-5), 138.1 (CH, C-8), 134.1 (C_q, C-12), 133.8 (C_q, C-9), 132.1 (CH, C-10), 130.5 (C_q, C-7), 129.0 (CH, C-11), 102.9 (CH_2, C-4), 100.5 (CH, C-2), 97.4 ppm (CH, C-6).

HRMS (ESI⁺): *m/z* calcd for $C_{14}H_{10}{}^{35}ClO_3{}^+$ [M + H⁺]: 261.0313; found: 261.0313.

IR (neat, ATR): $\tilde{v}$ = 1632, 1549, 1486, 1420, 1400, 1360, 1223, 1198, 1026, 944, 836, 820 cm⁻¹.

(*E*)-6-(3-Fluorobenzylidene)benzo[*d*][1,3]dioxol-5(6*H*)-one (1f) was prepared (*GP3*) from **4f** (0.360 g, 1.46 mmol) and silver(I) oxide (1.02 g, 4.40 mmol) in diethyl ether (40 mL) to yield the *o*QM **1f** (0.101 g, 0.410 mmol, 28%) as yellow-brown crystals; m.p. >105 °C (dec.).
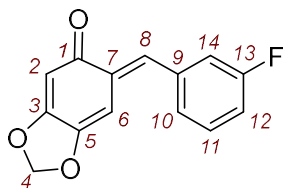
1f (CG313)

¹H NMR (400 MHz, d_6-DMSO): δ 7.62 (s, 1 H, 8-H), 7.54–7.48 (m, 1 H, 11-H), 7.44–7.41 (m, 2 H, 10-H and 14-H), 7.29–7.24 (m, 1 H, 12-H), 6.67 (s, 1 H, 6-H), 6.08 (s, 2 H, 4-H), 5.97 ppm (s, 1 H, 2-H).

¹³C{¹H} NMR (101 MHz, d_6-DMSO): δ 184.0 (C_q, C-1), 162.2 (C_q, d, $^1J_{C,F}$ = 244.4 Hz, C-13), 161.8 (C_q, C-3), 147.4 (C_q, C-5), 137.9 (CH, d, $^4J_{C,F}$ = 2.6 Hz, C-8), 137.2 (C_q, d, $^3J_{C,F}$ = 8.0 Hz, C-9), 130.9 (C_q, C-7), 130.9 (CH, d, $^3J_{C,F}$ = 8.5 Hz, C-11), 126.4 (CH, d, $^4J_{C,F}$ = 2.8 Hz, C-10), 116.7 (CH, d, $^2J_{C,F}$ = 21.9 Hz, C-14), 116.2 (CH, d, $^2J_{C,F}$ = 21.2 Hz, C-12), 102.9 (CH_2, C-4), 100.4 (CH, C-2), 97.4 ppm (CH, C-6).

¹⁹F NMR (376 MHz, d_6-DMSO): δ −112.44 to −112.51 ppm (m).

HRMS (pos. ESI): *m/z* calcd for $C_{14}H_{10}FO_3{}^+$ [M + H⁺]: 245.0608; found: 245.0608.

IR (neat, ATR): $\tilde{v}$ 2926, 1634, 1624, 1580, 1550, 1427, 1404, 1366, 1212, 1027, 936, 866, 838, 818, 776, 756, 679 cm⁻¹.

(*E*)-6-(4-(Trifluoromethyl)benzylidene)benzo[*d*][1,3]dioxol-5(6*H*)-one (1g) was prepared (*GP3*) from **4g** (0.785 g, 2.65 mmol) and silver(I) oxide (1.84 g, 7.94 mmol) in diethyl ether (80 mL) to give the *o*QM **1g** (0.308 g, 1.05 mmol, 40%) as yellow crystals; m.p. 145 °C.
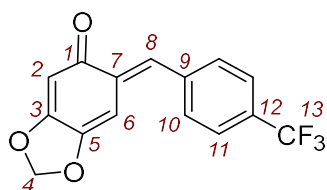
1g (CG329)

¹H NMR (400 MHz, d_6-DMSO): δ 7.82–7.77 (m, 4 H, 10-H and 11-H), 7.68 (s, 1 H, 8-H), 6.66 (s, 1 H, 6-H), 6.09 (s, 2 H, 4-H), 5.99 ppm (s, 1 H, 2-H).

¹³C{¹H} NMR (101 MHz, d_6-DMSO): δ 184.0 (C_q, C-1), 162.0 (C_q, C-3), 147.8 (C_q, C-5), 139.0 (C_q, C-9), 137.3 (CH, C-8), 131.6 (C_q, C-7), 130.9 (CH, C-10), 128.9 (C_q, q, $^2J_{C,F}$ = 31.9 Hz, C-12), 125.7–125.6 (CH, m, C-11), 124.1 (C_q, q, $^1J_{C,F}$ = 272 Hz, C-13), 103.1 (CH_2, C-4), 100.4 (CH, C-2), 97.1 ppm (CH, C-6).

¹⁹F NMR (377 MHz, d_6-DMSO): δ = −61.2 ppm.

HRMS (pos. ESI): m/z calcd for $C_{15}H_{10}F_3O_3^+$ [M + H$^+$]: 295.0577; found: 295.0575.

IR (neat, ATR): $\tilde{v}$ 2927, 1628, 1552, 1420, 1318, 1224, 1200, 1161, 1106, 1064, 1033, 1015, 951, 834, 824, 662 cm^{-1}.

(*E*)-6-(4-Nitrobenzylidene)benzo[*d*][1,3]dioxol-5(6*H*)-one (1h) was prepared (*GP3*) from **4h** (0.300 g, 1.10 mmol) and silver(I) oxide (0.763 g, 3.29 mmol) in diethyl ether (40 mL). The reaction mixture was filtered, and the collected solid was washed with acetone (25 mL). The combined organic phases were evaporated to dryness and the red residue was dissolved in acetone (30 mL). The volume of the solution reduced to one third of the initial volume. Upon cooling **1h** precipitated as red crystals (0.075 g, 0.280 mmol, 25%); m.p. >170 °C (dec.).

1h (CG330_2)   av216
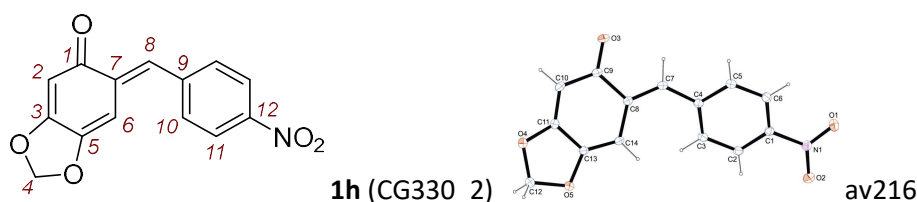
¹H NMR (400 MHz, d_6-DMSO): δ 8.27 (d, J = 8.9 Hz, 2 H, 11-H), 7.84 (d, J = 8.9 Hz, 2 H, 10-H), 7.68 (s, 1 H, 8-H), 6.67 (s, 1 H, 6-H), 6.11 (s, 2 H, 4-H), 6.01 ppm (s, 1 H, 2-H).

¹³C{¹H} NMR (101 MHz, d_6-DMSO): δ 184.0 (C_q, C-1), 162.0 (C_q, C-3), 148.3 (C_q, C-5), 147.1 (C_q, C-12), 141.7 (C_q, C-9), 136.3 (CH, C-8), 132.2 (C_q, C-7), 131.4 (CH, C-10), 123.8 (CH, C-11), 103.2 (CH_2, C-4), 100.4 (CH, C-2), 97.0 ppm (CH, C-6).

HRMS (neg. ESI): m/z calcd for $C_{14}H_{10}NO_5^-$ [M + H$^-$]: 272.0564; found: 272.0564.

IR (neat, ATR): $\tilde{v}$ 2924, 1621, 1586, 1540, 1506, 1423, 1338, 1222, 1108, 1032, 949, 912, 850, 748, 676 cm^{-1}.

6-((Perfluorophenyl)methyl)-7a-((6-((perfluorophenyl)methyl)benzo[*d*][1,3]dioxol-5-yl)oxy)benzo-[*d*][1,3]dioxol-5(7a*H*)-one (5) was prepared (*GP3*) from **4i** (0.900 g, 2.83 mmol) and silver(I) oxide (1.97 g, 8.50 mmol) in diethyl ether (90 mL) to deliver **5** (0.685 g, 76%) as yellow crystals; m.p. 118 °C (dec.).

_____
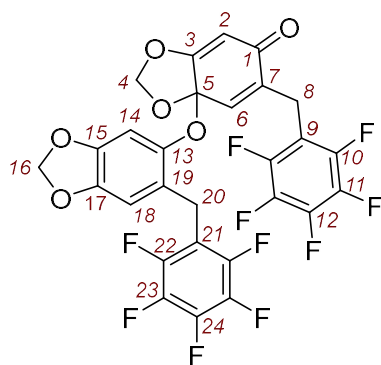
5 (LW04)
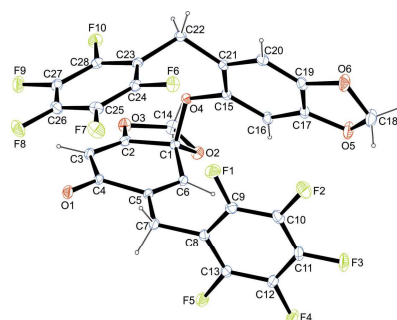
bv341

¹H NMR (600 MHz, CDCl₃): δ 6.76 (s, 1 H), 6.48 (s, 1 H), 6.26 (s, 1 H), 5.93–5.69 (m, 5 H), 3.78–3.58 ppm (m, 4 H).

IR (neat, ATR): $\tilde{\nu}$ 1685, 1656, 1635, 1518, 1503, 1484, 1208, 1159, 1120, 1030, 1013, 998, 960, 894, 864 cm⁻¹.

Elemental Analysis: Calcd (%) for $C_{28}H_{12}F_{10}O_6$: C 53.01, H 1.91; found: C 53.00, H 1.98.

5.2.3. Products of Reactions of *ortho*-Quinone Methides with Nucleophiles

General Procedure (GP4):

A solution of the nucleophile (1.0 to 1.5 equiv.) in d_6-DMSO (1.0 mL) was mixed with *o*QM **1** in a standard GC vial by sonication. Then, the reaction mixture was left for the specified reaction time at room temperature (23 °C). Subsequently, the mixture was quenched with sat. aq. ammonium chloride solution (1 mL), diluted with water (5 mL) and extracted with diethyl ether (4 × 10 mL). The combined organic phases were washed with water (4 × 10 mL) and dried over MgSO₄. The solvent was removed under reduced pressure at the rotary evaporator. The residue was further purified either by chromatography or crystallization and characterized by spectroscopic methods.

5a-Hydroxy-10-(4-methoxyphenyl)-7,7-dimethyl-5a,6,7,8,9a,10-hexahydro-9*H*-[1,3]dioxolo[4,5-b]xanthen-9-one (6ba) was synthesized by mixing **1b** (257 mg, 1.00 mmol) and **2a** (190 mg, 1.07 mmol) in DMSO (5 mL). The reaction mixture was stirred for 15 h. Aqueous workup (*GP4*) gave a crude product which was purified by column chromatography (silica gel, eluent: *n*-pentane:EtOAc = 8:2) to give **6ba** (355 mg, 90%) as a white solid; m.p. 167 °C (dec.).
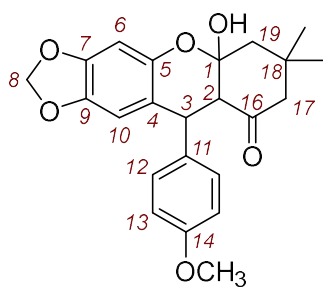
6ba (CG307)
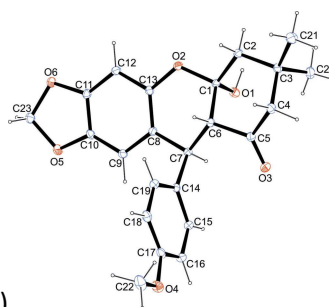
av494

_____

R_f (*n*-pentane/EtOAc 8:2, silica, UV) = 0.30.

¹H NMR (800 MHz, CDCl₃): δ 7.17 (d, *J* = 8.4 Hz, 2 H, 12-H), 6.80 (d, *J* = 8.9 Hz, 2 H, 13-H), 6.36 (s, 1 H, 6-H), 6.18 (s, 1 H, 10-H), 5.84 (d, *J* = 1.4 Hz, 1 H, 8-Hᵃ), 5.81 (d, *J* = 1.4 Hz, 1 H, 8-Hᵇ), 4.39 (d, *J* = 11.6 Hz, 1 H, 3-H), 3.77 (s, 3 H, 14-OCH₃), 3.07 (d, *J* = 11.6 Hz, 1 H, 2-H), 2.40 (s, 1 H, 1-OH), 2.34 (d, *J* = 12.6 Hz, 1 H, 17-Hᵃ), 2.29 (d, *J* = 14.4 Hz, 1 H, 19-Hᵃ), 2.14 (d, *J* = 12.6 Hz, 1 H, 17-Hᵇ), 2.05 (d, *J* = 14.4 Hz, 1 H, 19-Hᵇ), 1.15 (s, 3 H, 18-CH₃ᵃ), 1.13 ppm (s, 3 H, 18-CH₃ᵇ).

¹³C{¹H} NMR (201 MHz, CDCl₃): δ 204.8 (C_q, C-16), 158.3 (C_q, C-14), 146.9 (C_q, C-7), 145.1 (C_q, C-5), 142.6 (C_q, C-9), 135.9 (C_q, C-11), 130.7 (CH, C-12), 118.3 (C_q, C-4), 113.9 (CH, C-13), 109.1 (CH, C-10), 101.1 (CH₂, C-8), 99.1 (C_q, C-1), 98.7 (CH, C-6), 58.3 (CH, C-2), 55.3 (CH₃, 14-OCH₃), 55.0 (CH₂, C-17), 49.7 (CH₂, C-19), 36.8 (CH, C-3), 33.9 (C_q, C-18), 33.4 (CH₃, 18-CH₃), 27.2 ppm (CH₃, 18-CH₃).

HRMS (neg. ESI): *m/z* calcd for C₂₃H₂₃O₆⁻ [M − H⁺]: 395.1500; found: 395.1497.

IR (neat, ATR): ṽ 3419, 1712, 1610, 1500, 1478, 1242, 1175, 1150, 1038, 1004, 930, 856 cm⁻¹.

1-(6-Hydroxy-8-(4-methoxyphenyl)-6-methyl-7,8-dihydro-6*H*-[1,3]dioxolo[4,5-*g*]chromen-7-yl)ethan-1-one (6bb) was prepared according to *GP4* (reaction time: 4 h) from **1b** (7.0 mg, 0.027 mmol) and **2b** (4.2 mg, 0.030 mmol). The crude product was purified by preparative TLC (silica gel, eluent: *n*-pentane:EtOAc = 8:2) to give **6bb** (4.2 mg, 44%) as a colorless oil; mixture of diastereomers (d.r. = 86:14).

6bb (CG202F1)

R_f (*n*-pentane/EtOAc 8:2, silica, UV) = 0.50.

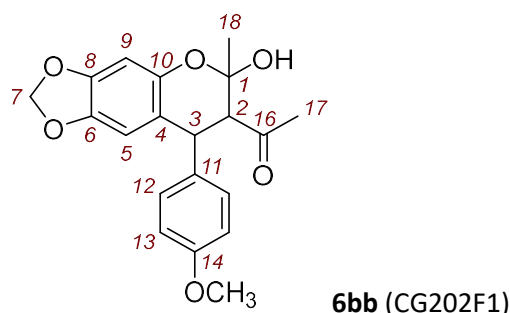**¹H NMR** (800 MHz, CDCl₃): δ 7.08 (d, *J* = 8.8 Hz, 2 H, 12-Hᵐᵃʲᵒʳ), 7.04 (d, *J* = 8.7 Hz, 2 H, 12-Hᵐⁱⁿᵒʳ), 6.86 (d, *J* = 8.8 Hz, 2 H, 13-Hᵐᵃʲᵒʳ), 6.81 (d, *J* = 8.8 Hz, 2 H, 13-Hᵐⁱⁿᵒʳ), 6.43 (s, 1 H, 9-Hᵐᵃʲᵒʳ), 6.39 (s, 1 H, 9-Hᵐⁱⁿᵒʳ), 6.14 (d, *J* = 1.0 Hz, 1 H, 5-Hᵐⁱⁿᵒʳ), 6.12 (d, *J* = 1.0 Hz, 1 H, 5-Hᵐᵃʲᵒʳ), 5.85–5.82 (m, 2 H, 7-Hᵐᵃʲᵒʳ⁺ᵐⁱⁿᵒʳ), 4.21 (d, *J* = 12.3 Hz, 2 H, 3-H), 4.01 (s, 2 H, 1-OH), 3.81 (s, 3 H, 14-OCH₃ᵐᵃʲᵒʳ), 3.79 (s, 3 H, 14-OCH₃ᵐⁱⁿᵒʳ), 3.39 (d, *J* = 11.9 Hz, 1 H, 2-Hᵐⁱⁿᵒʳ), 3.22 (d, *J* = 12.1 Hz, 1 H, 2-Hᵐᵃʲᵒʳ), 1.98 (s, 3 H, 17-Hᵐⁱⁿᵒʳ), 1.84 (s, 3 H, 17-Hᵐᵃʲᵒʳ), 1.56 (s, 3 H, 18-Hᵐᵃʲᵒʳ), 1.49 ppm (s, 3 H, 18-Hᵐⁱⁿᵒʳ).

¹³C{¹H} NMR (201 MHz, CDCl₃): δ 213.4 (C=O, C-16ᵐᵃʲᵒʳ), 208.7 (C=O, C-16ᵐⁱⁿᵒʳ), 159.1 (C_q, C-14ᵐᵃʲᵒʳ), 158.7 (C_q, C-14ᵐⁱⁿᵒʳ), 147.5 (C_q, C-8ᵐⁱⁿᵒʳ), 147.2 (C_q, C-8ᵐᵃʲᵒʳ), 146.2 (C_q, C-4, 2C), 142.3 (C_q, C-6ᵐⁱⁿᵒʳ), 142.3 (C_q, C-6ᵐᵃʲᵒʳ), 134.3 (C_q, C-11ᵐⁱⁿᵒʳ), 133.2 (C_q, C-11ᵐᵃʲᵒʳ), 130.1 (CH, C-12ᵐᵃʲᵒʳ), 130.1 (CH, C-12ᵐⁱⁿᵒʳ), 116.6 (C_q, C-10ᵐᵃʲᵒʳ), 116.5 (C_q, C-10ᵐⁱⁿᵒʳ), 114.6 (CH, C-13ᵐᵃʲᵒʳ), 114.3 (CH, C-13ᵐⁱⁿᵒʳ), 108.3 (CH, C-5ᵐⁱⁿᵒʳ), 107.8 (CH, C-5ᵐᵃʲᵒʳ), 101.2 (CH₂, C-7ᵐⁱⁿᵒʳ), 101.2 (CH₂, C-7ᵐᵃʲᵒʳ), 99.0 (CH, C-9ᵐⁱⁿᵒʳ), 98.8 (CH, C-9ᵐᵃʲᵒʳ), 98.6 (C_q, C-1ᵐⁱⁿᵒʳ), 95.4 (C_q, C-1ᵐᵃʲᵒʳ), 61.7 (CH, C-2ᵐⁱⁿᵒʳ), 60.8 (CH, C-2ᵐᵃʲᵒʳ), 55.4 (CH₃, 14-OCH₃ᵐᵃʲᵒʳ), 55.4 (CH₃, 14-OCH₃ᵐⁱⁿᵒʳ), 44.0 (CH, C-3ᵐⁱⁿᵒʳ), 43.3 (CH, C-3ᵐᵃʲᵒʳ), 34.4 (CH₃, C-17ᵐⁱⁿᵒʳ), 33.2 (CH₃, C-17ᵐᵃʲᵒʳ), 27.7 (CH₃, C-18ᵐᵃʲᵒʳ), 21.6 ppm (CH₃, C-18ᵐⁱⁿᵒʳ).

HRMS (EI): *m/z* calcd for C₂₀H₂₀O₆•⁺ [M•⁺]: 356.1254; found: 356.1246.

Ethyl 6-hydroxy-8-(4-methoxyphenyl)-6-methyl-7,8-dihydro-6*H*-[1,3]dioxolo[4,5-*g*]chromene-7-carboxylate (6bc) was prepared according to *GP4* (reaction time: 2 h) from **1b** (13.0 mg, 0.051 mmol) and **2c** (10.2 mg, 0.061 mmol). The crude product was purified by preparative TLC (silica gel, eluent: *n*-pentane:EtOAc = 7:3) to give **6bc** (12.7 mg, 64%) as a colorless oil; mixture of diastereomers (d.r. = 87:13).
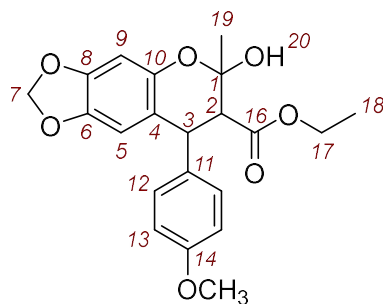

6bc (CG229)

R$_f$ (*n*-pentane/EtOAc 7:3, silica, UV) = 0.75.

^{1}H NMR (400 MHz, CDCl$_3$): *δ* 7.08 (d, *J* = 8.8 Hz, 2 H, 12-H^{major}), 7.06 (d, *J* = 4.6 Hz, 2 H, 12-H^{minor}), 6.84 (d, *J* = 8.8 Hz, 2 H, 13-H^{major}), 6.81 (d, *J* = 4.0 Hz, 2 H, 13-H^{minor}), 6.43 (s, 1 H, 9-H^{major}), 6.41 (s, 1 H, 9-H^{minor}), 6.14 (d, *J* = 1.0 Hz, 1 H, 5-H$^{major+minor}$), 5.85–5.81 (m, 2 H, 7-H$^{major+minor}$), 4.33 (d, *J* = 12.3 Hz, 1 H, 3-H^{major}), 4.24 (d, *J* = 11.9 Hz, 1 H, 3-H^{minor}), 4.04–3.98 (m, 4 H, 17-H$^{major+minor}$), 3.80 (s, 3 H, 14-OCH$_3$^{major}), 3.79 (s, 3 H, 14-OCH$_3$^{minor}), 3.67 (s, 2 H, 1-OH), 3.03 (d, *J* = 11.5 Hz, 1 H, 2-H^{minor}), 2.96 (d, *J* = 12.3 Hz, 1 H, 2-H^{major}), 1.63 (s, 3 H, 19-H^{major}), 1.58 (s, 3 H, 19-H^{minor}), 1.06 (t, *J* = 7.1 Hz, 3 H, 18-H^{minor}), 1.01 ppm (t, *J* = 7.1 Hz, 3 H, 18-H^{major}).

^{13}C{^{1}H} NMR (101 MHz, CDCl$_3$): *δ* 173.3 (C$_q$, C-16^{major}), 171.0 (C=O, C-16^{minor}), 159.0 (C$_q$, C-14^{major}), 158.9 (C$_q$, C-14^{minor}), 147.6 (C$_q$, C-6^{minor}), 147.3 (C$_q$, C-4^{minor}), 147.1 (C$_q$, C-6^{major}), 146.1 (C$_q$, C-4^{major}), 142.3 (C$_q$, C-8, C-8$^{major+minor}$), 133.8 (C$_q$, C-11^{minor}), 133.4 (C$_q$, C-11^{major}), 130.3 (CH, C-12^{major}), 130.1 (CH, C-12^{minor}), 116.5 (C$_q$, C-10^{major}), 115.9 (C$_q$, C-10^{minor}), 114.2 (CH, C-13^{major}), 114.2 (CH, C-13^{minor}), 108.3 (CH, C-5^{minor}), 108.1 (CH, C-5^{major}), 101.2 (CH$_2$, C-7^{minor}), 101.1 (CH$_2$, C-7^{major}), 98.8 (CH, C-9^{major}), 98.7 (CH, C-9^{minor}), 95.5 (C$_q$, C-1$^{major+minor}$), 61.3 (CH$_2$, C-17^{major}), 61.2 (CH$_2$, C-17^{minor}), 57.9 (CH, C-2^{minor}), 55.5 (CH, C-2^{major}), 55.4 (CH$_3$, 14-OCH$_3$^{major}), 55.4 (CH$_3$, 14-OCH$_3$^{minor}), 44.5 (CH, C-3^{minor}), 42.2 (CH, C-3^{major}), 27.8 (CH$_3$, C-19^{major}), 21.0 (CH$_3$, C-19^{minor}), 14.2 (CH$_3$, C-18^{minor}), 14.1 ppm (CH$_3$, C-18^{major}).

HRMS (EI): *m/z* calcd for C$_{21}$H$_{22}$O$_7$$^{•+}$ [M$^{•+}$]: 386.1360; found: 386.1363.

6-Amino-8-(4-methoxyphenyl)-8*H*-[1,3]dioxolo[4,5-*g*]chromene-7-carbonitrile (6bd) was prepared according to *GP4* (reaction time: 2 h) from **1b** (15.0 mg, 0.059 mmol) and **2d** (7.3 mg, 0.070 mmol). was prepared according to *GP4* (reaction time: 2 h). The crude product was purified by preparative TLC (silica gel, eluent: *n*-pentane:EtOAc:NEt$_3$ = 70:29:1) to give **6bd** (14.7 mg, 77%) as a colorless oil (known compound: ref. [6]).

6bd (CG225)

R_f (*n*-pentane/EtOAc/NEt$_3$ 70:29:1, silica, UV) = 0.20.

^{1}H NMR (800 MHz, CDCl$_3$): δ 7.10 (d, *J* = 8.7 Hz, 2 H, 12-H), 6.85 (d, *J* = 8.8 Hz, 2 H, 13-H), 6.50 (s, 1 H, 9-H), 6.34 (s, 1 H, 5-H), 5.92 (d, *J* = 1.5 Hz, 1 H, 7-H^a), 5.89 (d, *J* = 1.3 Hz, 1 H, 7-H^b), 4.58 (s, 1 H, 3-H), 4.53 (s, 2 H, 1-NH$_2$), 3.78 ppm (s, 3 H, 14-OCH$_3$).

^{13}C{^{1}H} NMR (201 MHz, CDCl$_3$): δ 159.1 (C$_q$, C-1), 158.9 (C$_q$, C-14), 147.3 (C$_q$, C-8), 144.9 (C$_q$, C-6), 143.1 (CH, C-10), 137.0 (C$_q$, C-11), 129.0 (CH, C-12), 120.0 (C$_q$, C-15), 115.3 (C$_q$, C-4), 114.3 (CH, C-13), 107.9 (CH, C-5), 101.8 (CH$_2$, C-7), 98.0 (CH, C-9), 61.0 (C$_q$, C-2), 55.4 (CH$_3$, 14-OCH$_3$), 40.6 ppm (CH, C-3).

HRMS (EI): *m/z* calcd for C$_{18}$H$_{14}$N$_2$O$_4$$^{•+}$ [M$^{•+}$]: 322.0948; found: 322.0949.
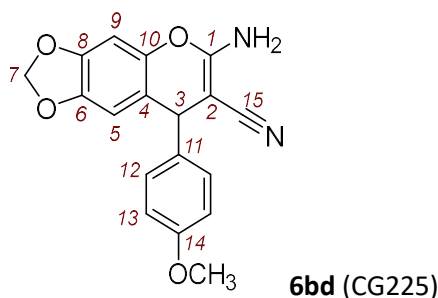
IR (neat, ATR): ṽ 2922, 2189, 1718, 1655, 1605, 1508, 1480, 1395, 1244, 1174, 1152, 1029, 831, 727 cm^{-1}.

Ethyl 2-cyano-3-(6-hydroxybenzo[*d*][1,3]dioxol-5-yl)-3-(4-methoxyphenyl)propanoate (7be) and 8-(4-Methoxyphenyl)-6-oxo-7,8-dihydro-6*H*-[1,3]dioxolo[4,5-*g*]chromene-7-carbonitrile (6be) were obtained according to *GP4* (reaction time: 12 h) from **1b** (20.0 mg, 0.078 mmol) and **2e** (12.4 mg, 0.082 mmol). The crude product was purified by preparative TLC (silica gel, eluent: *n*-pentane:EtOAc = 8:2) to yield **7be** (11.8 mg, 41%, mixture of diastereomers: d.r. = 54:46) and **6be** (9.5 mg, 38%, mixture of diastereomers. d.r. = 55:45).

7be (CG415_1)

R_f (*n*-pentane/EtOAc 8:2, silica, UV) = 0.15.

^{1}H NMR (599 MHz, CDCl$_3$): δ = 7.35 (d, *J* = 8.7 Hz, 2 H, 10-H^{major}), 7.24 (d, *J* = 8.7 Hz, 2 H, 10-H^{minor}), 6.88 (d, *J* = 8.8 Hz, 2 H, 11-H^{major}), 6.83 (d, *J* = 8.8 Hz, 2 H, 11-H^{minor}), 6.75 (s, 1 H, 6-H^{minor}), 6.55 (s, 1 H, 6-H^{major}), 6.37 (s, 1 H, 2-H^{minor}), 6.36 (s, 1 H, 2-H^{major}), 5.88 (s, 2 H, 4-H^{minor}), 5.86 (m, 2 H, 4-H^{major}), 5.39 (br s, 1 H, 1-OH^{minor}), 5.30 (br s, 1 H, 1OH^{major}), 4.96 (d, *J* = 8.2 Hz, 2 H, 8-H$^{major+minor}$), 4.47 (d, *J* = 8.2 Hz, 1 H, 14-H^{major}), 4.36 (d, *J* = 8.5 Hz, 1 H, 14-H^{minor}), 4.16–4.11 (m, 4 H, 16-H$^{major+minor}$), 3.79 (s, 3 H, 13-H^{major}), 3.77 (s, 3 H, 13-H^{minor}), 1.17 (t, *J* = 7.1 Hz, 3 H, 17-H^{minor}), 1.13 ppm (t, *J* = 7.2 Hz, 3 H, 17-H^{major}).

^{13}C{^{1}H} NMR (151 MHz, CDCl$_3$): δ 166.0 (C$_q$, C-15^{minor}), 165.7 (C$_q$, C-15^{major}), 159.1 (C$_q$, C-12^{major}), 159.0 (C$_q$, C-12^{minor}), 148.1 (C$_q$, C-1^{minor}), 147.6 (C$_q$, C-1^{major}), 147.5 (C$_q$, C-3^{minor}), 147.4 (C$_q$, C-3^{major}), 142.1 (C$_q$, C-5^{minor}), 141.9 (C$_q$, C-5^{major}), 131.5 (C$_q$, C-9^{minor}), 130.2 (C$_q$, C-9^{major}), 129.6 (CH, C-10^{major}), 129.0 (CH, C-10^{minor}), 118.6 (C$_q$, C-7^{major}), 118.3 (C$_q$, C-7^{minor}), 116.4 (C$_q$, C-18^{major}), 116.2 (C$_q$, C-18^{minor}), 114.3 (CH, C-

11^{major}), 114.3 (CH, C-11^{minor}), 108.7 (CH, C-6^{major}), 108.3 (CH, C-6^{minor}), 101.5 (CH$_2$, C-4^{minor}), 101.4 (CH2, C-4^{major}), 99.3 (CH, C-2^{minor}), 98.7 (CH, C-2^{major}), 63.3 (CH$_2$, C-16^{minor}), 63.0 (CH$_2$, C-16^{major}), 55.4 (CH$_3$, C-13^{minor}), 55.4 (CH$_3$, C-13^{major}), 44.2 (CH, C-8^{major}), 44.0 (CH, C-8^{minor}), 42.8 (CH, C-14^{minor}), 42.1 (CH, C-14^{major}), 13.9 (CH$_3$, C-17^{major}), 13.9 ppm (CH$_3$, C-17^{minor}).

HRMS (EI): *m/z* calcd for C$_{20}$H$_{19}$NO$_6$$^{•+}$ [M$^{•+}$]: 369.1207; found: 369.1210.

6be (CG415_2)

R$_f$ (*n*-pentane/EtOAc 8:2, silica, UV) = 0.

¹H NMR (800 MHz, *d*$_6$-DMSO): δ 7.26 (d, *J* = 8.8 Hz, 2 H, 11-H^{minor}), 7.07–7.01 (m, 4 H, 11-H^{major}, 12-H^{major}), 6.99 (s, 1 H, 3-H^{minor}), 6.96 (s, 1 H, 3-H^{major}), 6.93 (d, *J* = 8.8 Hz, 2 H, 12-H^{minor}), 6.89 (s, 1 H, 7-H^{major}), 6.08–6.03 (m, 2 H, 5-H^{major}), 6.03–6.01 (m, 2 H, 5-H^{minor}), 5.95 (d, *J* = 1.2 Hz, 1 H, 7-H^{minor}), 5.32 (d, *J* = 6.2 Hz, 1 H, 14-H^{major}), 5.24 (d, *J* = 12.9 Hz, 1 H, 14-H^{minor}), 4.84 (d, *J* = 12.9 Hz, 1 H, 9-H^{minor}), 4.71 (d, *J* = 6.1 Hz, 1 H, 9-H^{major}), 3.80 (s, 3 H, 13-OCH$_3$^{minor}), 3.73 ppm (s, 3 H, 13-OCH$_3$^{major}).

¹³C{¹H} NMR (201 MHz, *d*$_6$-DMSO): δ 161.9 (C$_q$, C-1^{minor}), 161.9 (C$_q$ C-1^{major}), 159.2 (C$_q$, C-13^{major}), 159.0 (C$_q$, C-13^{minor}), 147.7 (C$_q$, C-4^{minor}), 147.4 (C$_q$, C-4^{major}), 144.7 (C$_q$, C-2^{minor}), 144.7 (C$_q$, C-6^{minor}), 144.6 (C$_q$, C-2^{major}), 144.2 (C$_q$, C-6^{major}), 130.0 (CH, C-11^{minor}), 129.4 (CH, C-10^{minor}), 128.9 (CH, C-10^{major}), 128.7 (CH, C-11^{major}), 117.6 (C$_q$, C-8^{major}), 116.3 (C$_q$, C-8^{minor}), 115.5 (C$_q$, C-15^{major}), 115.1 (C$_q$, C-15^{minor}), 114.6 (CH, C-12^{major}), 114.4 (CH, C-12^{minor}), 107.3 (CH, C-7^{major}), 106.4 (CH, C-7^{minor}), 102.1 (CH$_2$, C-5^{minor}), 102.0 (CH$_2$, C-5^{major}), 98.9 (CH, C-3^{minor}), 98.8 (CH, C-3^{major}), 55.1 (CH$_3$, C-14^{major}), 55.1 (CH$_3$, C-14^{minor}), 42.1 (CH, C-9^{major}), 42.0 (CH, C-9^{minor}), 40.4 (CH, C-14^{minor}), 40.0 ppm (CH, C-14^{major}).

HRMS (EI): *m/z* calcd for C$_{18}$H$_{13}$NO$_5$$^{•+}$ [M$^{•+}$]: 323.0788; found: 323.0792.
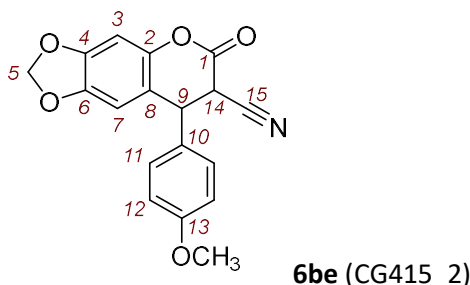
Ethyl 8-(4-methoxyphenyl)-6-oxo-7,8-dihydro-6*H*-[1,3]dioxolo[4,5-*g*]chromene-7-carboxylate (6bf) was prepared according to *GP4* (reaction time: 30 min) from **1b** (14.0 mg, 0.055 mmol) and **2f** (11.4 mg, 0.057 mmol). The crude product was purified by preparative TLC (silica gel, eluent: *n*-pentane:EtOAc = 8:2) to give **6bf** (15.3 mg, 75%) as a colorless oil.

6bf (CG201_2)

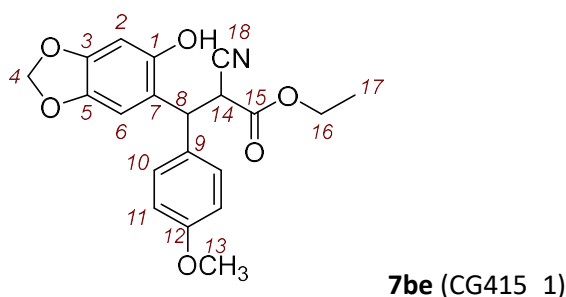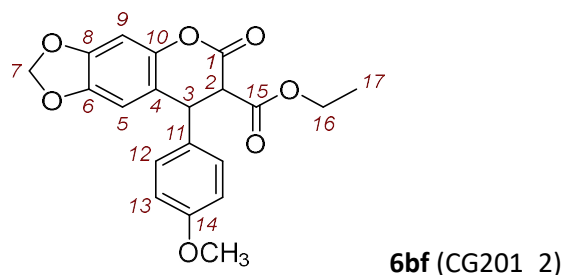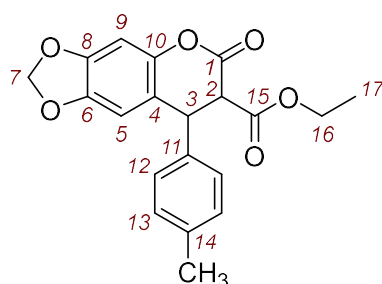*R*$_f$ (*n*-pentane/EtOAc 8:2, silica, UV) = 0.50.

¹H NMR (599 MHz, CDCl$_3$): δ 7.07 (d, *J* = 8.8 Hz, 2 H, 12-H), 6.86 (d, *J* = 8.8 Hz, 2 H, 13-H), 6.66 (s, 1 H, 9-H), 6.37 (s, 1 H, 5-H), 5.95 (s, 2 H, 7-H), 4.55 (d, *J* = 7.8 Hz, 1 H, 3-H), 4.16–4.06 (m, 2 H, 16-H), 3.86 (d, *J* = 7.8 Hz, 1 H, 2-H), 3.79 (s, 3 H, 14-OCH$_3$), 1.11 ppm (t, *J* = 7.1 Hz, 3 H, 17-H).

^{13}C{^{1}H} NMR (151 MHz, CDCl$_3$): δ 167.0 (C$_q$, C-15), 164.5 (C$_q$, C-1), 159.4 (C$_q$, C-14), 147.9 (C$_q$, C-8), 145.6 (C$_q$, C-10), 144.9 (C$_q$, C-6), 130.3 (C$_q$, C-11), 129.1 (CH, C-12), 116.7 (C$_q$, C-4), 114.7 (CH, C-13), 107.7 (CH, C-5), 102.0 (CH$_2$, C-7), 99.1 (CH, C-9), 62.2 (CH$_2$, C-16), 55.4 (CH$_3$, 14-OCH$_3$), 54.3 (CH, C-2), 43.6 (CH, C-3), 14.1 ppm (CH$_3$, C-17).

HRMS (neg. ESI): *m/z* calcd for C$_{20}$H$_{17}$O$_7^-$ [M − H$^+$]: 369.0980; found: 369.0983.

IR (neat, ATR): ṽ 2918, 1769, 1735, 1611, 1511, 1480, 1436, 1250, 1150, 1030, 934, 835, 736 cm^{-1}.

Ethyl 6-oxo-8-(*p*-tolyl)-7,8-dihydro-6*H*-[1,3]dioxolo[4,5-*g*]chromene-7-carboxylate (6cf) was prepared according to *GP4* (reaction time: 30 min) from **1c** (9.0 mg, 0.037 mmol) and **2f** (8.2 mg, 0.041 mmol). The crude product was purified by preparative TLC (silica gel, eluent: *n*-pentane:EtOAc = 8:2) to furnish **6cf** (10.4 mg, 78%) as a colorless oil.

6cf (CG316)

R_f (*n*-pentane/EtOAc 8:2, silica, UV) = 0.75.

^{1}H NMR (600 MHz, CDCl$_3$): δ 7.14 (d, *J* = 7.8 Hz, 2 H, 12-H), 7.03 (d, *J* = 8.2 Hz, 2 H, 13-H), 6.66 (s, 1 H, 9-H), 6.38 (s, 1 H, 5-H), 5.95 (s, 2 H, 7-H), 4.57 (d, *J* = 7.5 Hz, 1 H, 3-H), 4.16–4.07 (m, 2 H, 16-H), 3.88 (d, *J* = 7.5 Hz, 1 H, 2-H), 2.32 (s, 3 H, 14-CH$_3$), 1.11 ppm (t, *J* = 7.1 Hz, 3 H, 17-H).

^{13}C{^{1}H} NMR (151 MHz, CDCl$_3$): δ 167.0 (C$_q$, C-15), 164.5 (C$_q$, C-1), 147.9 (C$_q$, C-8), 145.7 (C$_q$, C-10), 144.9 (C$_q$, C-6), 137.9 (C$_q$, C-11), 135.4 (C$_q$, C-14), 130.0 (CH, C-12), 127.8 (CH, C-13), 116.5 (C$_q$, C-4), 107.7 (CH, C-5), 102.0 (CH$_2$, C-7), 99.1 (CH, C-9), 62.3 (CH$_2$, C-16), 54.2 (CH, C-2), 44.0 (CH, C-3), 21.2 (CH$_3$, 14-CH$_3$), 14.0 ppm (CH$_3$, C-17).

HRMS (EI): *m/z* calcd for C$_{20}$H$_{18}$O$_6$$^{•+}$ [M$^{•+}$]: 354.1098; found: 354.1096.

IR (neat, ATR): ṽ 2983, 1906, 1770, 1736, 1503, 1480, 1436, 1256, 1149, 1032, 935, 862, 733 cm^{-1}.

6-Amino-8-phenyl-8*H*-[1,3]dioxolo[4,5-*g*]chromene-7-carbonitrile (6dd) was prepared according to *GP4* (reaction time: 2 h) from **1d** (10.9 mg, 0.048 mmol) and **2d** (5.1 mg, 0.049 mmol) to yield after aq. workup but without further purification **6dd** (10.3 mg, 73%) as a yellow oil (known compound: ref. [7]).

6dd (CG387_2)

^{1}H NMR (600 MHz, CD$_2$Cl$_2$): δ 7.37–7.31 (m, 2 H, 13-H), 7.26 (t, *J* = 7.3 Hz, 1 H, 14-H), 7.22–7.20 (m, 2 H, 12-H), 6.54 (s, 1 H, 9-H), 6.35 (s, 1 H, 5-H), 5.93 (d, *J* = 1.3 Hz, 1 H, 7-H), 5.89 (d, *J* = 1.3 Hz, 1 H, 7-H), 4.63–4.62 (m, 3 H, 3-H and 1-NH$_2$).

_____

13C{1H} NMR (151 MHz, CD$_2$Cl$_2$): δ 159.6 (C$_q$, C-1), 147.6 (C$_q$, C-8), 145.3 (C$_q$, C-11), 145.2 (C$_q$, C-6), 143.4 (C$_q$, C-10), 129.2 (CH, C-13), 128.2 (CH, C-12), 127.7 (CH, C-14), 119.9 (C$_q$, C-15), 115.3 (C$_q$, C-4), 107.9 (CH, C-5), 102.3 (CH$_2$, C-7), 98.2 (CH, C-9), 60.6 (C$_q$, C-2), 41.6 ppm (CH, C-3).

HRMS (EI): *m/z* calcd for C$_{17}$H$_{12}$N$_2$O$_3$$^{\bullet+}$ [M$^{\bullet+}$]: 292.0842; found: 292.0844.

IR (neat, ATR): $\tilde{v}$ 3453, 3324, 2193, 1658, 1598, 1500, 1479, 1452, 1395, 1245, 1180, 1152, 1035, 934, 701 cm^{-1}.

Ethyl 6-oxo-8-phenyl-7,8-dihydro-6*H*-[1,3]dioxolo[4,5-*g*]chromene-7-carboxylate (6df) was prepared according to *GP4* (reaction time: 30 min) from **1d** (9.0 mg, 0.040 mmol) and **2f** (8.7 mg, 0.044 mmol). The crude product was purified by preparative TLC (silica gel, eluent: *n*-pentane:EtOAc = 8:2) to give **6df** (6.5 mg, 48%) as a colorless oil.

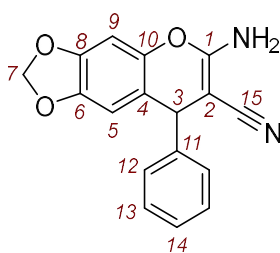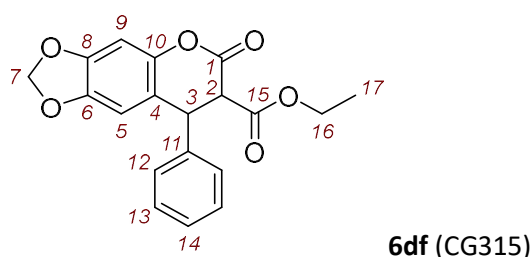**6df** (CG315)

R_f (*n*-pentane/EtOAc 8:2, silica, UV) = 0.65.

1H NMR (800 MHz, CDCl$_3$): δ 7.34 (t, *J* = 7.4 Hz, 2 H, 13-H), 7.29 (t, *J* = 7.4 Hz, 1 H, 14-H), 7.15 (d, *J* = 7.2 Hz, 2 H, 12-H), 6.68 (s, 1 H, 9-H), 6.38 (s, 1 H, 5-H), 5.96 (m, 2 H, 7-H), 4.61 (d, *J* = 7.5 Hz, 1 H, 3-H), 4.15–4.08 (m, 2 H, 16-H), 3.91 (d, *J* = 7.5 Hz, 1 H, 2-H), 1.10 ppm (t, *J* = 7.2 Hz, 3 H, 17-H).

13C{1H} NMR (201 MHz, CDCl$_3$): δ 166.9 (C$_q$, C-15), 164.3 (C$_q$, C-1), 148.0 (C$_q$, C-8), 145.8 (C$_q$, C-10), 144.9 (C$_q$, C-6), 138.5 (C$_q$, C-11), 129.4 (CH, C-13), 128.2 (CH, C-14), 128.0 (CH, C-12), 116.3 (C$_q$, C-4), 107.8 (CH, C-5), 102.0 (CH$_2$, C-7), 99.1 (CH, C-9), 62.3 (CH$_2$, C-16), 54.1 (CH, C-2), 44.4 (CH, C-3), 14.0 ppm (CH$_3$, C-17).

HRMS (EI): *m/z* calcd for C$_{19}$H$_{16}$O$_6$$^{\bullet+}$ [M$^{\bullet+}$]: 340.0941; found: 340.0945.

IR (neat, ATR): $\tilde{v}$ 2984, 2905, 1771, 1736, 1482, 1437, 1257, 1152, 1033, 935, 864, 701 cm^{-1}.

Ethyl 8-(4-chlorophenyl)-6-oxo-7,8-dihydro-6*H*-[1,3]dioxolo[4,5-*g*]chromene-7-carboxylate (6ef) was prepared according to *GP4* (reaction time: 30 min) from **1e** (9.1 mg, 0.035 mmol) and **2f** (7.5 mg, 0.038 mmol). The crude product was purified by preparative TLC (silica gel, eluent: *n*-pentane:EtOAc = 8:2) to give **6ef** (9.8 mg, 75%) as a colorless oil.

6ef (CG314)

R_f (*n*-pentane/EtOAc 8:2, silica, UV) = 0.65.

^{1}H NMR (600 MHz, CDCl$_3$): δ 7.32 (d, J = 8.7 Hz, 2 H, 12-H), 7.10 (d, J = 8.7 Hz, 2 H, 13-H), 6.67 (s, 1 H, 9-H), 6.35 (s, 1 H, 5-H), 5.97 (s, 2 H, 7-H), 4.59 (d, J = 7.5 Hz, 1 H, 3-H), 4.17–4.08 (m, 2 H, 16-H), 3.85 (d, J = 7.5 Hz, 1 H, 2-H), 1.12 ppm (t, J = 7.1 Hz, 3 H, 17-H).

^{13}C{^{1}H} NMR (151 MHz, CDCl$_3$): δ 166.7 (C$_q$, C-15), 164.0 (C$_q$, C-1), 148.2 (C$_q$, C-8), 145.7 (C$_q$, C-10), 145.0 (C$_q$, C-6), 137.0 (C$_q$, C-11), 134.2 (C$_q$, C-14), 129.6 (CH, C-12), 129.4 (CH, C-13), 115.7 (C$_q$, C-4), 107.5 (CH, C-5), 102.1 (CH$_2$, C-7), 99.2 (CH, C-9), 62.5 (CH$_2$, C-16), 54.0 (CH, C-2), 43.7 (CH, C-3), 14.1 ppm (CH$_3$, C-17).

HRMS (EI): *m/z* calcd for C$_{19}$H$_{15}$^{35}ClO$_6$$^{\bullet+}$ [M$^{\bullet+}$]: 374.0552; found: 374.0550.
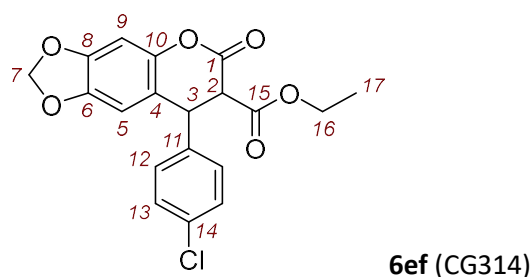
IR (neat, ATR): $\tilde{\nu}$ 2983, 2905, 1771, 1735, 1480, 1436, 1257, 1151, 1092, 1032, 1014, 935, 911, 862, 836, 728 cm^{-1}.

7-(4-Methoxyphenyl)-6-phenyl-6,7-dihydro-[1,3]dioxolo[4,5-*f*]benzofuran (8')

According to *GP4*, *o*QM **1b** (15.0 mg, 0.059 mmol), potassium *tert*-butoxide (7.9 mg, 0.070 mmol), and benzyl trifluoromethyl sulfone (17.3 mg, 0.077 mmol) were mixed in d_6-DMSO. After 4 h at r.t. and aq. workup, a residue was obtained that was further purified by preparative TLC (SiO$_2$, eluent: *n*-pentane:EtOAc = 8:2) to give **8'** as a colorless oil (12.8 mg, 63%).

8' (CG226)
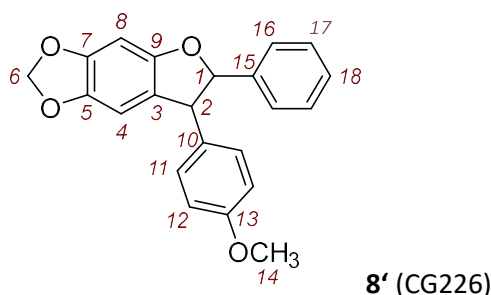
R_f (*n*-pentane/EtOAc 8:2, silica, UV) = 0.80.

^{1}H NMR (400 MHz, CDCl$_3$) δ 7.37–7.30 (m, 5 H, 16-H, 17-H, and 18-H), 7.10 (d, J = 8.8 Hz, 2 H, 11-H), 6.87 (d, J = 8.8 Hz, 2 H, 12-H), 6.54 (s, 1 H, 8-H), 6.42 (d, J = 1.2 Hz, 1 H, 4-H), 5.92 (d, J = 1.4 Hz, 1 H, 6-H), 5.91 (d, J = 1.4 Hz, 1 H, 6-H), 5.47 (d, J = 8.4 Hz, 1 H, 1-H), 4.46–4.38 (m, 1 H, 2-H), 3.81 ppm (s, 3 H, 14-H).

^{13}C{^{1}H} NMR (101 MHz, CDCl$_3$): δ = 159.0 (C$_q$, C-13), 154.5 (C$_q$, C-9), 148.0 (C$_q$, C-7), 142.2 (C$_q$, C-5), 140.9 (C$_q$, C-15), 134.1 (C$_q$, C-10), 129.4 (CH, C-11), 128.7 (CH, C-17), 128.3 (CH, C-18), 125.9 (CH, C-16), 121.5 (C$_q$, C-3), 114.4 (CH, C-12), 105.3 (CH, C-4), 101.4 (CH$_2$, C-6), 94.0 (CH, C-1), 93.1 (CH, C-8), 57.4 (CH, C-2), 55.4 ppm (CH$_3$, C-14).

HRMS (EI): *m/z* calcd for C$_{22}$H$_{18}$O$_4$$^{\bullet+}$ [M$^{\bullet+}$]: 346.1200; found: 346.1198.

(4-Methoxyphenyl)(7-(4-methoxyphenyl)-6,7-dihydro-[1,3]dioxolo[4,5-*f*]benzofuran-6-yl)methanone (9')

According to *GP4*, *o*QM **1b** (16.0 mg, 0.062 mmol), and the sulfonium ylide **9** (14.4 mg, 0.068 mmol) were mixed in d_6-DMSO. After 6 h at r.t. and aq. workup, a residue was obtained that was further purified by preparative TLC (silica gel, eluent: *n*-pentane:EtOAc = 8:2) to give diastereomerically pure **9'** (24.0 mg, 96%) as a colorless oil.

_____

9' (CG310)

R_f (*n*-pentane/EtOAc 8:2, silica, UV) = 0.60.

^{1}H NMR (600 MHz, CDCl$_3$): δ 7.91 (d, J = 9.1 Hz, 2 H, 17-H), 7.15 (d, J = 8.8 Hz, 2 H, 11-H), 6.92 (d, J = 8.9 Hz, 2 H, 18-H), 6.87 (d, J = 8.8 Hz, 2 H, 12-H), 6.54 (s, 1 H, 8-H), 6.41 (s, 1 H, 4-H), 5.90 (d, J = 1.5 Hz, 1 H, 6-H), 5.88 (d, J = 1.3 Hz, 1 H, 6-H), 5.72 (d, J = 6.3 Hz, 1 H, 1-H), 4.79 (d, J = 6.5 Hz, 1 H, 2-H), 3.87 (s, 3 H, 20-H), 3.80 (s, 3 H, 14-H).

^{13}C{^{1}H} NMR (151 MHz, CDCl$_3$): δ 193.4 (C$_q$, C-15), 164.1 (C$_q$, C-19), 159.0 (C$_q$, C-13), 153.8 (C$_q$, C-9), 148.1 (C$_q$, C-7), 142.5 (C$_q$, C-5), 134.6 (C$_q$, C-10), 131.7 (CH, C-17), 129.2 (CH, C-11), 127.4 (C$_q$, C-16), 120.7 (C$_q$, C-3), 114.4 (CH, C-12), 114.0 (CH, C-18), 105.1 (CH, C-4), 101.5 (CH$_2$, C-6), 93.3 (CH, C-8), 91.5 (CH, C-1), 55.7 (CH$_3$, C-20), 55.5 (CH$_3$, C-14), 50.7 (CH, C-2).

HRMS (EI): *m/z* calcd for C$_{24}$H$_{20}$O$_6$$^{\bullet+}$ [M$^{\bullet+}$]: 404.1254; found: 404.1252.
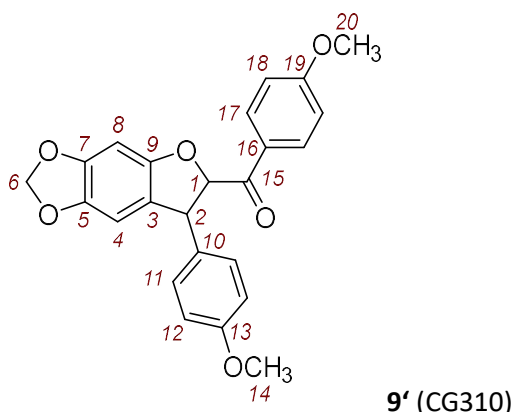
IR (neat, ATR): $\tilde{v}$ 2899, 2839, 1682, 1598, 1511, 1471, 1454, 1243, 1168, 1141, 1032, 964, 937, 908, 831, 727 cm^{-1}.

Ethyl 3-(6-hydroxybenzo[d][1,3]dioxol-5-yl)-3-(4-methoxyphenyl)-2-(triphenyl-λ^5-phosphaneylidene)propanoate (10')

According to *GP4*, *o*QM **1b** (15.0 mg, 0.059 mmol) and the phosphonium ylide **10** (22.4 mg, 0.064 mmol) were mixed in DMSO (5 mL). After 48 h at ambient temperature and aq. workup, a residue was obtained that was further purified by crystallization from *n*-hexane/CH$_2$Cl$_2$ to give **10'** (22.0 mg, 0.036 mmol, 62%) as a white solid; m.p. 138 °C.

10' (CG240_2)
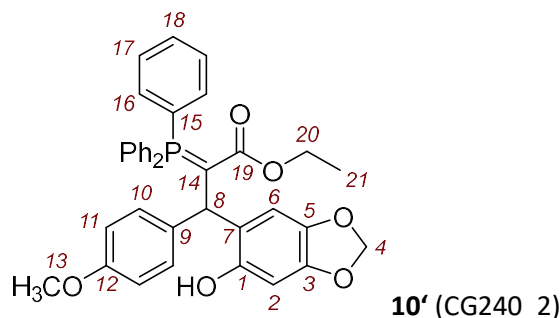
^{1}H NMR (400 MHz, CDCl$_3$): δ 10.44 (s, 1 H, 1-OH), 7.61–7.55 (m, 9 H, 16-H and 18-H), 7.50–7.46 (m, 6 H, 17-H), 7.26 (d, J = 8.9 Hz, 2 H, 10-H), 6.80 (d, J = 8.9 Hz, 2 H, 11-H), 6.52 (s, 1 H, 2-H), 5.82 (d, ^2J = 1.5 Hz, 1 H, 4-H^a), 5.76 (d, ^2J = 1.5 Hz, 1 H, 4-H^b), 5.01 (br s, 1 H, 6-H), 4.25 (br d, $^3J_{H,P}$ = 17.3 Hz, 1 H, 8-H), 3.76 (s, 3 H, 13-H), 3.73–3.52 (m, 2 H, 20-H), 0.39 ppm (t, J = 7.1 Hz, 3 H, 21-H).

^{13}C{^{1}H} NMR (101 MHz, CDCl$_3$): δ 171.2 (C$_q$, d, $^2J_{C,P}$ = 13.3 Hz, C-19), 157.5 (C$_q$, C-12), 151.6 (C$_q$, C-1), 146.5 (C$_q$, C-3), 139.4 (C$_q$, C-5), 135.7 (C$_q$, d, $^3J_{C,P}$ = 8.5 Hz, C-9), 134.0 (CH, d, $^2J_{C,P}$ = 9.6 Hz, C-16), 132.2

_____

(CH, d, $^4J_{C,P}$ = 2.9 Hz, C-18), 128.9 (CH, d, $^3J_{C,P}$ = 12.1 Hz, C-17), 128.6 (C$_q$, d, $^1J_{C,P}$ = 12.1 Hz, C-15), 128.5 (CH, C-10), 127.5 (C$_q$, d, $^1J_{C,P}$ = 90.7 Hz, C-14), 122.4 (C$_q$, d, $^3J_{C,P}$ = 2.3 Hz, C-7), 113.5 (CH, C-11), 110.0 (CH, C-2), 100.6 (CH$_2$, C-4), 100.0 (CH, C-6), 58.7 (CH$_2$, C-20), 55.3 (CH$_3$, C-13), 47.2 (CH, d, $^2J_{C,P}$ = 4.2 Hz, C-8), 13.9 ppm (CH$_3$, C-21).

HRMS (pos. ESI): *m/z* calcd for C$_{37}$H$_{34}$O$_6$P$^+$ [M + H$^+$]: 605.2088; found: 605.2094.

IR (neat, ATR): $\tilde{v}$ 2888, 1627, 1583, 1504, 1480, 1436, 1367, 1295, 1249, 1144, 1100, 1034, 937, 749, 714, 690 cm^{-1}.

6-(((3,5-Bis(trifluoromethyl)phenyl)thio)(4-methoxyphenyl)methyl)benzo[*d*][1,3]dioxol-5-ol (11')

According to *GP4*, *o*QM **1b** (9.0 mg, 0.035 mmol), potassium *tert*-butoxide (4.2 mg, 0.037 mmol), and 3,5-bis(trifluoromethyl)benzenethiol (10.9 mg, 0.044 mmol) were mixed in d_6-DMSO. After 1 h at r.t. and aq. workup, a residue was obtained that was further purified by column chromatography (silica gel, eluent: *n*-pentane:EtOAc = 9:1) to give **11'** (15.3 mg, 87%) as a yellow oil.

11' (CG363)

R_f (*n*-pentane/EtOAc 9:1, silica, UV) = 0.20.

^{1}H NMR (400 MHz, CDCl$_3$): δ 7.62 (s, 2 H, 15-H), 7.59 (s, 1 H, 17-H), 7.37 (d, *J* = 8.9 Hz, 2 H, 10-H), 6.87 (d, *J* 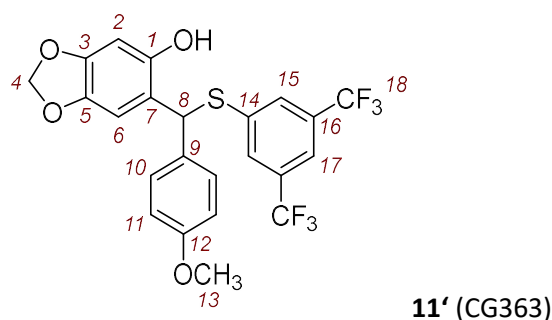= 8.9 Hz, 2 H, 11-H), 6.80 (s, 1 H, 6-H), 6.40 (s, 1 H, 2-H), 5.94 (s, 1 H, 8-H), 5.88 (d, *J* = 1.4 Hz, 1 H, 4-H), 5.87 (d, *J* = 1.4 Hz, 1 H, 4-H), 3.79 ppm (s, 3 H, 13-H).

^{13}C{^{1}H} NMR (101 MHz, CDCl$_3$): δ 159.4 (C$_q$, C-12), 148.2 (C$_q$, C-1), 148.0 (C$_q$, C-3), 142.2 (C$_q$, C-5), 139.6 (C$_q$, C-14), 131.9 (C$_q$, C-16, q, $^2J_{C,F}$ = 33.4 Hz), 130.4 (C$_q$, C-9), 129.7 (CH, C-10), 129.2 (CH, C-15, q, $^3J_{C,F}$ = 2.9 Hz), 123.0 (C-F, C-18, q, $^1J_{C,F}$ = 272.9 Hz), 120.1 – 119.8 (m, CH, 17-C), 117.6 (C$_q$, C-7), 114.4 (CH, C-11), 108.6 (CH, C-6), 101.5 (CH$_2$, C-4), 98.9 (CH, C-2), 55.5 (C-13), 50.2 ppm (C-8).

^{19}F NMR (377 MHz, CDCl$_3$): δ –63.1 ppm.

HRMS (neg. ESI): *m/z* calcd for C$_{23}$H$_{16}$ClF$_6$O$_4$S$^-$ [M + Cl$^-$]: 537.0368; found: 537.0365.

IR (neat, ATR): $\tilde{v}$ 3379, 2915, 1608, 1509, 1486, 1440, 1352, 1276, 1176, 1132, 1038, 876, 843, 825, 682 cm^{-1}.

6-((4-Methoxyphenyl)(propylamino)methyl)benzo[*d*][1,3]dioxol-5-ol (12c')

According to *GP4*, *o*QM **1b** (10.0 mg, 0.039 mmol) and the primary amine **2k** (2.5 mg, 0.043 mmol) were mixed in DMSO. After 1 h at r.t. and aq. workup **12c'** (9.0 mg, 73%) was obtained as a yellow oil.

12c' (CG218)
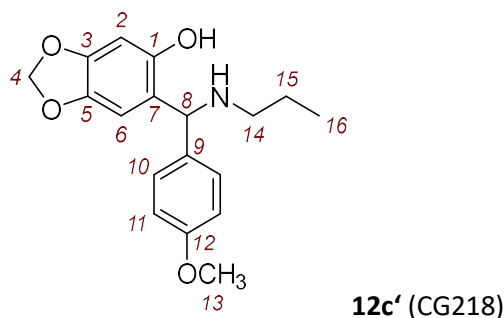
¹H NMR (600 MHz, CDCl$_3$): δ 7.25 (d, J = 8.3 Hz, 2 H, 10-H), 6.87 (d, J = 8.3 Hz, 2 H, 11-H), 6.43 (s, 1 H, 2-H), 6.29 (s, 1 H, 6-H), 5.83 (d, J = 2.0 Hz, 1 H, 4-H), 5.80 (d, J = 2.0 Hz, 1 H, 4-H), 4.73 (s, 1 H, 8-H), 3.79 (s, 3 H, 13-H), 2.67 (t, J = 7.2 Hz, 2 H, 14-H), 1.65–1.51 (m, 2 H, 15-H), 0.94 ppm (t, J = 7.4 Hz, 3 H, 16-H). resonances of 1-OH, and NH could not be assigned presumably because of significant signal broadening.

¹³C{¹H} NMR (151 MHz, CDCl$_3$): δ 159.3 (C$_q$, C-12), 153.1 (C$_q$, C-1), 147.6 (C$_q$, C-3), 140.3 (C$_q$, C-5), 134.5 (C$_q$, C-9), 128.6 (CH, C-10), 116.3 (C$_q$, C-7), 114.4 (CH, C-11), 108.3 (CH, C-6), 100.9 (CH$_2$, C-4), 99.2 (CH, C-2), 67.4 (CH, C-8), 55.4 (CH$_3$, C-13), 50.0 (CH$_2$, C-14), 22.9 (CH$_2$, C-15), 11.8 ppm (CH$_3$, C-16).

HRMS (pos. ESI): m/z calcd for C$_{18}$H$_{22}$NO$_4^+$ [M + H$^+$]: 316.1543; found: 316.1545.

IR (neat, ATR): $\tilde{v}$ 2960, 2874, 1630, 1609, 1510, 1475, 1410, 1246, 1177, 1035, 935, 833, 765 cm^{-1}.

8-(4-Methoxyphenyl)-8*H*-[1,3]dioxolo[4',5':4,5]benzo[1,2-*e*][1,3]oxazin-6-amine (13)

According to *GP4*, *o*QM **1b** (15.0 mg, 0.059 mmol), potassium *tert*-butoxide (7.2 mg, 0.064 mmol), and cyanamide (3.0 mg, 0.071 mmol) were mixed in d_6-DMSO. After 30 min at r.t. and subsequent aq. workup, a residue was obtained that was further purified by crystallization from *n*-pentane/CH$_2$Cl$_2$ to give **13** (14.0 mg, 80%) as a white solid; m.p. 176 °C.

13 (CG577_DMSO)

¹H NMR (400 MHz, d_6-DMSO): δ 7.13 (d, J = 8.7 Hz, 2 H, 10-H), 6.85 (d, J = 8.8 Hz, 2 H, 11-H), 6.59 (s, 1 H, 2-H), 6.50 (s, 1 H, 6-H), 6.00–5.90 (m, 2 H, 4-H), 5.88 (s, 2 H, 14-NH$_2$), 5.29 (s, 1 H, 8-H), 3.71 ppm (s, 3 H, 13-H).

¹³C{¹H} NMR (101 MHz, d_6-DMSO): δ 158.0 (C$_q$, C-12), 149.0 (C$_q$, C-14), 146.2 (C$_q$, C-3), 143.2 (C$_q$, C-5), 143.0 (C$_q$, C-1), 138.5 (C$_q$, C-9), 127.8 (CH, C-10), 116.7 (C$_q$, C-7), 113.6 (CH, C-11), 105.9 (CH, C-6), 101.1 (CH$_2$, C-4), 97.1 (CH, C-2), 56.4 (CH, C-8), 55.0 ppm (CH$_3$, C-13).
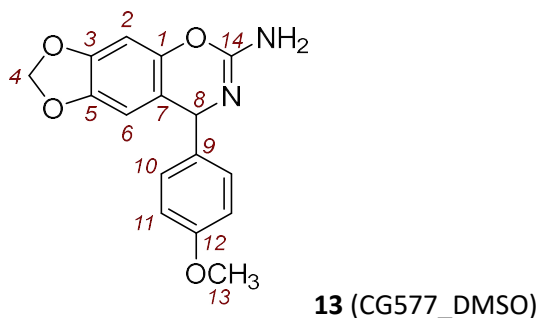
HRMS (pos. ESI): m/z calcd for C$_{16}$H$_{15}$N$_2$O$_4^+$ [M + H$^+$]: 299.1026; found: 299.1028.

IR (neat, ATR): $\tilde{v}$ 3436, 3093, 2903, 1696, 1608, 1507, 1482, 1360, 1252, 1242, 1153, 1085, 1033, 1008, 927, 842, 809 cm^{-1}.

1-((6-Hydroxybenzo[*d*][1,3]dioxol-5-yl)(4-methoxyphenyl)methyl)pyridin-2(1*H*)-one (14)

According to *GP4*, *o*QM **1b** (15.0 mg, 0.059 mmol), potassium *tert*-butoxide (7.2 mg, 0.064 mmol), and 2-pyridone (6.1 mg, 0.064 mmol) were mixed in d_6-DMSO. After 2 h at r.t. and subsequent aq. workup, a residue was obtained that was further purified by crystallization from *n*-pentane/CH$_2$Cl$_2$ to give **14** (8.0 mg, 39%) as a beige solid; m.p. 190 °C (dec.).

14 (CG571)
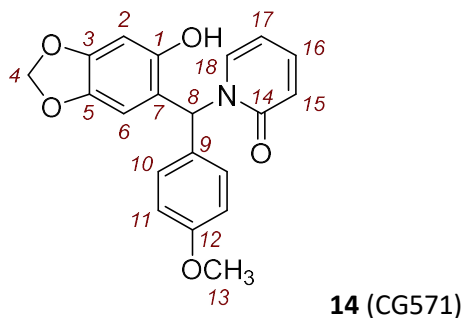
1H NMR (400 MHz, d_6-DMSO): δ 9.52 (s, 1 H, 1-H), 7.42–7.38 (m, 1 H, 16-H), 7.24 (dd, *J* = 7.0, 2.1 Hz, 1 H, 18-H), 7.19 (s, 1 H, 8-H), 6.93 (s, 4 H, 10-H and 11-H), 6.48 (s, 1 H, 2-H), 6.38 (dd, *J* = 9.4, 1.9 Hz, 1 H, 15-H), 6.22–6.15 (m, 1 H, 17-H), 6.14 (s, 1 H, 6-H), 5.91 (s, 2 H, 4-H), 3.74 ppm (s, 3 H, 13-H).
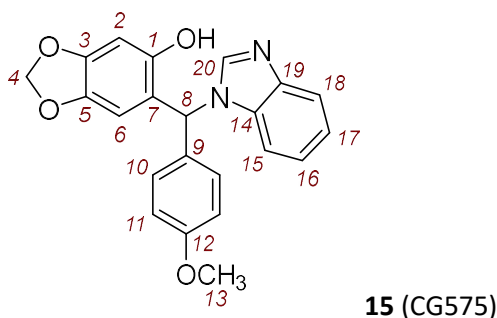
13C{1H} NMR (101 MHz, d_6-DMSO): δ 161.1 (C$_q$, C-14), 158.4 (C$_q$, C-12), 150.3 (C$_q$, C-1), 147.3 (C$_q$, C-3), 139.7 (C$_q$, C-5), 139.4 (CH, C-16), 136.2 (CH, C-18), 131.0 (C$_q$, C-9), 128.9 (CH, C-10), 119.6 (CH, C-15), 116.9 (C$_q$, C-7), 114.0 (CH, C-11), 108.8 (CH, C-6), 104.9 (CH, C-17), 101.0 (CH$_2$, C-4), 97.8 (CH, C-2), 56.5 (CH, C-8), 55.1 ppm (CH$_3$, C-13).

HRMS (neg. ESI): *m/z* calcd for C$_{20}$H$_{16}$NO$_5^-$ [M − H$^+$]: 350.1034; found: 350.1033.

IR (neat, ATR): ṽ 2924, 2873, 1647, 1562, 1536, 1515, 1499, 1443, 1263, 1244, 1171, 1045, 1024, 941, 860, 780 cm^{-1}.

6-((1*H*-Benzo[*d*]imidazol-1-yl)(4-methoxyphenyl)methyl)benzo[*d*][1,3]dioxol-5-ol (15)

According to *GP4*, *o*QM **1b** (15.0 mg, 0.059 mmol), potassium *tert*-butoxide (7.2 mg, 0.064 mmol), and benzimidazole (7.6 mg, 0.064 mmol) were mixed in d_6-DMSO. After 30 min at r.t. and subsequent aq. workup, a residue was obtained that was further purified by crystallization from *n*-pentane/CH$_2$Cl$_2$ to give **15** (19.0 mg, 86%) as a beige solid; m.p. 215 °C (dec.).

15 (CG575)

1H NMR (400 MHz, d_6-DMSO): δ 9.65 (s, 1 H, 1-OH), 7.84 (s, 1 H, 20-H), 7.66 (dd, *J* = 5.9, 1.9 Hz, 1 H, 18-H), 7.29–7.21 (m, 1 H, 15-H), 7.21–7.13 (m, 2 H, 16-H and 17-H), 7.08 (d, *J* = 8.6 Hz, 2 H, 10-H), 7.02 (s, 1 H, 8-H), 6.93 (d, *J* = 8.9 Hz, 2 H, 11-H), 6.52 (s, 1 H, 2-H), 6.30 (s, 1 H, 6-H), 5.91 (s, 2 H, 4-H), 3.74 ppm (s, 3 H, 13-H).

13C{1H} NMR (101 MHz, d_6-DMSO): δ 158.8 (C$_q$, C-12), 150.0 (C$_q$, C-1), 147.5 (C$_q$, C-3), 143.7 (C$_q$, C-19), 142.8 (CH, C-20), 139.9 (C$_q$, C-5), 133.9 (C$_q$, C-14), 130.4 (C$_q$, C-9), 128.9 (CH, C-10), 122.3 (CH, C-16),

121.6 (CH, C-17), 119.5 (CH, C-18), 116.5 (C$_q$, C-7), 114.1 (CH, C-11), 111.0 (CH, C-15), 107.9 (CH, C-6), 101.0 (CH$_2$, C-4), 97.8 (CH, C-2), 56.4 (CH, C-8), 55.1 ppm (CH$_3$, C-13).

HRMS (neg. ESI): *m/z* calcd for C$_{22}$H$_{17}$N$_2$O$_4^-$ [M − H$^+$]: 373.1194; found: 373.1193.

IR (neat, ATR): $\tilde{v}$ 2901, 1611, 1514, 1454, 1250, 1218, 1172, 1034, 928, 858, 804, 785, 744 cm^{-1}.

2-((6-Hydroxybenzo[*d*][1,3]dioxol-5-yl)(4-methoxyphenyl)methyl)-1,3-dimesityl-1*H*-imidazol-3-ium chloride (16)

Under an atmosphere of dry argon, a mixture of the *o*QM **1b** (18.0 mg, 0.070 mmol) and the *N*-heterocyclic carbene IMes (21.4 mg, 0.070 mmol) in dry *d*$_8$-THF (1 mL) was stirred for 15 min at ambient temperature. The reaction mixture was quenched with 2 M aq. HCl (3 mL) and extracted with dichloromethane (3 × 10 mL). The organic phases were combined, and the solvent was removed under reduced pressure. The residue was dissolved in a minimum volume of dichloromethane. Upon addition of *n*-pentane, **16** (29.4 mg, 70%) precipitated as an off-white solid; m.p. 212 °C.

16 (CG687)
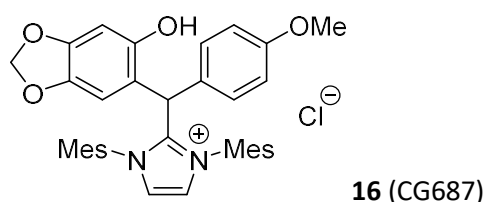
¹H NMR (600 MHz, CDCl$_3$): δ 10.51 (s, 1 H, OH), 7.43 (s, 2 H), 7.06 (s, 1 H), 6.93–6.92 (m, 2 H), 6.76 (d, *J* = 8.8 Hz, 2 H), 6.66–6.66 (m, 2 H), 6.61 (d, *J* = 8.8 Hz, 2 H), 5.82 (s, 1 H), 5.63 (s, 1 H), 5.58–5.54 (m, 2 H), 3.71 (s, 3 H), 2.30 (s, 6 H), 2.24 (s, 6 H), 1.71 ppm (s, 6 H).

¹³C{¹H} NMR (151 MHz, CDCl$_3$): δ 159.2, 150.5, 149.6, 147.5, 140.9, 139.5, 135.3, 134.2, 130.7, 130.1, 129.7, 129.6, 129.4, 124.5, 114.1, 111.3, 108.1, 100.7, 98.9, 55.46, 55.4, 42.7, 21.1, 18.4, 17.8 ppm.

HRMS (pos. ESI): *m/z* calcd for C$_{36}$H$_{37}$N$_2$O$_4^+$ [M$^+$]: 561.2748; found: 561.2740.

IR (neat, ATR): $\tilde{v}$ 2917, 1609, 1512, 1489, 1439, 1269, 1251, 1181, 1170, 1032, 935, 861, 797, 776 cm^{-1}.

7-(4-Methoxyphenyl)-[1,3]dioxolo[4,5-*f*]benzofuran-6-amine (17)

According to *GP4*, *o*QM **1b** (23.0 mg, 0.090 mmol) and sodium cyanide (6.6 mg, 0.13 mmol) were mixed in *d*$_6$-DMSO. After 1 h at r.t. and subsequent aq. workup, a residue was obtained that was further purified by preparative TLC (silica gel, eluent: *n*-pentane:EtOAc:NEt$_3$ = 80:19:1) to give **17** (13.8 mg, 54%) as a green viscous liquid.

17 (CG361)
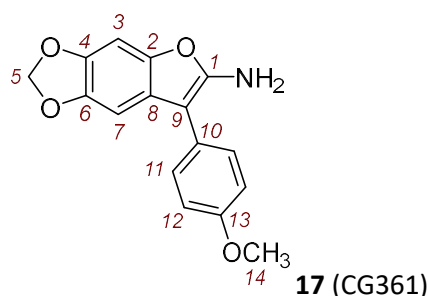
R$_f$ (*n*-pentane/EtOAc/NEt$_3$ 80:19:1, silica, UV) = 0.30.

¹H NMR (400 MHz, CDCl₃): δ 7.42 (d, *J* = 8.9 Hz, 2 H, 11-H), 7.01 (d, *J* = 8.9 Hz, 2 H, 12-H), 6.90 (s, 1 H, 7-H), 6.87 (s, 1 H, 3-H), 5.93 (s, 2 H, 5-H), 4.08 (s, 2 H, 1-NH₂), 3.85 ppm (s, 3 H, 14-H).

¹³C{¹H} NMR (101 MHz, CDCl₃): δ 158.1 (C$_q$, C-13), 152.6 (C$_q$, C-1), 144.3 (C$_q$, C-4), 144.3 (C$_q$, C-2), 143.3 (C$_q$, C-6), 128.8 (CH, C-11), 125.5 (C$_q$, C-10), 123.5 (C$_q$, C-8), 114.8 (CH, C-12), 101.0 (CH₂, C-5), 97.4 (CH, C-7), 95.5 (C$_q$, C-9), 93.4 (CH, C-3), 55.5 ppm (CH₃, C-14).

HRMS (EI): *m/z* calcd for C₁₆H₁₃NO₄•⁺ [M•⁺]: 283.0839; found: 283.0839.

N-(*tert*-Butyl)-7-(4-methoxyphenyl)-[1,3]dioxolo[4,5-*f*]benzofuran-6-amine (18)

A mixture of *o*QM **1b** (50.0 mg, 0.20 mmol) and *tert*-butyl isocyanide (21.1 mg, 0.25 mmol) in dichloromethane (1 mL) was stirred at ambient temperature for 120 h. The solvent was removed under reduced pressure and the residue was purified by preparative TLC preparative TLC (silica gel, eluent: *n*-pentane:EtOAc:NEt₃ = 85:13:2) to give **18** (35.0 mg, 52%) as a colorless oil.

18 (CG640)
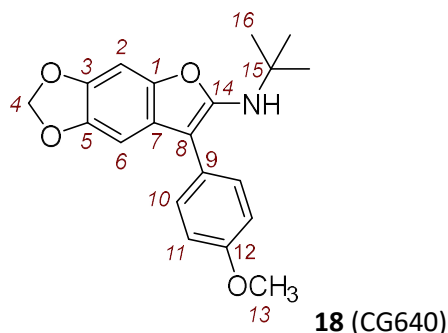
¹H NMR (400 MHz, CD₂Cl₂): δ 7.39 (d, *J* = 8.9 Hz, 2 H, 10-H), 7.00 (d, *J* = 8.9 Hz, 2 H, 11-H), 6.91 (d, *J* = 0.5 Hz, 1 H, 2-H), 6.85 (d, *J* = 0.5 Hz, 1 H, 6-H), 5.92 (s, 2 H, 4-H), 3.96 (s, 1 H, 14-NH), 3.84 (s, 3 H, 13-H), 1.31 ppm (s, 9 H, 16-H).

¹³C{¹H} NMR (101 MHz, CD₂Cl₂): δ 158.6 (C$_q$, C-12), 154.6 (C$_q$, C-14), 145.3 (C$_q$, C-1), 144.5 (C$_q$, C-3), 143.9 (C$_q$, C-5), 129.6 (CH, C-10), 125.9 (C$_q$, C-9), 123.3 (C$_q$, C-7), 114.9 (CH, C-11), 101.4 (CH₂, C-4), 100.8 (C$_q$, C-8), 97.4 (CH, C-6), 93.5 (CH, C-2), 55.7 (CH₃, C-13), 53.9 (C$_q$, C-15), 30.6 ppm (CH₃, C-16).

HRMS (EI): *m/z* calcd for C₂₀H₂₁NO₄•⁺ [M•⁺]: 339.1465; found: 339.1468.

IR (neat, ATR): ṽ 3371, 2964, 1749, 1601, 1516, 1461, 1247, 1175, 1145, 1035, 943, 835 cm⁻¹.

5.2.4. UV/Vis Spectra of *ortho*-Quinone Methides

Quinone methide solutions [7–14 mM in dry DMSO or dichloromethane (DCM)] were added stepwise to known volumes of the same solvent. The absorbances *A* of the *o*QM solutions were detected by using a *J&M* TIDAS diode array spectrophotometer (connected to a Hellma quartz probe with a path length *d* = 0.5 cm).

Molar absorption coefficients ε (M⁻¹ cm⁻¹) were determined from the slopes of linear correlations of absorbance with *o*QM concentrations by assuming the validity of the Beer-Lambert law [Equation (S1)].

$$\lg (I_0/I) = A = \varepsilon \, d \, c \qquad \text{(S1)}$$

1a — In DMSO:
λ_{max} = 504 nm
ε = 2.11 × 10^4 M^{-1} cm^{-1}

1b — In DMSO:
λ_{max} = 435 nm
ε = 1.00 × 10^4 M^{-1} cm^{-1}
In DCM:
λ_{max} = 430 nm
ε = 1.21 × 10^4 M^{-1} cm^{-1}

1c — In DMSO:
λ_{max} = 342 nm
λ_{max} = 424 nm
ε = 1.21 × 10^4 M^{-1} cm^{-1}
ε = 1.06 × 10^4 M^{-1} cm^{-1}

1d — In DMSO:
λ_{max} = 328 nm
λ_{max} = 419 nm
ε = 9.97 × 10^3 M^{-1} cm^{-1}
ε = 7.13 × 10^3 M^{-1} cm^{-1}
In DCM:
λ_{max} = 323nm
λ_{max} = 413 nm
ε = 9.58 × 10^3 M^{-1} cm^{-1}
ε = 7.05 × 10^3 M^{-1} cm^{-1}

1e — In DMSO:
λ_{max} = 335 nm
λ_{max} = 421 nm
ε = 1.43 × 10^4 M^{-1} cm^{-1}
ε = 1.10 × 10^4 M^{-1} cm^{-1}

1f — In DMSO:
λ_{max} = 327 nm
λ_{max} = 417 nm
ε = 1.36 × 10^4 M^{-1} cm^{-1}
ε = 9.02 × 10^3 M^{-1} cm^{-1}

In DMSO:

λ_{max} = 323 nm
λ_{max} = 419 nm
ε = 1.35 × 10^4 M^{-1} cm^{-1}
ε = 8.13 × 10^3 M^{-1} cm^{-1}

In DMSO:

λ_{max} = 335 nm
λ_{max} = 437 nm
ε = 1.51 × 10^4 M^{-1} cm^{-1}
ε = 1.12 × 10^4 M^{-1} cm^{-1}
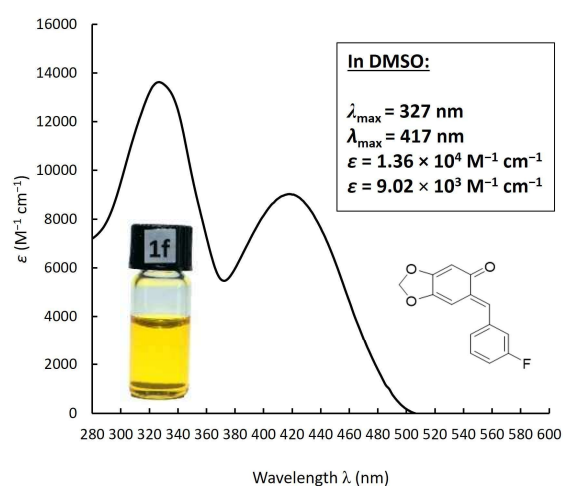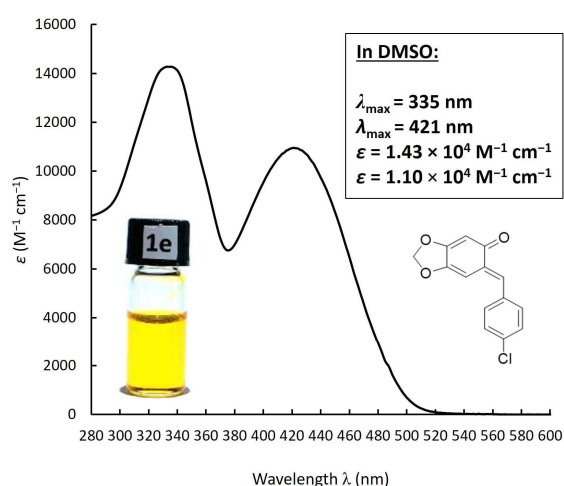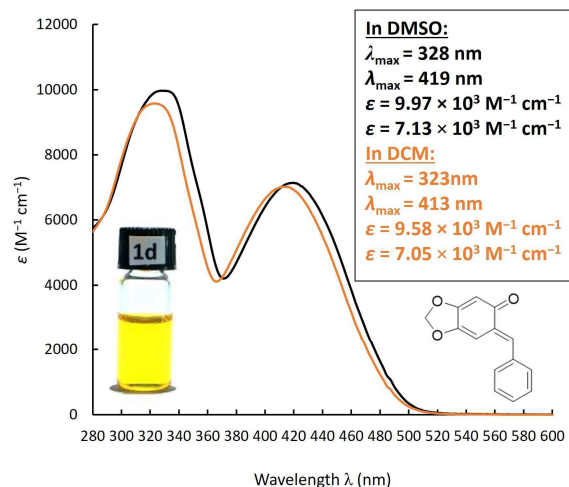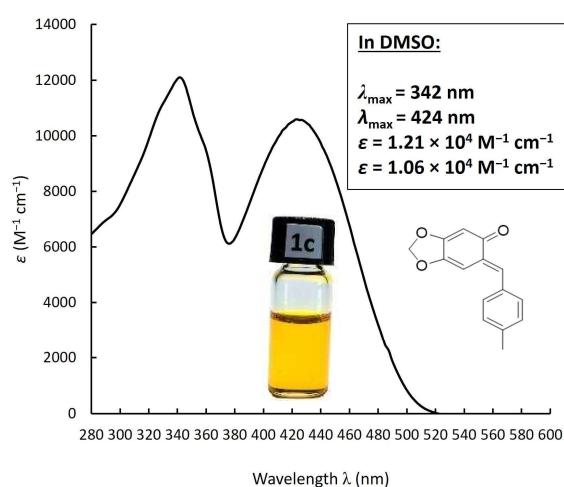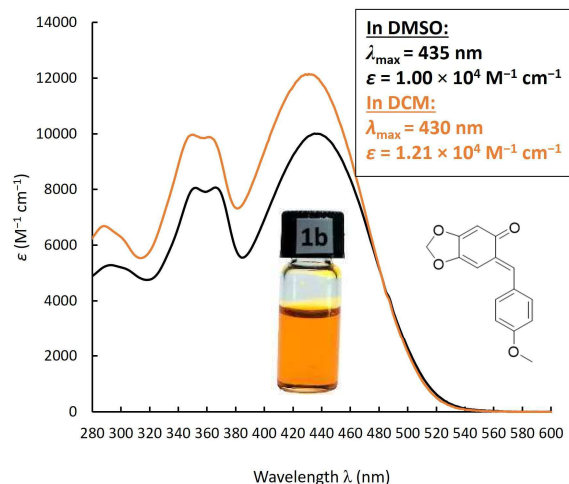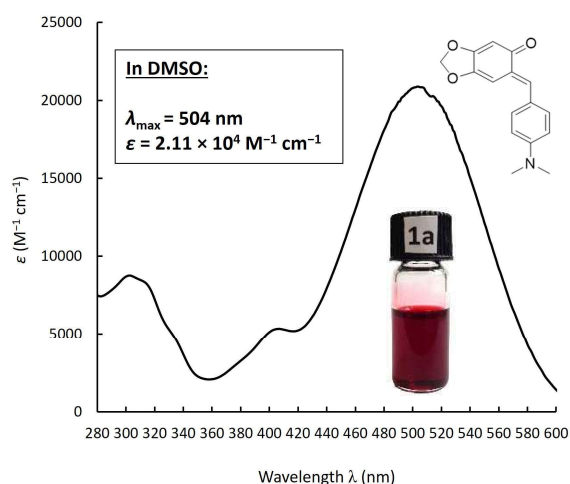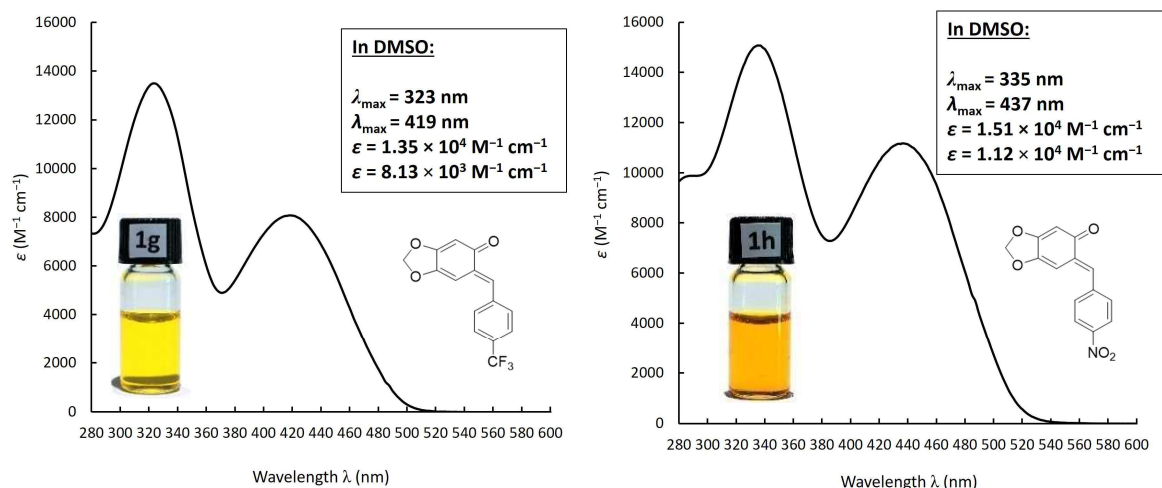
5.2.5. Cyclic voltammetry measurements of *ortho*-Quinone Methides

The reduction potentials of *o*QMs (E_p^{red}) were determined in acetonitrile on a CH Instruments 630E electrochemical analyzer using a 2 mm diameter platinum working electrode, a platinum wire counter electrode and an Ag wire pseudo-reference electrode applying a scan rate of 0.1 V/s. Cyclic voltammetry measurements were performed in deaerated acetonitrile solutions containing 0.1 M tetra-*n*-butylammonium perchlorate, the *o*QMs ($c \approx 1 \times 10^{-3}$ M), and ferrocene ($c = 7.5 \times 10^{-4}$ M) as an internal standard. The $E_{1/2}$(fc$^+$/fc in MeCN) = +0.382 V[8] was used to calibrate E_p^{red} (**1** in MeCN) vs SCE.

Only peak potentials E_p^{red} could be determined due to the non-reversibility of the *o*QM reduction.

_____
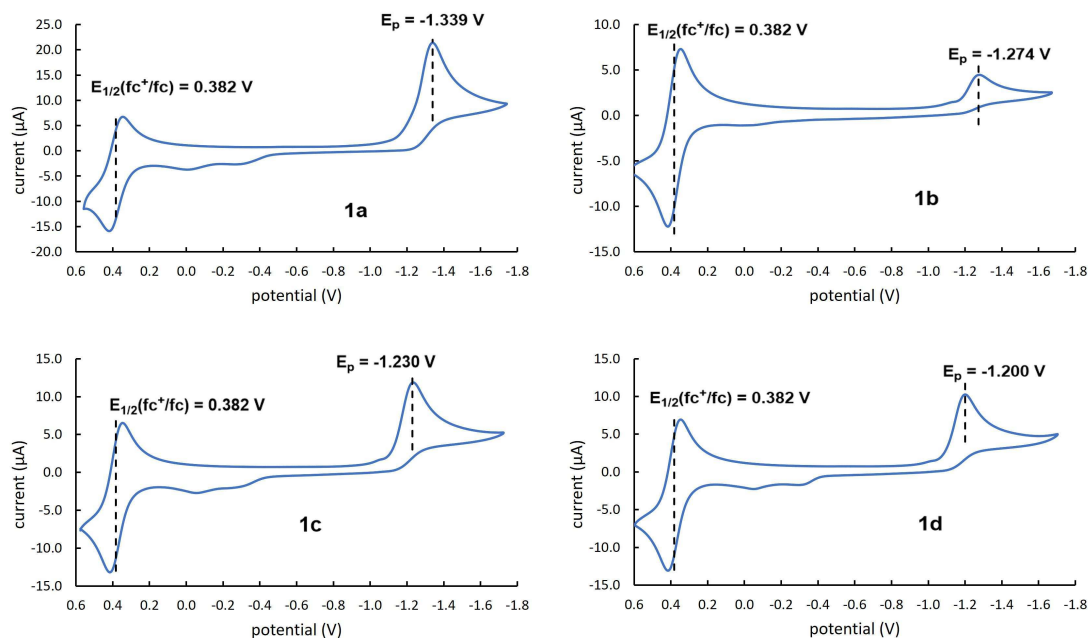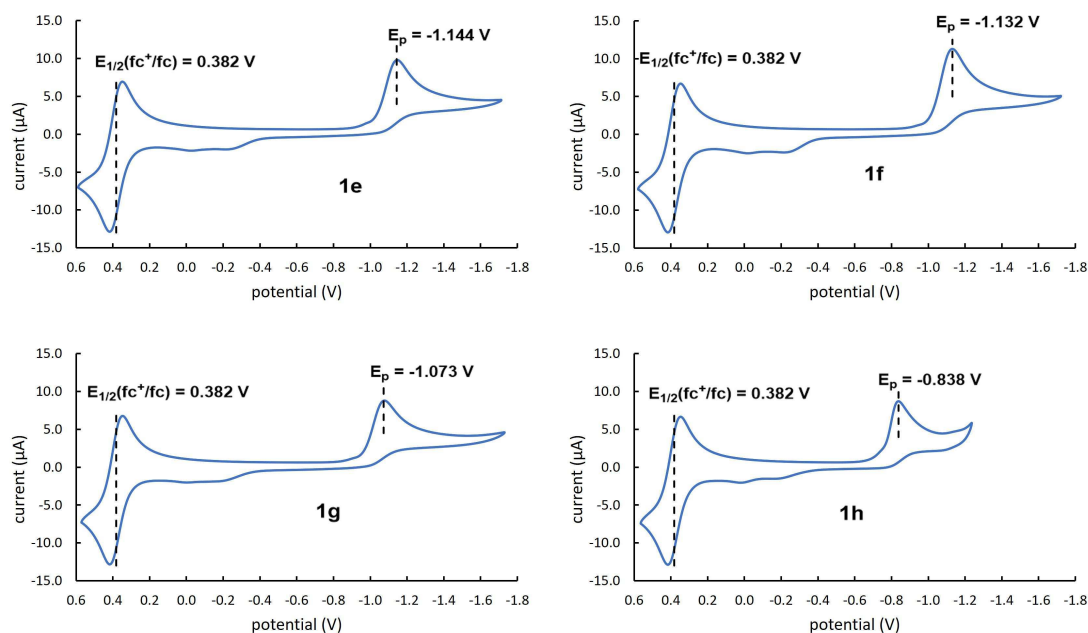
5.2.6. Kinetics of the Reactions of *o*QMs with Carbanions (Reference Nucleophiles)

Kinetic measurements were performed by harnessing UV/Vis photometry on AppliedPhotophysics SX.20 stopped-flow instruments as well as on a conventional J&M TIDAS diode array spectrophotometer, which was controlled by TIDASDAQ3 (v3) software and connected to a Hellma 661.502-QX quartz Suprasil immersion probe (light path d = 5 mm) via fiber optic cables and standard SMA connectors. The temperature (20.0 ± 0.2 °C) was maintained constant by using circulating bath cryostats.

All solutions were prepared by using dry DMSO (ThermoScientific, DMSO 99.7+%, extra dry, over molecular sieve, AcroSeal) and kept under an atmosphere of dry nitrogen. When carbanions were used as the nucleophiles, the kinetic measurements for each *o*QM/nucleophile combination were performed with or without added 18-crown-6 ether (18-c-6) and in some cases with additional CH-acid.

1a + **2a** in DMSO (stopped-flow method, detection at 504 nm) CG302

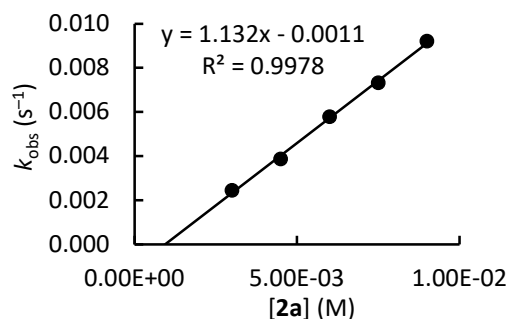| [**1a**]$_0$ (M)	[**2a**]$_0$ (M)	[18-c-6]$_0$ (M)	k_{obs} (s^{-1})
2.92×10^{-5}	3.00×10^{-3}		2.45×10^{-3}
2.92×10^{-5}	4.50×10^{-3}	4.95×10^{-3}	3.86×10^{-3}
2.92×10^{-5}	6.00×10^{-3}		5.78×10^{-3}
2.92×10^{-5}	7.50×10^{-3}	8.25×10^{-3}	7.32×10^{-3}
2.92×10^{-5}	9.00×10^{-3}		9.21×10^{-3}

$$k_2 = (1.13 \pm 0.03) \text{ M}^{-1} \text{ s}^{-1}$$

1a + **2b** in DMSO (stopped-flow method, detection at 504 nm) CG299
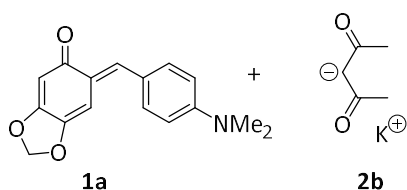
[**1a**]$_0$ (M)	[**2b**]$_0$ (M)	[18-c-6]$_0$ (M)	$k_{obs}{}^a$ (s^{-1})
2.82×10^{-5}	1.20×10^{-3}		2.19×10^{-2}
2.82×10^{-5}	1.80×10^{-3}	1.98×10^{-3}	3.32×10^{-2}
2.82×10^{-5}	2.40×10^{-3}		4.36×10^{-2}
2.82×10^{-5}	3.00×10^{-3}	3.30×10^{-3}	5.58×10^{-2}
2.82×10^{-5}	3.60×10^{-3}		6.58×10^{-2}

^{a} Only the first half-life time was evaluated.

$$k_2 = (1.84 \pm 0.03) \times 10^1 \text{ M}^{-1} \text{ s}^{-1}$$
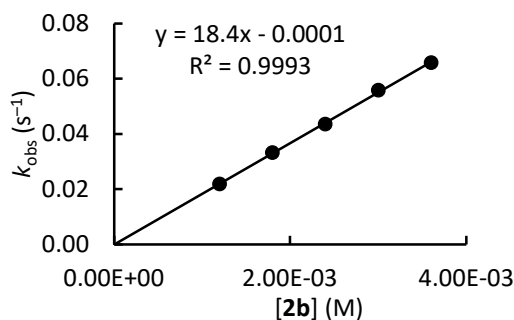
1a + **2c** in DMSO (stopped-flow method, detection at 504 nm) CG298
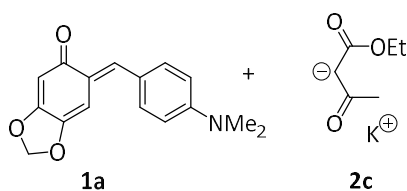
[**1a**]$_0$ (M)	[**2c**]$_0$ (M)	[18-c-6]$_0$ (M)	k_{obs} (s^{-1})
3.06×10^{-5}	9.00×10^{-4}		4.60×10^{-2}
3.06×10^{-5}	1.35×10^{-3}	1.49×10^{-3}	6.63×10^{-2}
3.06×10^{-5}	1.80×10^{-3}		8.54×10^{-2}
3.06×10^{-5}	2.25×10^{-3}	2.48×10^{-3}	1.06×10^{-1}
3.06×10^{-5}	2.70×10^{-3}		1.26×10^{-1}

$$k_2 = (4.44 \pm 0.03) \times 10^1 \text{ M}^{-1} \text{ s}^{-1}$$
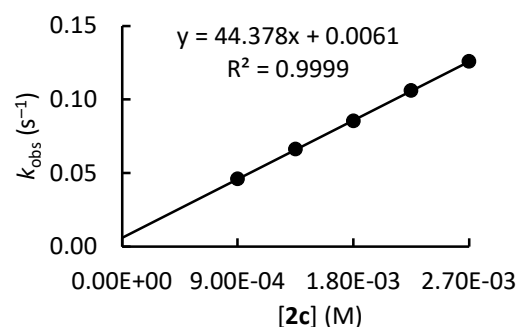
_____

1a + **2d** in DMSO (stopped-flow method, detection at 504 nm) CG297
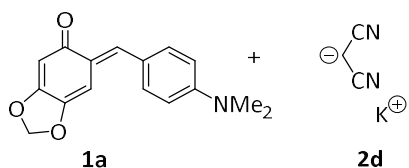
[**1a**]$_0$ (M)	[**2d**]$_0$ (M)	[18-c-6]$_0$ (M)	k_{obs}[a] (s^{-1})
2.87×10^{-5}	6.00×10^{-4}		3.55×10^{-1}
2.87×10^{-5}	9.00×10^{-4}	9.90×10^{-4}	5.36×10^{-1}
2.87×10^{-5}	1.20×10^{-3}		6.93×10^{-1}
2.87×10^{-5}	1.50×10^{-3}	1.65×10^{-3}	8.71×10^{-1}
2.87×10^{-5}	1.80×10^{-3}		1.02
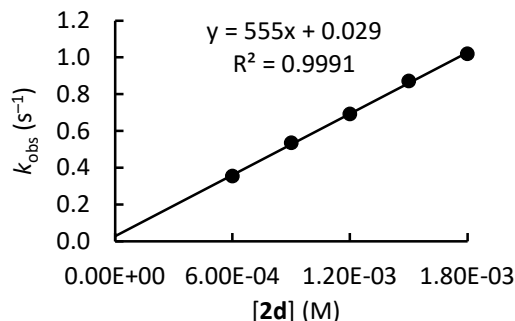
[a] Only the first half-life time was evaluated.

$$k_2 = (5.55 \pm 0.10) \times 10^2 \text{ M}^{-1} \text{ s}^{-1}$$

1a + **2e** in DMSO (stopped-flow method, detection at 504 nm) CG296
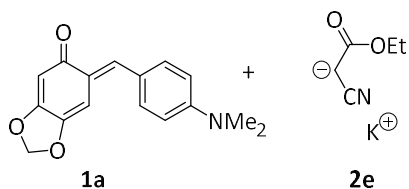
[**1a**]$_0$ (M)	[**2e**]$_0$ (M)	[18-c-6]$_0$ (M)	k_{obs}[a] (s^{-1})
2.82×10^{-5}	6.00×10^{-4}		2.59×10^{-1}
2.82×10^{-5}	9.00×10^{-4}	9.90×10^{-4}	3.80×10^{-1}
2.82×10^{-5}	1.20×10^{-3}		5.08×10^{-1}
2.82×10^{-5}	1.50×10^{-3}	1.65×10^{-3}	6.24×10^{-1}
2.82×10^{-5}	1.80×10^{-3}		7.57×10^{-1}
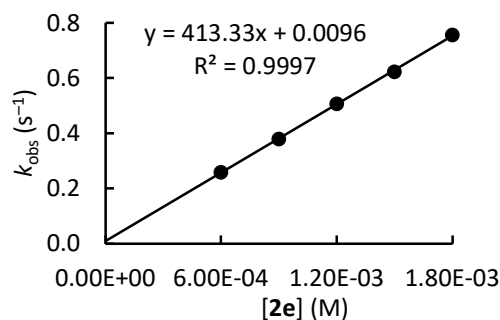
[a] Only the first half-life time was evaluated.

$$k_2 = (4.13 \pm 0.04) \times 10^2 \text{ M}^{-1} \text{ s}^{-1}$$

**1a** + **2f** in DMSO (stopped-flow method, detection at 504 nm) CG295
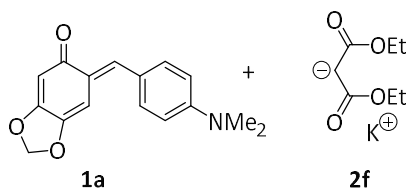
[**1a**]$_0$ (M)	[**2f**]$_0$ (M)	[18-c-6]$_0$ (M)	k_{obs} (s^{-1})
2.82×10^{-5}	6.00×10^{-4}		8.53×10^{-2}
2.82×10^{-5}	9.00×10^{-4}	9.90×10^{-4}	1.24×10^{-1}
2.82×10^{-5}	1.20×10^{-3}		1.64×10^{-1}
2.82×10^{-5}	1.50×10^{-3}	1.65×10^{-3}	2.10×10^{-1}
2.82×10^{-5}	1.80×10^{-3}		2.49×10^{-1}
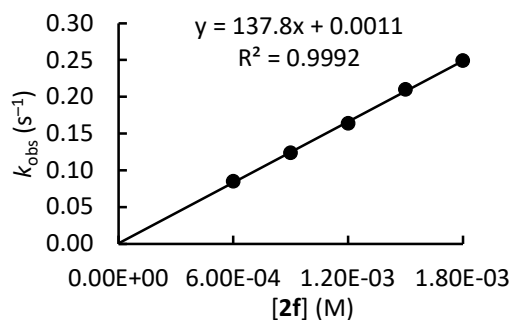
$$k_2 = (1.38 \pm 0.02) \times 10^2 \text{ M}^{-1} \text{ s}^{-1}$$

_____

1b + **2a** in DMSO (stopped-flow method, detection at 440 nm) CG208
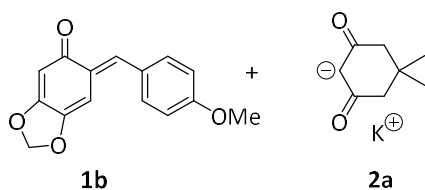
$[\mathbf{1b}]_0$ (M)	$[\mathbf{2a}]_0$ (M)	$[18\text{-c-6}]_0$ (M)	k_{obs} (s^{-1})
4.8×10^{-5}	1.00×10^{-3}		3.53×10^{-3}
4.8×10^{-5}	1.50×10^{-3}	1.65×10^{-3}	5.35×10^{-3}
4.8×10^{-5}	2.00×10^{-3}		7.69×10^{-3}
4.8×10^{-5}	2.50×10^{-3}	2.75×10^{-3}	9.17×10^{-3}

$$k_2 = (3.85 \pm 0.22) \text{ M}^{-1} \text{ s}^{-1}$$
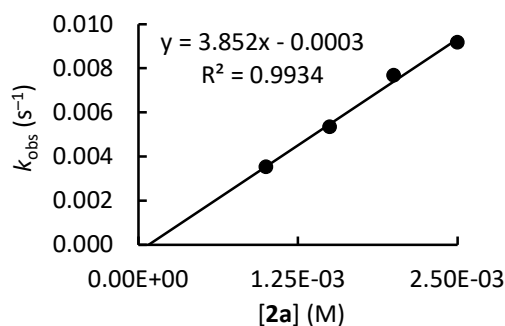
1b + **2b** in DMSO (stopped-flow method, detection at 443 nm) CG207
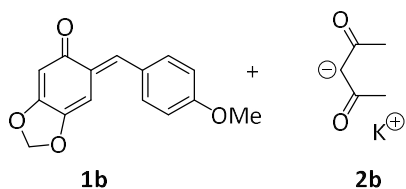
$[\mathbf{1b}]_0$ (M)	$[\mathbf{2b}]_0$ (M)	$[18\text{-c-6}]_0$ (M)	k_{obs} (s^{-1})
4.50×10^{-5}	1.00×10^{-3}		1.17×10^{-1}
4.50×10^{-5}	1.50×10^{-3}	1.65×10^{-3}	1.60×10^{-1}
4.50×10^{-5}	2.00×10^{-3}		2.00×10^{-1}
4.50×10^{-5}	2.50×10^{-3}	2.75×10^{-3}	2.37×10^{-1}

$$k_2 = (8.00 \pm 0.19) \times 10^1 \text{ M}^{-1} \text{ s}^{-1}$$
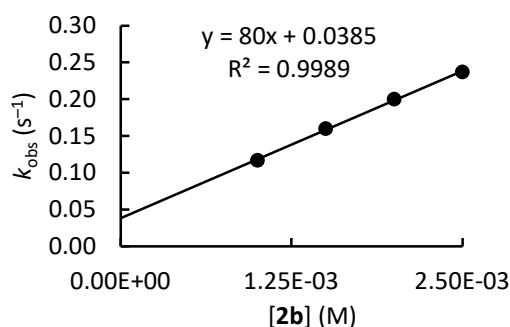
1b + **2c** in DMSO (stopped-flow method, detection at 453 nm) CG206
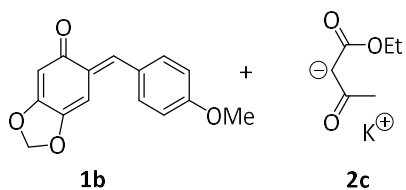
$[\mathbf{1b}]_0$ (M)	$[\mathbf{2c}]_0$ (M)	$[18\text{-c-6}]_0$ (M)	k_{obs} (s^{-1})
4.40×10^{-5}	1.00×10^{-3}		2.18×10^{-1}
4.40×10^{-5}	1.50×10^{-3}	1.65×10^{-3}	2.92×10^{-1}
4.40×10^{-5}	2.00×10^{-3}		3.94×10^{-1}
4.40×10^{-5}	2.50×10^{-3}	2.75×10^{-3}	5.17×10^{-1}

$$k_2 = (2.00 \pm 0.15 \times 10^2 \text{ M}^{-1} \text{ s}^{-1}$$
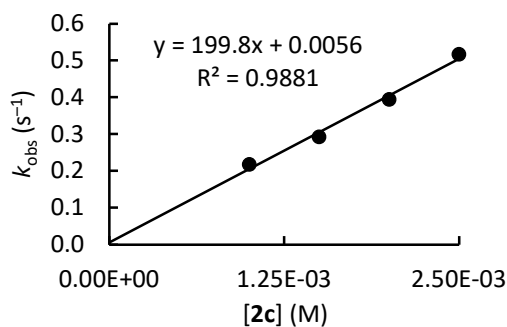
1b + **2d** in DMSO (stopped-flow method, detection at 440 nm) CG205

$[\mathbf{1b}]_0$ (M)	$[\mathbf{2d}]_0$ (M)	$[\text{18-c-6}]_0$ (M)	k_{obs} (s^{-1})
6.00×10^{-5}	1.00×10^{-3}		2.14
6.00×10^{-5}	1.50×10^{-3}	1.65×10^{-3}	3.19
6.00×10^{-5}	2.00×10^{-3}		4.08
6.00×10^{-5}	2.50×10^{-3}	2.75×10^{-3}	5.05
6.00×10^{-5}	3.00×10^{-3}		6.01

$k_2 = (1.92 \pm 0.02) \times 10^3$ M^{-1} s^{-1}
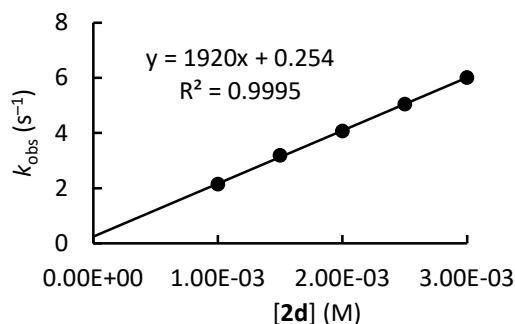
1b + **2e** in DMSO (stopped-flow method, detection at 440 nm) CG204_1
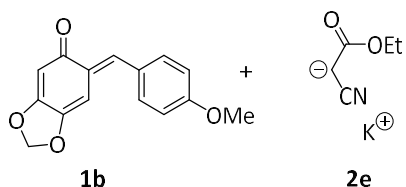
$[\mathbf{1b}]_0$ (M)	$[\mathbf{2e}]_0$ (M)	$[\text{18-c-6}]_0$ (M)	k_{obs} (s^{-1})
6.00×10^{-5}	1.00×10^{-3}		1.79
6.00×10^{-5}	1.50×10^{-3}	1.65×10^{-3}	2.43
6.00×10^{-5}	2.00×10^{-3}		3.14
6.00×10^{-5}	2.50×10^{-3}	2.75×10^{-3}	3.79
6.00×10^{-5}	3.00×10^{-3}		4.50

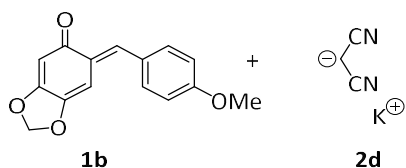$k_2 = (1.36 \pm 0.01) \times 10^3$ M^{-1} s^{-1}
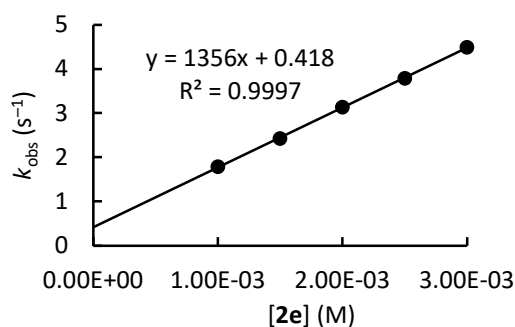
1b + **2f** in DMSO (stopped-flow method, detection at 440 nm) CG203_1
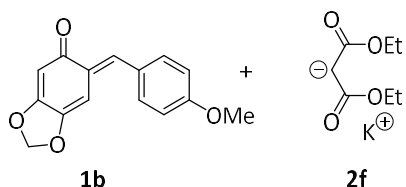
$[\mathbf{1b}]_0$ (M)	$[\mathbf{2f}]_0$ (M)	$[\text{18-c-6}]_0$ (M)	k_{obs} (s^{-1})
4.5×10^{-5}	1.00×10^{-3}		9.72×10^{-1}
4.5×10^{-5}	1.50×10^{-3}	1.65×10^{-3}	1.39
4.5×10^{-5}	2.00×10^{-3}		1.67
4.5×10^{-5}	2.50×10^{-3}	2.75×10^{-3}	2.30

$k_2 = (8.53 \pm 0.96) \times 10^2$ M^{-1} s^{-1}
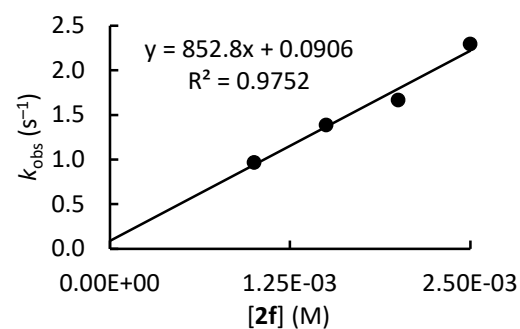
_____

1c + **2a** in DMSO (stopped-flow method, detection at 424 nm) CG265
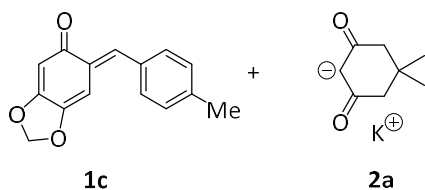
[**1c**]$_0$ (M)	[**2a**]$_0$ (M)	[18-c-6]$_0$ (M)	k_{obs} (s^{-1})
5.10×10^{-5}	1.00×10^{-3}		9.59×10^{-3}
5.10×10^{-5}	1.50×10^{-3}	1.65×10^{-3}	1.25×10^{-2}
5.10×10^{-5}	2.00×10^{-3}		1.50×10^{-2}
5.10×10^{-5}	2.50×10^{-3}	2.75×10^{-3}	1.81×10^{-2}
5.10×10^{-5}	3.00×10^{-3}		2.11×10^{-2}

$$k_2 = (5.72 \pm 0.11)\ \text{M}^{-1}\ \text{s}^{-1}$$
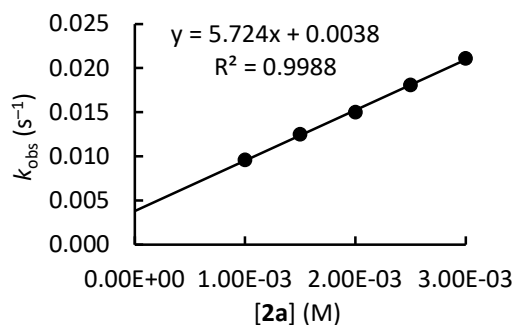
1c + **2b** in DMSO (stopped-flow method, detection at 424 nm) CG264
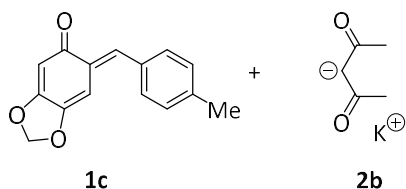
[**1c**]$_0$ (M)	[**2b**]$_0$ (M)	[18-c-6]$_0$ (M)	k_{obs} (s^{-1})
4.43×10^{-5}	1.00×10^{-3}		1.88×10^{-1}
4.43×10^{-5}	1.50×10^{-3}	1.65×10^{-3}	2.85×10^{-1}
4.43×10^{-5}	2.00×10^{-3}		3.61×10^{-1}
4.43×10^{-5}	2.50×10^{-3}	2.75×10^{-3}	4.39×10^{-1}
4.43×10^{-5}	3.00×10^{-3}		5.10×10^{-1}

$$k_2 = (1.60 \pm 0.05) \times 10^2\ \text{M}^{-1}\ \text{s}^{-1}$$
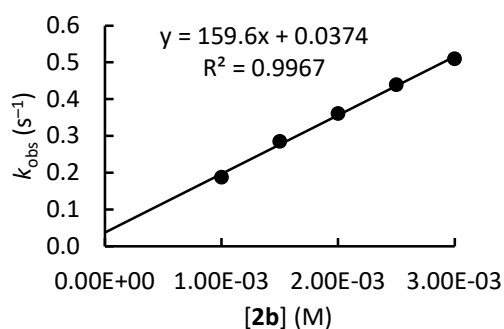
1c + **2c** in DMSO (stopped-flow method, detection at 424 nm) CG263
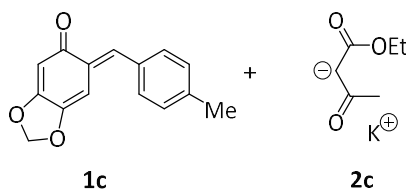
[**1c**]$_0$ (M)	[**2c**]$_0$ (M)	[18-c-6]$_0$ (M)	k_{obs} (s^{-1})
4.53×10^{-5}	1.00×10^{-3}		5.70×10^{-1}
4.53×10^{-5}	1.50×10^{-3}	1.65×10^{-3}	8.30×10^{-1}
4.53×10^{-5}	2.00×10^{-3}		1.03
4.53×10^{-5}	2.50×10^{-3}	2.75×10^{-3}	1.27

$$k_2 = (4.60 \pm 0.15) \times 10^2\ \text{M}^{-1}\ \text{s}^{-1}$$
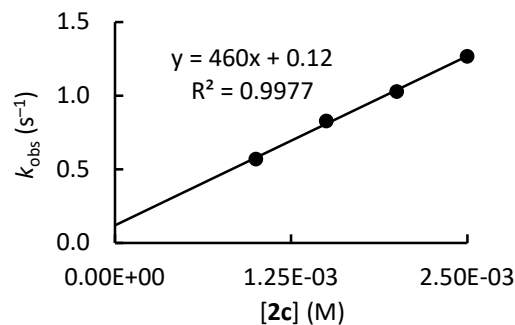
1c + **2d** in DMSO (stopped-flow method, detection at 424 nm) CG261

1c   **2d**

[1c]$_0$ (M)	[2d]$_0$ (M)	[18-c-6]$_0$ (M)	k_{obs} (s^{-1})
5.10×10^{-5}	1.00×10^{-3}		3.34
5.10×10^{-5}	1.50×10^{-3}	1.65×10^{-3}	4.71
5.10×10^{-5}	2.00×10^{-3}		6.37
5.10×10^{-5}	2.50×10^{-3}	2.75×10^{-3}	7.69
5.10×10^{-5}	3.00×10^{-3}		9.21

$$k_2 = (2.94 \pm 0.05) \times 10^3 \text{ M}^{-1} \text{ s}^{-1}$$

y = 2944x + 0.376
R^2 = 0.9991
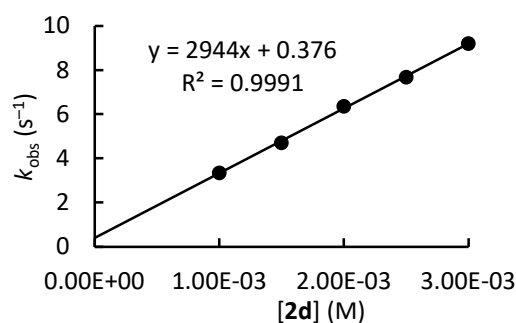
1c + **2e** in DMSO (stopped-flow method, detection at 424 nm) CG262

1c   **2e**
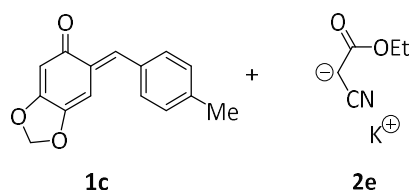
[1c]$_0$ (M)	[2e]$_0$ (M)	[18-c-6]$_0$ (M)	k_{obs} (s^{-1})
5.00×10^{-5}	1.00×10^{-3}		3.31
5.00×10^{-5}	1.50×10^{-3}	1.65×10^{-3}	4.79
5.00×10^{-5}	2.00×10^{-3}		6.34
5.00×10^{-5}	2.50×10^{-3}	2.75×10^{-3}	7.58
5.00×10^{-5}	3.00×10^{-3}		8.79

$$k_2 = (2.75 \pm 0.09) \times 10^3 \text{ M}^{-1} \text{ s}^{-1}$$

y = 2750x + 0.662
R^2 = 0.9969
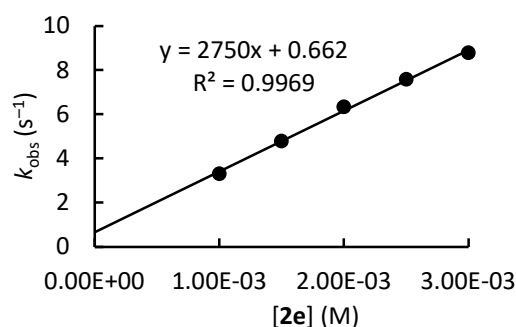
1c + **2f** in DMSO (stopped-flow method, detection at 424 nm) CG260

1c   **2f**

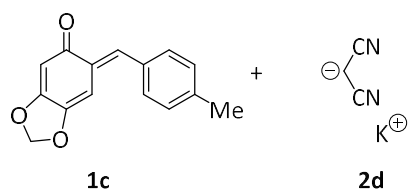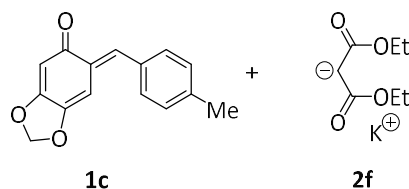| [1c]$_0$ (M)	[2f]$_0$ (M)	[18-c-6]$_0$ (M)	k_{obs} (s^{-1})
4.34×10^{-5}	1.00×10^{-3}		1.52
4.34×10^{-5}	1.50×10^{-3}	1.65×10^{-3}	2.14
4.34×10^{-5}	2.00×10^{-3}		2.59
4.34×10^{-5}	2.50×10^{-3}	2.75×10^{-3}	3.39

$$k_2 = (1.21 \pm 0.09) \times 10^3 \text{ M}^{-1} \text{ s}^{-1}$$
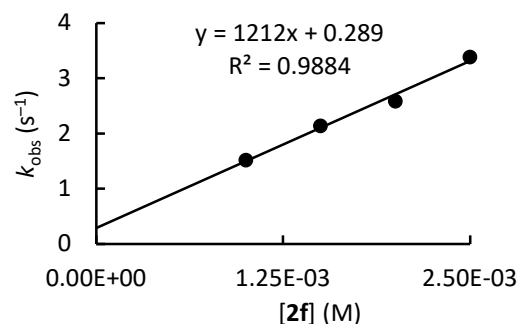
y = 1212x + 0.289
R^2 = 0.9884

1d + **2a** in DMSO (stopped-flow method, detection at 419 nm) CG280

236

1d   **2a**
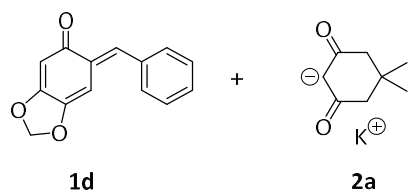
[**1d**]$_0$ (M)	[**2a**]$_0$ (M)	[18-c-6]$_0$ (M)	k_{obs} (s^{-1})
7.00×10^{-5}	1.25×10^{-3}		1.91×10^{-2}
7.00×10^{-5}	1.88×10^{-3}	2.06×10^{-3}	2.84×10^{-2}
7.00×10^{-5}	2.50×10^{-3}		3.63×10^{-2}
7.00×10^{-5}	3.13×10^{-3}	3.44×10^{-3}	4.57×10^{-2}
7.00×10^{-5}	3.75×10^{-3}		5.26×10^{-2}

$$k_2 = (1.35 \pm 0.04) \times 10^1 \ M^{-1} s^{-1}$$

y = 13.488x + 0.0027
R^2 = 0.9978
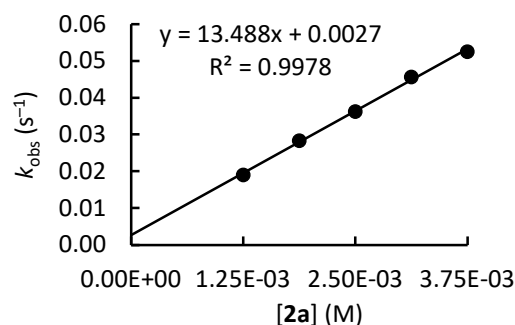
1d + **2b** in DMSO (stopped-flow method, detection at 419 nm) CG279

1d   **2b**
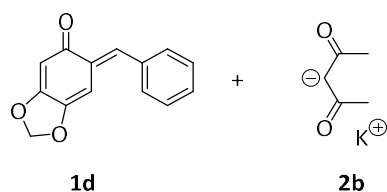
[**1d**]$_0$ (M)	[**2b**]$_0$ (M)	[18-c-6]$_0$ (M)	k_{obs} (s^{-1})
7.00×10^{-5}	1.25×10^{-3}		3.72×10^{-1}
7.00×10^{-5}	1.88×10^{-3}	2.06×10^{-3}	5.59×10^{-1}
7.00×10^{-5}	2.50×10^{-3}		7.20×10^{-1}
7.00×10^{-5}	3.13×10^{-3}	3.44×10^{-3}	9.14×10^{-1}
7.00×10^{-5}	3.75×10^{-3}		1.06

$$k_2 = (2.77 \pm 0.07) \times 10^2 \ M^{-1} s^{-1}$$

y = 276.96x + 0.0326
R^2 = 0.9983
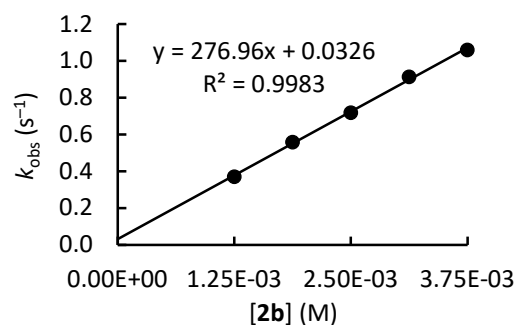
1d + **2c** in DMSO (stopped-flow method, detection at 419 nm) CG278_1

1d   **2c**
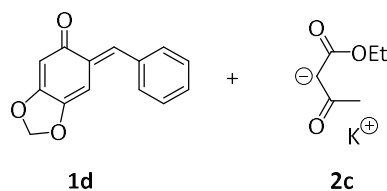
[**1d**]$_0$ (M)	[**2c**]$_0$ (M)	[18-c-6]$_0$ (M)	k_{obs} (s^{-1})
6.86×10^{-5}	1.25×10^{-3}		1.06
6.86×10^{-5}	1.88×10^{-3}	2.06×10^{-3}	1.59
6.86×10^{-5}	2.50×10^{-3}		2.01
6.86×10^{-5}	3.13×10^{-3}	3.44×10^{-3}	2.60

$$k_2 = (8.06 \pm 0.35) \times 10^2 \ M^{-1} s^{-1}$$
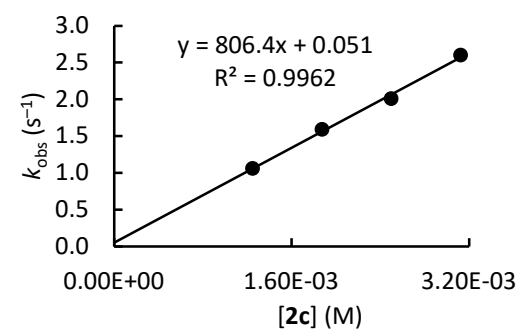
y = 806.4x + 0.051
R^2 = 0.9962

1d + **2d** in DMSO (stopped-flow method, detection at 419 nm) CG274

_____
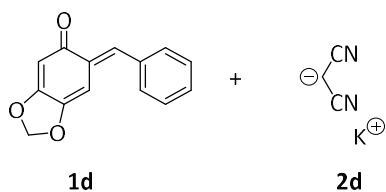
[**1d**]$_0$ (M)	[**2d**]$_0$ (M)	[18-c-6]$_0$ (M)	k_{obs} (s^{-1})
7.14×10^{-5}	1.25×10^{-3}		5.52
7.14×10^{-5}	1.88×10^{-3}	2.06×10^{-3}	7.91
7.14×10^{-5}	2.50×10^{-3}		1.05×10^1
7.14×10^{-5}	3.13×10^{-3}	3.44×10^{-3}	1.26×10^1
7.14×10^{-5}	3.75×10^{-3}		1.51×10^1

$$k_2 = (3.82 \pm 0.06) \times 10^3 \text{ M}^{-1}\text{ s}^{-1}$$
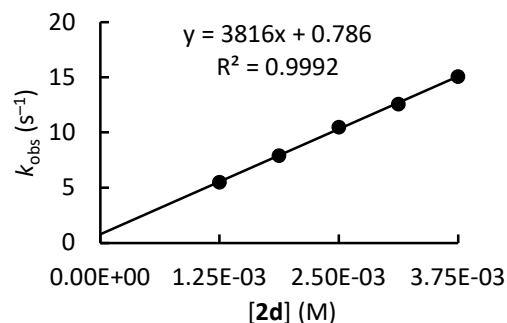
1d + **2e** in DMSO (stopped-flow method, detection at 419 nm) CG275
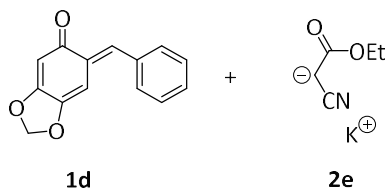
[**1d**]$_0$ (M)	[**2e**]$_0$ (M)	[18-c-6]$_0$ (M)	k_{obs} (s^{-1})
7.00×10^{-5}	1.25×10^{-3}		6.40
7.00×10^{-5}	1.88×10^{-3}	2.06×10^{-3}	9.15
7.00×10^{-5}	2.50×10^{-3}		1.23×10^1
7.00×10^{-5}	3.13×10^{-3}	3.44×10^{-3}	1.49×10^1
7.00×10^{-5}	3.75×10^{-3}		1.78×10^1

$$k_2 = (4.57 \pm 0.07) \times 10^3 \text{ M}^{-1}\text{ s}^{-1}$$
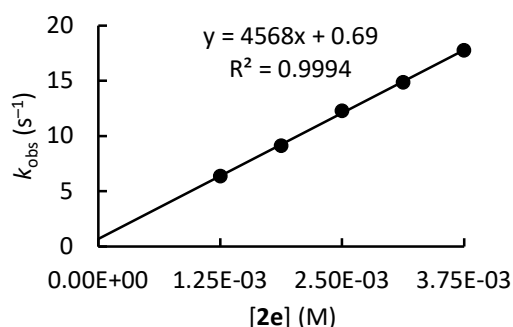
**1d** + **2f** in DMSO (stopped-flow method, detection at 419 nm) CG273

[**1d**]$_0$ (M)	[**2f**]$_0$ (M)	[18-c-6]$_0$ (M)	k_{obs} (s^{-1})
7.42×10^{-5}	1.25×10^{-3}		3.96
7.42×10^{-5}	1.88×10^{-3}	2.06×10^{-3}	5.98
7.42×10^{-5}	2.50×10^{-3}		7.23
7.42×10^{-5}	3.13×10^{-3}	3.44×10^{-3}	9.48

$$k_2 = (2.85 \pm 0.21) \times 10^3 \text{ M}^{-1}\text{ s}^{-1}$$
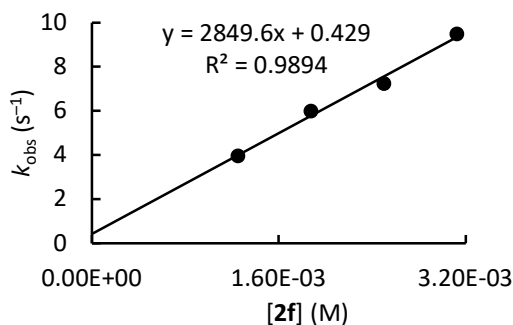
1e + **2a** in DMSO (stopped-flow method, detection at 421 nm) CG326
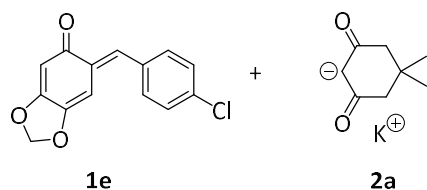
[1e]$_0$ (M)	[2a]$_0$ (M)	[18-c-6]$_0$ (M)	k_{obs} (s^{-1})
4.27×10^{-5}	1.00×10^{-3}		2.74×10^{-2}
4.27×10^{-5}	1.50×10^{-3}	1.65×10^{-3}	4.01×10^{-2}
4.27×10^{-5}	2.00×10^{-3}		5.19×10^{-2}
4.27×10^{-5}	2.50×10^{-3}	2.75×10^{-3}	6.63×10^{-2}
4.27×10^{-5}	3.00×10^{-3}		7.81×10^{-2}

$$k_2 = (2.55 \pm 0.04) \times 10^1 \text{ M}^{-1} \text{ s}^{-1}$$
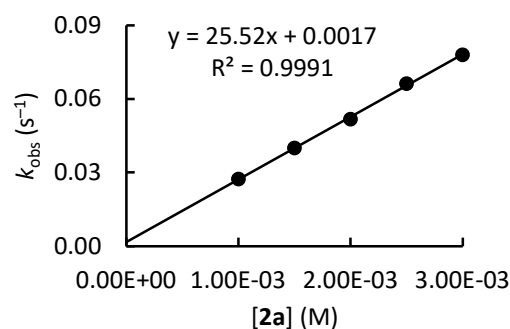
**1e** + **2b** in DMSO (stopped-flow method, detection at 421 nm) CG325
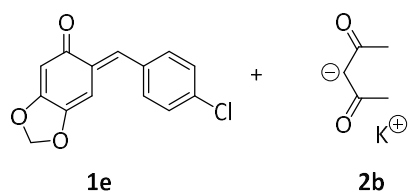
[1e]$_0$ (M)	[2b]$_0$ (M)	[18-c-6]$_0$ (M)	k_{obs} (s^{-1})
4.55×10^{-5}	1.00×10^{-3}		6.32×10^{-1}
4.55×10^{-5}	1.50×10^{-3}	1.65×10^{-3}	9.25×10^{-1}
4.55×10^{-5}	2.00×10^{-3}		1.17
4.55×10^{-5}	2.50×10^{-3}	2.75×10^{-3}	1.44

$$k_2 = (5.34 \pm 0.13) \times 10^2 \text{ M}^{-1} \text{ s}^{-1}$$
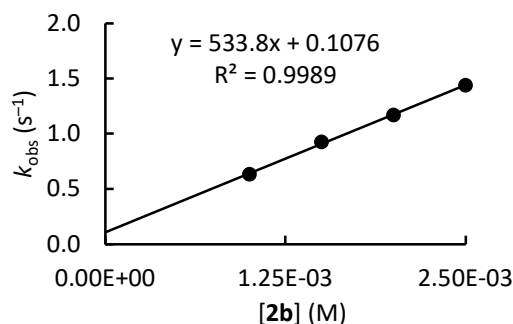
1e + **2c** in DMSO (stopped-flow method, detection at 421 nm) CG324
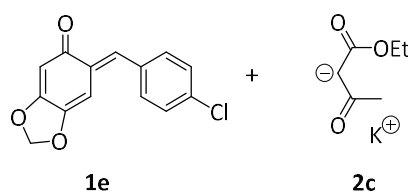
[1e]$_0$ (M)	[2c]$_0$ (M)	[18-c-6]$_0$ (M)	k_{obs} (s^{-1})
4.55×10^{-5}	5.00×10^{-4}		9.82×10^{-1}
4.55×10^{-5}	7.50×10^{-4}	8.25×10^{-4}	1.44
4.55×10^{-5}	1.00×10^{-3}		1.84
4.55×10^{-5}	1.25×10^{-3}	1.38×10^{-3}	2.24

$$k_2 = (1.67 \pm 0.04) \times 10^3 \text{ M}^{-1} \text{ s}^{-1}$$
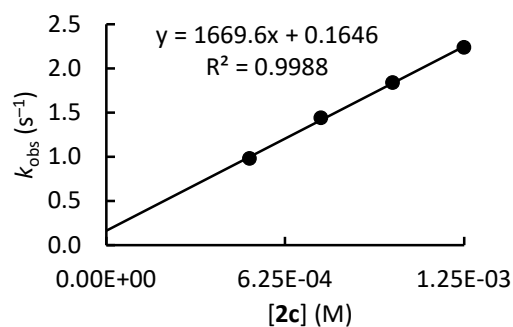
1e + **2d** in DMSO (stopped-flow method, detection at 421 nm) CG319
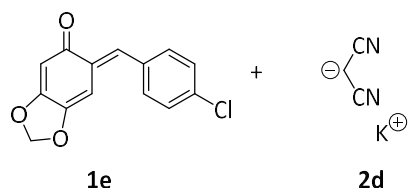
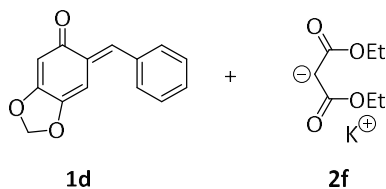| [1e]$_0$ (M)	[2d]$_0$ (M)	[18-c-6]$_0$ (M)	k_{obs} (s^{-1})
3.82×10^{-5}	5.00×10^{-4}		4.16
3.82×10^{-5}	7.50×10^{-4}	8.25×10^{-4}	6.14
3.82×10^{-5}	1.00×10^{-3}		8.09
3.82×10^{-5}	1.25×10^{-3}	1.38×10^{-3}	1.01×10^1
3.82×10^{-5}	1.50×10^{-3}		1.19×10^1

$$k_2 = (7.78 \pm 0.08) \times 10^3 \text{ M}^{-1}\text{ s}^{-1}$$
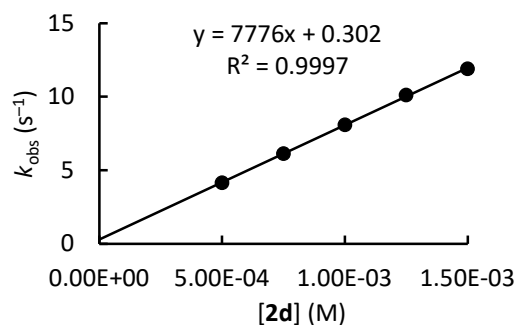
**1e** + **2e** in DMSO (stopped-flow method, detection at 421 nm) CG323
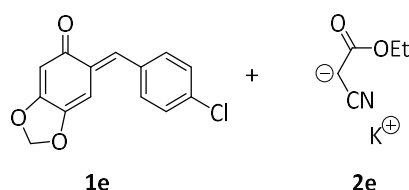
[1e]$_0$ (M)	[2e]$_0$ (M)	[18-c-6]$_0$ (M)	k_{obs} (s^{-1})
4.00×10^{-5}	5.00×10^{-4}		6.14
4.00×10^{-5}	7.50×10^{-4}	8.25×10^{-4}	9.14
4.00×10^{-5}	1.00×10^{-3}		1.19×10^1
4.00×10^{-5}	1.25×10^{-3}	1.38×10^{-3}	1.49×10^1
4.00×10^{-5}	1.50×10^{-3}		1.78×10^1

$$k_2 = (1.16 \pm 0.01) \times 10^4 \text{ M}^{-1}\text{ s}^{-1}$$
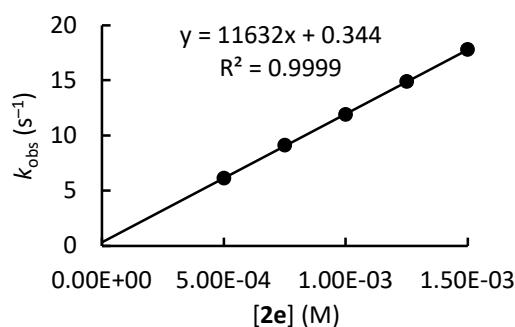
1e + **2f** in DMSO (stopped-flow method, detection at 421 nm) CG318
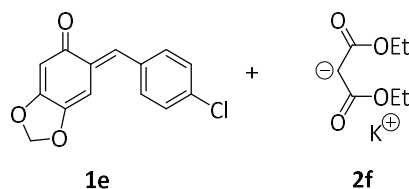
[1e]$_0$ (M)	[2f]$_0$ (M)	[18-c-6]$_0$ (M)	k_{obs} (s^{-1})
4.00×10^{-5}	1.00×10^{-3}		9.15
4.00×10^{-5}	1.50×10^{-3}	1.65×10^{-3}	1.39×10^1
4.00×10^{-5}	2.00×10^{-3}		1.66×10^1
4.00×10^{-5}	2.50×10^{-3}	2.75×10^{-3}	2.21×10^1

$$k_2 = (8.31 \pm 0.73) \times 10^3 \text{ M}^{-1}\text{ s}^{-1}$$
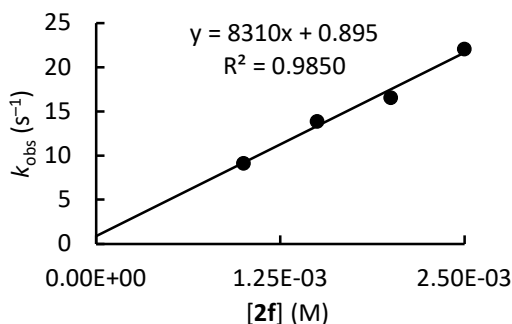
_____

1f + **2a** in DMSO (stopped-flow method, detection at 417 nm) CG342
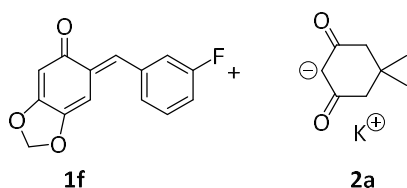
[**1f**]$_0$ (M)	[**2a**]$_0$ (M)	[18-c-6]$_0$ (M)	k_{obs} (s^{-1})
5.88×10^{-5}	1.25×10^{-3}		3.91×10^{-2}
5.88×10^{-5}	1.88×10^{-3}	2.06×10^{-3}	5.85×10^{-2}
5.88×10^{-5}	2.50×10^{-3}		7.55×10^{-2}
5.88×10^{-5}	3.13×10^{-3}	3.44×10^{-3}	9.73×10^{-2}
5.88×10^{-5}	3.75×10^{-3}		1.13×10^{-1}

$$k_2 = (2.99 \pm 0.08) \times 10^1 \text{ M}^{-1} \text{ s}^{-1}$$
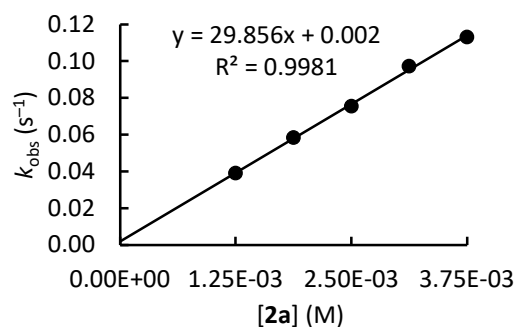
1f + **2b** in DMSO (stopped-flow method, detection at 417 nm) CG339
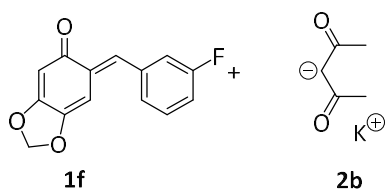
[**1f**]$_0$ (M)	[**2b**]$_0$ (M)	[18-c-6]$_0$ (M)	k_{obs} (s^{-1})
5.88×10^{-5}	1.25×10^{-3}		8.48×10^{-1}
5.88×10^{-5}	1.88×10^{-3}	2.06×10^{-3}	1.25
5.88×10^{-5}	2.50×10^{-3}		1.63
5.88×10^{-5}	3.13×10^{-3}	3.44×10^{-3}	2.05
5.88×10^{-5}	3.75×10^{-3}		2.39

$$k_2 = (6.21 \pm 0.10) \times 10^2 \text{ M}^{-1} \text{ s}^{-1}$$
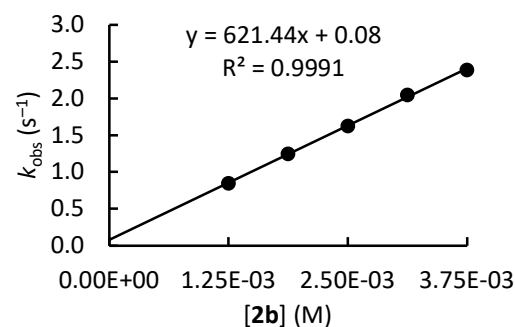
1f + **2c** in DMSO (stopped-flow method, detection at 417 nm) CG341
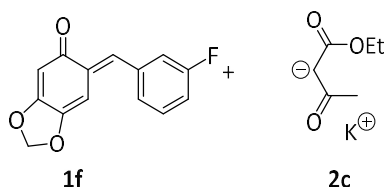
[**1f**]$_0$ (M)	[**2c**]$_0$ (M)	[18-c-6]$_0$ (M)	k_{obs} (s^{-1})
5.88×10^{-5}	6.25×10^{-4}		1.35
5.88×10^{-5}	9.40×10^{-4}	1.03×10^{-3}	1.92
5.88×10^{-5}	1.25×10^{-3}		2.51
5.88×10^{-5}	1.57×10^{-3}	1.72×10^{-3}	3.07

$$k_2 = (1.83 \pm 0.02) \times 10^3 \text{ M}^{-1} \text{ s}^{-1}$$
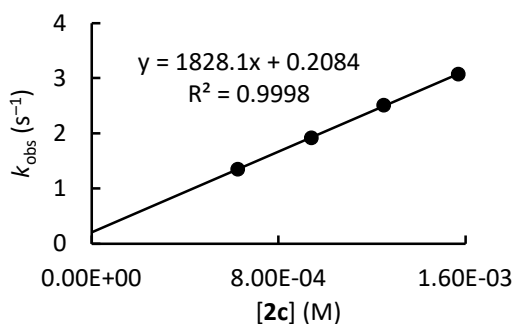
241

_____

1f + **2d** in DMSO (stopped-flow method, detection at 417 nm) CG338
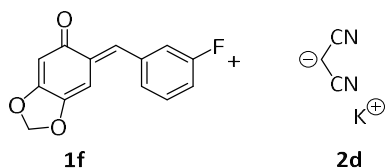
$[1f]_0$ (M)	$[2d]_0$ (M)	$[18\text{-}c\text{-}6]_0$ (M)	k_{obs} (s^{-1})
5.76×10^{-5}	6.25×10^{-4}		4.77
5.76×10^{-5}	9.40×10^{-4}	1.03×10^{-3}	6.74
5.76×10^{-5}	1.25×10^{-3}		9.04
5.76×10^{-5}	1.57×10^{-3}	1.72×10^{-3}	1.08×10^1
5.76×10^{-5}	1.88×10^{-3}		1.27×10^1

$$k_2 = (6.34 \pm 0.16) \times 10^3 \text{ M}^{-1} \text{ s}^{-1}$$

y = 6343.1x + 0.8621
R^2 = 0.9980
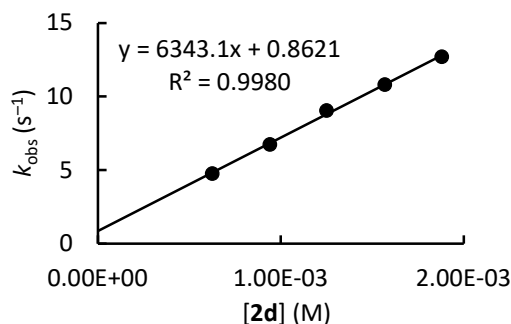
1f + **2e** in DMSO (stopped-flow method, detection at 417 nm) CG340
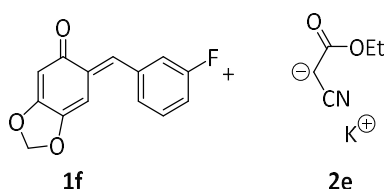
$[1f]_0$ (M)	$[2e]_0$ (M)	$[18\text{-}c\text{-}6]_0$ (M)	k_{obs} (s^{-1})
5.76×10^{-5}	6.25×10^{-4}		7.07
5.76×10^{-5}	9.40×10^{-4}	1.03×10^{-3}	9.85
5.76×10^{-5}	1.25×10^{-3}		1.29×10^1
5.76×10^{-5}	1.57×10^{-3}	1.72×10^{-3}	1.49×10^1

$$k_2 = (8.43 \pm 0.53) \times 10^3 \text{ M}^{-1} \text{ s}^{-1}$$

y = 8434.5x + 1.9337
R^2 = 0.9923
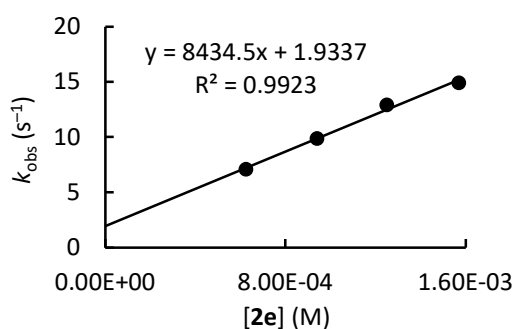
1f + **2f** in DMSO (stopped-flow method, detection at 417 nm) CG337
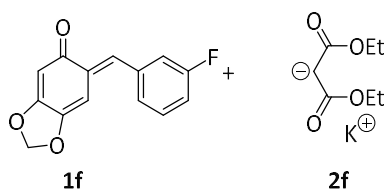
$[1f]_0$ (M)	$[2f]_0$ (M)	$[18\text{-}c\text{-}6]_0$ (M)	k_{obs} (s^{-1})
5.54×10^{-5}	6.25×10^{-4}		6.54
5.54×10^{-5}	9.40×10^{-4}	1.03×10^{-3}	9.41
5.54×10^{-5}	1.25×10^{-3}		1.16×10^1
5.54×10^{-5}	1.57×10^{-3}	1.72×10^{-3}	1.43×10^1

$$k_2 = (8.10 \pm 0.26) \times 10^3 \text{ M}^{-1} \text{ s}^{-1}$$

y = 8099.7x + 1.5833
R^2 = 0.9979

_____
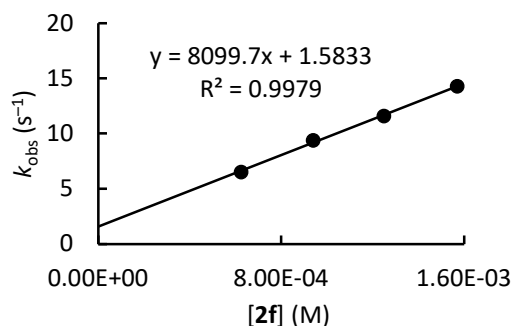
1g + **2a** in DMSO (stopped-flow method, detection at 419 nm) CG336
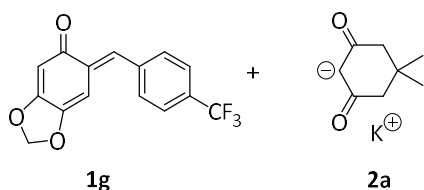
$[\mathbf{1g}]_0$ (M)	$[\mathbf{2a}]_0$ (M)	$[\text{18-c-6}]_0$ (M)	k_{obs} (s^{-1})
6.82×10^{-5}	1.25×10^{-3}		7.20×10^{-2}
6.82×10^{-5}	1.88×10^{-3}	2.06×10^{-3}	1.03×10^{-1}
6.82×10^{-5}	2.50×10^{-3}		1.37×10^{-1}
6.82×10^{-5}	3.13×10^{-3}	3.44×10^{-3}	1.68×10^{-1}
6.82×10^{-5}	3.75×10^{-3}		2.04×10^{-1}

$$k_2 = (5.26 \pm 0.08) \times 10^1 \text{ M}^{-1} \text{ s}^{-1}$$
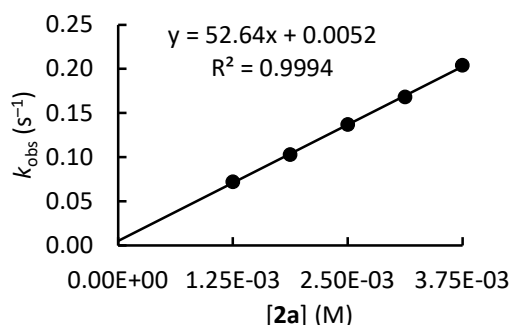
**1g** + **2b** in DMSO (stopped-flow method, detection at 419 nm) CG335

$[\mathbf{1g}]_0$ (M)	$[\mathbf{2b}]_0$ (M)	$[\text{18-c-6}]_0$ (M)	k_{obs} (s^{-1})
6.94×10^{-5}	1.25×10^{-3}		1.62
6.94×10^{-5}	1.88×10^{-3}	2.06×10^{-3}	2.40
6.94×10^{-5}	2.50×10^{-3}		3.13
6.94×10^{-5}	3.13×10^{-3}	3.44×10^{-3}	3.88
6.94×10^{-5}	3.75×10^{-3}		4.61

$$k_2 = (1.19 \pm 0.01) \times 10^3 \text{ M}^{-1} \text{ s}^{-1}$$
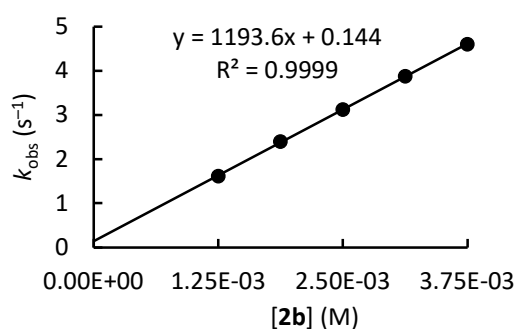
**1g** + **2c** in DMSO (stopped-flow method, detection at 419 nm) CG334
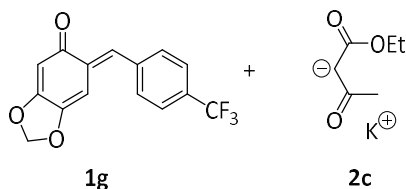
$[\mathbf{1g}]_0$ (M)	$[\mathbf{2c}]_0$ (M)	$[\text{18-c-6}]_0$ (M)	k_{obs} (s^{-1})
5.70×10^{-5}	6.25×10^{-4}		2.52
5.70×10^{-5}	9.40×10^{-4}	1.03×10^{-3}	4.01
5.70×10^{-5}	1.25×10^{-3}		5.16
5.70×10^{-5}	1.57×10^{-3}	1.72×10^{-3}	6.47
5.70×10^{-5}	1.88×10^{-3}		7.58

$$k_2 = (4.01 \pm 0.01) \times 10^3 \text{ M}^{-1} \text{ s}^{-1}$$
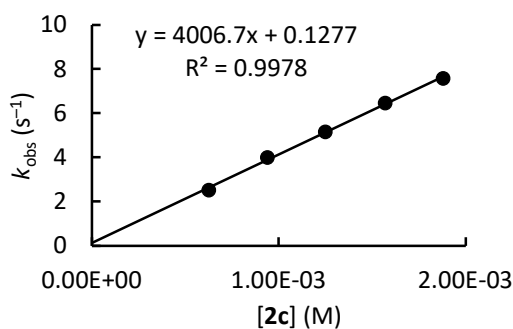
_____

1g + **2d** in DMSO (stopped-flow method, detection at 419 nm) CG332

[**1g**]$_0$ (M)	[**2d**]$_0$ (M)	[18-c-6]$_0$ (M)	k_{obs} (s^{-1})
5.58×10^{-5}	6.25×10^{-4}		7.69
5.58×10^{-5}	9.40×10^{-4}	1.03×10^{-3}	1.17×10^1
5.58×10^{-5}	1.25×10^{-3}		1.57×10^1
5.58×10^{-5}	1.57×10^{-3}	1.72×10^{-3}	1.93×10^1
5.58×10^{-5}	1.88×10^{-3}		2.30×10^1

$k_2 = (1.22 \pm 0.02) \times 10^4$ M^{-1} s^{-1}
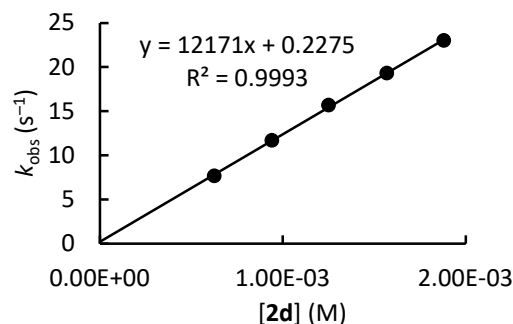
1g + **2e** in DMSO (stopped-flow method, detection at 419 nm) CG333
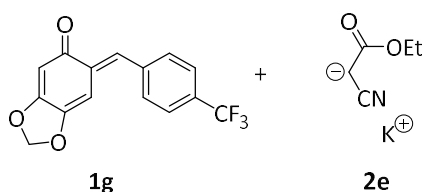
[**1g**]$_0$ (M)	[**2e**]$_0$ (M)	[18-c-6]$_0$ (M)	k_{obs} (s^{-1})
5.58×10^{-5}	6.25×10^{-4}		1.45×10^1
5.58×10^{-5}	9.40×10^{-4}	1.03×10^{-3}	2.13×10^1
5.58×10^{-5}	1.25×10^{-3}		2.85×10^1
5.58×10^{-5}	1.57×10^{-3}	1.72×10^{-3}	3.49×10^1
5.58×10^{-5}	1.88×10^{-3}		4.20×10^1

$k_2 = (2.18 \pm 0.03) \times 10^4$ M^{-1} s^{-1}
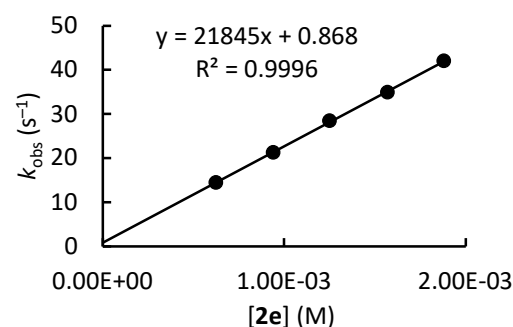
1g + **2f** in DMSO (stopped-flow method, detection at 419 nm) CG331
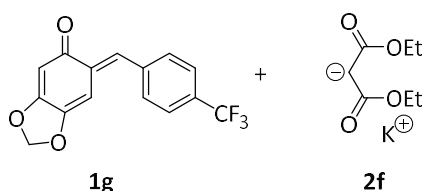
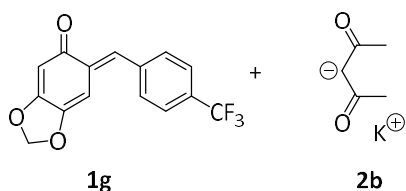| [**1g**]$_0$ (M)	[**2f**]$_0$ (M)	[18-c-6]$_0$ (M)	k_{obs} (s^{-1})
5.33×10^{-5}	6.25×10^{-4}		1.30×10^1
5.33×10^{-5}	9.40×10^{-4}	1.03×10^{-3}	1.96×10^1
5.33×10^{-5}	1.25×10^{-3}		2.40×10^1
5.33×10^{-5}	1.57×10^{-3}	1.72×10^{-3}	3.12×10^1

$k_2 = (1.88 \pm 0.11) \times 10^4$ M^{-1} s^{-1}
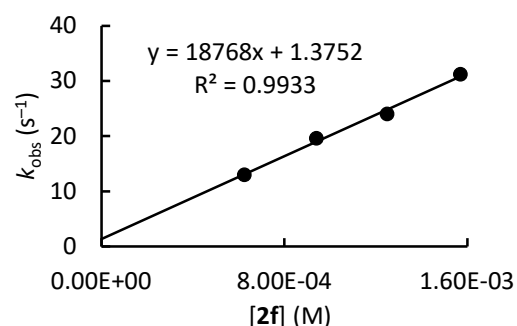
_____

1h + **2a** in DMSO (stopped-flow method, detection at 437 nm) CG402
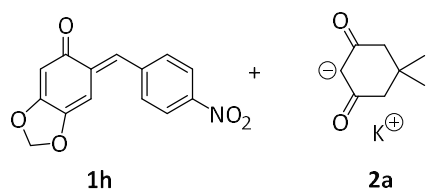
[**1h**]$_0$ (M)	[**2a**]$_0$ (M)	[18-c-6]$_0$ (M)	k_{obs} (s^{-1})
3.93×10^{-5}	1.75×10^{-3}		1.65×10^{-1}
3.93×10^{-5}	2.63×10^{-3}	2.89×10^{-3}	2.49×10^{-1}
3.93×10^{-5}	3.50×10^{-3}		3.40×10^{-1}
3.93×10^{-5}	4.38×10^{-3}	4.81×10^{-3}	4.19×10^{-1}
3.93×10^{-5}	5.25×10^{-3}		5.04×10^{-1}

$$k_2 = (9.69 \pm 0.11) \times 10^1 \text{ M}^{-1} \text{ s}^{-1}$$
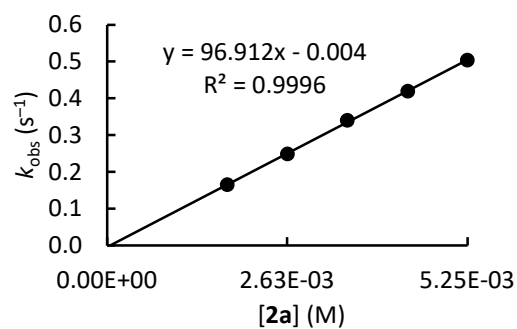
**1h** + **2b** in DMSO (stopped-flow method, detection at 437 nm) CG346
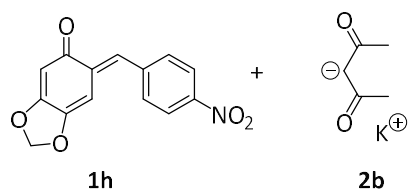
[**1h**]$_0$ (M)	[**2b**]$_0$ (M)	[18-c-6]$_0$ (M)	k_{obs} (s^{-1})
5.63×10^{-5}	1.00×10^{-3}		2.20
5.63×10^{-5}	1.50×10^{-3}	1.65×10^{-3}	3.32
5.63×10^{-5}	2.00×10^{-3}		4.48
5.63×10^{-5}	2.50×10^{-3}	2.75×10^{-3}	5.59

$$k_2 = (2.27 \pm 0.01) \times 10^3 \text{ M}^{-1} \text{ s}^{-1}$$
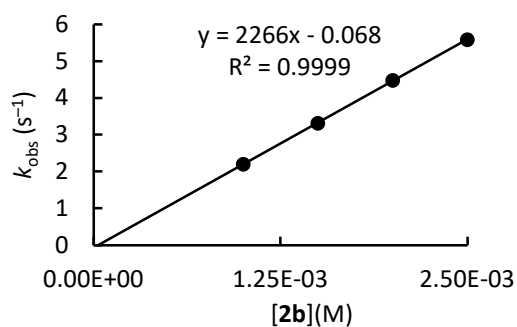
1h + **2c** in DMSO (stopped-flow method, detection at 437 nm) CG345
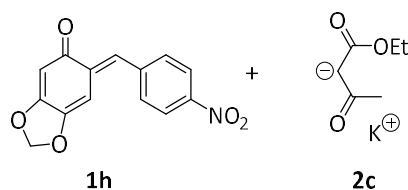
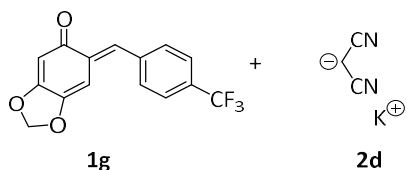
[**1h**]$_0$ (M)	[**2c**]$_0$ (M)	[18-c-6]$_0$ (M)	k_{obs} (s^{-1})
5.63×10^{-5}	5.00×10^{-4}		4.03
5.63×10^{-5}	7.50×10^{-4}	8.25×10^{-4}	5.97
5.63×10^{-5}	1.00×10^{-3}		7.97
5.63×10^{-5}	1.25×10^{-3}	1.38×10^{-3}	9.91
5.63×10^{-5}	1.50×10^{-3}		1.16×10^1

$$k_2 = (7.63 \pm 0.13) \times 10^3 \text{ M}^{-1} \text{ s}^{-1}$$
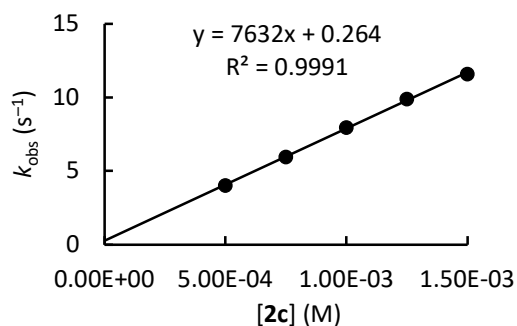
_____

1h + **2d** in DMSO (stopped-flow method, detection at 437 nm) CG344
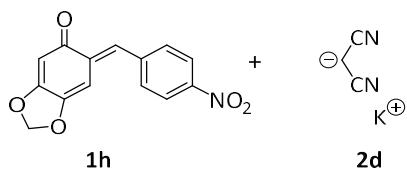
$[\mathbf{1h}]_0$ (M)	$[\mathbf{2d}]_0$ (M)	$[\text{18-c-6}]_0$ (M)	k_{obs} (s^{-1})
4.30×10^{-5}	5.00×10^{-4}		1.08×10^1
4.30×10^{-5}	7.50×10^{-4}	8.25×10^{-4}	1.56×10^1
4.30×10^{-5}	1.00×10^{-3}		2.13×10^1
4.30×10^{-5}	1.25×10^{-3}	1.38×10^{-3}	2.61×10^1
4.30×10^{-5}	1.50×10^{-3}		3.14×10^1

$$k_2 = (2.07 \pm 0.03) \times 10^4 \text{ M}^{-1} \text{ s}^{-1}$$
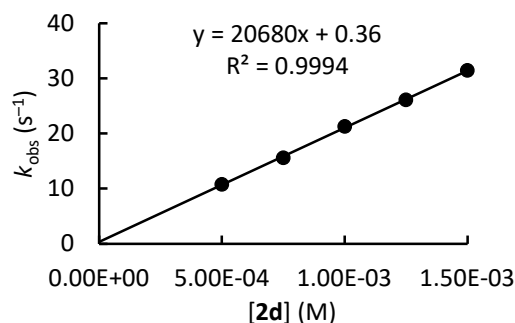
1h + **2e** in DMSO (stopped-flow method, detection at 437 nm) CG347
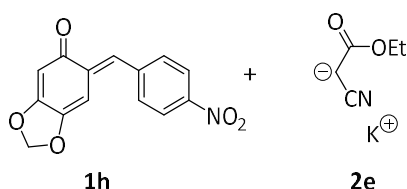
$[\mathbf{1h}]_0$ (M)	$[\mathbf{2e}]_0$ (M)	$[\text{18-c-6}]_0$ (M)	k_{obs} (s^{-1})
5.36×10^{-5}	5.00×10^{-4}		1.85×10^1
5.36×10^{-5}	7.50×10^{-4}	8.25×10^{-4}	2.72×10^1
5.36×10^{-5}	1.00×10^{-3}		3.63×10^1
5.36×10^{-5}	1.25×10^{-3}	1.38×10^{-3}	4.43×10^1
5.36×10^{-5}	1.50×10^{-3}		5.38×10^1

$$k_2 = (3.51 \pm 0.05) \times 10^4 \text{ M}^{-1} \text{ s}^{-1}$$
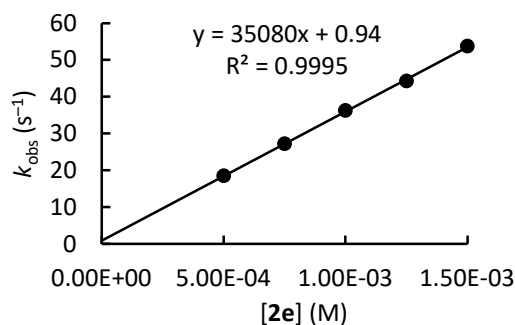
**1h** + **2f** in DMSO (stopped-flow method, detection at 437 nm) CG343
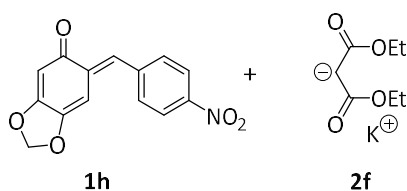
$[\mathbf{1h}]_0$ (M)	$[\mathbf{2f}]_0$ (M)	$[\text{18-c-6}]_0$ (M)	k_{obs} (s^{-1})
4.20×10^{-5}	5.00×10^{-4}		2.30×10^1
4.20×10^{-5}	7.50×10^{-4}	8.25×10^{-4}	3.52×10^1
4.20×10^{-5}	1.00×10^{-3}		4.38×10^1
4.20×10^{-5}	1.25×10^{-3}	1.38×10^{-3}	5.66×10^1

$$k_2 = (4.38 \pm 0.22) \times 10^4 \text{ M}^{-1} \text{ s}^{-1}$$
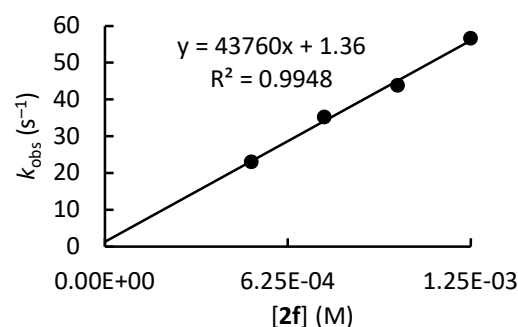
5.2.7. Kinetics of the Reactions of *o*QM 1b with Miscellaneous Nucleophiles

1b + **8** in DMSO (stopped-flow method, detection at 440 nm) CG223

[**1b**]$_0$ (M)	[**8**]$_0$ (M)	k_{obs} (s^{-1})
5.40×10^{-5}	1.00×10^{-3}	3.08×10^{-1}
5.40×10^{-5}	1.50×10^{-3}	4.33×10^{-1}
5.40×10^{-5}	2.00×10^{-3}	5.78×10^{-1}
5.40×10^{-5}	2.50×10^{-3}	6.92×10^{-1}

k_2 = (2.59 ± 0.08) × 10^2 M^{-1} s^{-1}
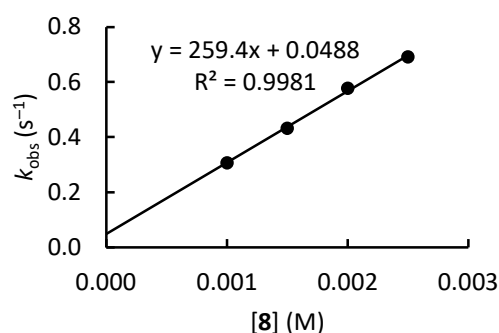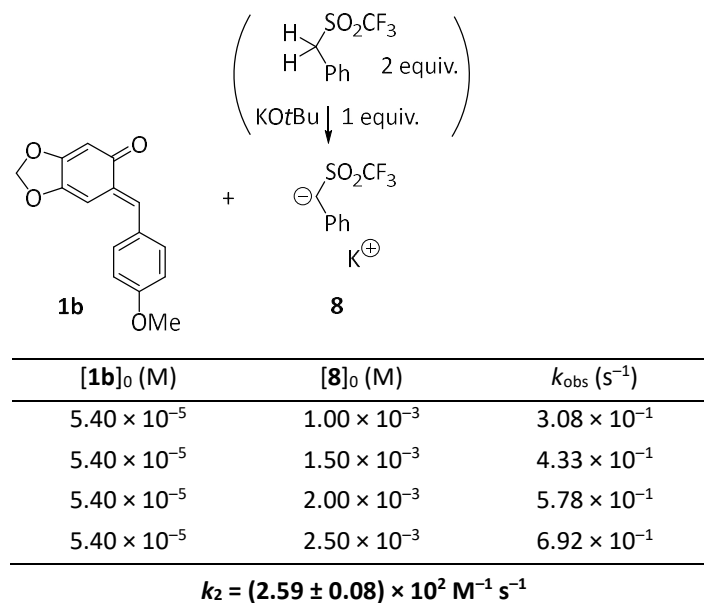
1b + **9** in DMSO (stopped-flow method, detection at 440 nm) CG230

[**1b**]$_0$ (M)	[**9**]$_0$ (M)	k_{obs} (s^{-1})
5.80×10^{-5}	1.00×10^{-3}	4.07×10^{-3}
5.80×10^{-5}	1.50×10^{-3}	6.19×10^{-3}
5.80×10^{-5}	2.00×10^{-3}	8.08×10^{-3}
5.80×10^{-5}	2.50×10^{-3}	1.06×10^{-2}
5.80×10^{-5}	3.00×10^{-3}	1.28×10^{-2}

k_2 = (4.37 ± 0.11) M^{-1} s^{-1}
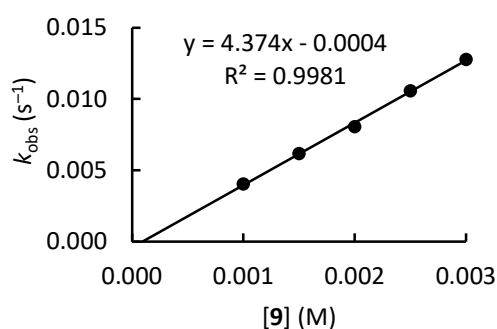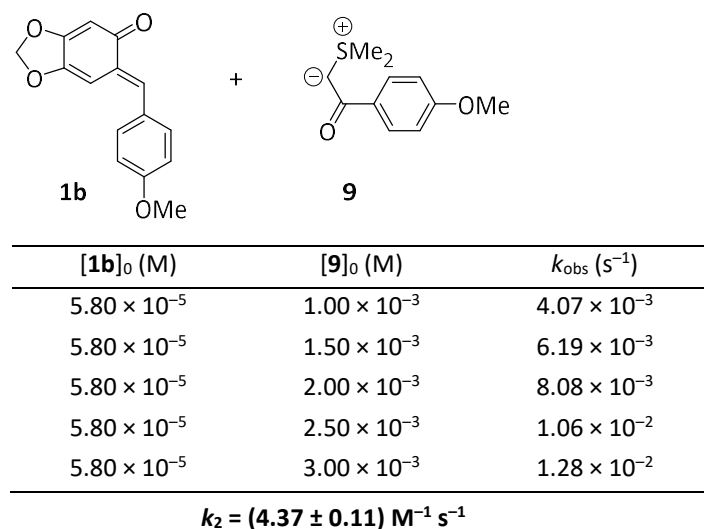
1b + **10** in DMSO (conventional photometry, detected at 440 nm) CG235
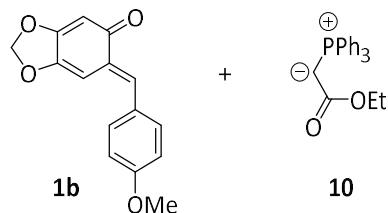
[**1b**]$_0$ (M)	[**10**]$_0$ (M)	k_{obs} (s^{-1})
5.40×10^{-5}	4.54×10^{-3}	7.96×10^{-5}
5.40×10^{-5}	6.71×10^{-3}	1.20×10^{-4}
5.40×10^{-5}	7.85×10^{-3}	1.32×10^{-4}
5.40×10^{-5}	8.83×10^{-3}	1.45×10^{-4}

$$k_2 = (1.52 \pm 0.13) \times 10^{-2} \text{ M}^{-1} \text{ s}^{-1}$$
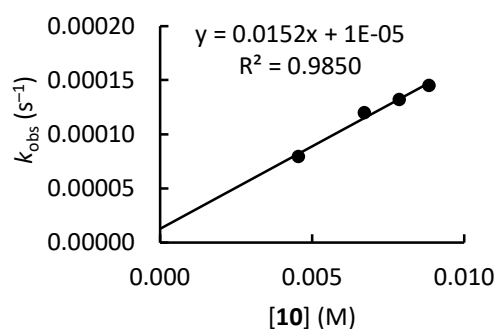
1b + **11** in DMSO (stopped-flow method, detection at 440 nm) CG231
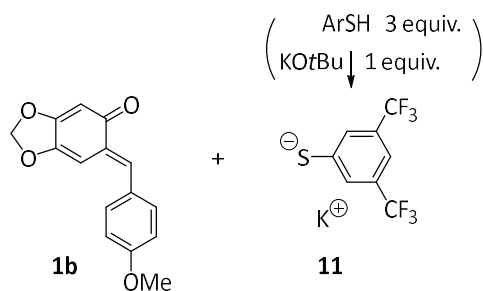
[**1b**]$_0$ (M)	[**11**]$_0$ (M)	k_{obs} (s^{-1})
6.00×10^{-5}	5.00×10^{-4}	1.17×10^{1}
6.00×10^{-5}	7.50×10^{-4}	1.90×10^{1}
6.00×10^{-5}	1.00×10^{-3}	2.72×10^{1}
6.00×10^{-5}	1.25×10^{-3}	3.48×10^{1}
6.00×10^{-5}	1.50×10^{-3}	4.34×10^{1}

$$k_2 = (3.17 \pm 0.05) \times 10^{4} \text{ M}^{-1} \text{ s}^{-1}$$

_____
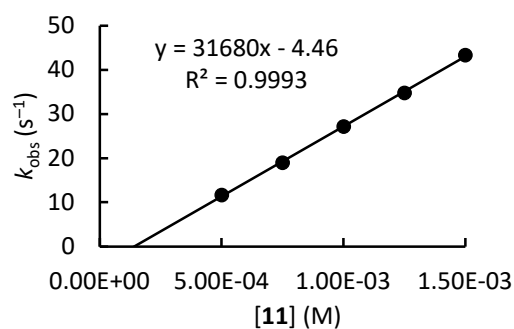
1b + **12a** in DMSO (stopped-flow method, detection at 440 nm) CG209
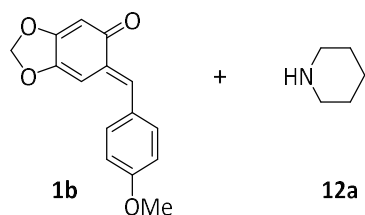
$[\mathbf{1b}]_0$ (M)	$[\mathbf{12a}]_0$ (M)	k_{obs} (s^{-1})
4.70×10^{-5}	1.00×10^{-3}	4.31×10^{-1}
4.70×10^{-5}	1.50×10^{-3}	6.54×10^{-1}
4.70×10^{-5}	2.00×10^{-3}	8.76×10^{-1}
4.70×10^{-5}	2.50×10^{-3}	1.09

$$k_2 = (4.40 \pm 0.03) \times 10^2 \ M^{-1} \ s^{-1}$$
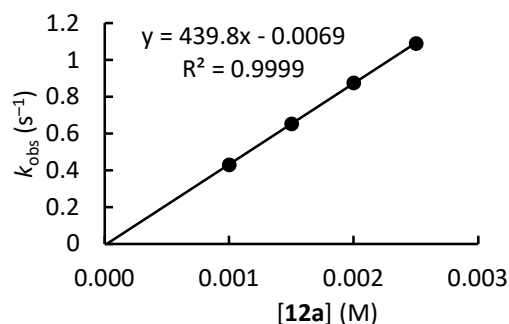
1b + **12b** in DMSO (stopped-flow method, detection at 440 nm) CG210
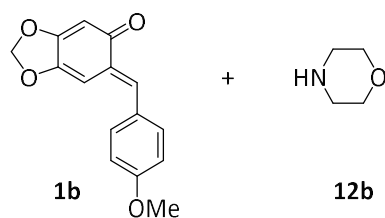
$[\mathbf{1b}]_0$ (M)	$[\mathbf{12b}]_0$ (M)	k_{obs} (s^{-1})
4.30×10^{-5}	1.00×10^{-3}	1.35×10^{-1}
4.30×10^{-5}	1.50×10^{-3}	2.04×10^{-1}
4.30×10^{-5}	2.00×10^{-3}	2.70×10^{-1}
4.30×10^{-5}	2.50×10^{-3}	3.41×10^{-1}

$$k_2 = (1.37 \pm 0.02) \times 10^2 \ M^{-1} \ s^{-1}$$
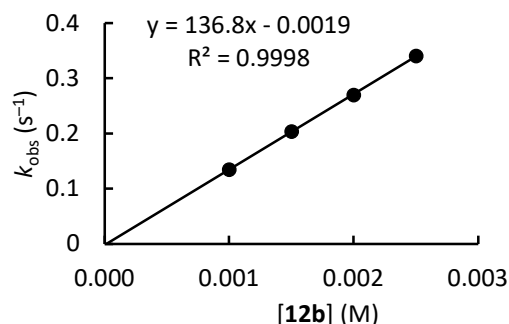
1b + **12c** in DMSO (stopped-flow method, detection at 440 nm) CG212
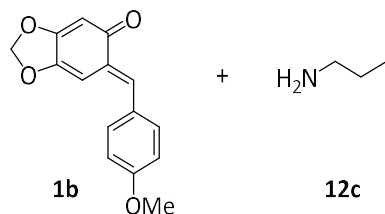
$[\mathbf{1b}]_0$ (M)	$[\mathbf{12c}]_0$ (M)	k_{obs} (s^{-1})
4.40×10^{-5}	2.50×10^{-3}	5.73×10^{-2}
4.40×10^{-5}	3.00×10^{-3}	6.77×10^{-2}
4.40×10^{-5}	3.50×10^{-3}	7.76×10^{-2}
4.40×10^{-5}	4.00×10^{-3}	8.79×10^{-2}

$$k_2 = (2.03 \pm 0.01) \times 10^1 \ M^{-1} \ s^{-1}$$

_____
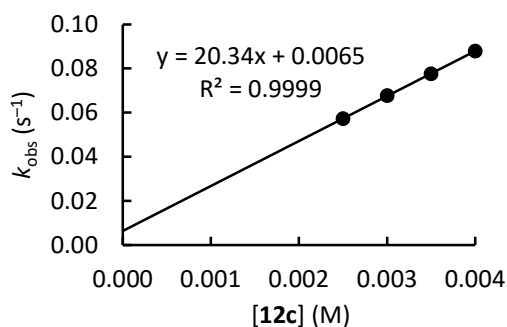
1b + **12d** in DMSO (stopped-flow method, detection at 440 nm) CG211
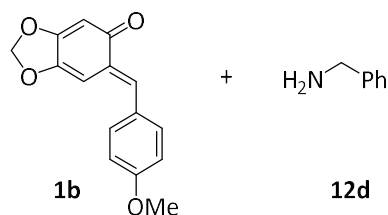
$[1b]_0$ (M)	$[12d]_0$ (M)	k_{obs} (s^{-1})
4.30×10^{-5}	2.50×10^{-3}	3.19×10^{-2}
4.30×10^{-5}	3.00×10^{-3}	3.76×10^{-2}
4.30×10^{-5}	3.50×10^{-3}	4.31×10^{-2}
4.30×10^{-5}	4.00×10^{-3}	4.87×10^{-2}

$k_2 = (1.12 \pm 0.01) \times 10^1$ M^{-1} s^{-1}
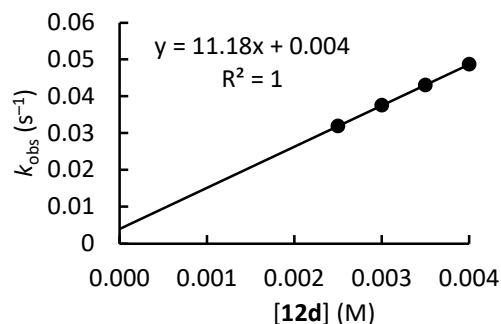
1b + **12e** in DMSO (stopped-flow method, detection at 440 nm) CG215
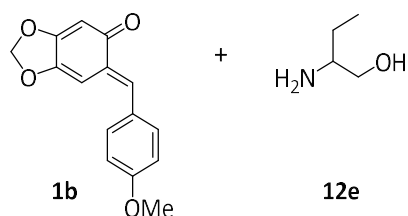
$[1b]_0$ (M)	$[12e]_0$ (M)	k_{obs} (s^{-1})
3.80×10^{-5}	2.50×10^{-3}	1.14×10^{-2}
3.80×10^{-5}	3.00×10^{-3}	1.28×10^{-2}
3.80×10^{-5}	3.50×10^{-3}	1.44×10^{-2}
3.80×10^{-5}	4.00×10^{-3}	1.63×10^{-2}

$k_2 = (3.26 \pm 0.16)$ M^{-1} s^{-1}
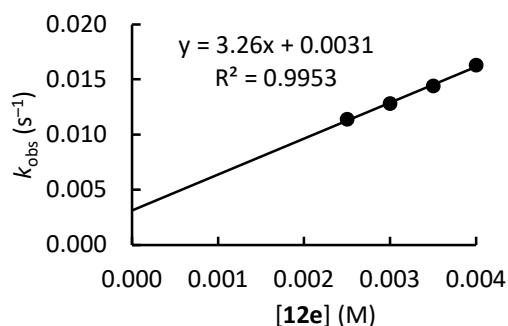
1b + **12f** in DMSO (conventional photometry, detection at 440 nm) CG214
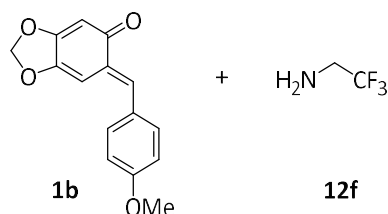
$[1b]_0$ (M)	$[12f]_0$ (M)	k_{obs} (s^{-1})
5.98×10^{-5}	2.61×10^{-3}	4.98×10^{-4}
4.98×10^{-5}	4.97×10^{-3}	8.53×10^{-4}
5.15×10^{-5}	7.38×10^{-3}	1.20×10^{-3}
4.89×10^{-5}	9.61×10^{-3}	1.49×10^{-3}

$k_2 = (1.42 \pm 0.03) \times 10^{-1}$ M^{-1} s^{-1}

_____
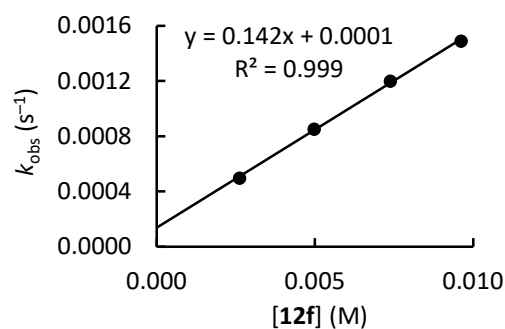
5.2.8. Single Crystal X-Ray Structure Determination

(*E*)-6-(4-(Dimethylamino)benzylidene)benzo[*d*][1,3]dioxol-5(6*H*)-one (1a)
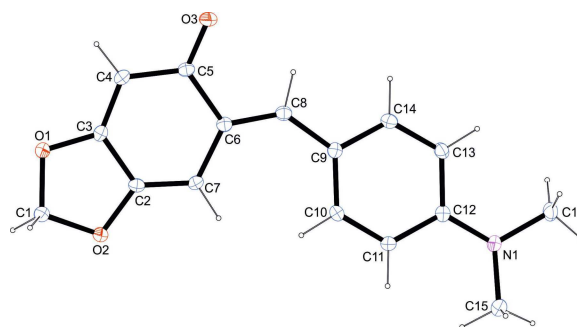
1a (cv086/CCDC 2386679, CG252)

net formula	$C_{16}H_{15}NO_3$
M_r/g mol^{-1}	269.29
crystal size/mm	0.090 × 0.050 × 0.010
T/K	173.(2)
radiation	MoKα
diffractometer	'Bruker D8 Venture TXS'
crystal system	monoclinic
space group	'P 1 21/c 1'
a/Å	7.4428(6)
b/Å	6.1255(4)
c/Å	28.022(2)
α/°	90
β/°	94.503(3)
γ/°	90
V/Å^3	1273.60(17)
Z	4
calc. density/g cm^{-3}	1.404
μ/mm^{-1}	0.098
absorption correction	Multi-Scan
transmission factor range	0.96–1.00
refls. measured	13622
R_{int}	0.0507
mean $\sigma(I)/I$	0.0330
θ range	2.745–25.339
observed refls.	1842
x, y (weighting scheme)	0.0403, 0.6767
hydrogen refinement	constr
refls in refinement	2325
parameters	183
restraints	0
$R(F_{obs})$	0.0434
$R_w(F^2)$	0.1031
S	1.063
shift/error$_{max}$	0.001
max. electron density/e Å^{-3}	0.198
min. electron density/e Å^{-3}	−0.195

_____

(*E*)-6-(4-Methylbenzylidene)benzo[*d*][1,3]dioxol-5(6H)-one (1c)
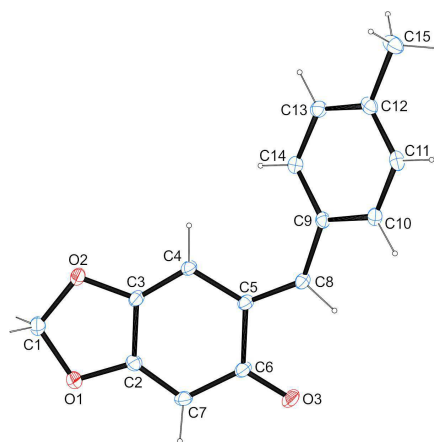
1c (zv536/CCDC 2386677, LL05)

net formula	$C_{15}H_{12}O_3$
M_r/g mol^{-1}	240.25
crystal size/mm	0.120 × 0.090 × 0.030
T/K	173.(2)
radiation	MoKα
diffractometer	'Bruker D8 Venture TXS'
crystal system	monoclinic
space group	'P 1 21/c 1'
a/Å	12.0012(6)
b/Å	6.8353(3)
c/Å	14.5744(7)
α/°	90
β/°	106.242(2)
γ/°	90
V/Å^3	1147.85(9)
Z	4
calc. density/g cm^{-3}	1.390
μ/mm^{-1}	0.097
absorption correction	Multi-Scan
transmission factor range	0.97–1.00
refls. measured	21953
R_{int}	0.0356
mean σ(I)/I	0.0199
θ range	2.911–27.482
observed refls.	2271
x, y (weighting scheme)	0.0518, 0.3898
hydrogen refinement	constr
refls in refinement	2617
parameters	164
restraints	0
$R(F_{obs})$	0.0399
$R_w(F^2)$	0.1083
S	1.068
shift/error$_{max}$	0.001
max. electron density/e Å^{-3}	0.230
min. electron density/e Å^{-3}	−0.174

(*E*)-6-(4-Nitrobenzylidene)benzo[*d*][1,3]dioxol-5(6*H*)-one (1h)
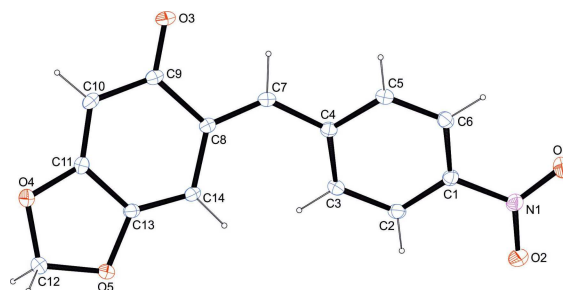
1h (av216/CCDC 2386678, CG330_2)

net formula	$C_{14}H_9NO_5$
M_r/g mol^{-1}	271.22
crystal size/mm	0.100 × 0.080 × 0.040
T/K	173.(2)
radiation	MoKα
diffractometer	'Bruker D8 Venture TXS'
crystal system	monoclinic
space group	'P 1 21/c 1'
a/Å	11.9087(7)
b/Å	6.9259(4)
c/Å	14.1427(9)
α/°	90
β/°	102.090(2)
γ/°	90
V/Å^3	1140.60(12)
Z	4
calc. density/g cm^{-3}	1.579
μ/mm^{-1}	0.122
absorption correction	Multi-Scan
transmission factor range	0.81–0.99
refls. measured	15422
R_{int}	0.0428
mean σ(I)/I	0.0295
θ range	2.946–26.369
observed refls.	2018
x, y (weighting scheme)	0.0412, 0.5614
hydrogen refinement	constr
refls in refinement	2331
parameters	181
restraints	0
$R(F_{obs})$	0.0384
$R_w(F^2)$	0.1000
S	1.082
shift/error$_{max}$	0.001
max. electron density/e Å^{-3}	0.248
min. electron density/e Å^{-3}	−0.169

_____

6-((Perfluorophenyl)methyl)-7a-((6-((perfluorophenyl)methyl)benzo[d][1,3]dioxol-5-yl)oxy)benzo-[d][1,3]dioxol-5(7aH)-one (5)
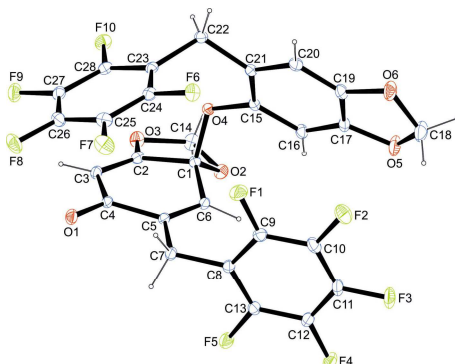
5 (bv341/CCDC 2386680, LW04)

net formula	$C_{28}H_{12}F_{10}O_6$
M_r/g mol^{-1}	634.38
crystal size/mm	$0.160 \times 0.140 \times 0.070$
T/K	173.(2)
radiation	MoKα
diffractometer	'Bruker D8 Venture TXS'
crystal system	triclinic
space group	'P -1'
a/Å	9.1211(5)
b/Å	10.7331(6)
c/Å	12.3894(6)
α/°	91.229(2)
β/°	91.311(2)
γ/°	99.466(2)
V/Å^3	1195.67(11)
Z	2
calc. density/g cm^{-3}	1.762
μ/mm^{-1}	0.174
absorption correction	Multi-Scan
transmission factor range	0.92–0.99
refls. measured	21157
R_{int}	0.0367
mean $\sigma(I)/I$	0.0357
θ range	2.265–27.485
observed refls.	4701
x, y (weighting scheme)	0.0396, 0.6054
hydrogen refinement	constr
refls in refinement	5469
parameters	397
restraints	0
$R(F_{obs})$	0.0369
$R_w(F^2)$	0.0982
S	1.038
shift/error$_{max}$	0.001
max electron density/e Å^{-3}	0.321
min electron density/e Å^{-3}	−0.227

_____

5a-Hydroxy-10-(4-methoxyphenyl)-7,7-dimethyl-5a,6,7,8,9a,10-hexahydro-9*H*-[1,3]dioxolo[4,5-*b*]xanthen-9-one (6ba)
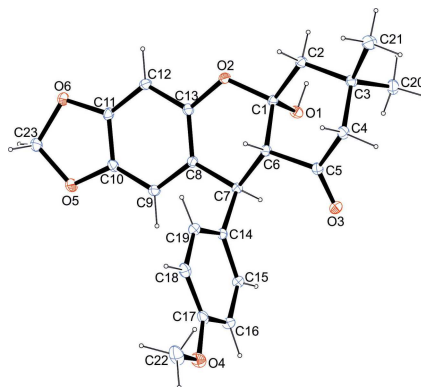
6ba (av494/CCDC 2386681, CG307)

net formula	$C_{23}H_{24}O_6$
M_r/g mol^{-1}	396.42
crystal size/mm	0.110 × 0.090 × 0.070
T/K	173.(2)
radiation	MoKα
diffractometer	'Bruker D8 Venture TXS'
crystal system	monoclinic
space group	'P 1 21/n 1'
a/Å	11.6639(12)
b/Å	11.7932(14)
c/Å	13.9997(15)
α/°	90
β/°	99.733(3)
γ/°	90
V/Å^3	1898.0(4)
Z	4
calc. density/g cm^{-3}	1.387
μ/mm^{-1}	0.100
absorption correction	Multi-Scan
transmission factor range	0.90–0.99
refls. measured	31621
R_{int}	0.0655
mean $\sigma(I)/I$	0.0409
θ range	3.031–26.361
observed refls.	3434
x, y (weighting scheme)	0.0387, 1.0812
hydrogen refinement	mixed
refls in refinement	3881
parameters	269
restraints	0
$R(F_{obs})$	0.0411
$R_w(F^2)$	0.1057
S	1.051
shift/error$_{max}$	0.001
max electron density/e Å^{-3}	0.290
min electron density/e Å^{-3}	−0.206

5.3. References

[1]   R. Lucius, R. Loos and H. Mayr, *Angew. Chem. Int. Ed.*, **2002**, *41*, 91.

[2]   C. Hansch, A. Leo and R. W. Taft, *Chem. Rev.*, **1991**, *91*, 165.

[3]   B. Wu, M.-W. Chen, Z.-S. Ye, C.-B. Yu and Y.-G. Zhou, *Adv. Synth. Catal.*, **2014**, *356*, 383.

[4]   D. Mitchell, C. W. Doecke, L. A. Hay, T. M. Koenig and D. D. Wirth, *Tetrahedron Lett.*, **1995**, *36*, 5335.

[5]   L. Jurd, *Tetrahedron,* **1977**, *33*, 163.

[6]   M. Uyanik, K. Nishioka, R. Kondo and K. Ishihara, *Nat. Chem.*, **2020**, *12*, 353.

[7]   M. J. Heravi and M. Daraie, *Monatsh. Chem.*, **2014**, *145*, 1479.

[8]   J. Ruiz Aranzaes, M.-C. Daniel and D. Astruc, *Can. J. Chem.*, **2006**, *84*, 288.

Chapter 6. Asymmetric isochalcogenourea-catalysed (4+2)-cycloadditions of *ortho*-quinone methides and allenoates

A. Scheucher, C. Gross, M. Piringer, J. Novacek, A. R. Ofial, M. Waser, *Org. Biomol. Chem.* **2025**, *23*, 827.

https://doi.org/10.1039/D4OB01855A

Copyright

Parts of the supporting information are shown in section 6.2. A complete version of the electronic supporting information (*ESI*) is accessible under the following link:

https://doi.org/10.1039/D4OB01855A

The raw data of kinetic measurements that support the findings of this study are openly available in Open Data LMU under the following link:

https://doi.org/10.5282/ubm/data.545

6.1. Copies of Manuscript

PAPER

Check for updates

Asymmetric isochalcogenourea-catalysed (4 + 2)-cycloadditions of *ortho*-quinone methides and allenoates†

Anna Scheucher,[a] Christoph Gross,[b] Magdalena Piringer,[a] Johanna Novacek,[c] Armin R. Ofial [ID][b] and Mario Waser [ID] *[a]

Chiral isochalcogenoureas (*i.e.* isothioureas and isoselenoureas) catalyse the asymmetric (4 + 2)-cyclo-addition of various allenoates with *ortho*-quinone methides. This approach provides straightforward access to different chromane derivatives with high enantioselectivities, good yields, and control of the configuration of the exocyclic double bond. Furthermore, some of the novel *ortho*-quinone methides used herein were successfully integrated into the Mayr reactivity scale by determining their electrophilicity parameter.

Introduction

Allenoates **1** have been established as versatile reagents for various (formal) cycloaddition reactions over the course of the last three decades.[1,2] Upon using chiral Lewis base (LB) organocatalysts,[3] which form an activated betaine intermediate *via* addition to the β-carbon of the allenoate (Scheme 1A), reactions between allenoates and dipolar (vinylogous) acceptors (E-Nu) can lead to structurally diverse carbo- and heterocycles in a stereoselective manner.[4] Remarkably, the nature of the catalyst usually has a strong influence on the reaction pathway, thus allowing for orthogonal outcomes depending on the used class of catalysts.[5–10] Most commonly, (chiral) tertiary phosphines are the Lewis bases of choice for allenoate activations.[5,6] Besides, also tertiary amines[7] or N-heterocyclic carbenes (NHCs)[8] have proven their potential for allenoate-based cycloadditions. Very recently, we have shown that chiral isochalcogenoureas (IChUs, Scheme 1B), *i.e.* isothioureas (ITUs)[11] and isoselenoureas (ISeU),[12] hold much potential for the activation of allenoates, too.[10] Interestingly, in our studies we found that these easily accessible bench-stable Lewis bases allow for complementary reaction pathways as compared to the established phosphine- and amine-catalysed protocols.[9,10]

[a]Institute of Organic Chemistry, Johannes Kepler University Linz, Altenbergerstrasse 69, 4040 Linz, Austria. E-mail: mario.waser@jku.at
[b]Department Chemie, Ludwig-Maximilians-Universität München, Butenandtstr. 5-13, 81377 München, Germany
[c]Institute of Analytical and General Chemistry, Johannes Kepler University Linz, Altenbergerstrasse 69, 4040 Linz, Austria
†Electronic supplementary information (ESI) available: Experimental procedures, analytical details, VCD investigations, kinetic measurements. See DOI: https://doi.org/10.1039/d4ob01855a

More specifically, so far we have investigated cycloaddition reactions between allenoates and four different classes of Michael acceptors and in all cases we exclusively observed (4 + 2)-heterocycloadditions leading to the formation of highly
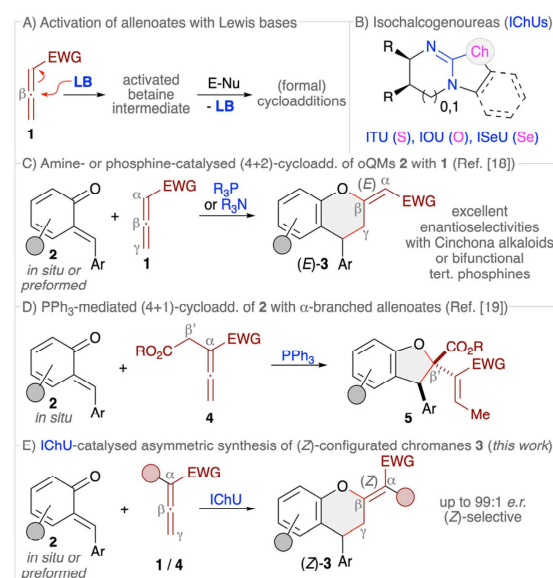
Scheme 1 (A) General concept of LB-activation of allenoates; (B) iso-chalcogenoureas; (C) established amine- and phosphine-catalysed (4 + 2)-cycloadditions of *o*-quinone methides **2** with allenoates **1**; (D) our recently developed PPh₃-mediated (4 + 1)-cycloaddition of α-branched allenoates **4**; (E) the herein investigated IChU-catalysed synthesis of chromanes **3**.

This journal is © The Royal Society of Chemistry 2025

Org. Biomol. Chem., 2025, **23**, 827–834 | **827**

functionalised dihydropyrans with a (*Z*)-configured exocyclic double bond.[10] In sharp contrast, phosphine catalysis often leads to (3 + 2)-carbocyclisations[2,13] while tertiary amines can give analogous (4 + 2)-heterocycloadditions but with (*E*)-configured double bonds instead.[14] Thus, IChUs represent a powerful alternative catalyst platform for asymmetric allenoate cycloadditions which provides an entry to chiral targets that are not easily accessible with the classically used Lewis base organocatalysts.

ortho-Quinone methides (*o*QMs, **2**) are intensively investigated building blocks that can undergo various heterocycloaddition reactions.[15] These reactive and often rather unstable compounds can either be formed *in situ* and then immediately be trapped by nucleophiles or dienophiles. Or, less frequently, *o*QMs have been preformed and used directly. (4 + 2)-Cycloadditions of *o*QMs[16] can lead to highly functionalised chiral chromane[17] derivatives **3**, and it was recently shown that reactions between allenoates and *o*QMs in the presence of either chiral tertiary amines (*i.e.* Cinchona alkaloids) or chiral bifunctional tertiary phosphines can lead to the formation of chromanes **3** with an (*E*)-configured exocyclic double bond (Scheme 1C).[18] Interestingly, we recently found that the reaction of α-alkyloxycarbonylmethyl-substituted allenoates **4** with *o*QMs **2** in the presence of triphenylphosphine resulted in the formation of dihydrobenzofurans **5** *via* a (4 + 1)-cycloaddition instead (Scheme 1D),[19] thus underscoring the diversity of possible reaction pathways that allenoates can enter. Considering these recent results from other groups and ourselves, which demonstrate that cycloadditions of allenoates and *o*QMs can lead to various highly decorated aryl-fused oxygenated heterocycles straightforwardly, we were now wondering whether it is possible to carry out such reactions under IChU catalysis as well. Based on our recent observations,[10] we concluded that this approach should give us predominately access to the (*Z*)-configured chromanes **3** instead of the already established (*E*)-configured ones.[18] In addition, we were wondering if the presence of α- or γ-substituents will be tolerated without affecting the overall cycloaddition pathway too, in contrast to the mentioned differences when using phosphine catalysis (compare Scheme 1C and D).[18c,19] Overall such an approach should thus provide an entry to the densely functionalised chiral products **3** in a highly selective manner (Scheme 1E).

Results and discussion

Electrophilic reactivities of *o*QMs

According to the general mechanism depicted in Scheme 1A, Lewis base addition to the electrophilic allenoates **1**[6] as well as the subsequent trapping of the nucleophilic betaine intermediate by sufficiently reactive electrophiles are the key bimolecular reactions that need to be understood to rationally optimise the cycloaddition reactions. In the context of this work, insight into the electrophilic reactivity of *ortho*-quinone methides **2** is crucial to define the scope of the IChU-catalysed synthesis of chromanes.

The Munich team recently synthesised a series of prototypical *o*QMs **2** formally derived from sesamol (= 3,4-methylendioxyphenol) and various acceptor- and donor-substituted benzaldehydes, studied their reactivities toward reference nucleophiles, and finally characterised the electrophilicities *E* of *o*QMs **2** on the Mayr reactivity scale.[20] To cover further *o*QMs used in this work, we set out to include heteroaryl-substituted *o*QMs with furanyl (*o*QM1), pyrrolyl (*o*QM2), and indolyl (*o*QM3) moieties as well as with extended π-system (*o*QM4) (Scheme 2). The second-order rate constants k_2 of addition reactions of carbanions (reference nucleophiles) to these *o*QMs in DMSO at 20 °C were determined by using (stopped-flow) photometric methods. Then, the electrophilicities *E* of *o*QM1–*o*QM4 were calculated from the experimentally determined k_2 and the reported nucleophilicity parameters (*N* and s_N)[21] of the reference nucleophiles according to the Mayr–Patz equation (see ESI, Section 1† for details).

The *p*-anisyl-substituted *o*QM **2a** (*E* = −15.20)[20] was used in the optimisation and screening studies of this work. Supplementing the Mayr electrophilicity scale[21c] by the *ortho*-quinone methides *o*QM1–*o*QM4 shows that all *o*QMs are
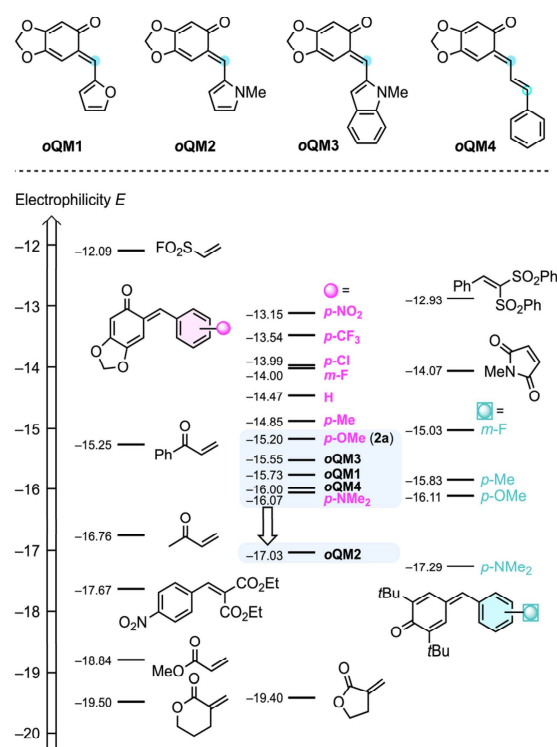
Scheme 2 Comparing the Mayr electrophilicities *E* of *o*QM1–*o*QM4 with those of aryl-substituted *o*QMs (such as **2a**), *para*-quinone methides, and further Michael acceptors (with data from ref. 20 and 21*c*). Compounds are ordered according to their *E* parameters with increasing reactivity from bottom to the top. Top line: blue dots mark the electrophilic positions of *o*QM1–*o*QM4.

828 | *Org. Biomol. Chem.*, 2025, **23**, 827–834

This journal is © The Royal Society of Chemistry 2025

Organic & Biomolecular Chemistry

Paper

located in a narrow reactivity range (Scheme 2). For *o*QM1 (*E* = −15.73), *o*QM3 (*E* = −15.55), and *o*QM4 (*E* = −16.00) it can be anticipated that they may perform comparably well as **2a** or the only slightly less electrophilic *p*-(dimethylamino)-substituted *o*QM (*E* = −16.07).[20] Allene ketones were successfully shown to undergo phosphine-catalysed (4 + 2) annulations with *o*QM4.[18c] However, due to the low regioselectivity of the ambident *o*QM4 in reactions with nucleophiles (see ESI, Section 12†), we excluded *o*QM4 from further studies in this work. Similarly, low regioselectivities for the attack of C-nucleophiles at vinyl *para*-quinone methides were reported previously.[22] The *N*-methylpyrrol-2-yl-substituted *o*QM2 is by almost two orders of magnitude less electrophilic than the standard *o*QM **2a**. Successful (4 + 2)-heterocycloadditions with *o*QM **2a** would, therefore, significantly enhance the reactivity range of *o*QMs that could be used for the IChU-catalysed reactions with allenoates.

Cycloadditions with preformed stabilised *o*QMs

We started our investigations on the allenoate cycloadditions by using the stabilised electron-rich benzodioxole-based *o*QMs **2**. A first screening and optimisation of reaction conditions was carried out using *o*QM **2a** and the unbranched allenoate **1a** (Table 1).

Testing the four different catalysts depicted in Fig. 1 under conditions similar to those established for IChU-catalysed allenoate (4 + 2)-cycloadditions with various Michael acceptors,[10] we observed a likewise reactivity trend herein as well (entries 1–4). While BTM (**ITU1**, entry 1) did not allow for any product formation, the 6-ring-based HBTM (**ITU2**, entry 2), HyperBTM (**ITU3**, entry 3), and its selenium-containing analogue (**ISeU**, entry 4) promoted the (4 + 2)-cycloaddition well. This difference in reactivity between the BTM motif and the
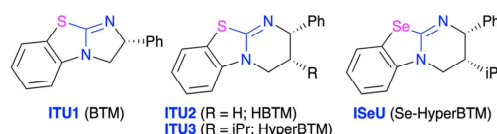

Fig. 1 IChUs used herein.

HBTM/HyperBTM scaffold can most likely be rationalised by the lower nucleophilicity of 5-ring-based isothioureas,[23] thus slowing down the initial addition to the allenoate (we recently showed that this step has a rather high activation barrier, which most likely also explains the need for higher reaction temperatures[10]). Interestingly, we not only observed the formation of the anticipated chromane **3a** [with the (*Z*)-isomer being the major one; the configuration of the double bond was assigned by NOESY NMR experiments], but also notable amounts of the chromene **6a** (originating from an initial α-attack of the allenoate to the benzylic position of the *o*QM). This observation is in sharp contrast to our previous studies, where analogous α-addition-based products were obtained in minute amounts only (if formed at all). Noteworthy, the enantioselectivity for the targeted (*Z*)-**3a** was very high, independent of the used catalyst (entries 2–4). On the other hand, the catalyst scaffold, as well as the reaction conditions (entries 2–10) had an influence on the product distribution. Overall, it turned out that HyperBTM (**ITU3**) is the Lewis base of choice. Using 20 mol% of this catalyst in toluene at 80 °C allows for around 60% (*Z*)-**3a** selectivity, besides approx. 10% of the (*E*)-diastereomer and slightly less than 30% of **6a** (entry 3). Interestingly, the two side-products (*E*)-**3a** (83 : 17 er) and **6a** (74 : 26 er) were obtained with significantly lower enantioselectivities as compared to the major product (*Z*)-**3a** (99 : 1 er).

Table 1 Optimisation of the (4 + 2)-cycloaddition of allenoate **1a** with *o*QM **2a** [a]

Entry	IChU (mol%)	Solv.	*T* (°C)	(*Z*)-**3a** [b] (%)	(*Z*)-**3a** er[c]	(*E*)-**3a** [b] (%)	**6a** [b] (%)
1	**ITU1** (20%)	Tol.	80	—	—	—	—
2	**ITU2** (20%)	Tol.	80	48	99 : 1	8	32
3	**ITU3 (20%)**	**Tol.**	**80**	**61 (59)**[d]	**99 : 1**	**7 (83 : 17)**[c]	**28 (74 : 26)**[c]
4	**ISeU** (20%)	Tol.	80	59	99 : 1	13	26
5	**ITU3** (10%)	Tol.	80	54	99 : 1	9	28
6	**ITU3** (20%)	Tol.	40	52	99 : 1	7	20
7	**ITU3** (20%)	Tol.	120	51	99 : 1	8	25
8	**ITU3** (20%)	DCM	80	33	99 : 1	8	29
9	**ITU3** (20%)	THF	80	58	99 : 1	10	29
10	**ITU3** (20%)	Tol.[e]	80	29	99 : 1	4	26

[a] Unless otherwise stated, reactions were run for 24 h using 0.15 mmol **1a** and 0.1 mmol **2a** in the presence of the given catalyst in the indicated solvent (*c* = 0.02 M with respect to **2a**) under N$_2$ at the indicated temperature (tol. = toluene; DCM = dichloromethane; THF = tetrahydrofuran). [b] Calculated from the ^{1}H NMR spectrum of the crude product using mesitylene as an internal standard (IST). [c] Enantiomeric ratio determined by HPLC using a chiral stationary phase. [d] Isolated yield. [e] With added Cs$_2$CO$_3$ (1 equiv.).

This journal is © The Royal Society of Chemistry 2025

Org. Biomol. Chem., 2025, **23**, 827–834 | **829**

260

Changing the solvent (entries 8 and 9), adding base (as exemplified for Cs_2CO_3; entry 10), and varying the temperature (entries 6 and 7) did not allow for any better results and lower catalyst loading (entry 5) resulted in a reduced yield too. Gratifyingly, the (*Z*)-isomer could easily be separated from the other two cycloaddition side-products by means of a simple silica gel column chromatography, thus giving (*Z*)-**3a** in a moderate isolated yield of 59% with excellent enantioselectivity (entry 3).

With suited asymmetric conditions for the synthesis of (*Z*)-**3a** at hand, we next investigated the application scope by using various sesamol-derived *o*QMs **2** as well as different allenoates **1** and **4** (Scheme 3). Varying the ester group of allenoates **1** first (see products **3a–f**) showed that *t*-butyl esters allow for the highest yields with reduced amounts of the α-addition products **6**. This can be explained by the higher steric shielding of the α-position, thus preventing formation of compounds **6** while making the γ-position more accessible. Accordingly, testing of different *o*QMs was then carried out with the *t*-butyl allenoate as the cycloaddition partner. As shown for products **3g–3p** various (hetero)aryl groups were well tolerated and in each case the level of enantioselectivity was very high. However, the method came to its limits when using

γ-substituted allenoates. In this case the reaction was found to be rather messy and the only distinct product that could be obtained in trace amounts and with very low er was the chromene **6s** (formed *via* α-attack of the activated allenoate to QM). Remarkably when using α-branched allenoates **4** instead again the formation of the chromane skeleton **3** was the dominant transformation (see products **3q** and **3r**). This is in sharp contrast to our previous observations when reacting such allenoates with *in situ* generated *o*QMs (Scheme 1D)[19] and OH-containing *para*-QMs[24] in the presence of phosphine catalysts, thus underscoring the generality and functional group tolerance of the IChU-catalysed (4 + 2)-cycloaddition. Interestingly, herein the isoselenourea derivative **ISeU** allowed for higher yields and again the enantioselectivity was nearly perfect.

Cycloadditions with *in situ* generated *o*QMs

When using less stabilised *o*QMs these transient species are usually generated *in situ* from different easily accessible precursors.[13] One straightforward approach that should be compatible with our Lewis base-catalysis strategy relies on the use of α-(arylsulfonyl)methyl-substituted β-naphthols **7** under basic conditions, which leads to the formation of the corresponding *o*QMs *via* elimination of an arylsulfinic acid. This strategy was recently also utilised in our (4 + 1)-cycloaddition of allenoates **4** (Scheme 1D)[19] and we thus set out to explore the possibility of applying this to IChU-catalysed allenoate cycloadditions. By starting from the precursor **7a** and the parent allenoate **1a** we first optimised the synthesis of product **3aa** (Table 2). We initially set the reaction temperature to 40 °C as we know from previous investigations with compounds **7** that higher temperatures usually lead to a relatively fast decomposition of the corresponding *o*QMs. First test reactions with the three isothiourea catalysts **ITU1–3** under basic conditions showed a similar reactivity trend as compared to the stabilised *o*QM **2a** (compare entries 1–3 of both tables). Again HyperBTM (**ITU3**) was best suited giving the targeted (*Z*)-**3aa** with moderate NMR yield and excellent enantioselectivity (entry 3). Interestingly, formation of the (*E*)-diastereoisomer and the α-addition product **6aa** was less pronounced as compared to the use of **2a**. Unfortunately, lower catalyst loading was again not well tolerated (entry 4). Interestingly however, in this case **ISeU** was found to be higher yielding (entry 5). Some further optimisation of reaction conditions was first carried out with **ITU3** (entries 6–8) showing that an excess of 3 equiv. of allenoate is beneficial, while increased or decreased temperature did not allow for any improvement (a few other solvents or bases were tested too but did not allow for any improvement). Finally, using **ISeU** in combination with 3 equiv. of **1a** and 1 equiv. of Cs_2CO_3 in toluene at 40 °C allowed for the synthesis of (*Z*)-**3aa** in 77% isolated yield with 99 : 1 er and only minor quantities of the other cycloaddition side products (entry 9).

Investigating the asymmetric application scope for the cycloaddition starting from *o*QM precursors **7** (Scheme 4) showed that various naphthol-based derivatives are well tolerated, as exemplified for products **3aa–aj**. Unfortunately, however, the method comes to its limits when utilising simple
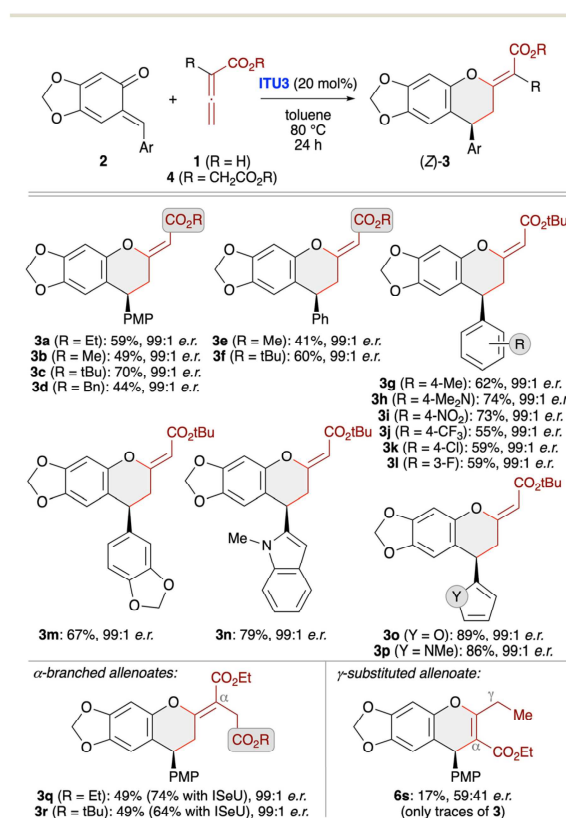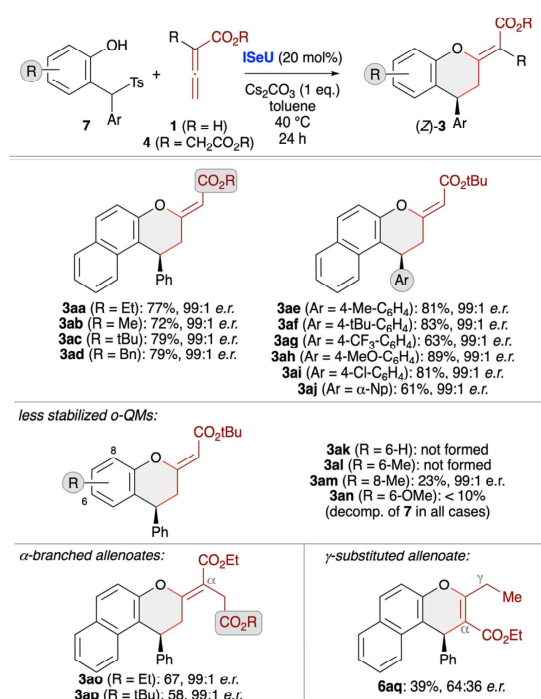

Scheme 3 Asymmetric application scope testing various stabilised *o*QMs and different allenoates using (2*S*,3*R*)-HyperBTM (**ITU3**; conditions as specified in entry 3, Table 1).

Table 2 Optimisation of the (4 + 2)-cycloaddition of allenoate **1a** with *o*QM precursors **7a** [a]

Entry	IChU (mol%)	T (°C)	(Z)-**3aa** [b] (%)	(Z)-**3aa** er [c]	(E)-**3aa** [b] (%)	**6aa** [b] (%)
1	**ITU1** (20%)	40	—	—	—	—
2	**ITU2** (20%)	40	29	97:3	8	5
3	**ITU3** (20%)	40	54	99:1	8	4
4	**ITU3** (10%)	40	19	98:2	5	3
5	**ISeU** (20%)	40	77	99:1	12	4
6	**ITU3** (20%) [d]	40	72	99:1	12	4
7	**ITU3** (20%) [d]	60	60	99:1	10	5
8	**ITU3** (20%) [d]	25	56	99:1	11	4
9	**ISeU** (20%) [d]	40	79 (77) [e]	99:1	12 (63:37) [c]	3 (56:44) [c]

[a] Unless otherwise stated, reactions were run for 24 h using 0.15 mmol **1a** and 0.1 mmol **7a** in the presence of the given catalyst in toluene under N_2 at the indicated temperature. [b] Calculated from the ^{1}H NMR spectrum of the crude product using mesitylene as an internal standard (IST). [c] Enantiomeric ratio determined by HPLC using a chiral stationary phase. [d] Using 3 equiv. of allenoate **1a**. [e] Isolated yield.

Scheme 4 Asymmetric application scope using *in situ* generated *o*QMs (accessed from compounds **7**) and different allenoates in the presence of (2S,3R)-SeHyperBTM (**ISeU**; conditions as detailed in entry 9, Table 2).
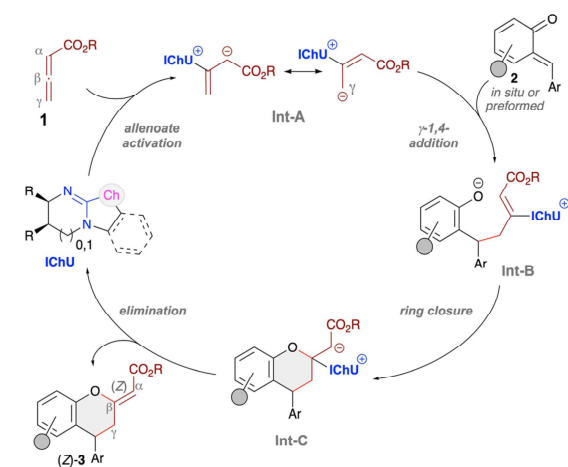
phenol-based QM precursors that yield less stable and thus more easily decomposing *o*QMs. While products **3ak** and **3al** could not be accessed at all and **3an** was only detected in trace amounts, the 8-Me-containing **3am** could at least be obtained in low yield (but with very high enantioselectivity). In all these

cases we observed a very pronounced formation of unidentified side-products originating from the decomposition of the *in situ* formed quinone methides. Using α-branched allenoates **4** allowed for the selective (4 + 2)-cycloaddition as well, as demonstrated for the synthesis of chromanes **3ao** and **3ap**. Again, this result is in sharp contrast to our recent phosphine-catalysed (4 + 1)-cycloaddition protocol (Scheme 1D),[19] underscoring the orthogonal catalytic potential of different Lewis bases for allenoate activation. Finally, analogous to the use of preformed *o*QMs (see product **6r**, Scheme 3), the use of γ-branched allenoates resulted in the formation of the chromene skeleton herein as well, but with low yield and unsatisfying enantioselectivity only (product **6aq**).

We have not been able to obtain crystals of the enantioenriched products **3** that would have allowed for an unambiguous assignment of their absolute configuration by means of single crystal X-ray diffraction. Thus we recorded vibrational circular dichroism (VCD)[25] spectra of both enantiomers of compound **3e** and compared the experimental spectra with those calculated from DFT optimised structures which strongly supports the absolute configuration depicted in Scheme 3.[26] This sense of configuration of the major enantiomer is in full accordance with our recent observations of IChU-catalysed allenoate-based (4 + 2)-cycloadditions where we always observed this orientation of the substituent on the stereogenic center in position 4 of tetrahydropyran ring when using the (2S,3R)-configured **ITU3** or **ISeU**.[10] Furthermore, comparison of the optical rotation of our (Z)-configured products **3** with reported structurally similar (E)-configured ones[18] support this sense of configuration as well and we therefore assigned all other products in analogy.

Mechanistically, we proposed that the herein reported stereoselective syntheses of chromanes **3** follow the established pathway for our recently introduced IChU-catalysed (4 + 2)-cycloadditions of allenoates with different Michael acceptors

This journal is © The Royal Society of Chemistry 2025

Org. Biomol. Chem., 2025, **23**, 827–834 | **831**

262

Scheme 5 Mechanistic proposal.[10]

(Scheme 5).[10] More specifically, the IChU first activates the allenoates **1** giving the resonance-stabilised **Int-A**. This chiral intermediate then undergoes 1,4-addition to the *o*QM **2** with its γ-carbon, giving **Int-B**. This is also the step that controls the configuration of products **3**. As stated above, so far we have always observed the same sense of induction when using the same enantiomers of our catalysts, thus substantiating a very high level of catalyst control and a very well defined **Int-A**. **Int-B** then undergoes ring-closure and final IChU-elimination which also sets the configuration of the exocyclic double bond. Interestingly, while other Lewis base catalysts usually favour (*E*)-configured double bonds in such transformations,[18] IChUs show pronounced (*Z*)-selectivity, a kinetic phenomenon which we could also recently support by DFT calculations.[10a]

Follow-up transformations

Finally, we also carried out some test reactions to demonstrate the suitability of products **3** to serve as starting materials for further transformations. As outlined in Scheme 6, the exocyclic
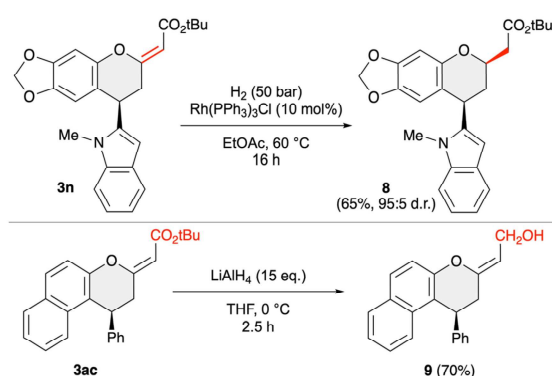
double bond can be selectively hydrogenated under homogeneous conditions by using Wilkinson's catalyst. In this way product **8** was obtained with high diastereoselectivity; the *cis* configuration of the 2-acetyl group and the 4-indolyl substituent was determined by NOESY experiments. Furthermore, the ester functionality can be reduced to the primary alcohol **9** by using an excess of LiAlH$_4$. It should be stated that neither of these two transformations have been optimised further, but in our opinion they represent a proof-of-concept to demonstrate the suitability of compounds **3** for further manipulations.

Conclusions

Isothioureas (ITUs) and isoselenoureas (ISeUs) were successfully employed as chiral Lewis base catalysts for asymmetric (4 + 2)-cycloadditions of various allenoates with different *ortho*-quinone methides. This approach allows for the synthesis of chromanes **3** with (*Z*)-configured exocyclic double bonds in high enantioselectivities and good isolated yields. Accompanying VCD studies supported the assignment of the absolute configuration of the products. Furthermore, the electrophilicity parameters of some heteroaryl-substituted and π-extended *ortho*-quinone methides were successfully determined. These quantitative reactivity data hint to the reactivity range which the electrophilic component in the (4 + 2)-cycloadditions needs to cover. This knowledge should allow us to identify additional suitable reaction partners for such allenoate-based cycloadditions in the future, which can be selected based on their reported electrophilicity parameters *E*.

Experimental details[26]

General procedure using preformed *o*QMs 2

A flame dried N$_2$-flushed flask was charged with **ITU3** (20 mol%), the respective *o*QM **2** (0.1 mmol, 1 equiv.) and toluene (5 mL, 0.02 mol L^{-1}), directly followed by the addition of the allenoate **1** or **4** (0.15 mmol, 1.5 equiv.). The reaction mixture was then stirred at 80 °C for 24 h. After cooling, the mixture was filtered through a Na$_2$SO$_4$ plug. The solvent was removed under reduced pressure to yield the crude products **3a–q**. Purification *via* preparative TLC (heptane : EtOAc = 2 : 1) gave the products in the reported yields and enantiopurities.

General procedure using *o*QM precursors 7

A N$_2$-flushed and flame-dried flask was charged with **ISeU** (20 mol%), Cs$_2$CO$_3$ (0.1 mmol, 1 equiv.), the respective *o*QM precursor **7** (0.1 mmol, 1 equiv.) and toluene (5 mL, 0.02 mol L^{-1}). The allenoate (0.3 mmol, 3 equiv.) was added and the mixture was heated to 40 °C and stirred for 24 h. After cooling to r.t., the mixture was filtered through a Na$_2$SO$_4$ plug and the solvent was removed under reduced pressure to give the crude products **3**. Purification *via* preparative TLC (heptane : EtOAc = 2 : 1) gave the products in the reported yields and enantiopurities.

Scheme 6 Reductive follow-up transformations of compounds **3**.

832 | *Org. Biomol. Chem.*, 2025, **23**, 827–834

This journal is © The Royal Society of Chemistry 2025

263

Paper

Author contributions

A. S., C. G., and M. P. carried out all the syntheses, method development and analysis of the compounds. C. G. characterised the electrophilicites of the *o*QMs. J. N. carried out the VCD measurements and accompanying calculations. A. R. O. and M. W. initiated and supervised the project and wrote the manuscript with contributions from all authors.

Data availability

The data supporting this article have been included as part of the ESI.† Raw data of the individual kinetic measurements that support the findings of this study are openly available in Open Data LMU at **https://doi.org/10.5282/ubm/data.545**.

Conflicts of interest

There are no conflicts to declare.

Acknowledgements

References

1 (*a*) X. Lu, C. Zhang and Z. Xu, *Acc. Chem. Res.*, 2001, **34**, 535; (*b*) S. Ma, *Chem. Rev.*, 2005, **105**, 2829; (*c*) B. J. Cowen and S. J. Miller, *Chem. Soc. Rev.*, 2009, **38**, 3102; (*d*) S. Yu and S. Ma, *Angew. Chem., Int. Ed.*, 2012, **51**, 3074; (*e*) Y. C. Fan and O. Kwon, *Chem. Commun.*, 2013, **49**, 11588; (*f*) Y. Xiao, Y. Sung, H. Guo and O. Kwon, *Beilstein J. Org. Chem.*, 2014, **10**, 2089; (*g*) Z. Wang, X. Xu and O. Kwon, *Chem. Soc. Rev.*, 2014, **43**, 2927; (*h*) F. López and J. Mascareñas, *Chem. Soc. Rev.*, 2014, **43**, 2904; (*i*) Y. Wei and M. Shi, *Org. Chem. Front.*, 2017, **4**, 1876; (*j*) E.-Q. Li and Y. Huang, *Chem. Commun.*, 2020, **56**, 680; (*k*) R. Hajinasiri, *Tetrahedron*, 2022, **126**, 133053; (*l*) M. Alonso and P. Almendros, *Adv. Synth. Catal.*, 2023, **365**, 1332.

2 Pioneering report introducing Lewis base-catalysed cycloadditions of allenoates: C. Zhang and X. Lu, *J. Org. Chem.*, 1995, **60**, 2906.

3 (*a*) M. J. Gaunt and C. C. C. Johansson, *Chem. Rev.*, 2007, **107**, 5596; (*b*) G. C. Fu, *Acc. Chem. Res.*, 2000, **33**, 412; (*c*) S. France, D. J. Guerin, S. J. Miller and T. Lectka, *Chem. Rev.*, 2003, **103**, 2985; (*d*) S. E. Denmark and G. L. Beutner, *Angew. Chem., Int. Ed.*, 2008, **47**, 1560; (*e*) J. E. Taylor, S. D. Bull and J. M. J. Williams, *Chem. Soc. Rev.*, 2012, **41**, 2109.

4 M. Shi, Y. Wei, M.-X. Zhao and J. Zhang, *Organocatalytic Cycloadditions for Synthesis of Carbo- and Heterocycles*, Wiley-VCH, Weinheim, 2018.

5 For illustrative reviews on chiral phosphine organocatalysis including allenoate applications, too: (*a*) J. L. Methot and W. R. Roush, *Adv. Synth. Catal.*, 2004, **346**, 1035; (*b*) A. Voituriez, A. Marinetti and M. Gicquel, *Synlett*, 2015, 142; (*c*) H. Li and Y. Lu, *Asian J. Org. Chem.*, 2017, **6**, 1130; (*d*) H. Ni, W.-L. Chan and Y. Lu, *Chem. Rev.*, 2018, **118**, 9344; (*e*) H. Guo, Y. C. Fan, Z. Sun, Y. Wu and O. Kwon, *Chem. Rev.*, 2018, **118**, 10049; (*f*) Y. Huang, J. Liao, W. Wang, H. Liu and H. Guo, *Chem. Commun.*, 2020, **56**, 15235; (*g*) C. Xie, A. J. Smaligo, X.-R. Song and O. Kwon, *ACS Cent. Sci.*, 2021, **7**, 536.

6 For reactivities of tertiary phosphines towards allenoates: (*a*) F. An, H. Jangra, Y. Wei, M. Shi, H. Zipse and A. R. Ofial, *Chem. Commun.*, 2022, **58**, 3358; (*b*) F. An, J. Brossette, H. Jangra, Y. Wei, M. Shi, H. Zipse and A. R. Ofial, *Chem. Sci.*, 2024, **15**, 18111.

7 Early reports describing the use of chiral tert. amines for allenoate reactions: (*a*) J.-B. Denis, G. Masson, P. Retailleau and J. Zhu, *Angew. Chem., Int. Ed.*, 2011, **50**, 5356; (*b*) X. Wang, T. Fang and X. Tong, *Angew. Chem., Int. Ed.*, 2011, **50**, 5361; (*c*) K. D. Ashtekar, R. J. Staples and B. Borhan, *Org. Lett.*, 2011, **13**, 5732; (*d*) C.-K. Pei, Y. Jiang, Y. Wei and M. Shi, *Angew. Chem., Int. Ed.*, 2012, **51**, 11328; (*e*) C.-K. Pei and M. Shi, *Chem. – Eur. J.*, 2012, **18**, 6712.

8 Early examples on the use of NHCs for allenoate-based cycloadditions: (*a*) L. Sun, T. Wang and S. Ye, *Chin. J. Chem.*, 2012, **30**, 190; (*b*) Y. Hu, S. Li, Z. Wang, Y. Yao, T. Li, C. Yu and C. Yao, *J. Org. Chem.*, 2018, **83**, 3361; (*c*) S. S. Lopez, A. A. Jaworski and K. A. Scheidt, *J. Org. Chem.*, 2018, **83**, 14637.

9 Illustrative studies reporting complementary outcomes when using different Lewis bases for allenoate cycloadditions: (*a*) G.-T. Huang, T. Lankau and C.-H. Yu, *J. Org. Chem.*, 2014, **79**, 1700; (*b*) L.-J. Yang, S. Li, S. Wang, J. Nie and J.-A. Ma, *J. Org. Chem.*, 2014, **79**, 3547; (*c*) G.-T. Huang, Z. Lankau and C.-H. Yu, *Org. Biomol. Chem.*, 2014, **12**, 7297; (*d*) Y. Li, S. Du, Z. Du and C. Chen, *RSC Adv.*, 2016, **6**, 82260.

10 (*a*) L. S. Vogl, P. Mayer, R. Robiette and M. Waser, *Angew. Chem., Int. Ed.*, 2024, **63**, e202315345; (*b*) M. Piringer, M. Hofer, L. S. Vogl, P. Mayer and M. Waser, *Adv. Synth. Catal.*, 2024, **366**, 2115; (*c*) M. Waser, *Chem. Lett.*, 2024, **53**, upae168.

11 For reviews on isothiourea catalysis: (*a*) J. Merad, J.-M. Pons, O. Chuzel and C. Bressy, *Eur. J. Org. Chem.*, 2016, 5589; (*b*) V. B. Birman, *Aldrichimica Acta*, 2016, **49**, 23; (*c*) W. C. Hartley, T. J. C. O'Riordan and A. D. Smith, *Synthesis*, 2017, **49**, 3303; (*d*) A. Biswas, H. Mondal and M. S. Maji, *J. Heterocycl. Chem.*, 2020, **57**, 3818;

This journal is © The Royal Society of Chemistry 2025

Org. Biomol. Chem., 2025, **23**, 827–834 | **833**

264

(*e*) C. McLaughlin and A. D. Smith, *Chem. – Eur. J.*, 2021, **27**, 1533; (*f*) J. Bitai, M. T. Westwood and A. D. Smith, *Org. Biomol. Chem.*, 2021, **19**, 2366; (*g*) A. J. Nimmo, C. M. Young and A. D. Smith, *Isothiourea Catalysis – New Opportunities for Asymmetric Synthesis*, in *Asymmetric Organocatalysis: New Strategies, Catalysts, and Opportunities*, ed. Ł. Albrecht, A. Albrecht and L. Dell'Amico, Wiley-VCH, Weinheim, 2023, ch. 5, p. 151.

12 Seminal study on the use of isoselenoureas: C. M. Young, A. Elmi, D. J. Pascoe, R. K. Morris, C. McLaughlin, A. M. Woods, A. B. Frost, A. Houpliere, K. B. Ling, T. K. Smith, A. M. Z. Slawin, P. H. Willoughby, S. Cockroft and A. D. Smith, *Angew. Chem., Int. Ed.*, 2020, **59**, 3705.

13 (*a*) R. Ma, G. Song, Q. Xi, L. Yang, E.-Q. Li and Z. Duan, *Chin. J. Org. Chem.*, 2019, **39**, 2196; (*b*) S. Anwar, L.-T. Lin, V. Srinivasadesikan, V. B. Gudise and K. Chen, *RSC Adv.*, 2021, **11**, 38648.

14 (*a*) K. D. Ashtekar, R. J. Staples and B. Borhan, *Org. Lett.*, 2011, **13**, 5732; (*b*) X. Wang, T. Fang and X. Tong, *Angew. Chem., Int. Ed.*, 2011, **50**, 5361; (*c*) C. K. Pei, Y. Jiang and M. Shi, *Org. Biomol. Chem.*, 2012, **10**, 4355; (*d*) C.-K. Pei, Y. Jiang, Y. Wei and M. Shi, *Angew. Chem., Int. Ed.*, 2012, **51**, 11328; (*e*) C. Wang, H. Jia, C. Zhang, Z. Gao, L. Zhou, C. Yuan, Y. Xiao and H. Guo, *J. Org. Chem.*, 2017, **82**, 633.

15 (*a*) W.-J. Bai, J.-G. David, Z.-G. Feng, M. G. Weaver, K.-L. Wu and T. R. R. Pettus, *Acc. Chem. Res.*, 2014, **47**, 3655; (*b*) M. S. Singh, A. Nagaraju, N. Anand and S. Chowdhury, *RSC Adv.*, 2014, **4**, 55924; (*c*) L. Caruana, M. Fochi and L. Bernardi, *Molecules*, 2015, **20**, 11733; (*d*) D. V. Osipov, V. A. Osyanin and Y. N. Klimochkin, *Russ. Chem. Rev.*, 2017, **86**, 625; (*e*) X. Li, Z. Li and J. Sun, *Nat. Synth.*, 2022, **1**, 426.

16 Early asymmetric (4 + 2)-annulations of *o*QMs using different starting materials and catalysis modes: (*a*) C.-C. Hsiao, H.-H. Liao and M. Rueping, *Angew. Chem., Int. Ed.*, 2014, **53**, 13258; (*b*) O. El-Sepelgy, S. Haseloff, S. K. Alamsetti and C. Schneider, *Angew. Chem., Int. Ed.*, 2014, **53**, 7923; (*c*) S. Saha and C. Schneider, *Org. Lett.*, 2015, **17**, 648; (*d*) L. Caruana, M. Mondatori, V. Corti, S. Morales, A. Mazzanti, M. Fochi and L. Bernardi, *Chem. –*

Eur. J., 2015, **21**, 603; (*e*) D. Zhou, K. Mao, J. Zhang, B. Yan, W. Wang and H. Xie, *Tetrahedron Lett.*, 2016, **57**, 5649; (*f*) Y. Zhu, W.-Z. Zhang, L. Zhang and S. Luo, *Chem. – Eur. J.*, 2017, **23**, 1253; (*g*) H. Hu, Y. Liu, J. Guo, L. Lin, Y. Xu, X. Liu and X. Feng, *Chem. Commun.*, 2015, **51**, 3835; (*h*) S. K. Alamsetti, M. Spanka and C. Schneider, *Angew. Chem., Int. Ed.*, 2016, **55**, 2392.

17 (*a*) *Chemistry of Heterocyclic Compounds: Chromans and Tocopherols*, ed. G. P. Ellis and I. M. Lockhart, Wiley Interscience, New York, 1981, vol. 36; (*b*) H. C. Shen, *Tetrahedron*, 2009, **65**, 3931; (*c*) T. Rosenau and S. Böhmdorfer, ortho-Quinone Methides in Tocopherol Chemistry, in *Quinone Methides*, ed. S. Rokita, Wiley, Hoboken (NJ), 2009, ch. 6, p. 163.

18 (4 + 2)-Cycloadditions of allenoates with *o*QMs: (*a*) Y.-H. Deng, W.-D. Chu, X.-Z. Zhang, X. Yan, K.-Y. Yu, L.-L. Yang, H. Huang and C.-A. Fan, *J. Org. Chem.*, 2017, **82**, 5433; (*b*) P. Chen, K. Wang, W. Guo, X. Liu, Y. Liu and C. Li, *Angew. Chem., Int. Ed.*, 2017, **56**, 3689; (*c*) Z. Wang, T. Wang, W. Yao and Y. Lu, *Org. Lett.*, 2017, **19**, 4126.

19 K. Zielke and M. Waser, *Org. Lett.*, 2018, **20**, 768.

20 C. Gross, A. Eitzinger, N. Hampel, P. Mayer and A. R. Ofial, *Chem. – Eur. J.*, 2024, e202403785, DOI: **10.1002/chem.202403785**.

21 (*a*) R. Lucius, R. Loos and H. Mayr, *Angew. Chem., Int. Ed.*, 2002, **41**, 91; (*b*) H. Mayr, *Tetrahedron*, 2015, **71**, 5095; (*c*) A collection of published reactivity parameters N, sN, and E is freely accessible at: **https://www.cup.lmu.de/oc/mayr/reaktionsdatenbank2/** (accessed Nov 5, 2024).

22 A. Eitzinger, R. J. Mayer, N. Hampel, P. Mayer, M. Waser and A. R. Ofial, *Org. Lett.*, 2020, **22**, 2182.

23 B. Maji, C. Joanesse, T. A. Nigst, A. D. Smith and H. Mayr, *J. Org. Chem.*, 2011, **76**, 5104.

24 K. Zielke, O. Kováč, M. Winter, J. Pospíšil and M. Waser, *Chem. – Eur. J.*, 2019, **25**, 8163.

25 For illustrative reviews: (*a*) C. Merten, T. P. Golub and N. M. Kreienborg, *J. Org. Chem.*, 2019, **84**, 8797; (*b*) C. Merten, *Eur. J. Org. Chem.*, 2020, 5892.

26 See ESI for further details.†

834 | *Org. Biomol. Chem.*, 2025, **23**, 827–834

This journal is © The Royal Society of Chemistry 2025

265

6.2. Supporting Information

6.2.1. Additional Table and Supplementary Figures

The kinetics of oQM + carbanion reactions (Fig. S1A) were monitored photometrically at the absorbance maxima of the colored oQMs by using stopped-flow or conventional UV/VIS spectroscopy. The carbanions were used in at least ten-fold excess over the oQMs, which allows for pseudo-first order reactions conditions. First-order rate constants k_{obs} (s^{-1}) were derived by least squares-fitting of the mono-exponential decay function $A = A_0 \exp(-k_{obs}t) + C$ to the time-dependent experimental absorbances A_t (Fig. S1B). The second order rate constants k_2^{exp} ($M^{-1}\ s^{-1}$) were then calculated as the slopes of the linear correlations of k_{obs} (s^{-1}) with four to five different carbanion concentrations (Fig. S1C). The second-order rate constants of all kinetically investigated oQM/carbanion combinations are listed in Table S1.
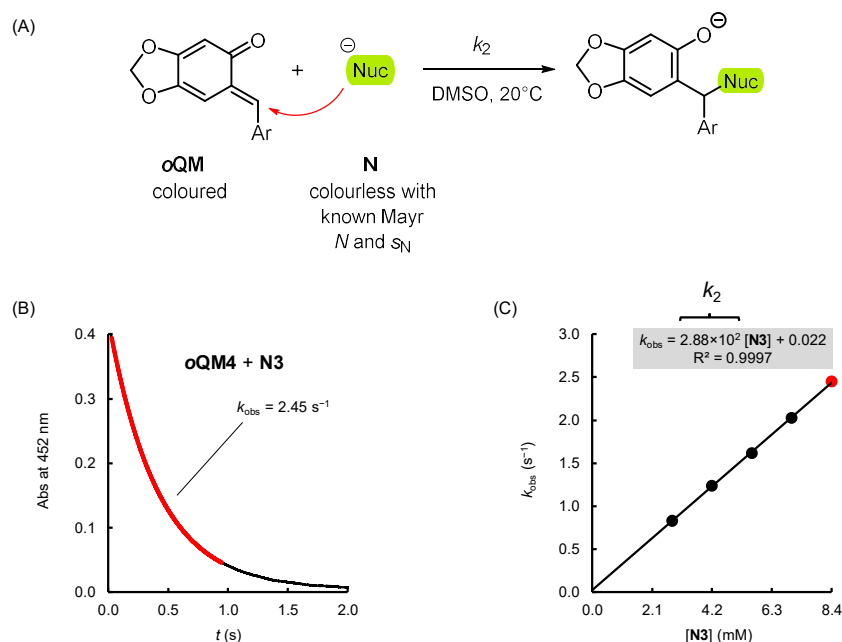

Fig. S1. (A) Carbon-carbon bond-forming reaction of an oQM with an anionic nucleophile. (B) Time-dependent decay of the oQM absorbance of **oQM4** ([**oQM4**]$_0$ = 2.50 × 10^{-5} M) at 452 nm for the reaction with the carbanionic nucleophile **N3** ([**N3**]$_0$ = 2.40 × 10^{-3} M) in DMSO at 20°C and determination of the observed rate constant. (C) Linear correlation of experimentally determined first-order rate constants k_{obs} (s^{-1}) with the concentration of **N3** as required by the relationship $k_{obs} = k_2$[**N**]. The slope of the linear correlation corresponds to the second-order rate constant k_2 ($M^{-1}\ s^{-1}$).

Rearranging the Mayr-Patz equation (1)

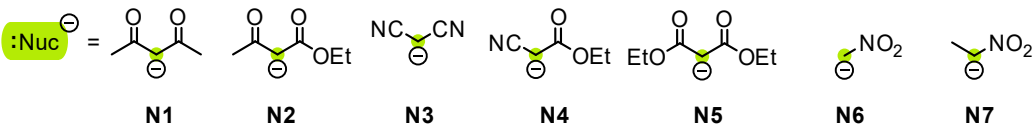$$\lg k_2(20\ °C) = s_N(N + E) \qquad\qquad (1)$$

to equation (2)

$$(\lg k_2)/s_N = N + E \qquad\qquad (2)$$

_____

enables to depict the kinetic data of Table S1 as linear correlations (Figs. S2–S5) which illustrate the results of the least-square minimizations $\Delta^2 = (\lg k_2^{exp} - s_N(N + E))^2$ to calculate the electrophilicity E of the *o*QMs. The least-squares minimizations used the experimental second-order rate constants k_2^{exp} in DMSO at 20 °C from Table S1 and the reported nucleophile-specific reactivity parameters N and s_N of the reference nucleophiles **N1**–**N7** from ref. [1] as input in an MS Excel spreadsheet. The E parameter was defined as an adjustable variable and optimized for the individual *o*QMs by using the MS Excel Solver (GRG algorithm).

Table S1: Summary of experimentally determined second-order rate constants k_2^{exp} for the reactions of *o*QM1–*o*QM4 with carbanions **N1**–**N7** (reference nucleophiles) in DMSO at 20°C.

Nucleophiles	N (s_N)	k_2^{exp} (M^{-1} s^{-1})			
		*o*QM1	*o*QM2	*o*QM3	*o*QM4[a]
N1	17.64 (0.73)	3.84×10^1	7.92	6.00×10^1	n.d.
N2	18.82 (0.69)	1.08×10^2	1.28×10^1	1.57×10^2	6.27×10^1
N3	19.36 (0.67)	4.37×10^2	n.d.	6.50×10^2	2.40×10^2
N4	19.62 (0.67)	4.30×10^2	8.94×10^1	n.d.	2.88×10^2
N5	20.22 (0.65)	3.06×10^2	n.d.	4.89×10^2	3.32×10^2
N6	20.71 (0.60)	n.d.	8.04×10^1	n.d.	n.d.
N7	21.54 (0.62)	4.93×10^3	3.02×10^2	3.82×10^3	4.38×10^3
Electrophilicity E of *o*QM		−15.73	−17.03	−15.55	−16.00[a]

[a] Kinetic data for *o*QM4 reflect the overall reactivity of the ambient electrophile.

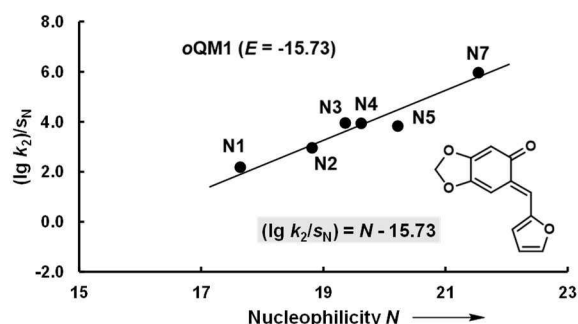The slopes in Figs. S2–S5 were set to unity as required by Equation (1).

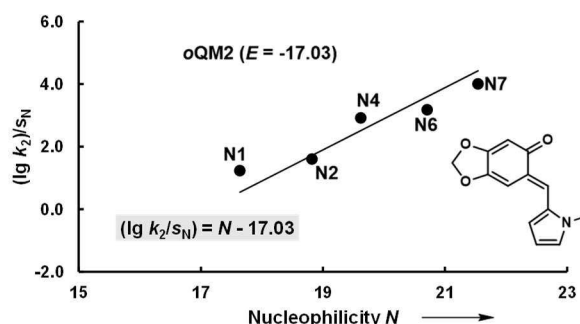**Fig. S2**. Correlation of lg k_2^{exp}/s_N vs. N for *o*QM *o*QM1.

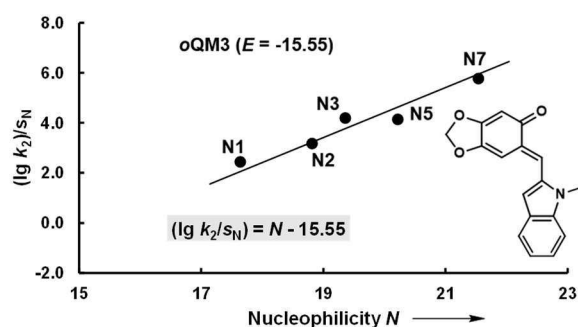**Fig. S3**. Correlation of lg k_2^{exp}/s_N vs. N for *o*QM *o*QM2.

_____

Fig. S4. Correlation of lg k_2^{exp}/s_N vs. N for *o*QM **oQM3**.
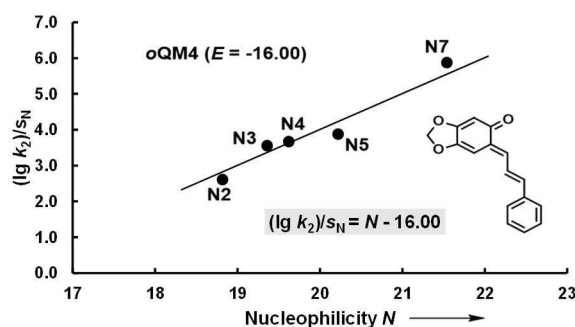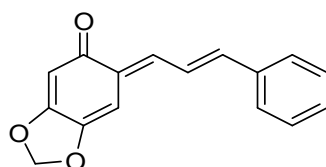

Fig. S5. Correlation of lg k_2^{exp}/s_N vs. N for *o*QM **oQM4**.

6.2.2. Synthesis of Hetero(aryl)- and Cinnamyl-substituted *ortho*-Quinone Methides

(*Z*)-6-((E)-3-Phenylallylidene)benzo[*d*][1,3]dioxol-5(6*H*)-one (*o*QM4) was synthesized according to a literature procedure.[2] NMR spectroscopic data agree with those described in ref. [2].


oQM4 (CG373)

¹H NMR (400 MHz, d_6-acetone): δ 7.73 (d, J = 6.7 Hz, 2 H), 7.67 (dd, J = 15.2, 12.3 Hz, 1 H), 7.46–7.35 (m, 4 H), 7.25 (d, J = 15.2 Hz, 1 H), 6.94 (s, 1 H), 6.05 (s, 2 H), 5.79 ppm (s, 1 H).

¹³C{¹H} NMR (101 MHz, d_6-acetone): δ 184.5, 162.4, 146.6, 144.0, 140.1, 137.7, 131.5, 130.2, 129.7, 128.6, 124.6, 103.4, 101.5, 98.7 ppm.

IR (neat, ATR): $\tilde{v}$ 3054, 2917, 1618, 1591, 1524, 1427, 1365, 1227, 1208, 1093, 974, 957, 862, 811, 749, 690 cm⁻¹.

HRMS (EI): *m/z* calcd for $C_{16}H_{12}O_3^{\bullet+}$ [M⁺]: 252.0781; found: 252.0779.

The hetero(aryl)-substituted **oQMs 1-3** were synthesized based on the established synthetic methodology in ref. [3] with slight modifications.
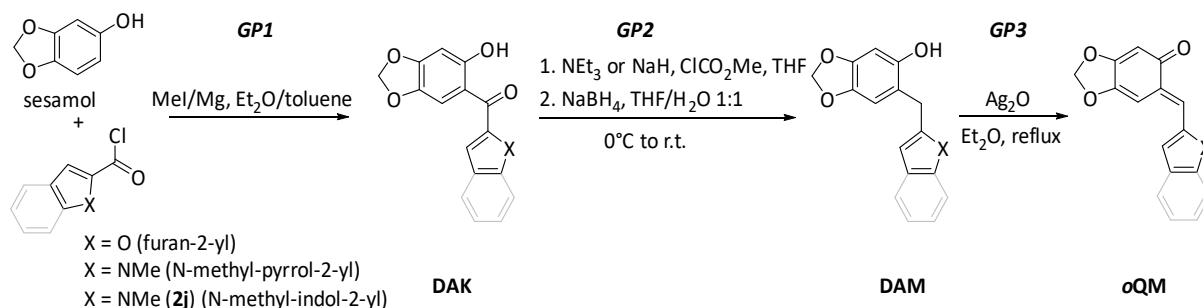
Furan-2-yl(6-hydroxybenzo[*d*][1,3]dioxol-5-yl)methanone (DAK1) was prepared (*GP1*) from magnesium (0.40 g, 16 mmol), methyl iodide (3.85 g, 27.1 mmol), sesamol (1.50 g, 10.9 mmol), and 2-

furoyl chloride (1.42 g, 10.9 mmol). Purification of the crude material by flash chromatography (silica gel, *n*-pentane:EtOAc = 19:1) gave **DAK1** as two yellow fractions. One pure fraction as yellow crystals (0.035 g) that was used for spectroscopic analysis and a crude product (2.40 g), which was directly used in the next step without further purification; m.p. 103 °C.
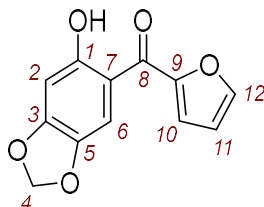

DAK1 (CG454_1)

¹H NMR (400 MHz, CDCl₃): δ 13.27 (s, 1 H, 1-OH), 7.79 (s, 1 H, 6-H), 7.70 (dd, *J* = 1.7, 0.8 Hz, 1 H, 12-H), 7.37 (dd, *J* = 3.6, 0.8 Hz, 1 H, 10-H), 6.61 (dd, *J* = 3.6, 1.8 Hz, 1 H, 11-H), 6.51 (s, 1 H, 2-H), 6.01 ppm (s, 2 H, 4-H).

¹³C{¹H} NMR (101 MHz, CDCl₃): δ 183.0 (C_q, C-8), 164.3 (C_q, C-1), 154.6 (C_q, C-3), 152.6 (C_q, C-9), 146.7 (CH, C-12), 140.9 (C_q, C-5), 120.1 (CH, C-10), 112.5 (CH, C-11), 110.9 (C_q, C-7), 108.3 (CH, C-6), 102.1 (CH_2, C-4), 99.0 ppm (CH, C-2).

IR (neat, ATR): ṽ 3132, 2921, 1734, 1621, 1583, 1481, 1463, 1419, 1326, 1252, 1213, 1167, 1031, 1021, 927, 864, 827, 771, 752, 706 cm⁻¹.

HRMS (EI): *m/z* calcd for $C_{12}H_8O_5^{\bullet+}$ [M•⁺]: 232.0366; found: 232.0365.

(6-Hydroxybenzo[*d*][1,3]dioxol-5-yl)(1-methyl-1*H*-pyrrol-2-yl)methanone (DAK2) was prepared (*GP1*) from magnesium (0.34 g, 14 mmol), methyl iodide (3.34 g, 23.5 mmol), sesamol (1.30 g, 9.41 mmol), and pyrrole 2-carbonyl chloride (1.49 g, 10.4 mmol). Purification of the crude material by flash chromatography (silica gel, *n*-pentane:EtOAc = 19:1 → 9:1) and crystallization (from *n*-hexane/CH₂Cl₂) gave **DAK2** (0.360 g, 16%) as yellow crystals; m.p. 104 °C.
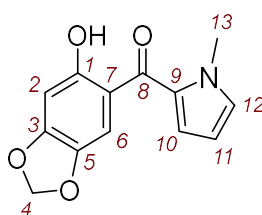
DAK2 (CG484)

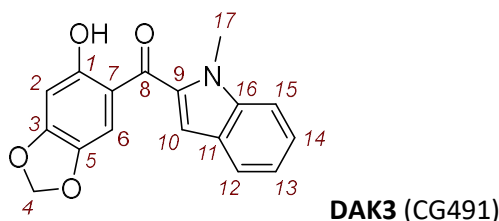*R*f (silica, *n*-pentane/EtOAc = 19:1, UV) = 0.30.
¹H NMR (400 MHz, CDCl₃): δ 12.77 (s, 1 H, 1-H), 7.34 (s, 1 H, 6-H), 6.90–6.89 (m, 1 H, 12-H), 6.78–6.76 (m, 1 H, 10-H), 6.51 (s, 1 H, 2-H), 6.20–6.18 (m, 1 H, 11-H), 5.98 (s, 2 H, 4-H), 3.93 ppm (s, 3 H, 13-H).

¹³C {¹H} NMR (101 MHz, CDCl₃): δ 187.8 (C_q, C-8), 162.1 (C_q, C-1), 153.5 (C_q, C-3), 140.2 (C_q, C-5), 130.9 (CH, C-12), 129.7 (C_q, C-9), 121.1 (CH, C-10), 112.8 (C_q, C-7), 109.8 (CH, C-6), 108.4 (CH, C-11), 101.8 (CH_2, C-4), 98.9 (CH, C-2), 36.9 ppm (CH_3, C-13).

IR (neat, ATR): ṽ 2918, 1624, 1580, 1483, 1405, 1295, 1244, 1194, 1140, 1078, 1031, 931, 874, 863, 832, 732, 689 cm⁻¹.

HRMS (EI): *m/z* calcd for $C_{13}H_{11}NO_4^{\bullet+}$ [M•⁺]: 245.0683; found: 245.0683.

(6-Hydroxybenzo[*d*][1,3]dioxol-5-yl)(1-methyl-1*H*-indol-2-yl)methanone (DAK3) was prepared (*GP1*) from magnesium (0.37 g, 15 mmol), methyl iodide (3.60 g, 25.4 mmol), sesamol (1.40 g, 10.1 mmol), and indole 2-carbonyl chloride (2.16 g, 11.1 mmol, added portion by portion to the reaction mixture). Purification of the crude material by flash chromatography (silica gel, *n*-pentane:EtOAc = 19:1 → 9:1) and crystallization (from *n*-hexane/CH$_2$Cl$_2$) gave **DAK3** (1.29 g, 43%) as yellow crystals; m.p. 179 °C.

DAK3 (CG491)

R_f (silica, *n*-pentane/EtOAc = 19:1, UV) = 0.40.

^{1}H NMR (400 MHz, CDCl$_3$): δ 12.91 (s, 1 H, 1-H), 7.72–7.69 (m, 1 H, 12-H), 7.44–7.38 (m, 3 H, 6-H, 14-H, and 15-H), 7.21–7.17 (m, 1 H, 13-H), 7.00 (s, 1 H, 10-H), 6.56 (s, 1 H, 2-H), 6.01 (s, 2 H, 4-H), 3.98 ppm (s, 3 H, 17-H).
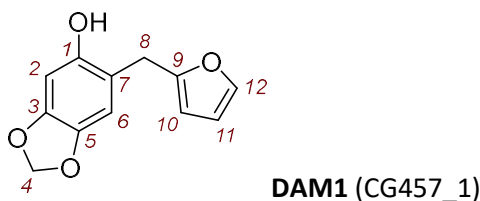
^{13}C{^{1}H} NMR (101 MHz, CDCl$_3$): δ 190.0 (C$_q$, C-8), 163.2 (C$_q$, C-1), 154.5 (C$_q$, C-3), 140.5 (C$_q$, C-5), 139.9 (C$_q$, C-16), 134.6 (C$_q$, C-9), 126.2 (C$_q$, C-11), 125.6 (CH, C-14), 122.7 (CH, C-12), 121.0 (CH, C-13), 113.1 (C$_q$, C-7), 112.1 (CH, C-10), 110.4 (CH, C-15), 110.0 (CH, C-6), 102.1 (CH$_2$, C-4), 98.9 (CH, C-2), 31.9 ppm (CH$_3$, C-17).

IR (neat, ATR): $\tilde{v}$ 2904, 1619, 1585, 1509, 1474, 1430, 1385, 1309, 1246, 1229, 1187, 1166, 1038, 939, 845, 734 cm^{-1}.

HRMS (EI): *m/z* calcd for C$_{17}$H$_{13}$NO$_4$$^{\bullet+}$ [M$^{\bullet+}$]: 295.0839; found: 295.0839.

6-(Furan-2-ylmethyl)benzo[*d*][1,3]dioxol-5-ol (DAM1) was prepared (*GP2*) from crude **DAK1** (2.40 g, approx. 10 mmol), triethylamine (1.57 g, 15.5 mmol), methyl chloroformate (1.12 g, 11.9 mmol) in THF (40 mL). After filtration, the solvent was removed under reduced pressure at the rotary evaporator and purification of the crude material by flash chromatography (silica gel, eluent: *n*-pentane:EtOAc = 8:2) yielded the carbonate [1.13 g, 3.89 mmol, R_f (silica, *n*-pentane/EtOAc 8:2, UV) = 0.2].

The carbonate (1.13 g, 3.89 mmol) was dissolved in THF (20 mL) and sodium borohydride (0.589 g, 15.6 mmol, in 20 mL water) was added. Purification of the crude material by flash chromatography (silica gel, eluent: *n*-pentane:EtOAc = 8:2) furnished **DAM1** (0.790 g, 93%, calculated from the carbonate) as a colorless oil.


DAM1 (CG457_1)

R_f (silica, pentane/EtOAc 8:2, UV) = 0.60.

^{1}H NMR (600 MHz, CDCl$_3$): δ 7.34–7.33 (m, 1 H, 12-H), 6.62 (s, 1 H, 6-H), 6.44 (s, 1 H, 2-H), 6.30–6.29 (m, 1 H, 11-H), 6.06–6.05 (m, 1 H, 10-H), 5.89 (s, 2 H, 4-H), 5.00 (s, 1 H, 1-OH), 3.87 ppm (s, 2 H, 8-H).

^{13}C{^{1}H} NMR (151 MHz, CDCl$_3$): δ 153.7 (C$_q$, C-9), 148.4 (C$_q$, C-1), 147.1 (C$_q$, C-3), 141.8 (CH, C-12), 141.7 (C$_q$, C-5), 116.3 (C$_q$, C-7), 110.6 (CH, C-11), 109.7 (CH, C-6), 106.2 (CH, C-10), 101.2 (CH$_2$, C-4), 99.1 (CH, C-2), 29.3 ppm (CH$_2$, C-8).

HRMS (EI): *m/z* calcd for C$_{12}$H$_{10}$O$_4$$^{\bullet+}$ [M$^{\bullet+}$]: 218.0574; found: 218.0572.

6-((1-Methyl-1*H*-pyrrol-2-yl)methyl)benzo[*d*][1,3]dioxol-5-ol (DAM2) was prepared (*GP2*) from **DAK2** (0.360 g, 1.47 mmol), sodium hydride (60% dispersion in mineral oil, 0.088 g, 2.21 mmol), methyl chloroformate (0.160 g, 1.69 mmol) in THF (30 mL). After filtration, the solution was reduced to half of the volume by solvent evaporation at the rotary evaporator. Then, sodium borohydride (0.222 g, 5.87 mmol in 15 mL water) was added. Purification of the crude material by flash chromatography (silica gel, eluent: *n*-pentane:EtOAc = 8:2) furnished **DAM2** (0.312 g, 92%) as a colorless oil.

DAM2 (CG488)
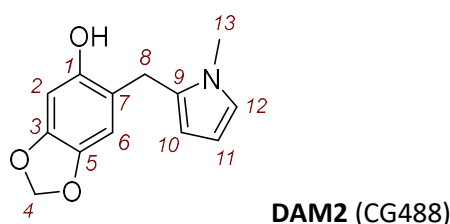
R_f (silica, n-*pentane*/EtOAc 8:2, UV) = 0.40.
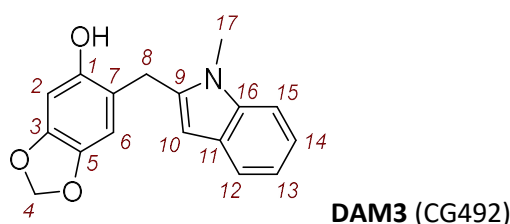
^{1}H NMR (400 MHz, CDCl$_3$): δ 6.61–6.60 (m, 1 H, 12-H), 6.56 (s, 1 H, 6-H), 6.40 (s, 1 H, 2-H), 6.07 (t, *J* = 3.1 Hz, 1 H, 11-H), 6.00–5.98 (m, 1 H, 10-H), 5.88 (s, 2 H, 4-H), 5.11 (s, 1 H, 1-OH), 3.86 (s, 2 H, 8-H), 3.45 ppm (s, 3 H, 13-H).

^{13}C{^{1}H} NMR (101 MHz, CDCl$_3$): δ 149.3 (C$_q$, C-1), 147.0 (C$_q$, C-3), 141.6 (C$_q$, C-5), 129.7 (C$_q$, C-9), 123.3 (CH, C-12), 116.4 (C$_q$, C-7), 109.5 (CH, C-6), 107.7 (CH, C-10), 107.2 (CH, C-11), 101.1 (CH$_2$, C-4), 99.2 (CH, C-2), 34.1 (CH$_3$, C-13), 29.0 ppm (CH$_2$, C-8).

IR (neat, ATR): $\tilde{v}$ 3438, 2894, 1633, 1503, 1483, 1444, 1297, 1168, 1037, 934, 854, 761, 713 cm^{-1}.

HRMS (EI): *m/z* calcd for C$_{13}$H$_{13}$NO$_3$$^{\bullet+}$ [M$^{\bullet+}$]: 231.0890; found: 231.0889.

6-((1-Methyl-1*H*-indol-2-yl)methyl)benzo[*d*][1,3]dioxol-5-ol (DAM3) was prepared (*GP2*) from **DAK3** (1.29 g, 4.37 mmol), triethylamine (0.796 g, 7.87 mmol), methyl chloroformate (0.620 g, 6.56 mmol) in THF (40 mL). After filtration, the solution was reduced to half of the volume by solvent evaporation at the rotary evaporator before sodium borohydride (1.32 g, 34.9 mmol in 20 mL water) was added. Purification of the crude material by flash chromatography (silica gel, eluent: *n*-pentane:EtOAc = 9:1→8:2) furnished **DAM3** (1.14 g, 93%) as an off-white solid; m.p. 134 °C.


DAM3 (CG492)

^{1}H NMR (400 MHz, CDCl$_3$): δ 7.56–7.54 (m, 1 H, 12-H), 7.29–7.27 (m, 1 H, 15-H), 7.22–7.18 (m, 1 H, 14-H), 7.13–7.08 (m, 1 H, 13-H), 6.58 (s, 1 H, 6-H), 6.42 (s, 1 H, 2-H), 6.32 (q, *J* = 0.9 Hz, 1 H, 10-H), 5.90 (s, 2 H, 4-H), 4.89 (s, 1 H, 1-OH), 4.04 (s, 2 H, 8-H), 3.62 ppm (s, 3 H, 17-H).

^{13}C{^{1}H} NMR (101 MHz, CDCl$_3$): δ 148.7 (C$_q$, C-1), 147.1 (C$_q$, C-3), 141.9 (C$_q$, C-5), 138.2 (C$_q$, C-9), 138.2 (C$_q$, C-16), 127.8 (C$_q$, C-11), 121.4 (CH, C-14), 120.3 (CH, C-12), 119.7 (CH, C-13), 116.1 (C$_q$, C-7), 109.7 (CH, C-6), 109.1 (CH, C-15), 101.3 (CH$_2$, C-4), 100.7 (CH, C-10), 99.1 (CH, C-2), 29.9 (CH$_3$, C-17), 28.7 ppm (CH$_2$, C-8).

IR (neat, ATR): $\tilde{\nu}$ 3566, 2921, 1502, 1477, 1275, 1175, 1112, 1036, 929, 874, 860, 744 cm^{-1}.

HRMS (EI): *m/z* calcd for C$_{17}$H$_{15}$NO$_3$$^{\bullet+}$ [M$^{\bullet+}$]: 281.1046; found: 281.1047.

(*E*)-6-(Furan-2-ylmethylene)benzo[*d*][1,3]dioxol-5(6*H*)-one (*o*QM1) was prepared (*GP3*) from **DAM1** (0.750 g, 3.44 mmol) and silver(I) oxide (2.39 g, 10.3 mmol) in diethyl ether (80 mL) to yield *o*QM1 (0.230 g, 31%) as red crystals; m.p. >127 °C (dec.).
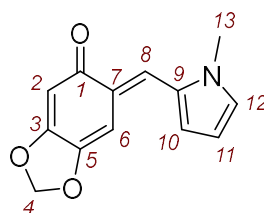

*o*QM1 (CG459)
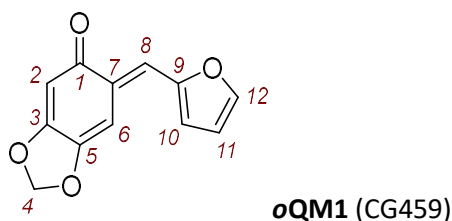
^{1}H NMR (400 MHz, d_6-DMSO): δ 8.03 (d, *J* = 1.9 Hz, 1 H, 12-H), 7.34 (s, 1 H, 8-H), 7.23 (d, *J* = 3.5 Hz, 1 H, 10-H), 7.15 (s, 1 H, 6-H), 6.74 (dd, *J* = 3.5, 1.9 Hz, 1 H, 11-H), 6.08 (s, 2 H, 4-H), 5.92 ppm (s, 1 H, 2-H).

^{13}C{^{1}H} NMR (101 MHz, d_6-DMSO): δ 183.8 (C$_q$, C-1), 161.3 (C$_q$, C-3), 152.1 (C$_q$, C-9), 147.7 (CH, C-12), 146.1 (C$_q$, C-5), 126.0 (C$_q$, C-7), 123.8 (CH, C-8), 121.3 (CH, C-10), 113.5 (CH, C-11), 102.8 (CH$_2$, C-4), 100.3 (CH, C-2), 98.9 ppm (CH, C-6).

IR (neat, ATR): $\tilde{\nu}$ 3124, 1628, 1561, 1518, 1466, 1420, 1348, 1220, 1026, 1009, 945, 931, 849, 827, 746, 706 cm^{-1}.

HRMS (EI): *m/z* calcd for C$_{12}$H$_8$O$_4$$^{\bullet+}$ [M$^{\bullet+}$]: 216.0417; found: 216.0416.

(*E*)-6-((1-Methyl-1*H*-pyrrol-2-yl)methylene)benzo[*d*][1,3]dioxol-5(6*H*)-one (*o*QM2) was prepared (*GP3*) from **DAM2** (0.310 g, 1.34 mmol) and silver(I) oxide (0.932 g, 4.02 mmol) in diethyl ether (40 mL). The reaction mixture was filtered, and the filtration residue was washed with acetone (100 mL). The combined organic phases were evaporated to dryness. The red residue was dissolved in acetone (30 mL). The volume of the acetone solution was reduced to ca. 10 mL by solvent evaporation at the rotary evaporator, which led to precipitation of *o*QM2 (0.121 g, 39%) as dark red crystals; m.p. >120 °C (dec.).
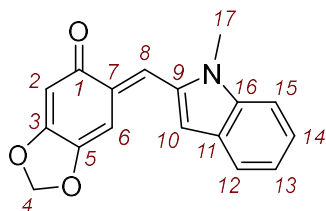
***o*QM2** (CG489)

^{1}H NMR (400 MHz, d_6-DMSO): δ 7.61 (s, 1 H, 8-H), 7.23 (br s, 1 H, 12-H), 6.96 (d, *J* = 4.5 Hz, 1 H, 10-H), 6.88 (s, 1 H, 6-H), 6.29–6.28 (m, 1 H, 11-H), 6.04 (s, 2 H, 4-H), 5.90 (s, 1 H, 2-H), 3.74 ppm (s, 3 H, 13-H).

^{13}C{^{1}H} NMR (101 MHz, d_6-DMSO): δ 183.3 (C_q, C-1), 160.8 (C_q, C-3), 145.1 (C_q, C-5), 129.9 (CH, C-12), 129.1 (C_q, C-9), 127.1 (CH, C-8), 124.3 (C_q, C-7), 116.1 (CH, C-10), 110.8 (CH, C-11), 102.3 (CH_2, C-4), 100.7 (CH, C-2), 99.1 (CH, C-6), 34.0 ppm (CH_3, C-13).

IR (neat, ATR): ṽ 3100, 1617, 1532, 1518, 1484, 1432, 1421, 1374, 1344, 1280, 1212, 1077, 1028, 944, 870, 841, 719, 704 cm^{-1}.

HRMS (pos. ESI): *m/z* calcd for $C_{13}H_{12}NO_3^+$ [M + H$^+$]: 230.0812; found: 230.0818.

(*E*)-6-((1-Methyl-1*H*-indol-2-yl)methylene)benzo[*d*][1,3]dioxol-5(6*H*)-one (*o*QM3) was prepared (*GP3*) from **DAM3** (1.14 g, 4.05 mmol) and silver(I) oxide (2.82 g, 12.2 mmol) in diethyl ether (80 mL). The reaction mixture was filtered, and the filtration residue was washed with acetone (500 mL). The combined organic phases were evaporated to dryness. The red residue was dissolved in acetone (150 mL). The volume of the acetone solution was reduced to ca. 50 mL by solvent evaporation at the rotary evaporator, which led to precipitation of *o*QM3 (0.730 g, 65%) as claret-red crystals; m.p. >135 °C (dec.).

***o*QM3** (CG495)

^{1}H NMR (800 MHz, d_6-DMSO): δ 7.74 (s, 1 H, 8-H), 7.63 (d, *J* = 7.9 Hz, 1 H, 12-H), 7.53 (d, *J* = 8.4 Hz, 1 H, 15-H), 7.27–7.25 (m, 1 H, 14-H), 7.21 (s, 1 H, 10-H), 7.09–7.07 (m, 1 H, 13-H), 6.99 (s, 1 H, 6-H), 6.10 (s, 2 H, 4-H), 5.99 (s, 1 H, 2-H), 3.83 ppm (s, 3 H, 17-H).

^{13}C{^{1}H} NMR (201 MHz, d_6-DMSO): δ 183.6 (C_q, C-1), 161.5 (C_q, C-3), 147.1 (C_q, C-5), 138.7 (C_q, C-16), 134.3 (C_q, C-9), 129.3 (C_q, C-7), 127.7 (C_q, C-11), 126.5 (CH, C-8), 124.1 (CH, C-14), 121.5 (CH, C-12), 120.3 (CH, C-13), 110.3 (CH, C-15), 107.2 (CH, C-10), 102.9 (CH_2, C-4), 100.5 (CH, C-2), 98.6 (CH, C-6), 29.9 ppm (CH_3, C-17).

IR (neat, ATR): ṽ 2899, 1619, 1530, 1423, 1368, 1351, 1324, 1212, 1180, 1152, 1040, 947, 725, 702, 688 cm^{-1}.

HRMS (EI): *m/z* calcd for $C_{17}H_{13}NO_3^{•+}$ [M$^{•+}$]: 279.0890; found: 279.0897.
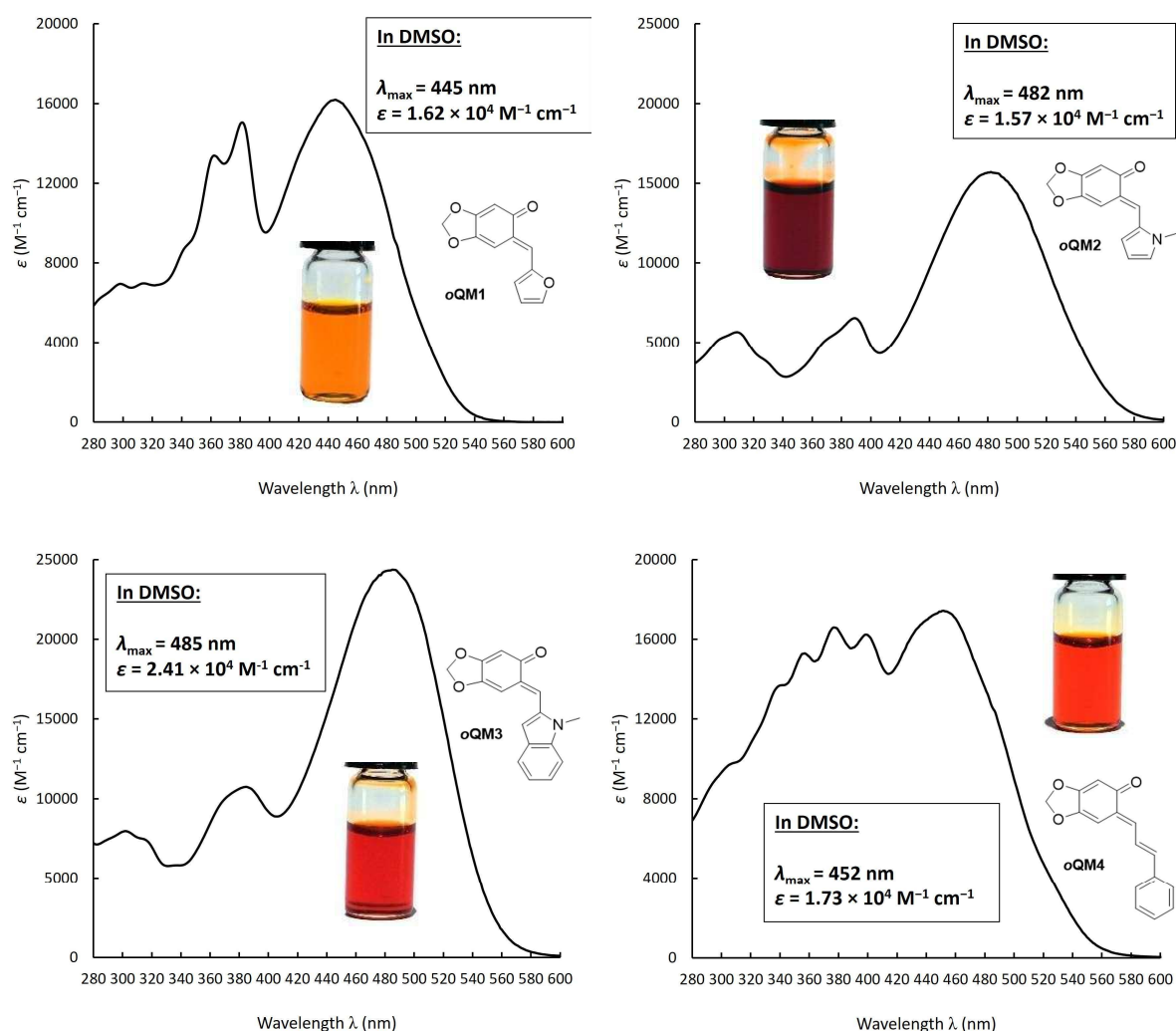
6.2.3. UV/Vis Spectra and Molar Absorption Coefficients of *o*QMs

UV/Vis photometric measurements were carried out using a J&M TIDAS diode array spectrophotometer, which was controlled by TIDASDAQ3 (v3) software and connected to a Hellma 661.502-QX quartz Suprasil immersion probe (light path *d* = 5 mm) via fiber optic cables and standard SMA connectors.

Quinone methide solutions [9–14 mM] in dry DMSO were added stepwise to known volumes of the same solvent. The absorbances *A* of the *o*QM solutions were detected by using a *J&M* TIDAS diode array spectrophotometer (connected to a Hellma quartz probe with a path length *d* = 0.5 cm).

Molar absorption coefficients ε (M^{-1} cm^{-1}) were determined from the slopes of linear correlations of absorbance with *o*QM concentrations by assuming the validity of the Beer-Lambert law [Equation (S1)].

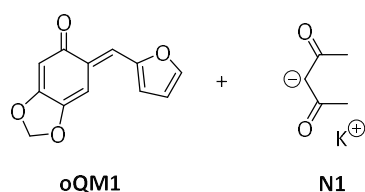$$\lg (I_0/I) = A = \varepsilon\, d\, c \qquad\qquad (S1)$$

6.2.4. Kinetics of the Reactions of *o*QMs with Carbanions (Reference Nucleophiles)

For kinetic measurements the reactions of *o*QMs with carbanionic nucleophiles were monitored by UV/Vis photometry on AppliedPhotophysics SX.20 stopped-flow (SF) instruments as well as on a conventional J&M TIDAS diode array spectrophotometer, which was controlled by TIDASDAQ3 (v3) software and connected to a Hellma 661.502-QX quartz Suprasil immersion probe (light path d = 5 mm) via fiber optic cables and standard SMA connectors. The temperature (20.0 ± 0.2 °C) was maintained constant by using circulating bath cryostats.
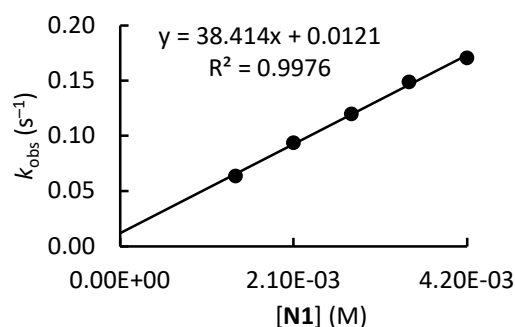
All solutions were prepared by using dry DMSO (ThermoScientific, DMSO 99.7+%, extra dry, over molecular sieve, AcroSeal) and kept under an atmosphere of dry nitrogen. When carbanions were used as the nucleophiles, the kinetic measurements for each *o*QM/nucleophile combination were performed with or without added 18-crown-6 ether (18-c-6) and in some cases with additional CH-acid.

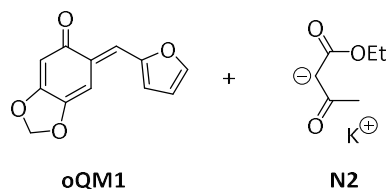**oQM1** + **N1** in DMSO (20 °C, stopped-flow method, detection at 445 nm) CG472

[**oQM1**]$_0$ (M)	[**N1**]$_0$ (M)	[18-c-6]$_0$ (M)	k_{obs} (s^{-1})
3.70 × 10^{-5}	1.40 × 10^{-3}		6.40 × 10^{-2}
3.70 × 10^{-5}	2.10 × 10^{-3}	2.31 × 10^{-3}	9.41 × 10^{-2}
3.70 × 10^{-5}	2.80 × 10^{-3}		1.20 × 10^{-1}
3.70 × 10^{-5}	3.50 × 10^{-3}	3.85 × 10^{-3}	1.49 × 10^{-1}
3.70 × 10^{-5}	4.20 × 10^{-3}		1.71 × 10^{-1}

$$k_2 = (3.84 \pm 0.11) \times 10^1 \text{ M}^{-1} \text{ s}^{-1}$$

oQM1 + **N2** in DMSO (20 °C, stopped-flow method, detection at 445 nm) CG471
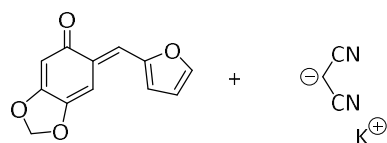

[**oQM1**]$_0$ (M)	[**N2**]$_0$ (M)	[18-c-6]$_0$ (M)	k_{obs} (s^{-1})
3.83 × 10^{-5}	7.00 × 10^{-4}		9.51 × 10^{-2}
3.83 × 10^{-5}	1.05 × 10^{-3}	1.16 × 10^{-3}	1.37 × 10^{-1}
3.83 × 10^{-5}	1.40 × 10^{-3}		1.74 × 10^{-1}
3.83 × 10^{-5}	1.75 × 10^{-3}	1.93 × 10^{-3}	2.09 × 10^{-1}

$$k_2 = (1.08 \pm 0.03) \times 10^2 \text{ M}^{-1} \text{ s}^{-1}$$

oQM1 + **N3** in DMSO (20 °C, stopped-flow method, detection at 445 nm) CG468

[oQM1]$_0$ (M)	[N3]$_0$ (M)	[18-c-6]$_0$ (M)	k_{obs} (s^{-1})
2.96×10^{-5}	3.50×10^{-4}		1.72×10^{-1}
2.96×10^{-5}	5.25×10^{-4}	5.78×10^{-4}	2.49×10^{-1}
2.96×10^{-5}	7.00×10^{-4}		3.27×10^{-1}
2.96×10^{-5}	8.75×10^{-4}	9.63×10^{-4}	4.04×10^{-1}
2.96×10^{-5}	1.05×10^{-3}		4.77×10^{-1}

$$k_2 = (4.37 \pm 0.03) \times 10^2 \text{ M}^{-1} \text{ s}^{-1}$$

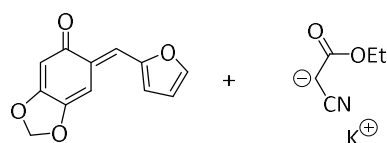**oQM1** + **N4** in DMSO (20 °C, stopped-flow method, detection at 445 nm) CG469

[oQM1]$_0$ (M)	[N4]$_0$ (M)	[18-c-6]$_0$ (M)	k_{obs} (s^{-1})
2.96×10^{-5}	3.50×10^{-4}		1.80×10^{-1}
2.96×10^{-5}	5.25×10^{-4}	5.78×10^{-4}	2.68×10^{-1}
2.96×10^{-5}	7.00×10^{-4}		3.40×10^{-1}
2.96×10^{-5}	8.75×10^{-4}	9.63×10^{-4}	4.16×10^{-1}
2.96×10^{-5}	1.05×10^{-3}		4.82×10^{-1}

$$k_2 = (4.30 \pm 0.12) \times 10^2 \text{ M}^{-1} \text{ s}^{-1}$$

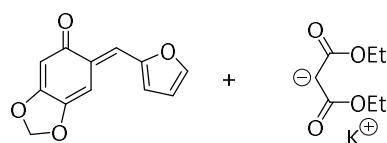**oQM1** + **N5** in DMSO (20 °C, stopped-flow method, detection at 445 nm) CG470

[oQM1]$_0$ (M)	[N5]$_0$ (M)	[18-c-6]$_0$ (M)	k_{obs} (s^{-1})
2.96×10^{-5}	3.50×10^{-4}		1.23×10^{-1}
2.96×10^{-5}	5.25×10^{-4}	5.78×10^{-4}	1.81×10^{-1}
2.96×10^{-5}	7.00×10^{-4}		2.32×10^{-1}
2.96×10^{-5}	8.75×10^{-4}	9.63×10^{-4}	2.87×10^{-1}
2.96×10^{-5}	1.05×10^{-3}		3.38×10^{-1}

$$k_2 = (3.06 \pm 0.04) \times 10^2 \text{ M}^{-1} \text{ s}^{-1}$$

oQM1 + **N7** in DMSO (20 °C, stopped-flow method, detection at 445 nm) CG473
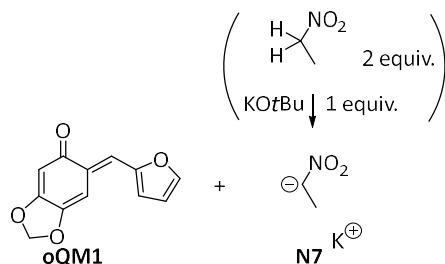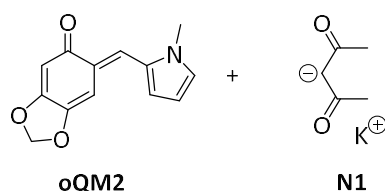
[**oQM1**]$_0$ (M)	[**N7**]$_0$ (M)	[18-c-6]$_0$ (M)	k_{obs} (s^{-1})
3.46×10^{-5}	7.00×10^{-4}		3.74
3.46×10^{-5}	1.05×10^{-3}	1.16×10^{-3}	5.63
3.46×10^{-5}	1.40×10^{-3}		7.08
3.46×10^{-5}	1.75×10^{-3}	1.93×10^{-3}	9.01

$$k_2 = (4.93 \pm 0.19) \times 10^3 \text{ M}^{-1} \text{ s}^{-1}$$

y = 4931.4x + 0.324
$R^2 = 0.9971$

oQM2 + **N1** in DMSO (20 °C, diode array detection at 482 nm) CG518

[**oQM2**]$_0$ (M)	[**N1**]$_0$ (M)	[18-c-6]$_0$ (M)	k_{obs} (s^{-1})
4.90×10^{-5}	8.87×10^{-4}		6.94×10^{-3}
4.90×10^{-5}	1.32×10^{-3}	1.45×10^{-3}	1.06×10^{-2}
5.10×10^{-5}	1.77×10^{-3}		1.41×10^{-2}
5.10×10^{-5}	2.15×10^{-3}	2.37×10^{-3}	1.74×10^{-2}
4.97×10^{-5}	2.60×10^{-3}		2.04×10^{-2}

$$k_2 = (7.92 \pm 0.19) \text{ M}^{-1} \text{ s}^{-1}$$

y = 7.9197x + 6E-05
$R^2 = 0.9983$

oQM2 + **N2** in DMSO (20 °C, stopped-flow method, detection at 482 nm) CG519

[**oQM2**]$_0$ (M)	[**N2**]$_0$ (M)	[18-c-6]$_0$ (M)	k_{obs}[a] (s^{-1})
4.78×10^{-5}	7.50×10^{-4}		1.33×10^{-2}
4.78×10^{-5}	1.13×10^{-3}	1.24×10^{-3}	1.88×10^{-2}
4.78×10^{-5}	1.50×10^{-3}		2.28×10^{-2}
4.78×10^{-5}	1.88×10^{-3}	2.06×10^{-3}	2.84×10^{-2}
4.78×10^{-5}	2.25×10^{-3}		3.25×10^{-2}

y = 12.803x + 0.0039
$R^2 = 0.9976$

[a] Only the first half-life time was used to determine k_{obs}.

$$k_2 = (1.28 \pm 0.04) \times 10^1 \text{ M}^{-1} \text{ s}^{-1}$$

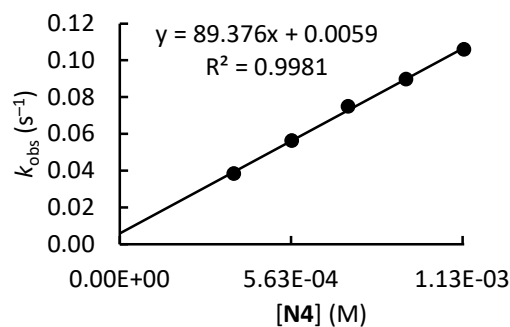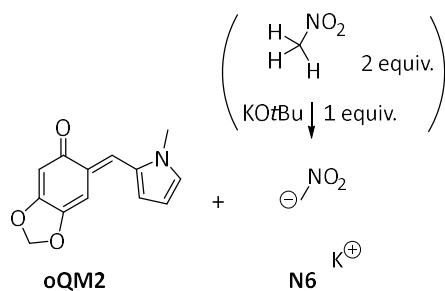**oQM2** + **N4** in DMSO (20 °C, stopped-flow method, detection at 482 nm) CG521

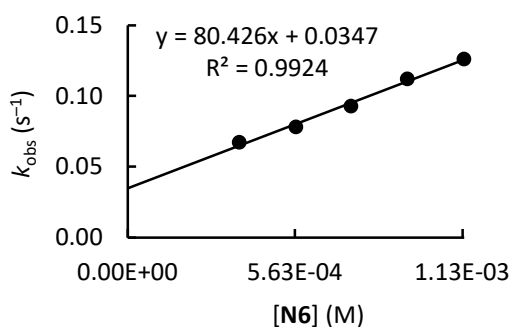| [oQM2]$_0$ (M)	[N4]$_0$ (M)	[18-c-6]$_0$ (M)	k_{obs}[a] (s^{-1})
4.33×10^{-5}	3.75×10^{-4}		3.85×10^{-2}
4.33×10^{-5}	5.65×10^{-4}	6.19×10^{-4}	5.63×10^{-2}
4.33×10^{-5}	7.50×10^{-4}		7.49×10^{-2}
4.33×10^{-5}	9.40×10^{-4}	1.03×10^{-3}	8.98×10^{-2}
4.33×10^{-5}	1.13×10^{-3}		1.06×10^{-1}

[a] Only the first half-life time was used to determine k_{obs}.

$$k_2 = (8.94 \pm 0.23) \times 10^1 \text{ M}^{-1} \text{ s}^{-1}$$

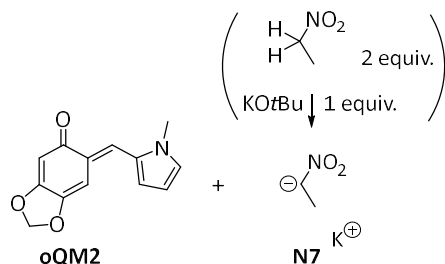**oQM2** + **N6** in DMSO (20 °C, stopped-flow method, detection at 482 nm) CG520

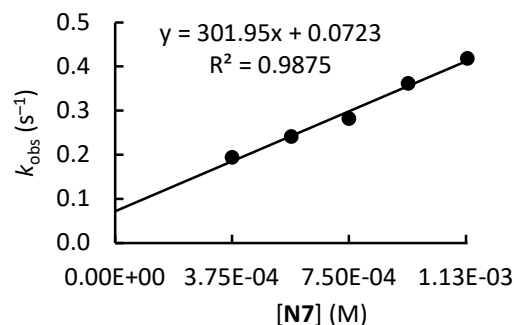| [oQM2]$_0$ (M)	[N6]$_0$ (M)	[18-c-6]$_0$ (M)	k_{obs} (s^{-1})
4.90×10^{-5}	3.75×10^{-4}		6.72×10^{-2}
4.90×10^{-5}	5.65×10^{-4}	6.19×10^{-4}	7.80×10^{-2}
4.90×10^{-5}	7.50×10^{-4}		9.29×10^{-2}
4.90×10^{-5}	9.40×10^{-4}	1.03×10^{-3}	1.12×10^{-1}
4.90×10^{-5}	1.13×10^{-3}		1.26×10^{-1}

$$k_2 = (8.04 \pm 0.41) \times 10^1 \text{ M}^{-1} \text{ s}^{-1}$$

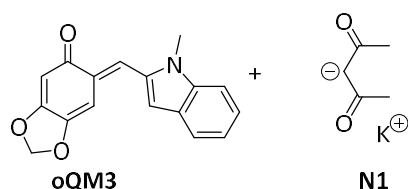**oQM2** + **N7** in DMSO (20 °C, stopped-flow method, detection at 482 nm) CG517

[oQM2]$_0$ (M)	[N7]$_0$ (M)	[18-c-6]$_0$ (M)	k_{obs} (s^{-1})
3.72×10^{-5}	3.75×10^{-4}		1.94×10^{-1}
3.72×10^{-5}	5.65×10^{-4}	6.19×10^{-4}	2.41×10^{-2}
3.72×10^{-5}	7.50×10^{-4}		2.82×10^{-2}
3.72×10^{-5}	9.40×10^{-4}	1.03×10^{-3}	3.62×10^{-1}
3.72×10^{-5}	1.13×10^{-3}		4.18×10^{-1}

$y = 301.95x + 0.0723$
$R^2 = 0.9875$

$$k_2 = (3.02 \pm 0.20) \times 10^2 \text{ M}^{-1} \text{ s}^{-1}$$

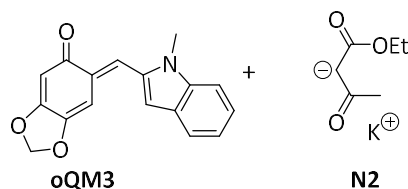**oQM3** + **N1** in DMSO (20 °C, diode array detection at 485 nm) CG514

[oQM3]$_0$ (M)	[N1]$_0$ (M)	[18-c-6]$_0$ (M)	k_{obs} (s^{-1})
2.46×10^{-5}	4.97×10^{-4}		3.26×10^{-2}
2.34×10^{-5}	7.39×10^{-4}	8.12×10^{-4}	4.20×10^{-2}
2.50×10^{-5}	1.00×10^{-3}		5.98×10^{-2}
2.30×10^{-5}	1.22×10^{-3}	1.34×10^{-3}	7.36×10^{-2}
2.42×10^{-5}	1.48×10^{-3}		9.02×10^{-2}

$y = 59.998x + 0.0004$
$R^2 = 0.9933$

$$k_2 = (6.00 \pm 0.28) \times 10^1 \text{ M}^{-1} \text{ s}^{-1}$$

oQM3 + **N2** in DMSO (20 °C, stopped-flow method, detection at 485 nm) CG513
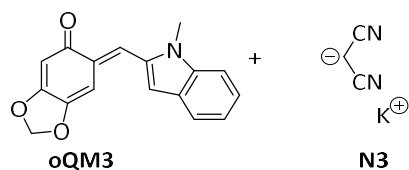
[oQM3]$_0$ (M)	[N2]$_0$ (M)	[18-c-6]$_0$ (M)	k_{obs} (s^{-1})
2.50×10^{-5}	5.00×10^{-4}		9.53×10^{-2}
2.17×10^{-5}	7.50×10^{-4}	8.25×10^{-4}	1.31×10^{-1}
2.01×10^{-5}	1.00×10^{-3}		1.69×10^{-1}
1.84×10^{-5}	1.25×10^{-3}	1.38×10^{-3}	2.15×10^{-1}
1.76×10^{-5}	1.50×10^{-3}		2.49×10^{-1}

$y = 156.56x + 0.0153$
$R^2 = 0.998$

$$k_2 = (1.57 \pm 0.04) \times 10^2 \text{ M}^{-1} \text{ s}^{-1}$$

oQM3 + **N3** in DMSO (20 °C, stopped-flow method, detection at 485 nm) CG508

_____

oQM3 + **N3**

[oQM3]$_0$ (M)	[N3]$_0$ (M)	[18-c-6]$_0$ (M)	k_{obs} (s^{-1})
2.09 × 10^{-5}	2.50 × 10^{-4}		2.62 × 10^{-1}
1.97 × 10^{-5}	3.75 × 10^{-4}	4.13 × 10^{-4}	3.59 × 10^{-1}
1.84 × 10^{-5}	5.00 × 10^{-4}		4.36 × 10^{-1}
1.76 × 10^{-5}	6.25 × 10^{-4}	6.88 × 10^{-4}	5.14 × 10^{-1}
1.62 × 10^{-5}	7.50 × 10^{-4}		5.91 × 10^{-1}

$y = 650.4x + 0.1072$
$R^2 = 0.9977$

$k_2 = (6.50 \pm 0.18) \times 10^2$ M^{-1} s^{-1}

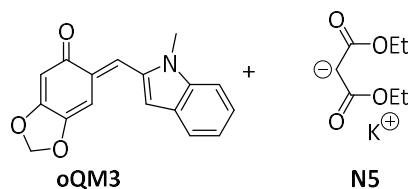**oQM3** + **N5** in DMSO (20 °C, stopped-flow method, detection at 485 nm) CG507

[oQM3]$_0$ (M)	[N5]$_0$ (M)	[18-c-6]$_0$ (M)	k_{obs} (s^{-1})
2.58 × 10^{-5}	2.50 × 10^{-4}		1.73 × 10^{-1}
2.46 × 10^{-5}	3.75 × 10^{-4}	4.13 × 10^{-4}	2.44 × 10^{-1}
2.34 × 10^{-5}	5.00 × 10^{-4}		3.06 × 10^{-1}
2.17 × 10^{-5}	6.25 × 10^{-4}	6.88 × 10^{-4}	3.56 × 10^{-1}

$y = 488.8x + 0.0559$
$R^2 = 0.9941$
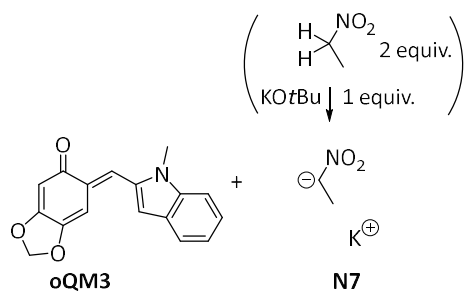
$k_2 = (4.89 \pm 0.27) \times 10^2$ M^{-1} s^{-1}

oQM3 + **N7** in DMSO (20 °C, stopped-flow method, detection at 485 nm) CG512

[oQM3]$_0$ (M)	[N7]$_0$ (M)	[18-c-6]$_0$ (M)	k_{obs} (s^{-1})
2.42 × 10^{-5}	2.50 × 10^{-4}		9.85 × 10^{-1}
2.13 × 10^{-5}	3.75 × 10^{-4}	4.13 × 10^{-4}	1.47
1.93 × 10^{-5}	5.00 × 10^{-4}		1.94
1.68 × 10^{-5}	6.25 × 10^{-4}	6.88 × 10^{-4}	2.42

$y = 3820x + 0.0325$
$R^2 = 1$

$k_2 = (3.82 \pm 0.02) \times 10^3$ M^{-1} s^{-1}

oQM4 + N2 in DMSO (20 °C, stopped-flow method, detection at 452 nm) CG378

$[oQM4]_0$ (M)	$[N2]_0^{[a]}$ (M)	$[18\text{-}c\text{-}6]_0$ (M)	k_{obs} (s^{-1})
6.55×10^{-5}	3.50×10^{-3}		2.32×10^{-1}
5.86×10^{-5}	5.25×10^{-3}	5.78×10^{-3}	3.55×10^{-1}
5.06×10^{-5}	7.00×10^{-3}		4.38×10^{-1}
4.60×10^{-5}	8.75×10^{-3}	9.63×10^{-3}	5.70×10^{-1}

[a] Additionally, the reaction mixtures contained an equimolar amount of the corresponding CH-acid.

$$k_2 = (6.27 \pm 0.37) \times 10^1 \text{ M}^{-1} \text{ s}^{-1}$$

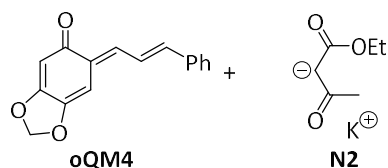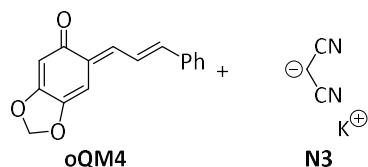**oQM4 + N3** in DMSO (20 °C, stopped-flow method, detection at 452 nm) CG377

$[oQM4]_0$ (M)	$[N3]_0^{[a]}$ (M)	$[18\text{-}c\text{-}6]_0$ (M)	k_{obs} (s^{-1})
5.98×10^{-5}	1.40×10^{-3}		3.37×10^{-1}
5.23×10^{-5}	2.10×10^{-3}	2.31×10^{-3}	5.02×10^{-1}
4.43×10^{-5}	2.80×10^{-3}		6.75×10^{-1}
3.85×10^{-5}	3.50×10^{-3}	3.85×10^{-3}	8.34×10^{-1}
3.33×10^{-5}	4.20×10^{-3}		1.01

[a] Additionally, the reaction mixtures contained an equimolar amount of the corresponding CH-acid.

$$k_2 = (2.40 \pm 0.02) \times 10^2 \text{ M}^{-1} \text{ s}^{-1}$$

oQM4 + N4 in DMSO (20 °C, stopped-flow method, detection at 452 nm) CG376

$[oQM4]_0$ (M)	$[N4]_0^{[a]}$ (M)	$[18\text{-}c\text{-}6]_0$ (M)	k_{obs} (s^{-1})
3.62×10^{-5}	2.80×10^{-3}		8.30×10^{-1}
3.40×10^{-5}	4.20×10^{-3}	4.62×10^{-3}	1.24
3.05×10^{-5}	5.60×10^{-3}		1.62
2.70×10^{-5}	7.00×10^{-3}	7.70×10^{-3}	2.03
2.41×10^{-5}	8.40×10^{-3}		2.45

[a] Additionally, the reaction mixtures contained an equimolar amount of the corresponding CH-acid.

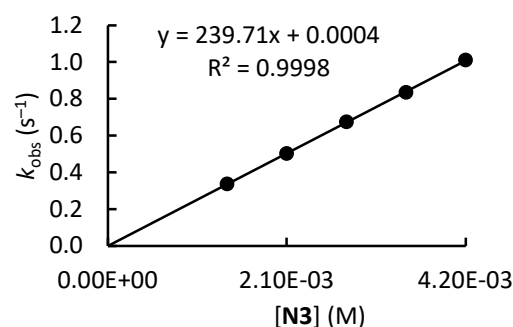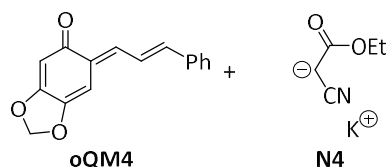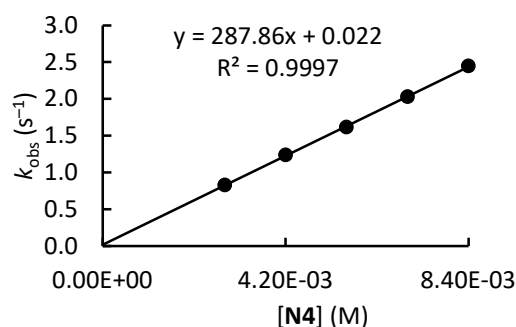$$k_2 = (2.88 \pm 0.03) \times 10^2 \text{ M}^{-1} \text{ s}^{-1}$$

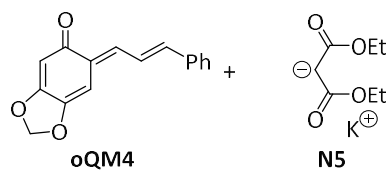***o*QM4** + **N5** in DMSO (20 °C, stopped-flow method, detection at 452 nm) CG379

[*o*QM4]$_0$ (M)	[**N5**]$_0^{[a]}$ (M)	[18-c-6]$_0$ (M)	k_{obs} (s^{-1})
3.10×10^{-5}	1.05×10^{-3}		3.50×10^{-1}
2.36×10^{-5}	1.58×10^{-3}	1.73×10^{-3}	5.45×10^{-1}
1.72×10^{-5}	2.10×10^{-3}		6.61×10^{-1}
1.26×10^{-5}	2.63×10^{-3}	2.89×10^{-3}	8.94×10^{-1}

[a] Additionally, the reaction mixtures contained an equimolar amount of the corresponding CH-acid.

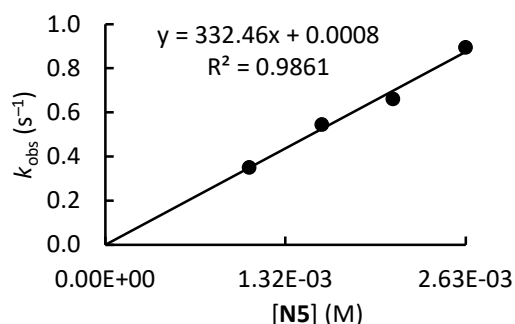$$k_2 = (3.32 \pm 0.28) \times 10^2 \text{ M}^{-1} \text{ s}^{-1}$$

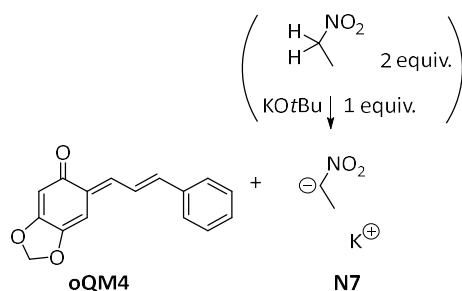***o*QM4** + **N7** in DMSO (20 °C, stopped-flow method, detection at 452 nm) CG375

[*o*QM4]$_0$ (M)	[**N7**]$_0$ (M)	[18-c-6]$_0$ (M)	k_{obs} (s^{-1})
3.68×10^{-5}	1.40×10^{-3}		5.23
3.40×10^{-5}	2.10×10^{-3}	2.31×10^{-3}	8.46
3.16×10^{-5}	2.80×10^{-3}		11.0
2.87×10^{-5}	3.50×10^{-3}	3.85×10^{-3}	14.6

$$k_2 = (4.38 \pm 0.20) \times 10^3 \text{ M}^{-1} \text{ s}^{-1}$$

6.3. References

[1]   R. Lucius, R. Loos and H. Mayr, *Angew. Chem. Int. Ed*. **2002**, *41*, 91.

[2]   L. M. Bishop, M. Winkler, K. N. Houk, R. G. Bergman and D. Trauner, *Chem. Eur. J.* **2008**, *14*, 5405.

[3]   C. Gross, A. Eitzinger, N. Hampel, P. Mayer, A. R. Ofial, *Chem. Eur. J.* **2025**, *31*, e202403785.

Chapter 7. [4+2] Cycloadditions of *ortho*-Quinone Methides with Enamines and Determining the Free Energy of Concert

Author contributions

All experimental work was performed by Christoph Gross. Peter Mayer performed the crystallographic analysis and visualization.

7.1. Introduction

The Diels–Alder reaction (DA) is one of the most powerful and widely applied methods for the formation of six-membered rings, involving a [4+2] cycloaddition between a conjugated diene and a dienophile.[1] These reactions are frequently employed in the stereoselective synthesis of natural products, pharmaceuticals, and other complex organo-functionalized compounds.[2] As a pericyclic reaction, it proceeds through a concerted, symmetry-allowed mechanism that can be predicted by the Woodward–Hoffmann rules.[3] However, stepwise mechanisms (biradical and zwitterionic) have also been proposed in some cases.[4] From a frontier molecular orbital (FMO) perspective, the classical Diels–Alder reaction is typically governed by the interaction of the HOMO of the diene with the LUMO of the dienophile[5], a scenario favored when the diene is electron-rich and the dienophile is electron-poor.

Expanding upon the classical framework, hetero-Diels–Alder (HDA) reactions introduce heteroatoms, such as oxygen or nitrogen into either the diene or the dienophile.[6] These variants broaden the synthetic utility of the reaction and enabling access to heterocyclic scaffolds.[7] Depending on the electronic nature of the reacting partners, the dominant FMO interaction may still involve the diene's HOMO and the dienophile's LUMO. However, in cases where the diene is electron-poor and the dienophile is electron-rich, the orbital interaction is reversed.[8] The HOMO of the dienophile now interacts with the LUMO of the diene. This type of transformation is referred to as an inverse electron-demand hetero-Diels–Alder reaction,[9] and is often encountered in reactions involving electron-deficient heterodienes.

A particularly interesting class of such heterodienes are *ortho*-quinone methides (*o*QMs).[10] Owing to high polarization and extended conjugation, these reactive compounds participate in a broad range of cycloaddition and nucleophilic addition reactions, enabling the formation of diverse chromane and benzopyran frameworks.[11] Their pronounced reactivity in [4+2] cycloadditions has long been exploited as a means to indirectly confirm their transient existence. In this context, a variety of dienophiles such as styrene, enol ethers, enamines and others have been employed in the literature to trap *o*QMs as stable Diels-Alder adducts.[12]

However, it is often challenging to unambiguously determine whether such annulation reactions proceed via a concerted or a stepwise mechanism. In this context, the present chapter explores how the Mayr–Patz equation (Equation 1)[13] can be employed to analyze and predict the reactivities of *o*QMs in [4+2] cycloadditions.

$$\lg k_2 \,(20°\text{C}) = s_\text{N}(N + E) \tag{1}$$

Equation (1) has proven to be a powerful and reliable tool for predicting the reaction rates of bimolecular electrophile–nucleophile combinations. It currently represents the most comprehensive framework for polar organic reactivity, with reactivity parameters established for over 1300 nucleophiles and 350 electrophiles in solution.[14] Second-order rate constants (k_2) are calculated using one electrophilicity parameter E and two nucleophile-specific, solvent-dependent parameters, the nucleophilicity N and the nucleophile-specific sensitivity parameter s_N. While the N and s_N values are derived from kinetic studies involving carbon-based reference electrophiles, the E parameters are determined from reactions with carbon-centered nucleophiles.[15]

It is important to note, however, that the derivation of these parameters is based on kinetic measurements of reactions in which only a single σ-bond is formed in the rate-determining step.[16] Consequently, the Mayr–Patz equation may not be directly applicable to multibond-forming processes such as concerted cycloadditions, where two σ-bonds are formed simultaneously. Therefore,

deviations between experimentally measured rate constants and those predicted by Equation (1) (assuming a hypothetical stepwise mechanism) can serve as a quantitative measure of the energy of concert $\Delta G^{\ddagger}_{concert}$ (Equation 2), offering insight into the degree of concertedness in the reaction pathway.[17]

$$\Delta G^{\ddagger}_{concert} = RT \ln(k_2^{exptl}/k_2^{Eq.(1)}) \qquad (2)$$

This approach was recently demonstrated by Mayr, Ofial, and co-workers in their study of 1,3-dipolar cycloadditions (Huisgen reactions) between diazoalkanes and various dipolarophiles[18,19] By applying Equation (1), they were able to show that many of these reactions proceed via concerted mechanisms, quantify the energy of concert, and proposed a new ordering principle for 1,3-dipolar cycloadditions.[19] In the present work, the Mayr–Patz equation will be utilized as a diagnostic tool to examine inverse-electron-demand hetero-[4+2] cycloadditions between *o*QMs (as electron-poor dienes) and nucleophilic and electron-rich dienophiles, such as enamines. This will allow us to assess the extent of concertedness in these reactions (see Scheme 1).
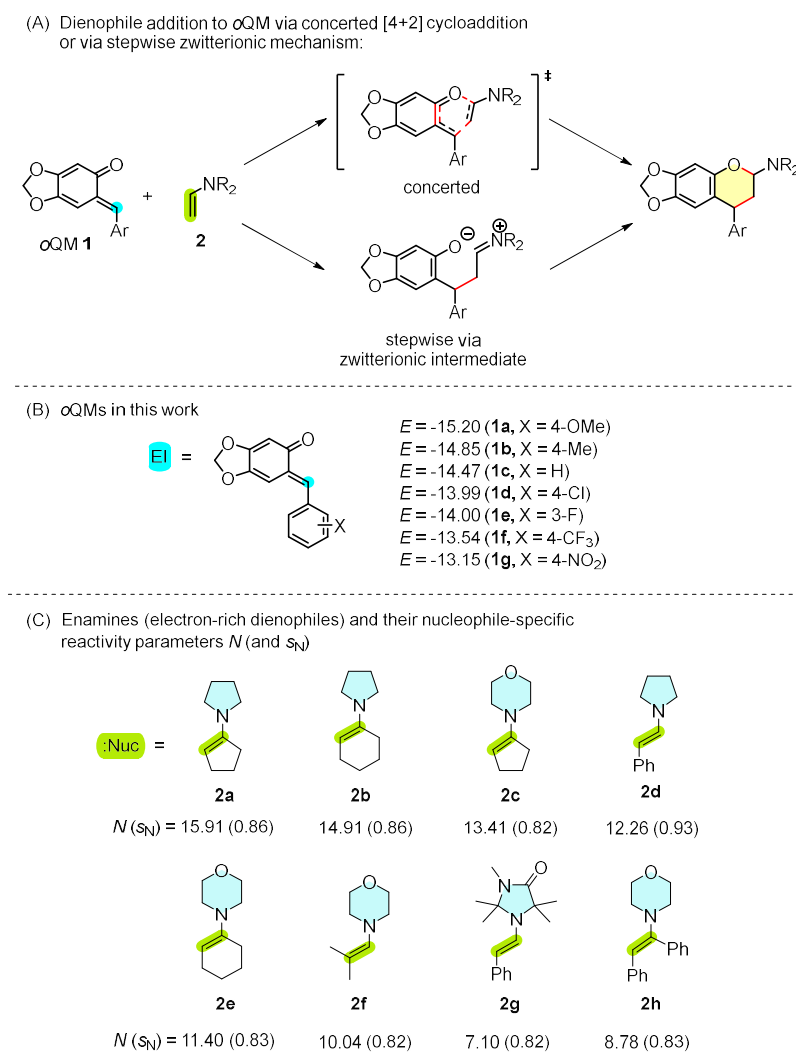

Scheme 1. (A) Illustration of an inverse hetero-Diels-Alder reaction of an *o*QM with an enamine (electron-rich dienophile) following either a concerted or stepwise mechanism. (B) Structures and electrophilicity parameters *E* of *o*QMs **1a-1g** (with *E* from ref. [20] or Chapter 5). (C) Enamines **2a-h** (electron-rich dienophiles) used in this work (nucleophilicity parameters *N* and sensitivity parameters s_N of enamines **2a-2f, 2h** in CH$_2$Cl$_2$, **2g** in MeCN from ref. [21, 22, 23, 24]).

7.2. Results and Discussion

Product Studies of *o*QMs with Enamines.

At first, *o*QMs were prepared according to the synthetic procedure reported in Chapter 5. Then, the products of reactions between preformed (*E*)-configured *o*QMs **1**[20] and electron-rich enamines **2** were investigated. These reactions typically afforded chromanes after reaction times of 30 minutes to 36 hours (Scheme 2).
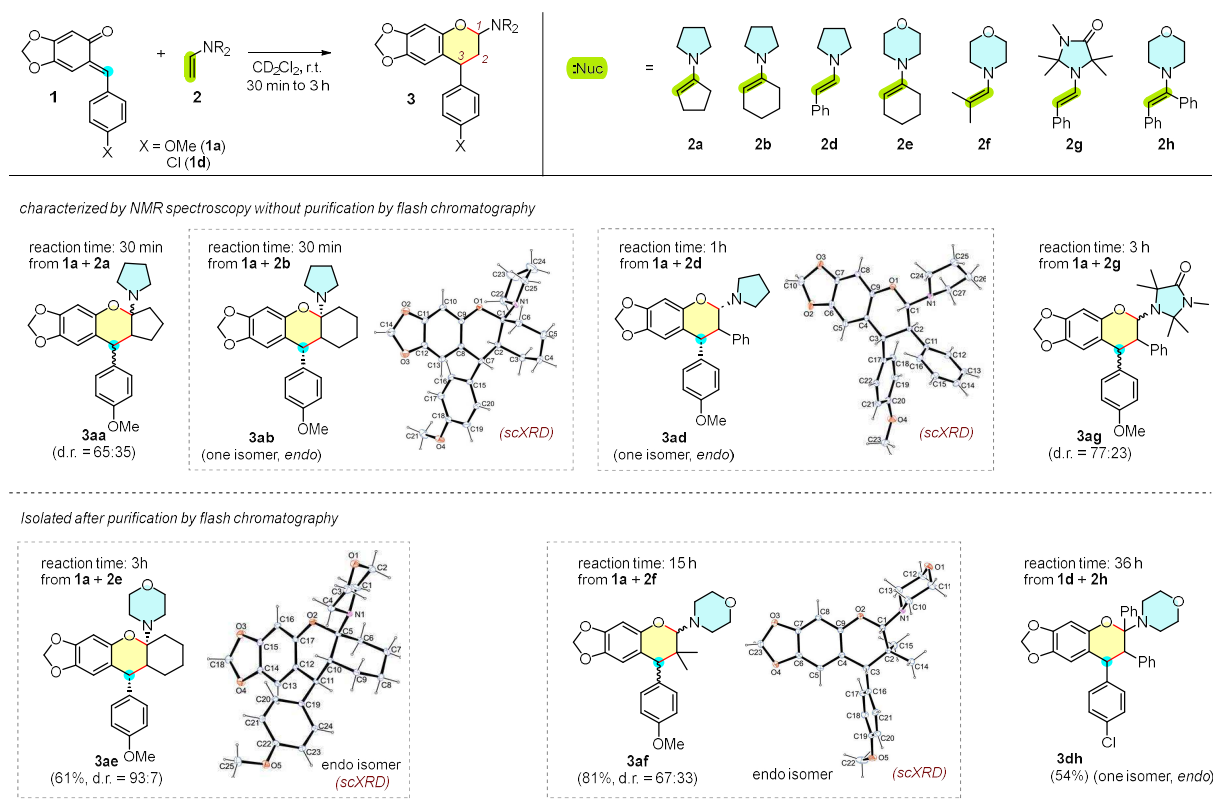

Scheme 2. Observed [4+2] cycloaddition products from the reactions of *o*QM **1a** and **1d** with enamines **2** in CH$_2$Cl$_2$ at 20°C. Yields refer to isolated products after purification with flash chromatography. Thermal ellipsoids of single crystal X-ray structures are shown on the 25% probability level (at 173 K).

The reactions were performed by mixing the *o*QMs with the enamines in CH$_2$Cl$_2$ under a nitrogen atmosphere at room temperature, typically using a slight excess of enamine (up to 1.3 equiv.). The crude reaction mixtures were analyzed after a reaction time of 30 min to 36 h and solvent exchange either directly by NMR-spectroscopy (in CD$_2$Cl$_2$) and high-resolution mass spectrometry (HRMS), or in some cases, after purification by flash chromatography prior to analysis. Diastereomeric ratios of all products were determined from their NMR spectra except of **3ae** and **3dh**. For the products **3aa**, **3ab**, **3ad** and **3ag** no isolated yields were determined. However, NMR analysis indicated nearly quantitative conversions of both reactants with only minor amounts of unreacted enamine detectable. Products **3ae**, **3af** and **3dh** were purified by flash chromatography and isolated in 61%, 81% and 54% yield, respectively.

The configuration of the *o*QMs in these reactions is particularly relevant, as literature reports suggest that (*E*)-configured *o*QMs preferentially lead to *endo*-configured cycloadducts (*cis*-chromanes).[25] This tendency is in accord with *Alder's endo rule* of favorable secondary orbital interactions.[26]

Consistently, the reactions furnished benzopyran derivatives with predominant formation of the *endo*-isomer. This outcome aligns with both theoretical expectations and experimental findings for related Diels-Alder reactions involving (*E*)-configured *o*QMs.[27] Reactions of **1a** with enamines **2b** and **2d** as well as **1d** with **2h**, yielded only one detectable isomer according to NMR analysis. Similarly, the reaction with enamine **2e** afforded cycloaddition product **3ae** with a high diastereoselectivity (d.r. = 93:7), indicating a strong preference for one isomer. For the corresponding products **3ab**, **3ad**, and **3ae** (major isomer) single crystals suitable for X-ray analysis were obtained via the vapor diffusion method (*n*-pentane/CH$_2$Cl$_2$ or *n*-pentane/Et$_2$O), unambiguously confirming the *endo*-configuration in all three cases. In contrast, reactions of *o*QM **1a** with enamines **2a** and **2f** gave approximately 2:1 isomeric mixtures of **3aa** and **3af**, respectively. A crystal of **3af** was isolated and its *endo*-configuration confirmed by scXRD. Similarly, the reaction of **1a** with **2g** gave product **3ag** in a 3:1 diastereomeric ratio based on NMR data. Although no crystals could be isolated for **3aa** and **3ag**, the stereochemical assignment of the major isomer can nonetheless be made with high confidence based on conformational analysis and NMR data.

In the crystal structure-verified cases of **3ab**, **3ad** and **3ae**, the aryl-substituent of the *o*QM and the aminoalkyl residue from the enamine are located on the same face of the chromane-ring, confirming the *cis*-(*endo*)-configuration. Notably, the chromane-ring adopts a half-chair conformation with the ring-protons 2-H and 3-H (see Scheme 3 for atom numbering) being in an antiperiplanar geometry, an arrangement which also gave rise to large vicinal coupling constants ($^3J \approx 9 - 11$ Hz, typically for dihedral angle $\phi = 180°$, according to Karplus relationship)[28] in their ^{1}H-NMR spectra. Since the major diastereomers of **3aa** and **3ag** exhibit similarly large vicinal coupling constants for the 2-H and 3-H protons in their ^{1}H NMR spectra, it is reasonable to conclude that these compounds also possess the *cis*-(*endo*)-configuration and adopt the same half-chair conformation of the chromane ring. For **3dh** no crystal structure could be obtained, but the NMR spectra showed only one isomer and the coupling constants observed for the ring protons are in good agreement with the other products, supporting an *endo*-assignment.

antiperiplanar geometry of two adjacent Protons
($\theta = 180°$, $^3J \approx 9\text{-}11$ Hz)
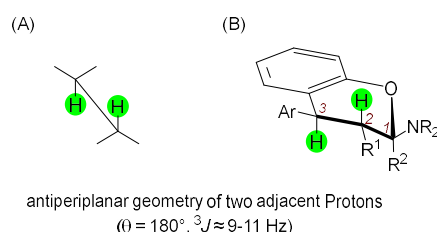
Scheme 3. Antiperiplanar geometry of two adjacent protons in vicinal coupling over three bonds (A) in an alkane and (B) in the chromane formed from the reaction of *o*QM with enamine which is in a characteristic half-chair conformation.

Taken together, the consistent stereochemical outcomes in scXRD-verified cases, the observed ^{1}H-NMR coupling patterns, and the conformational analysis of the chromane ring strongly support that *endo*-selectivity predominates across all examples, including those without direct crystallographic confirmation. To evaluate the stability of the diastereomeric ratio, a crystal of **3af** was dissolved in CD$_2$Cl$_2$ and monitored by NMR spectroscopy. No isomerization to the *exo*-form was observed, indicating that the diastereomeric distribution remains stable after isolation. Additional details on the cycloaddition products are provided in the experimental part (Section 7.4.3).

It is also worth noting that structurally related chromane-type products were reported in earlier studies by JURD[29], who demonstrated that Mannich bases in combination with ketones or aldehydes can generate both *o*QMs and enamines in situ. The resulting intermediates subsequently underwent [4+2] cycloadditions, to afford chromane systems of similar structural composition.

Kinetics of the Cycloaddition Reactions of *o*QMs with Enamines.

Next, kinetic investigations were carried out for the reactions of *o*QMs **1** with enamines **2**, for which nucleophilicity and electrophilicity parameters are known. The experimentally determined second-order rate constants of the [4+2] cycloadditions were then compared to rates calculated by the Mayr-Patz equation based on one-bond nucleophilicity and electrophilicity parameters, in order to examine the relationship between concerted and stepwise polar (formation of zwitterionic intermediate) reactions.

The *o*QMs are intensely colored compounds that strongly absorb in the visible region, with λ_{max} values ranging from 417 to 504 nm in DMSO[20], depending on their substitution pattern. To evaluate potential solvent effects on the absorption properties, UV–Vis spectra of *o*QMs **1a** and **1c** were also recorded in CH_2Cl_2 and CH_3CN. Only minor hypsochromic shifts were observed (λ_{max} for **1a**: 435 nm in DMSO, 430 nm in CH_2Cl_2, and 429 nm in CH_3CN; for **1c**: 417 nm in DMSO and 413 nm in CH_2Cl_2). Due to the only small solvent-dependent differences, a comprehensive screening of absorption spectra for all *o*QMs in various solvents was deemed unnecessary. Consequently, kinetics can be monitored via UV/Vis spectroscopy in the visible region at or near the known λ_{max} values. In cases where no specific absorption spectrum in the target solvent was available, the λ_{max} determined in DMSO was used. Kinetic measurements were performed by stopped-flow UV–Vis spectroscopy, following the decay of the *o*QM's characteristic visible band during reaction with enamines **2** (Figure 1A). All experiments were conducted at 20°C in CH_2Cl_2, CH_3CN, DMF, toluene, and 1,4-dioxane.

To establish pseudo-first-order conditions, the enamines were employed in at least a ten-fold excess relative to the *o*QMs concentration. The mono-exponential decrease in absorbance over time was fitted using the function $A = A_0 \exp(-k_{obs} t) + C$ yielding the observed first-order rate constants k_{obs} (s^{-1}) (Figure 1B). For each *o*QM enamine pair, first-order rate constants k_{obs} were determined at a minimum of four different enamine concentrations. The second-order rate constants (k_2^{exptl}) were then obtained from the slope of the linear correlation between k_{obs} and the enamine concentrations (Figure 1C).
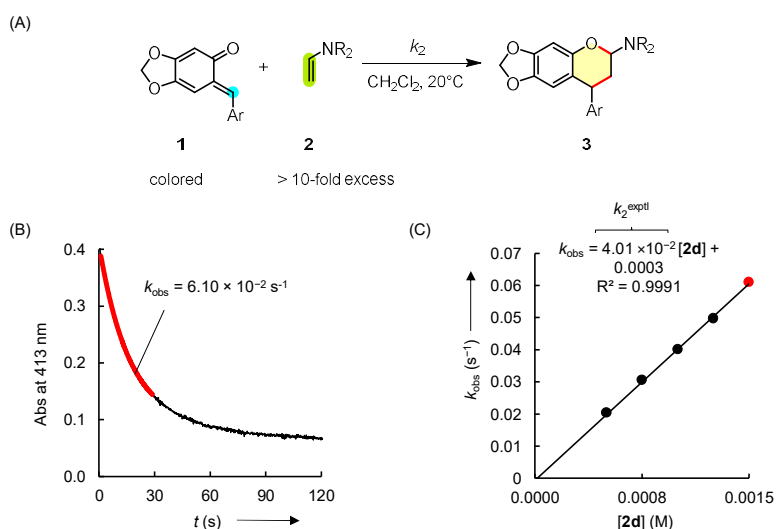

Figure 1. (A) [4+2] Cycloaddition of an *o*QM **1** with an enamine **2** in CH_2Cl_2 at 20 °C. (B): Time-dependent decay of the absorbance of **1c** ($[1c]_0 = 5.69 \times 10^{-5}$ M) at 413 nm for the reaction with **2d** ($[2d]_0 = 1.50 \times 10^{-3}$ M) in CH_2Cl_2 at 20°C. (C): Linear correlation of experimentally determined k_{obs} values with concentrations of **2d**, the slope represents the second-order rate constant k_2.

This methodology was applied to study the reactivity of *o*QM **1a** with enamines **2a-2g**, and of enamine **2d** with different *o*QMs **1a-1g**. Most experiments were carried out in CH_2Cl_2 but additional experiments

were monitored in CH_3CN, 1,4-dioxane, toluene, and DMF to explore the influence of solvent polarity on the reaction rates. The experimentally determined second-order rate constants k_2^{exptl}, along with the rate constants $k_2^{Eq.(1)}$ predicted by the Mayr–Patz equation, are summarized in Table 1, Table 2, and Table 3. Additional kinetic data, including linear plots for each electrophile–nucleophile combination and experimental details are provided in the experimental part (section 7.4.8).

Correlation Analysis.

Equation (1) allows the prediction of rates of electrophile nucleophile combinations and typically provides reliable estimates within two orders of magnitude. If the reactions of *o*QMs **1** with enamines **2** proceeded stepwise, with rate-determining formation of a zwitterionic intermediate, as illustrated in Scheme 1A, it is expected that the experimental rates match closely those which are calculated by Equation (1) (predicted with reactivity parameters N, s_N and E calibrated for single-bonding processes).

However, a comparison of the experimentally determined rate constants k_2^{exptl} with the calculated rate constants $k_2^{Eq.(1)}$ in Tables 1 and 2 reveals substantial discrepancies. For all measured combinations of enamines **2a-g** and *o*QMs **1a-g**, the experimental rates exceed the predicted ones by at least two orders of magnitude (i.e. $k_2^{exptl}/k_2^{Eq.(1)} > 100$). These pronounced deviations indicate that the observed kinetics measured via UV/Vis spectroscopy are not consistent with a stepwise mechanism involving rate-determining C–C bond formation between *o*QM and enamine.

Table 1. Experimental and calculated second-order rate constants k_2^{exptl} and $k_2^{Eq.(1)}$ for the reactions of *o*QM **1a** with enamines **2a-f** in CH_2Cl_2 and **2g** in MeCN at 20°C.

2	N (s_N)[a]	k_2^{exptl} $(M^{-1}s^{-1})$	$k_2^{Eq.(1)}$ [b] $(M^{-1}s^{-1})$	$k_2^{exptl}/k_2^{Eq.(1)}$	$\Delta G^{\ddagger}_{concert}$ $(kJ\,mol^{-1})$
2a	15.91 (0.86)	4.73×10^2	4.08	1.16×10^2	11.6
2b	14.91 (0.86)	2.69×10^2	5.63×10^{-1}	4.78×10^2	15.1
2c	13.41 (0.82)	6.41	3.41×10^{-2}	1.88×10^2	12.8
2d	12.26 (0.93)	3.11×10^1	1.84×10^{-3}	1.69×10^4	23.7
2e	11.40 (0.83)	2.48	7.01×10^{-4}	3.54×10^3	20.0
2f	10.04 (0.82)	3.84	5.87×10^{-5}	6.54×10^4	27.0
2g	7.10 (0.82)	1.09×10^1	2.28×10^{-7}	4.78×10^7	43.1

[a] Nucleophilicity parameters N (and s_N) taken from ref.[14].

[b] Second-order rate constants $k_2^{Eq.(1)}$ calculated by using Equation (1), reported nucleophile-specific parameters N and s_N (from ref. [14]), and electrophilicity parameters E (from ref.[14]).

Table 2. Experimental and calculated second-order rate constants k_2^{exptl} and $k_2^{Eq.(1)}$ for the reactions of enamine **2d** with *o*QMs **1a-g** in CH_2Cl_2 at 20°C.

1	$E^{[a]}$	k_2^{exptl} $(M^{-1}s^{-1})$	$k_2^{Eq.(1)\,[b]}$ $(M^{-1}s^{-1})$	$k_2^{exptl}/k_2^{Eq.(1)}$	$\Delta G^{\ddagger}_{concert}$ (kJ mol^{-1})
1a	−15.20	3.11×10^1	1.84×10^{-3}	1.69×10^4	23.7
1b	−14.86	3.23×10^1	3.90×10^{-3}	8.28×10^3	22.0
1c	−14.47	4.01×10^1	8.80×10^{-3}	4.56×10^3	20.5
1d	−13.99	4.90×10^1	2.46×10^{-2}	1.99×10^3	18.5
1e	−14.00	4.90×10^1	2.41×10^{-2}	2.03×10^3	18.5
1f	−13.54	7.75×10^1	6.45×10^{-2}	1.20×10^3	17.2
1g	−13.15	1.32×10^2	1.49×10^{-1}	8.86×10^2	16.5

[a] Electrophilicity parameters *E* taken from ref.[14].

[b] Second-order rate constants $k_2^{Eq.(1)}$ calculated by using Equation (1), reported nucleophile-specific parameters *N* and s_N (from ref. [14]), and electrophilicity parameters *E* (from ref.[14]).

Further, Figure 2 illustrates the discrepancy between experimental and predicted second-order rate constants. In Figure 2B, a Plot of (lg k_2)/s_N vs. *N* is shown for the reactions of *o*QM **1a** with enamines **2a-2g**. The black line represents the predicted rate constants $k_2^{Eq.(1)}$ for the rate-determining formation of the zwitterionic intermediates based on the reactivity parameters of *o*QM **1a** (*E* = −15.20) and the corresponding enamines **2a-2g** (*N*, s_N parameters in CH_2Cl_2 or MeCN, see Scheme 1C). The blue data points show the experimentally determined rate constants k_2^{exptl}. The deviations between experimental and predicted rate constants k_2^{exptl} and $k_2^{Eq.(1)}$ increase with decreasing nucleophilicity of the enamines.

For the more nucleophilic enamines **2a-2c** the difference ranges from a factor of 116 to 478, while for weaker enamines **2d-2f** it spans three and four orders of magnitude (factor 1,000-99,999). For the least nucleophilic enamine **2g** the observed rate exceeds the predicted value by even seven orders of magnitude (factor of over 10 million). A similar trend is evident in Figure 2C, where lg k_2 is plotted against the electrophilicity parameter *E*. Here, the reactivity of different *o*QMs **1a–1g** toward enamine **2d** is shown, with rate differences again spanning three to four orders of magnitude.

Consequently, the pronounced deviations between k_2^{exptl} and $k_2^{Eq.(1)}$ clearly suggest that the reactions are unlikely to proceed via a simple stepwise mechanism with an initial, rate-determining C-C bond formation. Instead, the data could be interpreted in a way that the reaction follows a multibonding process, possibly involving a concerted transition state.

To further explore this hypothesis, the so-called "energy of concert" was calculated using the term $\Delta G^{\ddagger}_{concert} = RT \ln(k_2^{exptl}/k_2^{Eq.(1)})$ (Equation 2) from the experimental and predicted second-order rate constants. The resulting values, which are listed in Table 1 and 2 (rightmost column), range from 11 to

43 kJ mol^{-1}, indicating that the energy difference depends on the nucleophilic and electrophilic reactivity parameters, respectively, and provides a quantitative measure of deviation from a stepwise mechanism.
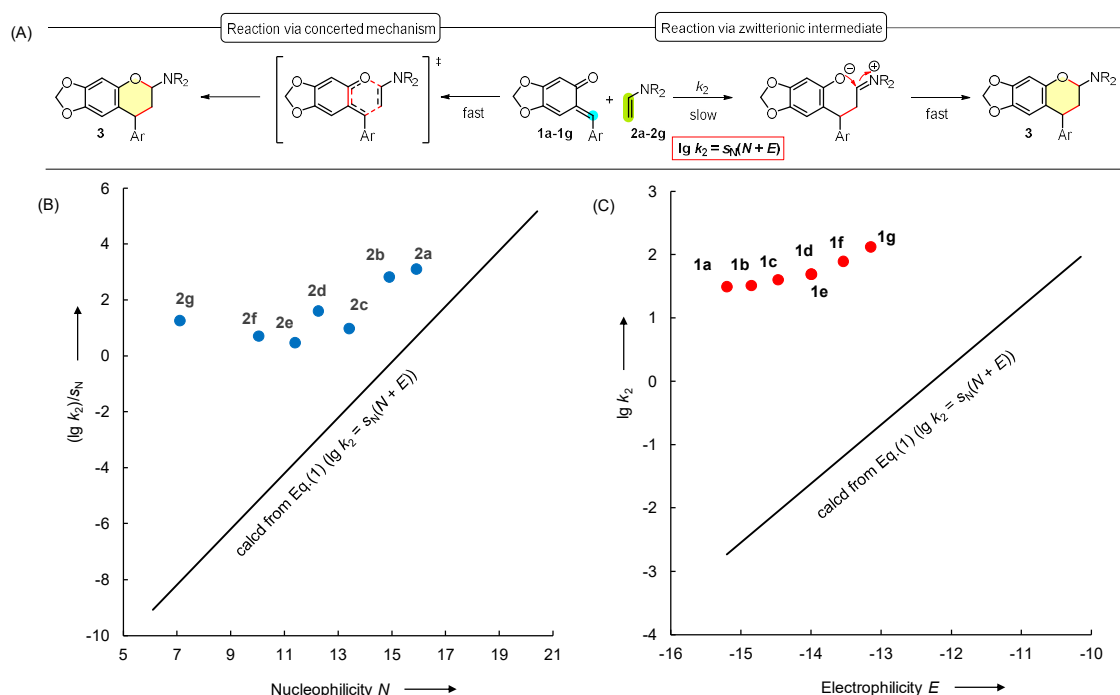

Figure 2. (A) Concerted or stepwise mechanism between *o*QMs **1** and enamines **2**. (B) Correlation of (lg k_2)/s_N for the reactions of *o*QM **1a** with enamines **2a-2g** against the nucleophilicity parameter N of the enamines. (C) Correlation of lg k_2 for the reactions of enamine **2d** with *o*QMs **1a-1g** against the electrophilicity parameter E of the *o*QMs.

Additionally, Figure 3 visualizes the relationship between the Gibbs activation energies $\Delta G^{\ddagger}$ and the nucleophilicity parameter N for the reactions of *o*QM **1a** with enamines **2a-2g**. The orange line represents the Gibbs activation energies $\Delta G^{\ddagger}_{Eq.(1)}$ derived from predicted rate constants for the stepwise mechanism, while the blue line shows the Gibbs activation energies $\Delta G^{\ddagger}_{exptl}$ of experimentally determined second-order rate constants. The difference between these two energies represents the energy of concert $\Delta G^{\ddagger}_{concert}$, as shown in the grey correlation line. Notably, this energy decreases with increasing nucleophilicity of the enamine. This trend might suggest that reactions with less nucleophilic enamines proceed via more synchronous transition states, while those with more nucleophilic enamines may involve more asynchronous bond formation. This hypothesis is further supported by a detailed quantum chemical study reported by Han, Peng and coworkers.[30] Their study focused on regioselectivity and asynchronicity in bond formation for the inverse-electron-demand hetero Diels-Alder reactions of simple *o*QMs with various dienophiles (styrene, methyl vinyl ether, methyl vinyl ketone). It was revealed that the asynchronicity increases with the electron-donating character of the dienophile substituents. This observation aligns with the trend described here, since nucleophilicity typically increases with electron-donating substituents. Hence, increasing nucleophilicity not only accelerates the reaction but also enhances the asynchronous nature of the transition state.

Interestingly, similar discrepancies between experimental and predicted rate constants as well as analogous trends in the synchronicity of bond formation have been discussed previously in 1,3-dipolar cycloadditions of diazo compounds with various dipolarphiles.[19] However, alternative explanations such as solvent effects cannot be ruled out at this stage and will be discussed in the following section.
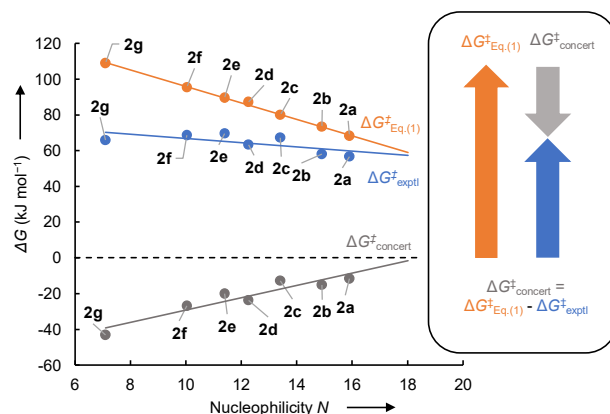
_____

Figure 3. Correlation of Gibbs activation energies $\Delta G^{\ddagger}$ for the reaction of *o*QM **1a** with enamines **2a-2g** (at 20°C in CH_2Cl_2) against the one-bond nucleophilicity parameters *N*. The difference between $\Delta G^{\ddagger}_{Eq.(1)}$ (orange line) and $\Delta G^{\ddagger}_{exptl}$ (blue line) is equal to the energy of concert $\Delta G^{\ddagger}_{concert}$ (grey line).

Hence, in order to further investigate the nature of the cycloaddition mechanism, second-order rate constants for the reactions of *o*QM **1a** with enamine **2d** were measured at 20°C in four additional solvents of varying polarity (CH_3CN, DMF, toluene, 1,4-dioxane). The reaction proceeded with comparable rate constants in the polar aprotic solvents (CH_2Cl_2, CH_3CN, DMF) and in the aprotic nonpolar solvent toluene, despite significant differences in their solvent polarity parameters $E_T(30)$ (Table 3). A moderate rate decrease of approximately 50% in comparison to the other solvents was observed in 1,4-dioxane. However, such deviations are still marginal and consistent with previously reported solvent effects in various Diels–Alder reactions.[8] Notably, it is well-established in the literature that [4+2]-cycloaddition reactions (Diels-Alder) are generally less sensitive to solvent polarity than stepwise polar reactions, expect in aqueous media, where significantly larger effects have been observed (attributed to hydrophobic interactions).[31] This limited solvent dependence is commonly attributed to the absence of significant charge separation in the transition state of concerted pericyclic processes that otherwise in stepwise reactions could be stabilized by polar protic/aprotic solvents.[32, 33]

Table 3. Second-order rate constants k_2^{exptl} of the reactions of *o*QM **1a** with enamine **2d** in five different solvents at 20°C.

solvent	$E_T(30)^{[a]}$	N (s_N) of **2d**	k_2^{exptl} (M^{-1} s^{-1})
$CH_2Cl_2^{[b]}$	40.7	12.26 (0.93)	3.11×10^1
CH_3CN	45.6	13.87 (0.87)	2.94×10^1
DMF	43.8	n.d.	2.65×10^1
1,4-Dioxane	36.0	n.d.	1.11×10^1
Toluene	33.9	n.d.	2.51×10^1

[a] $E_T(30)$ values were taken from ref. [33]

[b] Second-order rate constant k_2 in CH_2Cl_2 from Table 1.

The negligible solvent effect observed in this study is therefore fully consistent with the characteristic behavior of many concerted [4+2] cycloadditions. Thus, it can be concluded that the [4+2] cycloaddition reactions studied in this work do not significantly depend on the polarity of the solvent. This result further supports the hypothesis that *o*QM-enamine cycloadditions might follow a concerted mechanism without formation of a zwitterionic intermediate.

Moreover, Figure 4 illustrates the linear correlations between the logarithm of the experimentally observed second-order rate constants k_2^{exptl} for the reactions of *o*QMs **1a-1g** with enamine **2d** with the Hammett substituent constants and the reduction potentials E_p^{red} of *o*QMs **1a-1g**.[20] These linear correlations demonstrate that both the electronic nature of the substituents remote to the electrophilic center and the redox properties of the *o*QMs systematically influence the reaction rates and allow to further predict the reactivity of other novel *o*QMs with enamine **2d** in their cycloaddition reactions. It is expected, that this linear behavior could also be observed in the context of other enamines.
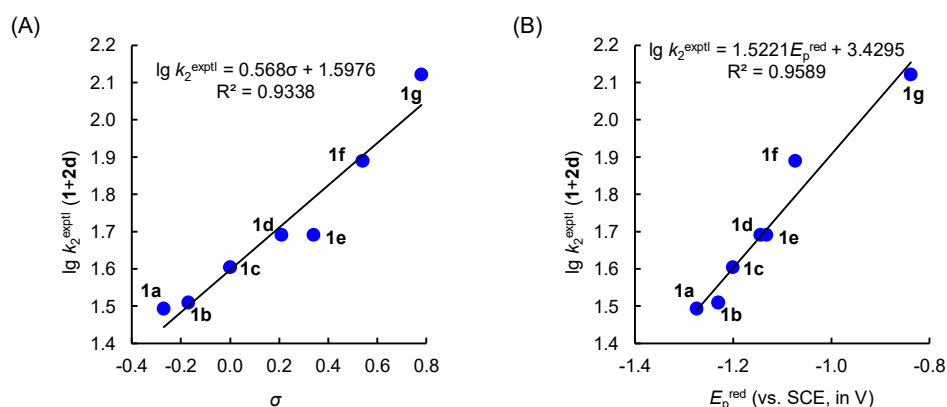
Figure 4. Linear correlation of the logarithm of measured rate constants lg k_2^{exptl} with (A) Hammett substituent constants σ and (B) experimental reduction potentials E_p^{red} of *o*QMs **1a**-**1g** for the reactions of *o*QMs **1a-1g** with enamine **2d**.

Although, the so far discussed experimental kinetic data in this Chapter is more consistent with a concerted mechanism, the possibility of a stepwise biradical pathway involving single-electron transfer (SET) was also considered.

For that reason, the one-electron oxidation potentials E_p^{ox} of the enamines **3** were measured via cyclic voltammetry in CH_3CN (see experimental part for details, section 7.4.6). Together with reported one-electron reduction potentials of *o*QMs **1**[20], these data were used to calculated Gibbs free energies for hypothetical electron transfer processes ΔG°_{ET}, using Equation (3).[34] These energies were then compared with the experimentally determined Gibbs energies of activation $\Delta G^{\ddagger}_{exptl}$, calculated from experimental second-order rate constants via the Eyring equation.[35]

$$\Delta G^{\circ}_{ET} = F(E^{ox} - E^{red}) \qquad (3)$$

As summarized in Table 4, the activation energies for all examined oQM-enamine couples are significantly lower than the corresponding Gibbs energies of electron transfer ΔG°_{ET} (energy of activation for an outer sphere SET process $\Delta G^{\ddagger}_{ET}$ was not calculated, but must be greater than ΔG°_{ET}). The difference between ΔG°_{ET} and $\Delta G^{\ddagger}_{exptl}$ exceeds for electrophile-nucleophile couples 50 kJ mol^{-1} which converted into rate constants results in a difference ten orders of magnitude or more. Consequently, it can be concluded that none of the herein experimentally observed reactions between *o*QMs **1** and enamines **2** proceeds via an SET pathway.

Table 4. Calculated Gibbs energies of electron transfer $\Delta G°_{ET}$ for the electrophile-nucleophile couples **1a** with **2a**-**2g** and **1a**-**1g** with **2d** are compared to their experimentally determined Gibbs activation energies $\Delta G^{\ddagger}_{exptl}$.

1a + 2	$\Delta G^{\ddagger}_{exptl}$ (kJ mol^{-1})	$\Delta G°_{ET}$ (kJ mol^{-1})	1 + 2d	$\Delta G^{\ddagger}_{exptl}$ (kJ mol^{-1})	$\Delta G°_{ET}$ (kJ mol^{-1})
2a	56.7	155.1	1a	63.4	156.2
2b	58.1	156.2	1b	63.3	152.0
2c	67.2	176.5	1c	62.8	149.1
2d	63.4	156.2	1d	62.3	143.7
2e	69.5	176.7	1e	62.3	142.5
2f	68.5	174.1	1f	61.2	136.8
2g	65.9	n.d.	1g	59.9	114.1

Scope of *o*QM Reactions with Further Types of Dienophiles.

After quantifying the cycloaddition rates of *o*QMs **1** with enamines **2**, the study was extended to reactions of **1** with other types of dienophiles to explore whether they proceed via stepwise or concerted mechanisms. In principle, the reactivity parameters (*E*, *N*, s_N) from Equation (1), can be used not only to rationalize reported electrophile-nucleophile combinations, but also to predict new reactions. Figure 5 presents a combined electrophilicity-nucleophilicity scale, which is arranged in a way that $E + N = -5$. Reactants located on the same horizontal level typically (to some degree dependent on the s_N parameter) react with rate constants between 10^{-3} and 10^{-6} M^{-1} s^{-1}, corresponding to half reaction times of 5 min to several days at 20°C in 1 M solutions.

The rule of thumb of *E+N* > −5 is generally considered as the lower threshold for observable reactivity given that only one new σ-bond is formed in the rate-determining step. However, if bond formation occurs via a multibonding process in a concerted reaction, considerably higher reaction rates may be observed, even when the *E* + *N* criterion is not fulfilled. Consequently, product formation under such conditions may indicate the operation of a multibonding pathway.

_____
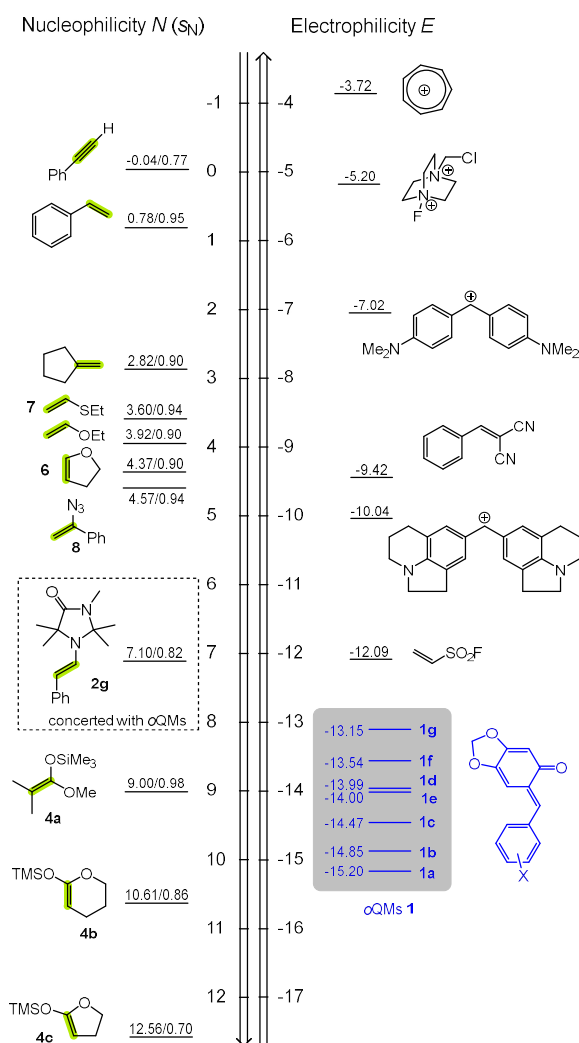
Figure 5. *o*QMs **1** are ranked according to their electrophilicity parameters *E* in the Mayr reactivity scales. The location of **1** can be used to identify useful nucleophilic reaction partners (see main text). (Nucleophile specific reactivity parameters *N* (s_N) in CH$_2$Cl$_2$ if not mentioned otherwise). Reactivity parameters taken from ref. [14].

Notably, reactions of *o*QM **1b** (*E* = −15.20) with styrene (*N*/s_N = 0.78/0.95)[14] and ethyl vinyl ether (*N*/s_N = 3.92/0.90)[14] under the formation of (dihydro)chromanes have been reported in the literature. In the case of styrene elevated temperatures (>100°C) were required[36], whereas the reaction with neat ethyl vinyl ether proceeded at room temperature after just 5 h in a yield of 67%.[12e] That is quite remarkable as this reaction should not take place under these simple reaction conditions according to Mayr's reactivity parameters. This deviation from the predicted behavior therefore indicates the operation of a non-stepwise mechanism. Supporting this, quantum chemical studies by Han, Peng and co-workers proposed that the reaction of a simple *o*QM with styrene follows an asynchronous concerted mechanism, while the reaction with methyl vinyl ether (structurally related to ethyl vinyl ether) proceeds through a highly asynchronous more zwitterionic-like mechanism.[30]

Building on these findings, reactions between *o*QMs **1** and silyl ketene acetals **4a-4c**, 2,3-dihydrofuran **6**, ethyl vinylsulfide **7** and α-azidostyrene **8** were investigated in CH$_2$Cl$_2$ at room temperature (Figure 6). It is worth noting, that the nucleophiles **6-8** have previously been studied in reactions with in situ generated *o*QMs.[37-39] However, these reported reactions were conducted under significantly different reaction conditions. The investigated reactions in this work were studied by simply mixing the reactants in dichloromethane under nitrogen atmosphere followed by purification using flash

chromatography, which furnished the desired cycloadducts in good to excellent yields (Figure 6). For example, *o*QM **1a** and enol ether **4a** reacted over 72 h to form a crude product that was filtered through a plug of basic Al_2O_3 which led to desilylation and the formation of the coumarin derivative **5aa** in a yield of 82%. Suitable crystals for single crystal X-ray diffraction (scXRD) were furnished by the vapor diffusion method (*n*-pentane/dichloromethane, +4°C) which showed a characteristic half-chair conformation of the chromane ring. The reaction of **1a** with **4b** formed after 60 h and desilylation the hemiacetal **5ab** (61% yield, d.r. = 75:25), while **1a** and **4c** produced the silylated acetal **5ac** in 56% yield (d.r. = 53:47) after approximately 1 h without desilylation. Based on the available structural data, it was not possible to clearly assign the *endo*- or *exo*-configuration of these two cycloadducts. Additionally, reaction of *o*QM **1f** with 2,3-dihydrofuran **6** gave acetal **6'** in 42% yield (d.r. = 67:33) after only 120 h. The major isomer shows *cis*-(*endo*)-configuration based on X-ray data and NMR coupling constants (4.3 – 5.3 Hz), consistent with a gauche arrangement of the ring protons 1-H, 2-H, 3-H (see Figure 6 for atom numbering, dihedral angle ф ≈ 60°, 2 – 6 Hz, Karplus relationship).[28] Cycloadducts **7'** and **8'**, derived from reactions of **1a** with ethyl vinyl sulfide **7** and **1g** with α-azidostyrene **8** were also obtained within a few days in moderate to good yields of 75% and 47%, respectively. In both cases, the ring protons of the chromane ring show vicinal coupling constants (^3J = 8.7 Hz) in the ^1H NMR spectra, that indicate antiperiplanar geometry.[28] For **8'**, this assignment was confirmed by scXRD, which also showed that the chromane ring adopts a half-chair conformation with the adjacent substituents being in a *cis*-configuration. Although no crystal structure was obtained for **7'**, the antiperiplanar position of the ring protons (^3J = 11 Hz) in analogy to those of **8'**, suggests that this product might also exist in an *endo*-configuration.

Overall, the observed selectivity toward *endo*-configured cycloadducts for some of these dienophiles, is in good agreement with the results obtained from reactions with enamines and supports the general preference for cis-fused chroman systems.

According to the Mayr scale (Figure 5), the reactions between *o*QM **1a** (*E*= −15.20) and silyl ketene acetals **4a-4c** (*N* = > 9) fall within or close to the predictive threshold *E* + *N* > −5 where reaction products with stepwise mechanisms can still be expected. This makes a mechanistic distinction between stepwise and concerted pathways difficult in these cases. However, the reactions involving *o*QMs **1** with dienophiles **6-8** proceeded despite much lower reactivity combinations (*E* +*N* < −5) where product formation would not be expected under the assumption of a rate-determining stepwise σ-bond-forming transition state. For example, the nucleophilic reactivity parameters *N* (and s_N) of ethyl vinyl sulfide **7** (*N*/s_N = 3.60/0.91) and α-azido styrene **8** (*N*/s_N = 4.57/0.94) were determined in the course of this study via kinetic experiments of their reactions with reference diarylcarbenium ions (see Section 7.3.1 for details). The corresponding reactivity difference between electrophile and nucleophile (*E* + *N*) falls for reactions with *o*QMs **1** and dienophiles **6-8** below *E*+*N* = −8.5. In the most favorable of these mismatches (combination **1g** with **8**), the calculated half-life time for a 0.02 M solution is approximately 230 years, whereas the product **8'** was isolated in a yield of 47 % after only seven days. This enormous difference between predicted and observed reactivity is a strong indication that the reaction proceeds most likely via a multicenter process in a concerted manner. Consequently, the same can be anticipated for the formation of cycloadducts **6'** and **7'**.

While the rule of thumb based on the *E* + *N* > −5 criterion provides a useful tool to identify successful electrophile-nucleophile combinations it could be considered to be an oversimplified approach to analyze reaction mechanisms. The Mayr-Patz equation, though highly predictive in many cases, may exhibit deviations, especially when reference systems are not involved. Therefore, definitive

_____

mechanistic insight would benefit from a combination of absolute kinetic measurements and quantum chemical calculations.
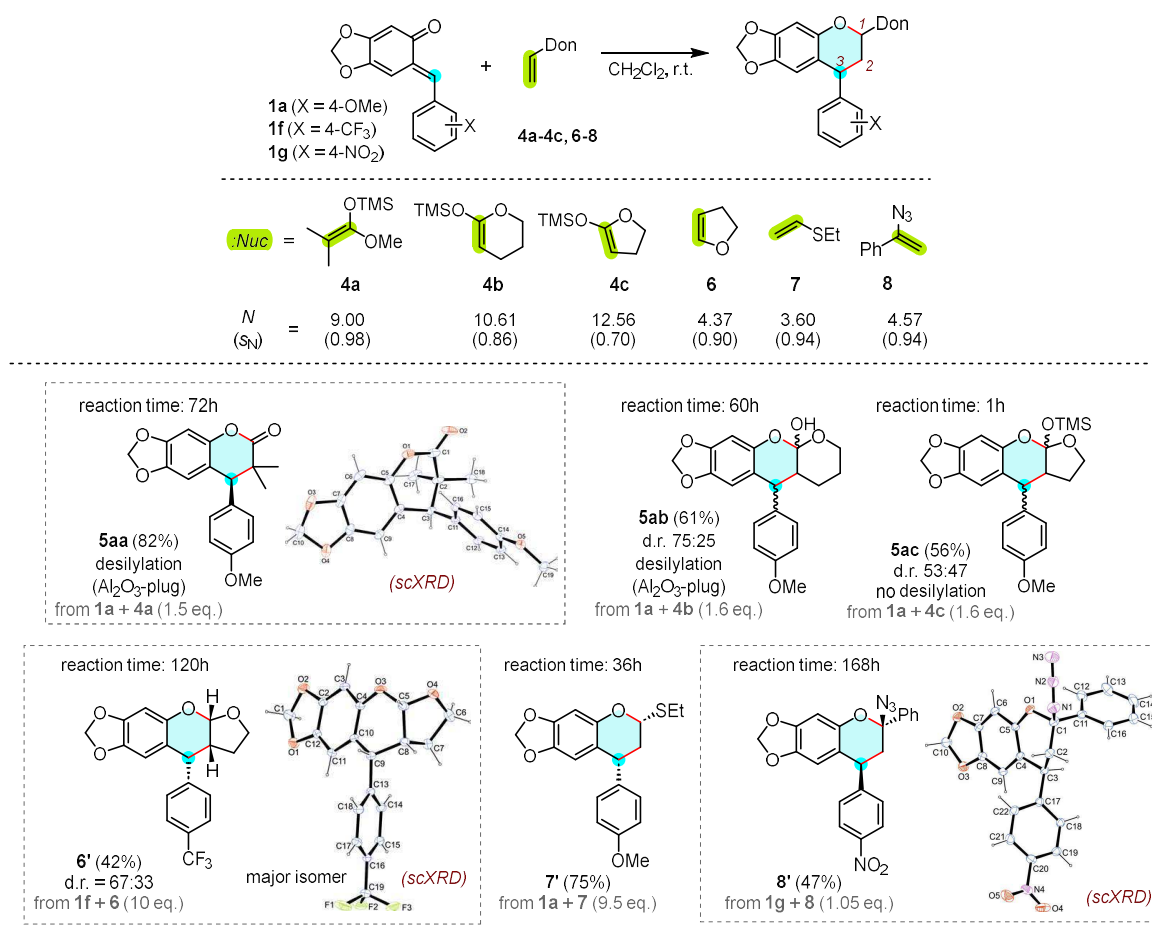

Figure 6. Observed cycloaddition products formed by the reactions of *o*QMs **1** with silyl ketene acetals **5** and further dienophiles **7-9** in CH_2Cl_2 at r.t. (Thermal ellipsoids of single crystal X-ray structures are shown on the 25% probability level (at 173 k)).

7.3. Conclusion

In summary, the linear free-energy relationship (1) was used as a tool for probing the mechanisms of the cycloadditions between *o*QMs and enamines. The difference in the activation barriers between a concerted and a stepwise mechanism involving zwitterionic intermediates can be interpreted as a measure of the energy of concert.

The investigated product studies showed that *o*QMs react with enamines as electron-rich dienophiles via [4+2] cycloadditions to form dihydrochromanes with strong preference for the *endo*-configuration and in accordance with literature reports. Kinetic measurements revealed that experimentally determined rate constants exceed those predicted for a stepwise mechanism (based on Equation (1)) by more than two orders of magnitude, thus suggesting the possible operation for a concerted mechanism.

Moreover, the magnitude of the observed rate enhancement (energy of concert) decreases with increasing reactivity of the enamines. This suggests that reactions with more nucleophilic enamines tend to proceed through increasingly asynchronous concerted transition states. This hypothesis is in

agreement with quantum chemical findings from Han and Peng, who observed that asynchronicity in *o*QM cycloadditions increases with the electron-donating nature (higher nucleophilic reactivity) of substituents on the alkene component.

In addition to these findings, solvent effects were also examined. Second-order rate constants for representative *o*QM-enamine reactions were measured in solvents of varying polarity. The results revealed only minimal differences in rate across aprotic polar and nonpolar solvents. These results are consistent with the well-documented insensitivity of many Diels-Alder reactions to solvent polarity and provide further support for a concerted cycloaddition mechanism in these systems.

Furthermore, product studies with *o*QMs were extended to other dienophiles, including enol ethers, vinyl sulfides and vinyl azides. In several of these cases, cycloaddition products were obtained even when the empirical rule $E + N > -5$ was not fulfilled, thus indicating the possible involvement of a multibond-forming transition state.

Future studies should focus on quantum chemical calculations to a broad set of *o*QM-dienophile combinations, with the goal of computing activation barriers for both concerted and stepwise pathways. If concerted mechanisms are energetically favored, further investigation could address the degree of concertedness and its dependency from the reactivity parameters (E and N). On the experimental side, additional kinetic studies could be performed, in particular with alternative dienophiles such as 1,3-dienes (could react via one of the two double bonds). Time-resolved NMR spectroscopy may offer as a valuable method for monitoring very slow cycloadditions of *o*QMs with dienophiles.

7.4. Experimental Part

7.4.1. Additional Table and Supplementary Figures

Reactivity parameters *N* (and *s*$_N$) of vinylic nucleophiles.

Nucleophilic reactivity parameters *N* (and *s*$_N$) were determined for ethyl vinyl sulfide **7** and α-azido styrene **8** from kinetic experiments of their reactions with colored benzhydrylium ions **9a-9f** in CH$_2$Cl$_2$ at 20°C (Figure 7). The ethyl vinyl sulfide **7** is a commercially available compound while α-azido styrene **8** was synthesized according to a literature procedure.[40]
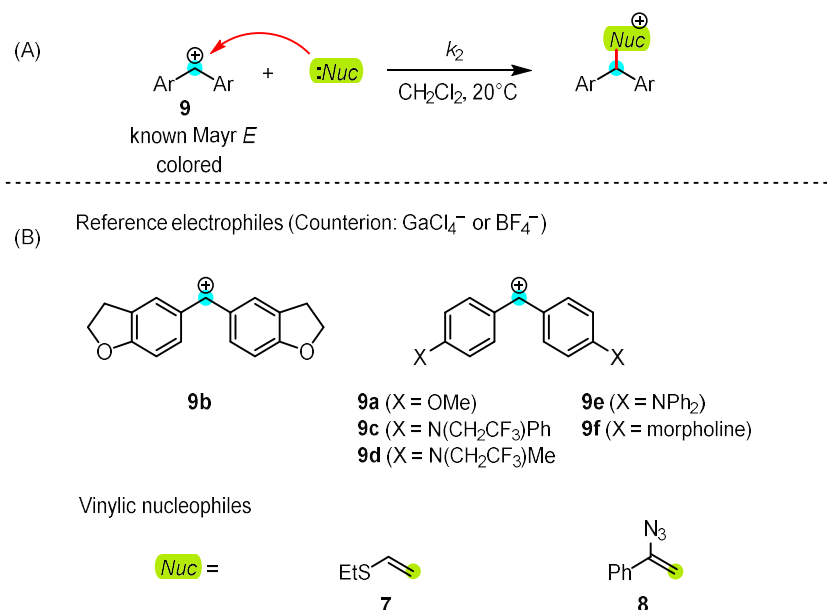
Figure 7. (A) Carbon-Carbon bond forming reaction between benzhydrylium ion **9** and vinylic nucleophile in CH$_2$Cl$_2$ at 20°C; (B) Reference electrophiles **9** used to determine reactivity parameters of vinylic nucleophiles **7** and **8**.

Benzhydrylium ion **9d** was used to characterize typical reaction products of the kinetically investigated carbon-carbon bond forming reactions of benzhydrylium ions **9** and α-azido styrene **8** (Figure 8A). The product study led after aqueous workup to formation of a secondary amide (see section 7.4.5 for more details). This reaction can be rationalized by the initial formation of an iminodiazolium ion and a subsequent Schmidt-rearrangement to a nitrilium ion and finally to the secondary amide by aqueous workup. (Figure 8B).
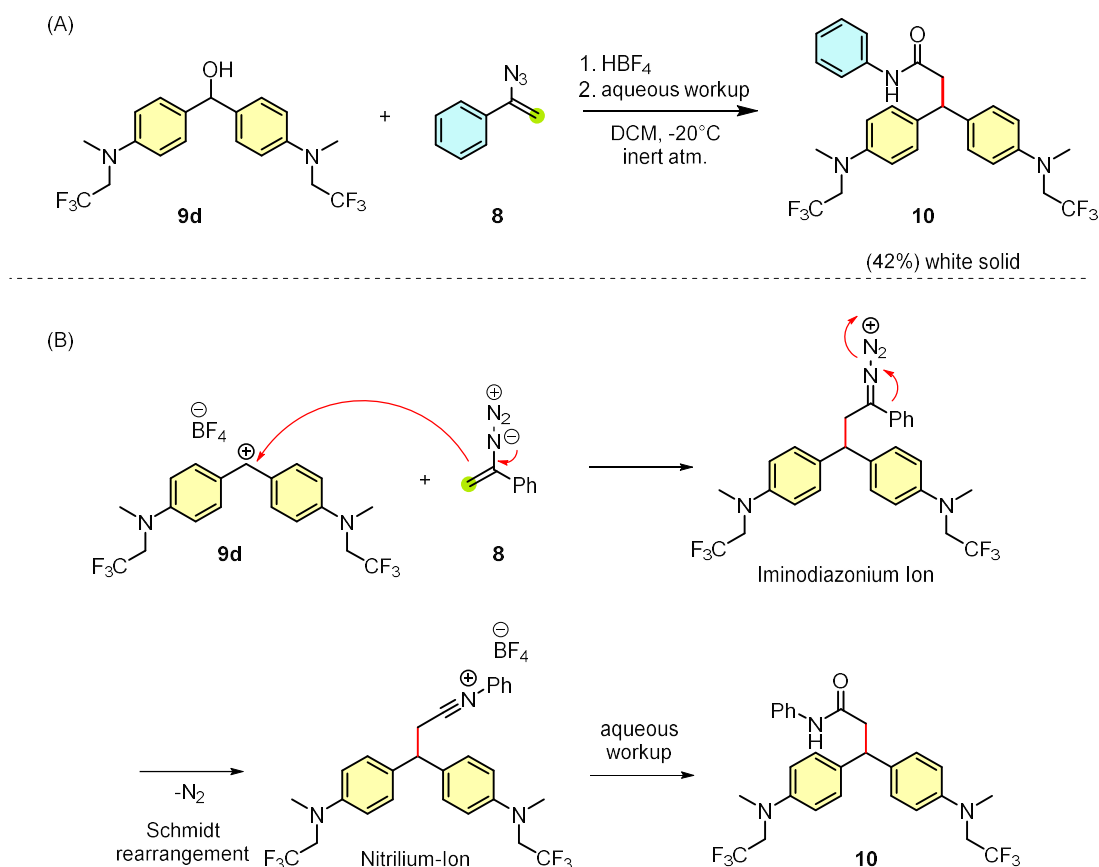
Figure 8. (A) Observed secondary amide **10** of carbon-carbon bond-forming reaction between benzhydrylium ion **9d** and α-azido styrene **8**. (B) Mechanism that leads to formation of product **10**.

Kinetic experiments of the reactions of benzhydrylium ions + vinylic nucleophiles were measured photometrically at the absorbance maxima of the colored benzhydrylium ions by using stopped-flow or conventional UV/Vis spectroscopy. The vinylic nucleophiles were used in at least three-fold excess over the benzhydrylium ions which ensures pseudo-first order reaction conditions (Figure 9A). Least squares-fitting of the mono-exponential decay functions $A = A_0 \exp(-k_{obs}t) + C$ to the time -dependent experimental absorbances allowed to determine the first-order rate constants k_{obs} (s^{-1}) (Figure 9B). This methodology was usually repeated with four to five different nucleophile concentrations and the second-order rate constants k_2^{exp} (M^{-1} s^{-1}) of the bimolecular reactions were then calculated as the slopes of linear correlations of k_{obs} vs the concentrations of the vinylic nucleophiles (Figure 9C) The second-order rate constants k_2^{exp} of all kinetically investigated reactions between benzhydrylium ions + vinylic nucleophiles are listed in Table 5. Details of the individual kinetic experiments are given in section 7.4.11.

(A)

$$9 \quad\quad 7 \text{ or } 8$$

colored   > 3-fold excess

(B)

$k_{obs} = 5.08 \times 10^{-3}\ s^{-1}$

(C)

$k_{obs} = 1.3315[8] + 0.0002$
$R^2 = 0.9997$
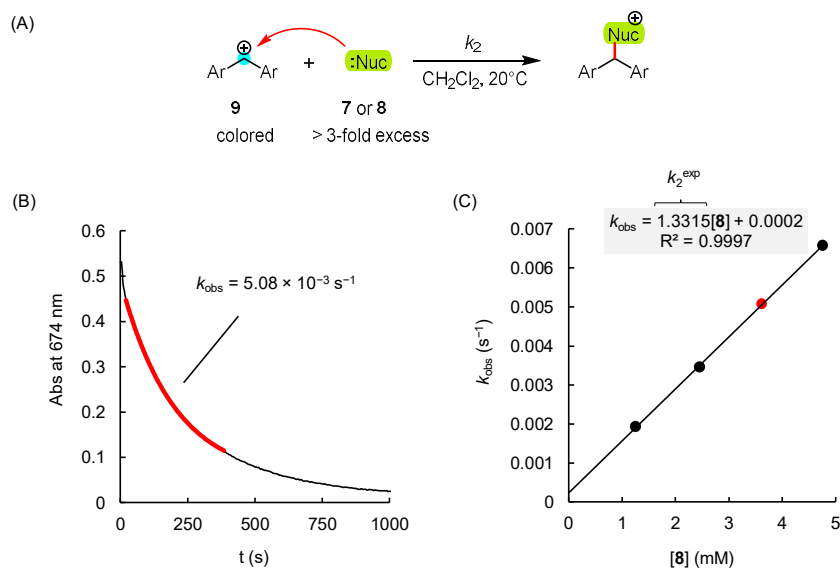
Figure 9. (A) Carbon-carbon bond-forming reaction of vinylic nucleophile with colored benzhydrylium ion in CH_2Cl_2 at 20°C. (B) Time-dependent decay of the benzhydrylium ion absorbance of benzhydrylium ion **9e** ($[9e]_0 = 5.55 \times 10^{-6}$ M) at 674 nm for the reaction with the nucleophile **8** ($[8]_0 = 3.62 \times 10^{-3}$ M) and determination of the observed first-order rate constant $k_{obs}.(s^{-1})$. (C) Linear correlation of experimentally determined k_{obs} values with the concentrations of nucleophile **8**. The slope represents the second-order rate constant k_2^{exp} ($M^{-1}\ s^{-1}$).

Table 5. Experimentally determined second-order rate constants k_2^{exp} for the reactions of vinylic nucleophiles **7** and **8** with benzhydrylium ions **9a**–**9f** (reference electrophiles) in CH_2Cl_2 at 20°C.

Electrophiles	E	k_2^{exp} ($M^{-1}\ s^{-1}$)	
		7	**8**
9a	0.00	2.20×10^3	n.d.
9b	−1.36	1.48×10^2	1.14×10^3
9c	−3.14	2.54	2.34×10^1
9d	−3.85	n.d.	2.65
9e	−4.72	n.d.	1.33
9f	−5.53	n.d.	1.05×10^{-1}
Nucleophilicity N and (s_N)		**3.60 (0.94)**	**4.57 (0.94)**

Nucleophilic reactivity parameters N (and s_N) of the vinylic nucleophiles **7** and **8** can then be calculated by the Mayr-Patz equation (1) and linear correlations of plots of lg k_2^{exp} vs Mayr electrophilicity E of the benzhydrylium ions (Figure 10A).[21] The nucleophiles-sensitivity parameter s_N is calculated as the slope of the linear correlation, while the intercept of the linear correlation with the abscissa (that is lg k_2^{exp} = 0) correspond to $N = -E$.

lg k_2(20 °C) = $s_N(N + E)$ (1)
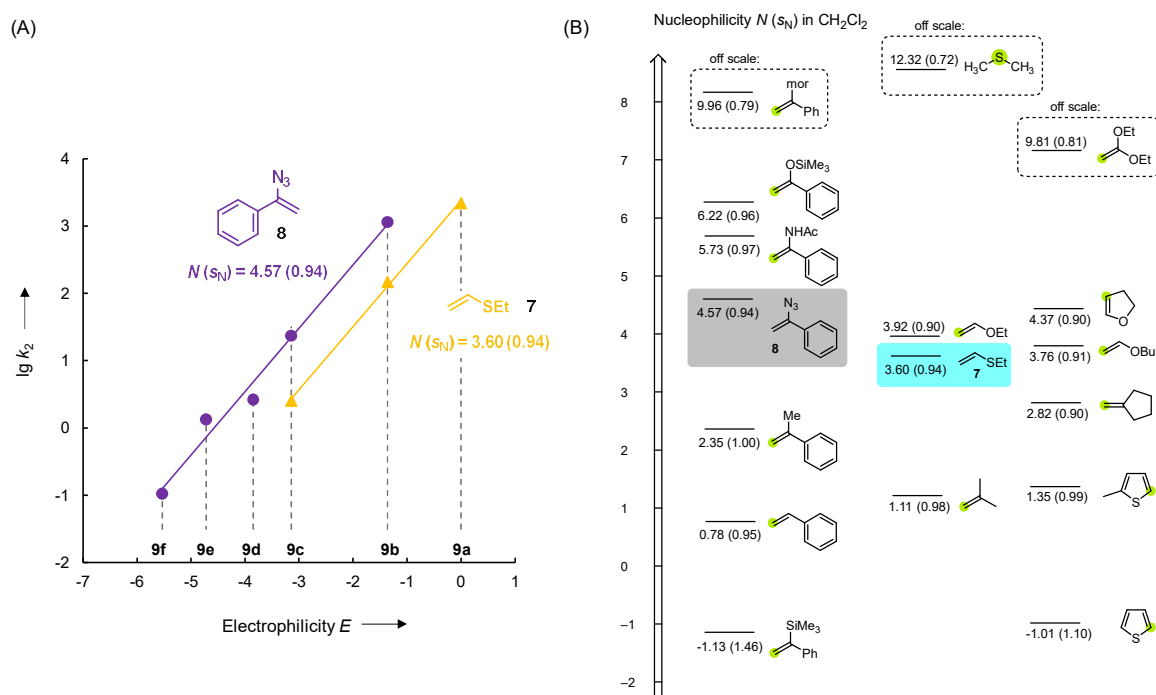
Figure 10. (A) Linear correlations of lg k_2 for the reactions of ethyl vinylsulfide **7** and α-azido styrene **8** with diarylcarbenium ions against the electrophilicity parameters E of **9a-9f** (CH$_2$Cl$_2$, 20 °C); (B) Embedding the reactivity parameters N (and s_N) of vinylic nucleophiles **7** and **8** on a reactivity scale and comparison to other novel vinylic compounds. Reactivity parameters taken from ref. [14].

Embedding the reactivity parameters N of the vinylic nucleophiles on a Mayr's reactivity scale (Figure 10B) shows that the ethyl vinyl sulfide **7** (N=3.60, s_N=0.94) is only slightly less reactive than the analogous ethyl vinyl ether (N=3.92, s_N=0.90) and the *n*-butyl vinyl ether (N=3.76, s_N=0.91) but more reactive than isobutylene (N=1.11, s_N=0.98). However, α-azido styrene **8** (N=4.57, s_N=0.94) is one order of magnitude more nucleophilic than ethyl vinyl sulfide **7** with identical s_N parameters. If α-azido styrene **8** is compared to structurally related compounds such as α-methyl styrene (N=2.35, s_N=1.00) and normal styrene (N=0.78, s_N=0.95) it is up to almost four orders of magnitude more reactive. Only species such as α-N-(acetamide) styrene, α-(trimethylsiloxy) styrene and α-N-(morpholino) styrene that carry very strong electron-donating functional groups close to the nucleophilic position exceed the reactivity of α-azido styrene. The pronounced reactivity of **8** can be explained by the azido group, which is an electron-withdrawing substituent and, depending on the molecular framework, can also act as a strong π-donor.[41] This effect as supported by DFT calculations[41] might rationalizes the high nucleophilic reactivity of **8**. Currently, further comprehensive reactivity studies involving additional vinyl azides are underway.

7.4.2. General

Commercial reagents and dry solvents (stored over molecular sieves) were used without further purification as purchased from Sigma-Aldrich or Acros Organics. Dichloromethane (DCM was dried over CaH_2, diethyl ether was dried over sodium and distilled. For thin-layer chromatography, silica gel plates with F-254 fluorescence indicator (Merck) were used. Purification by flash column chromatography was performed using Merck silica gel 60 (0.040–0.063 mm) with freshly distilled solvents.

Melting points were acquired using Büchi Melting Point B-560 devices and are not corrected.

Nuclear magnetic resonance (NMR) spectra were recorded on 400, 600, and 800 MHz spectrometers. NMR signals were assigned based on information from additional 2D NMR experiments (COSY, gHSQC, gHMBC). Residual solvent signals were used as internal reference (δ_H 7.26 ppm, δ_C 77.16 ppm for $CDCl_3$, δ_H 5.32 ppm, δ_C 53.84 ppm for CD_2Cl_2).

Infrared (IR) spectra were recorded on a Perkin Elmer Spectrum BX-59343 instrument with a Smiths Detection DuraSamplIR II Diamond ATR sensor or a Bruker Tensor 27 FT-IR instrument with a "Platinum" Diamond ATR sensor for detection in the range 4500–600 cm^{-1} as a film for liquids or neat for solids.

High resolution (HRMS) mass spectra were recorded on a Finnigan MAT 90, a Finnigan MAT 95, a JEOL MStation JMS 700, a Thermo Finnigan LTQ FT Ultra Fourier Transform ion cyclotron resonance, a Q Exactive GC Orbitrap GC/MS or a Thermo Fisher Scientific LTQ Orbitrap XL. For ionization of the samples, either electron-impact ionization (EI) or electrospray ionization (ESI) was applied.

UV/Vis photometric measurements were carried out using a J&M TIDAS diode array spectrophotometer, which was controlled by TIDASDAQ3 (v3) software and connected to a Hellma 661.502-QX quartz Suprasil immersion probe (light path d = 5 mm) via fiber optic cables and standard SMA connectors.

The oxidation potentials of enamines (E_p^{ox}) were determined in acetonitrile on a CH Instruments 630E electrochemical analyzer using a 2 mm diameter platinum working electrode, a platinum wire counter electrode and an Ag wire pseudo-reference electrode applying a scan rate of 0.1 V/s. Cyclic voltammetry measurements were performed in deaerated acetonitrile solutions containing 0.1 M tetra-*n*-butylammonium perchlorate, the enamines **3** ($c \approx 1 \times 10^{-3}$ M), and decamethyl ferrocene (c = 7.5×10^{-4} M) as an internal standard. The $E_{1/2}$(fc$^+$/fc in MeCN) = −0.125 V[42] was used to calibrate E_p^{ox} (**3** in MeCN) vs SCE.

Vinylazide **8** and *ortho*-quinone methides **1a-1g** were prepared according to literature procedures[20, 40], while enamines **2a-2h**, and enol ethers **4b-4c** were available through former group members.

7.4.3. Products of *ortho*-Quinone Methides with Enamines

General Procedure (*GP1*):

1.0-1.3 equivalents of enamine **2** were mixed with the *o*QM **1** in 5.0 mL of dry CH₂Cl₂ under argon at room temperature (23 °C) and stirred until decolorization (reaction times: 30 min – 36 h). The solvent was removed under vacuo and the remaining residue was either pure enough for NMR analysis or was further purified by flash column chromatography. Suitable crystals of the reaction products for single crystal X-Ray Diffraction (*scXRD*) were obtained from the vapor-diffusion method of *n*-pentane/CH₂Cl₂ mixtures.

1-(9-(4-methoxyphenyl)-7,8,8a,9-tetrahydrocyclopenta[b][1,3]dioxolo[4,5-g]chromen-5a(6H)-yl)pyrrolidine (3aa) was prepared according to *GP1* (reaction time: 30 min) from **1a** (23.8 mg, 0.093 mmol), and **2a** (13.4 mg, 0.098 mmol). The reaction mixture (dissolved in 0.8 mL CD₂Cl₂) was analyzed by NMR spectroscopy and HRMS. **3aa** was obtained as a mixture of diastereomers (d.r. = 65:35).

3aa (CG421)
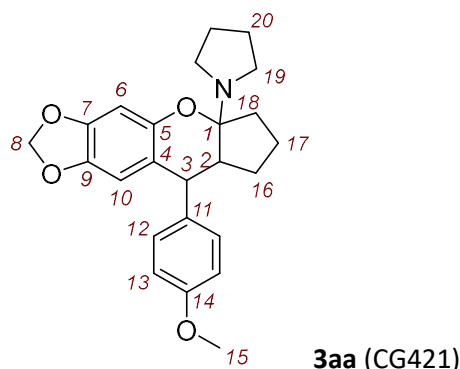
¹H NMR (400 MHz, CD₂Cl₂): δ 7.14 (d, *J* = 8.8 Hz, 2 H, 12-H^major), 7.11 (d, *J* = 8.8 Hz, 2 H, 12-H^minor), 6.89 (d, *J* = 8.8 Hz, 2 H, 13-H^major), 6.85 (d, *J* = 8.8 Hz, 2 H, 13-H^minor), 6.43 (s, 1 H, 6-H^major), 6.38 (s, 1 H, 6-H^minor), 6.31 (d, *J* = 1.1 Hz, 1 H, 10-H^minor), 6.05 (d, *J* = 1.1 Hz, 1 H, 10-H^major), 5.88 – 5.74 (m, 4 H, 8-H), 4.17 (d, *J* = 6.0 Hz, 1 H, 3-H^minor), 3.81 (s, 3 H, 15-H^major), 3.79 (s, 3 H, 15-H^minor), 3.56 (d, *J* = 9.6 Hz, 1 H, 3-H^major), 2.94 – 2.63 (m, 8 H, 19-H), 2.58 – 2.48 (m, 1 H, 2-H^major), 2.37 – 2.28 (m, 1 H, 2-H^minor), 2.21 – 1.21 ppm (m, 20 H, 16-H, 17-H, 18-H, 20-H).

¹³C{¹H} NMR (101 MHz, CD₂Cl₂): δ 158.9 (C_q, C-14^major), 158.8 (C_q, C-14^minor), 151.3 (C_q, C-5^major), 148.4 (C_q, C-5^minor), 147.0 (C_q, C-7^minor), 146.8 (C_q, C-7^major), 141.6 (C_q, C-9^minor), 141.6 (C_q, C-9^major), 135.3 (C_q, C-11^minor), 134.8 (C_q, C-11^major), 130.8 (CH, C-12^major), 130.8 (CH, C-12^minor), 121.9, 116.7, 114.2 (CH, C-13^major), 113.9 (CH, C-13^minor), 108.6 (CH, C-10^minor), 107.9 (CH, C-10^major), 103.1 (C_q, C-1^major), 101.3 (CH₂, C-8^minor), 101.2 (CH2, C-8^major), 100.1 (C_q, C-1^minor), 99.2 (CH, C-6^minor), 99.0 (CH, C-6^major), 55.6 (CH₃, C-15^major), 55.6 (CH₃, C-15^minor), 48.5 (CH, C-2^major), 46.8 (CH2, C-19^minor), 46.6 (CH, C-2^minor), 46.3 (CH, C-19^major), 46.2 (CH, C-3^major), 41.3 (CH, C-3^minor), 35.9, 30.5, 28.9, 26.2, 25.0, 24.4, 21.5, 19.9 ppm.

HRMS (pos. ESI): *m/z* calcd for C₂₄H₂₈NO₄⁺ [M + H⁺]: 394.2013; found: 394.2018.

1-(10-(4-methoxyphenyl)-6,7,8,9,9a,10-hexahydro-5aH-[1,3]dioxolo[4,5-b]xanthen-5a-yl)pyrrolidine (3ab) was prepared according to *GP1* (reaction time: 30 min) from **1a** (15.0 mg, 0.059 mmol), and **2b** (9.3 mg, 0.061 mmol). The reaction mixture (dissolved in 0.8 mL CD₂Cl₂) was

analyzed by NMR spectroscopy, HRMS and IR. **3ab** was obtained as one single diastereomer; Recrystallization from *n*-pentane/CH₂Cl₂ mixture afforded colorless crystals; m.p. 163 °C.

3ab (CG422)   av376
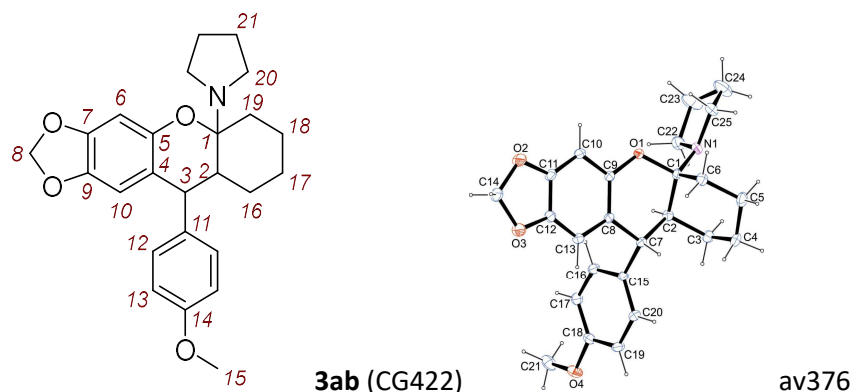
¹H NMR (400 MHz, CD₂Cl₂): δ 7.08 (d, *J* = 8.8 Hz, 2 H, 12-H), 6.85 (d, *J* = 8.8 Hz, 2 H, 13-H), 6.30 (s, 1 H, 6-H), 6.03 (d, *J* = 1.0 Hz, 1 H, 10-H), 5.78 (d, *J* = 1.4 Hz, 1 H, 8-H), 5.76 (d, *J* = 1.4 Hz, 1 H, 8-H), 4.01 (d, *J* = 10.9 Hz, 1 H, 3-H), 3.79 (s, 3 H, 15-H), 3.00 – 2.82 (m, 4 H, 20-H), 2.29 – 2.21 (m, 1 H, 2-H), 1.80 – 1.59 (m, 10 H, 16-H, 17-H, 18-H, 19-H, 21-H), 1.47 – 1.37 (m, 1 H, H-17), 1.34 – 1.24 ppm (m, 1 H, H-16).

¹³C{¹H} NMR (101 MHz, CD₂Cl₂): δ 158.8 (C$_q$, C-14), 150.2 (C$_q$, C-5), 147.0 (C$_q$, C-7), 141.0 (C$_q$, C-9), 137.2 (C$_q$, C-11), 130.6 (CH, C-12), 117.1 (C$_q$, C-4), 114.2 (CH, C-13), 108.9 (CH, C-10), 101.2 (CH₂, C-8), 98.1 (CH, C-6), 93.2 (C$_q$, C-1), 55.6 (CH₃, C-15), 44.1 (CH₂, C-20), 42.9 (CH, C-3), 42.6 (CH, C-2), 30.0, 25.1, 24.9 (CH₂, C-16), 23.6, 19.9 ppm (CH₂, C-17).

HRMS (pos. ESI): *m/z* calcd for C₂₅H₃₀NO₄⁺ [M + H⁺]: 408.2170; found: 408.2176.

IR (neat, ATR): ṽ 2932, 1509, 1476, 1428, 1244, 1143, 1035, 996, 888, 861, 831, 796 cm⁻¹.

**1-(8-(4-methoxyphenyl)-7-phenyl-7,8-dihydro-6H-[1,3]dioxolo[4,5-g]chromen-6-yl)pyrrolidine (3ad)** was prepared according to *GP1* (reaction time: 1 h) from **1a** (23.0 mg, 0.090 mmol), and **2d** (16.3 mg, 0.094 mmol). The reaction mixture (dissolved in 0.8 mL CD₂Cl₂) was analyzed by NMR spectroscopy, HRMS and IR. **3ad** was obtained as one single diastereomer; Recrystallization from *n*-pentane/CH₂Cl₂ mixture afforded colorless crystals; m.p. 132 °C.

3ad (CG430)   av409
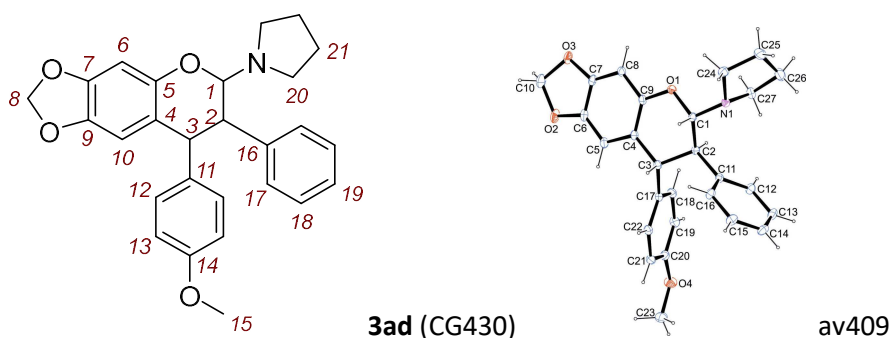
¹H NMR (800 MHz, CD₂Cl₂): δ 7.19 (t, *J* = 7.3 Hz, 2 H, 18-H), 7.16 – 7.11 (m, 1 H, 19-H), 7.00 – 6.93 (m, 2 H, 17-H), 6.78 (d, *J* = 8.8 Hz, 2 H, 12-H), 6.68 (d, *J* = 8.8 Hz, 2 H, 13-H), 6.44 (s, 1 H, 6-H), 6.08 (s, 1 H, 10-H), 5.88 – 5.79 (m, 2 H, 8-H), 5.21 (d, *J* = 9.9 Hz, 1 H, 1-H), 4.14 (d, *J* = 10.2 Hz, 1 H, 3-H), 3.71 (s, 3 H, 15-H), 3.14 (dd, *J* = 11.2, 9.8 Hz, 1 H, 2-H), 2.99 – 2.89 (m, 4 H, 20-H), 1.73 – 1.63 ppm (m, 4 H, 21-H).

¹³C{¹H} NMR (201 MHz, CD₂Cl₂): δ 158.6 (C$_q$, C-14), 150.7 (C$_q$, C-5), 147.1 (C$_q$, C-7), 141.7 (C$_q$, C-16), 141.6 (C$_q$, C-9), 135.8 (C$_q$, C-11), 130.2 (CH, C-12), 128.7 (CH, C-17), 128.4 (CH, C-18), 126.5 (CH, C-19),

118.9 (C_q, C-4), 113.8 (CH, C-13), 108.7 (CH, C-10), 101.4 (CH_2, C-8), 98.4 (CH, C-6), 92.9 (CH, C-1), 55.4 (CH_3, C-15), 52.8 (CH, C-2), 51.7 (CH, C-3), 46.6 (CH_2, C-20), 25.1 ppm (CH_2, C-21).

HRMS (pos. ESI): *m/z* calcd for $C_{27}H_{28}NO_4^+$ [M + H$^+$]: 430.2013; found: 430.2027.

IR (neat, ATR): $\tilde{v}$ 2964, 1611, 1510, 1476, 1239, 1174, 1143, 1034, 938, 918, 751, 699 cm^{-1}.

4-(10-(4-methoxyphenyl)-6,7,8,9,9a,10-hexahydro-5aH-[1,3]dioxolo[4,5-b]xanthen-5a-yl)morpholine (3ae) was prepared according to *GP1* (reaction time: 3 h) from **1a** (17.0 mg, 0.066 mmol), and **2e** (11.6 mg, 0.070 mmol). The reaction mixture was further purified by column chromatography (silica gel, eluent: *n*-pentane:EtOAc:NEt₃ = 80:19:1) to give **3ae** as two separate diastereomers (d.r. = 93:7, major isomer (18.2 mg, 65%), minor isomer (1.2 mg, 4%)). Recrystallization of the major diastereomer from *n*-pentane/CH₂Cl₂ mixture afforded colorless crystals; m.p. 200 °C.

3ae (CG712)   cv196
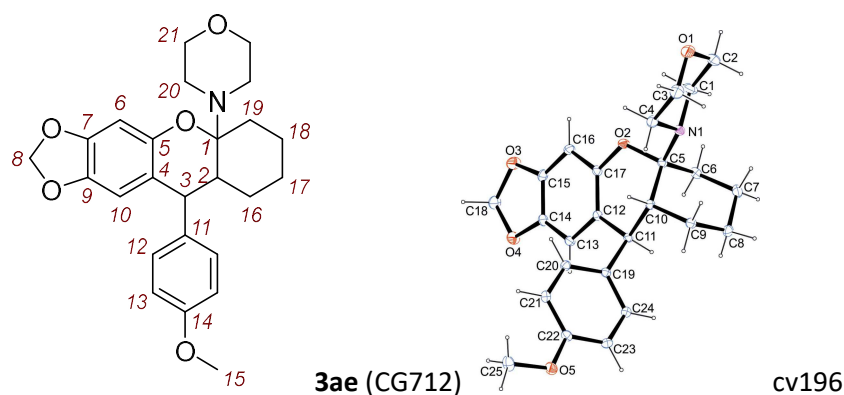
Major Isomer: **3ae** (CG712F1)

R_f (*n*-pentane/EtOAc/NEt₃ = 80:19:1, silica, UV) = 0.70.

¹H NMR (400 MHz, CD₂Cl₂): δ 7.08 (d, *J* = 8.7 Hz, 2 H, 12-H), 6.83 (d, *J* = 8.8 Hz, 2 H, 13-H), 6.34 (s, 1 H, 6-H), 6.14 (s, 1 H, 10-H), 5.82 (d, *J* = 1.3 Hz, 1 H, 8-H^a), 5.80 (d, *J* = 1.4 Hz, 1 H, 8-H^b), 3.95 (d, *J* = 8.4 Hz, 1 H, 3-H), 3.78 (s, 3 H, 15-H), 3.49 (s, 4 H, 21-H), 2.86 – 2.47 (m, 4 H, 20-H), 2.35 (dt, *J* = 9.0, 5.0 Hz, 1 H, 2-H), 1.88 – 1.57 (m, 6 H), 1.46 – 1.26 ppm (m, 2 H).

¹³C{¹H} NMR (101 MHz, CD₂Cl₂): δ 158.6 (C_q, C-14), 148.7 (C_q, C-5), 147.1 (C_q, C-7), 141.4 (C_q, C-9), 137.5 (C_q, C-11), 130.5 (CH, C-12), 116.2 (C_q, C-4), 114.0 (CH, C-13), 109.2 (CH, C-10), 101.3 (CH_2, C-8), 98.3 (CH, C-6), 92.1 (C_q, C-1), 67.5 (CH_2, C-21), 55.6 (CH_3, C-15), 44.9 (CH_2, C-20), 43.9 (CH, C-3), 40.0 (CH, C-2), 27.5 (CH_2), 27.4 (CH_2), 22.9 (CH_2), 21.4 ppm (CH_2).

HRMS (pos. ESI): *m/z* calcd for $C_{25}H_{30}NO_5^+$ [M + H$^+$]: 424.2118; found: 424.2104.

IR (neat, ATR): $\tilde{v}$ 2932, 1610, 1509, 1477, 1242, 1145, 1116, 1033, 938, 832, 797, 711 cm^{-1}.

Minor Isomer: **3ae** (CG712F2)

R_f (*n*-pentane/EtOAc/NEt₃ = 80:19:1, silica, UV) = 0.65.

¹H NMR (400 MHz, CD₂Cl₂): δ 7.04 (d, *J* = 8.6 Hz, 2 H, 12-H), 6.85 (d, *J* = 8.9 Hz, 2 H, 13-H), 6.36 (m, 2 H, 6-H, 10-H), 5.84 (dd, *J* = 11.3, 1.4 Hz, 2 H, 8-H), 4.42 (d, *J* = 5.3 Hz, 1 H, 3-H), 3.79 (s, 3 H, 15-H), 3.67 – 3.57 (m, 2 H), 3.56 – 3.49 (m, 2 H), 2.72 – 2.66 (m, 4 H), 2.02 – 1.68 (m, 2 H), 1.65 – 1.49 (m, 3 H), 1.46 – 1.34 (m, 1 H), 1.22 – 1.08 (m, 2 H), 1.06 – 0.92 ppm (m, 1 H).

13C{1H} NMR (101 MHz, CD2Cl2): δ 158.8 (Cq, C-14), 147.4 (Cq, C-5), 146.7 (Cq, C-7), 141.5 (Cq, C-9), 134.1 (Cq, C-11), 131.6 (CH, C-12), 117.0 (Cq, C-4), 113.8 (CH, C-13), 108.6 (CH, C-10), 101.3 (CH2, C-8), 98.8 (CH, C-6), 90.2 (CH, C-1), 68.0 (CH2), 55.6 (CH3, C-15), 45.5 (CH2), 42.2 (CH, C-3), 39.6 (CH, C-2), 27.4 (CH2), 25.5 (CH2), 24.4 (CH2), 22.6 ppm (CH2).

4-(8-(4-methoxyphenyl)-7,7-dimethyl-7,8-dihydro-6H-[1,3]dioxolo[4,5-g]chromen-6-yl)morpholine (3af) was prepared according to *GP1* (reaction time: 15 h) from **1a** (20.0 mg, 0.078 mmol), and **2f** (11.6 mg, 0.082 mmol). The reaction mixture was further purified by column chromatography (silica gel, eluent: *n*-pentane:EtOAc:NEt3 = 80:19:1) to give **3af** (25.1 mg, 81%) as a white solid; mixture of diastereomers (d.r. = 67:33). Recrystallization from *n*-pentane/CH2Cl2 mixture afforded colorless crystals of the endo isomer.
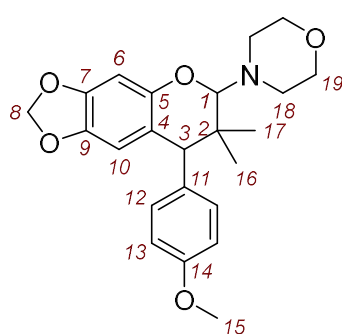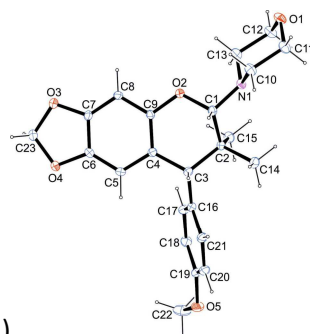
3af (CG289_2)   av381

1H NMR (400 MHz, CD2Cl2): δ 7.07 – 6.90 (m, 4 H, 12-H), 6.85 (d, *J* = 8.9 Hz, 2 H, 13-H^minor), 6.79 (d, *J* = 8.9 Hz, 2 H, 13-H^major), 6.43 (s, 1 H, 6-H^major), 6.40 (s, 1 H, 6-H^minor), 6.23 (d, *J* = 1.1 Hz, 1 H, 10-H^major), 6.12 (d, *J* = 1.1 Hz, 1 H, 10-H^minor), 5.85 – 5.79 (m, 4 H, 8-H), 4.34 (s, 1 H, 1-H^minor), 4.33 (s, 1 H, 1-H^major), 3.90 (s, 1 H, 3-H^minor), 3.80 (s, 3 H, 15-H^minor), 3.76 (s, 3 H, 15-H^major), 3.71 – 3.65 (m, 4 H, 19-H^minor), 3.64 – 3.58 (m, 4 H, 19-H^major), 3.55 (s, 1 H, 3-H^major), 3.12 – 3.04 (m, 2 H, 18-H^minor), 3.03 – 2.93 (m, 2 H, 18-H^major), 2.80 – 2.72 (m, 2 H, 18-H^minor), 2.70 – 2.60 (m, 2 H, 18-H^major), 1.10 (s, 3 H, 17-H^major), 0.93 (s, 3 H, 17-H^minor), 0.84 (s, 3 H, 16-H^minor), 0.80 ppm (s, 3 H, 16-H^major).

13C{1H} NMR (101 MHz, CD2Cl2): δ 159.0 (CH, C-14^minor), 158.7 (CH, C-14^major), 150.8 (Cq, C-5^minor), 149.8 (Cq, C-5^major), 147.4 (Cq, C-7^major), 147.0 (Cq, C-7^minor), 141.8 (Cq, C-9^major), 141.6 (Cq, C-9^minor), 135.4 (Cq, C-11), 132.2 (CH, C-12^minor), 131.8 (CH, C-13^major), 117.2 (Cq, C-4^minor), 116.2 (Cq, C-4^major), 113.3 (CH, C-13), 109.3 (CH, C-10^major), 109.1 (CH, C-10^minor), 101.4 (CH2, C-8), 100.3 (CH, C-1^minor), 98.0 (CH, C-6^minor), 97.7 (CH, C-6^major), 95.4 (CH, C-1^major), 67.7 (CH2, C-19^minor), 67.7 (CH2, C-19^major), 56.5 (CH, C-3^minor), 55.6 (CH3, C-15^minor), 55.6 (CH3, C-15^major, CH, C-3^major), 51.1 (CH2, C-18^minor), 50.9 (CH2, C-18^major), 37.5 (Cq, C-2^minor), 37.1 (Cq, C-2^major), 24.8 (CH3, C-17^major), 24.2 (CH3, C-17^minor), 24.2 (CH3, C-16^major), 16.3 ppm (CH3, C-16^minor).

HRMS (pos. ESI): *m/z* calcd for C23H28NO5+ [M + H+]: 398.1962; found: 398.1965.

1-(8-(4-methoxyphenyl)-7-phenyl-7,8-dihydro-6H-[1,3]dioxolo[4,5-g]chromen-6-yl)-2,2,3,5,5-pentamethylimidazolidin-4-one (3ag) was prepared according to *GP1* (reaction time: 3 h) from **1a** (15.0 mg, 0.059 mmol), and **2g** (15.9 mg, 0.061 mmol). The reaction mixture (dissolved in 0.8 mL CD2Cl2) was analyzed by NMR spectroscopy and HRMS. **3ag** was obtained as a mixture of diastereomers (d.r. = 77:23).
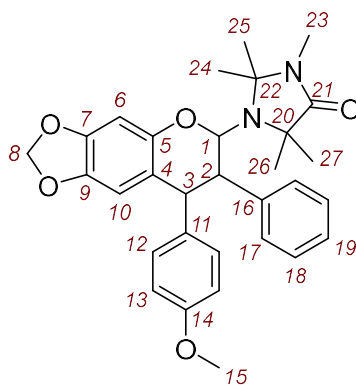
3ag (CG428)

¹H NMR (400 MHz, CD₂Cl₂): δ 7.19 – 7.06 (m, 6 H, 18-H, 19-H), 6.90 – 6.83 (m, 2 H, 17-H^{minor}), 6.76 (d, J = 9.0 Hz, 2 H, 12-H^{minor}), 6.73 – 6.67 (m, 4 H, 13-H^{minor}, 17-H^{major}), 6.63 (d, J = 8.8 Hz, 2 H, 13-H^{major}), 6.48 (d, J = 8.8 Hz, 2 H, 12-H^{major}), 6.41 (s, 1 H, 6-H^{major}), 6.39 (s, 1 H, 10-H^{major}), 6.38 (s, 1 H, 6-H^{minor}), 6.07 (d, J = 1.0 Hz, 1 H, 10-H^{minor}), 5.87 (d, J = 1.3 Hz, 1 H, 8-H^{major}), 5.84 (d, J = 1.3 Hz, 1 H, 8-H^{major}), 5.82 (d, J = 1.3 Hz, 1 H, 8-H^{minor}), 5.81 (d, J = 1.3 Hz, 1 H, 8-H^{minor}), 5.71 (d, J = 11.4 Hz, 1 H, 1-H^{major}), 5.57 (d, J = 10.5 Hz, 1 H, 1-H^{minor}), 4.08 – 4.01 (m, 2 H, 3-H), 3.82 (dd, J = 11.4, 4.8 Hz, 1 H, 2-H^{major}), 3.74 (s, 3 H, 15-H^{minor}), 3.73 (s, 3 H, 15-H^{major}), 3.43 (dd, J = 12.5, 5.4 Hz, 1 H, 2-H^{minor}), 2.72 (s, 3 H, 23-H^{minor}), 2.71 (s, 3 H, 23-H^{major}), 1.41 (s, 6 H, 22-CH₃), 1.33 (s, 6 H, 20-CH₃), 1.30 (s, 6 H, 22-CH₃), 1.09 ppm (s, 6 H, 20-CH₃).

¹³C{¹H} NMR (101 MHz, CD₂Cl₂): δ 174.2 (C=O, C-21), 158.8 (C$_q$, C-14^{major}), 158.7 (C$_q$, C-14^{minor}), 150.0 (C$_q$, C-5^{minor}), 149.5 (C$_q$, C-5^{major}), 147.7 (C$_q$, C-7^{major}), 147.1 (C$_q$, C-7^{minor}), 141.8 (C$_q$, C-9^{minor}), 141.6 (C$_q$, C-9^{major}), 140.1 (C$_q$, C-16), 135.6 (C$_q$, C-11^{minor}), 132.8 (C$_q$, C-11^{major}), 131.3 (CH, C-12^{major}), 130.4 (CH, C-12^{minor}), 129.8 (CH, C-17^{major}), 129.5 (CH, C-17^{minor}), 127.8 (CH, C-18^{minor}), 127.7 (CH, C-18^{major}), 126.6 (CH, C-19^{major}), 126.5 (CH, C-19^{minor}), 118.8 (C$_q$, C-4^{minor}), 117.5 (C$_q$, C-4^{major}), 113.9 (CH, C-13^{minor}), 113.2 (CH, C-13^{major}), 108.5 (CH, C-10^{minor}), 108.0 (CH, C-10^{major}), 101.4 (CH₂, C-8), 98.6 (CH, C-6^{minor}), 98.6 (CH, C-6^{major}), 89.2 (CH, C-1^{minor}), 84.9 (CH, C-1^{major}), 78.3 (C$_q$, C-22), 61.5 (C$_q$, C-20), 55.5 (CH₃, C-15^{minor}), 55.5 (CH₃, C-15^{major}), 53.7 (CH, C-3^{minor}), 52.1 (CH, C-2^{minor}), 50.8 (CH, C-3^{major}), 47.4 (CH, C-2^{major}), 28.9 (CH₃), 27.7 (CH₃), 27.4 (CH₃), 26.9 (CH₃), 25.1 ppm (CH₃, C-23).

HRMS (pos. ESI): *m/z* calcd for C₃₁H₃₅N₂O₅⁺ [M + H⁺]: 515.2541; found: 515.2556.

4-(8-(4-chlorophenyl)-6,7-diphenyl-7,8-dihydro-6H-[1,3]dioxolo[4,5-g]chromen-6-yl)morpholine (3dh) was prepared according to *GP1* (reaction time: 36 h) from **1d** (17.0 mg, 0.065 mmol), and **2h** (18.2 mg, 0.068 mmol). The reaction mixture was further purified by column chromatography (silica gel, eluent: *n*-pentane:EtOAc = 9:1) to give **3dh** (18.2 mg, 54%) as a white solid; m.p. >150 °C (dec.).
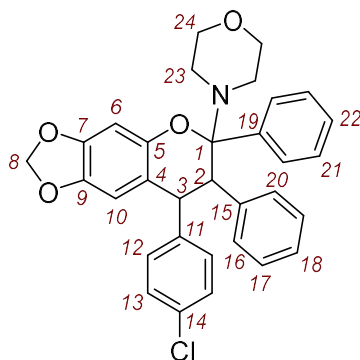
3dh (CG713F1)

R_f (*n*-pentane/EtOAc 9:1, silica, UV) = 0.60.

¹H NMR (400 MHz, CD₂Cl₂): δ 7.30 – 7.23 (m, 1 H), 7.22 – 7.14 (m, 2 H), 7.10 (d, *J* = 8.7 Hz, 2 H), 7.08 – 6.92 (m, 7 H,), 6.79 – 6.69 (m, 2 H, 16-H), 6.63 (s, 1 H, 6-H), 5.94 (d, *J* = 1.0 Hz, 1 H, 10-H), 5.89 – 5.86 (m, 2 H, 8-H), 4.13 (d, *J* = 10.2 Hz, 1 H, 2-H), 3.95 (d, *J* = 10.6 Hz, 1 H, 3-H), 3.56 – 3.46 (m, 4 H, 24-H), 3.12 – 2.97 (m, 2 H, 23-H), 2.64 – 2.55 ppm (m, 2 H, 23-H).

¹³C{¹H} NMR (101 MHz, CD₂Cl₂): δ 149.9 (C$_q$, C-5), 147.9 (C$_q$, C-7), 142.0 (C$_q$, C-11), 141.8 (C$_q$, C-9), 138.1 (C$_q$, C-15), 137.8 (C$_q$, C-19), 132.2 (C$_q$, C-14), 131.4 (CH, C-13), 131.1 (CH, C-16), 129.4 (CH, C-22), 128.6 (CH, C-12), 128.2 (CH, C-17), 127.4 (CH, C-20), 127.3 (CH, C-21), 126.9 (CH, C-18), 117.4 (C$_q$, C-4), 108.6 (CH, C-10), 101.6 (CH₂, C-8), 98.3 (C$_q$, C-1), 97.7 (CH, C-6), 67.2 (CH₂, C-24), 48.8 (CH, C-2), 47.6 (CH₂, C-23), 45.3 ppm (CH, C-3).

HRMS (pos. ESI): *m/z* calcd for $C_{32}H_{29}ClNO_4^+$ [M + H⁺]: 526.1780; found: 526.1784.

IR (neat, ATR): $\tilde{v}$ 2858, 1477, 1426, 1144, 1113, 1032 938, 922, 896, 779, 725, 700 cm⁻¹.

7.4.4. Products of *ortho*-Quinone Methides with further Dienophiles

General Procedure (*GP2*):

1.0-1.3 equivalents of enol ether **4** were mixed with the *o*QM **1** in 5.0 ml of dry CH₂Cl₂ under argon and stirred for up to 72 hours. The reaction mixture was filtered through a plug of Al₂O₃ and the solvent was removed under reduced pressure. The remaining residue was purified by flash column chromatography. Suitable crystals of the reaction products for single crystal X-Ray Diffraction (*scXRD*) were obtained from the vapor-diffusion method of *n*-pentane/CH₂Cl₂ mixtures (at +4°C).

8-(4-methoxyphenyl)-7,7-dimethyl-7,8-dihydro-6H-[1,3]dioxolo[4,5-g]chromen-6-one **(5aa)** was prepared according to *GP2* (reaction time: 72 h) from **1a** (30.0 mg, 0.12 mmol), and **4a** (30.6 mg, 0.18 mmol). The reaction mixture was further purified by column chromatography (silica gel, eluent: *n*-pentane:EtOAc = 8:2) to give **5aa** (32.0 mg, 82%) as a colorless solid; m.p. 124 °C.
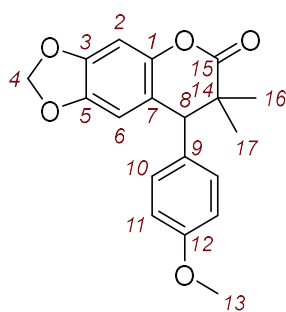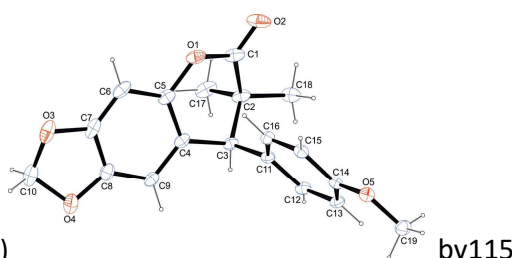
5aa (CG477)   bv115

¹H NMR (400 MHz, CDCl₃): δ 6.97 (d, *J* = 8.7 Hz, 2 H, 10-H), 6.80 (d, *J* = 8.8 Hz, 2 H, 11-H), 6.64 (s, 1 H, 2-H), 6.50 (s, 1 H, 6-H), 5.96 – 5.88 (m, 2 H, 4-H), 3.75 (s, 3 H, 13-H), 3.62 (s, 1 H, 8-H), 1.32 (s, 3 H), 1.08 ppm (s, 3 H).

¹³C{¹H} NMR (101 MHz, CDCl₃): δ 173.3 (C=O, C-15), 159.0 (C$_q$, C-12), 147.4 (C$_q$, C-3), 145.1 (C$_q$, C-1), 144.5 (C$_q$, C-5), 132.0 (C$_q$, C-9), 129.2 (CH, C-10), 118.4 (C$_q$, C-7), 114.3 (CH, C-11), 108.1 (CH, C-6), 101.7 (CH₂, C-4), 98.7 (CH, C-2), 55.4 (CH₃, C-13), 53.9 (CH, C-8), 42.0 (C$_q$, C-14), 26.2, 22.6 ppm.

HRMS (EI): *m/z* calcd for $C_{19}H_{18}O_5^{\bullet+}$ [M•⁺]: 326.1149; found: 326.1148.

IR (film, ATR): $\tilde{v}$ 2927, 1758, 1512, 1481, 1439, 1248, 1171, 1148, 1097, 1033, 936, 831 cm⁻¹.

10-(4-methoxyphenyl)-8,9,9a,10-tetrahydro-5aH,7H-[1,3]dioxolo[4,5-g]pyrano[2,3-b]chromen-5a-ol (5ab) was prepared according to *GP2* (reaction time: 60 h) from **1a** (30.0 mg, 0.12 mmol), and **4b** (32.3 mg, 0.19 mmol). The reaction mixture was further purified by column chromatography (silica gel, eluent: *n*-pentane:EtOAc = 8:2→5:5) to give **5ab** (26.0 mg, 61%) as a colorless oil; mixture of diastereomers (d.r. = 75:25).

5ab (CG487)
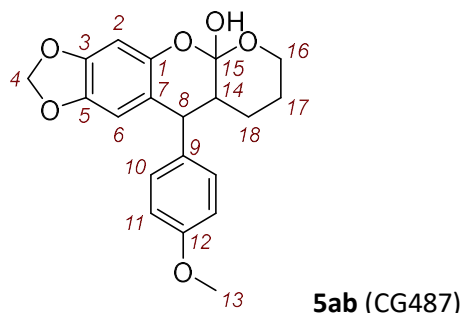
R_f (*n*-pentane/EtOAc 1:1, silica, UV) = 0.40.

^{1}H NMR (600 MHz, CDCl$_3$): δ 7.01 (d, *J* = 8.7 Hz, 2 H, 10-H^{minor}), 6.99 (d, *J* = 8.7 Hz, 2 H, 10-H^{major}), 6.86 (d, *J* = 8.7 Hz, 2 H, 11-H^{minor}), 6.79 (d, *J* = 8.7 Hz, 2 H, 11-H^{major}), 6.65 (s, 1 H, 2-H^{major}), 6.63 (s, 1 H, 2-H^{minor}), 6.56 (s, 1 H, 6-H^{major}), 6.32 (s, 1 H, 6-H^{minor}), 5.97 – 5.89 (m, 4 H, 4-H), 4.02 (d, *J* = 6.3 Hz, 1 H, 8-H^{major}), 3.94 (d, *J* = 7.2 Hz, 1 H, 8-H^{minor}), 3.79 (s, 3 H, 13-H^{minor}), 3.75 (s, 3 H, 13-H^{major}), 3.69 – 3.57 (m, 4 H, 16-H), 3.00 – 2.94 (m, 1 H, 14-H^{major}), 2.94 – 2.89 (m, 1 H, 14-H^{minor}), 1.83 – 1.63 (m, 6 H, 17-H, 18-H), 1.51 (s, 2 H, 15-H), 1.45 – 1.37 ppm (m, 2 H, 17-H).

^{13}C{^{1}H} NMR (151 MHz, CDCl$_3$): δ 170.5 (C$_q$, C-15^{major}), 170.2 (C$_q$, C-15^{minor}), 159.1 (C$_q$, C-12^{major}), 159.0 (C$_q$, C-12^{minor}), 147.6 (C$_q$, C-3^{major}), 147.5 (C$_q$, C-3^{minor}), 145.5 (C$_q$, C-1^{major}), 145.4 (C$_q$, C-1^{minor}), 144.5 (C$_q$, C-5^{minor}), 144.5 (C$_q$, C-5^{major}), 132.4 (C$_q$, C-9^{minor}), 130.6 (C$_q$, C-9^{major}), 128.9 (C-10, 2C), 119.7 (C$_q$, C-7^{major}), 117.7 (C$_q$, C-7^{minor}), 114.6 (CH, C-11^{minor}), 114.5 (CH, C-11^{major}), 108.1 (CH, C-6^{minor}), 107.3 (CH, C-6^{major}), 101.8 (CH$_2$, C-4^{minor}), 101.8 (CH$_2$, C-4^{major}), 99.1 (CH, C-2^{major}), 98.8 (CH, C-2^{minor}), 62.6 (CH$_2$, C-16^{major}), 62.3 (CH$_2$, C-16^{minor}), 55.4 (CH$_3$, C-13^{minor}), 55.4 (CH$_3$, C-13^{major}), 46.7 (CH, C-14^{minor}), 45.5 (CH, C-8, 2C), 44.6 (CH, C-14^{major}), 30.7 (CH$_2$, C-18^{major}), 29.8 (CH$_2$, C-18^{minor}), 25.8 (CH$_2$, C-17^{minor}), 24.0 ppm (CH$_2$, C-17^{major}).

HRMS (EI): *m/z* calcd for C$_{20}$H$_{20}$O$_6$$^{\bullet+}$ [M$^{\bullet+}$]: 356.1255; found: 356.1255.

IR (film, ATR): $\tilde{v}$ 3416, 2928, 1758, 1512, 1480, 1440, 1251, 1151, 1033, 935, 834, 732 cm^{-1}.

((9-(4-methoxyphenyl)-7,8,8a,9-tetrahydro-5aH-[1,3]dioxolo[4,5-g]furo[2,3-b]chromen-5a-yl)oxy)trimethylsilane (5ac) was prepared by mixing of **1a** (32.0 mg, 0.12 mmol), and **4c** (31.1 mg, 0.2 mmol) in 5 ml CH$_2$Cl$_2$ under argon atmosphere. After 1 h the solvent was removed under reduced pressure and the crude was further purified by column chromatography (silica/*n*-pentane:EtOAc 8:2 → 7:3) to give **5ac** as a colorless oil (28.0 mg, 56%); mixture of diastereomers (d.r. = 53:47).

5ac (CG499_1)

^{1}H NMR (400 MHz, CDCl$_3$): δ 7.18 (d, *J* = 8.5 Hz, 2 H, 10-H[major]), 7.05 (d, *J* = 8.5 Hz, 2 H, 10-H[minor]), 6.82 (d, *J* = 8.9 Hz, 2 H, 11-H[major]), 6.78 (d, *J* = 8.9 Hz, 2 H, 11-H[minor]), 6.74 (s, 1 H, 6-H[minor]), 6.70 (s, 1 H, 6-H[major]), 6.36 (s, 1 H, 2-H[minor]), 6.36 (s, 1 H, 2-H[major]), 5.91 (s, 2 H, 4-H[minor]), 5.90 – 5.85 (m, 2 H, 4-H[major]), 4.82 (d, *J* = 5.5 Hz, 1 H, 8-H[minor]), 4.53 (d, *J* = 8.9 Hz, 1 H, 8-H[major]), 4.23 – 3.84 (m, 4 H, 16-H), 3.77 (s, 3 H, 13-H[major]), 3.76 (s, 3 H, 13-H[minor]), 3.37 – 3.24 (m, 1 H, 14-H[major]), 3.23 – 3.10 (m, 1 H, 14-H[minor]), 2.44 – 1.96 (m, 4 H, 15-H), 0.23 (s, 9 H, 18-H[major]), 0.13 ppm (s, 9 H, 18-H[minor]).

^{13}C{^{1}H} NMR (101 MHz, CDCl$_3$): δ 178.3 (C$_q$, C-17[minor]), 177.8 (C$_q$, C-17[major]), 158.4 (C$_q$, C-12[minor]), 158.3 (C$_q$, C-12[major]), 147.7 (C$_q$, C-1[minor]), 147.5 (C$_q$, C-1[major]), 146.4 (C$_q$, C-3[major]), 146.4 (C$_q$, C-3[minor]), 141.9 (C$_q$, C-5[major]), 141.6 (C$_q$, C-5[minor]), 134.0 (C$_q$, C-9[major]), 133.4 (C$_q$, C-9[minor]), 129.6 (CH, C-10[minor]), 129.4 (CH, C-10[major]), 125.3 (C$_q$, C-7[minor]), 125.2 (C$_q$, C-7[major]), 113.9 (CH, C-11[minor]), 113.8 (CH, C-11[major]), 108.4 (CH, C-6[major]), 107.6 (CH, C-6[minor]), 101.3 (CH$_2$, C-4[major]), 101.2 (CH$_2$, C-4[minor]), 101.2 (CH, C-2[minor]), 100.8 (CH, C-2[major]), 66.5 (CH$_2$, C-16[minor]), 66.3 (CH$_2$, C-16[major]), 55.4 (CH$_3$, C-13[minor]), 55.3 (CH$_3$, C-13[major]), 43.9 (CH, C-8[major]), 43.7 (CH, C-14[minor]), 43.4 (CH, C-8[minor]), 43.1 (CH, C-14[major]), 28.4 (CH$_2$, C-15[major]), 26.8 (CH$_2$, C-15[minor]), 0.6 (CH$_3$, C-18[major]), 0.4 ppm (CH$_3$, C-18[minor]).

HRMS (EI): *m/z* calcd for C$_{22}$H$_{26}$O$_6$Si$^{\bullet+}$ [M$^{\bullet+}$]: 414.1494; found: 414.1496.

9-(4-(trifluoromethyl)phenyl)-5a,7,8,8a-tetrahydro-9H-[1,3]dioxolo[4,5-g]furo[2,3-b]chromene (6') was prepared by mixing of **1f** (20.0 mg, 0.068 mmol), and **6** (47.6 mg, 0.680 mmol) in 5 ml CH$_2$Cl$_2$. After 120 h the solvent was removed under reduced pressure and the crude was further purified by column chromatography (silica/*n*-pentane:EtOAc 9:1) to give **6'** as two separate diastereomers (7.0 mg, 28% and 3.5 mg, 14%) each as a colorless oil. Crystallization of the major isomer by the vapor diffusion method from a *n*-pentane/Et$_2$O mixture (at +4°C) afforded suitable crystals for X-Ray diffraction.

6' (CG710)   cv213

Major Isomer: **6'** (CG710F2)

^{1}H NMR (400 MHz, CDCl$_3$): δ 7.62 (d, *J* = 8.3 Hz, 2 H, 13-H), 7.36 (d, *J* = 8.2 Hz, 2 H, 12-H), 6.50 (s, 1 H, 6-H), 6.23 (s, 1 H, 10-H), 5.89 (d, *J* = 1.3 Hz, 1 H, 8-H[a]), 5.86 (d, *J* = 1.3 Hz, 1 H, 8-H[b]), 5.70 (d, *J* = 4.3 Hz,

_____

1 H, 1-H), 4.55 (d, *J* = 5.3 Hz, 1 H, 3-H), 4.13 (td, *J* = 9.0, 2.4 Hz, 1 H, 17-H^a), 3.93 – 3.82 (m, 1 H, 17-H^b), 2.78 – 2.66 (m, 1 H, 2-H), 1.96 – 1.81 (m, 1 H, 16-H^a), 1.62 – 1.50 ppm (m, 1 H, 16-H^b).

^{13}C{^{1}H} NMR (101 MHz, CDCl$_3$): *δ* 148.0 (C$_q$, C-5), 147.5 (C$_q$, C-7), 145.9 (C$_q$, C-11, q, $^5J_{C,F}$ = 1.3 Hz), 142.2 (C$_q$, C-9), 129.7 (C$_q$, C-14, q, $^2J_{C,F}$ = 32.9 Hz), 129.6 (CH, C-12), 125.8 (CH, C-13, q, $^3J_{C,F}$ = 3.8 Hz), 124.3 (C$_q$, C-15, q, $^1J_{C,F}$ = 272.2 Hz), 114.0 (C$_q$, C-4), 107.6 (CH, C-10), 101.4 (CH, C-1), 101.3 (CH$_2$, C-8), 99.4 (CH, C-6), 68.5 (CH$_2$, C-17), 44.7 (CH, C-2), 42.4 (CH, C-3), 25.2 ppm (CH$_2$, C-16).

^{19}F NMR (376 MHz, CDCl$_3$): *δ* -62.53 (s, 3 F, 15-F)

HRMS (EI): *m/z* calcd for C$_{19}$H$_{15}$F$_3$O$_4$$^{•+}$ [M$^{•+}$]: 364.0917; found: 364.0916.
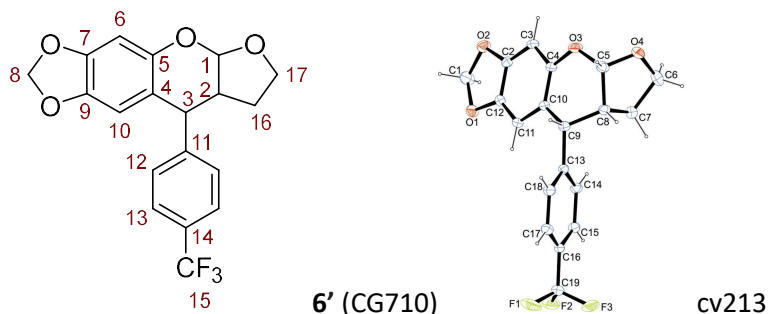
IR (neat, ATR): $\tilde{v}$ 2900, 1619, 1481, 1435, 1325, 1240, 1162, 1122, 1068, 1037, 936, 889 cm^{-1}.

Minor Isomer: **6'** (CG710F3)

^{1}H NMR (400 MHz, CDCl$_3$): *δ* = 7.56 (d, *J* = 8.0 Hz, 2 H, 13-H), 7.26 (d, *J* = 8.6 Hz, 2 H, 12-H), 6.54 (s, 1 H, 6-H), 6.38 (s, 1 H, 10-H), 5.90 (d, *J* = 1.5 Hz, 1 H, 8-H^a), 5.89 (d, *J* = 1.4 Hz, 1 H, 8-H^b), 5.51 (d, *J* = 4.9 Hz, 1 H, 1-H), 4.09 (td, *J* = 8.8, 4.4 Hz, 1 H, 17-H^a), 4.03 (d, *J* = 2.9 Hz, 1 H, 3-H), 3.94 (q, *J* = 8.0 Hz, 1 H, 17-H^b), 2.77 – 2.66 (m, 1 H, 2-H), 2.27 – 2.14 (m, 1 H, 16-H^a), 1.89 – 1.75 ppm (m, 1 H, 16-H^b).

^{13}C{^{1}H} NMR (101 MHz, CDCl$_3$): *δ* = 148.3 (C$_q$, C-11, q, $^5J_{C,F}$ = 1.3 Hz), 147.9 (C$_q$, C-5), 147.9 (C$_q$, C-7), 142.6 (C$_q$, C-9), 129.3 (C$_q$, C-14, q, $^2J_{C,F}$ = 32.6 Hz), 128.3 (CH, C-12), 125.9 (CH, C-13, q, $^3J_{C,F}$ = 3.8 Hz), 114.1 (C$_q$, C-4), 108.6 (CH, C-10), 101.3 (CH$_2$, C-8), 100.0 (CH, C-1), 99.6 (CH, C-6), 67.8 (CH$_2$, C-17), 46.1 (CH, C-2), 44.1 (CH, C-3) 29.1 ppm (CH$_2$, C-16). Signal for C-15 (CF$_3$-group) could not be assigned, hidden in signal noise!

^{19}F NMR (376 MHz, CDCl$_3$): *δ* -62.53 (s, 3 F, 15-F)

HRMS (EI): *m/z* calcd for C$_{19}$H$_{15}$F$_3$O$_4$$^{•+}$ [M$^{•+}$]: 364.0917; found: 364.0916.

IR (film, ATR): $\tilde{v}$ 2897, 1618, 1481, 1443, 1325, 1158, 1121, 1068, 1038, 938, 892, 843 cm^{-1}.

6-(ethylthio)-8-(4-methoxyphenyl)-7,8-dihydro-6H-[1,3]dioxolo[4,5-g]chromene (7') was prepared by mixing of **1a** (50.0 mg, 0.195 mmol), and **7** (163 mg, 1.85 mmol) in 5 ml CH$_2$Cl$_2$. After 36 h the solvent was removed under reduced pressure and the crude was further purified by column chromatography (silica/*n*-pentane:EtOAc 9:1) to give **7'** as a white solid (50.3 mg, 0.146 mmol, 75%); m.p. 100°C.

7' (CG618)

R$_f$ (*n*-pentane/EtOAc 9:1, silica, UV) = 0.50.

^{1}H NMR (400 MHz, CD$_2$Cl$_2$): *δ* 7.09 (d, *J* = 8.7 Hz, 2 H, 10-H), 6.86 (d, *J* = 8.8 Hz, 2 H, 11-H), 6.41 (s, 1 H, 2-H), 6.14 (d, *J* = 0.8 Hz, 1 H, 6-H), 5.87 – 5.80 (m, 2 H, 4-H), 5.30 (dd, *J* = 11.0, 2.2 Hz, 1 H, 15-H), 4.08

(dd, *J* = 11.0, 6.6 Hz, 1 H, 8-H), 3.79 (s, 3 H, 13-H), 2.92 – 2.70 (m, 2 H, 16-H), 2.45 – 2.35 (m, 1 H, 14-H), 2.19 – 2.03 (m, 1 H, 14-H), 1.34 ppm (t, *J* = 7.4 Hz, 3 H).

^{13}C{^{1}H} NMR (101 MHz, CD$_2$Cl$_2$): δ 159.0 (C$_q$, C-12), 149.8 (C$_q$, C-1), 147.1 (C$_q$, C-3), 142.3 (C$_q$, C-5), 136.5 (C$_q$, C-9), 129.8 (CH, C-10), 118.3 (C$_q$, C-7), 114.4 (CH, C-11), 108.5 (CH, C-6), 101.5 (CH$_2$, C-4), 98.7 (CH, C-2), 81.2 (CH, C-15), 55.6 (CH$_3$, C-13), 42.5 (CH, C-8), 38.8 (CH$_2$, C-14), 25.0 (CH$_2$, C-16), 15.4 ppm (CH$_3$, C-17).

HRMS (EI): *m/z* calcd for C$_{19}$H$_{20}$O$_4$S$^{•+}$ [M$^{•+}$]: 344.1077; found: 344.1074.

IR (neat, ATR): ṽ 2927, 1613, 1518, 1474, 1246, 1183, 1172, 1142, 1031, 907, 891, 827 cm^{-1}.

6-azido-8-(4-nitrophenyl)-6-phenyl-7,8-dihydro-6H-[1,3]dioxolo[4,5-g]chromene (8') was prepared by mixing of **1g** (21.0 mg, 0.077 mmol), and **8** (11.8 mg, 0.081 mmol) in 5 ml CH$_2$Cl$_2$. After 7 days the solvent was removed under reduced pressure and the crude was further purified by column chromatography (silica/*n*-pentane:EtOAc 95:5) and recrystallized from Et$_2$O (slow evaporation) to give **8'** as colorless crystals (15.0 mg, 47%); m.p. 136 °C.

8' (CG680F3)   cv119

^{1}H NMR (600 MHz, CDCl$_3$): δ 8.18 (d, *J* = 8.8 Hz, 2 H, 13-H), 7.50 (dd, *J* = 8.2, 1.5 Hz, 2 H, 16-H), 7.46 – 7.39 (m, 3 H, 17-H, 18-H), 7.34 (d, *J* = 8.8 Hz, 2 H, 12-H), 6.70 (s, 1 H, 6-H), 6.10 (s, 1 H, 10-H), 5.95 – 5.90 (m, 2 H, 8-H), 3.89 (dd, *J* = 8.7, 6.3 Hz, 1 H, 3-H), 2.62 (dd, *J* = 13.9, 6.5 Hz, 1 H, 2-H), 2.39 ppm (dd, *J* = 13.9, 8.5 Hz, 1 H, 2-H).

^{13}C{^{1}H} NMR (151 MHz, CDCl$_3$): δ 151.8 (C$_q$, C-11), 148.0 (C$_q$, C-7), 147.9 (C$_q$, C-5), 147.0 (C$_q$, C-14), 142.9 (C$_q$, C-9), 139.2 (C$_q$ C-15), 129.7 (CH, C-12), 129.3 (CH, C-18), 129.1 (CH, C-17), 125.6 (CH, C-16), 124.0 (CH, C-13), 114.2 (C$_q$, C-4), 108.1 (CH, C-10), 101.5 (CH$_2$, C-8), 99.1 (CH, C-6), 93.3 (C$_q$, C-1), 41.1 (CH$_2$, C-2), 39.6 ppm (CH, C-3).

HRMS (EI): *m/z* calcd for C$_{22}$H$_{16}$N$_4$O$_5$$^{•+}$ [M$^{•+}$]: 416.1116; found: 416.1104.
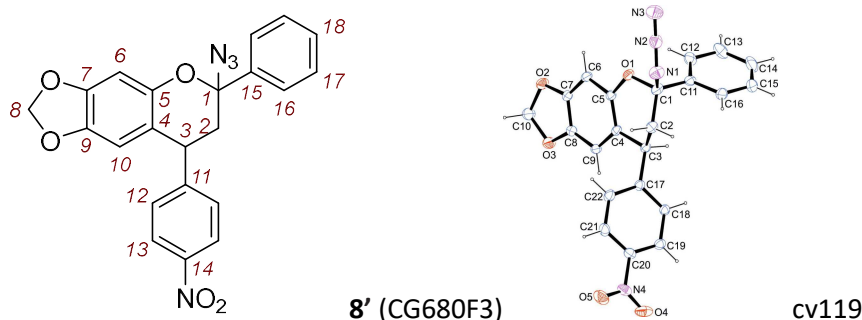
IR (neat, ATR): ṽ 2890, 2112, 1519, 1481, 1347, 1245, 1153, 1037, 939, 856, 733, 697 cm^{-1}.

7.4.5. Reaction Product of Benzhydrylium Ion with α-azido styrene

3,3-bis(4-(methyl(2,2,2-trifluoroethyl)amino)phenyl)-N-phenylpropanamide (10) was prepared by mixing of **9d** [preformed in 8 mL CH$_2$Cl$_2$ from Ar$_2$CH-OH (0.033 g, 0.081 mmol) and addition of HBF$_4$·Et$_2$O (12 μl, 0.089 mmol) at -20°C] and α-azido styrene **8** (dissolved in 2 mL CH$_2$Cl$_2$) under nitrogen atmosphere at -20°C. After 60 min the reaction was quenched by addition of aqueous hydrochloric acid (2 M). The reaction mixture was extracted with 3 × 10 mL of CH$_2$Cl$_2$ and the combined organic phases were washed with 10 mL brine, dried (MgSO$_4$) and the solvent was removed under reduced pressure. The crude was further purified by column chromatography (basic Al$_2$O$_3$/*n*-pentane:EtOAc:NEt$_3$ 80:18:2 and silica/*n*-pentane:EtOAc:NEt$_3$ 70:28:2) to give **10** as a white solid (18.0 mg, 42%); m.p. 138°C.

10 (CG734_1)
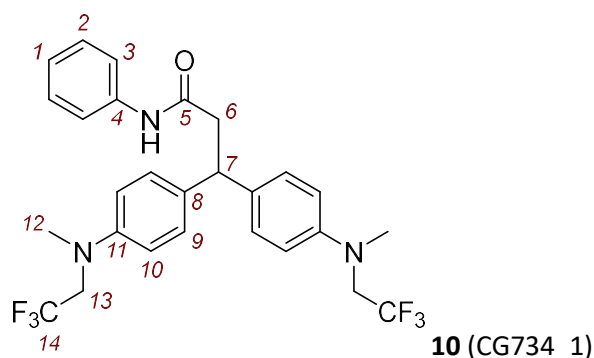
^{1}H NMR (400 MHz, CD$_2$Cl$_2$): δ 7.31 (d, *J* = 7.1 Hz, 2 H, 3-H), 7.28 − 7.21 (m, 2 H, 2-H), 7.15 (d, *J* = 8.8 Hz, 4 H, 9-H), 7.10 − 7.01 (m, 2 H, 1-H, 4-NH), 6.74 (d, *J* = 8.9 Hz, 4 H, 10-H), 4.44 (t, *J* = 7.8 Hz, 1 H, 7-H), 3.84 (q, *J* = 9.1 Hz, 4 H, 13-H), 3.05 − 2.96 ppm (m, 8 H, 6-H, 12-H).

^{13}C{^{1}H} NMR (101 MHz, CD$_2$Cl$_2$): δ 169.9 (C=O, C-5), 147.7 (C$_q$, C-11), 138.4 (C$_q$, C-4), 134.3 (C$_q$, C-8), 129.2 (CH, C-2), 128.6 (CH, C-9), 126.2 (C-F, C-14, q, $^1J_{C,F}$ = 283.0 Hz), 124.4 (CH, C-1), 120.2 (CH, C-3), 113.3 (CH, C-10, q, $^5J_{C,F}$ = 0.9 Hz), 54.6 (CH$_2$, C-13, q, $^2J_{C,F}$ = 32.3 Hz), 45.9 (CH, C-7), 44.7 (CH$_2$, C-6), 39.5 ppm (CH$_3$, C-12, q, $^4J_{C,F}$ = 1.0 Hz).

^{19}F NMR (376 MHz, CD$_2$Cl$_2$): δ -70.96 (t, *J* = 9.1 Hz, 3 F, 14-F).

HRMS (pos. ESI): *m/z* calcd for C$_{27}$H$_{27}$F$_6$N$_3$NaO$^+$ [M + Na$^+$]: 541.1951; found: 541.1963.

IR (neat, ATR): ṽ 3257, 2917, 1658, 1602, 1552 1517, 1371, 1264, 1139, 1093, 987, 789 cm^{-1}.

_____

7.4.6. Cyclic Voltammetry – Oxidation Potentials of Enamines

Only peak potentials E_p^{ox} could be determined due to the non-reversibility of the Enamine oxidation.
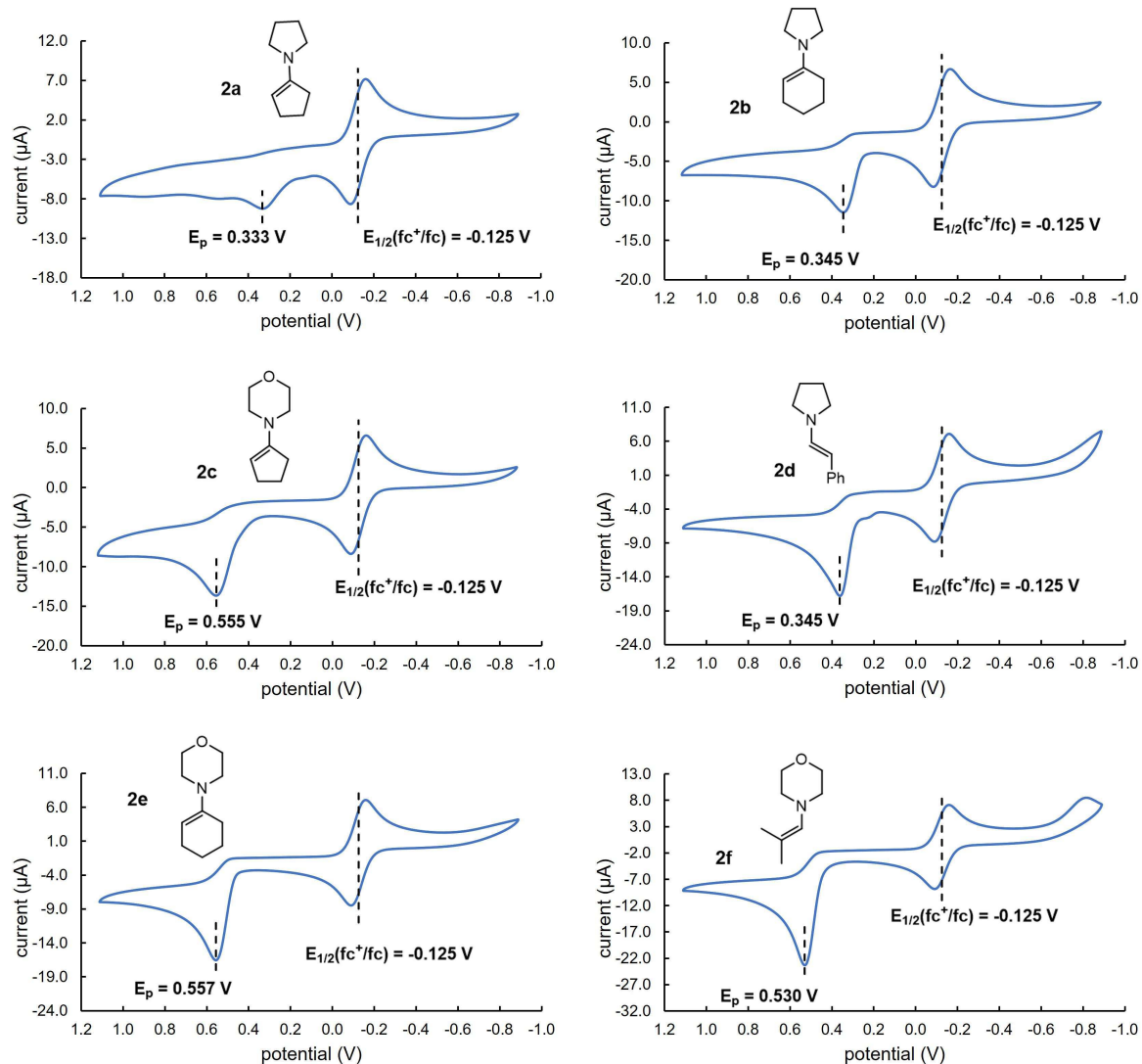
7.4.7. Single Crystal X-Ray Structure Determination

The X-ray intensity data of **3ab** (av376), **3ad** (av409), **3ae** (cv196), **3af** (av381), **5aa** (bv115), **6'** (cv213) and **8'** (cv119), were measured on a Bruker D8 Venture TXS system equipped with a multilayer mirror monochromator and a Mo Kα rotating anode X-ray tube (λ = 0.71073 Å). The frames were integrated with the Bruker SAINT software package.[43] Data were corrected for absorption effects using the Multi-Scan method (SADABS).[44] The structure was solved and refined using the Bruker SHELXTL Software Package.[45] All hydrogen atoms have been calculated in ideal geometry riding on their parent atoms. The structure of **3af** (av381), has been refined as a 2-component perfect inversion twin. All figures have been drawn at the 25% ellipsoid probability level.[46] The asymmetric unit of **3ad** (av409), **3af** (av381) and **3ab** (av376) contains two formula units, one of which has been depicted in the figures.

_____

1-(10-(4-methoxyphenyl)-6,7,8,9,9a,10-hexahydro-5aH-[1,3]dioxolo[4,5-b]xanthen-5a-yl)pyrrolidine (3ab)
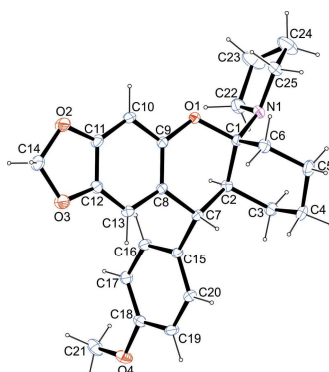
3ab (av376, CG422)

net formula	$C_{25}H_{29}NO_4$
M_r/g mol^{-1}	407.49
crystal size/mm	0.160 × 0.140 × 0.090
T/K	173.(2)
radiation	MoKα
diffractometer	'Bruker D8 Venture TXS'
crystal system	triclinic
space group	'P -1'
a/Å	9.9745(6)
b/Å	11.4487(7)
c/Å	18.5014(12)
α/°	91.786(2)
β/°	96.737(2)
γ/°	90.095(2)
V/Å^3	2097.1(2)
Z	4
calc. density/g cm^{-3}	1.291
μ/mm^{-1}	0.087
absorption correction	Multi-Scan
transmission factor range	0.94–0.99
refls. measured	37159
R_{int}	0.0418
mean σ(I)/I	0.0388
θ range	2.842–27.102
observed refls.	7442
x, y (weighting scheme)	0.0612, 1.0479
hydrogen refinement	constr
Flack parameter	?
refls in refinement	9234
parameters	543
restraints	0
$R(F_{obs})$	0.0534
$R_w(F^2)$	0.1458
S	1.057
shift/error$_{max}$	0.001
max electron density/e Å^{-3}	0.401
min electron density/e Å^{-3}	−0.263

_____

1-(8-(4-methoxyphenyl)-7-phenyl-7,8-dihydro-6H-[1,3]dioxolo[4,5-g]chromen-6-yl)pyrrolidine (3ad)
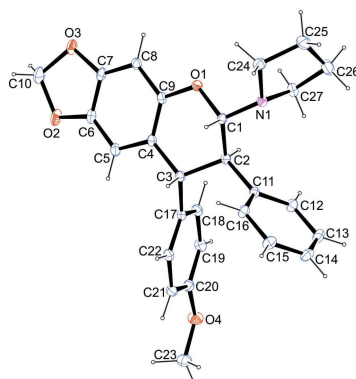
3ad (av409, CG430)

net formula	$C_{27}H_{27}NO_4$
M_r/g mol^{-1}	429.49
crystal size/mm	0.160 × 0.140 × 0.070
T/K	173.(2)
radiation	MoKα
diffractometer	'Bruker D8 Venture TXS'
crystal system	triclinic
space group	'P -1'
a/Å	9.3188(3)
b/Å	11.2818(3)
c/Å	20.8884(6)
α/°	91.4210(10)
β/°	91.3950(10)
γ/°	90.2740(10)
V/Å^3	2194.70(11)
Z	4
calc. density/g cm^{-3}	1.300
μ/mm^{-1}	0.087
absorption correction	Multi-Scan
transmission factor range	0.96–0.99
refls. measured	39340
R_{int}	0.0316
mean $\sigma(I)/I$	0.0323
θ range	2.626–27.484
observed refls.	8241
x, y (weighting scheme)	0.0447, 1.0906
hydrogen refinement	constr
Flack parameter	?
refls in refinement	10024
parameters	579
restraints	0
$R(F_{obs})$	0.0450
$R_w(F^2)$	0.1161
S	1.035
shift/error$_{max}$	0.001
max electron density/e Å^{-3}	0.556
min electron density/e Å^{-3}	−0.276

_____

4-(10-(4-methoxyphenyl)-6,7,8,9,9a,10-hexahydro-5aH-[1,3]dioxolo[4,5-b]xanthen-5a-yl)morpholine (3ae)
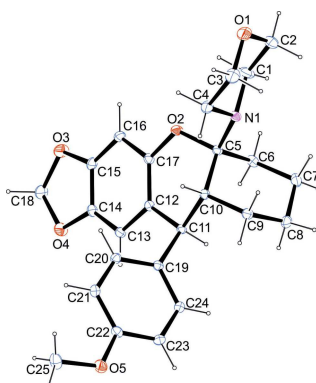
3ae (cv196, CG712F1)

net formula	$C_{25}H_{29}NO_5$
M_r/g mol^{-1}	423.49
crystal size/mm	0.200 × 0.140 × 0.100
T/K	173.(2)
radiation	MoKα
diffractometer	'Bruker D8 Venture TXS'
crystal system	triclinic
space group	'P -1'
a/Å	8.8887(6)
b/Å	9.7219(7)
c/Å	13.8965(9)
$α$/°	99.338(2)
$β$/°	102.164(2)
$γ$/°	111.613(2)
V/Å^3	1052.67(13)
Z	2
calc. density/g cm^{-3}	1.336
$μ$/mm^{-1}	0.093
absorption correction	Multi-Scan
transmission factor range	0.92–0.99
refls. measured	18687
R_{int}	0.0448
mean σ(I)/I	0.0417
θ range	3.361–27.485
observed refls.	4008
x, y (weighting scheme)	0.0315, 0.5516
hydrogen refinement	constr
Flack parameter	?
refls in refinement	4823
parameters	281
restraints	0
$R(F_{obs})$	0.0450
$R_w(F^2)$	0.1099
S	1.051
shift/error$_{max}$	0.001
max electron density/e Å^{-3}	0.332
min electron density/e Å^{-3}	−0.224

_____

4-(8-(4-methoxyphenyl)-7,7-dimethyl-7,8-dihydro-6H-[1,3]dioxolo[4,5-g]chromen-6-yl)morpholine (3af)
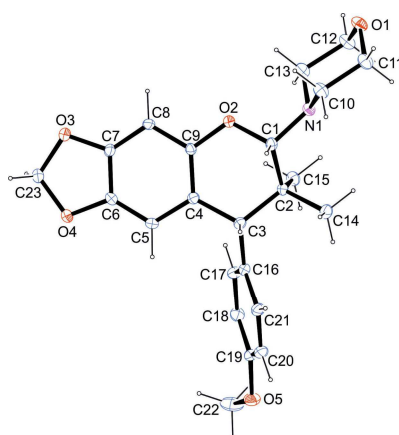
3af (av381, CG289_2)

net formula	$C_{23}H_{27}NO_5$
M_r/g mol^{-1}	397.45
crystal size/mm	0.180 × 0.080 × 0.070
T/K	173.(2)
radiation	MoKα
diffractometer	'Bruker D8 Venture TXS'
crystal system	triclinic
space group	'P 1'
a/Å	6.0808(2)
b/Å	11.9064(4)
c/Å	14.2793(4)
α/°	79.2240(10)
β/°	86.4640(10)
γ/°	85.1590(10)
V/Å^3	1010.86(6)
Z	2
calc. density/g cm^{-3}	1.306
μ/mm^{-1}	0.092
absorption correction	Multi-Scan
transmission factor range	0.97–0.99
refls. measured	17398
R_{int}	0.0276
mean $\sigma(I)/I$	0.0372
θ range	3.106–26.368
observed refls.	7293
x, y (weighting scheme)	0.0427, 0.2093
hydrogen refinement	constr
Flack parameter	0.5
refls in refinement	7842
parameters	529
restraints	3
$R(F_{obs})$	0.0383
$R_w(F^2)$	0.0913
S	1.049
shift/error$_{max}$	0.001
max electron density/e Å^{-3}	0.158
min electron density/e Å^{-3}	−0.178

8-(4-methoxyphenyl)-7,7-dimethyl-7,8-dihydro-6H-[1,3]dioxolo[4,5-g]chromen-6-one (5aa)
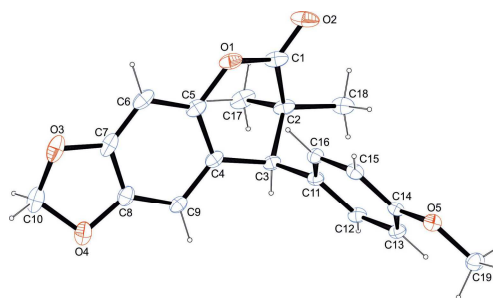
5aa (bv115, CG477)

net formula	$C_{19}H_{18}O_5$
M_r/g mol^{-1}	326.33
crystal size/mm	0.100 × 0.080 × 0.050
T/K	173.(2)
radiation	MoKα
diffractometer	'Bruker D8 Venture TXS'
crystal system	monoclinic
space group	'P 1 21/c 1'
a/Å	16.391(2)
b/Å	7.5698(10)
c/Å	12.8361(15)
α/°	90
β/°	92.448(4)
γ/°	90
V/Å^3	1591.2(3)
Z	4
calc. density/g cm^{-3}	1.362
μ/mm^{-1}	0.099
absorption correction	Multi-Scan
transmission factor range	0.92–0.99
refls. measured	25629
R_{int}	0.0613
mean σ(I)/I	0.0417
θ range	3.125–27.100
observed refls.	2860
x, y (weighting scheme)	0.0708, 0.7034
hydrogen refinement	constr
Flack parameter	?
refls in refinement	3492
parameters	220
restraints	0
$R(F_{obs})$	0.0511
$R_w(F^2)$	0.1549
S	1.109
shift/error$_{max}$	0.001
max electron density/e Å^{-3}	0.241
min electron density/e Å^{-3}	−0.323

_____

9-(4-(trifluoromethyl)phenyl)-5a,7,8,8a-tetrahydro-9H-[1,3]dioxolo[4,5-g]furo[2,3-b]chromene (6')
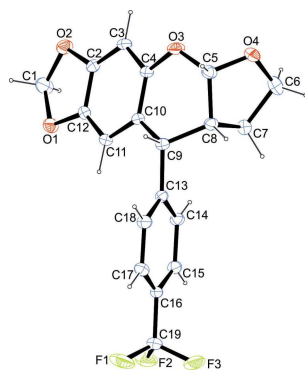
6' (cv213, CG710F2)

net formula	$C_{19}H_{15}F_3O_4$
M_r/g mol^{-1}	364.31
crystal size/mm	0.170 × 0.060 × 0.030
T/K	173.(2)
radiation	MoKα
diffractometer	'Bruker D8 Venture TXS'
crystal system	triclinic
space group	'P -1'
a/Å	9.0263(5)
b/Å	9.6710(5)
c/Å	10.5832(6)
α/°	93.995(2)
β/°	102.675(2)
γ/°	115.417(2)
V/Å^3	799.89(8)
Z	2
calc. density/g cm^{-3}	1.513
μ/mm^{-1}	0.128
absorption correction	Multi-Scan
transmission factor range	0.96–1.00
refls. measured	13818
R_{int}	0.0321
mean $\sigma(I)/I$	0.0297
θ range	3.110–26.370
observed refls.	2876
x, y (weighting scheme)	0.0964, 0.5667
hydrogen refinement	constr
Flack parameter	?
refls in refinement	3265
parameters	235
restraints	0
$R(F_{obs})$	0.0597
$R_w(F^2)$	0.1830
S	1.081
shift/error$_{max}$	0.001
max electron density/e Å^{-3}	0.670
min electron density/e Å^{-3}	−0.502

6-azido-8-(4-nitrophenyl)-6-phenyl-7,8-dihydro-6H-[1,3]dioxolo[4,5-g]chromene (8')
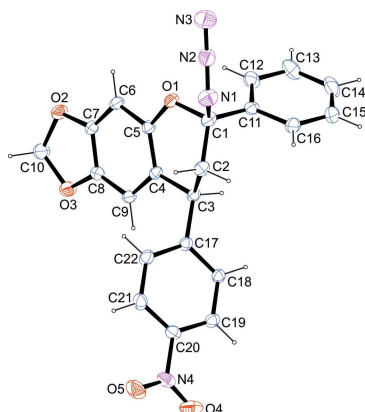
8' (cv119, CG680F3)

net formula	$C_{22}H_{16}N_4O_5$
M_r/g mol^{-1}	416.39
crystal size/mm	0.190 × 0.170 × 0.150
T/K	173.(2)
radiation	MoKα
diffractometer	'Bruker D8 Venture TXS'
crystal system	monoclinic
space group	'C 1 2/c 1'
a/Å	19.4261(7)
b/Å	9.2943(4)
c/Å	22.0217(9)
α/°	90
β/°	102.2100(10)
γ/°	90
V/Å^3	3886.1(3)
Z	8
calc. density/g cm^{-3}	1.423
μ/mm^{-1}	0.104
absorption correction	Multi-Scan
transmission factor range	0.93–0.98
refls. measured	33073
R_{int}	0.0393
mean σ(I)/I	0.0258
θ range	2.534–26.727
observed refls.	3384
x, y (weighting scheme)	0.0709, 5.3151
hydrogen refinement	constr
Flack parameter	?
refls in refinement	4125
parameters	280
restraints	0
$R(F_{obs})$	0.0516
$R_w(F^2)$	0.1544
S	1.026
shift/error$_{max}$	0.001
max electron density/e Å^{-3}	0.503
min electron density/e Å^{-3}	−0.273

7.4.8. Kinetics of the Reactions of *o*QMs with Enamines

Kinetic measurements were performed by harnessing UV/Vis photometry on AppliedPhotophysics SX.20 stopped-flow instruments The temperature (20.0 ± 0.2 °C) was maintained constant by using circulating bath cryostats. All solutions were prepared by using dry CH_2Cl_2 (Dichloromethane, Sigma-Aldrich, for HPLC, ≥ 99.8%), stirred for two weeks over sulfuric acid (96%), separated, washed and distilled over CaH_2) or dry CH_3CN (ThermoScientific, CH_3CN 99.7+%, extra dry, over molecular sieve, AcroSeal) and kept under an atmosphere of dry nitrogen.

1a + **2a** in CH_2Cl_2 (stopped-flow method, detection at 430 nm) CG245
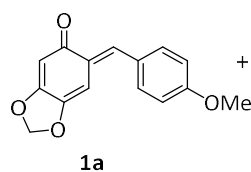
[**1a**]$_0$ (M)	[**2a**]$_0$ (M)	k_{obs} (s^{-1})
5.21×10^{-5}	1.00×10^{-3}	4.30×10^{-1}
5.21×10^{-5}	1.50×10^{-3}	7.03×10^{-1}
5.21×10^{-5}	2.00×10^{-3}	8.77×10^{-1}
5.21×10^{-5}	2.50×10^{-3}	1.13
5.21×10^{-5}	3.00×10^{-3}	1.40

$$k_2 = 4.73 \times 10^2 \text{ M}^{-1} \text{ s}^{-1}$$
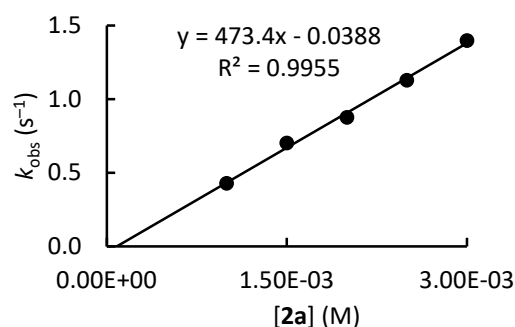
1a + **2b** in CH_2Cl_2 (stopped-flow method, detection at 430 nm) CG244_1
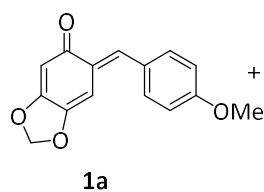
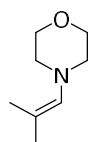| [**1a**]$_0$ (M)	[**2b**]$_0$ (M)	k_{obs} (s^{-1})
5.95×10^{-5}	1.00×10^{-3}	1.86×10^{-1}
5.95×10^{-5}	2.00×10^{-3}	4.22×10^{-1}
5.95×10^{-5}	2.50×10^{-3}	5.65×10^{-1}
5.95×10^{-5}	3.00×10^{-3}	7.30×10^{-1}

$$k_2 = 2.69 \times 10^2 \text{ M}^{-1} \text{ s}^{-1}$$
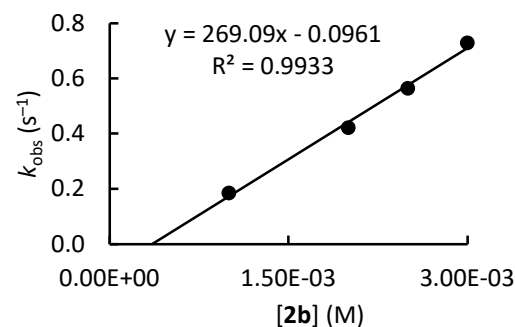
1a + **2c** in CH₂Cl₂ (stopped-flow method, detection at 430 nm) CG246
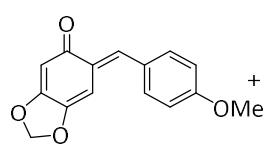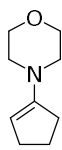
[**1a**]$_0$ (M)	[**2c**]$_0$ (M)	k_{obs} (s^{-1})
3.72×10^{-5}	1.00×10^{-3}	5.76×10^{-3}
3.72×10^{-5}	1.50×10^{-3}	8.75×10^{-3}
3.72×10^{-5}	2.50×10^{-3}	1.49×10^{-2}
3.72×10^{-5}	3.00×10^{-3}	1.87×10^{-2}

$$k_2 = 6.41 \times 10^0 \text{ M}^{-1} \text{ s}^{-1}$$
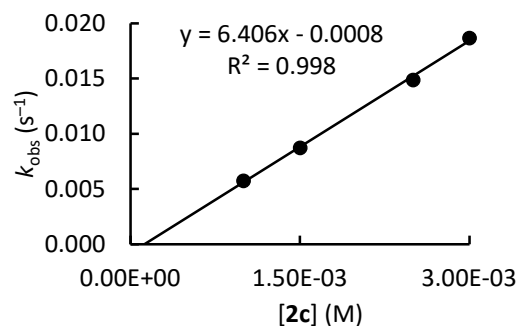
1a + **2d** in CH₂Cl₂ (stopped-flow method, detection at 430 nm) CG355
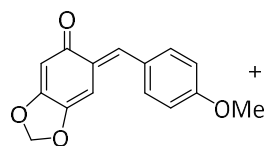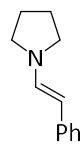
[**1a**]$_0$ (M)	[**2d**]$_0$ (M)	k_{obs} (s^{-1})
5.21×10^{-5}	1.00×10^{-3}	2.88×10^{-2}
5.21×10^{-5}	1.50×10^{-3}	4.36×10^{-2}
5.21×10^{-5}	2.00×10^{-3}	6.06×10^{-2}
5.21×10^{-5}	2.50×10^{-3}	7.52×10^{-2}
5.21×10^{-5}	3.00×10^{-3}	9.07×10^{-2}

$$k_2 = 3.11 \times 10^1 \text{ M}^{-1} \text{ s}^{-1}$$
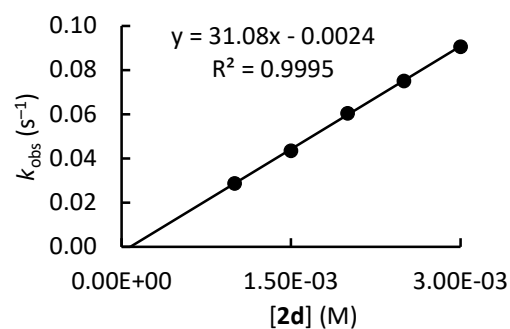
1a + **2d** in MeCN (stopped-flow method, detection at 429 nm) CG510
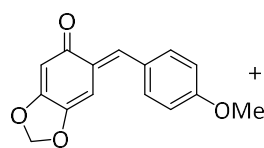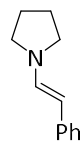
[**1a**]$_0$ (M)	[**2d**]$_0$ (M)	k_{obs} (s^{-1})
6.03×10^{-5}	5.00×10^{-4}	1.55×10^{-2}
5.79×10^{-5}	7.50×10^{-4}	2.18×10^{-2}
5.70×10^{-5}	1.00×10^{-3}	2.91×10^{-2}
5.62×10^{-5}	1.25×10^{-3}	3.74×10^{-2}
5.54×10^{-5}	1.50×10^{-3}	4.45×10^{-2}

$$k_2 = 2.94 \times 10^1 \text{ M}^{-1} \text{ s}^{-1}$$
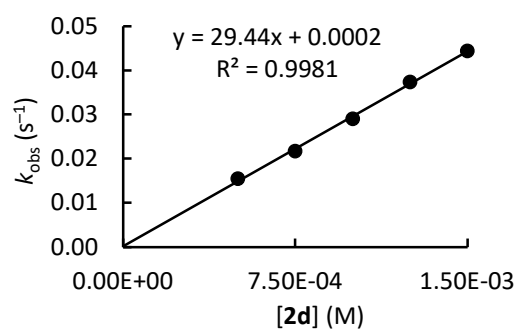
_____

1a + **2d** in Toluene (stopped-flow method, detection at 430 nm) CG736
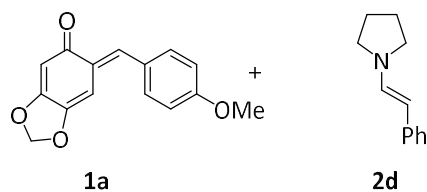
[**1a**]$_0$ (M)	[**2d**]$_0$ (M)	k_{obs} (s^{-1})
1.00×10^{-4}	2.00×10^{-3}	3.91×10^{-2}
1.00×10^{-4}	3.00×10^{-3}	6.76×10^{-2}
1.00×10^{-4}	4.00×10^{-3}	8.89×10^{-2}
1.00×10^{-4}	5.00×10^{-3}	1.15×10^{-1}
1.00×10^{-4}	6.00×10^{-3}	1.41×10^{-1}

$k_2 = 2.51 \times 10^1$ M^{-1} s^{-1}

y = 25.12x - 0.0102
R^2 = 0.9986
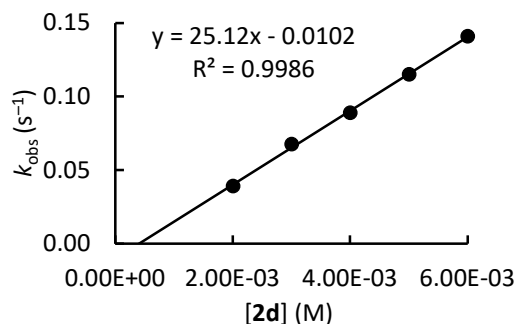
1a + **2d** in 1,4–Dioxane (stopped-flow method, detection at 430 nm) CG737
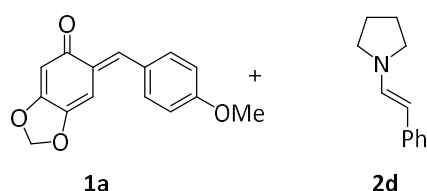
[**1a**]$_0$ (M)	[**2d**]$_0$ (M)	k_{obs} (s^{-1})
1.00×10^{-4}	1.00×10^{-3}	8.38×10^{-3}
1.00×10^{-4}	1.50×10^{-3}	1.32×10^{-2}
1.00×10^{-4}	2.50×10^{-3}	2.53×10^{-2}
1.00×10^{-4}	3.00×10^{-3}	3.04×10^{-2}

$k_2 = 1.12 \times 10^1$ M^{-1} s^{-1}

y = 11.228x - 0.0031
R^2 = 0.9984
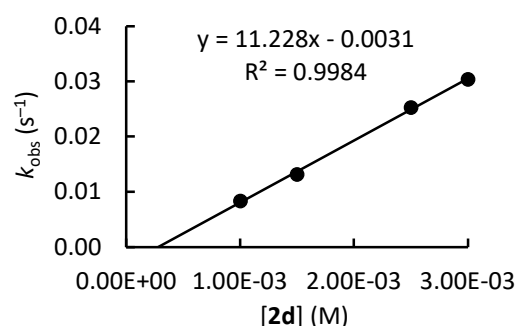
1a + **2d** in DMF (stopped-flow method, detection at 430 nm) CG738
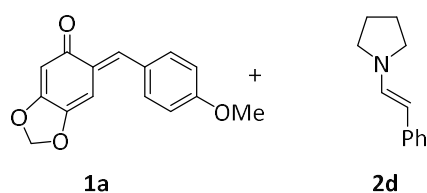
[**1a**]$_0$ (M)	[**2d**]$_0$ (M)	k_{obs} (s^{-1})
1.00×10^{-4}	1.00×10^{-3}	2.63×10^{-2}
1.00×10^{-4}	1.50×10^{-3}	4.53×10^{-2}
1.00×10^{-4}	2.50×10^{-3}	5.87×10^{-2}
1.00×10^{-4}	2.50×10^{-3}	6.89×10^{-2}
1.00×10^{-4}	3.00×10^{-3}	8.08×10^{-2}

$k_2 = 2.65 \times 10^1$ M^{-1} s^{-1}
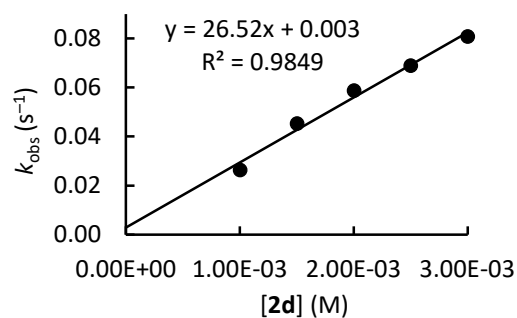
y = 26.52x + 0.003
R^2 = 0.9849

_____

1a + **2e** in CH_2Cl_2 (stopped-flow method, detection at 430 nm) CG247_3
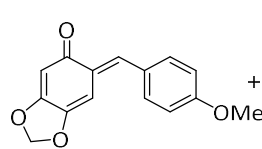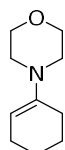
[**1a**]$_0$ (M)	[**2e**]$_0$ (M)	k_{obs} (s^{-1})
6.86×10^{-5}	2.50×10^{-3}	3.47×10^{-3}
6.86×10^{-5}	3.75×10^{-3}	6.62×10^{-3}
6.36×10^{-5}	5.00×10^{-3}	8.73×10^{-3}
6.36×10^{-5}	6.25×10^{-3}	1.31×10^{-2}

$$k_2 = 2.48 \times 10^0 \text{ M}^{-1} \text{ s}^{-1}$$
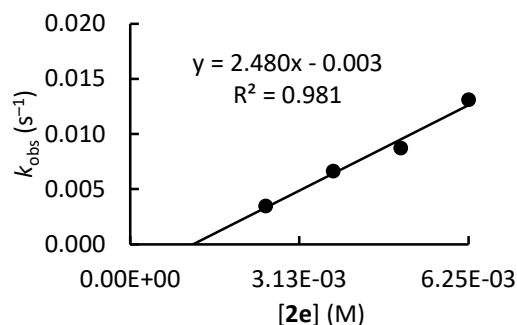
1a + **2f** in CH_2Cl_2 (stopped-flow method, detection at 430 nm) CG248
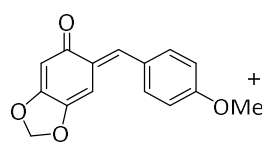
[**1a**]$_0$ (M)	[**2f**]$_0$ (M)	k_{obs} (s^{-1})
4.21×10^{-5}	1.25×10^{-3}	4.59×10^{-3}
4.21×10^{-5}	2.50×10^{-3}	8.40×10^{-3}
4.21×10^{-5}	3.75×10^{-3}	1.34×10^{-2}
4.21×10^{-5}	5.00×10^{-3}	1.84×10^{-2}
4.21×10^{-5}	6.25×10^{-3}	2.36×10^{-2}

$$k_2 = 3.84 \times 10^0 \text{ M}^{-1} \text{ s}^{-1}$$
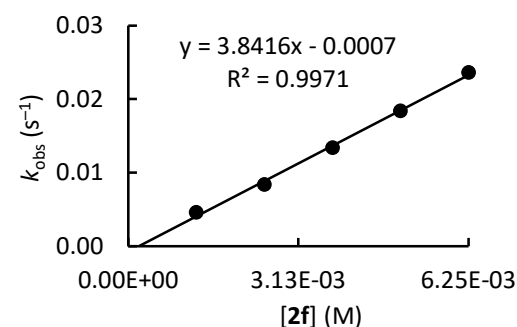
1a + **2g** in MeCN (stopped-flow method, detection at 429 nm) CG423
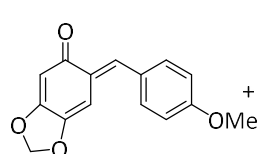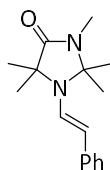
[**1a**]$_0$ (M)	[**2g**]$_0$ (M)	k_{obs} (s^{-1})
3.24×10^{-5}	1.00×10^{-3}	8.59×10^{-3}
3.24×10^{-5}	1.50×10^{-3}	1.57×10^{-2}
3.24×10^{-5}	2.00×10^{-3}	2.14×10^{-2}
3.24×10^{-5}	2.50×10^{-3}	2.55×10^{-2}
3.24×10^{-5}	3.00×10^{-3}	3.10×10^{-2}

$$k_2 = 1.09 \times 10^1 \text{ M}^{-1} \text{ s}^{-1}$$

_____
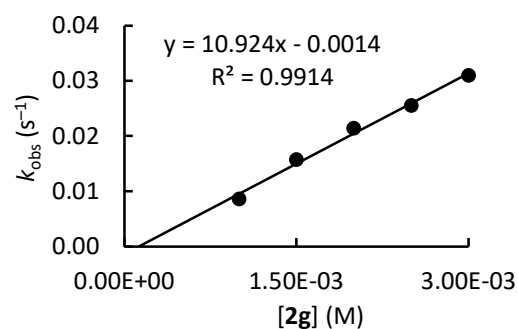
1b + **2d** in CH$_2$Cl$_2$ (stopped-flow method, detection at 420 nm) CG622
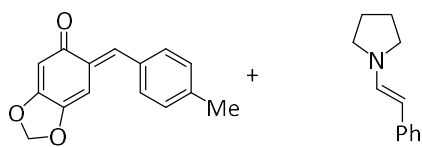
[**1b**]$_0$ (M)	[**2d**]$_0$ (M)	k_{obs} (s^{-1})
6.61×10^{-5}	5.00×10^{-4}	1.43×10^{-2}
6.61×10^{-5}	7.50×10^{-4}	2.27×10^{-2}
6.61×10^{-5}	1.00×10^{-3}	3.01×10^{-2}
6.61×10^{-5}	1.25×10^{-3}	3.84×10^{-2}
6.61×10^{-5}	1.50×10^{-3}	4.68×10^{-2}

k_2 = 3.23 × 10^1 M^{-1} s^{-1}

y = 32.28x - 0.0018
R² = 0.9996
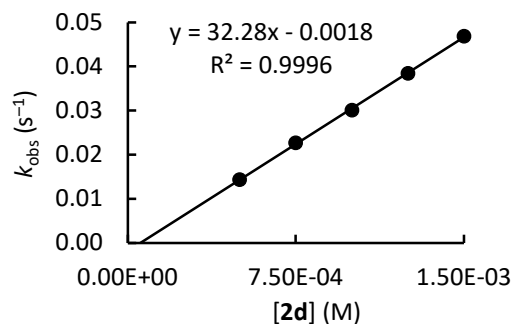
1c + **2d** in CH$_2$Cl$_2$ (stopped-flow method, detection at 413 nm) CG623
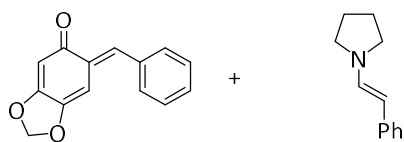
[**1c**]$_0$ (M)	[**2d**]$_0$ (M)	k_{obs} (s^{-1})
5.69×10^{-5}	5.00×10^{-4}	2.05×10^{-2}
5.69×10^{-5}	7.50×10^{-4}	3.06×10^{-2}
5.69×10^{-5}	1.00×10^{-3}	4.01×10^{-2}
5.69×10^{-5}	1.25×10^{-3}	4.98×10^{-2}
5.69×10^{-5}	1.50×10^{-3}	6.10×10^{-2}

k_2 = 4.01 × 10^1 M^{-1} s^{-1}

y = 40.08x + 0.0003
R² = 0.9991
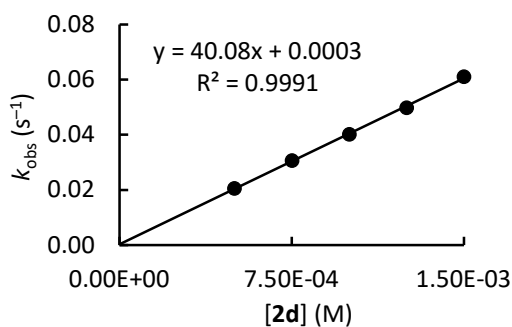
1c + **2f** in CH$_2$Cl$_2$ (stopped-flow method, detection at 413 nm) CG413
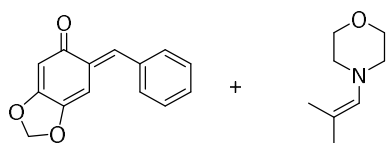
[**1c**]$_0$ (M)	[**2f**]$_0$ (M)	k_{obs} (s^{-1})
9.83×10^{-5}	4.90×10^{-3}	2.49×10^{-2}
9.83×10^{-5}	7.35×10^{-3}	3.47×10^{-2}
9.83×10^{-5}	9.80×10^{-3}	4.74×10^{-2}
9.83×10^{-5}	1.23×10^{-2}	5.94×10^{-2}
9.83×10^{-5}	1.47×10^{-2}	7.19×10^{-2}

k_2 = 4.83 × 10^0 M^{-1} s^{-1}
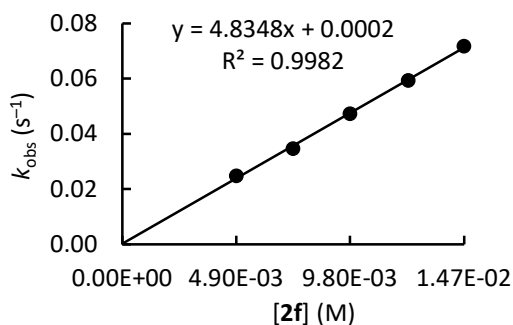
y = 4.8348x + 0.0002
R² = 0.9982

_____

1d + **2d** in CH_2Cl_2 (stopped-flow method, detection at 420 nm) CG624
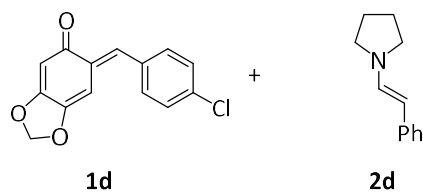
[**1d**]$_0$ (M)	[**2d**]$_0$ (M)	k_{obs} (s^{-1})
3.29×10^{-5}	5.00×10^{-4}	2.88×10^{-2}
3.29×10^{-5}	7.50×10^{-4}	3.81×10^{-2}
3.29×10^{-5}	1.00×10^{-3}	5.21×10^{-2}
3.29×10^{-5}	1.25×10^{-3}	6.61×10^{-2}
3.29×10^{-5}	1.50×10^{-3}	7.60×10^{-2}

$$k_2 = 4.90 \times 10^1 \text{ M}^{-1} \text{ s}^{-1}$$
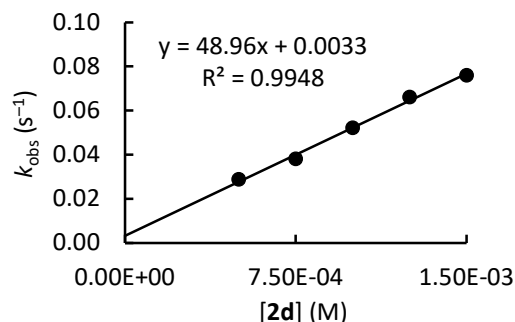
1e + **2d** in CH_2Cl_2 (stopped-flow method, detection at 417 nm) CG625
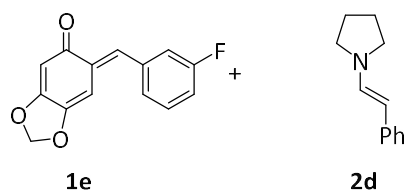
[**1e**]$_0$ (M)	[**2d**]$_0$ (M)	k_{obs} (s^{-1})
6.65×10^{-5}	7.50×10^{-4}	4.81×10^{-2}
6.65×10^{-5}	1.13×10^{-3}	6.89×10^{-2}
6.65×10^{-5}	1.50×10^{-3}	8.84×10^{-2}
6.65×10^{-5}	1.88×10^{-3}	1.05×10^{-1}
6.65×10^{-5}	2.25×10^{-3}	1.22×10^{-1}

$$k_2 = 4.90 \times 10^1 \text{ M}^{-1} \text{ s}^{-1}$$
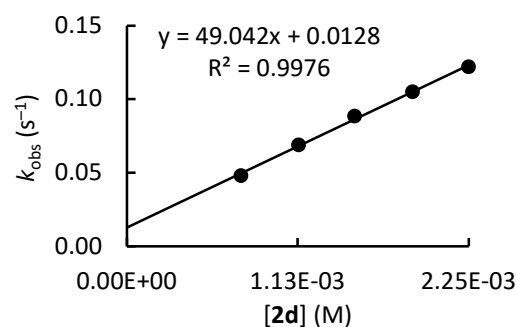
1f + **2d** in CH_2Cl_2 (stopped-flow method, detection at 420 nm) CG626
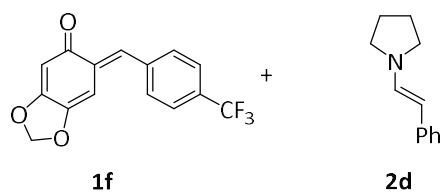
[**1f**]$_0$ (M)	[**2d**]$_0$ (M)	k_{obs} (s^{-1})
8.67×10^{-5}	7.50×10^{-4}	6.25×10^{-2}
8.67×10^{-5}	1.13×10^{-3}	9.23×10^{-2}
8.67×10^{-5}	1.50×10^{-3}	1.22×10^{-1}
8.67×10^{-5}	1.88×10^{-3}	1.48×10^{-1}
8.67×10^{-5}	2.25×10^{-3}	1.80×10^{-1}

$$k_2 = 7.75 \times 10^1 \text{ M}^{-1} \text{ s}^{-1}$$
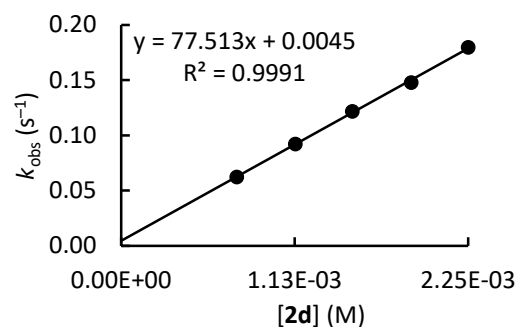
1g + **2d** in CH_2Cl_2 (stopped-flow method, detection at 435 nm) CG627
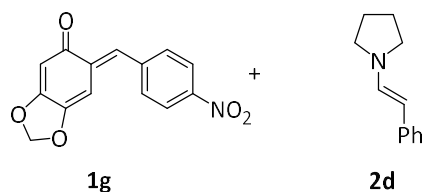
[**1g**]$_0$ (M)	[**2d**]$_0$ (M)	k_{obs} (s^{-1})
4.48×10^{-5}	5.00×10^{-4}	7.18×10^{-2}
4.48×10^{-5}	7.50×10^{-4}	1.09×10^{-1}
4.48×10^{-5}	1.00×10^{-3}	1.37×10^{-1}
4.48×10^{-5}	1.25×10^{-3}	1.71×10^{-1}
4.48×10^{-5}	1.50×10^{-3}	2.06×10^{-1}

$$k_2 = 1.32 \times 10^2 \ M^{-1} \ s^{-1}$$
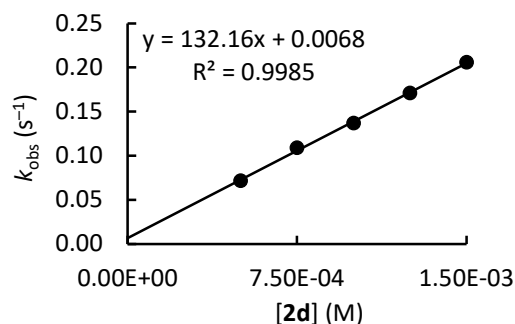
7.4.9. Kinetics of the Reactions of Benzhydrylium Ions with ethyl vinylsulfide and α-azido styrene

Kinetic measurements were performed by harnessing UV/Vis photometry on AppliedPhotophysics SX.20 stopped-flow instruments as well as on a conventional J&M TIDAS diode array spectrophotometer, which was controlled by TIDASDAQ3 (v3) software and connected to a Hellma 661.502-QX quartz Suprasil immersion probe (light path d = 5 mm) via fiber optic cables and standard SMA connectors. The temperature (20.0 ± 0.2 °C) was maintained constant by using circulating bath cryostats. All solutions were prepared by using dry CH_2Cl_2 (Dichloromethane, Sigma-Aldrich, for HPLC, ≥ 99.8%), stirred for two weeks over sulfuric acid (96%), separated, washed and distilled over CaH_2) and kept under an atmosphere of dry nitrogen.

7 + **9a** (generated in solution from Ar_2CH–Cl + 3 equiv. $GaCl_3$) in CH_2Cl_2 (conventional photometry, detection at 512 nm) CG724
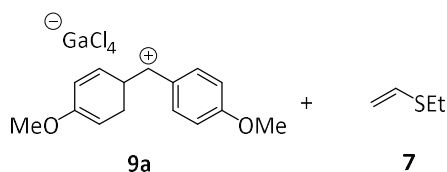
[**9a**]$_0$ (M)	[**7**]$_0$ (M)	k_{obs} (s^{-1})
1.61×10^{-5}	4.84×10^{-5}	1.21×10^{-1}
1.60×10^{-5}	7.99×10^{-5}	1.95×10^{-1}
1.60×10^{-5}	1.20×10^{-4}	2.74×10^{-1}
1.59×10^{-5}	1.43×10^{-4}	3.23×10^{-1}
1.59×10^{-5}	1.59×10^{-4}	3.72×10^{-1}

$$k_2 = 2.20 \times 10^3 \ M^{-1} \ s^{-1}$$
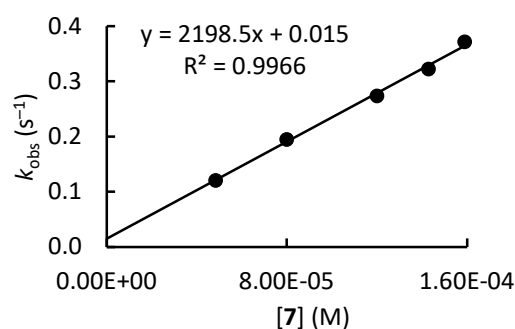
_____

7 + 9b (generated in solution from $Ar_2CH–Cl$ + 3 equiv. $GaCl_3$) in CH_2Cl_2 (conventional photometry, detection at 535 nm) CG723
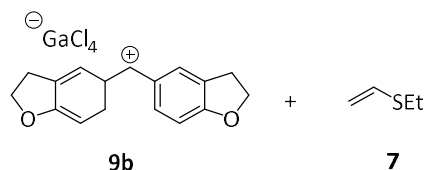
[9b]$_0$ (M)	[7]$_0$ (M)	k_{obs} (s^{-1})
1.52×10^{-5}	1.52×10^{-4}	2.52×10^{-2}
1.54×10^{-5}	2.30×10^{-4}	3.43×10^{-2}
1.53×10^{-5}	3.06×10^{-4}	4.51×10^{-2}
1.53×10^{-5}	3.83×10^{-4}	5.83×10^{-2}
1.52×10^{-5}	4.57×10^{-4}	6.97×10^{-2}

$$k_2 = 1.48 \times 10^2 \text{ M}^{-1} \text{ s}^{-1}$$

y = 148.04x + 0.0013
R^2 = 0.9954
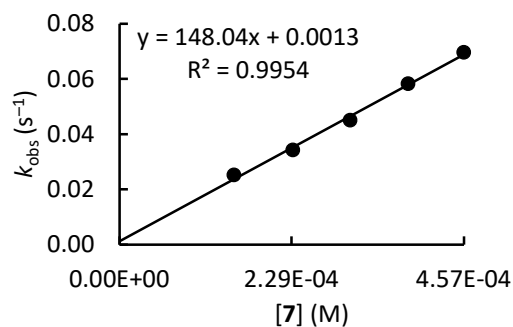
9c + 7 in CH_2Cl_2 (stopped-flow method, detection at 601 nm) CG634
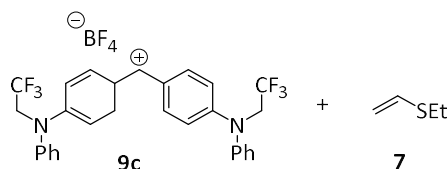
[9c]$_0$ (M)	[7]$_0$ (M)	k_{obs} (s^{-1})
2.62×10^{-6}	5.00×10^{-3}	1.17×10^{-2}
2.30×10^{-6}	7.50×10^{-3}	1.81×10^{-2}
2.22×10^{-6}	1.00×10^{-2}	2.44×10^{-2}
2.14×10^{-6}	1.25×10^{-2}	3.12×10^{-2}
2.07×10^{-6}	1.50×10^{-2}	3.69×10^{-2}

$$k_2 = 2.54 \text{ M}^{-1} \text{ s}^{-1}$$

y = 2.54x - 0.0009
R^2 = 0.9994
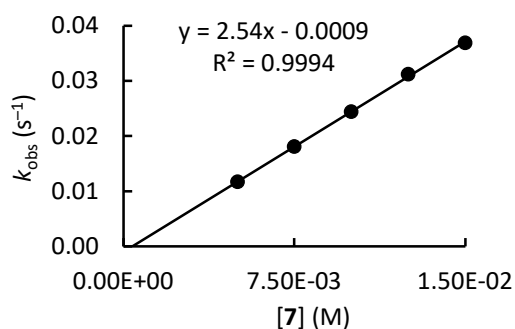
8 + 9b (generated in solution from $Ar_2CH–Cl$ + 3 equiv. $GaCl_3$) in CH_2Cl_2 (conventional photometry, detection at 535 nm) CG725
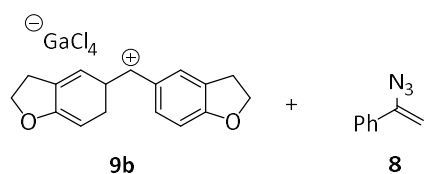
[9b]$_0$ (M)	[8]$_0$ (M)	k_{obs} (s^{-1})
1.37×10^{-5}	4.10×10^{-5}	5.68×10^{-2}
1.36×10^{-5}	6.82×10^{-5}	8.83×10^{-2}
1.37×10^{-5}	1.03×10^{-4}	1.23×10^{-1}
1.37×10^{-5}	1.23×10^{-4}	1.48×10^{-1}
1.37×10^{-5}	1.37×10^{-4}	1.69×10^{-1}

$$k_2 = 1.14 \times 10^3 \text{ M}^{-1} \text{ s}^{-1}$$
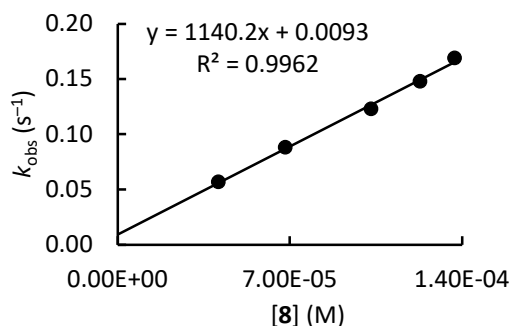
y = 1140.2x + 0.0093
R^2 = 0.9962

_____

9c + **8** in CH_2Cl_2 (stopped-flow method, detection at 601 nm) CG679
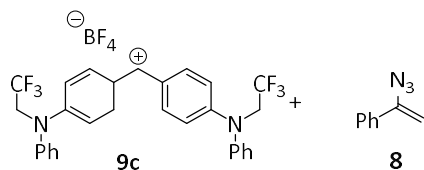
$[\mathbf{9c}]_0$ (M)	$[\mathbf{8}]_0$ (M)	k_{obs} (s^{-1})
3.73×10^{-6}	5.00×10^{-4}	1.29×10^{-2}
3.10×10^{-6}	7.50×10^{-4}	1.90×10^{-2}
3.10×10^{-6}	1.00×10^{-3}	2.33×10^{-2}
3.02×10^{-6}	1.25×10^{-3}	3.03×10^{-2}
2.86×10^{-6}	1.50×10^{-3}	3.65×10^{-2}

$$k_2 = 2.34 \times 10^1 \text{ M}^{-1} \text{ s}^{-1}$$

y = 23.4x + 0.001
R² = 0.9953
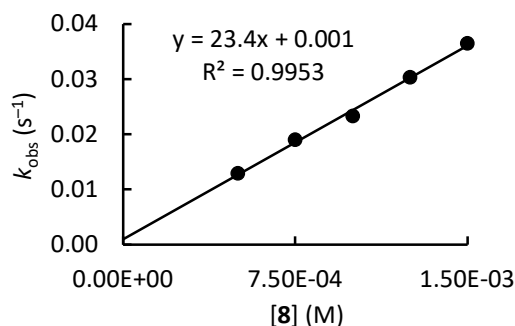
9d + **8** in CH_2Cl_2 (conventional photometry, detection at 593 nm) CG726
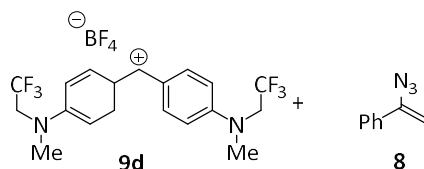
$[\mathbf{9d}]_0$ (M)	$[\mathbf{8}]_0$ (M)	k_{obs} (s^{-1})
1.19×10^{-5}	9.00×10^{-4}	2.70×10^{-3}
1.24×10^{-5}	1.33×10^{-3}	4.01×10^{-3}
1.27×10^{-5}	1.76×10^{-3}	5.10×10^{-3}
1.27×10^{-5}	2.18×10^{-3}	6.25×10^{-3}
1.26×10^{-5}	2.60×10^{-3}	7.21×10^{-3}

$$k_2 = 2.65 \text{ M}^{-1} \text{ s}^{-1}$$

y = 2.65x + 0.0004
R² = 0.9978
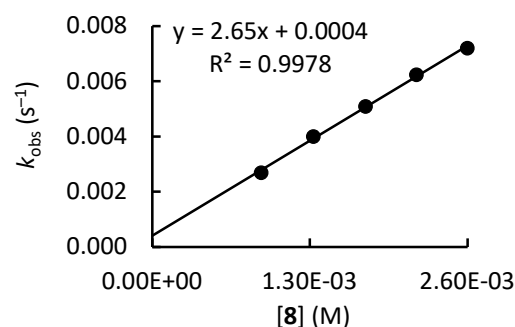
9e + **8** in CH_2Cl_2 (conventional photometry, detection at 674 nm) CG727
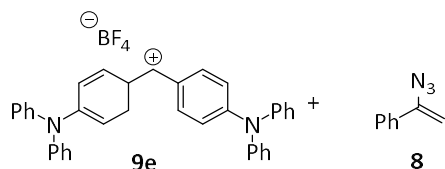
$[\mathbf{9e}]_0$ (M)	$[\mathbf{8}]_0$ (M)	k_{obs} (s^{-1})
1.08×10^{-5}	1.25×10^{-3}	1.92×10^{-3}
1.08×10^{-5}	2.45×10^{-3}	3.45×10^{-3}
1.11×10^{-5}	3.62×10^{-3}	5.08×10^{-3}
1.03×10^{-5}	4.76×10^{-3}	6.57×10^{-3}

$$k_2 = 1.33 \text{ M}^{-1} \text{ s}^{-1}$$
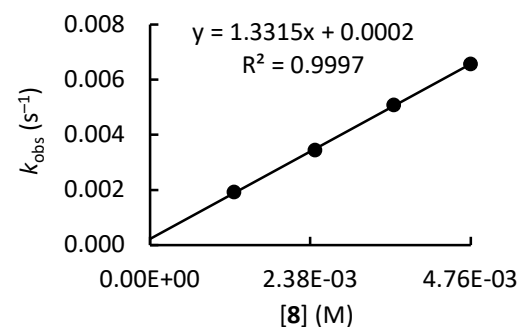
y = 1.3315x + 0.0002
R² = 0.9997

_____

9f + **8** in CH_2Cl_2 (conventional photometry, detection at 620 nm) CG728
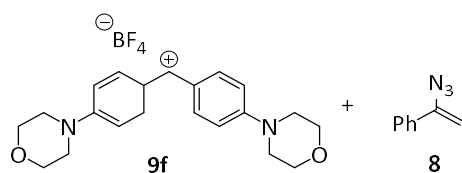
[**9f**]$_0$ (M)	[**8**]$_0$ (M)	k_{obs} (s^{-1})
8.47×10^{-6}	7.94×10^{-4}	8.25×10^{-5}
7.71×10^{-6}	1.22×10^{-3}	1.35×10^{-4}
8.11×10^{-6}	1.63×10^{-3}	1.69×10^{-4}
8.22×10^{-6}	1.87×10^{-3}	1.98×10^{-4}

$$k_2 = 1.05 \times 10^{-1} \text{ M}^{-1} \text{ s}^{-1}$$

_____
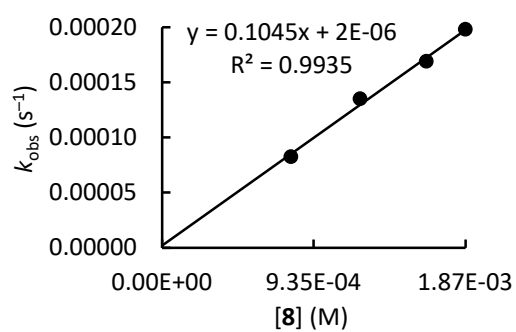
7.4.10. Copies of ^{1}H, ^{13}C and ^{19}F NMR Spectra
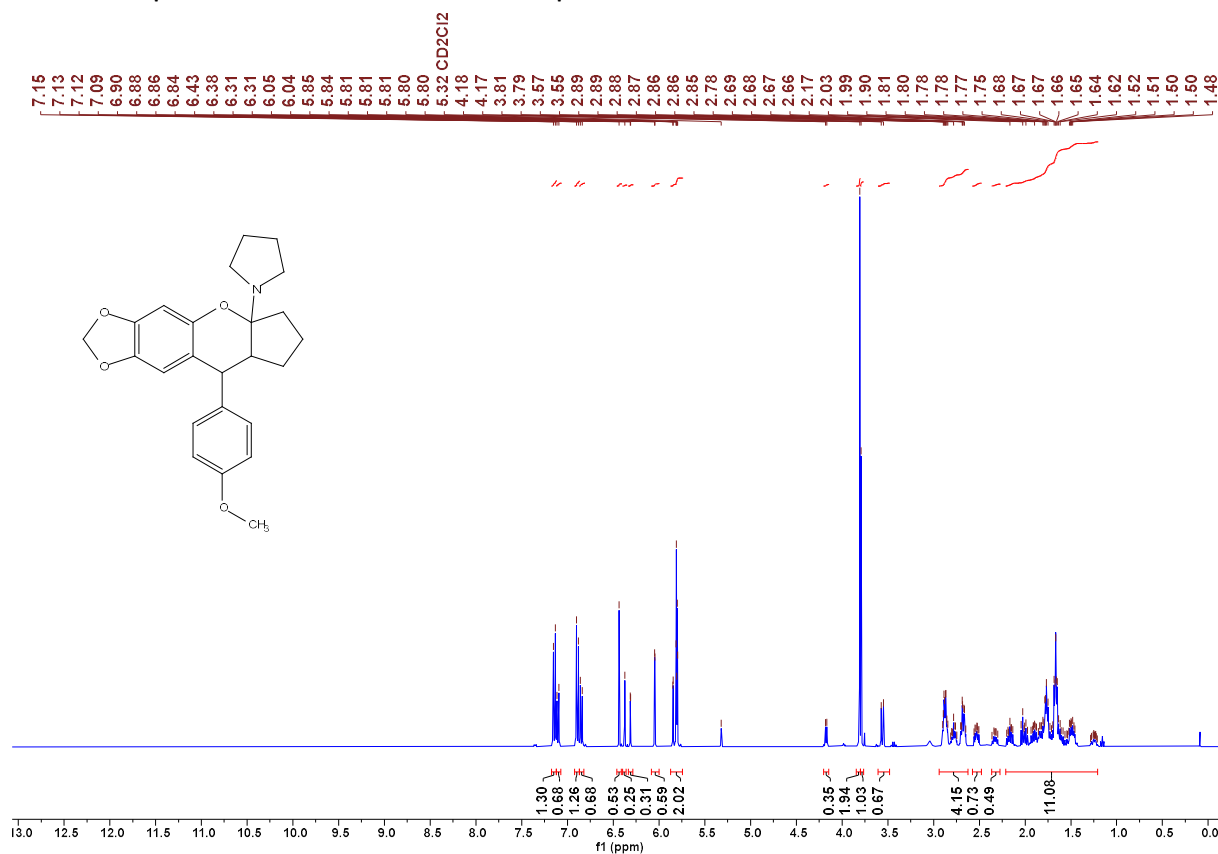
Figure S 11. ^{1}H NMR spectrum of **3aa** in CD$_2$Cl$_2$ (400 MHz) CG421
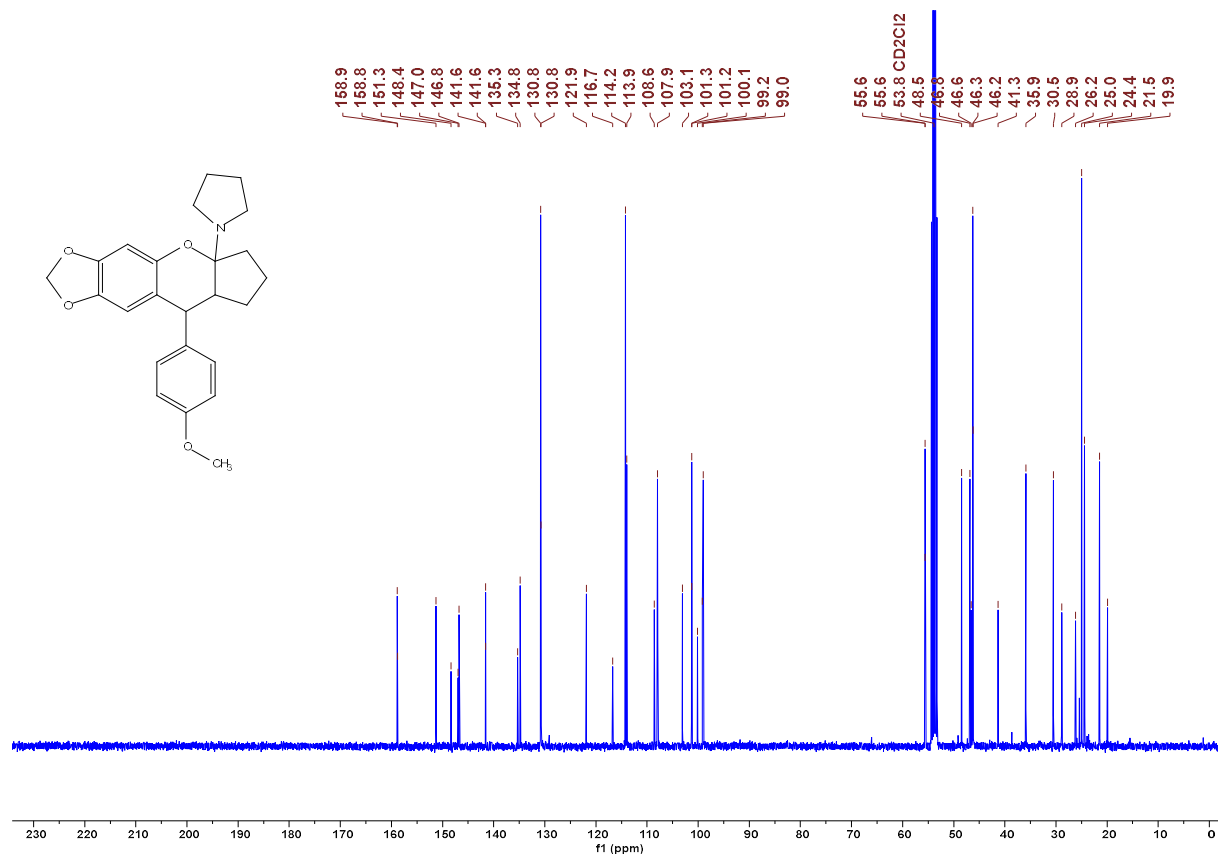
Figure S 12. ^{13}C NMR spectrum of **3aa** in CD$_2$Cl$_2$ (101 MHz) CG421
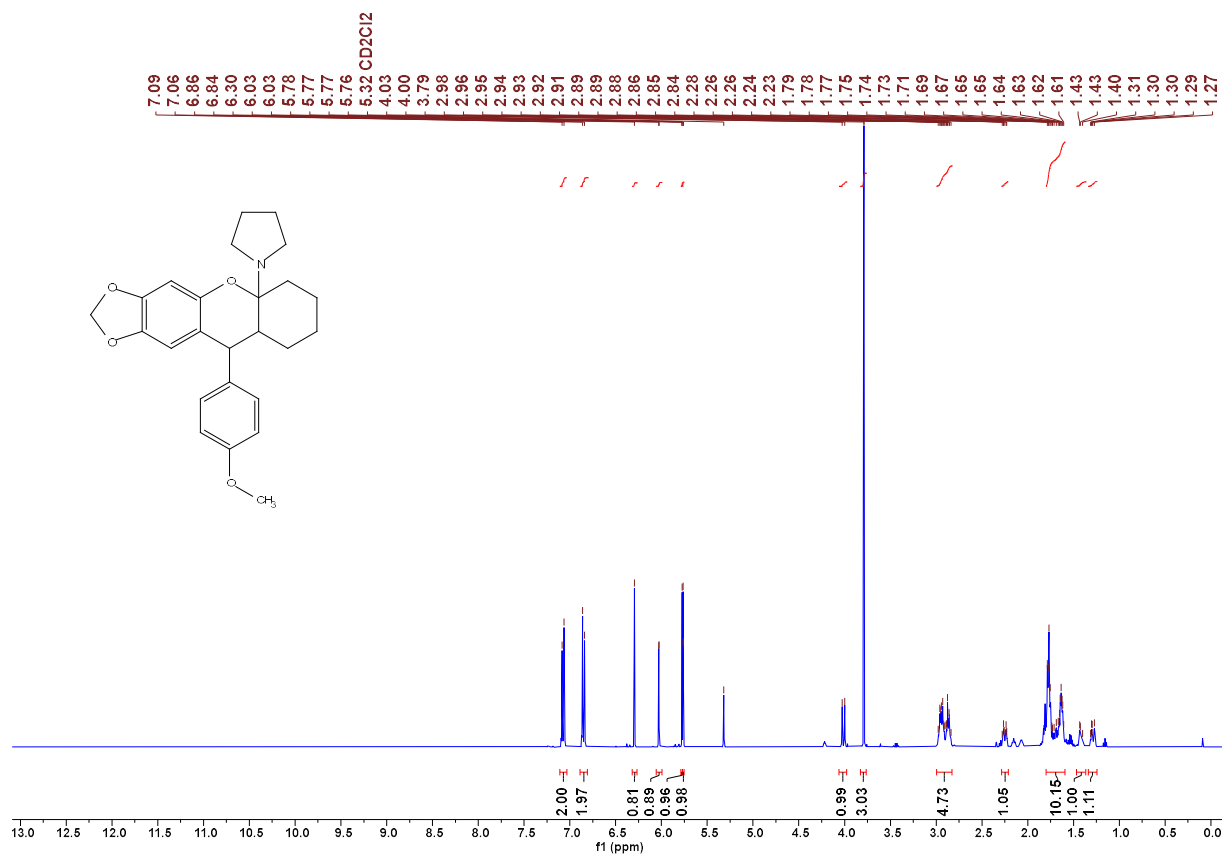
Figure S 13. ^{1}H NMR spectrum of **3ab** in CD$_2$Cl$_2$ (400 MHz) CG422
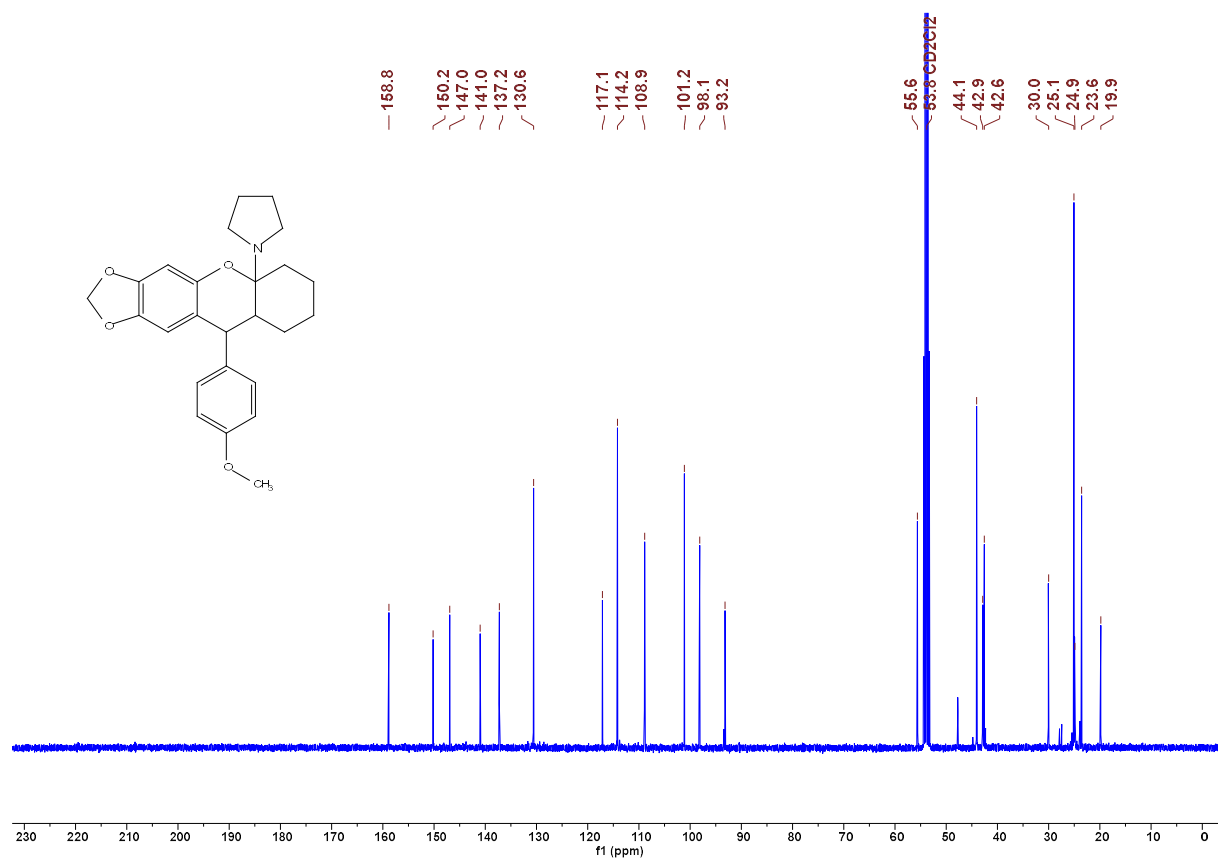
Figure S 14. ^{13}C NMR spectrum of **3ab** in CD$_2$Cl$_2$ (101 MHz) CG422
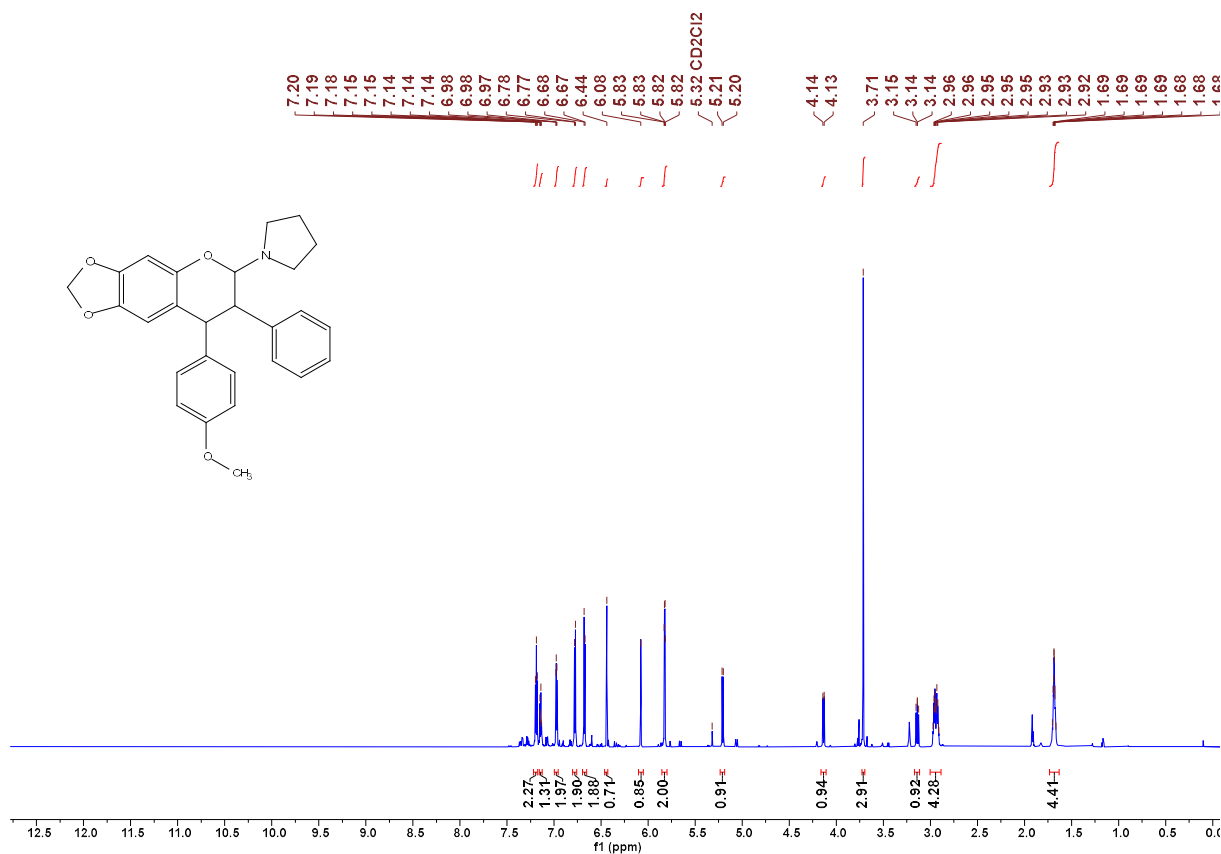
Figure S 15. ^{1}H NMR spectrum of **3ad** in CD$_2$Cl$_2$ (800 MHz) CG430
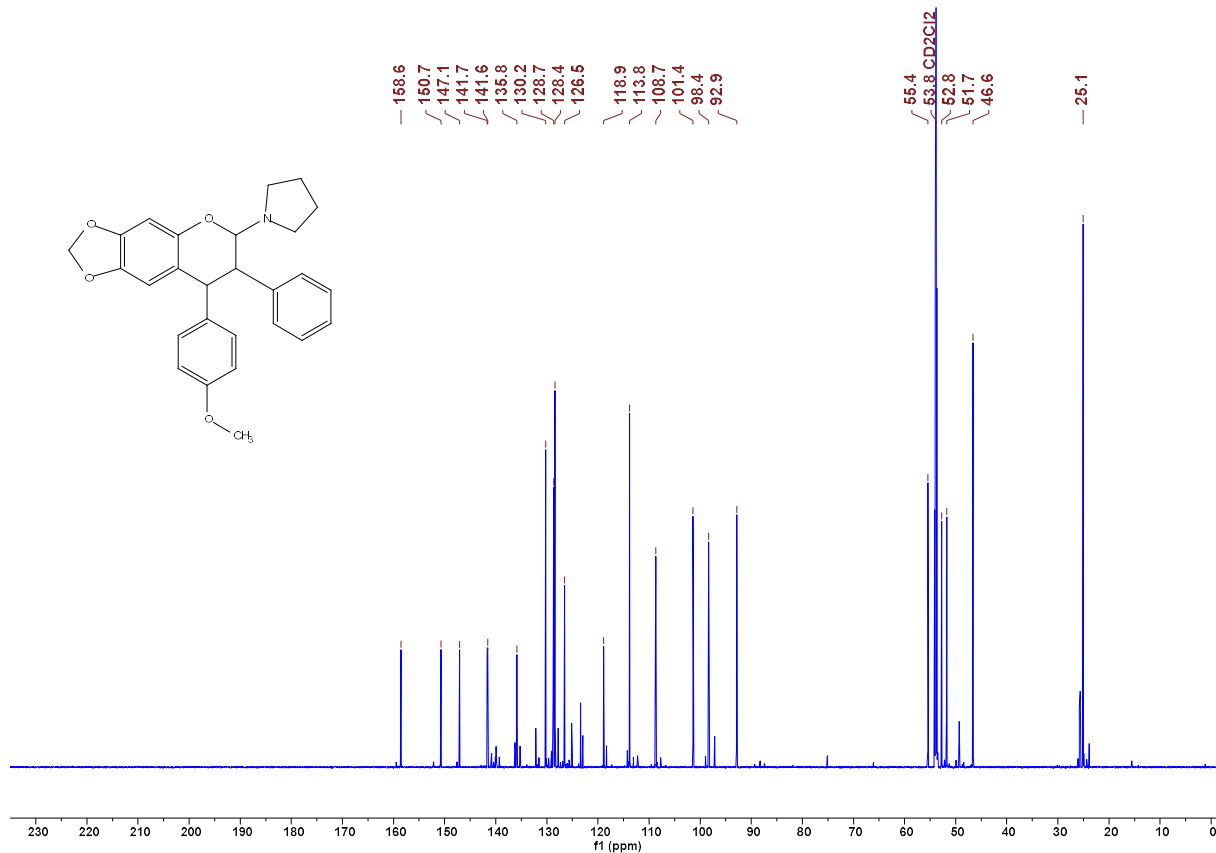
Figure S 16. ^{13}C NMR spectrum of **3ad** in CD$_2$Cl$_2$ (201 MHz) CG430
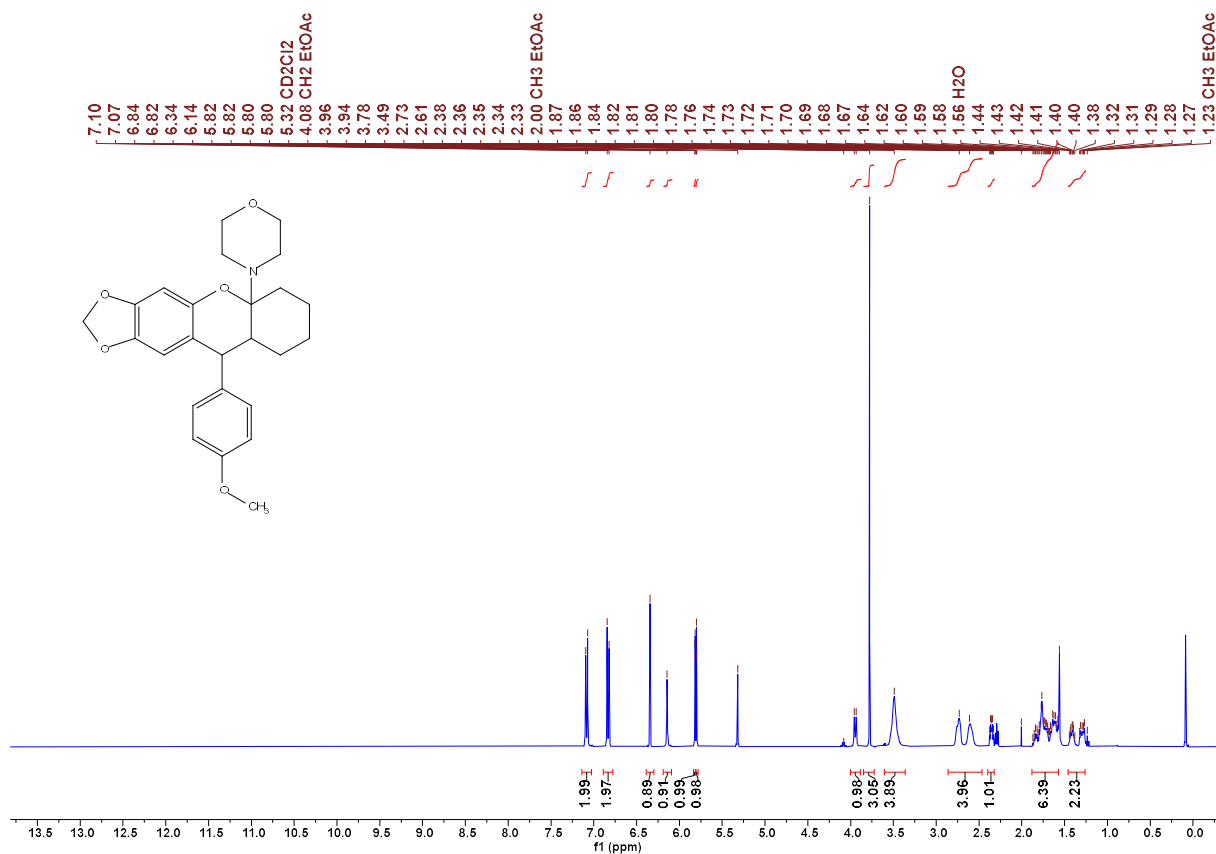
Figure S 17. ^{1}H NMR spectrum of **3ae** (major isomer) in CD$_2$Cl$_2$ (400 MHz) CG712F1
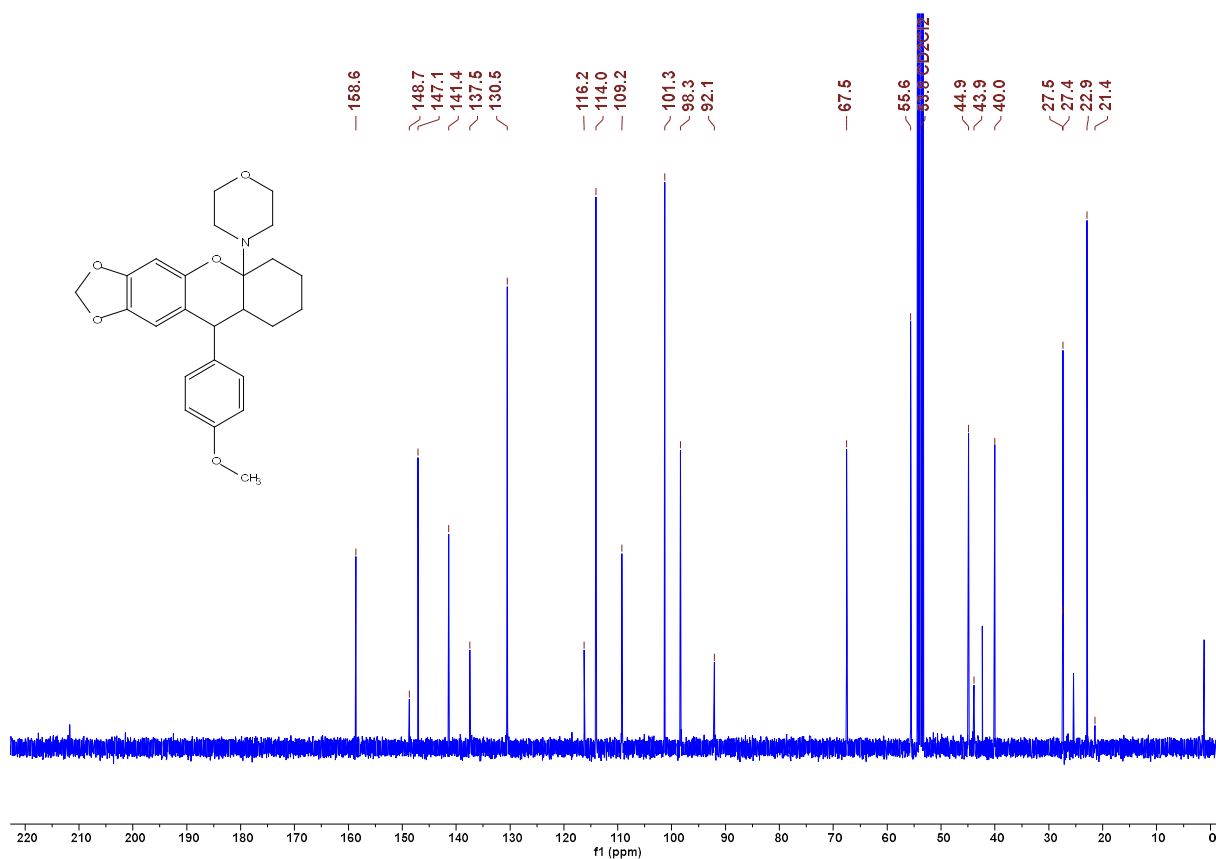
Figure S 18. ^{13}C NMR spectrum of **3ae** (major isomer) in CD$_2$Cl$_2$ (101 MHz) CG712F1
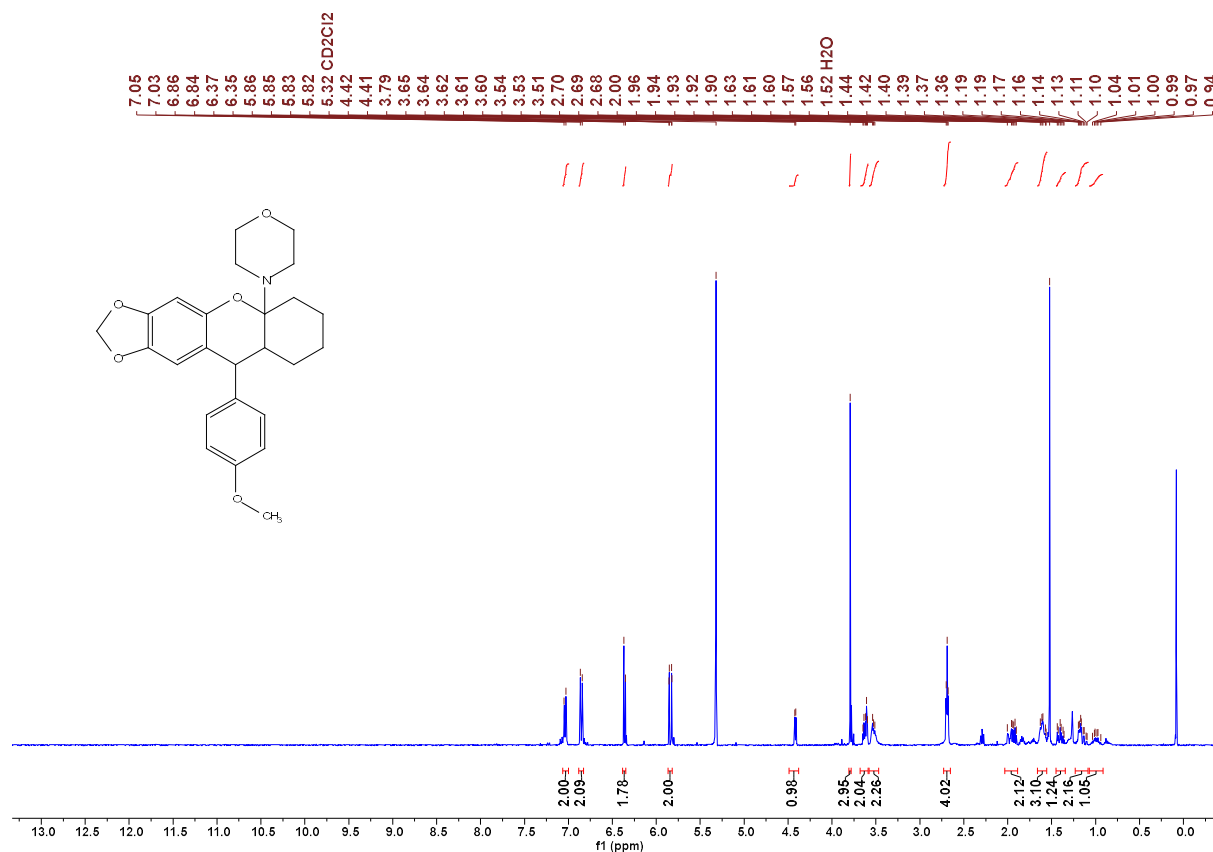
Figure S 19. ^{1}H NMR spectrum of **3ae** (minor isomer) in CD$_2$Cl$_2$ (400 MHz) CG712F2
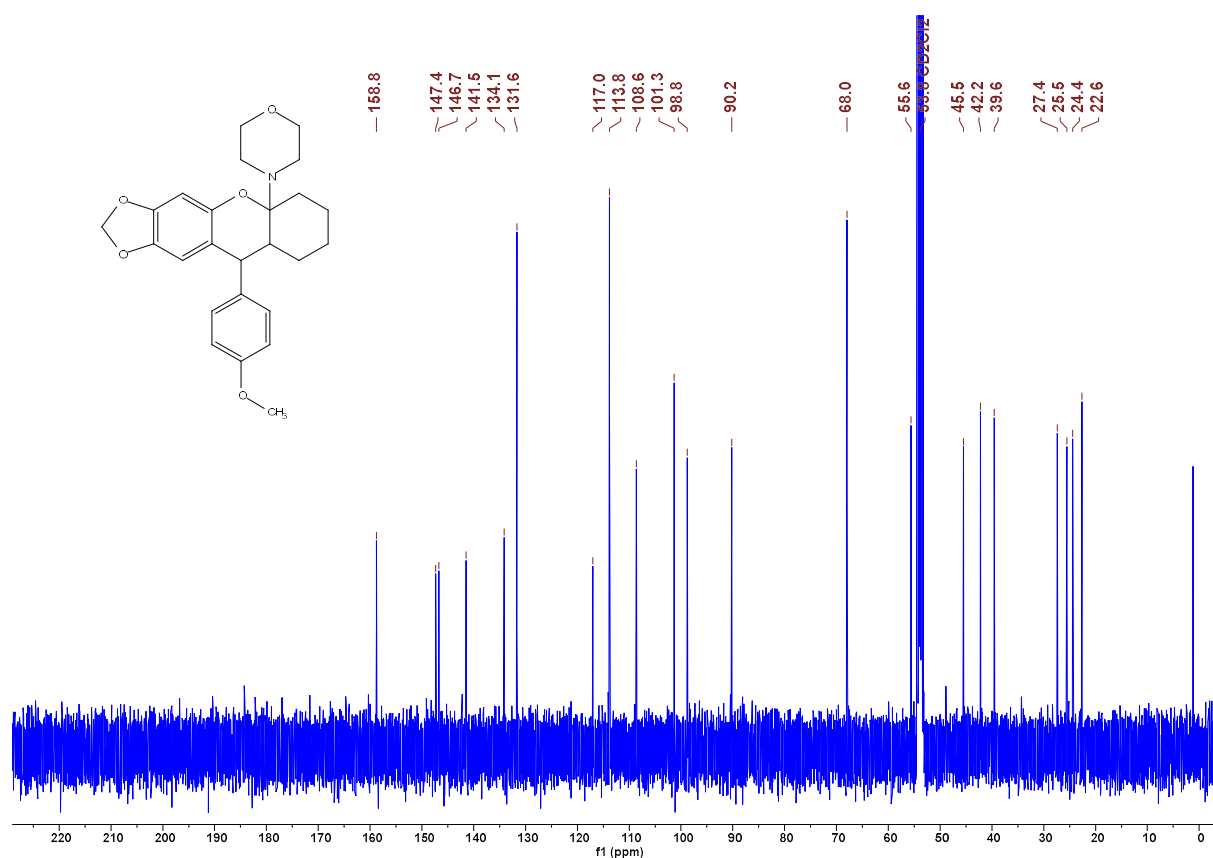
Figure S 20. ^{13}C NMR spectrum of **3ae** (minor isomer) in CD$_2$Cl$_2$ (101 MHz) CG712F2

Figure S 21. ^{1}H NMR spectrum of **3af** in CD$_2$Cl$_2$ (400 MHz) CG289_2

Figure S 22. ^{13}C NMR spectrum of **3af** in CD$_2$Cl$_2$ (101 MHz) CG289_2

Figure S 23. ^{1}H NMR spectrum of **3ag** in CD$_2$Cl$_2$ (400 MHz) CG428

Figure S 24. ^{13}C NMR spectrum of **3ag** in CD$_2$Cl$_2$ (101 MHz) CG428

Figure S 25. ^{1}H NMR spectrum of **3dh** in CD$_2$Cl$_2$ (400 MHz) CG713F1

Figure S 26. ^{13}C NMR spectrum of **3dh** in CD$_2$Cl$_2$ (101 MHz) CG713F1

342

Figure S 27. ^{1}H NMR spectrum of **5aa** in CDCl₃ (400 MHz) CG477_1
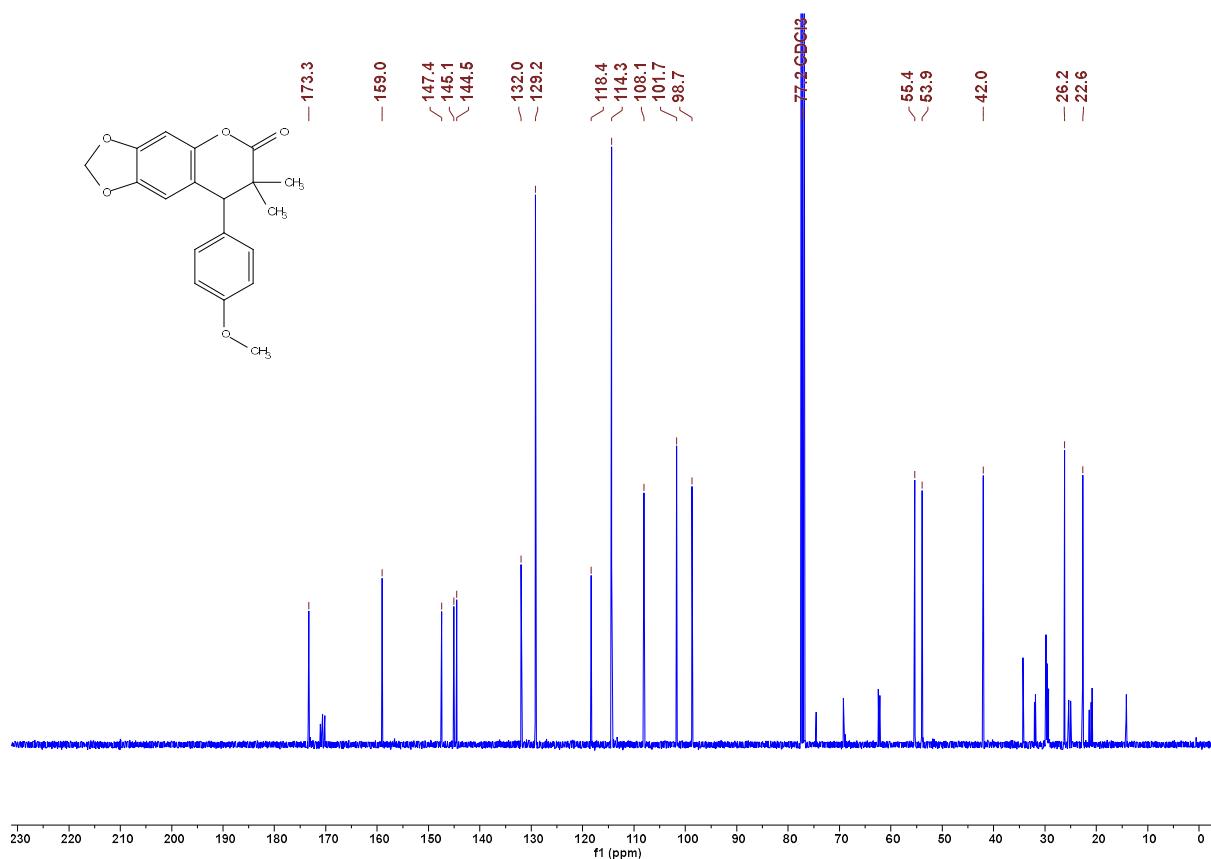
Figure S 28. ^{13}C NMR spectrum of **5aa** in CDCl₃ (101 MHz) CG477_1
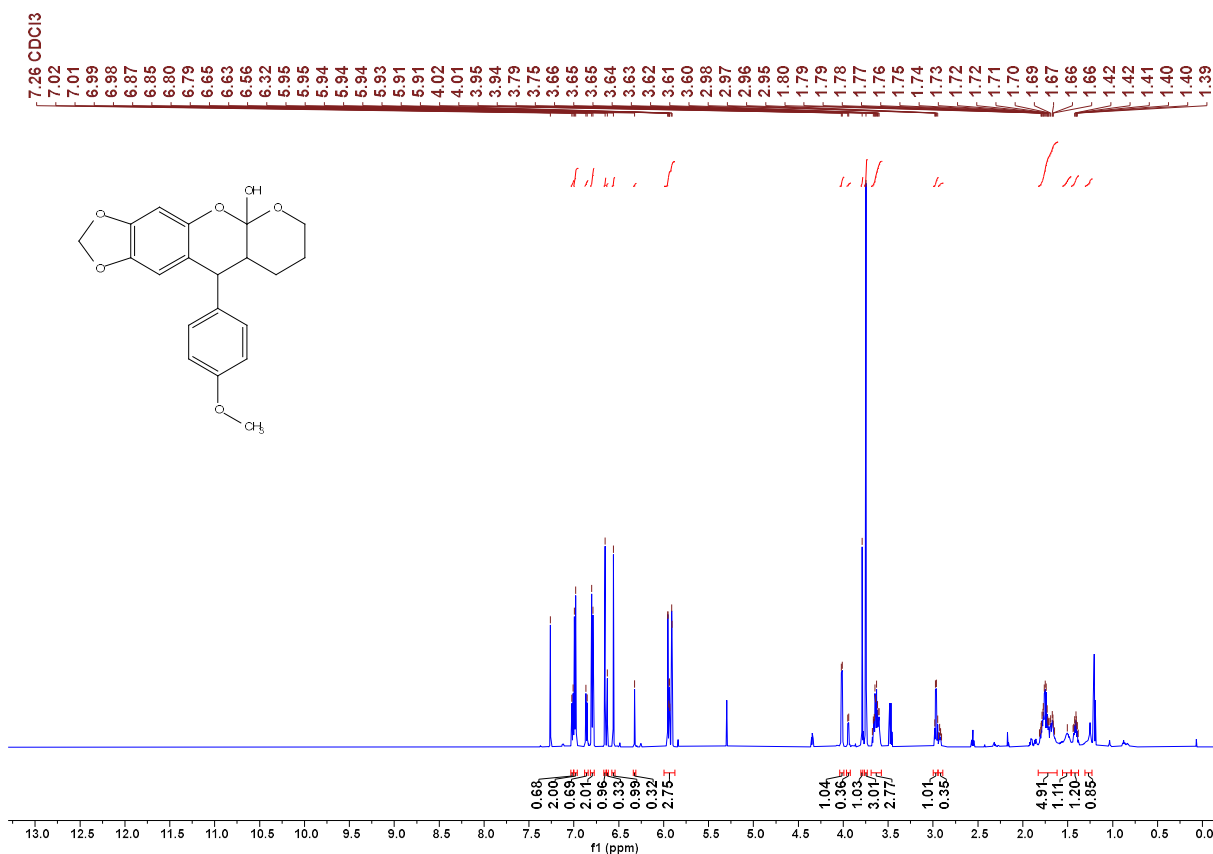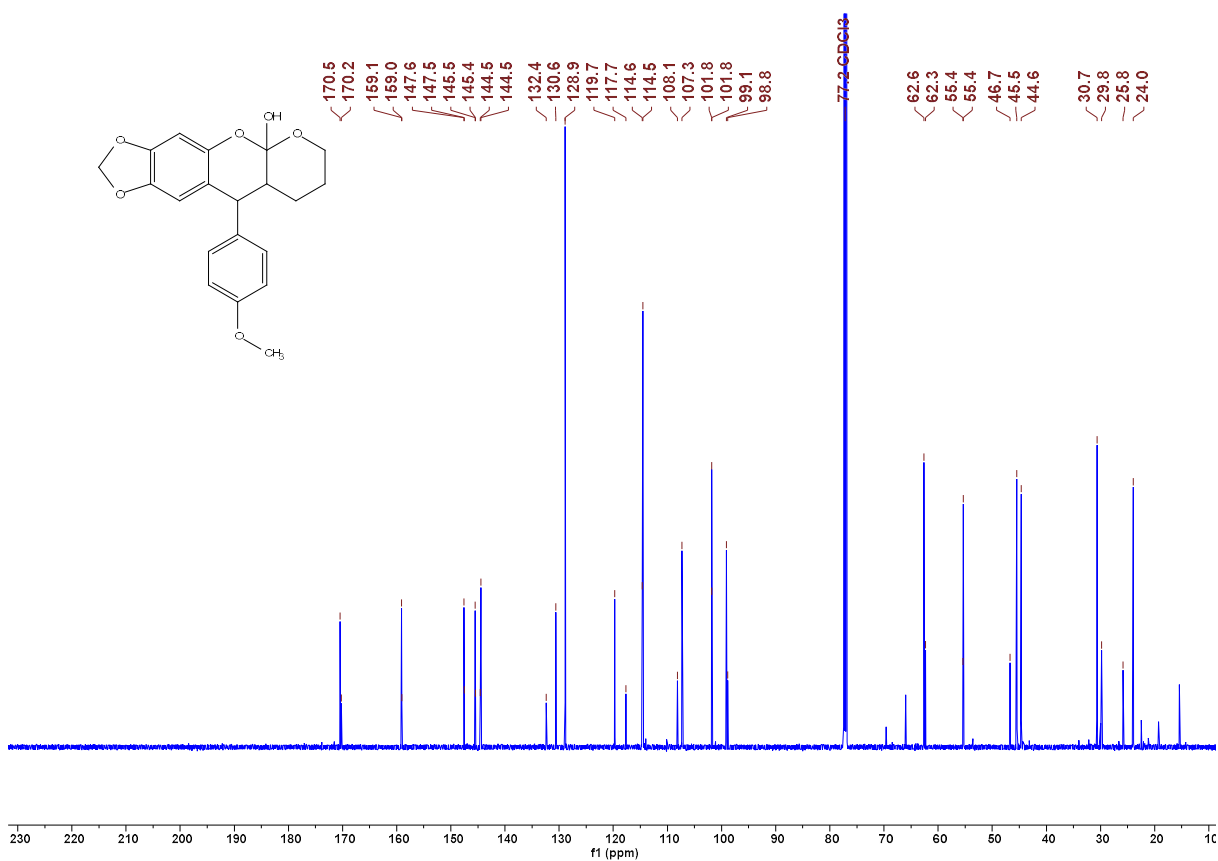
Figure S 29. ^{1}H NMR spectrum of **5ab** in CDCl$_3$ (600 MHz) CG487

Figure S 30. ^{13}C NMR spectrum of **5ab** in CDCl$_3$ (151 MHz) CG487
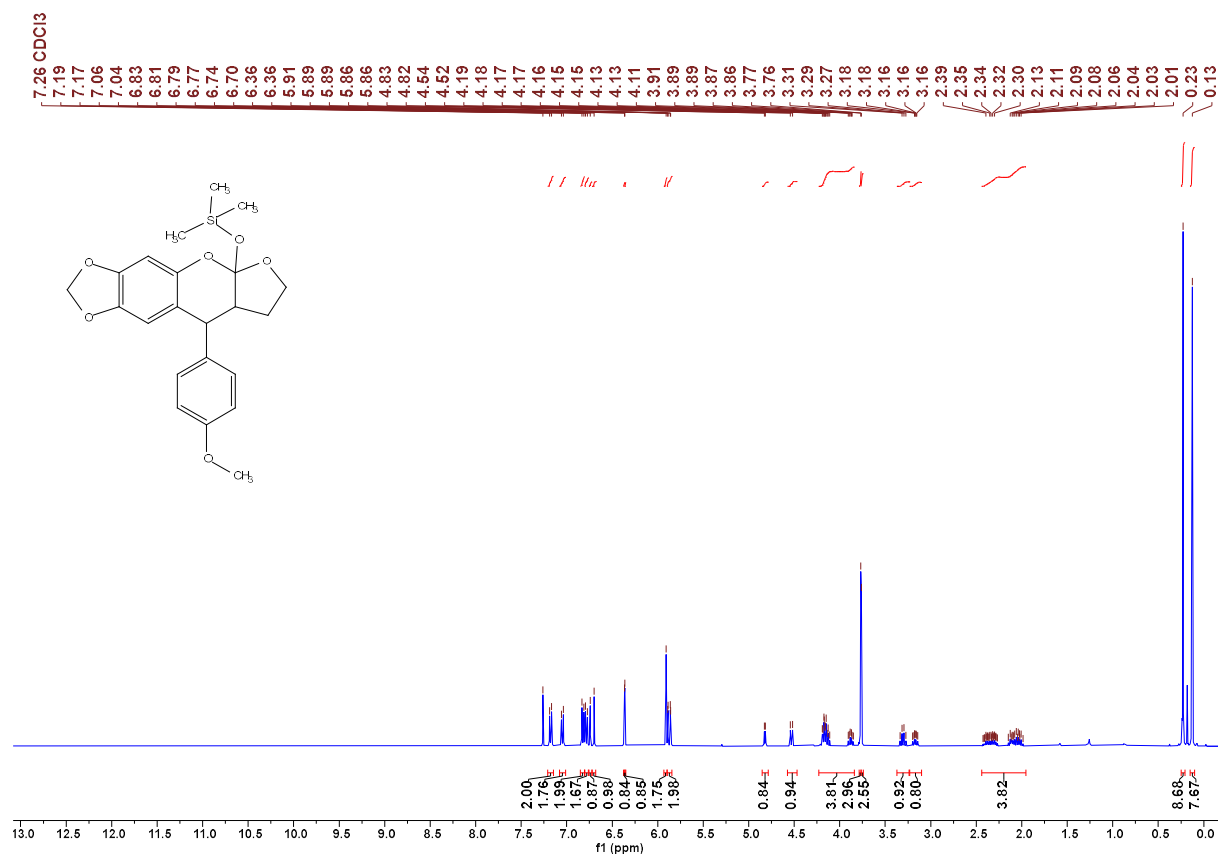
Figure S 31. ^{1}H NMR spectrum of **5ac** in CDCl$_3$ (400 MHz) CG499_1
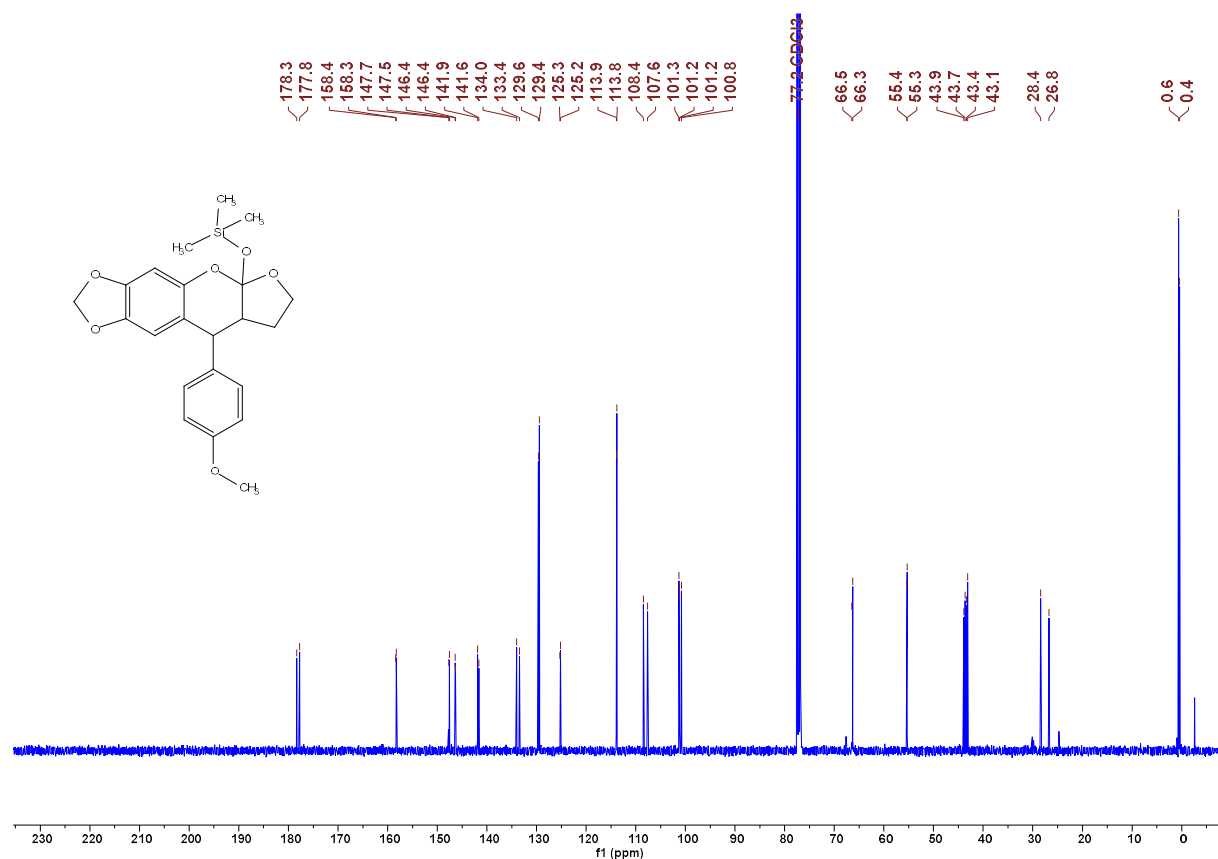

Figure S 32. ^{13}C NMR spectrum of **5ac** in CDCl$_3$ (101 MHz) CG499_1
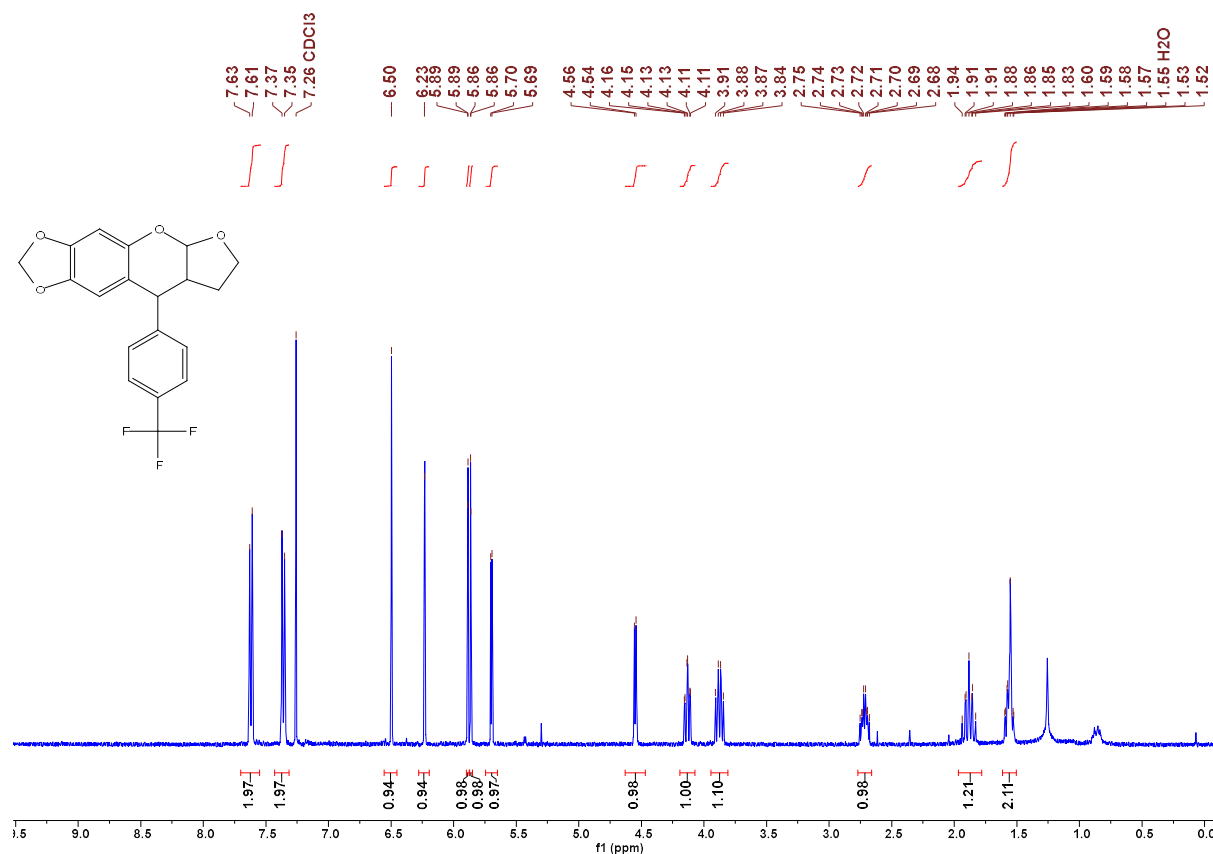
_____

Figure S 33. ^{1}H NMR spectrum of **6'** (major isomer) in CDCl₃ (400 MHz) CG710F2
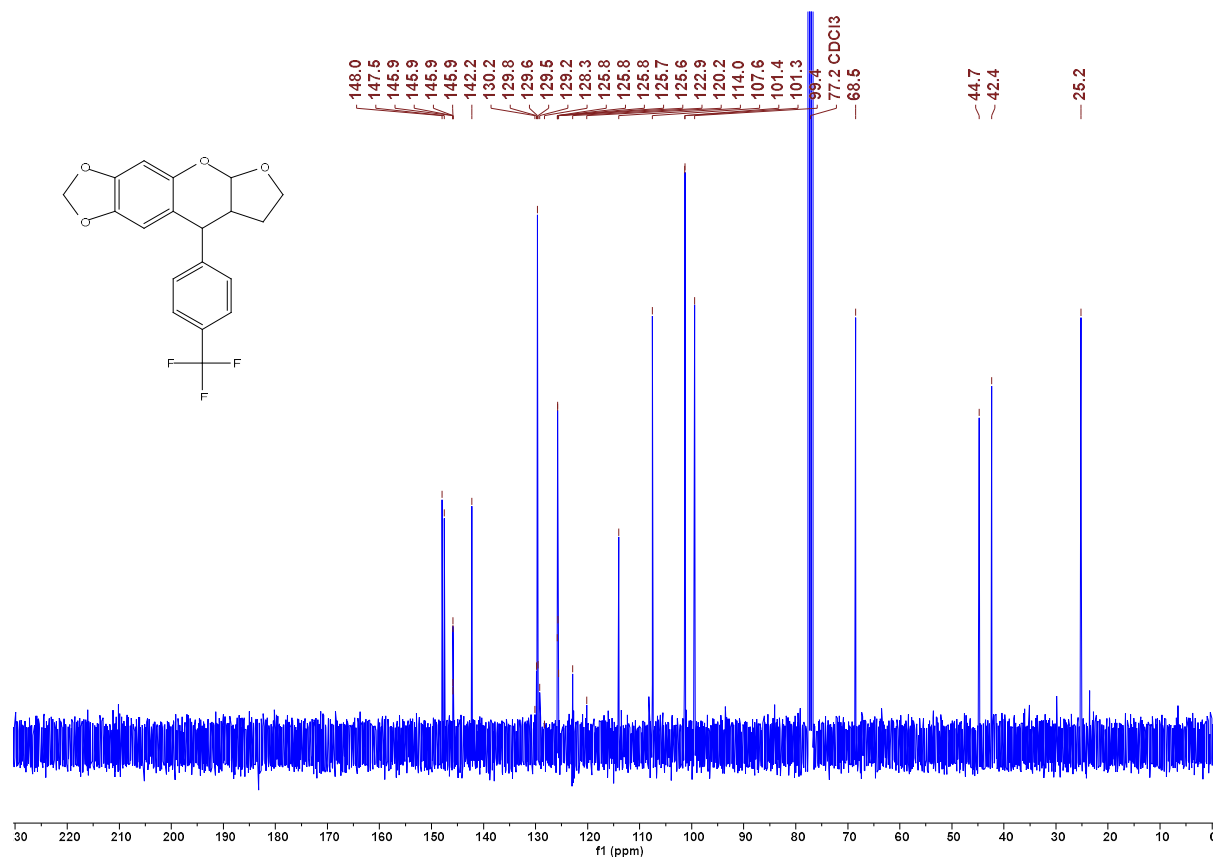

Figure S 34. ^{13}C NMR spectrum of **6'** (major isomer) in CDCl₃ (101 MHz) CG710F2
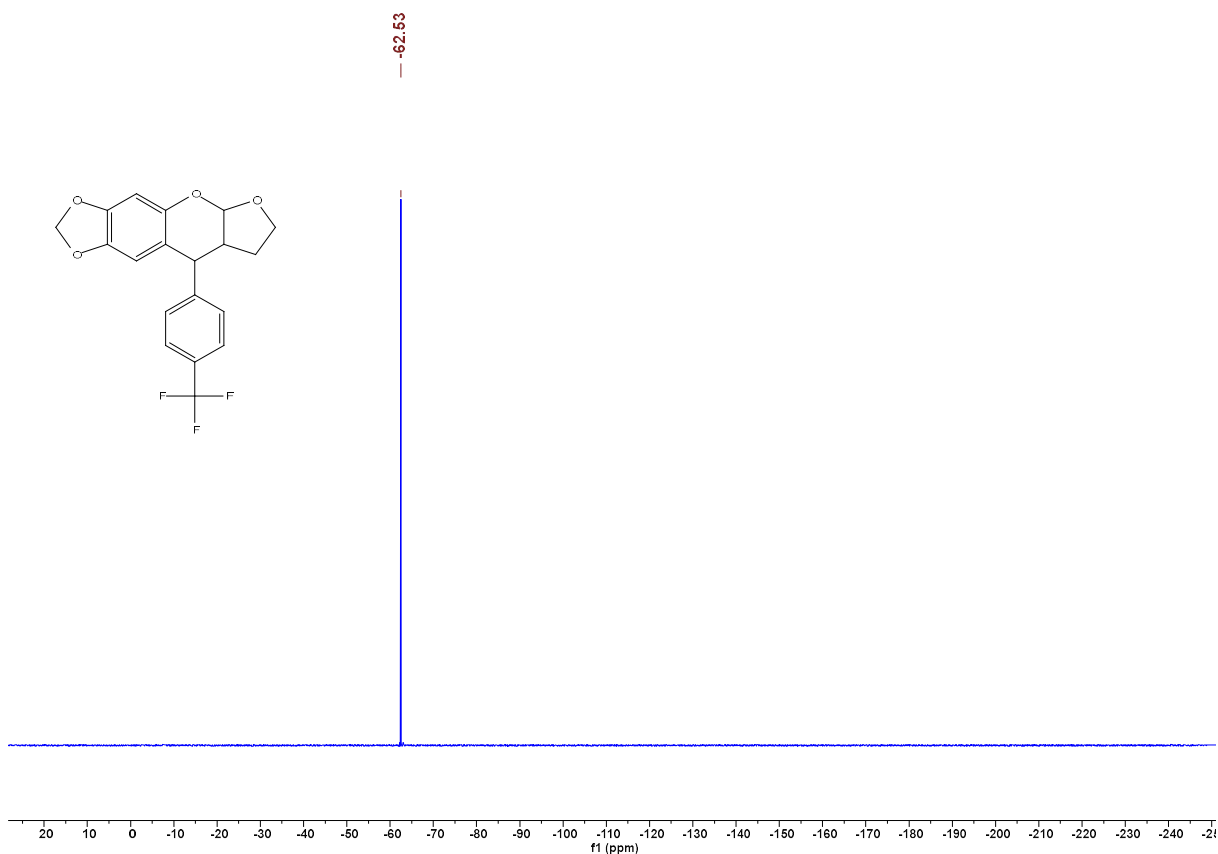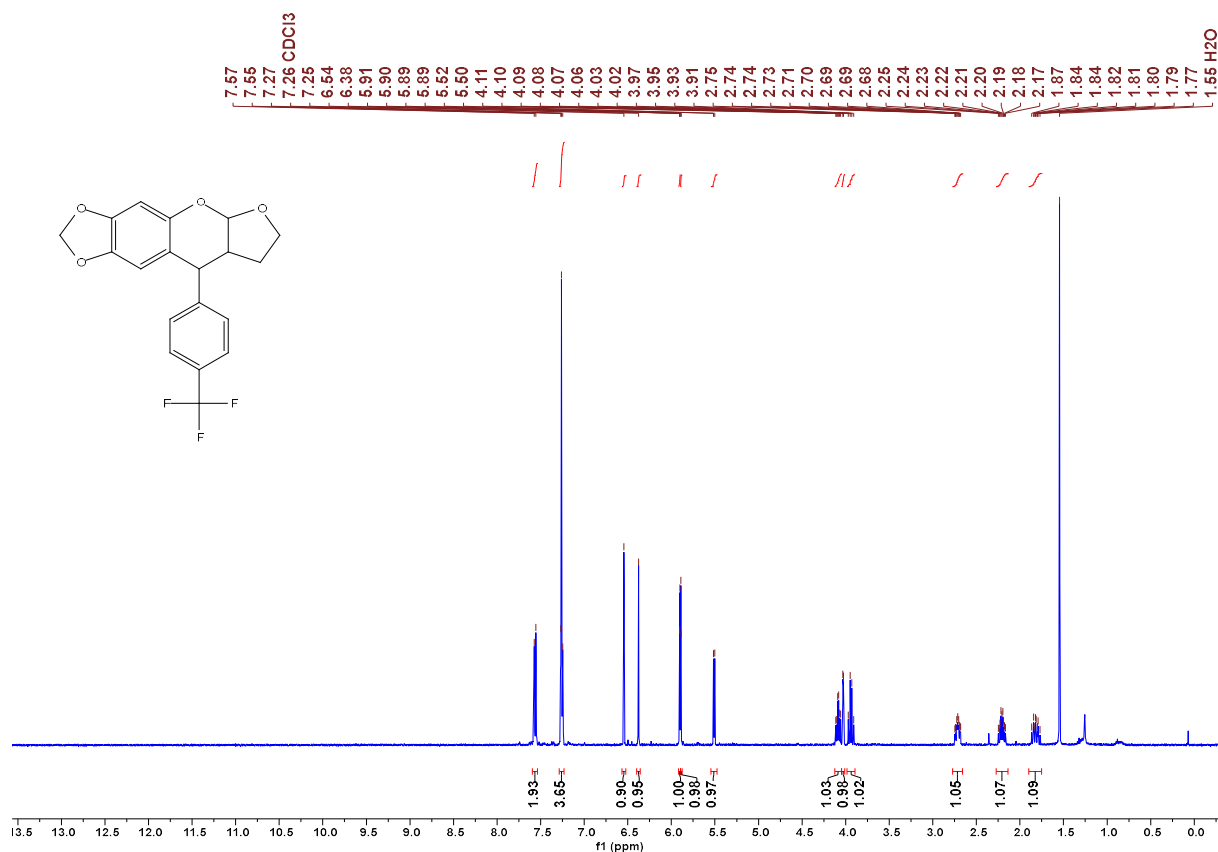
Figure S 35. ^{19}F NMR spectrum of **6'** (major isomer) in CDCl$_3$ (376 MHz) CG710F2

Figure S 36. ^{1}H NMR spectrum of **6'** (minor isomer) in CDCl$_3$ (400 MHz) CG710F3

Figure S 37. ^{13}C NMR spectrum of **6'** (minor isomer) in CDCl$_3$ (101 MHz) CG710F3

Figure S 38. ^{19}F NMR spectrum of **6'** (minor isomer) in CDCl$_3$ (376 MHz) CG710F3

_____
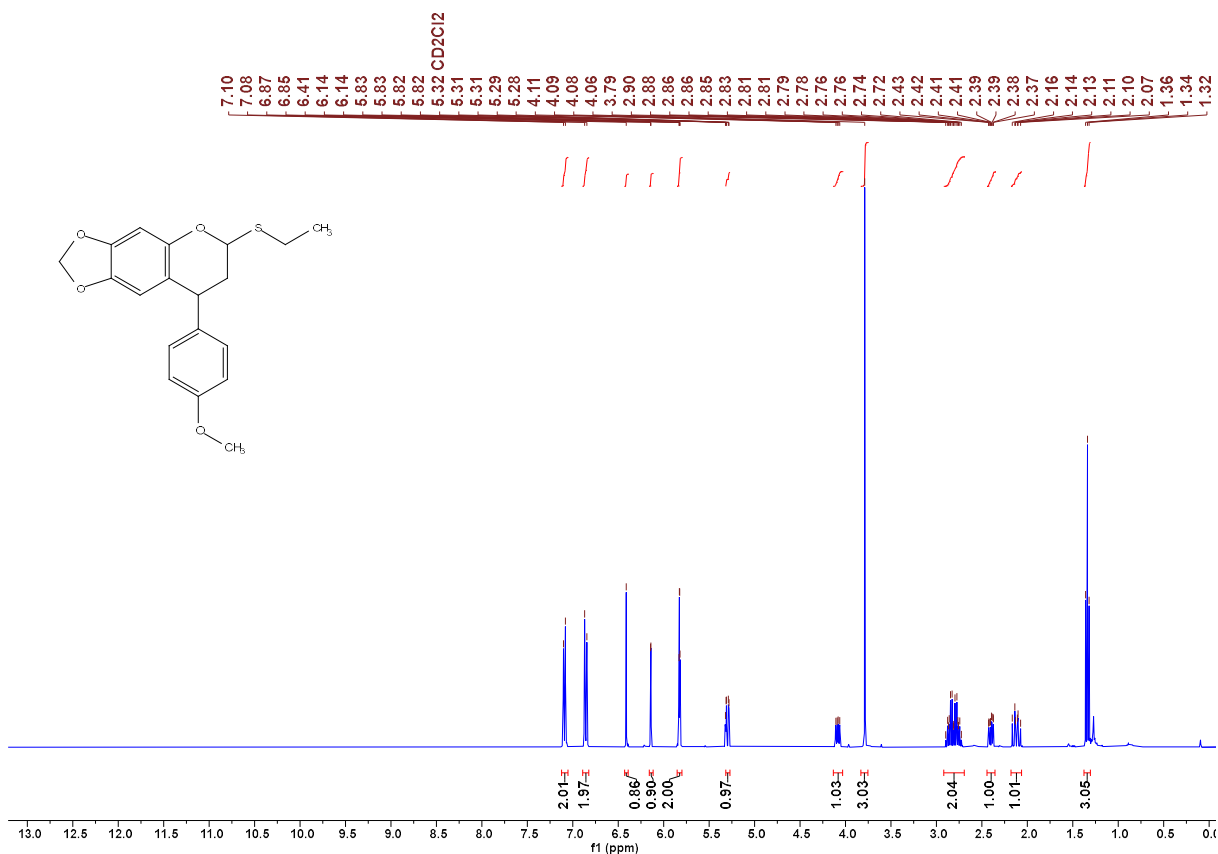
Figure S 39. ^{1}H NMR spectrum of **7'** in CD$_2$Cl$_2$ (400 MHz) CG618
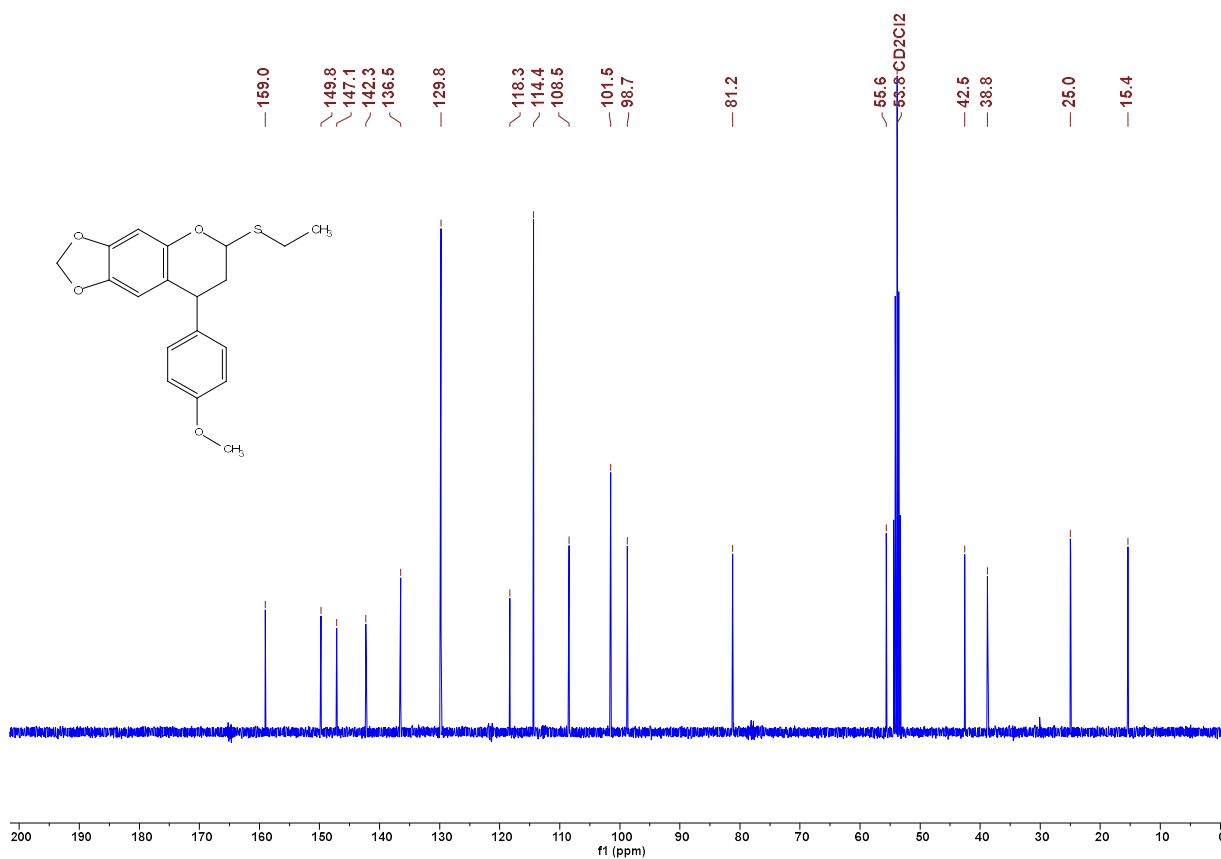
Figure S 40. ^{13}C NMR spectrum of **7'** in CD$_2$Cl$_2$ (101 MHz) CG618

349

_____

Figure S 41. ^{1}H NMR spectrum of **8'** in CDCl$_3$ (600 MHz) CG680F3

Figure S 42. ^{13}C NMR spectrum of **8'** in CDCl$_3$ (101 MHz) CG680F3
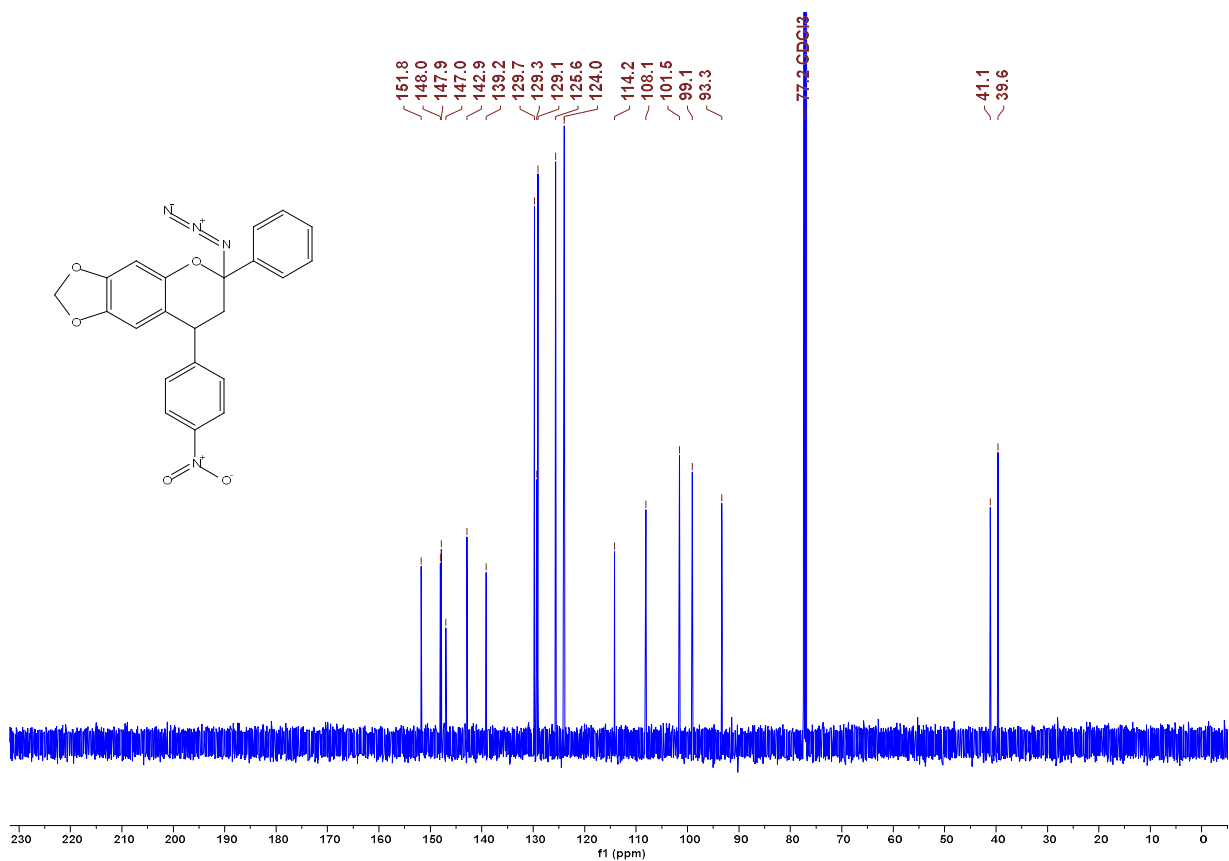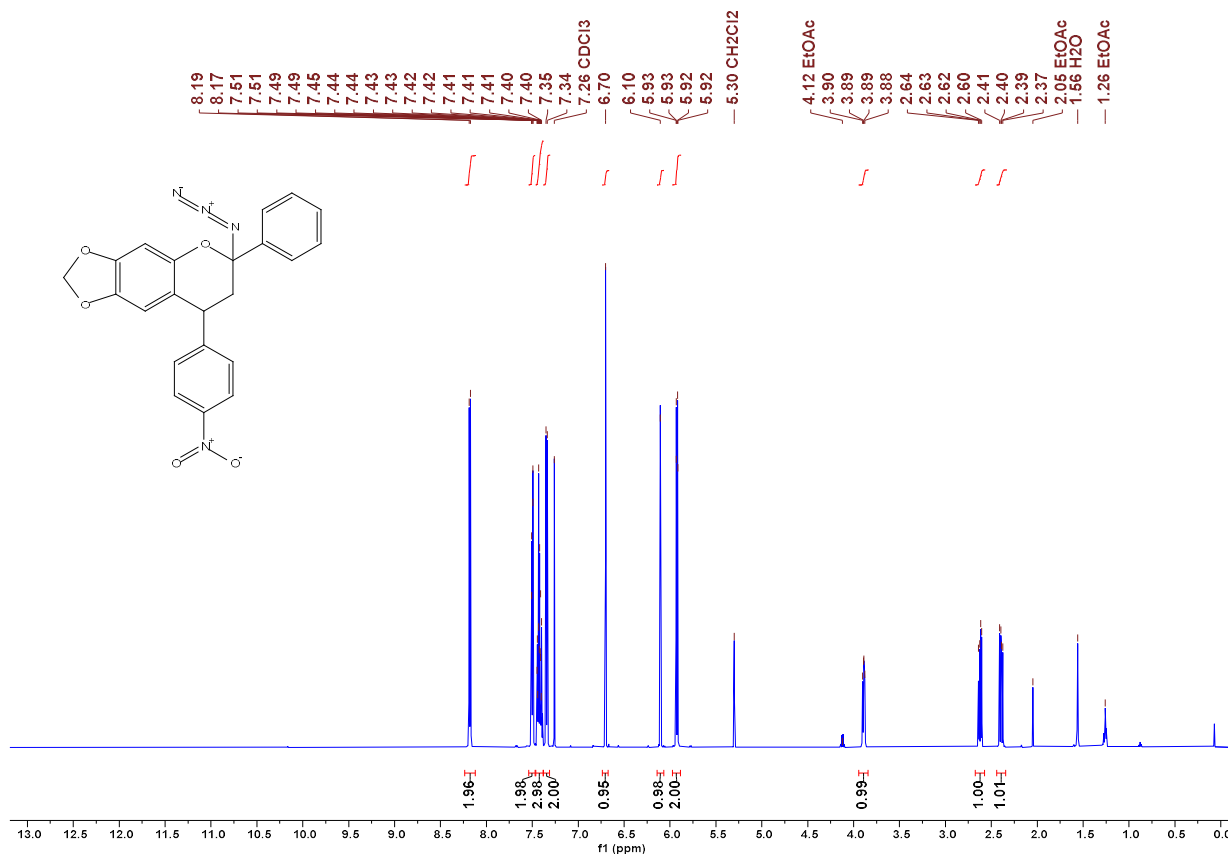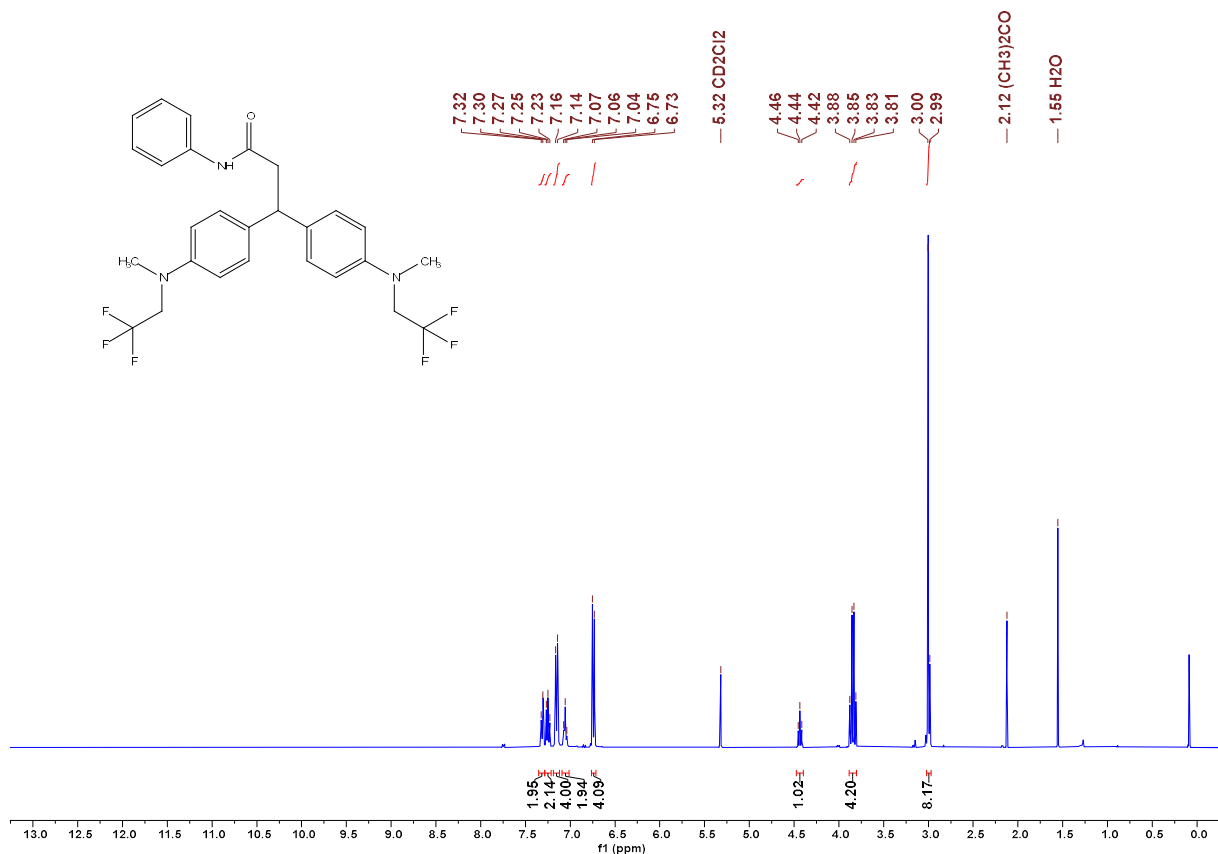
Figure S 43. ^{1}H NMR spectrum of **10** in CD$_2$Cl$_2$ (400 MHz) CG734_1
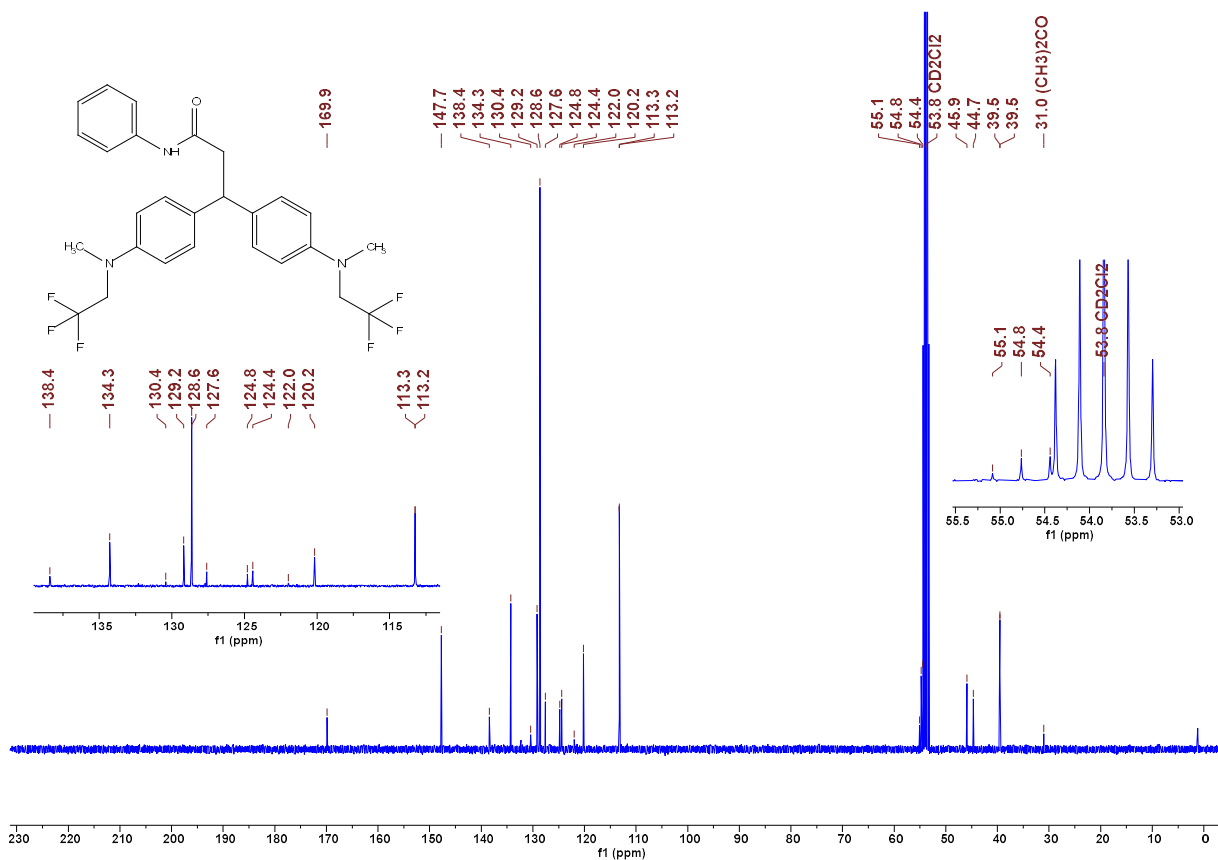
Figure S 44. ^{13}C NMR spectrum of **10** in CD$_2$Cl$_2$ (101 MHz) CG734_1
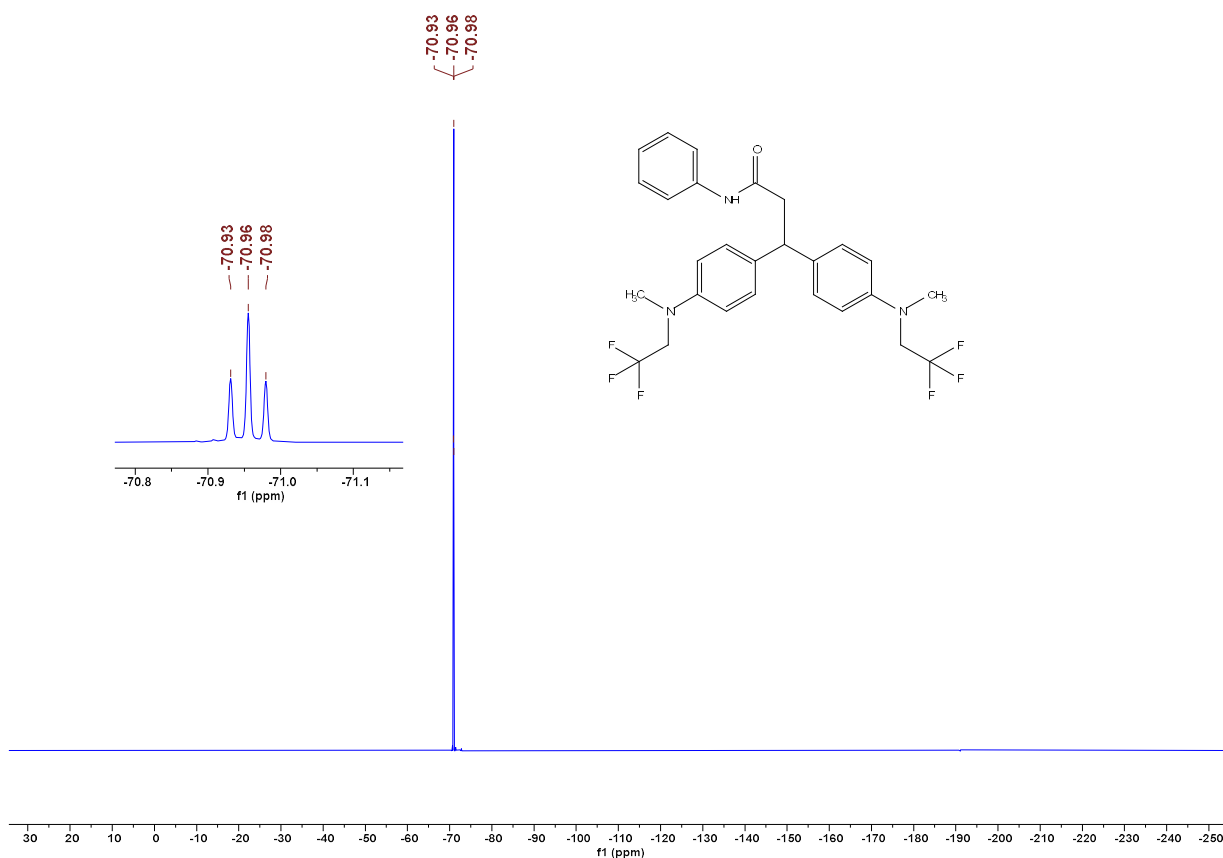
_____

Figure S 45. ^{19}F NMR spectrum of **10** in CD$_2$Cl$_2$ (376 MHz) CG734_1

7.5. References

[1]   a) S. Kobayashi, K. A. Jørgensen, *Cycloaddition reactions in organic synthesis*, Wiley-VCH, Weinheim, **2002**; b) S. Ma (Ed.) *Handbook of cyclization reactions*, Wiley-VCH, Weinheim, **2010**; c) J. A. Berson, *Tetrahedron* **1992**, *48*, 3; d) O. Diels, K. Alder, *Justus Liebigs Ann. Chem.* **1928**, *460*, 98.

[2]   a) K. C. Nicolaou, S. A. Snyder, T. Montagnon, G. Vassilikogiannakis, *Angew. Chem. Int. Ed.* **2002**, *41*, 1668; b) K.-I. Takao, R. Munakata, K. Tadano, *Chem. Rev.* **2005**, *105*, 4779; c) H. Oikawa, T. Tokiwano, *Nat. Prod. Rep.* **2004**, *21*, 321; d) A. A. Sara, U.-F. Um-e-Farwa, A. Saeed, M. Kalesse, *Synthesis* **2022**, *54*, 975; e) A. Rana, A. Mishra, S. K. Awasthi, *RSC Adv.* **2025**, *15*, 4496; f) T. J. Yeingst, A. M. Helton, D. J. Hayes, *Macromol. Biosci.* **2024**, *24*, e2400274; g) N. Zydziak, B. Yameen, C. Barner-Kowollik, *Polym. Chem.* **2013**, *4*, 4072; h) S. Munirasu, J. Albuerne, A. Boschetti-de-Fierro, V. Abetz, *Macromol. Rapid Commun.* **2010**, *31*, 574.

[3]   a) R. Hoffmann, R. B. Woodward, *J. Am. Chem. Soc.* **1965**, *87*, 2046; b) R. Hoffmann, R. B. Woodward, *Acc. Chem. Res.* **1968**, *1*, 17; c) R. B. Woodward, R. Hoffmann, *Angew. Chem. Int. Ed. Engl.* **1969**, *8*, 781.

[4]   a) V. Branchadell, J. Font, A. G. Moglioni, C. Ochoa de Echagüen, A. Oliva, R. M. Ortuño, J. Veciana, J. Vidal-Gancedo, *J. Am. Chem. Soc.* **1997**, *119*, 9992; b) M. Bobrowski, A. Liwo, S. Ołdziej, D. Jeziorek, T. Ossowski, *J. Am. Chem. Soc.* **2000**, *122*, 8112; c) S. Lakhdar, F. Terrier, D. Vichard, G. Berionni, N. El Guesmi, R. Goumont, T. Boubaker, *Chem. Eur. J.* **2010**, *16*, 5681.d) M. Linder, T. Brinck, *J. Org. Chem.* **2012**, *77*, 6563; e) M. Linder, A. J. Johansson, T. Brinck, *Org. Lett.* **2012**, *14*, 118; f) R. Jasiński, *Symmetry* **2021**, *13*, 1911.

[5]   K. N. Houk, *Acc. Chem. Res.* **1975**, *8*, 361.

[6]   S. B. Needleman, M. C. Chang Kuo, *Chem. Rev.* **1962**, *62*, 405.

[7]   a) D. L. Boger, *Chem. Rev.* **1986**, *86*, 781; b) K. A. Jørgensen, *Eur. J. Org. Chem.* **2004**, *2004*, 2093; c) H. Waldmann, *Synthesis* **1994**, *1994*, 535; d) H. Pellissier, *Tetrahedron* **2009**, *65*, 2839; e) K. A. Jørgensen, *Angew. Chem. Int. Ed.* **2000**, *39*, 3558.

[8]   J. Sauer, R. Sustmann, *Angew. Chem. Int. Ed. Engl.* **1980**, *19*, 779.

[9]   a) Z. M. Png, H. Zeng, Q. Ye, J. Xu, *Chem. Asian J.* **2017**, *12*, 2142; b) M. Xie, L. Lin, X. Feng, *Chem. Rec.* **2017**, *17*, 1184; c) A. Pałasz, *Top. Curr. Chem.* **2016**, *374*, 24; d) X. Jiang, R. Wang, *Chem. Rev.* **2013**, *113*, 5515; e) V. Laina-Martín, J. A. Fernández-Salas, J. Alemán, *Chem. Eur. J.* **2021**, *27*, 12509; f) J. Zhang, V. Shukla, D. L. Boger, *J. Org. Chem.* **2019**, *84*, 9397.

[10]   S. E. Rokita, *Quinone methides*, Wiley, Hoboken, N.J, **2009**.

[11]   W.-J. Bai, J. G. David, Z.-G. Feng, M. G. Weaver, K.-L. Wu, T. R. R. Pettus, *Acc. Chem. Res.* **2014**, *47*, 3655.

[12]   a) V. A. Osyanin, A. V. Lukashenko, D. V. Osipov, *Russ. Chem. Rev.* **2021**, *90*, 324; b) K. Tanaka, K. Ueno, Y. Tanaka, N. Ohtsuka, Y. Asada, M. Kishimoto, S. Sunaga, Y. Hoshino, K. Honda, *Synlett* **2020**, *31*, 1197; c) V. A. Nuraini, V. Falasca, D. S. Wenholz, D. S. Black, N. Kumar, *RSC Adv.* **2025**, *15*, 2912. d) A. Arduini, A. Pochini, R. Ungaro, P. Domiano, *J. Chem. Soc., Perkin Trans. 1* **1986**, 1391; e) L. Jurd, *Tetrahedron* **1977**, *33*, 163.

[13]   a) H. Mayr, M. Patz, *Angew. Chem. Int. Ed. Engl.* **1994**, *33*, 938; *Angew. Chem.* **1994**, *106*, 990; b) C. L. Perrin, I. Agranat, A. Bagno, S. E. Braslavsky, P. A. Fernandes, J.-F. Gal, G. C. Lloyd-Jones, H. Mayr, J. R. Murdoch, N. S. Nudelman, L. Radom, Z. Rappaport, M.-F. Ruasse, H.-U. Siehl, Y. Takeuchi, T. T. Tidwell, E. Uggerud, I. H. Williams *Pure Appl. Chem.* **2022**, *94*, 353.

[14]   Reactivity parameters *E*, *N* and s_N can be retrieved at https://www.cup.lmu.de/oc/mayr/reaktionsdatenbank2/, which is a freely accessible website (accessed on 28/06/2025)

[15]   a) H. Mayr, A. R. Ofial, *J. Phys. Org. Chem.* **2008**, *21*, 584; b) H. Mayr, A. R. Ofial, *Pure Appl. Chem.* **2005**, *77*, 1807; c) H. Mayr, *Tetrahedron* **2015**, *71*, 5095.

[16]   H. Mayr, B. Kempf, A. R. Ofial, *Acc. Chem. Res.* **2003**, *36*, 66.

[17]   a) W. v. E. Doering, W. R. Roth, R. Breuckmann, L. Figge, H.-W. Lennartz, W.-D. Fessner, H. Prinzbach, *Chem. Ber.* **1988**, *121*, 1; b) M. Hartnagel, K. Grimm, H. Mayr, *Liebigs Ann.* **1997**, *1997*, 71; c) H. Mayr, A. R. Ofial, J. Sauer, B. Schmied, *Eur. J. Org. Chem.* **2000**, *2000*, 2013; d) C. Fichtner, H. Mayr, *J. Chem. Soc., Perkin Trans. 2* **2002**, 1441; c) D. S. Allgäuer, P. Mayer, H. Mayr, *J. Am. Chem. Soc.* **2013**, *135*, 15216.

[18]   H. Jangra, Q. Chen, E. Fuks, I. Zenz, P. Mayer, A. R. Ofial, H. Zipse, H. Mayr, *J. Am. Chem. Soc.* **2018**, *140*, 16758.

[19]   L. Li, R. J. Mayer, A. R. Ofial, H. Mayr, *J. Am. Chem. Soc.* **2023**, *145*, 7416.

[20]   C. Gross, A. Eitzinger, N. Hampel, P. Mayer, A. R. Ofial, *Chem. Eur. J.* **2025**, *31*, e202403785.

[21]   H. Mayr, T. Bug, M. F. Gotta, N. Hering, B. Irrgang, B. Janker, B. Kempf, R. Loos, A. R. Ofial, G. Remennikov, H. Schimmel, *J. Am. Chem. Soc.* **2001**, *123*, 9500.

[22]   B. Kempf, N. Hampel, A. R. Ofial, H. Mayr, *Chem. Eur. J.* **2003**, *9*, 2209.

[23]   D. S. Timofeeva, R. J. Mayer, P. Mayer, A. R. Ofial, H. Mayr, *Chem. Eur. J.* **2018**, *24*, 5901.

[24]   M. J. Hensinger, A. Eitzinger, O. Trapp, A. R. Ofial, *Chem. Eur. J.* **2024**, *30*, e202302764.

[25]   R. W. van de Water, T. R. Pettus, *Tetrahedron* **2002**, *58*, 5367.

[26]   a) L. M. Stephenson, D. E. Smith, S. P. Current, *J. Org. Chem.* **1982**, *47*, 4170; b) A. Arrieta, F. P. Cossío, B. Lecea, *J. Org. Chem.* **2001**, *66*, 6178.

[27]   a) A. Arduini, A. Bosi, A. Pochini, R. Ungaro, *Tetrahedron* **1985**, *41*, 3095; b) T. Inoue, S. Inoue, K. Sato, *Bull. Chem. Soc. Jpn.* **1990**, *63*, 1062; c) K. Akkarasereenon, K. Tangdenpaisal, S. Ruchirawat, P. Ploypradith, *Org. Biomol. Chem.* **2020**, *18*, 8854.

[28]   a) M. Karplus, *J. Chem. Phys.* **1959**, *30*, 11; b) M. Karplus, *J. Am. Chem. Soc.* **1963**, *85*, 2870; c) H. Friebolin, *Ein- und zweidimensionale NMR-Spektroskopie. Eine Einführung*, Wiley-VCH, Weinheim, **2013**.

[29]   L. Jurd, *J. Heterocycl. Chem.* **1988**, *25*, 89.

[30]   H. Wang, Y. Wang, K.-L. Han, X.-J. Peng, *J. Org. Chem.* **2005**, *70*, 4910.

[31]   R. Breslow, *Acc. Chem. Res.* **1991**, *24*, 159.

[32]   M. F. Ruiz-Lopez, X. Assfeld, J. I. Garcia, J. A. Mayoral, L. Salvatella, *J. Am. Chem. Soc.* **1993**, *115*, 8780.

[33]   C. Reichardt, T. Welton, *Solvents and solvent effects in organic chemistry*, Wiley-VCH, Weinheim, **2011**.

[34]   X. Guo, H. Mayr, *J. Am. Chem. Soc.* **2013**, *135*, 12377.

[35]   K. J. Laidler, *Pure Appl. Chem.* **1996**, *68*, 149.

[36]   Y. F. Wong, Z. Wang, W.-X. Hong, J. Sun, *Tetrahedron* **2016**, *72*, 2748.

[37]   C. D. Bray, *Org. Biomol. Chem.* **2008**, *6*, 2815.

[38]   a) A. k. Shaikh, A. J. A. Cobb, G. Varvounis, *Org. Lett.* **2012**, *14*, 584; b) A. F. Barrero, J. F. Quílez del Moral, M. Mar Herrador, P. Arteaga, M. Cortés, J. Benites, A. Rosellón, *Tetrahedron* **2006**, *62*, 6012.

[39]   N. Thirupathi, C.-H. Tung, Z. Xu, *Adv. Synth.Catal.* **2018**, *360*, 3585.

[40]   Y.-F. Wang, M. Hu, H. Hayashi, B. Xing, S. Chiba, *Org. Lett.* **2016**, *18*, 992.

[41]   H. Jawale, S. Mistry, C. Conder, P. G. Wenthold, *J. Org. Chem.* **2022**, *87*, 985.

[42]   J. Ruiz Aranzaes, M.-C. Daniel, D. Astruc, *Can. J. Chem*., **2006**, *84*, 288.

[43]   *SAINT*, Bruker AXS Inc., Madison, Wisconsin, USA, **2012**.

[44]   Sheldrick, G. M., SADABS, University of Göttingen (Germany), **1996**.

[45]   G. M. Sheldrick, *Acta Cryst.* **2015**, *A71*, 3.

[46]   L. J. Farrugia, *J. Appl. Cryst.*, **2012**, *45*, 849.

Chapter 8. Conclusion and Outlook

Overall, the reactivity data established in this thesis underscore the potential of both *para*- and *ortho*-QMs as versatile and practical electrophiles in organic synthesis. These findings provide a valuable reference framework for comparing QMs to other classes of electrophiles, for predicting the reactivity of novel derivatives and for optimizing their application in organic synthesis as well as their use as molecular probes in biochemical studies. In addition, some of the QMs studied herein may serve as new standard electrophiles for future applications of the Mayr-Patz equation in nucleophile characterization.

Moreover, the established reactivity data can also support data-driven reactivity modeling.[1] Incorporating these results into machine learning algorithms could enable fast and accurate predictions of reaction outcomes and facilitate the targeted discovery of new electrophile-nucleophile combinations.[2]

Future research should aim to expand this work to other structural variants of quinone methides, especially to aza-quinone methides (aza-QMs) (Figure 1). These compounds feature an imine group in place of the carbonyl moiety within the QM scaffold. Both *para*- and *ortho*-aza-QMs have shown potentials as highly reactive intermediates in synthesis of natural products, pharmaceuticals and materials.[3] However, their transient nature and the lack of efficient synthetic methods have hampered their overall development and prevented detailed kinetic and spectroscopic characterization. Hence, developing stabilized aza-QMs that can be isolated and spectroscopically characterized would therefore represent a major breakthrough. This would not only enable systematic reactivity studies and quantitative parameterization using the Mayr-Patz methodology but also broaden their synthetic applications.
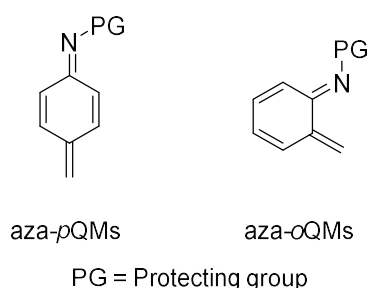

aza-*p*QMs   aza-*o*QMs

PG = Protecting group

Figure 1. *Para*- and *ortho*-aza-quinone methides (aza-*p*QMs and aza-*o*QMs), structural variants of normal QMs.

In addition, future efforts could target reactivity investigations of natural products that contain QM motifs, such as di- and triterpenes.[4] Understanding the electrophilic reactivity of these naturally occurring QMs is essential for elucidating their biological activity and assessing their therapeutic potential.

Given their ability to form reversible covalent bonds with nucleophiles[5], QMs also qualify as promising tools for probing dynamic molecular networks.[6] Within the concept of Dynamic Covalent Chemistry (DCC), this reversible binding has so far been primarily studied on aza-Michael additions. Notably, studies by Rokita et al. have demonstrated that QMs can migrate along duplex DNA strands before becoming covalently fixed at thermodynamically preferred nucleophilic sites.[7] This dynamic behavior holds significant potential for applications in target-selective therapeutics, adaptive molecular recognition and biological sensing.[8]

Importantly, thermodynamic control plays a central role in directing QM migration, particularly in non-equilibrium systems. To harness this behavior for controlled chemical processes, it would be essential to analyze kinetics and thermodynamics of QMs toward standardized carbon-, nitrogen-, sulfur-, and phosphorus-based nucleophiles/Lewis bases according to physical organic methodology. These studies should ideally be conducted under conditions that mimic relevant external chemical and physical triggers that affect molecular networks. Integrating electrophilic reactivity data (electrophilic reactivities) with quantitative thermodynamic descriptors (equilibrium constants K, Lewis acidities) could help to rationally design directionally controlled and switchable QM systems that operate across multidimensional scaffolds such as nucleic acids and peptides.

References.

[1] M. Vahl, J. Proppe, *Phys. Chem. Chem. Phys.* **2023**, *25*, 2717.

[2] a) S. A. Cuesta, M. Moreno, R. A. López, J. R. Mora, J. L. Paz, E. A. Márquez, *J. Chem. Inf. Model.* **2023**, *63*, 507; b) Y. Liu, Q. Yang, J. Cheng, L. Zhang, S. Luo, J.-P. Cheng, *ChemPhysChem* **2023**, *24*, e202300162.

[3] a) K. Wojciechowski, *Eur. J. Org. Chem.* **2001**, *2001*, 3587; b) H.-H. Liao, S. Miñoza, S.-C. Lee, M. Rueping, *Chem. Eur. J.* **2022**, *28*, e202201112; c) B. Yang, S. Gao, *Chem. Soc. Rev.* **2018**, *47*, 7926.

[4] a) S. E. Rokita, *Quinone Methides*, Wiley, Hoboken, (NJ), **2009**; b) T. N. Purdy, B. S. Moore, A. L. Lukowski, *J. Nat. Prod.* **2022**, *85*, 688; c) J. Gao, Q. Chen, Q. Zhang, *Nat. Prod. Rep.* **2025**, Advance Article (doi.org/10.1039/d5np00044k); d) L.-N. Gao, K. Zheng, H.-Y. Chen, Y.-N. Gao, Z.-Z. Li, C. He, S.-H. Huang, R. Hong, M. Bian, Z.-J. Liu, *Org. Biomol. Chem.* **2025**, *23*, 2775.

[5] a) R. Lucius, *Dissertation*, *Ludwig-Maximilians-Universität München*, München, Germany, **2001**, (https://doi.org/10.5282/edoc.257); b) S. Arumugam, V. V. Popik, *J. Am. Chem. Soc.* **2012**, *134*, 8408.

[6] S. Otto, *Acc. Chem. Res.* **2012**, *45*, 2200.

[7] a) F. Fakhari, S. E. Rokita, *Nat. Commun.* **2014**, *5*, 5591; b) C. Huang, Y. Liu, S. E. Rokita, *Signal Transduct. Target. Ther.* **2016**, *1*, 16009.

[8] A. Minard, D. Liano, X. Wang, M. Di Antonio, *Bioorg. Med. Chem.* **2019**, *27*, 2298.